SOCIETÀ NAZIONALE DI SCIENZE, LETTERE E ARTI IN NAPOLI
MEMORIE DELL'ACCADEMIA
DI SCIENZE FISICHE E MATEMATICHE

LIGUORI EDITORE

SOCIETÀ NAZIONALE DI SCIENZE, LETTERE E ARTI IN NAPOLI
MEMORIE DELL'ACCADEMIA
DI SCIENZE FISICHE E MATEMATICHE
7

TSUTOMU KAWASAKI (Ph. D.)

THEORY OF CHROMATOGRAPHY

LIGUORI EDITORE

Il presente volume è stato realizzato con il contributo della Regione Campania
e del Ministero per i Beni Culturali

Tutti i diritti sono riservati. Nessuna parte di questa pubblicazione può essere tradotta, riprodotta, copiata o trasmessa senza l'autorizzazione scritta dell'editore. Fotocopie per uso personale del lettore possono essere effettuate nei limiti del 15% di ciascun volume/fascicolo di periodico dietro pagamento alla SIAE del compenso previsto dall'art. 68, comma 4, della legge 22 aprile 1941 n. 633 ovvero dall'accordo stipulato tra SIAE, AIE, SNS e CNA, CONFARTIGIANATO, CASA, CLAAI, CONFCOMMERCIO, CONFESERCENTI il 18 dicembre 2000. Le riproduzioni ad uso differente da quello personale potranno avvenire, per un numero di pagine non superiori al 15% del presente volume, solo a seguito di specifica autorizzazione rilasciata da AIDRO, via delle Erbe 2, 20121 Milano, telefax 02 809506, e-mail aidro@iol.it.

Prima edizione italiana Gennaio 2004
Liguori Editore, Srl
via Posillipo 394
I 80123 Napoli

http://www.liguori.it

Copyright © Liguori Editore, S.r.l. 2004

Kawasaki, Tsutomu :
Theory of Chromatography/Tsutomu Kawasaki
Napoli : Liguori, 2004
ISBN 88 - 207 - 3651 - 9

Ristampe:

9 8 7 6 5 4 3 2 1 0 2012 2011 2010 2009 2008 2007 2006 2005 2004

Questo volume è stato stampato in Italia dalle Officine Grafiche Liguori - Napoli
su carta inalterabile, priva di acidi, a PH neutro, conforme alle norme Iso 9706 ∞.

Acknowledgments

I am very grateful to Prof.G.Bernardi for having suggested originally a series of investigations leading to this monograph and for his continuous interest and encouragement since the first encounter of nearly forty years ago. This happened as follows. I had completed four years of the graduate course involving the last two years of the stay in Department of Biophysics and Biochemistry, Faculty of Science, University of Tokyo, Tokyo, and I was immediately before the completion of two successive years of the master course in the laboratory of Prof.H.Noda in the same department. As for that epoch (about forty years ago), the education performed in the department, especially in the laboratory of Prof.Noda, was highly original and specific, demanding of the students all-round acquirements of certain levels of all of physical, chemical and biological sciences at the same time. I am grateful to Prof.Noda and all the staffs in his laboratory in that epoch for the original education and for useful discussions which led me to the foundation of a certain attitude vis-à-vis to the scientific research. It is in this background that Prof.Noda presented me Prof.Bernardi, who prepared me a post in his laboratory in the Centre de Recherches sur les Macromolécules (renamed as Institut Charles Sadron) in Strasbourg. Immediately after the completion of the master course, I removed to Strasbourg, and the study of hydroxyapatite chromatography started in collaboration with Prof.Bernardi by his suggestion. I am grateful to Prof.H.Benoit who kindly took his patience in critically reading the manuscripts of my first theoretical papers and who gave me very useful discussions with partitipations of both Prof.Bernardi and Prof.M.Daune to whom I am grateful also. After the stay of about three years in Strasbourg, I passed the total of about seven years again in the new laboratory of Prof.Bernardi in the Institut de Biologie Moléculaire (renamed as Institut Jacques Monod), Université Paris Ⅶ, Paris, with some interruptions by returning to Tokyo; some additional discussions with Prof.Benoit were continued in Paris. All the original experiments presented in Chapter Ⅶ were carried out directly by Mr.M. Niikura with a backup support by Mr.W.Kobayashi in Koken Bioscience Institute, Tokyo, to which I was belonging in some period. I wish to thank both of them as well as other staffs in the institute. Finally, I am grateful to Prof.H.Monma, Department of Applied Chemistry, Faculty of Engineering, Kogakuin University, Tokyo, for kindly providing me with useful knowledges about inorganic phosphate researches.

CONTENTS

XI *Abbreviations*

1 Chapter I.
Introduction
1 (A) A Sketch of Chromatography
33 (B) Perspective and the Current of Contents

39 Chapter II.
Ideal Isocratic Chromatography in the Absence of Axial Diffusion in the Column
39 (A) Fundamental Concept
43 (B) Variable s, $\hat{m}$ and ξ
45 (C) Gradient G, Trajectory T_0, and Trajectory T
52 (D) Measurements of C and χ
61 (E) Chromatogram as First Concept versus Abstract Flux, and Complementary Chromatogram as First Concept versus Complementary Abstract Flux
64 (F) Expression in Terms of Proper Time ξ: Chromatogram as Second Concept and Complementary Chromatogram as Second Concept versus Molecular Band as Flux
67 (G) Rewriting in Terms of Time η, Proper Time ξ, and Distance ζ

77 Chapter III.
Ideal Gradient Chromatography in the Absence of Axial Diffusion in the Column
77 (A) Gradient in the Liquid Phase and Gradient in the Solid Phase
81 (B) Unified View of Chromatography
83 (C) Usefulness of the ($\hat{m}$, s) Plane
87 (D) Expression of Gradient G in Terms of Projection B'($\hat{m}$) or B"(s)
89 (E) Capacity Ratio
90 (F) Chromatogram as First Concept versus Abstract Flux
94 (G) Expression in Terms of Proper Time ξ: Molecular Band as Flux
101 (H) Chromatogram as Second Concept versus Molecular Band as Flux
108 (I) The Case of Molecular Band with A Small Width
112 (J) Rewriting in Terms of Time η, Proper Time ξ, and Distance ζ

121 Chapter IV.
Actual Isocratic Chromatography in the Presence of Axial Diffusion in the Column
121 (A) Axial Diffusion in the Column and Trajectory T_0
121 (B) Chromatogram as Second Concept

124 (C) Derivation of Chromatogram as First Concept from Chromatogram as Second Concept

127 Chapter V.
Actual Gradient Chromatography in the Presence of Axial Diffusion in the Column
127 (A) Chromatogram as Second Concept
130 (B) Derivation of Chromatogram as First Concept from Chromatogram as Second Concept
132 (C) Concrete Form of Function $\Theta(s)$ or $\Xi(s) \equiv \Theta(s)/\Theta^{\circ}$: Balance between Axial Diffusion and Compression/Expansion of Band

137 Chapter VI.
Theory of Concentration Gradient Chromatography Combined with Competition Model
137 (A) Conclusion on the Theory of Concentration Gradient Chromatography
140 (B) Combination with Competition Model
141 (C) Relationship with Appendix XII(B)
143 (D) Relationship with Earlier Works

147 Chapter VII.
Experimental Verification of Dynamic Investigation
147 (A) Purpose
147 (B) Materials and Methods
148 (C) Test of Concentration Gradient
153 (D) Determination of Interstitial Volume, γ, per Unit Length of the Column
154 (E) Concentration Gradient Chromatography
167 (F) A Consideration

171 Chapter VIII.
Competition Model in Contrast with Hydroxyapatite Chromatography
171 (A) Background
178 (B) Competition Model and the Calculation of Adsorption Isotherm
191 (C) $\dot{B}(m)$ or $\dot{k}(m)$
193 (D) Quantitative Test of Competition model
203 (E) Importance of the Term, $\sum_{j=1}^{\nu} e^{E_j/kT}$, in Partition Function Ξ versus Energy, $-\varepsilon$, of Adsorption per Functional Group of Macromolecule
213 (F) Microheterogeneous Models of Collagen and Myosin
237 (G) Some Considerations on the Adsorption of Globular Proteins on the Hydroxyapatite Surface
240 (H) Relationships with Reversed-Phase and Ion-Exchange Chromatographies

245 Chapter IX.
Reversed-Phase Chromatography versus Competition Model
245 (A) Background

246 (B) General Aspect of Reversed-Phase Chromatography
261 (C) Analysis of the Experiment of Lochmüller and McGranaghan
284 (D) Analysis of the Experiment of Terabe et al.
286 (E) Analysis of the Experiment of Larmann et al.
312 (F) Analysis of the Experiment of Jandera

333 Chapter X.
Ion-Exchange Chromatography versus Competition Model
333 (A) General Aspect of Ion-Exchange Chromatography
350 (B) Alalysis of the Experiment of Kopaciewicz et al.
352 (C) Analysis of the Experiment of Baba et al.

377 APPENDIX

379 Appendix I.
Partial Differentiation of Compound Function

381 Appendix II.
Solutions of Differential Equations
381 (A) General Solution of Eq(3.31) When B Is Represented by Eq(3.32), and Other Similar Cases
381 (B) General Solution of Eq(3.77)
383 (C) Solution of Homogeneous Linear Partial Differential Equation of the Second Order with A Parabolic Form
386 (D) Solution of Eq(5.26) Combined with Eq(5.20)

387 Appendix III.
Complementary Arguments on Gradient Chromatography
387 (A) Complementary Chromatogram as First Concept versus Complementary Abstract Flux
390 (B) Complementary Chromatogram as Second Concept versus Molecular Band as Flux
391 (C) The Case of Molecular Band with A Small Width

393 Appendix IV.
Visual Understanding of the Relationship between Molecular Band and Chromatogram as First Concept versus Role of the Gradient
393 (A) General Case
407 (B) The Case of Molecular Band with A Small Width

411 Appendix V.
Some Arguments on Eq(5.14) or (5.14') in Connection with Eq(4.16)

415 Appendix VI.
Analysis of the Earlier Experiment

423 Appendix VII.
Justification of Eq(8.17)

425 Appendix VIII.
Reconsideration on the Methodology for the "Determination" of the Collagen Primary Structure versus Collagen Biosynthesis
425 (A) "Determination" of the Primary Structure
425 (B) Biosynthesis
427 (C) Possibility of Explaining the Heterogeneous Collagen Chromatograms (Figs 8.14 and 8.15) on the Basis of Other Models Than Microheterogeneous Model
429 (D) Comment on Some Experimental Data Giving An Apparent Impression of High Homogeneities of Both α_1 and α_2 Peptides

431 Appendix IX.
Experiment of Yamauchi et al. Manifesting A Heterogeneity of the Collagen Primary Structure

433 Appendix X.
Detail on the Calculation of Fig 8.19
433 (A) Calculation
436 (B) Some Comment

439 Appendix XI.
Theoretical Studies of Other Authors: Relationship with the Present Theory
439 (A) Isocratic Chromatography
453 (B) Gradient Chromatography
471 (C) Adsorption and Desorption Mechanism: Chemical Equilibrium Equation Model
479 (D) Models Insisting on the Predominant Role of the Mobile Phase for the Adsorption of Sample Molecule on the Adsorbent
485 (E) Solubility Parameter Model
486 (F) Statistical Mechanical Model

501 *References*

Abbreviations

RMT = resistance to mass transfer between mobile and stationary phases

TPV = theoretical point of view

EPV = experimental point of view

OPV = ordinary point of view

CPV = complementary point of view

OPV(CPV) = ordinary point of view induced from complementary point of view

CPV(OPV) = complementary point of view induced from ordinary point of view

OPV[CPV(OPV)] = ordinary point of view which is re-induced from complementary point of view induced from ordinary point of view

CPV[OPV(CPV)] = complementary point of view which is re-induced from ordinary point of view induced from complementary point of view

MB = molecular band

MB(o) = molecular band migrating on the column; suffix(o) implies "ordinariness"

MB(c) = molecular band migrating on the carrier liquid; suffix(c) implies "complement"

FCB = fundamental conceptual band

CGM1st = chromatogram as first concept

CGM2nd = chromatogram as second concept

χGM1st = complementary chromatogram as first concept

χGM2nd = complementary chromatogram as second concept

HPLC = high-performance liquid chromatography

HA = hydroxyapatite

M_m = molecular mass (used not only as abbreviation but also as symbol)

pI = isoelectric point

KP buffer = potassium phosphate buffer at pH≈6.8 i.e., an equimolar mixture of KH_2PO_4 and K_2HPO_4

NaP buffer = sodium phosphate buffer at pH≈6.8 i.e., an equimolar mixture of NaH_2PO_4 and Na_2HPO_4

AVFA = absolute value of free energy of adsorption

ACMCL = active component molecule from the carrier liquid (synonym of gradient substance)

LSS gradient = linear solvent strength gradient

PTH = phenylthiohydratoinine

SDS = sodium dodecylsulfate

OHAlHis = hydroxylaldolhistidine

THF = tetrahydrofuran

$MeCl_2$ = methylene chloride

ANC = acetonitrile

MtOH = methanol

DXN = 1,4-deoxane

LH-RH = luteinizing hormone releasing hormone

ACTH = adrenocorticotropic hormone

Na_4EDTA = sodium ethylenediaminetetraacetate

Chapter I. Introduction

(A) A Sketch of Chromatography

The Presence of Mobile and Stationary Phases. The general purpose of this monograph is to understand the fundamental principle of chromatography. Most rudimentarily, chromatography can be understood as a flow of sample molecules taking place in a two-phase system consisting of *mobile* and *stationary phases*. The stationary phase, in general, appears on the surfaces of the particles packed in the column and the mobile phase, filled with the carrier fluid, appears in the interstices among the particles. The packed particles may be replaced by a network structure constructed in the column.

In some instances, however, a model is applied in which the surface as stationary phase is replaced by a three-dimensional structure attached to the particles or the network, and it is assumed that the sample molecule is absorbed or dissolved in this structure instead of being adsorbed on the surface. The chromatography in which this model is believed to apply is called partition chromatography. The three-dimensional structure proposed in such a model, however, would result in an assembly of surfaces after all. This is because it is reasonable to consider that the molecule absorbed or dissolved in the three-dimensional structure is adsorbed on a surface or surfaces that is/are present within the structure eventually (even though the interval between face-to-face surfaces within the structure may be small). At least regarding the macromolecule (with molecular mass higher than the order of 10^3 dalton), it would be difficult to conceive partition chromatography.

The column may be replaced by other concepts like thin layer, paper etc. if chromatography is carried out on these supports. The carrier fluid may be liquid, gas or supercritical fluid.

In the chromatographic process, a sample molecule goes and returns frequently between mobile and stationary phases induced by thermal Brownian motion and, only in the fraction of time when it is staying in the mobile phase (while dissolving in the carrier fluid), the molecule is transported toward the outlet of the column by the flow of the carrier fluid; this is produced by the external force generated by a pump. With old type of chromatography, the gravity is often used instead of the pump as driving force. The assembly of the same molecular species in the sample mixture migrate on the column while forming a band at a rate lower than the migration rate of the carrier fluid, each molecule meanwhile repeating the frequent movement between the two phases. Between different molecular species with different fractions of time of stay in the mobile phase, the rates of migration on the column are different, and the chromatographic separation takes place between bands of different species. [In a special technique called frontal analysis, the molecular band with virtually infinite width is formed. We do not refer to this technique, however.]

Gradient. It is possible to bias the balance of the movement of sample molecules between mobile and stationary phases toward either phase by changing the environment sur-

rounding the molecules. Chromatography carried out while keeping the environment constant as a function of time is called *isocratic chromatography*. In the absence of mutual interactions among molecules (see the sudsequent subsection entitled "Analytical Chromatography with Low Molecular Density or Small Sample Loads"), the molecular band migrates at a constant rate on the column with isocratic chromatography. Chromatography carried out while changing the environment surrounding the sample molecules as a function of time is called *gradient chromatography*; *gradient* implies the gradual change of the environment. The abrupt change of the environment is called *step gradient*. Usually, the gradient is applied in such a way that the migration of the molecular band accelertates, and it is this case that is treated mainly in this monograph.

There are two types of gradient: the first and the second type bringing about *local* and *global* changes of the environment surrounding the sample molecules as functions of time, respectively. The first type involves two sub-types: *gradient in the stationary phase* and *gradient in the mobile phase*. This latter is also called as *concentration gradient*. Gradient in the stationary phase implies a (gradual) change of the property of packed particles taking place in the axial direction of the column. In order for the acceleration of the migration of the molecular band to occur, gradient in the stationary phase should be applied in such a way that the affinity of sample molecule for packed particles decreases when going from the inlet to the outlet of the column. In principle, gradient in the stationary phase is realizable not only by packing the column with particles with properties different from one another in the axial direction of the column but also by applying a temperature or another gradient between inlet and outlet of the column packed with homogeneous particles, provided that the affinity of sample molecule for packed particles depends on temperature or another field. A step gradient in the stationary phase can be realized by simply connecting columns with different properties in series.

Gradient in the mobile phase can be generated by supplying the column with the carrier fluid at the inlet while changing its composition or increasing the concentration of a certain component of the fluid as a function of time, provided that the affinity of sample molecule for packed particles in the column decreases with increase in concentration of the component under consideration coexisting with sample molecule (through a certain mechanism). Let us call this component as *gradient substance*. A concentration gradient now is formed between inlet and outlet of the column (in such a way that concentration decreases from the inlet to the outlet), and it migrates on the column at a rate equal to the migration rate of the carrier fluid, provided that the adsorption (or absorption with partition chromatography) of gradient substance on (in) packed particles in the column (called demixing) does not occur, or that its effect is negligible if demixing takes place actually. The concentration gradient passes the band of sample molecules migrating on the column since the rate of migration of the band, in general, is lower than the flow-rate of the carrier fluid or the migration rate of concentration gradient. The concentration of gradient substance at the position of the molecular band increases as a function of time, thus

bringing about the acceleration of the migration of the band.

The changes of the ambient temperature, the background pressure and other fields occurring globally in the chromatographic system can represent the second type of gradient, provided that the affinity of sample molecule for packed particles in the column depends on these agents. The migration of the molecular band can be accelerated by the second type of gradient.

This monograph is focused on column liquid chromatography for the case when the two-dimensional stationary phase takes place on the surfaces of the packed particles in the column. Whether the stationary phase is two- or three-dimensional, however, does not change the fundamental consideration on chromatography [cf. Appendix XI(A)]. With liquid chromatograaohy, the carrier fluid is limited to the carrier liquid, and mobile and stationary phases are synonymous to *liquid* and *solid phases*, respectively (but, for detail, see the subsequent subsection entitled "Resistance to Mass Transfer between Mobile and Stationary Phases"). Further, it is rare that the second type of gradient is applied [but see Appendix XI(B)], and we treat only the first type of gradient. Isocratic chromatography is regarded as an extreme case of the first type of gradient chromatography carried out by using an infinitesimal slope of gradient. It also is rare that the gradient in the stationary phase is applied in practice [cf. Appendix XI(B)]. Theoretically, however, it is important to consider the presences of both gradient in the mobile phase and gradient in the stationary phase. This is because the two gradients are conceptually both symmetric and complementary [cf. the subsequent Section(B)]; the consideration of the presences of the two gradients leads to a deeper insight into the principle of chromatography.

Analytical Chromatography with Low Molecular Density or Small Sample Loads. In this monograph, we only treat the case when the density of sample molecules in the column is low and when the mutual interactions among sample molecules are negligible. The mutual molecular interaction implies both geometrical and energetical [usually repulsive in appearance; cf. Chapter VIII(F)] interactions added to the simple exchange of energies of thermal motion between molecules (cf. Chapter VIII). At low molecular density, the adsorption isotherm (to the packed particles in the column) for any component of the sample mixture is linear, and the molecular band of any component migrates on the column independently of the presences of the other components. For developing the theory, it therefore is sufficient to consider the behavior of a single component. We mainly consider the case when a molecular band with a small width is formed initially at the inlet of the column; this is the usual experimental condition used in analytical chromatography (except the case of frontal analysis). In Chapter VIII(F), however, we touch slightly on the mutual interaction between sample molecules. The case when the flow-rate is constant is considered always. The flow-rate implies the volume of the carrier liquid passing a vertical section of the column per unit time (in units of volume/time) or the rate of migration of the carrier liquid passing the vertical section (in unit of lengh/time); the rate represents the mean rate in the presence of the flow heterogeneity. The compression of the liquid is as-

sumed to be negligible in practice if it takes place.

Gel Filtration Effect (also called as **Size Exclusion** or **Pore Exclusion Effect**). It sometimes happens that the effective interstitial volumes of the column (or the effective volumes of the mobile phase) are different between sample molecule and carrier liquid, or between sample molecules with different sizes. The latter phenomenon is called *gel filtration* effect, and it contributes to chromatographic separation. Theoretically, it also is possible that the effective interstitial volumes of the column are different between different components of the carrier liquid. In this monograph, however, we do not touch on these problems by simply assuming that the effective interstitial volumes are the same among all the substances interfering in chromatography. In fact, usually, the sizes of different components of the carrier liquids are comparable with one another, so that the effective interstitial volumes can be assumed to be also comparable. It therefore would not happen in practice that the liquid phase as environment surrounding sample molecules be perturbed, induced by different effective interstitial volumes among different components of the carrier liquid. Usually, the size of sample molecule is larger than or of the same order of magnitude as that of any component of the carrier liquid. In the former case, it in general is possible that the effective interstitial volume of the column for sample molecule is smaller than that for the carrier liquid. With regard to hydroxyapatite chromatography, however, we find experimentally no difference in effective interstitial volumes of the column among substances interfering in chromatography [cf. Chapter Ⅶ(D)]. With regard to reversed-phase chromatography, the gel filtration effect is much less feasible under adsorptive condition than under non-adsorptive condition [cf. Chapter Ⅸ(C)].

Apparent Equilibrium at the Center of Molecular Band: Equilibrium Theory versus Kinetic Theory. Let us begin with considering what happens if the rate of mass transfer between mobile and stationary phases is infinitesimal due to the presence of an infinite *resistance to mass transfer between the two phases* (abbreviated as RMT; cf. the subsequent subsection entitled "Resistance to Mass Transfer between Mobile and Stationary Phases"). In this hypothetical case, the molecules staying in mobile and stationary phases will continue staying in the same phases, respectively. Provided that a single molecular band with a small (virtualy infinitesimal) width is formed initially and that the enlargement of the width of the band due to diffusion in the axial direction of the column is negligible, then, with a lapse of time, the initial band will split into two bands: one of them will continue staying at the initial position and the other will migrate on the column at a rate equal to the flow rate. This means that the center of gravity of the two bands migrates on the column toward the outlet and that the standard deviation of the assembly of two bands around the center of gravity increases with migration of the center of gravity; the center of gravity is a concept conceivable by comparing the number of molecules contained in each band to weight.

To the contrary, if the rate of mass transfer between the two phases is infinite in the absence of RMT (i.e., if a thermodynamic equilibrium between the two phases is at-

tained in the band always), then the band (which we call equilibrium band) will migrate without splitting, and it always will be situated between the two bands which would take place in the presence of infinite RMT.

If molecular partitions (i.e., fractions of molecules) in mobile and stationary phases taking place in the initial band with infinitesimal rate of mass transfer are equal to those taking place in the equilibrium band, then the center of gravity between mobile and stationary phase molecular bands produced after splitting of the initial band will coincide with the position of the equilibrium band. In fact, denoting molecular partitions in mobile and stationary phases in the equilibrium band by B° and $1-B^\circ$ (where $0<B^\circ<1$), respectively, the equilibrium band will migrate on the column at a rate B° times as high as the rate of migration (equal to the flow-rate) of the mobile phase band; this is because the molecule is transported toward the outlet of the column by the flow of the carrier liquid only when it is staying in the mobile phase. It follows that the distance from the equilibrium band to the stationary phase band (or the distance between the equilibrium band and the initial position of all the bands) and the distance from the equilibrium band to the mobile phase band are proportional to B° and $1-B^\circ$, respectively. On the other hand, the total number of molecules contained in the stationary phase band and that of molecules contained in the mobile phase band are proportional to $1-B^\circ$ and B°, respectively. This means that the moments for the two splitting bands around the position of the equilibrium band are equal, both proportional to $B^\circ(1-B^\circ)$. In other words, the equilibrium band is situated at the center of gravity between the two splitting bands.

If the rate of mass transfer between the two phases is finite but high enough, the initial band will not split and a single band with a certain width will be obtained. Within such a band, a position always is involved which coincides with the position of the equilibrium band. It can be considered that both position and shape of the band under consideration are virtually independent of the partition of molecules between mobile and stationary phases that taked place initially in the band; this is because a large number of movements of molecules between the two phases are repeated in the band. As will be mentioned later, it can be deduced that the band is almost Gaussian in shape (i.e., that, in the band, the distribution in molecular density taking place in the axial direction of the column is almost Gaussian). This would mean that the position within the band coinciding with the position of the equilibrium band is also coinciding with the center of gravity of the band; the center of gravity now is identical with the center of symmetry (briefly, the center).

From the analogy to the consideration on the band with infinitesimal rate of mass transfer, the three following points can also be deduced. First, if the total band is considered to be a sum or superposition of the two bands formed in mobile and stationary phases, respectively, the position of the mobile phase band is shifting slightly to the flow direction (i.e., toward the outlet of the column) in comparison with the position of the stationary phase band. As a result, slightly excess partitions on average of molecules in

mobile and stationary phases (in comparison with the equilibrium partition) occur in front and rear halves of the band, respectively. Second, a thermodynamic equilibrium between mobile and stationary phases is attained apparently in the slice at the center of the total Gaussian band. The apparent thermodynamic equilibrium can be considered to occur at the center of the band even in the presence of axial moleculr diffusion in the column (which was assumed to be negligible in all the arguments above). This is because, due to symmetry in shape of the band, the effect of diffusion should be canceled out at the center of the band. Third, the width of the band increases monotonically with a lapse of time or with migration of the band on the column (as far as isocratic chromatography is concerned; for gradient chromatography, see below). This is true both when axial molecular diffusion in the column is negigible and when it is important.

Chromatography is feasible only when a single band with a small enough width of identical molecules is formed on the column. For this purpose, it is necessary (a) that axial molecular diffusion in the column occurs slowly enough and (b) that the deviation from equilibrium betwen mobile and stationary phases, if it takes place, is small enough. Condition(b) can be restated that the RMT is small enough, that the rate of mass transfer between the two phases is high enough, that the duration of a stay of the molecule in either phase is short enough, or that the molecule goes and returns frequently enough between the two phases. The smaller the deviation from equilibrium, the smaller the RMT, the higher the rate of mass transfer, the shorter the duration of a stay of the molecule in either phase, or the more frequent the movement of the molecule between the two phases, then the smaller is the effect of enlarging the width of the molecular band except for the effect arising from the axial molecular diffusion in the column.

Molecular diffusion in the axial direction of the column takes place actually in the carrier liquid or the mobile phase induced by a combination of thermal Brownian motion with the random motion of molecules brought about by a random heterogeneity of the flow of the carrier liquid; the random heterogeneity of the flow can be assumed to be induced by a number of fluid-mechanical factors taking place in the interstices among the packed particles in the column. This gives rise to axial diffusion of the molecules *as members of the molecular band*, which occurs only in fraction of time when molecules are staying in the mobile phase. Hereafter, let us call axial diffusion of the molecules as members of the band as *ordinary diffusion*, the enlargement of the width of the malecular band taking place, induced by a finite rate of mass transfer between mobile and stationary phases as *apparent diffusion*, and the enlargement of the width of the band taking place as a result of the coupling of ordinary and apparent diffusions as *diffusion* simply; only the case when both conditions(a) and (b) are fulfilled are treated. The terminology "axial diffusion" is also used, however, to represent the molecular diffusion (in the usual sense) taking place in the mobile phase (with explanatory notes if a confusion may occur).

In the absence of apparent diffusion, the initial molecular band with a small width would spread into a Gaussian band with a lapse of time or with migration on the column

induced by ordinary diffusion. It can be considered that ordinary diffusion is induced by Fick's first law and that this latter is induced by the presence of mean-free-path. [*Note.* Mean-free-path leads to diffusion constant [cf. eq(1.14)], and diffusion constant leads to Fick's first law, playing a role of the proportionality constant relating concentration gradient of molecules to flux of molecular flow brought about by concentration gradient; flux of molecular flow gives rise to ordinary molecular diffusion. The balance between the change in molecular concentration taking place with a lapse of time and the divergence of molecular flux brought about by concentration gradient to which another molecular flux brought about by the flow of the carrier liquid (produced by the external force) is added leads to a Gaussian molecular band if the initial band has a small width. The balance under consideration is called Fick's second law if the molecular flux brought about by the flow of the carrier liquid (produced by the external force) is absent.]

Mean-free-path under consideration is generated by the addition or subtraction of two distances. The first distance represents that corresponding to the component (in the axial direction of the column) of mean-free-path with respect to thermal Brownian motion of the molecule. The second distance represents that generated by a finite duration of stay of the molecule in a channel of the random liqid flow. It can be considered that the molecules goes and returns frequently across neighboring channels of the flow induced by thermal Brownian motion but that the duration of a stay in a channel is finite. In conclusion, the Gaussian shape of the molecular band is originating from mean-free-path taking place in the axial direction of the column.

Provided that ordinary diffusion is negligible and that the movement of the molecule between mobile and stationary phases is done frequently enough at a finite rate [condition (b)], the initial molecular band with a small width would also spread into a band with almost Gaussian shape induced by apparent diffusion. This is because, under condition(b), duration of a stay of the molecule in either phase plays a role of mean-free-path. The movement of the molecule in mean-free-path in the mobile phase occurs toward the outlet of the column relative to the mean movement of the molecule in the column, whereas the movement of the molecule in mean-free-path in the stationary phase occurs toward the inlet of the column relative to the mean movement of the molecule in the column. (The molecule in mean-free-path in the mobile phase is done at a rate equal to the flow-rate on average relative to the column, whereas the molecule in mean-free-path in the stationary phase continues staying at the same position of the column actually.) [For detail, see the subsequent subsection entitled "Diffusion Coefficient for Ordinary Diffusion and Diffusion Coefficient for Apparent Diffusion".]

In the presences of both ordinary and apparent diffusions, mean-free-path for ordinary diffusion taking place in the mobile phase, mean-free-path for apparent diffusion taking place in the mobile phase and mean-free-path for apparent diffusion taking place in the stationary phase together would give rise to a molecular band with almost Gaussian shape with a standard deviation larger than those for the bands taking place only due to ordina-

ry and aparent diffusions, respectively. [For detail, see the subsequent subsections entitled "Convolution Mechanism".]

With gradient chromatography, the axial diffusion taking place as a result of the coupling of ordinary and apparent diffusions can be considered to be balancing with the effect of different rates of migration of molecules taking place in different parts of the band where the environments surrounding molecules are different from one another. As a result, the width of the band does not always increase monotonically with a lapse of time or with migration on the column. Still the band can be considered to be almost Gaussian in shape (cf. the subsequent subsections entitled "Diffusion Coefficient for Ordinary Diffusion and Diffusion Coefficient for Apparent Diffusion" and "Quasi-Static Chromatography versus Nonequilibrium Thermodynamics", respectively).

Finally, it can be assumed that diffusion occurs rapidly enough in the vertical direction of the column for the molecular density to be regarded as being kept virtually uniform in this direction at any instant.

At a given moment, let us consider the total partition in the mobile phase of all the molecules in the molecular band. As the molecule is transported toward the outlet of the column by the flow of the carrier liquid only when it is staying in the mobile phase, the total molecular partition under consideration is numerically equal to the rate of migration of the band as a whole relative to the rate of migration of the carrier liquid. The relative rate of migration of the molecular band as a whole implies the average of the relative rates of migration of all the molecules forming the band. When the molecular band is Gaussian in shape, the molecular partition in the mobile phase taking place in the slice at the center of the band is numerically equal to the relative rate of migtation of the center of the band; this can be determined by the equilibrium theory (see above). Only in the presence of RMT, the kinetic theory interferes *in determining the width of the band.* Even in this instance, the kinetic theory does not make explicit appearance, hidden within the concept of diffusion coefficient with respect to total axial diffusion in the column (cf. the subsequent subsection entitled "Quasi-Static Chromatography versus Nonequilibrium Thermodynamics").

Convolution Mechanism. The convolution ,F_1*F_2, of two distributions F_1 and F_2 (as functions of L', respectively) can be defined as

$$(F_1*F_2)(L') = \int_{-\infty}^{\infty} F_1(L'-L'_2)F_2(L'_2)dL'_2$$

$$= \int_{-\infty}^{\infty} F_1(L'_1)F_2(L'-L'_1)dL'_1 \qquad (1.1)$$

In the middle of eq(1.1), $F_1(L'-L'_2)$ represents a distribution taking place along the L' axis with its mean position equal to L'_2 and $F_2(L'_2)$ represents the distribution (i.e., the frequency of occurrence) of mean position L'_2; L'_2 varies between $-\infty$ and ∞. Thus, convolution, F_1*F_2, represents a distribution as a sum or superposition of an infinite number of distributions F_1 the mean positions L'_2 of which are different from one another; the contribution of each F_1 (to the total distribution F_1*F_2) is represented by a distribution F_2. The extreme right-hand side of eq(1.1) manifests that the same total distribution F_1*F_2 can also be obtained if a distribution as a sum or superposition of an infinite number of distributions F_2 the mean positions L'_1 of which are different from one another is considered and if the contribution of each F_2 (to the total distribution F_1*F_2) is represented by a distribution F_1.

It is possible to extend eq(1.1) to

$$(F_1*F_2*\ldots*F_n)(L')$$

$$= \int_{-\infty}^{\infty}\cdots\int_{-\infty}^{\infty} F_1(L'-\sum_{i=2}^{n} L'_i)F_2(L'_2)\ldots F_n(L'_n)\prod_{i=2}^{n} dL'_i$$

$$= \int_{-\infty}^{\infty}\cdots\int_{-\infty}^{\infty} F_1(L'_1)F_2(L'-\sum_{i\neq 2} L'_i)F_3(L'_3)\ldots F_n(L'_n)\prod_{i\neq 2} dL'_i$$

$$\cdots$$

$$= \int_{-\infty}^{\infty}\cdots\int_{-\infty}^{\infty} F_1(L'_1)F_2(L'_2)\ldots F_{n-1}(L'_{n-1})F_n(L'-\sum_{i=1}^{n-1} L'_i)\prod_{i=1}^{n-1} dL'_i \qquad (1.2)$$

where it should be noted that F_i $(i=1,2,\ldots,n)$ are both commutative $(F_i*F_j=F_j*F_i)$ and associative $[(F_i*F_j)*F_k=F_i*(F_j*F_k)]$.

Let us consider the case when $F_i(L')$ represents a Gaussian distribution with standard deviation ρ_i or variance ρ_i^2:

$$F_i(L') = \frac{1}{\sqrt{2\pi}\ \rho_i}\exp(-\frac{L'^2}{2\rho_i^2}) \qquad (1.3)$$

where $i=1,2,\ldots,n$. It is easy to show that

$$(F_1*F_2*\ldots*F_n)(L') = \frac{1}{\sqrt{2\pi}\ (\rho_1^2+\rho_2^2+\ldots+\rho_n^2)^{1/2}} \exp\left(-\frac{L'^2}{2(\rho_1^2+\rho_2^2+\ldots+\rho_n^2)}\right) \quad (1.4)$$

By considering $L'-\acute{L}'$ (where $\acute{L}'$ represents a constant) instead of L', it is possible to rewrite eq(1.4) as

$$(F_1*F_2*\ldots*F_n)(L'-\acute{L}')$$

$$= \frac{1}{\sqrt{2\pi}\ (\rho_1^2+\rho_2^2+\ldots+\rho_n^2)^{1/2}} \exp\left(-\frac{(L'-\acute{L}')^2}{2(\rho_1^2+\rho_2^2+\ldots+\rho_n^2)}\right) \quad (1.4')$$

Eq(1.4) or (1.4') shows that the convolution of Gaussian distributions respectively with variances ρ_1^2, ρ_2^2, ..., ρ_n^2 generates a Gaussian distribution with variance ρ^2 represented as a sum of the original variances as

$$\rho^2 = \rho_1^2 + \rho_2^2 + \ldots + \rho_n^2 \quad (1.5)$$

Thus, the variances are additive with respect to the convolution among Gaussian distributions.

With regard to Gaussian molecular distribution brought about by ordinary diffusion (as a function axial position L' on the column or distance L' from the column inlet with the center of distribution at $L'=\acute{L}'$), the variance (denoted by $\bar{\rho}^2$) can in general be decomposed into a number of variances in such a way that

$$\bar{\rho}^2 = \sum_{\alpha} \bar{\rho}_\alpha^2 \quad (1.6)$$

This is because, at the moment when a Gaussian molecular distribution is expanding due to ordinary diffusion , all the slices of the distribution are being diffused to generate Gaussian distributions with identical widths among them (indicated by $\alpha = 1$), respectively; all the slices of all the Gaussian distributions indicated by $\alpha = 1$ are being diffused to generate Gaussian distributions with identical widths among them (indicated by $\alpha = 2$), respectively, and so on. The convolution can be made following any order of α values. The decomposition represented by eq(1.6) is of practical significance only if molecular diffusions indicated by different values of α take place by different mechanisms from one another. It should be noted, however, that an arbitrary decomposition of the diffusion mechanism into mechanisms that are not independent of one another does not reproduce the original distribution through a convolution.

It can be considered that the coupling of ordinary diffusion (bringing about a Gaussian distribution with variance $\bar{\rho}^2$) and apparent diffusion (bringing about a Gaussian distribution with variance $\bar{\bar{\rho}}^2$) to generate a Gaussian band (with variance ρ^2; deduced in the subsection entitled "Apparent Equilibrium at the Center of Molecular Band: Equilibrium Theory versus Kinetic Theory") occurs through a convolution mechanism fulfilling the relationship:

$$\rho^2 = \bar{\rho}^2 + \bar{\bar{\rho}}^2 \tag{1.7}$$

This is because any slice (with an infinitesimal width or variance) of Gaussian distribution with variance $\bar{\bar{\rho}}^2$ brought about by apparent diffusion can be considered to expand to a Gaussian distribution with a finite variance $\bar{\rho}^2$ when ordinary diffusion is coupled, thus giving rise to a Gaussian band with variance ρ^2 represented by eq(1.7). In the same fashion, any slice (with an infinitesimal width or variance) of Gaussian distribution with variance $\bar{\rho}^2$ brought about by ordinary diffusion would expand to a Gaussian distribution with a finite variance $\bar{\bar{\rho}}^2$ when apparent diffusion is coupled, thus giving rise to a Gaussian band with variance ρ^2 represented by eq(1.7).

Diffusion Coefficient for Ordinary Diffusion and Diffusion Coefficient for Apparent Diffusion. *New system of units*: In order to perform the efficient argument, let us introduce a new system of units according to which distance or length is represented in units of volume. Thus, the thickness of the slice of the column in which unit interstitial volume is involved is defined as *unit length expressed in units of volume.* When measuring any length, we imagine a column extending over the length and we express the length under consideration in terms of the total interstitial volumes of the column in imagination. Of course, this involves the special case when the length in question represents the distance from the inlet of an axial position of the column. In this instance, the distance expressed in new system of units represents the total interstitial volumes involved between the inlet and the position under consideration of the column. Let us consider that axial position L' on the column or distance L' from the column inlet (see the subsection entitled "Convolution Mechanism") is expressed in new system of units. Time is also represented in units of volume. Thus, the time necessary for the volume of carrier liquid equal to unit interstitial volume of the column to pass through a given position L' on the column is defined as *unit time expressed in units of volume.* In other words, the volume of the carrier liquid passing through a given axial position on the column is defined as time. Let us denote by Z the time expressed in new system of units. When measuring any time, we imagine a column and we express the time under consideration in terms of Z. The flow-rate i.e., the mean rate of migration of carrier liquid now is represented as unity (dimensionless).

Let us write x and t for general length and general time expressed in usual system of units, respectively, and let us write x as I when it is expressed in new system of units. We also write u for the flow-rate of the carrier liquid on the column (with dimension of length/time expressed in usual system of units). I and Z are related to x and t by

$$I = \gamma x \tag{1.8}$$

and

$$Z = \gamma ut \tag{1.9}$$

respectively, where γ (with dimensions of area in usual system of units) represents the

mean value of the interstitial volume per unit length of the column or the effective area of the column section; this fluctuates microscopically along the main axis of the column, contributing to bringing about random heterogeneity of the flow of the carrier liquid. When I represents L', x represents the distance (with dimension of length; written as L) from the inlet of any position on the column.

Representation of Einstein's equation in new system of units: By using new system of units, Einstein's equation relating ρ^2 to diffiusion coefficient Ψ° for total diffusion of the molecular band (present over both mobile and stationary phases), that relating $\bar{\rho}^2$ to diffuson coefficient $\bar{\Psi}^\circ$ with respect to ordinary diffusion of the band, that relating $\bar{\rho}_\alpha^2$ to diffusion coefficient $\bar{\Psi}^\circ_\alpha$ with respect to decomposed component α of ordinary diffusion of the band and that relating $\bar{\bar{\rho}}^2$ to diffusion coefficient $\bar{\bar{\Psi}}^\circ$ with respect to apparent diffusion of the band can be written as

$$\left.\begin{aligned} \rho^2 &= 2\Psi^\circ Z \\ \bar{\rho}^2 &= 2\bar{\Psi}^\circ Z \\ \bar{\rho}_\alpha^2 &= 2\bar{\Psi}^\circ_\alpha Z \\ \bar{\bar{\rho}}^2 &= 2\bar{\bar{\Psi}}^\circ Z \end{aligned}\right\} \quad \text{and} \qquad (1.10)$$

respectively; all the diffusion coefficients have dimensions of volume. By using eqs(1.6) and (1.7),

$$\bar{\Psi}^\circ = \sum_\alpha \bar{\Psi}^\circ_\alpha \qquad (1.11)$$

and

$$\Psi^\circ = \bar{\Psi}^\circ + \bar{\bar{\Psi}}^\circ \qquad (1.12)$$

are obtained, respectively. With isocratic chromatography, all the diffusion coefficients are constant, representing diffusion constants. With gradient chromatography, within the limit of the approximation of uniform equilibrium partition of molecules between mobile and stationray phases (see the subsequent paragraph), all the diffusion coefficients change with time Z since molecular partition between the two phases changes with Z.

Approximation of uniform equilibrium partition of molecules between mobile and stationary phases in the band: In the presence of RMT, molecular partition between the two phases is slightlty biased to mobile and stationary phases on average in front and rear halves of the molecular band compared with partition taking place, provided that a thermodynanic equilibrium is attained between the two phases, respectively (see the subsection entitled "Apparent Equilibrium at the Center of Molecular Band: Equilibrium Theory versus Kinetic Theory"). Moreover, with gradient chromatography, the environment surrounding the molecule is different from position to position in the band; this means that molecular

partition between the two phases is different from position to position in the band even when a thermodynamic equilibrium between the two phases is attained in any slice of the column. Under both condition(a) and (b) of chromatography (see the subsection referred to just above), however, let us introduce the approximation that molecular partition between the two phases taking place in any slice of the band is the same virtually, equal to the equilibrium partition taking place at the center of band with both isocratic and gradient chromatographies. (Let us denote the equilibrium molecular partitions in mobile and stationary phases by B° and $1-B^\circ$, respectively.) All the arguments below are performed by using this approximation, and the significance of the approximation will be considered later.

Representation of Ψ° *and* Ψ°_α: Writing $\bar{\Theta}^\circ$ for axial diffusion constant for ordinary molecular diffusion taking place in the mobile phase, Ψ° can be represented as

$$\Psi^\circ = B^\circ \bar{\Theta}^\circ \tag{1.13}$$

This is because the dimensions (volume=volume^2/volume) of both diffusion coefficient Ψ° and diffusion constant $\bar{\Theta}^\circ$ represent distance^2/time and the time for the molecule staying in the mobile phase is fraction B° of the total time for the molecule as member of the molecular band staying over both mobile and stationary phases. Similarly, writing $\bar{\Theta}^\circ_\alpha$ for diffusion constant for decomposed component α of ordinary diffusion taking place in the mobile phase, Ψ°_α can be represented as

$$\Psi^\circ_\alpha = B^\circ \bar{\Theta}^\circ_\alpha \tag{1.14}$$

By substituting both eqs(1.13) and (1.14) into eq(1.11),

$$\bar{\Theta}^\circ = \sum_\alpha \bar{\Theta}^\circ_\alpha \tag{1.15}$$

is obtained.

Preparation for the representation of Ψ°: Preliminarily, let us give Ψ° the meaning of diffusion coefficient for any one-dimensional free diffusion of molecules and let us call System 1 the space where diffusion takes place. Ψ° can be represented as

$$\Psi^\circ = b \cdot b/\iota = b^2/\iota = (b^2/\iota)^{1/2} \cdot (b^2/\iota)^{1/2} \tag{1.16}$$

The second term of eq(1.16) gives a definition of Ψ° where b stands for mean-free-path and b/ι for the mean rate of migration of the molecule from one end to the other of mean-free-path; ι represents mean-free-time. After all, Ψ° can be determinrd when both mean-free-path b and mean-free-time ι are given [third term of eq(1.16)]. Here, it is assumed that, if b, ι and Ψ° change with a lapse of time, the change occurs slowly enough. It is possible to divide the assembly of molecules submitted to diffusion into two groups, the one migrating toward a single direction and the other migrating toward the

opposite direction in mean-free-path. Both length of mean-free-path and duration of mean-free-time are equal between the two groups, and it is possible to interpret that first and second 1/2 times powered terms in the extreme right-hand side of eq(1.16) represent the contributions from the two groups of molecules, respectively. Thus, b and ι appearing in the first term represent mean-free-path and mean-free-time with respect to the group migrating toward a single direction, respectively, and b and ι appearing in the second term represent those for the group migrating toward the opposite direction, respectively. The reason why the two terms representing the contributions from the two groups of molecules, both of them, are bearing the same power of 1/2 comes from the fact that the behaviors of the two groups of molecules are symmetric.

Let us consider another system (called System 2) moving in parallel with the direction of diffusion at a rate of $-c/\iota$ relative to System 1 where c ($-b<c<b$) represents a constant provisionally (see below); c has a meaning of the change of distance between a given point of System 1 and a given point of System 2 taking place in mean-free-time ι. It is possible to reconsider that System 1 is moving at a rate equal to c/ι relative to System 2. Viewing from System 2, eq(1.16) can be rewritten as

$$\Phi^{\circ} = (b_{\mathrm{I}}^2/\iota)^{1/2}\cdot(b_{\mathrm{II}}^2/\iota)^{1/2} = b_{\mathrm{I}}b_{\mathrm{II}}/\iota \tag{1.17}$$

in which

$$b_{\mathrm{I}} = b + c \tag{1.18}$$

and

$$b_{\mathrm{II}} = b - c \tag{1.19}$$

showing that mean-free-paths, b_{I} and b_{II}, for molecules migrating to opposite directions are different by a factor of 2c.

The argument above holds even when c/ι or c is not constant, provided that it changes slowly enough fulfilling the following condition. Thus, the molecules under consideration are distributed in a small enough region in System 1, and the rate, $-c/\iota$, of movement of a given point of System 2 occurring when it passes one border of molecular distribution in System 1 is virtualy equal to that ocurrung when it passes the other border.

Representation of Φ°: Let us return to chromatography where Φ° represents diffusion coefficient for apparent diffusion for the molecules as members of the molecular band. The argument below is done for the purpose of calculating Φ°.

Let us denote by z_{I} the mean time necessary for a molecule to move from mobile to stationary phase. z_{I} has another meaning of mean-free-time for the molecule in the mobile phase (see the subsection entitled "Apparent Equilibrium at the Center of Molecular Band: Equilibrium Theory versus Kinetic Theory"). During mean-free-time z_{I}, the molecule moves in the flow direction along the corresponding mean-free-path (present in the mobile phase) at a mean rate equal to the flow-rate relative to the stationary phase; the

length of mean-free-path is equal to mean-free-time numerically (in new system of units). Similarly, let us denote by z_{II} the mean time necessary for a molecule to move from stationary to mobile phase. z_{II} has another meaning of mean-free-time for the molecule in the stationary phase. During mean-free-time z_{II}, the molecule moves in the direction opposite to the flow direction along the corresponding mean-free-path (present in the stationary phase) at a mean rate equal to the flow-rate relative to the mobile phase; the length of mean-free-path is again equal to mean-free-time numerically (in new system of units).

The molecule staying in the mobile phase during mean-free-time z_I and the molecule staying in the stationary phase during mean-free-time z_{II}, both of them, are members of the molecular band staying over both mobile and stationary phases. We calculate below mean-free-time ι_I and mean-free-path b_I for the molecule as member of the band taking place when it migrates toward the outlet of the column at a rate *higher* than the mean rate of migration of the band. We also calculate mean-free-time ι_{II} and mean-free-path b_{II} for the molecule under consideration taking place when it migrates toward the outlet of the column at a rate *lower* than the mean rate of migration of the band.

The calculation is done by using the approximation that an equilibrium between mobile and stationary phases is attained despite the fact that the rate of mass transfer between the two phases is finite (see the preceding paragraph beginning with the title: "Approximation of uniform equilibrium partition of molecules between mobile and stationary phases in the band"). With reference to the preceding paragraph beginning with the title: "Preparation for the representation of Φ°", it can be anticipated that $\iota_I = \iota_{II}$ $(= \iota)$ always, whereas both b_I and b_{II} should depend on the system (System 2) from which the system fixed to the center of molecular band (System 1) is observed. When System 2 is identical with System 1, then the relationship $b_I = b_{II}$ $(=b)$ can be anticipated to take place.

ι_I and ι_{II} can be calculated as

$$\iota_I = (1-B^{\circ})z_I \tag{1.20}$$

and

$$\iota_{II} = B^{\circ}z_{II} \tag{1.21}$$

respectively. Eq(1.20) manifests that mean-free-time ι_I effectively is a fraction, $1-B^{\circ}$, of mean time z_I necessary for a molecule to move from mobile to stationary phase; $1-B^{\circ}$ stands for the equilibrium molecular partition in the stationary phase. Therefore, provided that virtualy all the molecules are in the stationary phase in the equilibrium state ($1-B^{\circ} \rightarrow 1$ or $B^{\circ} \rightarrow 0$), then ι_I is almost equal to z_I ($\iota_I \rightarrow z_I$). Similarly, eq(1.21) manifests that mean-free-time ι_{II} effectively is a fraction, B°, of mean time z_{II} necessary for a molecule to move from stationary to mobile phase; B° stands for the equilibrium molecular partition in the mobile phase. Therefore, provided that virtualy all the molecules are in the mobile phase in the equilibrium state ($B^{\circ} \rightarrow 1$), then ι_{II} is almost equal to z_{II} ($\iota_{II} \rightarrow z_{II}$).

B° is a function of both z_I and z_{II}, which can be determined from the equilibrium condition:

$$\frac{z_{II}}{z_I} = \frac{1-B^\circ}{B^\circ} \tag{1.22}$$

as

$$B^\circ = \frac{z_I}{z_I + z_{II}} \tag{1.22'}$$

Combining both eqs(1.20) and (1.21) with the equilibrium condition [eq(1.22)] leads to

$$\iota_I = \iota_{II} = \iota = \frac{z_I z_{II}}{z_I + z_{II}} = \frac{z_i}{z_i/z_j + 1} \tag{1.23}$$

in which (i, j)=(I, II) or (II, I), and we wrote ι for either ι_I or ι_{II}. The conclusion obtained from eq(1.23) that ι_I and ι_{II} are equal to one another is just what is anticipated. Eq(1.23) shows that when either z_I or z_{II} tends to infinitesimal, then both ι_I and ι_{II} tend to infinitesimal. When $z_I \to 0$, then either z_I/z_{II}=finite [i.e., $z_{II} \to 0$, or B° (and $1-B^\circ$)=finite in general] or $z_I/z_{II}=0$ (i.e., z_{II}=finite or $B^\circ \to 0$; we do not consider the case when $z_{II}=\infty$ or the case when the mobile phase is independent of the stationary phase). The case when both $z_I \to 0$ and $z_{II} \to 0$ represents the case when RMT vanishes. Similarly, when $z_{II} \to 0$, then either z_{II}/z_I=finite [i.e., $z_I \to 0$, or $1-B^\circ$ (and B°)=finite in general] or $z_{II}/z_I=0$ (i.e., z_I=finite or $B^\circ \to 1$; we do not consider the case when $z_I=\infty$ or the case when the stationary phase is independent of the mobile phase). Arguing in the other direction, the condition of $\iota_I = \iota_{II}$ leads to the equilibrium condition [eq(1.22)] since both eqs(1.20) and (1.21) hold.

A certain system (System 2) should be present viewing from which the molecule migrates from one end to the other of mean-free-path b_I (toward the outlet of the column at a rate *higher* than the mean rate of migration of the band) only in fraction B° of mean-free-time ι_I $(=\iota)$ i.e., in fraction of time of stay in the mobile phase, and it migrates from one end to the other of the other mean-free-path b_{II} (toward the outlet of the column at a rate *lower* than the mean rate of migration of the band) only in fraction $1-B^\circ$ of mean-free-time ι_{II} $(=\iota)$ i.e., in fraction of time of stay in the stationary phase. b_I and b_{II} can be represented as

$$b_I = B^\circ \iota_I = B^\circ(1-B^\circ)z_I \tag{1.24}$$

and

$$b_{II} = (1-B^\circ)\iota_{II} = B^\circ(1-B^\circ)z_{II} \tag{1.25}$$

respevtively. Combining eqs(1.24) and (1.25) with either eq(1.22) or (1.23) leads to

$$\frac{b_{II}}{b_I} = \frac{1-B^\circ}{B^\circ} \tag{1.26}$$

Mean-free-path b with respect to all the molecules as member of the molecular band viewed from System 1 (fixed to the center of band) and the parameter c (which specifies the rate $-c/\iota$ of movement of System 2 relative to System 1) can be calculated by using eqs(1.18), (1.19), (1.23)-(1.26) as

$$b = \frac{b_I}{2B^\circ} = \frac{b_{II}}{2(1-B^\circ)} = \frac{\tau}{2} \tag{1.27}$$

and

$$c = [B^\circ-(1-B^\circ)]b = (2B^\circ-1)b \tag{1.28}$$

respectively. Therefore, when $B^\circ<1/2$, then c or $c/\iota<0$, $b_I<b$ and $b_{II}>b$; when $B^\circ=1/2$, then c or $c/\iota=0$ and $b_I=b_{II}=b$; and when $B^\circ>1/2$, then c or $c/\iota>0$, $b_I>b$ and $b_{II}<b$.

By using some part of eqs(1.20)-(1.26), eq(1.17) can be rewritten as

$$\begin{aligned}\bar{\Psi}^\circ &= [B^\circ(1-B^\circ)]^{3/2}\sqrt{z_I z_{II}} \\ &= B^\circ(1-B^\circ)^2 z_I = B^{\circ 2}(1-B^\circ)z_{II}\end{aligned} \tag{1.29}$$

In parallel with both eqs(1.13) and (1.14), it is possible to consider that apparent diffusion takes place in the mobile phase in appearance with diffusion coefficient $\bar{\Theta}^\circ$ and to write

$$\bar{\Psi}^\circ = B^\circ\bar{\Theta}^\circ \tag{1.30}$$

By using eq(1.29), $\bar{\Theta}^\circ$ can be represented as

$$\bar{\Theta}^\circ = \bar{\Psi}^\circ/B^\circ = (1-B^\circ)^2 z_I = B^\circ(1-B^\circ)z_{II} \tag{1.31}$$

Representation of diffusion coefficient Ψ° *and* Θ° *for total diffusion*: Ψ° [eq(1.12)] can be represented by using both eqs(1.13) and (1.29) as

$$\Psi^\circ = B^\circ\bar{\Theta}^\circ + B^\circ(1-B^\circ)^2 z_I = B^\circ\bar{\Theta}^\circ + B^{\circ 2}(1-B^\circ)z_{II} \tag{1.32}$$

and diffusion coefficient Θ° for total diffusion taking place in the mobile phase in appearance can be represented as

$$\begin{aligned}\Theta^\circ &= \Psi^\circ/B^\circ = \bar{\Theta}^\circ + \breve{\Theta}^\circ \\ &= \bar{\Theta}^\circ + (1-B^\circ)^2 z_I = \bar{\Theta}^\circ + B^\circ(1-B^\circ)z_{II}\end{aligned} \tag{1.33}$$

Significance of the approximation of uniform equilibrium partition of molecules between mobile and stationary phases in the band: Arguing in the other direction, it now is possible to reconsider that the convolution mechanism between ordinary and apparent diffusions (giving rise to a total Gaussian band) is a concept holding only on the basis of the approximation that the molecular partition between mobile and stationary phases taking place

in any slice of the band is the same virtually, equal to the equilibrium partition taking place at the center of band with both isocratic and gradient chromatographies. To be precise, the approximation is inconsistent with the actual situation, and such an inconsistency is compensated by the extraordinary property given to diffusion coefficient Ψ° or $\bar{\Theta}^\circ$ for apparaent diffusion. Thus, as axial diffusion in the column (in the usual sense) is feasible only in the mobile phase and not in the stationary phase, it can be demanded (a) that diffusion coefficient for the molecules in the mobile phase should be independent of molecular partition between mobile and stationary phases (which means that diffusion coefficient under consideration represents diffusion constant with both isocratic and gradient chromatographies) and (b) that diffusion coefficient for the molecules as members of the band (present over both mobile and stationary phases) should be represented by a product by molecular partition in the mobile phase of diffusion coefficient (=diffusion constant) for the molecules in the mobile phase. Diffusion coefficient Ψ° and diffusion constant Θ°, for ordinary diffusion fulfill both demands(a) and (b). [Demand(a) is fulfilled by the definition of $\bar{\Theta}^\circ$ and demand(b) is fulfilled by eq(1.13).] With regard to diffusion coefficients, Ψ° and $\bar{\Theta}^\circ$, for apparent diffusion, although demand(b) is fulfilled [see eq(1.30)], demand(a) is not fulfilled. In conclusion, not only diffusion coefficient Ψ° for the molecules as members of the band but also diffusion coefficient $\bar{\Theta}^\circ$ for the molecules in the mobile phase (in appearance) depend on B° [see both eqs(1.29) and (1.31)].

Nevertheless, the concept of convolution mechanism is highly essential, leading to the rudimentary understanding of the fundamental aspect of chromatography and it plays a central role in a series of theoretical studies developed by other authors [although the concept of convolution mechanism, itself, does not make explicit appearance in these studies, hidden within other concepts; see Appendix XI(A)].

Resistance to Mass Transfer between Mobile and Stationary Phases. There are at least three types:

Film resistance at the boundary of packed particle in the column (called *RMT type a*): It in general is assumed that a molecule has to overcome a resistance (called film resistance) for it to move from (to) the state where it is being transported by the carrier liquid to (from) the state where it is at rest relative to the packed particle in the column (in defiance of the liquid flow). Thus, as a result of fluid mechanics, it is apparent that the movement of the molecule between the two states proceeds in either direction at a finite rate while spending a finite time. It can be assumed that the film of RMT type a is wrapping the packed particle in the column and the rates of transfer of the molecule taking place in the two opposite directions are equal.

Resistance between the two states of molecule in the stationary phase, the state immediately after association to (or immediately before dissociation from) the adsorbent surface and the thermodynamically most stable state (called *RMT type b*): It can be assumed that a resistance consisting of at least two steps (Step 1 and 2) is present between the two states of molecule and that the transfer between these states is done in either direc-

tion at a finite rate while spending a finite time. The rate of transfer from the state immediately after association with the adsorbent surface to the thermodynamically most stable state is higher than the rate taking place in the opposite direction. It can be considered that, in Step 1, the molecule associated to the adsorbent surface moves to the more stable position and/or that the conformation [or the configuration; cf. Chapter Ⅷ(F)] of each molecule changes to the more stable one. The reverse process (which in general does not pass through the same way) is also conceivable. In Step 2, the chemical reaction (either binding or dissociation) between functional group of molecule and adsorbing site on the adsorbent surface proceeds at a finite rate. Steps 1 and 2 are not independent in general. [*Note.* It can be assumed that the effect of the movement of molecules taking place on the adsorbent surface (which may be regarded as diffusion) is much too small for it to directly enlarge the width of the molecular band in the axial direction of the column. Cf. the subsequent subsection entitled "Most General Chromatography in Hypothesis".]

Resistance brought about by the presence of the stagnant liquid inside the pore of packed particle in the column (called *RMT type c*): The packed particles in the column often are porous (usually with pore diameter of several nm to several times 10 nm; cf. Chapter Ⅸ), and the pores are open to the liquid phase, giving a large total effective area on the adsorbent surface. It can be assumed that the majority of adsorption and desorption phenomena take place inside the pores. As the liquid inside the pores is stagnant, the concept of mobile phase now applies only to the liquid outside the pores (and also outside the wrapping film of RTM type a), and it can be reconsidered that the liquid inside the pore and the solid phase together form a stationary phase. The liquid inside the pore plays a role of RMT. Thus, the movement of the molecule from (to) the boundary between outside and inside the pore to (from) the solid phase is done induced by a thermal Brownian motion. This is done in either direction at a finite rate while spending a finite time, and it can be assumed that the rates taking place in the two opposite directions are equal. [*Note 1.* It can be assumed that the effect of thermal Brownian diffusion of molecules taking place inside the pore is much too small for it to directly enlarge the width of the molecular band in the axial direction of the column. Cf. the subsequent subsection entitled "Most General Chromatography in Hypothesis". *Note 2.* Straightforward, the increase in axial molecular diffusion in the column brought about by the presence of the pores can simply be interpreted in terms of the increase in ordinary diffusion brought about by the enhancement of the random of the liquid flow. This is induced by intricate geometries of the column interstice added by the presence of the pores. In this consideration, only the coupling of ordinary diffusion to apparent diffusion taking place, induced by RMT type b is in problem. It, however, is difficult to consider that such a coupling takes place through a convolution mechanism. This is because the molecular flux induced by ordinary diffusion now cannot be coupled *uniformly* to apparent diffusion. It is only a special part of the molecular flux present inside the pore that can be coupled to apparent diffu-

sion. Such a situation leads to the concept of RMT taking place inside the pore. *Note 3.* With high-performance liquid chromatography(HPLC) of analytical type, it is common practice to use packed particles with a small diameter (e.g., five μm or even less). In this instance, the depth of the pore is much reduced, so that it can be assumed that RMT type c is much reduced. *Note 4.* Only in the absence of the pores, the liquid phase is completely sinonimous to the mobile phase.]

Times z_{I} and z_{II} as Sums of Times of Stay at Different Resistances to Mass Transfer That Are Joined in Series. Previously, it is necessary to make two preparations.

Preparartion 1. It is possible to consider that the total volume of a vertical slice of column packing is a sum of three volumes: (i) volume $\Delta L'$ occupied by the mobile phase, (ii) volume $\Delta L'_{\text{P}}$ occupied by the pores (to be precise, the open pores) inside the packed particles, and (iii) volume $\Delta L'_{\text{s}}$ occupied by the other part of the particles; the thickness of the film of RMT type a wrapping the particle can be assumed to be infinitesimal virtually. The parameter $\in_{\text{P}}$ defined by

$$\in_{\text{P}} \equiv \frac{\Delta L'_{\text{P}}}{\Delta L'_{\text{P}} + \Delta L'_{\text{s}}} \tag{1.34}$$

is called internal porosity, whereas the parameter $\in$ defined by

$$\in \equiv \frac{\Delta L'}{\Delta L' + \Delta L'_{\text{P}} + \Delta L'_{\text{s}}} \tag{1.35}$$

is called external porosity, total porosity, or void volume fraction of column packing conventionally.

Preparartion 2. In new system of units, time (in units of volume) is defined as volume of the carrier liquid passing through a given axial position on the column, and let us here call this time as *time type* α. In the above, it tacitly is considered that the column is fixed and that the carrier liquid moves. In contrast to this ordinary point of view, it is possible to consider that it is the carrier liquid that is fixed, and that both column container and packed particles in the column move in the direction opposite to the flow of carrier liquid (in the ordinary point of view) passing through the fixed carrier liquid (cf. Chapter II Fig 2.1). It now is possible to define another type of time (in units of volume) as sum of volumes of packed particles in the column passing through a given axial position on the fixed carrier liquid. Let us call this time as *time type* β. It is evident that time type β numerically is $(1-\in)/\in$ times as large as time type α when these represent the same duration of time; $(1-\in)/\in$ is called as *phase ratio.* It is possible to translate the movement of volume, X, of carrier liquid relative to the stationary phase (packed particles in the column) into time type α elapsing inside the mobile phase (carrier liquid) and to translate the latter into the former. To be symmetric, the movement of sum of volumes, $(1-\in)X/\in$, of packed particles relative to the mobile phase should be translated into time type β elapsing inside the stationary phase and the latter should be trans-

lated into the former. This means that, when the event taking place inside the mobile phase and that taking place inside the stationary phase are considered at the same time and if the former event is expressed in terms of time type α, then the latter should be expressed in terms of time type β [or $(1-\epsilon)/\epsilon$ times time type α] and vice versa. In this monograph, it is time type α rather than time type β that is used explicitly (only for comvenience' sake). Of course, it is possible to perform all the arguments by using explicitly a new system of units in which time type β is used instead of time type α [cf. eq(1.72')]. Hereafter as before, terminology "time" will be used to represent "time type α" unless a confusion occurs. Let us return to the main subject.

In the absence of the pores in the packed particles in the column, only RMT types a and b are joined in series. The time of stay of the molecule at RMT type a is independent of the direction of movement of the molecule, which we denote by z_a. Let us denote by $z_{b\,I}$ and $z_{b\,II}$ the times of stay of the molecule at RMT type b taking place on the way of transfer from the state immediately after association with the adsorbent surface to the thermodynamically most stable state and on the way of transfer in the opposite direction, respectively; $z_{b\,I} < z_{b\,II}$. It is possible to write

$$z_I = z_a + z_{b\,I} \tag{1.36}$$

and

$$z_{II} = z_a + z_{b\,II} \tag{1.37}$$

Let us consider the case when the packed particle in the column is spherical in shape with radius R and let us denote by ν the number of molecules adsorbed on the sphere surface per unit volume of the sphere. [$4\pi R^3 \nu/3$ represents the total number of molecules adsorbed on the sphere surface. Therefore, provided that the molecules entrapped by the particle are present inside the sphere instead of being adsorbed on the surface, ν would represent the mean density or concentration of molecules inside the sphere. In the presence of the pores, it is possible to consider that the molecules entrapped by the particle are present inside the sphere; see below.] The number, ω, of molecules passing in either direction over the wrapping film of RMT type a per unit time per unit area of the sphere surface per unit "density" ν can be represented as

$$\omega = \frac{4\pi R^3 \nu/3}{4\pi R^2[(1-\epsilon)/\epsilon] z_a \nu} = \frac{\epsilon}{1-\epsilon} \cdot \frac{R}{3z_a} \tag{1.38}$$

z_a can be expressed by using ω as

$$z_a = \frac{\epsilon}{1-\epsilon} \cdot \frac{R}{3\omega} \tag{1.38'}$$

In both eqs(1.38) and (1.38'), z_a represents time type α whereas $(1-\epsilon)z_a/\epsilon$ represents time type β. [*Note.* The reason why z_a represents time type α goes back to the fact

that z_I (or z_{II}) represents time type α and that z_I (or z_{II}) can be decomposed into a sum in which z_a is involved as a member [see eqs(1.36) or (1.37)]. The reason why z_I (or z_{II}) represents time type α can be found in eq(1.33), where the term $(1-B^\circ)^2 z_I$ [or $B^\circ(1-B^\circ)z_{II}$] in which z_I (or z_{II}) is involved represents diffusion coefficient for apparent diffusion taking place *in the mobile phase* in appearance. In conclusion, it is possible to consider that z_a represents time α *elapsing inside the mobile phase* (see "Preparation 2" above). The similar arguments will be feasible with respect to eqs(1.39)-(1.41), (1.43), (1.44), (1.50) and (1.51) where z_a is replaced by z_{bI}, z_{bII}, z_c, z_{pI} or z_{pII}.]

Denoting by λ_I and λ_{II} the rates of transfer of the molecule at RMT type b from the state immediately after association with the adsorbent surface to the thermodynamically most stable state and from latter to former states, then z_{bI} and z_{bII} can be expressed as

$$z_{bI} = \frac{\epsilon}{1-\epsilon} \cdot \frac{1}{\lambda_I} \tag{1.39}$$

and

$$z_{bII} = \frac{\epsilon}{1-\epsilon} \cdot \frac{1}{\lambda_{II}} \tag{1.40}$$

respectively; $\lambda_I > \lambda_{II}$. In eqs(1.39) and (1.40), z_{bI} and z_{bII} represent times type α whereas $(1-\epsilon)z_{bI}/\epsilon$ and $(1-\epsilon)z_{bII}/\epsilon$ represent times type β, respectively.

In the presence of the pores, RMT type c is added, at which the time of stay (denoted by z_c) of the molecule is independent of the direction of movement of the molecule.

When the packed particle in the column is spherical in shape with radius R, let us find the expression of z_c. Thus, by setting a spherical coordinate system with its origin coinciding with the center of sphere, it would be possible to reconsider that the thermal Brownian motions of all the molecules inside all the pores that are present within the spherical particle are done uniformly in the space with the coordinate system. Under such a consideration, the molecular diffusions taking place in either azimuthal or zenithal direction would be canceled out, and only the diffusion taking place in the radial direction would be effective, playing a role of RMT type c. It therefore would be possible to consider that the time necessary for the molecule to move the distance R between the center and the surface of the sphere by diffusion measures z_c. Let us denote by $\bar{\Theta}^\circ_P$ the diffusion constant for diffusion taking place in the sphere. As $\bar{\Theta}^\circ_P$ has dimensions of length^2/time (or those of volume in new system of units), it would be possible to consider that $\bar{\Theta}^\circ_P$ is proportional to R^2/z_c or it would be possible to write

$$z_c = \frac{\epsilon}{1-\epsilon} \cdot \frac{\eta R^2}{\bar{\Theta}^\circ_P} \tag{1.41}$$

in which η represents a positive constant; z_c and $(1-\epsilon)z_c/\epsilon$ represent times type α and β, respectively.

Taking into acount the intricate geometries of the pores, it would be reasonable to

assess on $\Theta^{\circ}{}_{P}$ the value smaller than that of thermal Brownian diffusion constant although the two values would be of the same order of magnitude. It is difficullt to evaluate η from the above consideration only. From the consideration of other authors [see Appendix XI(A)], it can be estimated that

$$\eta = 1/15 \tag{1.42}$$

RMT type b now is present inside the pore. Under such a situation, let us rewrite $z_{b\,I}$ and $z_{b\,II}$ as $z_{P\,I}$ and $z_{P\,II}$, respectively. Instead of eqs(1.39) and (1.40), we now have

$$z_{P\,I} = \frac{\epsilon}{1-\epsilon} \cdot \frac{1}{\lambda_{I}} \tag{1.43}$$

and

$$z_{P\,II} = \frac{\epsilon}{1-\epsilon} \cdot \frac{1}{\lambda_{II}} \tag{1.44}$$

respectively.

Let us introduce the approximation that either time $z_{P\,I}$ or $z_{P\,II}$ induces both finite time necessary for the molecule which came from the mobile phase and which has just passed over the film of RMT type a to pass over again the boundary between outside and inside of the pore and finite time necessary for the molecule coming from the inside of the pore to pass over the boundary to the outside [for detail, see below; let us call this approximation as Approximation(a)]. We now denote former and latter finite times by $z_{b\,I}$ and $z_{b\,II}$, respectively. In both absence and presence of the pores, $z_{b\,I}$ and $z_{b\,II}$ therefore represent times necessary for the molecule to pass over the boundary lying between the two states: the state just coming out of the film of RMT type a (toward the stationary phase) and the thermodynamically most stable state in the stationary phase. Due to Approximation(a), both $z_{b\,I}$ and $z_{b\,II}$ can be regarded as functions of either $z_{P\,I}$ or $z_{P\,II}$, and it is possible to write

$$z_{I} = z_{a} + z_{b\,I}(z_{P\,I} \text{ or } z_{P\,II}) + z_{c} \tag{1.45}$$

and

$$z_{II} = z_{a} + z_{b\,II}(z_{P\,I} \text{ or } z_{P\,II}) + z_{c} \tag{1.46}$$

With regard to the molecule in solution inside the pore, the concentration taking place in the neighborhood of the border to the outside would be lower than that taking place in the neighborhood of the solid surface actually. [The former concentration should be equal to the concentration taking place in the mobile phase because the time of stay of the molecule at the film resistance (RMT type a) is independent of the direction of movement of the molecule]. Only for the purpose of finding both functions $z_{b\,I}(z_{P\,I} \text{ or } z_{P\,II})$ and $z_{b\,II}(z_{P\,I} \text{ or } z_{P\,II})$, however, let us introduce the approximation that the molecular con-

centration inside the pore is uniform virtually, equal to that taking place in the mobile phase and that a thermodynamic equilibrium is attained at any instant inside the pore. [Let us call this approximation as Approximation(b).] Approximation(b) is consistent with the property of the film resistance (mentioned in the brackets above). Approximation(b) means that the molecular partition between liquid and solid phases inside the pore represents the equilibrium partition. Let us denote by B°_{P} and $1-B^{\circ}_{P}$ the equilibrium molecular partitions in liquid and solid phases inside the pore, respectively. The relationship between B°_{P} and B° will be considered later.

Thus, when the equilibrium molecular partition in the solid phase is $1-B^{\circ}_{P}$ inside the pore, the fraction of time for a molecule in the liquid phase to be able to move to the solid phase is $1-B^{\circ}_{P}$. As, in this instance, the equilibrium molecular partition in the liquid phase is B°_{P}, the fraction of time for an arbitrary molecule inside the pore (which can be present over both liquid and solid phases) to be able to stay in the liquid phase and, successively, to move to the solid phase is $B^{\circ}_{P}(1-B^{\circ}_{P})$. This means that the effective time that can be utilized by an arbitrary molecule inside the pore for a single movement from liquid to solid phase is represented by $B^{\circ}_{P}(1-B^{\circ}_{P})z_{P\,I}$. On the other hand, in order for the thermodynamic equilibrium inside the pore to be maintained, it is necessary that time $B^{\circ}_{P}(1-B^{\circ}_{P})z_{P\,I}$ be balanced with finite time $z_{b\,II}$ used for the molecule to go out of the pore; this leads to

$$B^{\circ}_{P}(1-B^{\circ}_{P})z_{P\,I} = z_{b\,II} \tag{1.47}$$

Similarly, the effective time that can be utilized by an arbitrary molecule inside the pore for a single movement from solid to liquid phase is represented by $B^{\circ}_{P}(1-B^{\circ}_{P})z_{P\,II}$, which is balanced with finite time $z_{b\,I}$ used for the molecule to enter the pore; this leads to

$$B^{\circ}_{P}(1-B^{\circ}_{P})z_{P\,II} = z_{b\,I} \tag{1.48}$$

By combining both eqs(1.47) and (1.48) with the equilibrium condition:

$$\frac{z_{P\,II}}{z_{P\,I}} = \frac{1-B^{\circ}_{P}}{B^{\circ}_{P}} \tag{1.49}$$

and using both eqs(1.43) and (1.44), then $z_{b\,I}$ and $z_{b\,II}$ as functions of either $z_{P\,I}$ or $z_{P\,II}$, or $z_{b\,I}$ and $z_{b\,II}$ as functions of either λ_{I} or λ_{II} are obtained; these can be written as

$$z_{b\,I} = B^{\circ}_{P}(1-B^{\circ}_{P})z_{P\,II} = (1-B^{\circ}_{P})^{2}z_{P\,I}$$

$$= B^{\circ}_{P}(1-B^{\circ}_{P})\,\frac{\epsilon}{1-\epsilon}\cdot\frac{1}{\lambda_{II}} = (1-B^{\circ}_{P})^{2}\,\frac{\epsilon}{1-\epsilon}\cdot\frac{1}{\lambda_{I}} \tag{1.50}$$

and

$$z_{b\,II} = B^{\circ}_{P}(1-B^{\circ}_{P})z_{P\,I} = B^{\circ}_{P}{}^{2}z_{P\,II}$$

$$= B^{\circ}_{P}(1-B^{\circ}_{P})\frac{\epsilon}{1-\epsilon}\cdot\frac{1}{\lambda_{I}} = B^{\circ}_{P}{}^{2}\frac{\epsilon}{1-\epsilon}\cdot\frac{1}{\lambda_{II}} \tag{1.51}$$

Eqs(1.50) and (1.51) (holding in the presence of the pores) can be compared with eqs (1.39) and (1.40) (holding in the absence of the pores), respectively.

It should be noted that Approximations(a) and (b) are equivalent. Thus, for Approximation(a) to hold, Approximation(b) is necessary, while, for Approximation(b) to hold Approximation(a) is necessary.

Relationship between B°_{P} *and* B°: Let us denote by $\hat{C}$, $\hat{\chi}_{P}$ and $\hat{\chi}_{s}$ the number of molecules that are present in the mobile phase, the number of molecules that are present in solution inside the pores and the number of molecules that are adsorbed on the solid surfaces inside the pores in the verical slice of column packing, respectively. B°_{P} and B° can be represented as

$$B^{\circ}_{P} = \frac{\hat{\chi}_{P}}{\hat{\chi}_{P}+\hat{\chi}_{s}} \tag{1.52}$$

and

$$B^{\circ} = \frac{\hat{C}}{\hat{C}+\hat{\chi}_{P}+\hat{\chi}_{s}} \tag{1.53}$$

respectively. Further, due to Approximation(b), the relationship:

$$\hat{C}/\Delta L' = \hat{\chi}_{P}/\Delta L'_{P} \tag{1.54}$$

is fulfilled.

From eqs(1.34), (1.35), (1.52)-(1.54),

$$B^{\circ}_{P}\frac{1-B^{\circ}}{B^{\circ}} = \epsilon_{P}\frac{1-\epsilon}{\epsilon} \tag{1.55}$$

can be derived. Eq(1.55) gives the relationship between B°_{P} and B°.

Finally, the equilibrium molecular partition, B°_{t}, in the total liquid phase (=mobile phase+liquid phase inside the pore) is conceivable; this can be written as

$$B^{\circ}_{t} = \frac{\hat{C}+\hat{\chi}_{P}}{\hat{C}+\hat{\chi}_{P}+\hat{\chi}_{s}} = B^{\circ} + \frac{1}{\Delta L'/\Delta L'_{P}+1/B^{\circ}_{P}} \tag{1.56}$$

As, usually, $\Delta L' \gg \Delta L'_{P}$ or $\hat{C} \gg \hat{\chi}_{P}$, then it can be considered that

$$B^{\circ}_{t} \approx B^{\circ} \tag{1.57}$$

[*Note.* It is possible to perform the argument above by replacing $\hat{C}$, $\hat{\chi}_{P}$ and $\hat{\chi}_{s}$ by C, χ_{P} and χ_{s}, respectively. For the symbols, see both Chapter II(A) and Appendix XI(A).]

Expression of Diffusion Coefficient Θ° or θ° in Usual System of Units. By using usu-

al system of units, let us rewrite times z_I, z_{II}, z_a, z_{bI}, z_{bII}, z_c, z_{PI} and z_{PII} (with dimensions of volume) as t_I, t_{II}, t_a, t_{bI}, t_{bII}, t_c, t_{PI} and t_{PII} (with dimension of time), respectively, and radius R of the spherical particle (with dimensions of volume) as $\hat{R}$ (with dimension of length). z_I, z_{II} etc. are related to t_I, t_{II} etc. through eq(1.9) into which z_I, z_{II} etc. are substituted for Z, and t_I, t_{II} etc. are substituted for t, respectively. R is related to $\hat{R}$ through eq(1.8) into which I and x are substituted for R and $\hat{R}$, respectively. Also by using usual system of units, let us rewrite the parameters $\bar{\Theta}^\circ$ [with dimensions of volume; eq(1.33)], ω [dimensionless; eq(1.38) or (1.38')], $\bar{\Theta}^\circ_P$ [with dimensions of volume; eq(1.41)], λ_I [with dimensions of volume^{-1}; eqs(1.39), (1.43) and (1.50)] and λ_{II} [with dimensions of volume^{-1}; eqs(1.40), (1.44) and (1.51)] as $\bar{D}^\circ$ (with dimensions of length^2/time), k_f (with dimension of length/time), $\bar{D}^\circ_P$ (with dimensions of length^2/time), v_I (with dimension of time^{-1}) and v_{II} (with dimension of time^{-1}), respectively. $\bar{\Theta}^\circ$, ω, $\bar{\Theta}^\circ_P$, λ_I and λ_{II} are related to $\bar{D}^\circ$, k_f, $\bar{D}^\circ_P$, v_I and v_{II} by

$$\left.\begin{aligned} \bar{\Theta}^\circ &= \gamma\,\bar{D}^\circ/u \\ \omega &= k_f/u \\ \bar{\Theta}^\circ_P &= \gamma\,\bar{D}^\circ_P/u \\ \lambda_I &= v_I/(\gamma\,u) \\ \lambda_{II} &= v_{II}/(\gamma\,u) \end{aligned}\right\} \qquad (1.58)$$

and

respectively.

Eq(1.33) can now be rewritten as

$$\Theta^\circ = \gamma\,\bar{D}^\circ/u + (1-B^\circ)^2\gamma\,ut_I = \gamma\,\bar{D}^\circ/u + B^\circ(1-B^\circ)\gamma\,ut_{II} \qquad (1.33')$$

In the absence of the pores, eq(1.36) combined with both eqs(1.38') and (1.39), and eq (1.37) combined with both eqs(1.38') and (1.40) can be rewritten as

$$t_I = \frac{\epsilon}{1-\epsilon}\left(\frac{\hat{R}}{3k_f} + \frac{1}{v_I}\right) \qquad (1.59)$$

and

$$t_{II} = \frac{\epsilon}{1-\epsilon}\left(\frac{\hat{R}}{3k_f} + \frac{1}{v_{II}}\right) \qquad (1.60)$$

respectively. In the presence of the pores, eq(1.45) combined with eqs(1.38'), (1.41)-(1.43) and (1.50), and eq(1.46) combined with eqs(1.38'), (1.41), (1.42), (1.44) and (1.51) can be rewritten as

$$\begin{aligned} t_I &= \frac{\epsilon}{1-\epsilon}\left(\frac{\hat{R}}{3k_f} + \frac{\hat{R}^2}{15\bar{D}^\circ_P} + \frac{B^\circ_P(1-B^\circ_P)}{v_{II}}\right) \\ &= \frac{\epsilon}{1-\epsilon}\left(\frac{\hat{R}}{3k_f} + \frac{\hat{R}^2}{15\bar{D}^\circ_P} + \frac{(1-B^\circ_P)^2}{v_I}\right) \end{aligned} \qquad (1.61)$$

and

$$t_{\parallel} = \frac{\epsilon}{1-\epsilon}\left(\frac{\hat{R}}{3k_f} + \frac{\hat{R}^2}{15\bar{D}^{\circ}_P} + \frac{B^{\circ}_P(1-B^{\circ}_P)}{v_{\parallel}}\right)$$

$$= \frac{\epsilon}{1-\epsilon}\left(\frac{\hat{R}}{3k_f} + \frac{\hat{R}^2}{15\bar{D}^{\circ}_P} + \frac{B^{\circ}_P{}^2}{v_{\parallel}}\right) \qquad (1.62)$$

respectively.

For comparison with the consideration of other authors[Appendix XI(A)], let us introduce diffusion coefficient θ° with dimension of length defined by

$$\theta^{\circ} = \Theta^{\circ}/\gamma \qquad (1.63)$$

By replacing Θ° with θ°, eq(1.33') can be rewriten as

$$\theta^{\circ} = \bar{D}^{\circ}/u + (1-B^{\circ})^2 u t_{\perp} = \bar{D}^{\circ}/u + B^{\circ}(1-B^{\circ})u t_{\parallel} \qquad (1.33'')$$

[*Nore 1.* Diffusion coefficient Θ° or θ° expressed in usual system of units, D°, (with dimensions of length^2/time) is conceivable, which can be represented as $D^{\circ}=u\Theta^{\circ}/\gamma = u\theta^{\circ}$. We do not use the concept of D° in this monograph, however. *Note 2.* $2\theta^{\circ}$ is called *height equivalent to a theoretical plate* at least with the isocratic case.]

Most General Chromatography in Hypothesis. For the purpose of attaining a better understanding of the argument, let us examine a most general hypothetical chromatography where ordinary molecular diffusion takes place in not only mobile phase but also stationary phase. Following the convolution mechanism taking place between the two types of ordinary diffusion, $\bar{p}^2$ can now be replaced by $\bar{p}^2 + \bar{p}'^2$ where $\bar{p}'^2$ represents the contribution from stationary phase ordinary diffusion to the total variance of the molecular band. Eq (1.7) can be extended to

$$\rho^2 = \bar{p}^2 + \bar{p}'^2 + \bar{\beta}^2 \qquad (1.64)$$

Einstein's equation relating $\bar{p}'^2$ to diffusion coefficient $\bar{\Psi}^{\circ}$' for stationary phase ordinary diffusion taking place in the molecular band can be written as

$$\bar{p}'^2 = 2\bar{\Psi}^{\circ}{}'Z \qquad (1.65)$$

which makes a pair with the second equality in eq(1.10). Eq(1.12) can be extended to

$$\Psi^{\circ} = \bar{\Psi}^{\circ} + \bar{\Psi}^{\circ}{}' + \bar{\Psi}^{\circ} \qquad (1.66)$$

Writing $\bar{\Theta}^{\circ}$' for axial diffusion constant for stationary phasse ordinary diffusion taking place in the stationary phase, $\bar{\Psi}^{\circ}$' can be represented as

$$\bar{\Psi}^{\circ}{}' = (1-B^{\circ})\bar{\Theta}^{\circ}{}' \qquad (1.67)$$

which makes a pair with eq(1.13).

It is possible to consider that apparent diffusion takes place in the stationary phase

in appearance with diffusion coefficient $\bar{\Theta}^{\circ\prime}$ and to write

$$\bar{\Psi}^{\circ} = (1-B^{\circ})\bar{\Theta}^{\circ\prime} \tag{1.68}$$

instead of eq(1.30). By using eq(1.29), diffusion coefficient $\bar{\Theta}^{\circ\prime}$ can be represented as

$$\bar{\Theta}^{\circ\prime} = \bar{\Psi}^{\circ}/(1-B^{\circ}) = B^{\circ}(1-B^{\circ})z_{\mathrm{I}} = B^{\circ 2}z_{\mathrm{II}} \tag{1.69}$$

which can be compared with eq(1.31).

Ψ° [eq(1.66)] can be represented by using eqs(1.13), (1.29) and (1.67) as

$$\begin{aligned}\Psi^{\circ} &= B^{\circ}\bar{\Theta}^{\circ} + (1-B^{\circ})\bar{\Theta}^{\circ\prime} + B^{\circ}(1-B^{\circ})^{2}z_{\mathrm{I}} \\ &= B^{\circ}\bar{\Theta}^{\circ} + (1-B^{\circ})\bar{\Theta}^{\circ\prime} + B^{\circ 2}(1-B^{\circ})z_{\mathrm{II}}\end{aligned} \tag{1.70}$$

It now is possible to consider either diffusion coefficient Θ° for total diffusion taking place in the mobile phase in appearance or diffusion coefficient $\Theta^{\circ\prime}$ for total diffusion taking place in the stationary phase in appearance. Θ° can be represented as

$$\begin{aligned}\Theta^{\circ} &= \Psi^{\circ}/B^{\circ} = \bar{\Theta}^{\circ} + \frac{1-B^{\circ}}{B^{\circ}}\bar{\Theta}^{\circ\prime} + \bar{\bar{\Theta}}^{\circ} \\ &= \bar{\Theta}^{\circ} + \frac{1-B^{\circ}}{B^{\circ}}\bar{\Theta}^{\circ\prime} + (1-B^{\circ})^{2}z_{\mathrm{I}} \\ &= \bar{\Theta}^{\circ} + \frac{1-B^{\circ}}{B^{\circ}}\bar{\Theta}^{\circ\prime} + B^{\circ}(1-B^{\circ})z_{\mathrm{II}}\end{aligned} \tag{1.71}$$

whereas $\Theta^{\circ\prime}$ can be represented as

$$\begin{aligned}\Theta^{\circ\prime} &= \Psi^{\circ}/(1-B^{\circ}) = \frac{B^{\circ}}{1-B^{\circ}}\bar{\Theta}^{\circ} + \bar{\Theta}^{\circ\prime} + \bar{\bar{\Theta}}^{\circ\prime} \\ &= \frac{B^{\circ}}{1-B^{\circ}}\bar{\Theta}^{\circ} + \bar{\Theta}^{\circ\prime} + B^{\circ}(1-B^{\circ})z_{\mathrm{I}} \\ &= \frac{B^{\circ}}{1-B^{\circ}}\bar{\Theta}^{\circ} + \bar{\Theta}^{\circ\prime} + B^{\circ 2}z_{\mathrm{II}}\end{aligned} \tag{1.72}$$

In new system of units where time type α is replaced with time type β, let us denote z_{I}, z_{II}, Ψ°, $\Theta^{\circ\prime}$, $\bar{\Theta}^{\circ}$, $\bar{\Theta}^{\circ\prime}$ and $\bar{\bar{\Theta}}^{\circ\prime}$ (written together as ζ) by z^{*}_{I}, z^{*}_{II}, $\Psi^{*\circ}$, $\Theta^{*\circ\prime}$, $\bar{\Theta}^{*\circ}$, $\bar{\Theta}^{*\circ\prime}$ and $\bar{\bar{\Theta}}^{*\circ\prime}$ (written together as ζ^{*}), respectively. ζ^{*} is related to ζ through

$$\zeta^{*} = \frac{\epsilon}{1-\epsilon}\zeta \tag{1.73}$$

By using eq(1.73), eq(1.72) can be rewritten as

$$\Theta^{*\circ\prime} = \Psi^{*\circ}/(1-B^\circ) = \frac{B^\circ}{1-B^\circ}\bar{\Theta}^{*\circ} + \bar{\Theta}^{*\circ\prime} + \bar{\bar{\Theta}}^{*\circ\prime}$$

$$= \frac{B^\circ}{1-B^\circ}\bar{\Theta}^{*\circ} + \bar{\Theta}^{*\circ\prime} + B^\circ(1-B^\circ)z^*_{\mathrm{I}}$$

$$= \frac{B^\circ}{1-B^\circ}\bar{\Theta}^{*\circ} + \bar{\Theta}^{*\circ\prime} + B^{\circ 2}z^*_{\mathrm{II}} \qquad (1.72')$$

It is eq(1.72') rather than eq(1.72) that is more symmetric to eq(1.71) conceptually.

[*Note.* More fundamentally, at least four types of new system of units are conceivable: type(i) where length is defined as interstitial volume of the column and time is defined as volume of the carrier liquid passing through a given position on the column; type(ii) where the definition of length is the same as in type(i) and time is defined as sum of volumes of packed particles in the column passing through a given position on the carrier liquid; type(iii) where length is defined as sum of volumes of packed particles in the column and the definition of time is the same as in type(i); and type(iv) where the definition of length is the same as in type(iii) and the definition of time is the same as in type (ii). Here, only new systems of units type(i) and (ii) are used as concepts.]

Quasi-Static Chromatography versus Nonequilibrium Thermodynamics. According to the general consideration in nonequilibrium therodynamics(1.1), it is possible to consider that the assembly of molecules submitting themselves to thermal Brownian diffusion following Fick's first law are a thermodynamic system in local equilibria although the equilibrium is not attained globally. It is evident that the consideration holds if the thermodynamic system is moving as a whole relative to another system i.e., if another molecular flux is added, viewed from the second system.

In the ideal case of *the absence of both RMT and any heterogeneity of the flow of the carrier liquid,* within the limit of the approximation of uniform molecular density in the vertical direction of the column (see the subsection entitled "Apparent Equilibrium at the Center of Molecular Band: Equilibrium Theory versus Kinetic Theory"), the molecular band migrating on the column can be considered to be a thermodynamic system in local equilibria and in nonequilibrium globally. Here, the column container plays a role of the second system in the general consideration in nonequilibrium thermodynamics, and local equilibrium means not only thermodynamic equilibrium between mobile and stationary phases attained in the vertical slice of the band but also the total equilibrium attained within the slice. Thus, the general consideration in nonequilibrium thermodynamics directly applies to chromatography, and it can be considered that the migration of the molecular band on the column is done *quasi-statically* while attaining local equilibria.

In the absence of RMT but in the presence of random hetertogeneity of the flow, within the limit of the aproximation of uniform molecular density in the vertical direction of the column, it is possible to consider that a thermodynamic equilibrium between mobile

and stationary phases is attained virtually in any slice of the band at any instant despite the fact that the total equilibrium is not attained within the slice; the band is in nonequilibrium globally. In chromatographic viewpoint, whether the total equilibrium is attained or not within the slice of the band is not important. What is important is that the migration of the band on the column is done quasi-statically in the sense that local equilibria *between mobile and stationary phases* are attained at any instant virtually.

With regard to gradient chromatography in connection with all the arguments performed above in this subsection, let us supplement the approximation that molecular partition between mobile and stationary phases taking place in any silce of the band is the same virtually, equal to the equilibrium partition taking place at the center of band. This approximation naturally is fulfilled with isocratic chromatography carried out in the absence of RMT.

In the presence of RMT, with addition of the approximation that the coupling of ordinary and apparent diffusions is done through a convolution mechanism to generate a Gaussian band, it again is possible to consider that the migration of the band on the column is done quasi-statically while attaining local equilibria *between the two phases*. This is because the convolution mechanism is a concept holding on the basis of the approximation that molecular partition between mobile and stationary phases taking place in any slice of the band is the same virtually, equal to the equilibrium partition taking place at the center of band with both isocratic and gradient chromatographies (see the subsection entitled "Diffusion Coefficient for Ordinary Diffusion and Diffusion Coefficient for Apparent Diffusion"). The supplemental approximation with gradient chromatography in the absence of RMT (see above) is incorporated in this approximation.

With isocratic chromatography in both absence and presence of RMT, the equilibrium molecular partitions, B^e and $1-B^e$, in mobile and stationary phases are constant during the time when the band is migrating on the column, respectively. This means that both apparent diffusion coefficients, $\bar{\Psi}^\circ$ [eq(1.29)] and $\bar{\Theta}^\circ$ [eq(1.31)], are constant during this time in the presence of RMT. In its absence (when $z_I = z_{II} = 0$), both $\bar{\Psi}^\circ$ and $\bar{\Theta}^\circ$ vanish. It follows that both diffusion coefficients for total diffusion, Ψ° [eq(1.32)] and Θ° [eq (1.33)], are constant. Thus, the problem of chromatography reduces to the problem equivalent to that of the assembly of molecules submitting themselves to one-dimensional free diffusion (in the usual sense), viewed from another system moving in parallel with the direction of diffusion at a constant rate relative to the assembly of molecules as a thermodynamic system.

With gradient chromatography in the absence of RMT, it is apparent that Θ° [eq (1.33)] is constant; this is because $\bar{\Theta}^\circ$ [eq(1.31)] vanishes in the absence of RMT when $z_I = z_{II} = 0$. Such a conclusion in appearance is not true, however, because it simply arises from the fundamental approximation of uniform equilibrium partition of molecules between mobile and stationary phases in the band. This approximation is necessary, on the one hand, for the convolution mechanism (giving rise to a Gaussian band) to be conceivable.

On the other hand, however, it only holds at the expense of the neglect of the effect on the bandwidth of different rates of migration of molecules taking place in different parts of the band (where the environments surrounding molecules are different from one another).

The expense of the neglect of the effect can be compensated by introducing another approximation. This states that the rate of increase (or decrease) of standard deviation of the Gaussian band can be represented as a sum of two quantities. The first quantity represents the rate of increase due to diffusion taking place, provided that there is no effect of the gradient (i.e., no effect of the differences in the environments surrounding the molecules at different positions in the band). The second quantity represents the rate of decrease (with negative value) or the rate of increase (with positive value) taking place due to the effect of the gradient (see above), provided that there is no axial diffusion in the column. Both quantities can be calculated without difficulty, and, from the equation representing the balance between the two quantities, diffusion coefficient Θ with which diffusion constant Θ° can be replaced can be derived [for detail, cf. Chapter V(C)].

With gradient chromatography in the presence of RMT, Θ° [eq(1.33)] is not constant. The effect on the bandwidth of different rates of migration of molecules taking place in different parts of the band still is neglected, however. In this instance also, the neglect of the effect can be compensated by the approximation of the introduction of the two quantities (see above). In order to reduce as much as possible the form of the equation representing the balance between the two quantities, let us introduce a further approximation in which Θ° [eq(1.33)] is replaced by a mean value of Θ° taking place in the whole process of chromatography. By using this approximation, diffusion coefficient Θ can be derived in the same fashon as in the absence of RMT [cf. Chapter V(C)].

With HPLC of analytical type where the diameter of the packed particles in the column is small, it can be assumed that RMT type c is much reduced (see the subsection entitled "Resistance to Mass Transfer between Mobile and Stationary Phases"). Further, it would be resonable to assume that RMT type b is also small except for the case when sample molecule "dives deeply" in the three-dimensional structure of the packed particle in the column. These imply that the change of Θ° [eq(1.33)] taking place in the whole process of chromatography is small since the contribution of $\tilde{\Theta}^\circ$[eq(1.31)] to Θ° can be considered to be small (unless RMT type a is important). The replacement of Θ° by its mean value would be a good approximation.

Hereafter, the symbol B° will be used only for isocratic chromatography. With gradient chromatography when B° changes with a lapse of time, the symbol B will be used instead.

Static Investigation and Dynamic Investigation. It is possible to divide the theoretical investigation on chromatography into two parts: static and dynanmic investigations.

In static investigation, a two-phase system *in equilibrium* consisting of liquid and solid phases equivalent to a slice of the column is hypothesized, and the adsorption and desorption mechanism taking place in the solid phase (i.e., on the adsorbent surface) is

studied. In the absence of the pores in the packed particles in the column, liquid and solid phases in static investigation correspond to mobile and stationary phases in dynamic investigation (see below), respectively. In the presence of the pores, the liquid phase in static investigation corresponds to the sum of mobile phase, film of RMT type a and stagnant liquid inside the pores in dynamic investigation, and the solid phase in the static investigation corresponds to the solid phase inside the pores in the dynamic investigation. Usually, however, volume $\Delta L'_P$ occupied by the pores is much smaller than volume $\Delta L'$ occupied by the mobile phase, and the liquid phase in static investigation corresponds to the sum of mobile phase and RMT film in dynamic investigation virtually [cf. eq(1.57)].

Ideally, for the study of the adsorption and desorption mechanism, the adsorption isotherm of sample molecule should first be calculated based on a certain model. Under condition of low molecular density or small sample loads, the adsorption isotherm is linear, and it is sufficient to consider the adsorption isotherm of a single component of interest while neglecting the presence of the other components in the sample mixture. This can be represented as a function of molecular concentration in the liquid phase, the property of the molecule under consideration and several factors characterizing both solid and liquid phases; the property of the molecule is a function of these factors. In order to connect static investigation to dynamic investigation, however, it is necessary to convert adsorption isotherm to partition of molecules in the liquid phase (i.e., the proportion in number of molecules staying in the liquid phase relative to the total number in the system) as a function of the property of the molecule and several factors characterizing both solid and liquid phases. Conventionally, however, it is common practice to consider capacity ratio (i.e., the ratio in number of molecules staying in the solid phase to those staying in the liquid phase) instead of molecular partition in the liquid phase, and, by a number of authors, attempt is made to calculate capacity ratio directly without touching on the concept of adsorption isotherm nor the concept of molecular partition in the liquid phase [cf. Appendix XI(C)-(F)].

How the property of the solid phase gives rise to a certain slope of adsorption isotherm or a certain partition of molecules in the liquid phase, in itself, is a problem out of chromatography. The concept of chromatography makes appearance when the property of the solid phase (i.e., the factors characterizing the solid phase) is given previously either uniformely or as a function of position along the main axis of the column. From a practical viewpoint, however, the situation is different as far as the liquid phase is concerned. Thus, it is the daily work of a number of chromatographers to control the property or composition of the liquid phase in order to obtain a good chromatographic separation; "composition of the liquid phase" is almost sinonimous to "concentration of gradient substance". Under such a situation, let us endow the concentration of gradient substance with the qualification as one of the elementary concepts establishing the total concept of chromatography. It is possible to say that the study of the mechanism regarding how the concentration of gradient substance regulates the slope of adsorption isotherm (or partition

of molecules in the liquid phase) performed when a certain solid phase is given is the main problem of static investigation.

Dynanic investigation implies the study of the migration of the molecular band on the column and the calculation of the chromatogram; cf. Chapter II(D)]. Within the limit of the approximation of quasi-static chromatography (see the subsection entitied "Quasi-Static Chromatography versus Nonequilibrium Thermodynamics"), dynamic inverstigation is feasible both when, previously, the equilibrium partition, B° (or B), of sample molecules in the liquid phase is calculated (by static investigation) or found empirically as a function of both property of the solid phase and property of the liquid phase (i.e., the concentration of gradient substance in the liquid phase) and when diffusion coefficient Θ° is given as a function of B° (or B). In dynamic investigation, the static concept of partition of sample molecules in the liquid phase is converted to the dynamic concept of the rate of migration of molecules relative to the rate of migration of the carrier liquid (cf. the last paragraph in the subsection entitled "Apparent Equilibrium at the Center of Molecular Band: Equilibrium Theory versus Kinetic Theory").

(B) Perspective and the Current of Contents

Perspective. The study begins with dynamic investigation(Chapter II-V), and static investigation begins with retardation with the introduction of *competition model* to specify the adsorption and desorption mechanism(Chapter VIII-X). The theoretical conclusion of pracical use obtained by combination of both static and dynamic investigations is summarized in Chapter VI [limiting ourselves to the usual case when only the gradient in the liquid phase (i.e., the concentration gradient) is applied] accompanying the experimental verification(Chapter VII).

Dynamic investigation is performed within the limit of the quasi-static approximation for the migration of the molecular band on the column, and the approximation of replacement of diffusion coefficient Θ° by its mean value is used with gradient chromatography [see the subsection entitled "Quasi-Static Chromatography versus Nonequilibrium Thermodynamics" in Section(A)]. When a molecular band with a small width is formed initially at the inlet of the column, provided that equilibrium partition B° (or B) of sample molecule is given previously as a function of both property of the solid phase and concentration of gradient substance in the liquid phase (either theoretically or empirically) and that the mean value of diffusion coefficient Θ° is also given previously, then the resultant chromatogram (or chromatographic peak) for sample molecule under consideration can be predicted or calculated under any experimental condition; capacity ratio is conceivable instead of B° (or B). The experimental condition implies the total length of the column, the property of the solid phase as a function of axial position on the column, and the concentration change of gradient substance taking place at the inlet of the column as a function of time. The change of concentration or the concentration gradient taking place at the col-

umn inlet may be either linear (with any slope or steepness) or curved (with any shape and steepness) as a function of time. The case when the concentration gradient is extremely steep such as bringing about a strong demixing effect is excluded from the theory, however [for demixing effect, cf. Chapter Ⅲ(A)]. The isocratic chromatography is involved as a special case of gradient chromatography. [*Note 1.* Account is not taken of the wall effect if it takes place inside the column container. Therefore, if time is expressed in terms of the volume of the carrier liquid being injected into the column [cf. the first paragraph beginning with the title of "New system of units" in the subsection entitled "Diffusion Coefficient for Ordinary Diffusion and Diffusion Coefficient for Apparent Diffusion" in Section(A)], the concentration change of gradient substance taking place at the column inlet as a function of time (or volume of the carrier liquid) for the column with a certain internal diameter is equivalent with the change taking place at twice the rate (or twice the steepness) for the coumn with a quarter the internal diameter. *Note 2.* How the chromatogram depends on the flow-rate applied is out of the problem of the present investigation. Thus, the investigation begins when once a constant flow-rate and the corresponding Θ° are given.]

As for static investigation, competition model is derived on the basis of a statistical mechanical concept; this states that adsorbing sites are arranged in some manner (usually with inter-site distances of the order of nm) on the surfaces of packed particles in the column and that sample molecules with functional adsorption groups and gradient substances compete for adsorption on the sites of packed particles. By using competition model, the adsorption isotherm of sample molecule can be calculated; this can be converted to equilibrium partition B° (or B) of sample molecule in the mobile phase as a function of concentration, m, of gradient substance in the mobile phase (when both property of sample molecule and property of the solid phase are given previously). B° (or B) in general increases monotonically from ≈ 0 to 1 with increase in m. Hence, by combining both static and dynamic investigations, a perfect theory of chromatography is established for the usual case when only the gradient in the mobile phase (i.e., the concentration gradient) is applied. Isocratic chromatography can now be regarded as a special case of concentration gradient chromatography. [*Note.* There are two considerations with regard to the conversion of adsorption isotherm to molecular partition B° (or B) in the mobile phase. In the first consideration, adsorption isotherm is converted to equilibrium molecular partition B°_1 in the liquid phase taking place in the two phase system hypothesized in static investigation [see the subsection entitled "Static Investigation and Dynamic Investigation" in Section(A)], and it is interpreted that B°_1 is equal to B° virtually [see eq (1.57)]. In the second consideration, adsorption isotherm is converted to B° directly. Thus, the parameter β [eq(8.50); measuring the ratio of the total area of the adsorbent surfaces to the total interstitial volumes in the two phase system hypothesized in static investigation] appears in the expression of B°_1 obtained by the conversion. It is possible, however, to modify the meaning assigned to β by considering, instead of the true area,

the apparent area of the adsorbent surface consisting of both true area and additional area in appearance representing the inside of the pore where the stagnant liquid is present. The value of β given the modified meaning, in general, is larger than that given the original meaning. In the second consideration, we give β the modified meaning. As a result, B°_{1} is modified to B°, or adsorption isotherm is converted to B° directly. It can be considered, however, that there is actually only a small difference between the two values of β with and without modification of the meaning and that B° is equal to B°_{1} virtually.]

It can finally be concluded that competition model is quite reasonable, explaining the adsorption and desorption mechanisms of a wide range of chromatographies in which three typicals: hydroxyapatite, reversed-phase and ion-exchange chromatographies are involved. With reversed-phase chromatography, both sample molecule and gradient substance are adsorbed "weakly" on the adsorbent surface while performing the competition, whereas, with ion-exchange chromatography, these are adsorbed "strongly" while performing the competition. In any chromatography, it is probable that the energy of adsorption per functional group of sample molecule is of the order of magnitude of kJ/mol to ten times kJ/mol. Further, on the basis of competition model, the following estimations can be made. Thus, with reversed-phase chromatography of polystyrene, the conformation of molecule in the adsorbed state is much more swollen than that taking place in the mobile phase. Whereas the molecular conformation of polystyrene on the reversed-phase surface is three-dimensional, those of n-alkanes, n-alkylbenzenes etc. with relatively low degrees of polymerization are either stretched or planar. The molecular conformations of both polyadenylate and polyphosphate with relatively low degrees of polymerization on the anion-exchanger surface are also either stretched or planar. On the hydroxyapatite surface, the molecular conformation of poly-L-lysine with relatively low degrees of polymerization is stretched, whereas those of denatured proteins and denatured DNA are perhaps three-dimensional.

The perfect theory of concentration gradient chromatography (obtained by combination of static and dynamic investigations; see above) is applied to the experimental analysis of multi-peak chromatograms of collagen and myosin obtained on hydroxyapatite columns. In contrast to these structural proteins, with globular proteins, chromatograms consisting of almost only one peak are obtained on hydroxyapatite columns usually. The multi-peak chromatograms leads to microheterogeneous models of collagen and myosin. With regard to type I collagen, the model states that the primary structures of the three peptide chains constructing the total collagen molecule are fluctuationg around mean or most-frequently-occurring structures that can be "determined" or "picked up" by using the organochemical method and that are consistent with the base sequences of the corresponding cDNA. It can be estimated that the probability that aspartic and glutamic residues are present at "correct" positions of the primary structures "determined" by the organochemical method is of the order of 80%. The tertiary structure of the total collagen molecule is rather simple represented by a triple helix of the three peptide chains, and it can be shown experi-

mentally that the same tertiary structure can be reproduced if the primary structures of the peptides are varied (except for some special amino or imino acid residues). Collagen is biosynthesized in an overwhelmingly large amount compared to globular proteins, and the equivocal primary structures of the peptide chains probably arise at a translational level of biosynthesis. The situation is different from the case of globular proteins with intricate tertiary structures that can be assumed to take place induced by the corresponding highly unequivocal primary structures of peptides, respectively. It can be assumed that similar microheterogeneous models apply to other types of collagen (that can genetically be distinguished from type I, respectively) as well as to myosin (which also is biosynthesized in an overwhelmingly large amount compared to globular proteins and has a rather simple tertiary structure in part). [*Note.* Microheterogeneous model of type I collagen was derived earlier. In this monograph, the model is re-discussed on the basis of the specified consideration on the adsorption and desorption mechanism taking place on the crystal surface of hydroxyapatite. For detail, see Chapter Ⅷ.]

Current of Contents. In Chapter Ⅱ and Ⅲ, in order to establish a fundamental concept of chromatography, ideal isocratic and gradient chromatographies, respectively, are treated under assumption that pointwise equilibria are attained at any instant between mobile and stationary phases in the molecular band and that there is no axial diffusion in the column. It should noted, however, that this assumption [originally used by Wilson, Weiss and Devault; see Appendix Ⅺ(A)] is unrealizable *in principle*; this is because the movement of a molecule between mobile and stationary phases is unrealizable in principle without accompanying the motion in the axial direction of the column. It is possible to consider that the actual molecular band migrating on the column is a sum of an infinite number of sub-bands with (almost) Gaussian shapes that behave independently of one another [in the absence of mutual interactions among molecules; see Section(A)]. The ideal chromatography under consideration is an abstract concept dealing with the behavior of the band defined as a sum of centers of the sub-bands. In the abstract band, the molecules move between the two phases at infinite rates without accompanying the motion in the axial direction of the column.

In Chapter Ⅱ, a number of concepts are introduced. These involve the following: "The symmetry between mobile and stationary phases", which is extended to "the symmetry between general ordinary and complementary considerations". "Reduced coordinate s on the column" and "reduced coordinate $\hat{m}$ on the carrier liquid". "The sum ξ of s and $\hat{m}$". The set of "s as distance", "$\hat{m}$ as time", and "ξ as proper time". The set of "$\hat{m}$ as distance", "s as time", and "ξ as proper time". "Gradient G". "Trajectory T_0" and "trajectory T". "Molecular band migrating on the column" and "molecular band migrating on the carrier liquid". "Chromatogram as first concept" and "chromatogram as second concept". "Complementary chromatogram as first concept" and "complementary chromatogram as second concept". "Contraction of time" and "chromatographic dilatation" etc. [*Note.* "Gradient G" is a concept intimately related to but different from that of "gradi-

ent".]

In Chapter III, a unified view of chromatography is established. In this view, any chromatography is characterized by a surface taking place in the three-dimensional ($\hat{m}$,s, B) space where B stands for both partition of molecules in the liquid phase and rate of migration of molecules relative to the rate of migration of the carrier liquid on the column [see Section(A)]. With the isocratic case, the surface represents a plane parallel to the ($\hat{m}$,s) plane. When only the gradient in the liquid phase is applied, the surface is parallel to the s axis. When only the graient in the solid phase is applied, the surface is parallel to the $\hat{m}$ axis. When both gradient in the liquid phase and gradient in the solid phase are applied at the same time, the surface is unparallel to both s and $\hat{m}$ axis. Chromatography proceeds along characteristic curves that are constrained on the characteristic surface while projecting itself on ($\hat{m}$,s), ($\hat{m}$,B) and (s,B) planes.

In Chapter IV and V, the theories developed in Chapter II and III for ideal isocratic and gradient chromatographies are extended to theories treating the actual case when axial diffusion takes place on the column, respectively.

In Chapter VI, limiting ourselves to the usual case when only the gradient in the mobile phase (i.e., the concentration gradient) is applird, the final conclusion on dynamic investigation on chromatography is summarized along with the conclusion obtained from the combination of dynamic investigation with static investigation which will be developed later based on competition model.

In Chapter VII (along with Appendix VI), the theoretical conclusion on dynamic investigation (summarized in Chapter VI) is verified experimentally for hydroxyapatite chromatography over wide ranges of experimental conditions, and the optimization of chromatography is argued.

In Chapter VIII, static investigation on chromatography begins, and this Chapter involves approximately four subjects. First, competition model is proposed on the basis of a statistical mechanical concept. Second, some quantitative tests of competition model are performed for hydroxyapatite chromatography with excellent fit with experiment. Third, multi-peak collagen chromatograms obtained on hydroxyapatite columns are analysed on the basis of the final theoretical conclusion (summarized in Chapter VI); this leads to microheterogeneous models of collagen and myosin (which also gives multi-peak chromatograms on hydroxyapatite columns). Last, it is shown theoretically that the adsorption and desorption mechanisms of reversed-phase and ion-exchange chromatographies can also be explained by competition model assuming that, with reversed phase chromatography, sample molecule and gradient substance are adsorbed "weakly" on the adsorbent surface while performing the competition, whereas, with ion-exchange chromatography, these are adsorbed "strongly" while performing the competition.

In Chapter IX and X, reversed-phase and ion-exchange chromatographies carried out by several authors are analyzed, and the competition mechanisms deduced theoretically in the last subject in Chapter VIII are verified, respectively. The studies in both Chapter IX

and X are performed in intimate connection with the theoretical studies of other authors presented in Appendix XI(C)-(F).

The studies in Chapter Ⅷ-X performed for the three typical chromatographies (hydroxyapatite, reversed-phase and ion-exchange chromatographies) are in harmony as a whole, representing the total static investigation of chromatography.

The earlier theoretical studies of other authors are summarized in Appendix XI with particular interest in the relationship with the present theory. Appendix XI(A) and (B) are for dynamic investigations on isocratic and gradient chromatographies, respectively. Appendix XI(C)-(F) are for static investigation where the models for the adsorption and desorption mechanism proposed by other authors are summarized. Each of them (except those that are not concrete enough) is compared with competition model to judge the validity of either model. It can be concluded that some model can be incorporated to competition model as a special case of this latter [see Appendix XI(C)]. Otherwise, along with the results of the experimental analyses performed in Chapter Ⅷ-X, it can be concluded that it is competition model (and not other models) that universally explains the adsorption and desorption mechanism of a wide range of chromatographies.

Chapter II. Ideal Isocratic Chromatography in the Absence of Axial Diffusion in the Column

(A) Fundamental Concept

The studies in this and the subsequent Chapter III are done on the basis of the assumption of pointwise equilibria and no axial diffusion in the column [see Chapter I (B)].

Let C and χ, respectively, be the numbers of sample molecules in mobile (or liquid) and stationary (or solid) phases per either unit interstitial volume of the column or unit volume of column packing. The total number, Ω, of molecules per either unit interstitial volume of the column or unit volume of column packing can be represented as

$$\Omega = C + \chi \tag{2.1}$$

We express C, χ and Ω by using a normalized unit in which total number of molecules loaded on the column is equal to unity. [What is important is that all C, χ and Ω are represented as numbers of molecules per certain common unit volume of the column. This may represent any part (or the total) of the vertical slice of column packing. In the argument performed in Appendix XI(A), however, C, χ and Ω are defined as numbers of molecules per unit volume of column packing, whereas, in Chapter VIII(C), C and Ω represent numbers per unit interstitial volume of the column (without normalization).]

Due to pointwise equilibria and no axial diffusion in the column, the rate of migration, R_F, of a molecule relative to the migration rate of the carrier liquid is equal to the fraction of time spending in the mobile phase. When considering an assembly of molecules, fraction of time can be replaced by partition:

$$B^\circ = C/\Omega \tag{2.2}$$

of molecules in the mobile phase. When adsorption isotherm is linear, partition B° takes place equally in any slice of the *molecular band*(MB) migrating on the column, and relative rate of migration, R_F, of any slice is the same, equal to B° numerically; the meaning of "slice" will be specified in the subsequent Section(C). As a result, MB as a whole migrates on the column without changing its shape at a constant relative rate R_F equal to B°. In the absence of axial diffusion in the column, the symbol B° will hereafter be used to represent both molecular partition, C/Ω, in the mobile phase and relative rate of migration, R_F, at the same time; B° is comprised between 0 and 1.

In Fig 2.1(a), the trapezoid drawn with solid lines (briefly, the solid trapezoid) represents an MB (i.e., the distribution of molecular density Ω forming a band) migrating from right to left on the hypothetical column with infinite length. The initial state of MB with its rear border keeping in contact with origin O on the column is represented by the trapezoid drawn with dotted lines (briefly, the dotted trapezoid). The downward-oriented arrow represents the present position of the slice of the carrier liquid which was present at origin O initially; this migrates at a rate equal to that of the carrier liquid or the

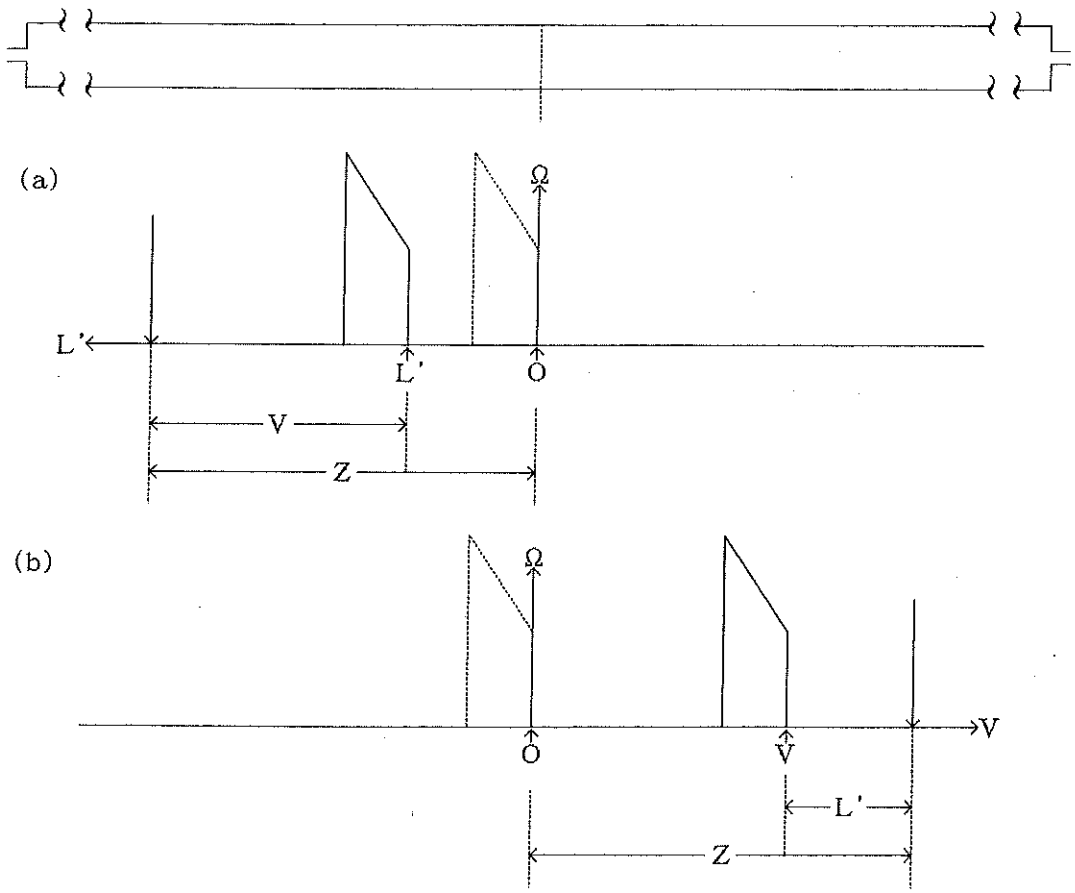


Fig 2.1. Migrations of MB (a) on the column to the left (OPV), and (b) on the carrier liquid to the right (CPV).

flow-rate. L' represents both the current coordinate calibrated on the hypothetical column along the main axis (in such a way that it increases from right to left) and the present position of the rear border of MB (i.e., the distance of this position from origin O). For convenience' sake, L' is expressed in terms of the sum of interstitial volumes involved between the position under consideration and origin O on the column. V represents the total volume of the carrier liquid that has passed the rear border of MB, whereas

$$Z = V + L' \tag{2.3}$$

represents the volume that has passed origin O on the column since the beginning of chromatography. (See Fig 2.1 drawn assuming that $B^\circ = 1/3$.)

Let us call the point of view based on the hypothetical column with infinite length as *theoretical point of view*(TPV) in contrast to *experimental point of view*(EPV) which is based on the actual column with finite length. The present theory will be developed in TPV mainly. Let us also call as *ordinary point of view*(OPV) the viewpoint in which Fig 2.1(a) is drawn where it is the column or the solid phase that is fixed; both carrier liquid and MB migrate to the left. EPV belongs in OPV. In Table 2.1, all the points of view that appear in this monograph are summarized.

In contrast to OPV, *complementary point of view*(CPV) in which Fig 2.1(b) is drawn is conceivable. In CPV (which belongs in TPV), it is the carrier liquid or the liquid phase that is fixed; both column and MB migrate to the right. As partition:

$$1 - B^\circ = \chi / \Omega \tag{2.4}$$

of molecules in the stationary phase takes place equally in any slice of MB, MB as a whole migrates without changing its shape at a relative rate (to the migration rate of the solid phase identical with the flow-rate) equal to $1 - B^\circ$ ($=2/3$). In Fig 2.1(b), solid and dotted trapezoids represent MB migrating on the carrier liquid and the initial state of MB with its front border keeping in contact with origin O on the carrier liquid, respectively; origin O on the carrier liquid is superposed on origin O on the column initially. The downward-oriented arrow represents the present position of the slice of the assembly of packed particles in the column, which was present at origin O on the carrier liquid initially. This migrates at a rate equal to the flow-rate in the directiion opposite to that of the flow of the carrier liquid taking place on the column. In Fig 2.1(b), V represents both the current coordinate calibrated on the carrier liquid along the main axis of the column (in such a way that it increases from left to right) and the present position of the front border of MB (i.e., the distance of this position from origin O). L' represents the sum of interstitial volumes of the column that have passed the front border of MB, whereas Z[eq (2.3)] represents the sum of interstitial volumes that have passed origin O on the carrier liquid since the beginning of chromatography.

The behavior of MB is describable in four ways by using (a) variable Z and L' in OPV [Fig 2.1(a)], (b) variable V and L' in OPV [Fig 2.1(a)], (c) variable Z and V in

Table 2.1

Summary of all the points of view.

Point of view	
EPV	OPV OPV[CPV(OPV)]
TPV	OPV CPV
	OPV(CPV) CPV(OPV)
	OPV[CPV(OPV)] CPV[OPV(CPV)]

CPV [Fig 2.1(b)], and (d) variable L' and V in CPV [Fig 2.1(b)]. Between each pair of variables above, the first can be interpreted to measure time elapsed since the beginning of chromatography, whereas the second measures distance of the position of MB from origin O along the current coordinate under consideration. It should be noted that there are two types of time: that associated with Z (called later as proper time) and that associated with V or L'. The terminologies OPV and CPV will be conserved hereafter as far as proper time (associated with Z) is used. When time (associated with V or L') is used, however, these will be modified to OPV(CPV) and CPV(OPV), respectively [see the subsequent Section(E)].

(B) Variable s, $\hat{m}$ and ξ

First definition of s. Let us hypothesize that the column container is stained with a color gradation with wave length of absorption increasing linearly in the flow direction along the main axis of the column. s is defined as difference in wave length of absorption between arbitrary position L' and origin O on the column, increasing linearly with increase in L' fulfilling

$$s = g'L' \tag{2.5}$$

in which g' (=tan α) stands for the slope of the color gradient [see Fig 2.2(a)]. In OPV, L' represents both the current coordinate calibrated on the column and the position of the rear border of MB [Section(A)], s represents these quantities in unit of wave length of absorption[Fig 2.2(a)]. The definition of s above is done, however, in association with the first definition of $\hat{m}$ which will be done below.

First definition of $\hat{m}$. Origin O on the hypothetical column with infinite length(TPV) corresponds to the inlet of the actual column(EPV). Suppose that, at the moment when the injection of the sample solution is completed at the inlet of the column or when the formation of the initial MB is completed with its rear border keeping in contact with the column inlet, the column is immediately supplied with a marker solution continuously at the inlet while increasing (from zero) the marker concentration linearly with increase in volume, Z, of supply. The development of MB on the column therefore is done by marker solution, where we asume that marker is unadsorbable and that it does not affect the adsorption and desorption of sample molecules at all. Let us define $\hat{m}$ as marker concentration. Denoting by g' the increase of $\hat{m}$ per unit volume of supply taking place at the inlet of the column, $\hat{m}$ can be represented as $\hat{m}=g'Z$. In this instance, $\hat{m}$ also increases linearly with increase in volume V of the carrier liquid passing the rear border of MB migrating on the column, fulfilling

$$\hat{m} = g'V \tag{2.6}$$

In CPV, V represents both the current coordinate calibrated on the carrier liquid and the

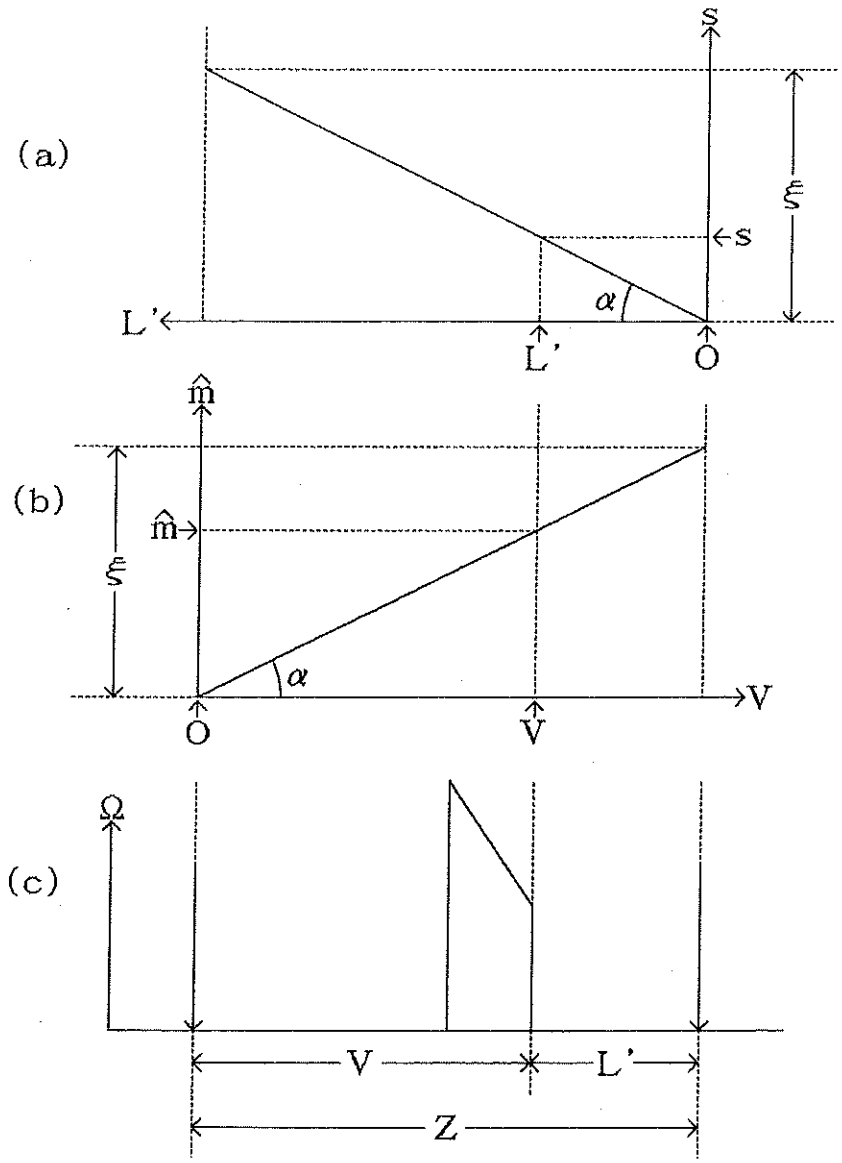


Fig 2.2. First definitions of (a) s, and (b) $\hat{m}$. Part(c) illustrates both Figs 2.1(a) and (b) at the same time.

position of the front border of MB migrating on the carrier liquid [Section(A)]. The marker concentration gradient is formed along the current coordinate V, and $\hat{m}$ represents both the current coordinate and the position of the front border of MB on the carrier liquid in unit of marker concentration [see Fig 2.2(b)]. We now identify numerically the slope g' of the color gradient and the slope g' of the marker gradient with one another by using a certain unit. Thus, both variable s and $\hat{m}$ have been defined in association with one another.

Second definition of s. s[eq(2.5)] is defined as difference of marker concentration, $\hat{m}$, between origin O and position L' on the column [see Fig 2.3(a)]. s now represents in unit of marker concentration both the current coordinate calibrated on the column and the position of the rear border of MB migrating on the column[Fig 2.3(a)].

Second definition of $\hat{m}$. $\hat{m}$[eq(2.6)] is defined as difference of wave length of absorption, s, between origin O and position V on the carrier liquid [see Fig 2.3(b)]. $\hat{m}$ now represents in unit of wave length of absorption both the current coordinate calibrated on the carrier liquid and the position of the front border of MB migrating on the carrier liquid[Fig 2.3(b)].

It should be noted that a set of variable s and $\hat{m}$ can be defined on the basis of the concept of either solid phase (combination of the first definition of s and the second definition of $\hat{m}$) or liquid phase (combination of the second definition of s and the first definition of $\hat{m}$). With gradient chromatography carried out by using only the gradient in the solid phase, it is convenient to define the set of s and $\hat{m}$ on the basis of the solid phase concept only. To the contrary, when only the gradient in the liquid phase is applied(usual case), it is convenient to define the set on the basis of the liquid phase concept only (cf. Chapter VI-Ⅷ).

Definition of ξ. ξ is defined as

$$\xi = g'Z = \hat{m} + s \tag{2.7}$$

All the arguments developed in Section(A) on the basis of variable V, L' and Z can be replaced by the arguments based on variable $\hat{m}$, s and ξ. As far as isocratic chromatography is concerned, the two arguments are identical. With gradient chromatography in which new concepts are added, respectively, to variable s and $\hat{m}$, a difference arises, and the argument based on variable $\hat{m}$, s and ξ are more useful [see the subsequent Chapter Ⅲ(C)]. In the subsequent Section(C)-(G), the argument on isocratic chromatography[Section(A)] will be continued by using $\hat{m}$, s and ξ in order for it to be connected to the argument on gradient chromatography which will be developed by using $\hat{m}$, s and ξ (Chapter Ⅲ).

(C) Gradient G, Trajectory T_0, and Trajectory T

Let us write MB(o) and MB(c) for MB when MB is interpreted to migrate on the

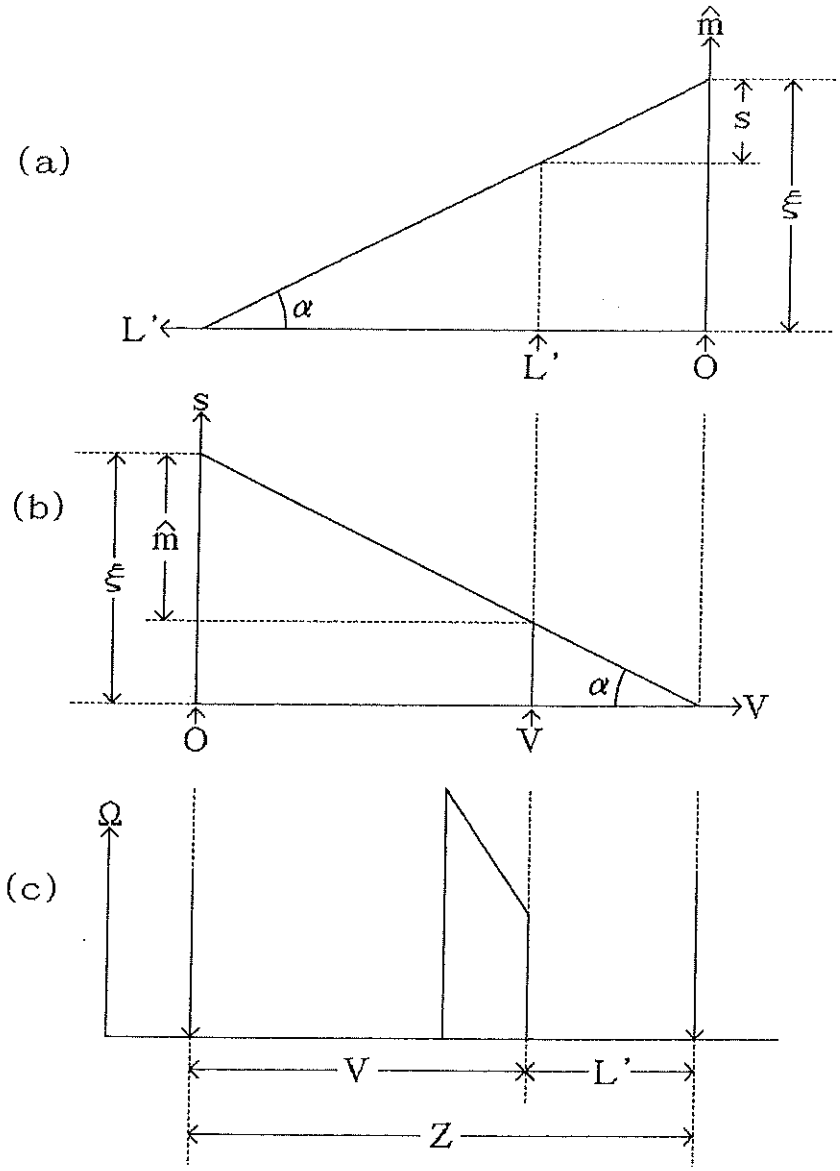


Fig 2.3. Second definitions of (a) s, and (b) $\hat{m}$. Part(c) illustrates both Figs 2.1(a) and (b) at the same time.

column[Fig 2.1(a); OPV] and the carrier liquid[Fig 2.1(b); CPV], respectively. Fig 2.4 reproduces Fig 2.1 in a different manner, where MB(o) and MB(c), being the mirror images of one another, are considered to represent projections on (s,Ω) and $(\hat{m},\Omega)$ planes of a *fundamental conceptual band*(FCB) present in the $(\hat{m},s,\Omega)$ space, respectively. FCB (to be precise, the curve representing FCB) is constrained on a plane parallel to the Ω axis the intersection of which with the $(\hat{m},s)$ plane defines a straight line with a slope of -45° on the $(\hat{m},s)$ plane; this intersects both $\hat{m}$ and s axes at coordinate ξ $(=\hat{m}+s)$. Let us call the straight line with slope of -45° as *gradient* G (see Fig 2.4). It is possible to consider that gradient G (which intersected origin O initially) migrates in either $\hat{m}$ or s direction at a constant rate equal to g' times the flow-rate, and that FCB migrates along gradient G at the same time while projecting itself on both (s,Ω) and $(\hat{m},\Omega)$ planes.

If gradient G is mapped to $(L',\hat{m})$ and (V,s) planes, it will coincide with marker gradient[Fig 2.3(a)] and color gradient[Fig 2.3(b)], respectively. To the contrary, if marker and color gradients are mapped to the $(\hat{m},s)$ plane, they will coincide with gradient G, respectively. Gradient G can also be mapped to the (V,L') plane while conserving the slope of -45°; it migrates in either V or L' direction at a rate equal to the flow-rate.

In Fig 2.4, point $\bar{P}$ corresponds to both the rear border of MB(o) migrating along s and front border of MB(c) migrating along $\hat{m}$. Point $\bar{P}$ (which stayed at origin O initially when gradient G intersected origin O) moves on the $(\hat{m},s)$ plne while staying on gradient G and keeping the sum of migration rates in $\hat{m}$ and s directions equal to g' times the flow-rate. Let us call the trajectory of point $\bar{P}$ drawn on the $(\hat{m},s)$ plne as *trajectory* T_0. Trajectory T_0 is linear with a slope of $B^{\circ}/(1-B^{\circ})$ because the rate of migration of MB(o) along s and the rate of migration of MB(c) along $\hat{m}$ are proportional to B° and $1-B^{\circ}$, respectively. If point $\bar{P}$ is mapped to the (V,L') plane, it will move on the plane while keeping the sum of migration rates in V and L' directions equal to the flow-rate drawing trajectory T_0.

Trajectory T_0 can be represented as

$$s = \frac{B^{\circ}}{1-B^{\circ}}\hat{m} \tag{2.8}$$

or, by using eq(2.7), as

$$\xi = \hat{m}+s = \hat{m}/(1-B^{\circ}) = s/B^{\circ} \tag{2.9}$$

Eq(2.9) manifests that both $\hat{m}$ and s (as coordinates of point $\bar{P}$; Fig 2.4) can be represented as functions of $\hat{m}+s$ or ξ; this arises from the fact that $\bar{P}$ stays on gradient G always. Rewriting $(\bar{\hat{m}},\bar{s})$ for the coordinate of $\bar{P}$, gradient G can be represented as

$$\hat{m}+s\ (=\bar{\hat{m}}+\bar{s}) = \bar{\hat{m}}/(1-B^{\circ}) = \bar{s}/B^{\circ} \tag{2.10}$$

[Fig 2.5(a)].

The parameter $S\equiv\int_{-\infty}^{s}\Omega\,ds$ represents the partial area of MB(o) with density Ω, the

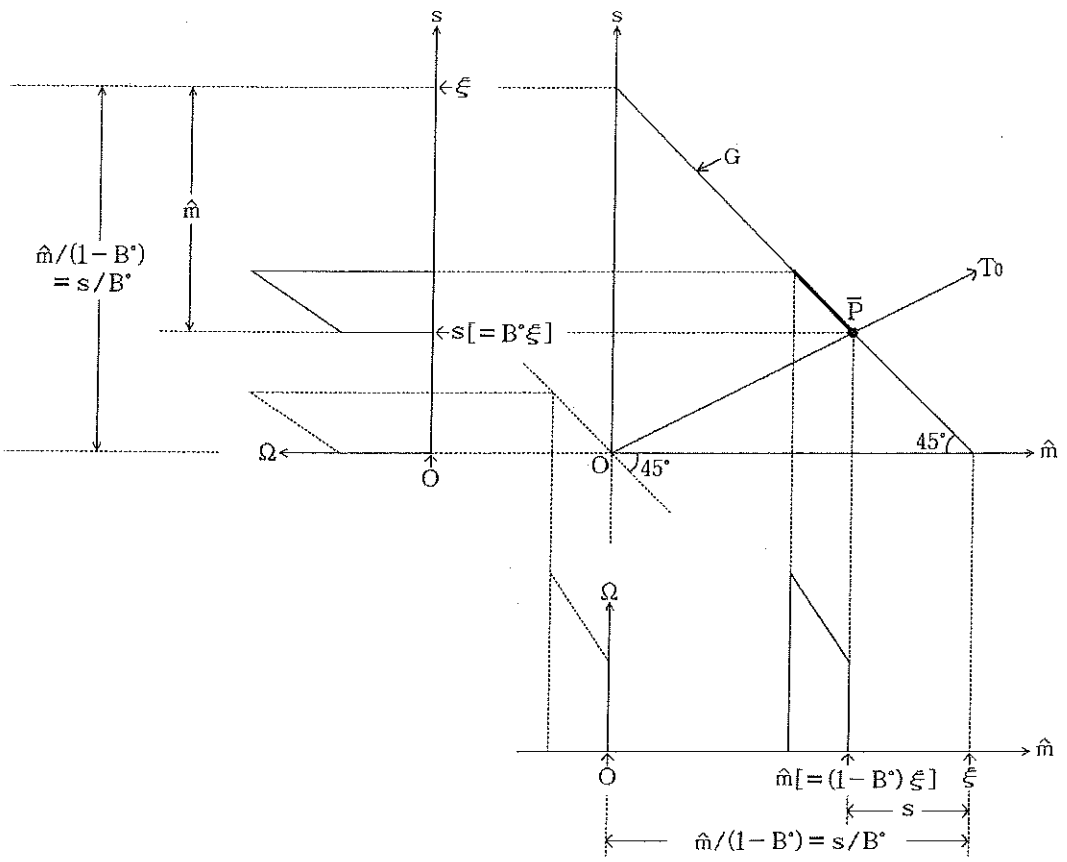


Fig 2.4. Another representation of Fig 2.1. Gradient G, FCB and trajectory T_0 are depicted.

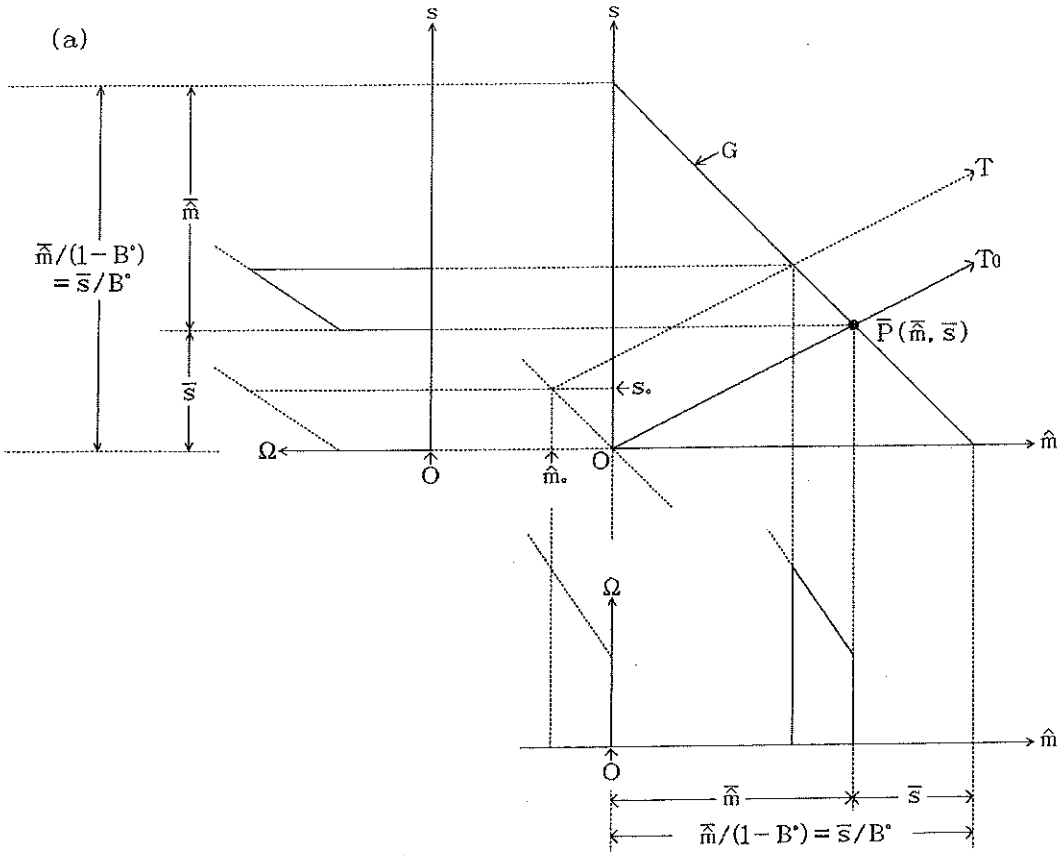


Fig 2.5. (a) Trajectory T_0 versus (b) Trajectory T.

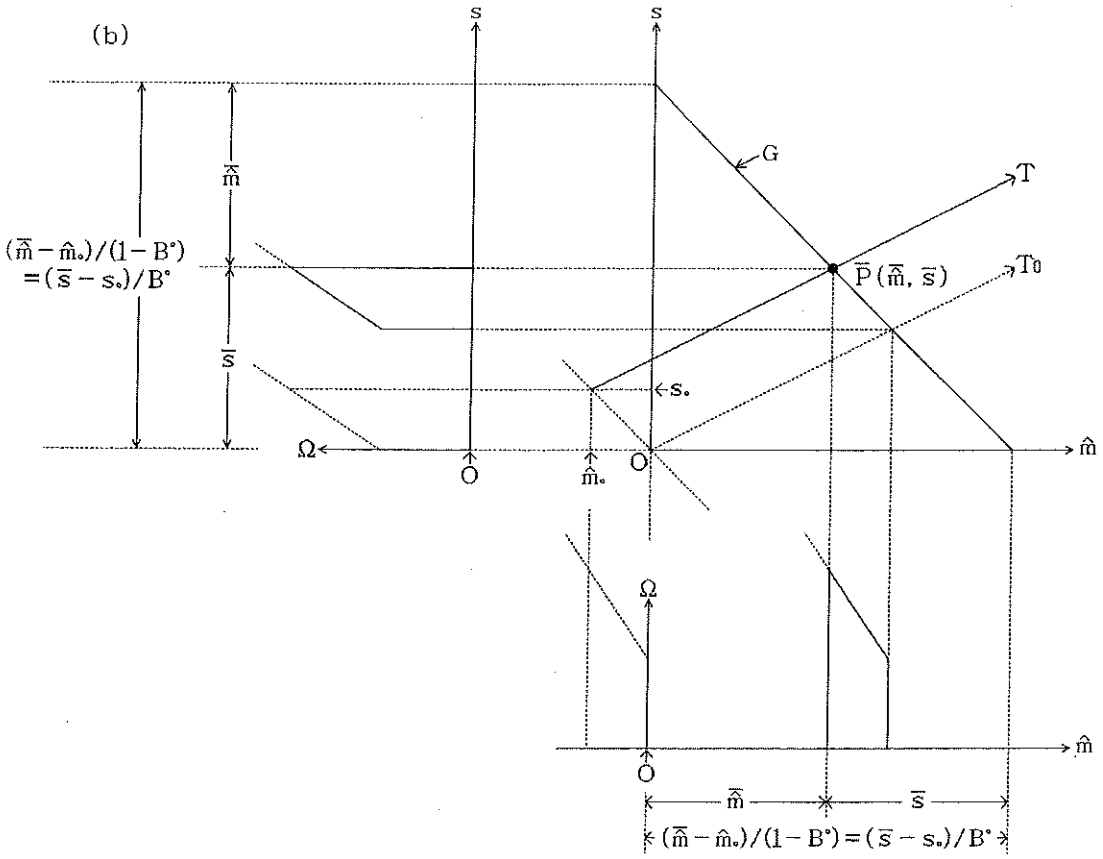

(b)
s
s
G
T
T0
$\bar{\bar{m}}$
$(\bar{\bar{m}} - \hat{m}_0)/(1 - B^*)$
$= (\bar{s} - s_0)/B^*$
$\bar{s}$
$\bar{P}(\bar{\bar{m}}, \bar{s})$
s_0
Ω
O
$\hat{m}_0$
O
$\hat{m}$
Ω
O
$\hat{m}$
$\bar{\bar{m}}$
$\bar{s}$
$(\bar{\bar{m}} - \hat{m}_0)/(1 - B^*) = (\bar{s} - s_0)/B^*$

Fig 2.5. (b)

total area being represented as $\int_{-\infty}^{\infty}\Omega\,ds=1$. Let us define the *slice* of MB(o) as slice inserted between two parts of MB(o) with areas S and S+dS (=S+Ωds), respectively. As for MB(c), S can be defined as $S\equiv\int_{\hat{m}}^{\infty}\Omega\,d\hat{m}$ with $\int_{-\infty}^{\infty}\Omega\,d\hat{m}=1$, and the corresponding *slice* of MB(c) can be defined as slice inserted between two parts of MB(c) with areas S and S+dS (=S−$\Omega\,d\hat{m}$). [This definition of the slice is valid even when the shape of MB(o) or MB(c) changes with its migration i.e., for the case of gradient chromatography (Chapter III) and for the case of both isocratic and gradient chromatographies taking place actually in the presence of axial diffusion in the column(Chapter IV and V).] Let us call the trajectory drawn by point $\bar{P}$ corresponding to any slice of MB(o) or MB(c) as *trajectory* T. Trajectory T does not necessarily begin at origin O [Fig 2.5(b)], and it can be represented, instead of eqs(2.8) and (2.9), as

$$s-s_o = \frac{B^o}{1-B^o}(\hat{m}-\hat{m}_o) \tag{2.11}$$

and

$$\xi = \hat{m}+s = (\hat{m}-\hat{m}_o)/(1-B^o) = (s-s_o)/B^o \tag{2.12}$$

respectively; $(\hat{m}_o, s_o)$ fulfilling

$$\hat{m}_o + s_o = 0 \tag{2.13}$$

stands for the initial coordinate of point $\bar{P}$ [see Fig 2.5(b)]. Rewriting $(\bar{\hat{m}}, \bar{s})$ for the coordinate of $\bar{P}$, gradient G can be represented, instead of eq(2.10), as

$$\hat{m}+s\ (=\bar{\hat{m}}+\bar{s}) = (\bar{\hat{m}}-\hat{m}_o)/(1-B^o) = (\bar{s}-s_o)/B^o \tag{2.14}$$

[see Fig 2.5(b)].

Writing

$$\Omega = F(s) \tag{2.15}$$

for the initial MB(o) (dotted trapezoid in the left part of Fig 2.4)

$$\Omega = F(s-B^o\xi) \tag{2.16}$$

represents MB(o) migrating on the column (solid trapezoid in the left part of Fig 2.4), where function F(X) is normalized [$\int_{-\infty}^{\infty}F(X)dX=1$], and it is defined that F(X)=0 when X<0. The initial MB(c) can be written as

$$\Omega = F(-\hat{m}) \tag{2.17}$$

(dotted trapezoid in the lower part of Fig 2.4), and MB(c) migrating on the carrier liquid can be represented as

$$\Omega = F[-(\hat{m}-(1-B^o)\xi)] \tag{2.18}$$

(solid trapezoid in the lower part of Fig 2.4). As a reflection of the fact that MB(o)[eq (2.16)] and MB(c)[eq(2.18)], respectively, are projections on (s, Ω) and $(\hat{m}, \Omega)$ planes of FCB migrating along gradient G, eq(2.18) can be derived by substituting $\xi - \hat{m}$ for s into eq(2.16), whereas eq(2.16) can be derived by substituting $\xi - s$ for $\hat{m}$ into eq(2.18). [Instead of eqs(2.16) and (2.18), it is possible to represent MB(o) and MB(c) as $\Omega = F[s - B^{\circ}\hat{m}/(1-B^{\circ})]$ and $\Omega = F[-\{\hat{m} - (1-B^{\circ})s/B^{\circ}\}]$, respectively. These expressions are not useful for our purpose, however.]

(D) Measurements of C and χ

Let us hypothesize to set a probe M at an arbitrary position s fixed on the hypothetical column with infinite length (TPV), and to monitor dencity C of molecules in the mobile or liquid phase as a function of liquid volume, $\hat{m}$, passing s (OPV; see Fig 2.6). Instead of $\hat{m}$, it is possible to consider ξ to represent liquid volume passing s; ξ is larger than $\hat{m}$ by a constant value of s [see eq(2.7)]. As far as the argument in this Section is concerned, it is only for convenience' sake that we choose $\hat{m}$ as liquid volume. [Until now the symbol s is used in three ways representing (a) current coordinate on the column, (b) position of the rear border of MB(o) migrating on the column, and (c) arbitrary position fixed on the column. s with sharp indicating a position on the s axis drawn in the left parts of both Figs 2.6(a) and (b) represents s as fixed position on the column. s indicating a position on the s axis drawn in the upper-middle part of Fig 2.6(c) represents both position of the rear border of MB(o) and arbitrary position fixed on the column at the same time.]

The trapezoids drawn in the left parts of both Figs 2.6(a) and (b) and the trapezoid drawn in the upper-middle part of Fig 2.6(c) represent an MB(o) (with density Ω) migrating on the column. When the front border of MB(o) reaches position s or $s^{\#}$, the monitoring begins [Fig 2.6(a) left part], and the left border of the registration diagram is completed [left border of the flat trapezoid in the lower part of Fig 2.6(a)]. This is superposed on the rear border of MB(c) [taller trapezoid in the lower part of Fig 2.6(a)]. The monitoring is completed when the rear border of MB(o) reaches position $s^{\#}$ or s [Fig 2.6 (c) upper-middle part] or when the front border of MB(c) coincides with the right border of the registration diagram [Fig 2,6(c) lower part] passing through the intermediate process [left and lower parts of Fig 2.6(b)]. Height or density of the registration diagram is B° (= 1/3) times as high as that of MB(c) or MB(o) at the corresponding part [Fig 2.6(c) lower part]; this arises from the fact that molecular density C in the liquid phase is B° times as high as total density Ω at the corresponding part [eq(2.2)]. Width Δ_c of the registration diagram is $1/B^{\circ}$ (=3) times as large as width Δ_o of MB(c) or MB(o):

$$\Delta_c = \Delta_o/B^{\circ} \tag{2.19}$$

[see Fig 2.6(c) lower part]. The registration diagram drawn in the lower part of Fig 2.6(c)

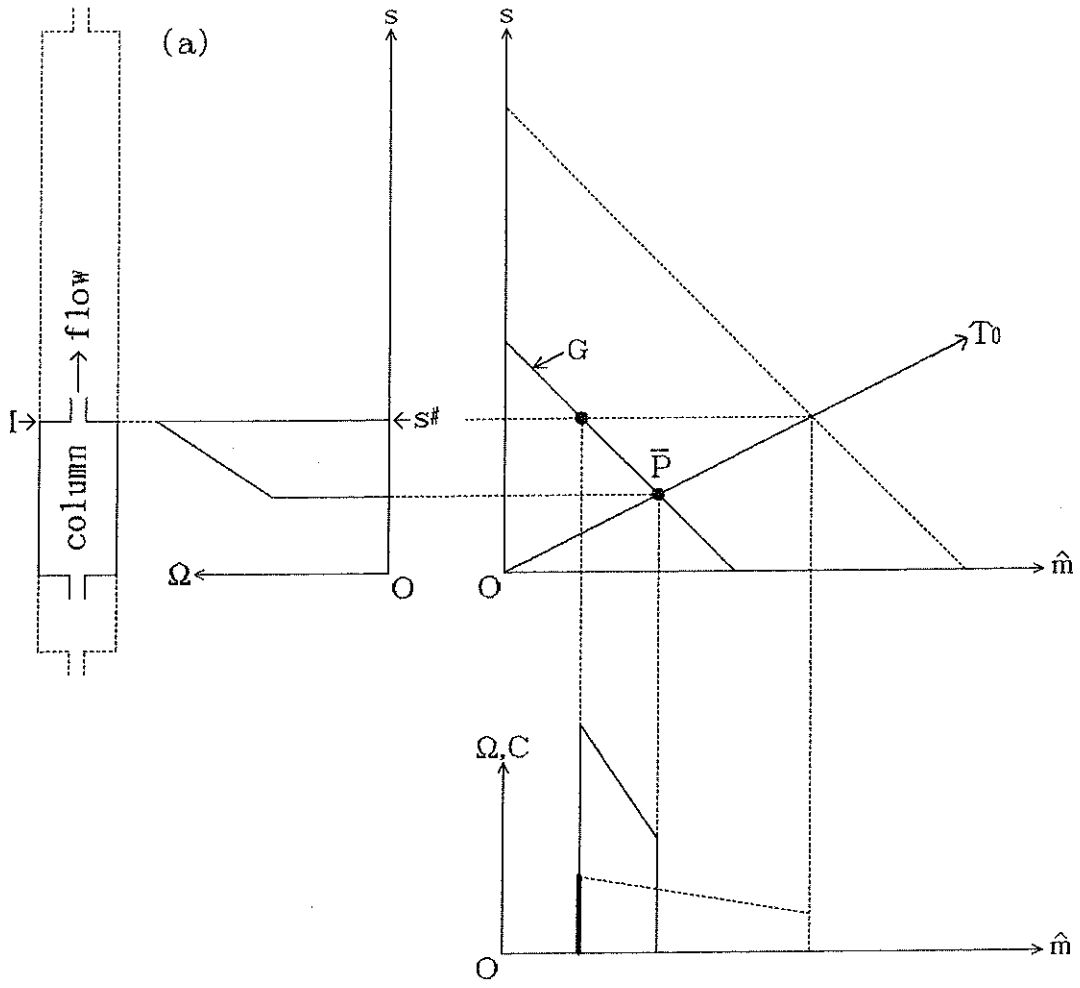


Fig 2.6. Measurement of molecular density C in the mobile or liquid phase by probe M fixed to the stationary phase, registering the completion of chromatogram.

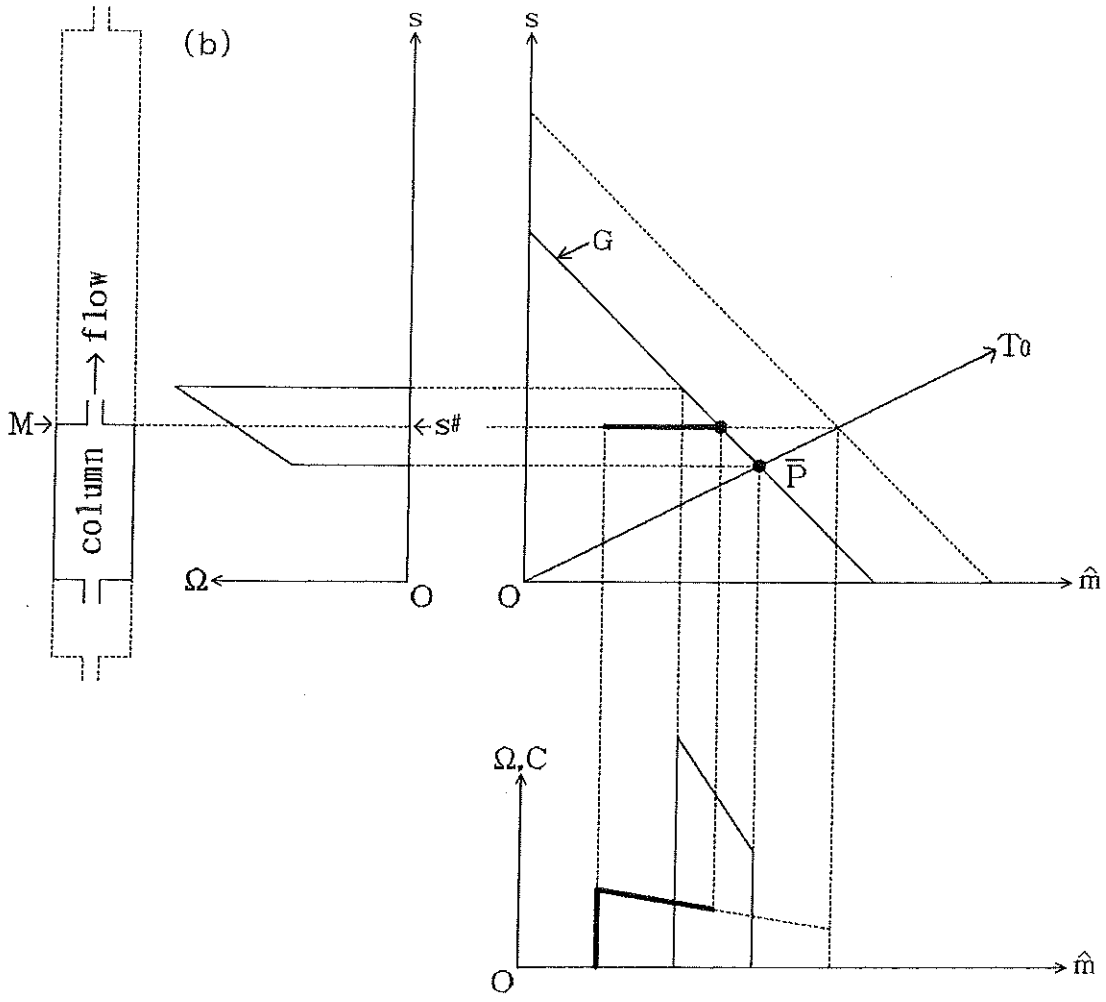


Fig 2.6. (b)

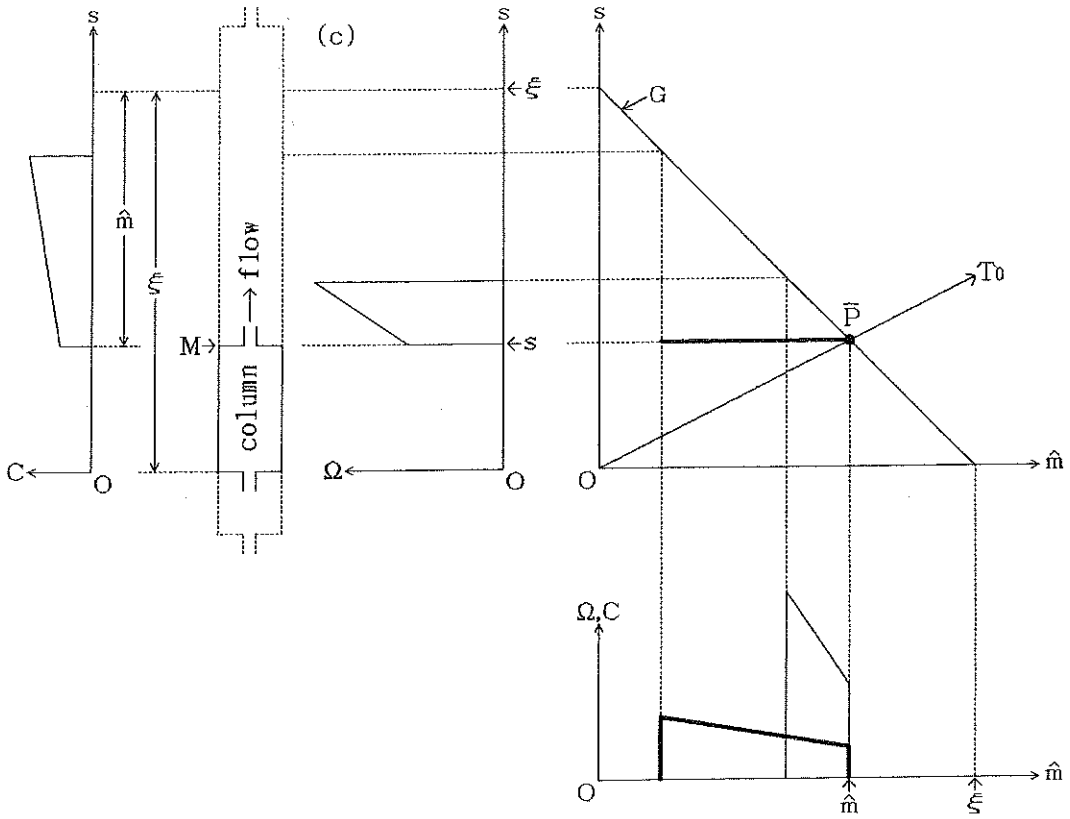

s
(c)
s
s
$\hat{\xi}$
G
$\hat{m}$
$\hat{\xi}$
flow
M
column
$\vec{P}$
To
s
C
O
Ω
O
O
$\hat{m}$
Ω,C
O
$\hat{m}$
$\hat{m}$
$\hat{\xi}$

Fig 2.6. (c)

is called a *chromatogram*.

When MB(o) [trapezoid in the upper-middle part of Fig 2.6(c)] is represented by eq (2.16) or when MB(c) [taller trapezoid in the lower part of Fig 2.6(c)] is represented by eq(2.18), then chromatogram [flat trapezoid in the lower part of Fig 2.6(c)] can be written as

$$C = B^{\circ}F[-B^{\circ}(\hat{m} - \frac{1-B^{\circ}}{B^{\circ}}s)] \qquad (2.20)$$

Let us call the chromatogram as expressed by using eq(2.20) as *chromatogram as first concept* (abbreviated as CGM1st); eq(2.20) can be regarded as a solution to the subsequent continuity equation, eq(2.23). [Instead of eq(2.20), it is possible to represent chromatogram as $C=B^{\circ}F[-B^{\circ}\{\hat{m}-(1-B^{\circ})\xi\}]$. This expression is not useful for our purpose, however. Cf. the argument with respect to eq(2.18).]

Actually, the monitoring is carried out in a flow-cell joined to the outlet of the column by using a fine tube with negligibly small total inner volume(EPV). In EPV, let us call volume $\hat{m}$ of the carrier liquid eluted from the outlet of the column as *elution volume*; CGM1st can be represented as a function of elution volume $\hat{m}$ [see Fig 2.6(c) lower part]. $\hat{m}$ also represents the elution volume at the right border of CGM1st [Fig 2.6(c) lower part]. Let us consider that the part [0,s] of the hypothetical column with infinite length represents the actual column, and that the part (s,∞) is empty. It is molecules in the mobile phase that is eluted out of the actual column, and the distribution taking place in the empty part (s,∞) of the molecules that have just been eluted out of the actual column represents the mirror image of CGM1st [see Fig 2.6(c) left part].

Again in EPV, let us call as *proper elution volume* the sum, ξ, of elution volume, $\hat{m}$, and total interstitial volume, s, of the column [eq(2.7); see Fig 2.6(c) left part]. At the beginning of chromatography when the rear border of MB(o) keeps in contact with the inlet of the column, proper elution volume ξ is equal to zero, whereas elution volume $\hat{m}$ is equal to minus the total interstitial volume s of the column.

Another probe M' floating in the carrier liquid and migrating on the hypothetical column with infinite length at a rate equal to the flow-rate is conceivable. Let us hypothesize to monitor density χ of molecules in the stationary or solid phase by using probe M' as a function of interstitial volume, s, of the column passing an arbitrary position, $\hat{m}$, fixed on the carrier liquid (CPV; see Fig 2.7). As far as the argument in this Section is concerned, it is only for convenience' sake that we choose s, instead of ξ, as interstitial volume passing $\hat{m}$. [Until now the symbol $\hat{m}$ is used in three ways representing (a) current coordinate on the carrier liquid, (b) position of the front border of MB(c) migrating on the carrier liquid, and (c) arbitrary position fixed on the carrier liquid. $\hat{m}$ with sharp indicating a position on the $\hat{m}$ axis drawn in the lower parts of Figs 2.7(a)-(c) represents $\hat{m}$ as fixed position on the carrier liquid. $\hat{m}$ indicating a position on the $\hat{m}$ axis drawn in the lower part of Fig 2.7(c') represents both position of the front border of MB(c) and

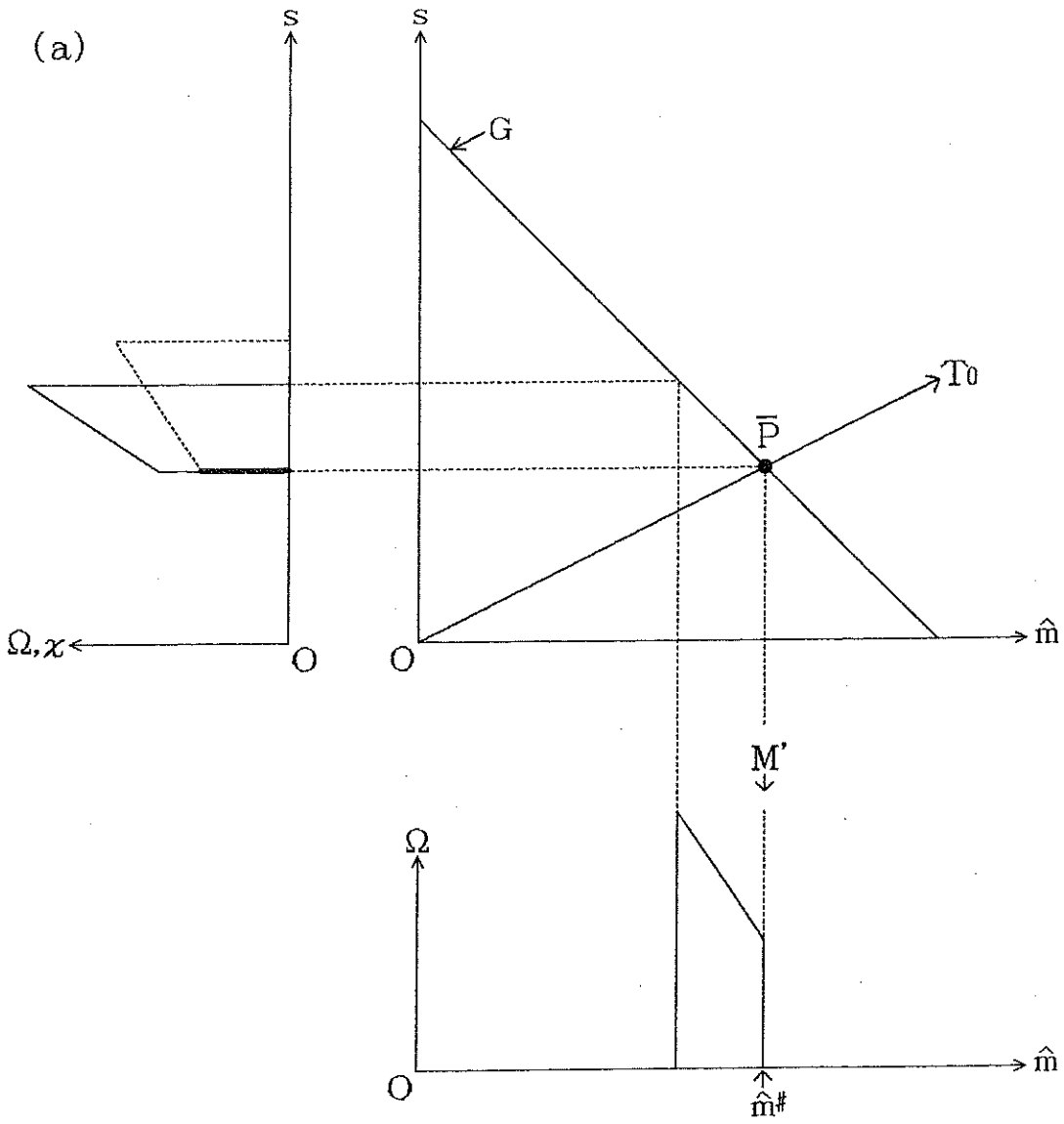


Fig 2.7. Measurement of molecular density χ in the stationary or solid phase by probe M' fixed to the mobile phase, registering the completion of complementary chromatogram.

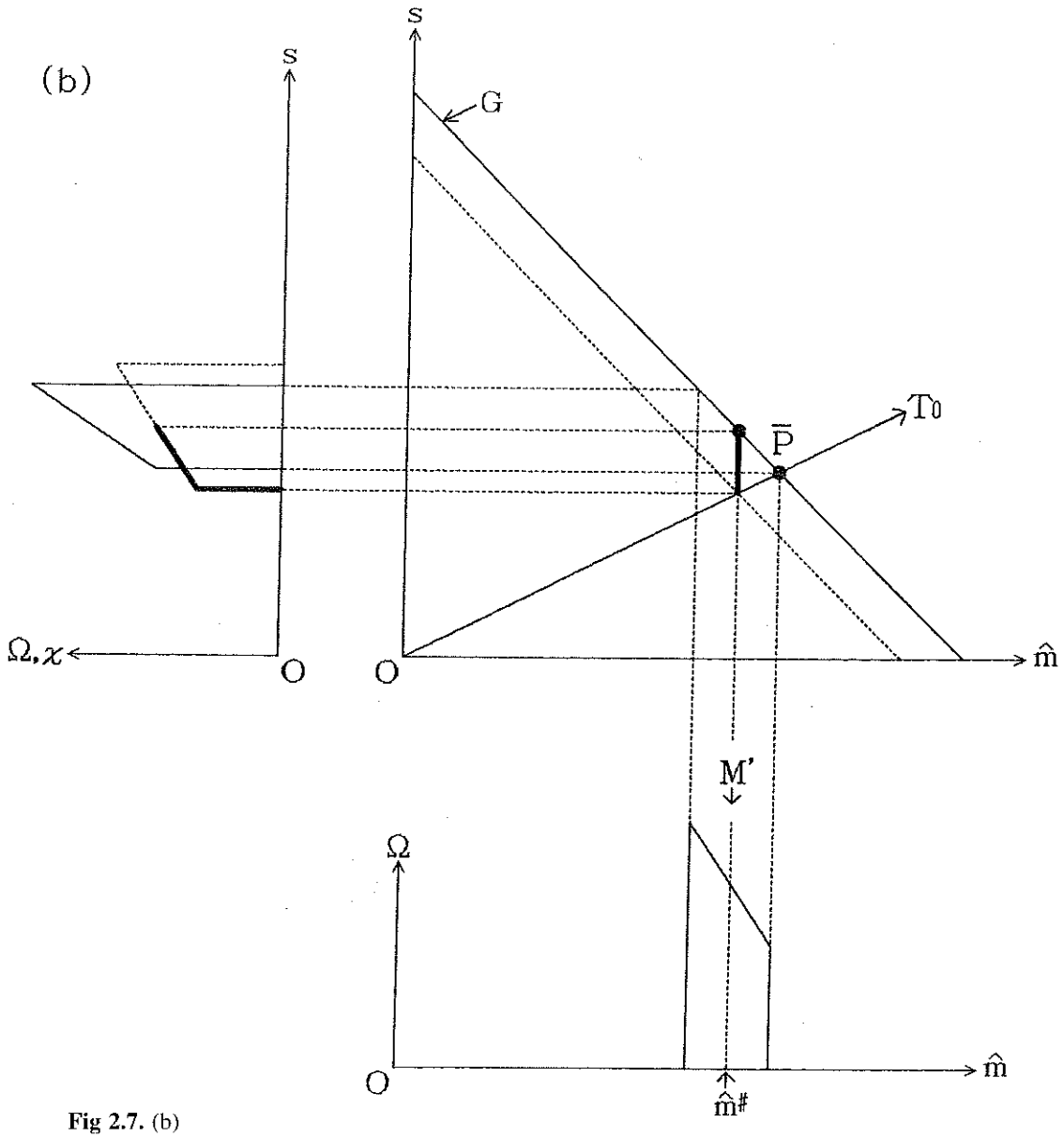


Fig 2.7. (b)

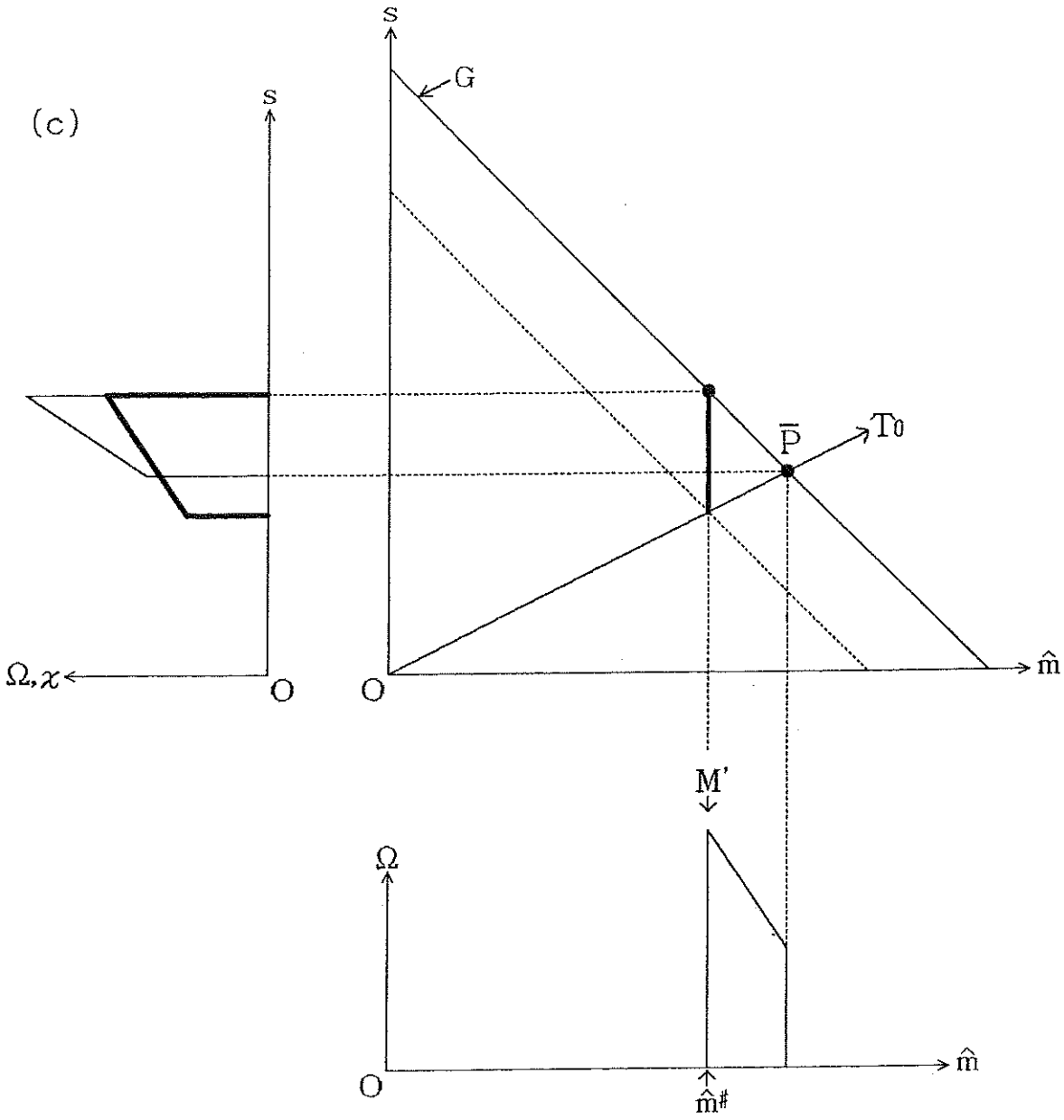


Fig 2.7. (c)

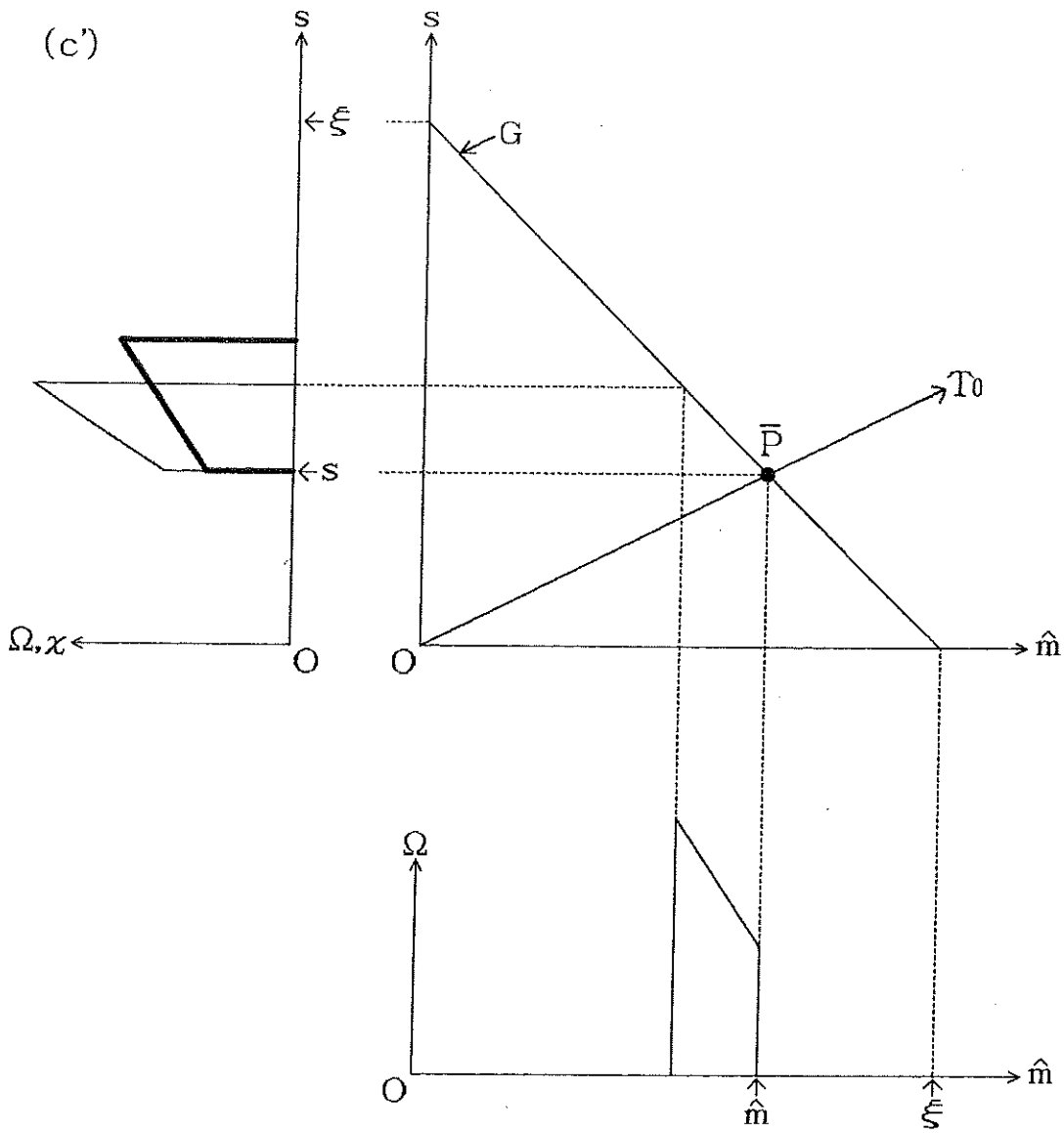


Fig 2.7. (c')

arbitrary position fixed on the carrier liquid at the same time.]

The trapezoids drawn in the lower parts of Figs 2.7(a)-(c) represent a MB(c) (with density Ω) migrating on the carrier liquid. When the front border of MB(c) reaches position $\hat{m}$ or $\hat{m}^*$, the monitoring begins [Fig 2.7(a) lower part], and the lower border of the registration diagram is completed [lower border of the flat trapezoid in the left part of Fig 2.7(a)]. This is superposed on the rear border of MB(o) [taller trapezoid in the left part of Fig 2.7(a)]. The monitoring is completed when the rear border of MB(c) reaches position $\hat{m}^*$ [Fig 2.7(c) lower part] or when the front border of MB(c) coincides with the upper border of the registration diagram [Fig 2.7(c) left part] passing through the intermediate process [lower and left parts of Fig 2.7(b)]. Height or densiy of the registration diagram is $1-B^\circ$ ($=2/3$) times as high as that of MB(c) or MB(o) at the corresponding part [Fig 2.7(c) left part]; this arizes from the fact that molecular density χ in the solid phase is $1-B^\circ$ times as high as total density Ω at the corresponding part [eq(2.4)]. Width Δ_χ of the registration diagram is $1/(1-B^\circ)$ ($=1.5$) times as large as width Δ_Ω of MB(c) or MB(o):

$$\Delta_\chi = \Delta_\Omega/(1-B^\circ) \tag{2.21}$$

[see Fig 2.7(c) left part]. To be symmetric with Fig 2.6(c), Fig 2.7(c) can be re-drawn as Fig 2.7(c') without changing the registration diagram. Let us call the registration diagram drawn in the left part of Fig 2.7(c) or (c') as a *complementary chromatogram*.

When MB(c) [trapezoid in the lower part of Fig 2.7(c')] is represented by eq(2.18) or when MB(o) [taller trapezoid in the left part of Fig 2.7(c')] is represented by eq(2.16), then complementary chromatogram [flat trapezoid in the left part of Fig 2.7(c')] can be written as

$$\chi = (1-B^\circ)\, F[(1-B^\circ)(s-\frac{B^\circ}{1-B^\circ}\hat{m})] \tag{2.22}$$

Due to both eqs(2.2) and (2.4), eq(2.22) is identical with eq(2.20). Let us call the complementary chromatogram as expressed by using eq(2.22) as *complementary chromatogram as first concept* (abbreviated as χGM1st); eq(2.22) can be regarded as a solution to the subsequent continuity equation, eq(2.25). [Instead of eq(2.22), it is possible to represent complementary chromatogram as $\chi=(1-B^\circ)F[(1-B^\circ)(s-B^\circ\xi)]$. This expression is not useful for our purpose, however. Cf. the argument with respect to eq(2.16).]

(E) Chromatogram as First Concept versus Abstract Flux, and Complementary Chromatogram as First Concept versus Complementary Abstract Flux

If a series of monitoring experiments of molecular density C [Section(D)] are carried out while changing position, s, of probe M to increase s (or while increasing length s of the column used; EPV), then CGM1st [flat trapezoid in the lower part of Fig 2.6(c)] will

migrate in the positive $\hat{m}$ direction. It now is possible to consider an *abstract flux* of molecules [with density C and rate, $(1-B^\circ)/B^\circ$, of migration] represented by eq(2.20); this migrates along *distance* $\hat{m}$ with a lapse of *time* s without changing the shape. It is eassy to find out that eq(2.20) is a solution to the conservation or continuity equation:

$$\mathrm{div}_{\hat{m}}\left(\frac{1-B^\circ}{B^\circ}C\right)+\frac{\partial C}{\partial s}=0 \tag{2.23}$$

obtained under initial condition:

$$\lim_{s\to 0} C = B^\circ F(-B^\circ \hat{m}) \tag{2.24}$$

In OPV (with EPV), eq(2.24) represents a change in molecular concentration, C, in the sample solution as a function of volume, $\hat{m}$, of injection, taking place immediately before the injection is effectuated at the inlet, $s=0$, of the column. It is assumed that the solvent of the sample solution is identical with the carrier liquid, and B° appearing in eq (2.24) represents the potential molecular partition in the liquid phase which would take place provided that the injection of the sample solution has been achieved. Immediately after the completion of the injection, the initial MB(o) or MB(c) is formed. This means that eq(2.24) represents in another way the fact that the initial MB(o) and MB(c) are represented by eqs(2.15) and (2.17), respectively. [*Note 1.* Volume of injection, in itself, should be represented by ξ (or Z) rather than by $\hat{m}$ (or V); cf. the argument with respect to the first definition of $\hat{m}$ performed in Section(B). $\hat{m}$, however, can now be interpreted to represent the volume of the solvent of the sample solution that has just passed the rear border of the initial MB(o) which keeps in contact with the inlet of the column; this is identical with the volume, ξ, of the solvent that has just passed the inlet of the column at the moment when the initial MB(o) is completed. In eq(2.24), $\hat{m}$ and ξ can be replaced by one another. In fact, eq(2.7) shows that $\hat{m}=\xi$ when s tends to infinitesimal. *Note 2.* In eq(2.23), both $\hat{m}$ and C are quantities with respect to the liquid phase, and eq(2.23) shows that a flux with density, C, in the liquid phase takes place in the liquid phase. The mirror image of chromatogram migrating along s [flat trapezoid in the left part of Fig 2.6(c)] will not arize directly from a simple continuity equation since s is a quantity with respect to the solid phase whereas C is concerned with the liquid phase.]

Let us call the point of view in which abstract flux[eq(2.20) or (2.23)] makes appearance as *complementary point of view induced from ordinary point of view*[CPV(OPV)]. The nomenclature symbolizes the fact that the concept of abstract flux (taking place along $\hat{m}$; CPV) is originating from the measurement of molecular density C in the liquid phase of MB(o) (with total density Ω) performed at fixed position s on the column (OPV) [see Section(D)]. Eq(2.20) as CGM1st can be re-interpreted, however, to represent molecular distribution C as a function of elution volume $\hat{m}$ obtained by using a column with length s (EPV), or molecular distribution C as a function of time $\hat{m}$ obtained at a given position

s on the hypothetical column with infinite length (TPV). Let us call the point of view in which the re-interpretation of CGM1st[eq(2.20)] is done as *ordinary point of view which is re-induced from complementary point of view induced from ordinary point of view* [OPV{CPV(OPV)}].

If a series of monitoring experiments of molecular density χ [Section(D)] are carried out while changing position, $\hat{m}$, of probe M' to increase $\hat{m}$, then χGM1st [flat trapezoid in the left part of Fig 2.7(c) or (c')] will migrate in the positive s direction. It is possible to consider a *complementary abstract flux* of molecules [with density χ and rate, $B^\circ/(1-B^\circ)$, of migration] represented by eq(2.22); this migrates along *distance* s with a lapse of *time* $\hat{m}$ without changing the shape. It is easy to find out that eq(2.22) is a solution to the conservation or continuity equation:

$$\mathrm{div}_s \left(\frac{B^\circ}{1-B^\circ} \chi \right) + \frac{\partial \chi}{\partial \hat{m}} = 0 \qquad (2.25)$$

obtained under initial condition:

$$\lim_{\hat{m} \to 0} \chi = (1-B^\circ) F[(1-B^\circ)s] \qquad (2.26)$$

where it should be noted that both s and χ are quantities with respect to the solid phase, and that s in eq(2.26) can be replaced by ξ. Eq(2.26) represents in another way the fact that the initial MB(o) and MB(c) are represented by eqs(2.15) and (2.17), respectively. Due to both eqs(2.2) and (2.4), eq(2.25) is identical with eq(2.23).

Let us call the point of view in which complementary abstract flux[eq(2.22) or (2.25)] makes appearance as *ordinary point of view induced from complementary point of view* [OPV(CPV)]. Eq(2.22) as χGM1st can be re-interpreted to represent molecular distribution χ as a function of time s obtained at a given position $\hat{m}$ on the carrier liquid. Let us call the point of view in which the re-interpretation of χGM1st[eq(2.22)] is done as *complementary point of view which is re-induced from ordinary point of view induced from complementary point of view*[CPV{OPV(CPV)}].

With reference to eqs(2.2) and (2.4), both eqs(2.23) and (2.25) can be re-expressed as

$$(\partial s/\partial \hat{m})_\Omega = -(\partial \Omega/\partial \hat{m})_s/(\partial \Omega/\partial s)_{\hat{m}} = B^\circ/(1-B^\circ) \qquad (2.27)$$

Molecular density Ω in any slice of MB(o) and MB(c) is constant when its shape is constant. Eq(2.27) therefore leads to

$$ds/d\hat{m} = B^\circ/(1-B^\circ) \qquad (2.28)$$

giving trajectory T_0[eq(2.8)] and T[eq(2.11)] as solutions obtained under initial conditions given by $\hat{m}=s=0$ and, by $\hat{m}=\hat{m}_0$ and $s=s_0$, respectively.

(F) Expression in Terms of Proper Time ξ : Chromatogram as Second Concept and Complementary Chromatogram as Second Concept versus Molecular Band as Flux

In contrast to time s[CPV(OPV); see eq(2.23)] or time $\hat{m}$[OPV(CPV); see eq(2.25)], ξ [Figs 2.6(c) and 2.7(c')] can be interpreted to represent time of another type. Let us call ξ as *proper time*. Time s and proper time ξ, and time $\hat{m}$ and proper time ξ are related to one another by eq(2.9) as

$$s = B^{\circ}\xi \tag{2.29}$$

and

$$\hat{m} = (1-B^{\circ})\xi \tag{2.30}$$

respectively.

In another interpretation, eqs(2.29) and (2.30) represent trajectory T_0 mapped to (ξ, s) and (ξ,$\hat{m}$) planes, respectively. [Eq(2.9) represents trajectory T_0 drawn on the ($\hat{m}$,s) plane, that mapped to the (ξ,s) plane, and that mapped to the (ξ,$\hat{m}$) plane at the same time. Eq(2.12) represents trajectory T drawn on the ($\hat{m}$,s) plane, that mapped to the (ξ, s) plane, and that mapped to the (ξ,$\hat{m}$) plane at the same time.] On the ($\hat{m}$,s) plane where trajectory T_0 or T is drawn, $\hat{m}$ and s represent time and distance, respectively [OPV(CPV)], or s and $\hat{m}$ represent time and distance, respectively[CPV(OPV)]. In contrast, on (ξ,s) and (ξ,$\hat{m}$) planes where trajectory T_0 or T is mapped, ξ represents proper time, and s and $\hat{m}$ represent distance in OPV and CPV, respectively.

Let us denote by ($\bar{\xi}$, $\bar{s}$) and ($\bar{\xi}$,$\bar{\hat{m}}$) the coordinates of point $\bar{P}$ (drawing trajectory T_0 or T) mapped to (ξ,s) and (ξ,$\hat{m}$) planes, respectively. Gradient G mapped to (ξ,s) and (ξ,$\hat{m}$) planes can be represented by using eq(2.10) or (2.14) into which ξ is substituted for $\hat{m}+s$ and $\bar{\xi}$ for $\bar{\hat{m}}+\bar{s}$ as

$$\xi \ (= \bar{\xi}) = \bar{s}/B^{\circ} \quad \text{or} \quad (\bar{s}-s_0)/B^{\circ} \tag{2.31}$$

(OPV) and

$$\xi \ (= \bar{\xi}) = \bar{\hat{m}}/(1-B^{\circ}) \quad \text{or} \quad (\bar{\hat{m}}-\hat{m}_0)/(1-B^{\circ}) \tag{2.32}$$

(CPV), respectively.

Fig 2.8(a) illustrates both trajectory T_0 and gradient G drawn on the ($\hat{m}$,s) plane, and Figs 2.8(b) and (c) illustrate those mapped to (ξ,s) and (ξ,$\hat{m}$) planes, respectively.

Executing the coordinate transformation: ($\hat{m}$,s)→(ξ,s) [i.e., by using Appendix I eq (A1.1) in which $u=\hat{m}$, $v=s$, $x(u,v)=\xi(\hat{m},s)\equiv\hat{m}+s$[eq(2.7)], $y(u,v)=s$ and $z=\Omega$] and with reference to eq(2.2), eq(2.23) can be transformed to

$$\mathrm{div}_s\,(B^{\circ}\Omega) + \partial\Omega/\partial\xi = 0 \tag{2.33}$$

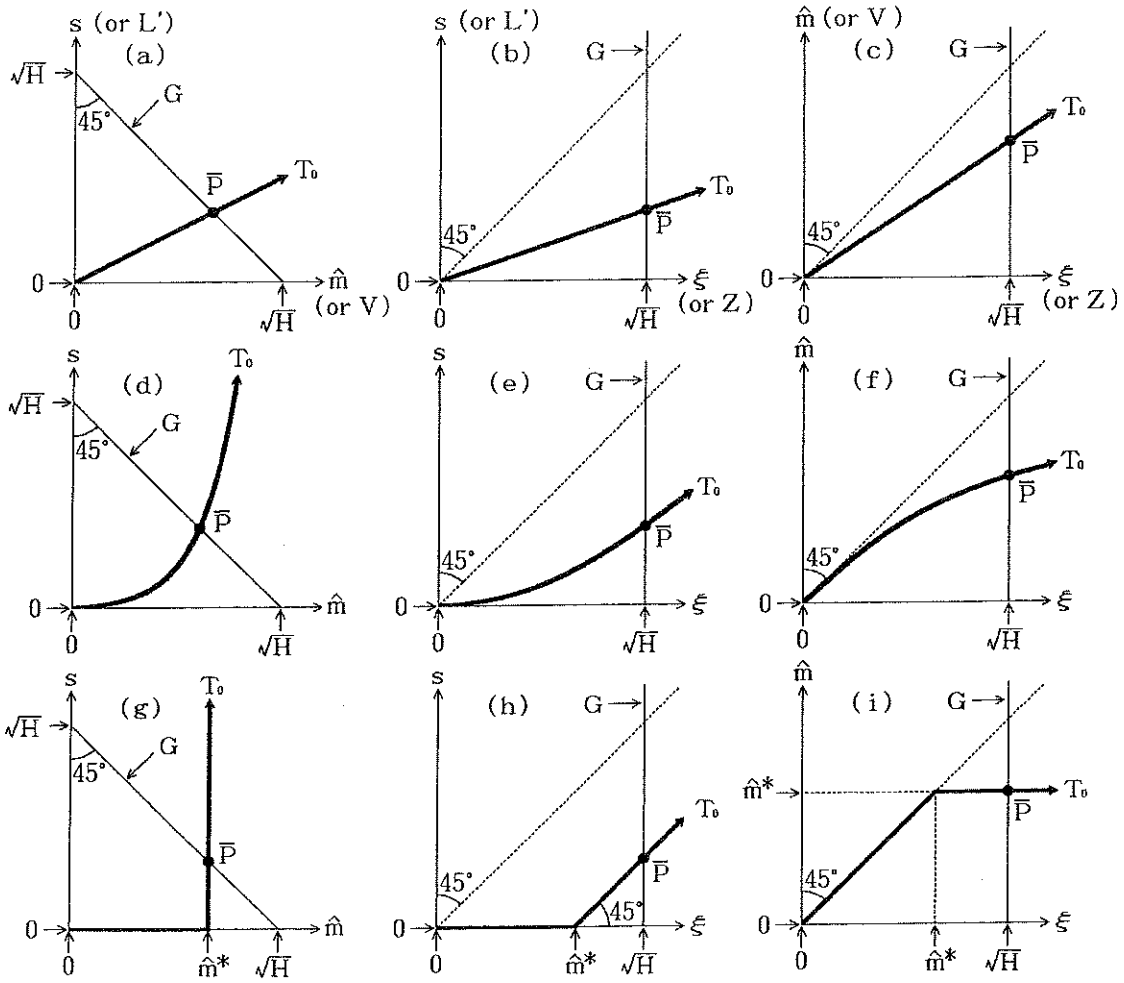


Fig 2.8. Both gradient G and trajectory T_0 drawn on ($\hat{m}$,s) [(a), (d) and (g)], (ξ,s) [(b), (e) and (h)], and (ξ,$\hat{m}$) [(c), (f) and (i)] planes. Part(a), (b) and (c), part(d), (e) and (f), and part(g), (h) and (i) correspond to Figs 3.2(a), (b) and (c), respectively. The tangent slope of trajectory T_0 on the ($\hat{m}$,s) plane is comprised between tan 0° (=0) and tan 90° (=∞), whereas that on either (ξ,s) or (ξ,$\hat{m}$) plane is comprised between tan 0° (=0) and tan 45° (=1).

On the other hand, executing the coordinate transformation: $(\hat{m},s)\rightarrow(\xi,\hat{m})$ [i.e., by using Appendix I eq(A1.1) in which $x(u,v)=\hat{m}$ and $y(u,v)=\xi(\hat{m},s)\equiv\hat{m}+s$ instead] and with reference to eq(2.2), eq(2.23) can be transformed to

$$\mathrm{div}_{\hat{m}}\,[(1-B^{\circ})\Omega]+\partial\Omega/\partial\xi=0 \tag{2.34}$$

Similarly but with reference to eq(2.4) instead of eq(2.2), eq(2.25) can also be transformed to both eqs(2.33) and (2.34). Eqs(2.33) and (2.34) represent MB(o) (OPV) and MB(c) (CPV) as fluxes of molecules with density Ω and rates, B° and $1-B^{\circ}$, of migration, respectively. In fact, under initial conditions given (when $\xi\rightarrow 0$) by eqs(2.15) and (2.17), eqs(2.33) and (2.34) have solutions given by eqs(2.16) and (2.18), respectively.

Eqs(2.33) and (2.34) can be re-expressed as

$$(\partial s/\partial\xi)_{\Omega}=-(\partial\Omega/\partial\xi)_{s}/(\partial\Omega/\partial s)_{\xi}=B^{\circ} \tag{2.33'}$$

and

$$(\partial\hat{m}/\partial\xi)_{\Omega}=-(\partial\Omega/\partial\xi)_{\hat{m}}/(\partial\Omega/\partial\hat{m})_{\xi}=1-B^{\circ} \tag{2.34'}$$

respectively. Eq(2.33') leads to

$$ds/d\xi=B^{\circ} \tag{2.35}$$

Under initial conditions given by $(\xi,s)=(0,0)$ and $(\xi,s)=(0,s_{o})$, eq(2.35) gives trajectory T_{0} [eq(2.29) or the equality between first and last terms in eq(2.9)] and trajectory T [the equality between first and last terms in eq(2.12)] mapped to the (ξ,s) plane, respectively. Similarly, eq(2.34') leads to

$$d\hat{m}/d\xi=1-B^{\circ} \tag{2.36}$$

Under initial conditions given by $(\xi,\hat{m})=(0,0)$ and $(\xi,\hat{m})=(0,\hat{m}_{o})$, eq(2.36) gives trajectory T_{0} [eq(2.30) or the equality between first and third terms in eq(2.9)] and trajectory T [the equality between first and third terms in eq(2.12)] mapped to the $(\xi,\hat{m})$ plane, respectively.

By combining eq(2.16) [solution of eq(2.33)] with eq(2.2)

$$C=B^{\circ}F[-B^{\circ}(\xi-s/B^{\circ})] \tag{2.37}$$

can be derived; this can be interpreted to represent molecular distribution C as a function of proper elution volume ξ obtained by using a column with length s (OPV, EPV) or molecular distribution C as a function of proper time ξ obtained at a given position s on the hypothetical column with infinite length (OPV, TPV). Let us call the molecular distribution given by eq(2.37) with the interpretation above as *chromatogram as second concept* (abbreviated as CGM2nd). Eq(2.37) can also be derived by substituting $\xi-s$ for $\hat{m}$ into eq(2.20), and, to the contrary, eq(2.20) can be derived by substituting $\hat{m}+s$ for ξ into eq(2.37). It is a natural conclusion that CGM2nd [concept in OPV; eq(2.37)] and

CGM1st as re-interpreted in OPV[CPV(OPV)] [eq(2.20)] are mutually derivable by shifting the origin of the time or proper time axis by a duration of time or proper time corresponding to the dead volume i.e., the interstitial volume of the column inserted between the initial position of MB(o) (coulmn inlet) and the position of measurement (column outlet). When s tends to infinitesimal, then eq(2.37) coincides with eq(2.24) into which ξ is substituted for $\hat{m}$. In eq(2.24), $\hat{m}$ can, in general, be replaced by ξ.

By combining eq(2.18) [solution of eq(2.34)] with eq(2.4)

$$\chi = (1-B^{\circ})F[(1-B^{\circ})(\xi - \frac{\hat{m}}{1-B^{\circ}})] \tag{2.38}$$

can be derived; this can be interpreted to represent molecular distribution χ as a function of proper time ξ obtained at a given position $\hat{m}$ on the carrier liquid (CPV). Let us call the molecular distribution given by eq(2.38) with the interpretation above as *complementary chromatogram as second concept* (abbreviated as χGM2nd). Eq(2.38) can also be derived by substituting $\xi - \hat{m}$ for s into eq(2.22), and, to the contrary, eq(2.22) can be derived by substituting $\hat{m}+s$ for ξ into eq(2.38). χGM2nd [concept in CPV; eq(2.38)] and χGM1st as re-interpreted in CPV[OPV(CPV)] [eq(2.22)] are mutually derivable by shifting the origin of the time or proper time axis by a duration of time or proper time corresponding to the volume of the carrier liquid inserted between the initial position of MB(c) and the position of measurement on the carrier liquid. When $\hat{m}$ tends to infinitesimal, then eq(2.38) coincides with eq(2.26) into which ξ is substituted for s. In eq(2.26), s can, in general, be replaced by ξ.

Fig 2.9 summarizes the relationships among the equations representing CGM1st, CGM2nd, χGM1st, χGM2nd, MB(o) and MB(c). The pictures reflected in OPV, CPV (OPV) and OPV[CPV(OPV)] are symmetric with those reflected in CPV, OPV(CPV) and CPV[OPV(CPV)], respectively, except for the fact that the initial molecular distribution takes place over positive coordinate values in OPV and negative coordinate values in CPV (OPV), whereas it takes place over negative coordinatre values in CPV and positive coordinate values in OPV(CPV). With gradient chromatography, another asymmetry will be added [see the subsequent Chapter Ⅲ(H)].

(G) Rewriting in Terms of Time η, Proper Time ξ, and Distance ζ

Denoting time, proper time and distance by η, ξ and ζ, respectively, it is possible to write

$$\left.\begin{aligned}(\eta,\zeta) &= (\hat{m},s) \quad [\text{in OPV(CPV)}]\\ (\eta,\zeta) &= (s,\hat{m}) \quad [\text{in CPV(OPV)}]\end{aligned}\right\} \tag{2.39}$$

and

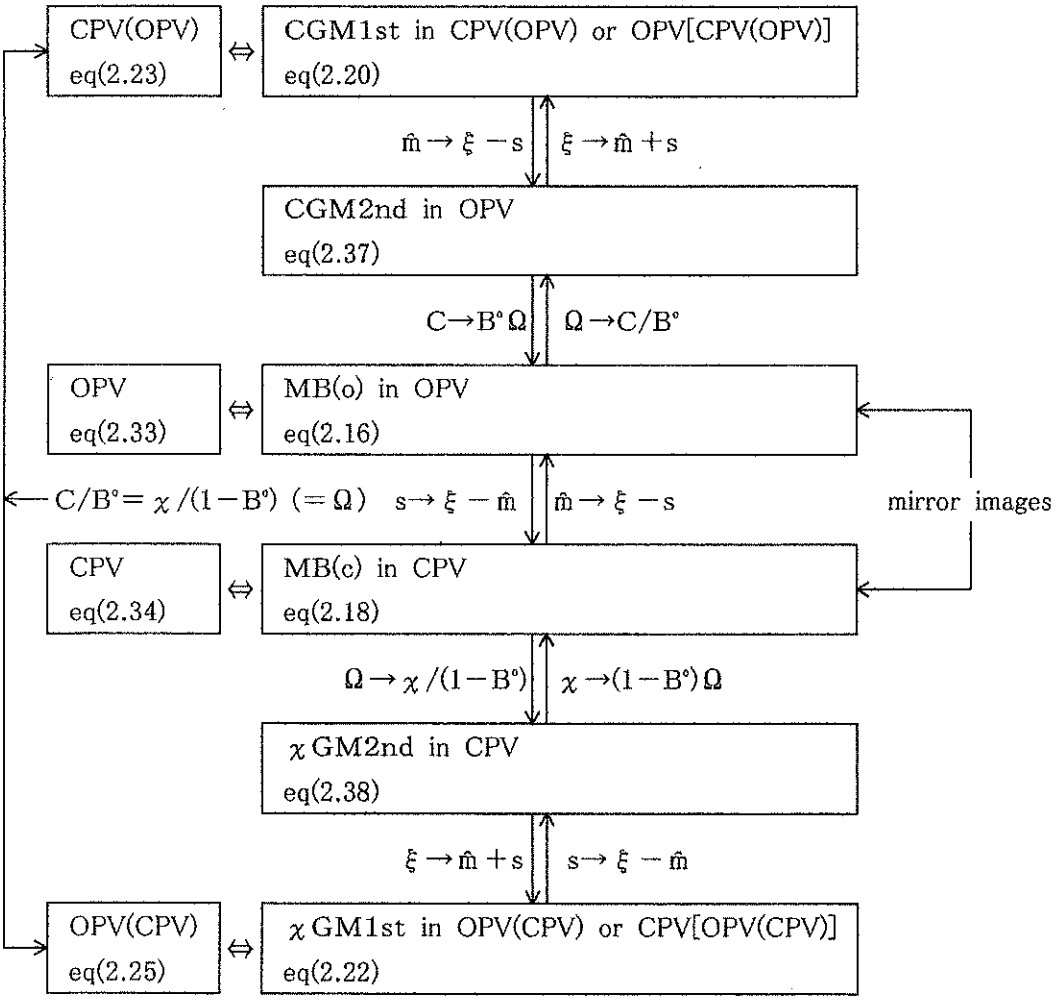


Fig 2.9. Relationships among the equations representing CGM1st, CGM2nd, χGM1st, χGM2nd, MB(o) and MB(c) with isocratic chromatography.

$$\xi = \eta + \zeta \tag{2.40}$$

which corresponds to eq(2.7), and to introduce the symbols $\bar{\eta}$, $\bar{\zeta}$, $\bar{\xi}$, η_0 and ζ_0 fulfilling

$$\left.\begin{aligned}(\bar{\eta},\bar{\zeta}) &= (\bar{\hat{m}},\bar{s}) \quad [\text{in OPV(CPV)}]\\ (\bar{\eta},\bar{\zeta}) &= (\bar{s},\bar{\hat{m}}) \quad [\text{in CPV(OPV)}]\end{aligned}\right\} \tag{2.41}$$

$$\bar{\xi} = \bar{\eta} + \bar{\zeta} \tag{2.42}$$

$$\left.\begin{aligned}(\eta_0,\zeta_0) &= (\hat{m}_0,s_0) \quad [\text{in OPV(CPV)}]\\ (\eta_0,\zeta_0) &= (s_0,\hat{m}_0) \quad [\text{in CPV(OPV)}]\end{aligned}\right\} \tag{2.43}$$

and

$$\eta_0 + \zeta_0 = 0 \tag{2.44}$$

which corresponds to eq(2.13). Further, let us introduce the following symbols:

$$\left.\begin{aligned}v^\circ &= B^\circ \quad [\text{when } (\eta,\zeta) = (\hat{m},s)]\\ v^\circ &= 1-B^\circ \quad [\text{when } (\eta,\zeta) = (s,\hat{m})]\end{aligned}\right\} \tag{2.45}$$

$$\left.\begin{aligned}\Lambda &= \chi \quad [\text{when } (\eta,\zeta) = (\hat{m},s)]\\ \Lambda &= C \quad [\text{when } (\eta,\zeta) = (s,\hat{m})]\end{aligned}\right\} \tag{2.46}$$

and

$$\left.\begin{aligned}f(X) &= F(X) \quad [\text{when } (\eta,\zeta) = (\hat{m},s)]\\ f(X) &= F(-X) \quad [\text{when } (\eta,\zeta) = (s,\hat{m})]\end{aligned}\right\} \tag{2.47}$$

Eq(2.28) and both eqs(2.35) and (2.36), representing trajectory T_0 or T, can be rewritten as

$$d\zeta/d\eta = v^\circ/(1-v^\circ) \tag{2.48}$$

and

$$d\zeta/d\xi = v^\circ \tag{2.49}$$

respectively.

Eq(2.8), eq(2.9) and both eqs(2.29) and (2.30), all representing trajectory T_0, can be rewritten as

$$\zeta = \frac{v^\circ}{1-v^\circ}\eta \tag{2.50}$$

$$\xi = \eta + \zeta = \zeta/v^\circ \tag{2.51}$$

and

$$\zeta = v^{\circ}\xi \tag{2.52}$$

respectively. As v° is comprised between 0 and 1, then $v^{\circ}/(1-v^{\circ})$ is comprised between 0 and ∞.

Eqs(2.11) and (2.12), both representing trajectory T, can be rewritten as

$$\zeta - \zeta_{\circ} = \frac{v^{\circ}}{1-v^{\circ}}(\eta - \eta_{\circ}) \tag{2.53}$$

and

$$\xi = \eta + \zeta = (\zeta - \zeta_{\circ})/v^{\circ} \tag{2.54}$$

respectively.

Eq(2.10), eq(2.14) and both eqs(2.31) and (2.32), all representing gradient G, can be rewritten as

$$\eta + \zeta \ (= \bar{\eta} + \bar{\zeta}) = \bar{\eta}/(1-v^{\circ}) = \bar{\zeta}/v^{\circ} \tag{2.55}$$

$$\eta + \zeta \ (= \bar{\eta} + \bar{\zeta}) = (\bar{\eta} - \eta_{\circ})/(1-v^{\circ}) = (\bar{\zeta} - \zeta_{\circ})/v^{\circ} \tag{2.56}$$

and

$$\xi \ (= \bar{\xi}) = \bar{\zeta}/v^{\circ} \quad \text{or} \quad (\bar{\zeta} - \zeta_{\circ})/v^{\circ} \tag{2.57}$$

respectively.

Both eqs(2.2) and (2.4) can be rewritten as

$$\Lambda = (1-v^{\circ})\Omega \tag{2.58}$$

Both eqs(2.19) and (2.21) as

$$\Delta_{\Lambda} = \Delta_{\Omega}/(1-v^{\circ}) \tag{2.59}$$

Both eqs(2.29) and (2.30), as interpreted to represent the relationship between time η and proper time ξ, as

$$\eta = (1-v^{\circ})\xi \tag{2.60}$$

Both eqs(2.23) and (2.25) can be rewritten as

$$\mathrm{div}_{\zeta}\left(\frac{v^{\circ}}{1-v^{\circ}}\Lambda\right) + \frac{\partial \Lambda}{\partial \eta} = 0 \tag{2.61}$$

Both eqs(2.24) and (2.26) as

$$\lim_{\eta \to 0} \Lambda = (1-v^{\circ})f[(1-v^{\circ})\zeta] \tag{2.62}$$

Both eqs(2.20) and (2.22) as

$$\Lambda = (1-v^\circ)f[(1-v^\circ)(\zeta - \frac{v^\circ}{1-v^\circ}\eta)] \quad (2.63)$$

Eq(2.27) as

$$(\partial \zeta / \partial \eta)_\Omega = v^\circ/(1-v^\circ) \quad (2.61')$$

Both eqs(2.33) and (2.34) can be rewritten as

$$\mathrm{div}_c\ (v^\circ \Omega) + \partial \Omega / \partial \xi = 0 \quad (2.64)$$

Both eqs(2.15) and (2.17) as

$$\lim_{\eta \to 0} \Omega = f(\zeta) \quad (2.65)$$

Both eqs(2.16) and (2.18) as

$$\Omega = f(\zeta - v^\circ \xi) \quad (2.66)$$

Both eqs(2.33') and (2.34') as

$$(\partial \zeta / \partial \xi)_\Omega = v^\circ \quad (2.64')$$

Both eqs(2.37) and (2.38) can be rewritten as

$$\Lambda = (1-v^\circ)f[(1-v^\circ)(\xi - \frac{\eta}{1-v^\circ})] \quad (2.67)$$

Exceptionally in eq(2.67), η represents distance i.e., either the distance from origin O on the column (when $\eta = s$ and $v^\circ = 1-B^\circ$; OPV) or the distance from origin O on the carrier liquid (when $\eta = \hat{m}$ and $v^\circ = B^\circ$; CPV). By substituting ζ for η, $1-v^\circ$ for v°, and $f(-X)$ for $f(X)$, eq(2.67) can be rewritten as

$$\Lambda = v^\circ f(\zeta - v^\circ \xi) \quad (2.67')$$

The informations given by eqs(2.58)-(2.60) are involved in the pair of eqs(2.63) and (2.66). In fact, in eq(2.63) or (2.66), the width of distribution Λ or Ω can be determined by the reciprocal of the constant ($1-v^\circ$ or unity) preceding variable ζ in function f; this leads to eq(2.59). Both eqs(2.63) and (2.66) also lead to eq(2.58) taking place, conjugate to eq(2.59). The position of distribution Λ or Ω can be determined by the factor $v^\circ \eta /(1-v^\circ)$ or $v^\circ \xi$ subtracted from variable ζ in function f. The fact that the molecular distribution in the abstract flux (with density Λ) is located at the same position as that of MB(c) or MB(o) (with density Ω) leads to $v^\circ \eta /(1-v^\circ) = v^\circ \xi$ or eq(2.60); we call both abstract flux and complementary abstract flux as abstract flux when variables η, ζ and ξ are used. Let us call as *contraction of time* the fact that time η is shorter than proper time ξ [eq(2.60)] and as *chromatographic dilatation* the fact that width Δ_Λ of the molecular distribution in the abstract flux is larger than width Δ_Ω of MB [eq(2.59)]. Con-

traction of time and chromatographic dilatation take place, conjugate to one another.

Important Consideration. In Fig 2.10(a)-(c), the behaviors of three abstract fluxes[eq (2.63)] taken at the same proper time ξ are compared. These are characterized by parameters v° with values of 0, 1/3 and 2/3, or by rates, $v^\circ/(1-v^\circ)$, of migration equal to 0[Fig 2.10(a)], 1/2[Fig 2.10(b)] and 2[Fig 2.10(c)] taking place along the distance axis ζ with a lapse of time η, respectively. Each abstract flux involves two subtypes, the one defined when $(\eta, \zeta)=(\hat{m}, s)$ with $v^\circ=B^\circ$ and $\Lambda=\chi$ [solid trapezoids drawn in the extreme-left parts of Figs 2.10(a)-(c)] and the other defined when $(\eta, \zeta)=(s, \hat{m})$ with $v^\circ=1-B^\circ$ and $\Lambda=C$ [mirror-imaged solid trapezoids drawn in the middle-left parts of Figs 2.10(a)-(c); see eqs(2.45)-(2.47)]. The dotted trapezoids drawn in extreme- and middle-left parts of Figs 2.10(b) and (c) represent the corresponding MB(o) and MB(c) [eq(2.66)], respectively; these are superposed on the solid trapezoids staying always at the initial positions in Fig 2.10(a). On the (η, ζ) plane, the two subtypes of abstract flux draw the same trajectory T_0 intersecting the η axis at an angle of $\tan^{-1}[v^\circ/(1-v^\circ)]$ [right parts of Figs 2.10(a)-(c)]; trajectory T_0 is superposed on the η axis in Fig 2.10(a). [See eq(2.50) or (2.51) representing trajectory T_0, and eq(2.55) representing gradient G in which $(\bar{\eta}, \bar{\zeta})$ stands for the coordinate of point $\bar{P}$ plotted in Fig 2.10.]

The events drawn in the extreme-left parts of Figs 2.10(b) and (c) are identical with those drawn in the middle-left parts of Figs 2.10(c) and (b), respectively. The event drawn in both extreme-left part of Fig 2.10(b) and middle-left part of Fig 2.10(c) is identical with that drawn as solid trapezoids in both left and lower parts of Fig 2.4. The rate, $v^\circ/(1-v^\circ)$, of migration of the event represented as tangent of the intersection angle of trajectory T_0 with the η axis increases following the order of Figs 2.10(a)-(c). This is conjugate to a decrease in time η at point $\bar{P}$ [contraction of time; eq(2.60)] and an increase in width Δ_Λ of the molecular distribution in the abstract flux [chromatographic dilatation; eq(2.59)].

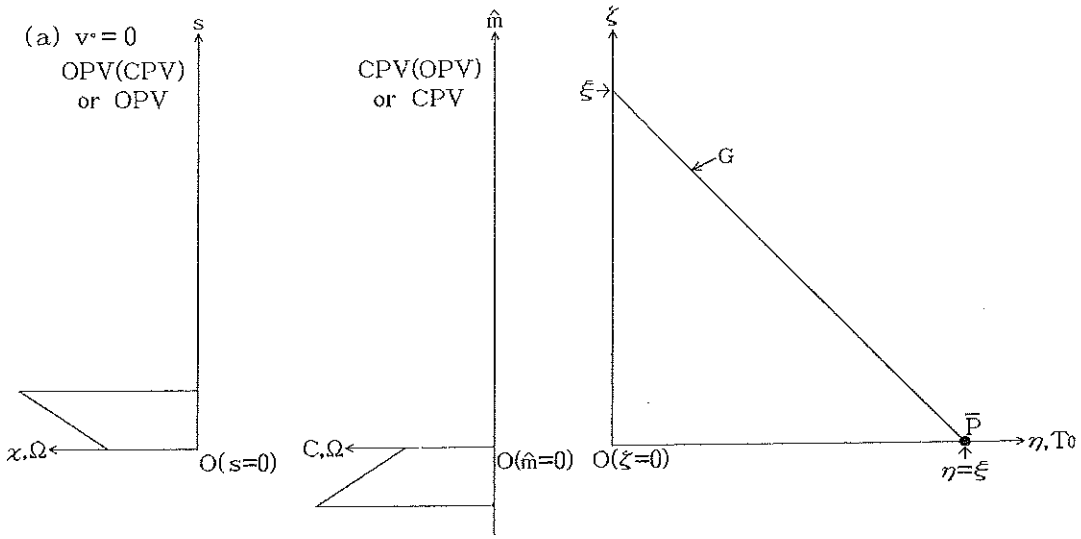


Fig 2.10. The behaviors of three abstract fluxes taken at the same proper time ξ. These are characterized by (a) $v^{\circ}=0$ or $v^{\circ}/(1-v^{\circ})=0$, (b) $v^{\circ}=1/3$ or $v^{\circ}/(1-v^{\circ})=1/2$, and (c) $v^{\circ}=2/3$ or $v^{\circ}/(1-v^{\circ})=2$.

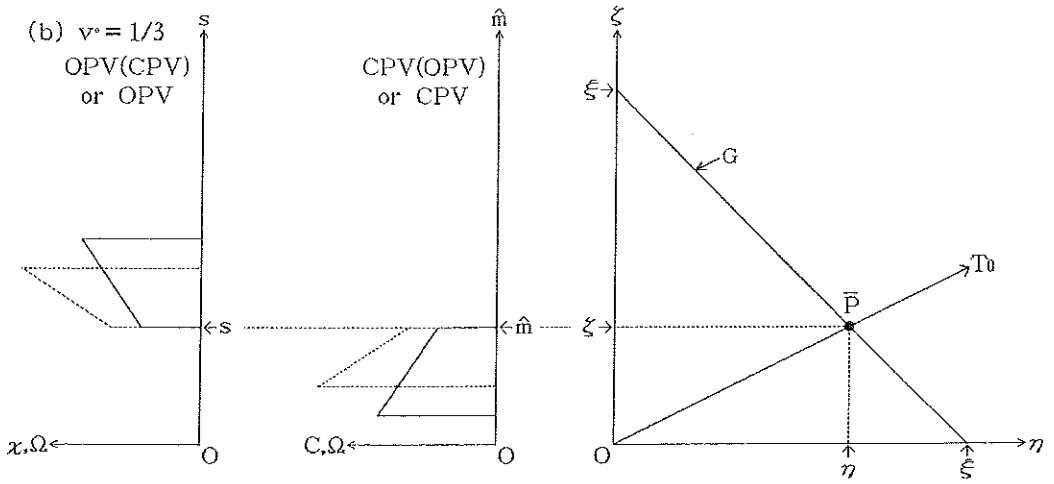


Fig 2.10. (b)

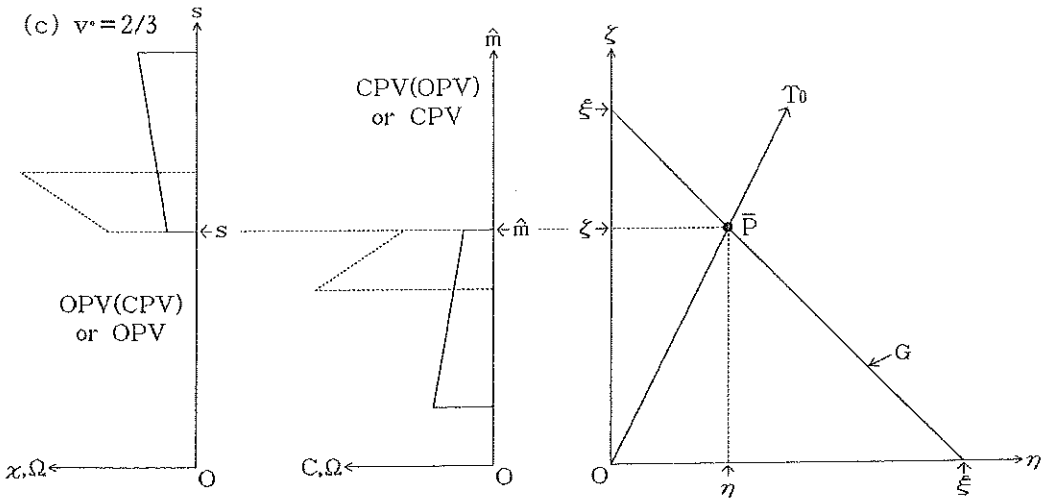


Fig 2.10. (c)

Chapter III. Ideal Gradient Chromatography in the Absence of Axial Diffusion in the Column

(A) Gradient in the Liquid Phase and Gradient in the Solid Phase

Usually with gradient chromatography, the migration of MB(o) along the s axis accelerates(OPV) and the migration of MB(c) along the $\hat{m}$ axis decelerates(CPV). Fig 3.1 illustrates both gradient G and trajectory T_0, where it is possible to consider that gradient G migrates in either $\hat{m}$ or s direction at a constant rate equal to g' times the flow-rate. Point $\bar{P}$ corresponding to both the rear border of MB(o) and the front border of MB(c) moves on the ($\hat{m}$,s) plane while staying on gradient G and keeping the sum of migration rates in $\hat{m}$ and s directions equal to g' times the flow-rate; this draws trajectory T_0 which is concave in shape (see Fig 3.1).

The Case of Gradient in the Liquid Phase. Let us first consider the case when the acceleration of the migration of MB(o) or the deceleration of the migration of MB(c) is achieved by using the gradient in the liquid phase or the concentration gradient [see Chapter I (A)]. We assume that, at the moment when the injection of sample solution is completed at the inlet of the column or when the formation of the initial MB(o) is completed with its rear border keeping in contact with the column inlet (EPV), then the column is immediately supplied with the carrier liquid continuously at its inlet while increasing concentration, m, of gradient substance [see Chapter I (A)] linearly or nonlinearly with increase in volume Z of supply. A concentration gradient with linear or nonlinear shape is then formed between inlet and outlet of the column (with concentration decreasing from inlet to outlet), and it migrates on the column at a rate almost (see below) equal to the flow-rate. The concentration gradient passes MB(o) because the rate of migration of MB(o), in general, is lower than that of the carrier liquid or the concentration gradient. Concentration m over which MB(o) is present increases with migration of MB(o), thus bringing about the acceleration of the migration. m under consideration can also be considered to increase linearly or nonlinearly with increase in volume, V, of the carrier liquid passing the rear border of MB(o).

Let us consider a series of experiments carried out by applying concentration gradients with similar shapes, each represented as a monotonically increasing function of V as $m = \phi(g'_{(i)}V)$ in which $g'_{(i)}$ is a positive constant measuring the mean slope or steepness of the concentration gradient applied in the i th experiment of the series. For each experiment, a hypothetical mean linear gradient represented as $\hat{m} = g'_{(i)}V$ is conceivable. If ϕ is a linear function represented as $\phi(g'_{(i)}V) = g'_{(i)}V$, then the concentration gradient applied is linear, coinciding with the hypothetical mean gradient (m coincides with $\hat{m}$). In the absence of concentration gradient, $\phi(g'_{(i)}V)$ is constant. Still the corresponding mean gradient, $\hat{m} = g'_{(i)}V$, is conceivable; this is because the absence of the concentration gradient is equivalent to the situation where the ability of gradient substance to suppress the adsorption of sample molecule is homogenized in the column, independent of the concen-

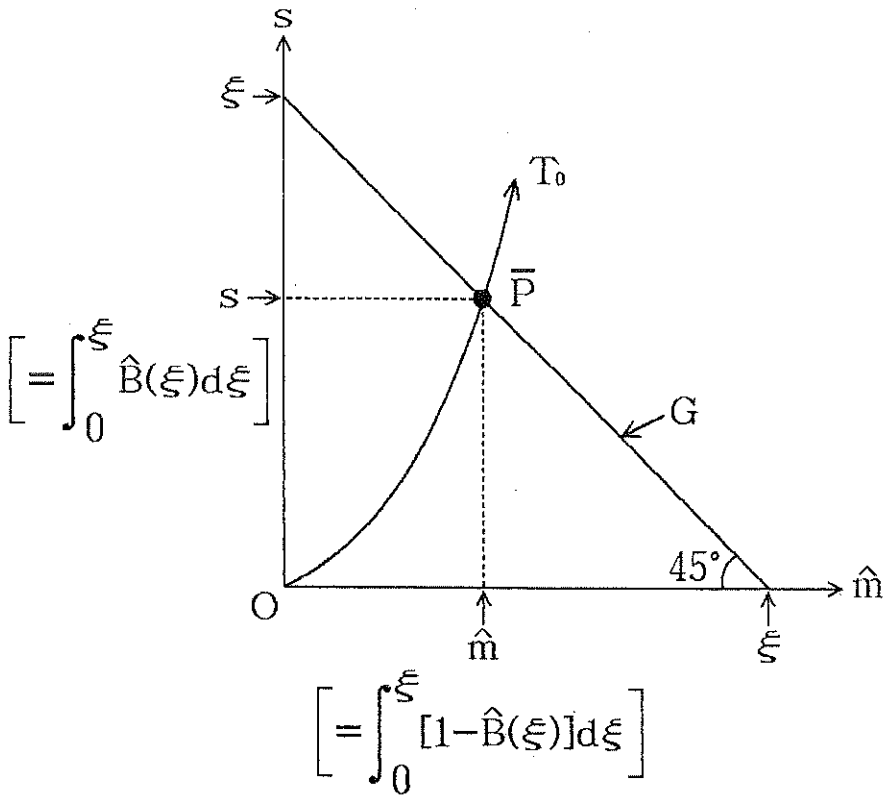


Fig 3.1. Gradient G and trajectory T_0.

tration of gradient substance. Omitting the suffix i and writing

$$m = \phi(\hat{m}) = \phi(g'V) \tag{3.1}$$

it is possible to consider that the hypothetical mean gradient is equivalent to the marker gradient[eq(2.6)]. Arguing in the other direction, it is possible to define g' previously as a mean slope of the concentration gradient. With the isocratic case, the definition dissolves. In order to maintain it, it is necessary to replace the definition by the definition as slope of the marker gradient. [In the argument above, it is considered that the initial concentration, m_{in}, of the concentration gradient is zero. If $m_{in} > 0$, the argument holds by replacing m by $m - m_{in}$.]

If gradient G drawn on the $(\hat{m},s)$ plane(Fig 3.1) is mapped to the $(L',\hat{m})$ plane, it will coincide with the mean concentration gradient or the concentration gradient itself for the linear case. To the contrary, if the mean concentration gradient or the concentration gradient with a linear shape formed on the $(L',\hat{m})$ plane is mapped to the $(\hat{m},s)$ plane, it will coincide with gradient G. [Cf. Fig 2.3(a).]

It often happens that gradient substance is partially adsorbed on the solid phase. The perturbation of the concentration gradient taking place induced by the adsorption (called solvent demixing) was argued classically by Drake and recently by Velayudhan and Ladisch [see Appendix XI(B)]. There is usually an upper limit of the amount of gradient substances that can be adsorbed per unit area of the adsorbent surface, however. Except just at the beginning of the gradient, concentration, m, in solution of gradient substances is high enough for the majority of substances to be in solution or in the liquid phase, and the demixing effect is negligible. The perturbation of the concentration gradient induced by adsorption and desorption of sample molecules is also negligible except at the beginning of the gradient because the total amount of sample molecules in the slice of the column usually is much smaller than that of gradient substances. Moreover, when considering the actual chromatography taking place in the presence of axial diffusion in the column, axial diffusion of gradient substances is negligible except for step gradient; this is because diffusion is canceled out between neighboring slices of the column. The concentration gradient therefore is very stable, and it migrates on the column without changing its shape at a rate equal to the flow-rate (except just at its beginning).

The fact that adsorption and desorption of sample molecules do not perturb the concentration gradient can be confirmed experimentally by monitoring the concentration gradient by the measurement of refractive index or electroconductivity of the solution passing the flow-cell set at the outlet of the column; this can be done simultaneously with the monitoring of density, C, of sample molecules [cf. Chapter II(D)] by the measurement of ultraviolet wave absorption, for instance, of the solution passing another flow-cell also set at the outlet of the column [connected in series to the flow-cell for the monitoring of the concentration gradient by using a fine tube the internal volume of which is negligibly small; cf. Chapter VII(B)]. The fact that concentration, m, in solution of gradient sub-

stance is high enough for the majority of substances to be in solution (except at the beginning of the gradient) can also be confirmed by the monitoring of the concentration gradient. In this instance, both shape and steepness of the gradient curve obtained by the monitoring experiment are identical with those obtained in the absence of the column (cf. Chapter Ⅶ Figs 7.1 and 7.2). The fact that the concentration gradient migrates on the column at a rate equal to the flow-rate (except at its beginning) can be confirmed by comparing retention times of the gradient curves obtained for columns with different total lengths [cf. Chapter Ⅷ(D)].

The Case of Gradient in the Solid Phase. Let us consider the case when the acceleration of the migration of MB(o) or the deceleration of the migration of MB(c) is achieved by using the gradient in the solid phase [see Chapter I (A)]. Instead of m, let us now introduce any parameter ρ corresponding in a one-to-one manner to the affinity of the solid phase for sample molecule. Representing ρ in such a way that it increases with decrease in the affinity, it is possible to consider that ρ is a monotonically increasing function of g'L' or s:

$$\rho = \phi(s) = \phi(g'L') \tag{3.2}$$

In eq(3.2), g' represents the mean slope or steepness of the ρ gradient, and the corresponding hypothetical mean linear gradient with slope g' is conceivable; this is identical with the color gradient expressed by using a certain unit[eq(2.5)]. In the absence of the ρ gradient, $\phi(s)$ or $\phi(g'L')$ is constant. Still the corresponding gradient[eq(2.5)] is conceivable because the absence of the ρ gradient is equivalent to the situation where the ability of the ρ gradient to suppress the adsorption of sample molecule is homogenized in the column, independent of the ρ value. The gradient[eq(2.5)] now simply represents the color gradient with which the column container is stained.

If gradient G drawn on the ($\tilde{m}$,s) plane(Fig 3.1) is mapped to the (V,s) plane, it will coincide with the mean ρ gradient or the ρ gradient itself for the linear case. To the contrary, if the mean ρ gradient or the ρ gradient with a linear shape formed on the (V,s) plane is mapped to the ($\tilde{m}$,s) plane, it will coincide with gradient G. [Cf. Fig 2.3 (b).]

The Case of Both Gradient in the Liquid Phase and Gradient in the Solid Phase. Let us examine the most general case when both the gradient in the liquid phase (i.e., the concentration gradient) and the gradient in the solid phase (i.e., the ρ gradient) are applied at the same time. Let us consider a series of experiments carried out by using both concentration gradients with similar shapes [each represented as a monotonicaly increasing function of V as $m = \phi(g'_{liquid(i)}V)$] and ρ gradients with similar shapes [each represented as a monotonically increasing function of L' as $\rho = \phi(g'_{solid(i)}L')$]. $g'_{liquid(i)}$ and $g'_{solid(i)}$ are positive constants measuring the mean slopes or steepnesses of the gradients formed in liquid and slolid phases in the i th experiment of the series, respectively; the ratio $g'_{liquid(i)}/g'_{solid(i)}$ is constant, independent of i. This ratio can be identified with unity by expressing

either gradient in a certain unit. Omitting the suffix i, the gradients in liquid and solid phases applied in any experiment can be represented by using eqs(3.1) and (3.2), respectively. A common parameter g' is involved in both eqs(3.1) and (3.2).

(B) Unified View of Chromatography

Let us denote by B both relative rate, R_F, of migration and partition, C/Ω, in the liquid phase of sample molecules in the column. B is comprised between 0 and 1 and, to be compatible with the argument developed in Section(A), B is a monotonically increasing function of both m and ρ; we assume that B tends to unity when either m or ρ approaches infinity. On the other hand, m and ρ are monotonically increasing functions of $\hat{m}$ [eq(3.1)] and s[eq(3.2)], respectively, from which it follows that B is a monotonically increasing function of both $\hat{m}$ and s:

$$B\ [=\ \dot{B}(m, \rho)]\ =\ \dot{B}[\phi(\hat{m}), \phi(s)] \tag{3.3}$$

representing a surface present in the $(\hat{m}, s, B)$ space (called a *characteristic surface*). [Eq (3.3) holds even in the absence of sample molecules if B or $\dot{B}$ is defined as potential molecular partition in the liquid phase which would take place provided that molecules are present.]

s and $\hat{m}$ components of the velocity of point $\dot{P}$ of drawing trajectory T_0 or T on the $(\hat{m}, s)$ plane are proportional to $\dot{B}[\phi(\hat{m}), \phi(s)]$ and $1-\dot{B}[\phi(\hat{m}), \phi(s)]$, respectively [see Fig 3.1; cf. both Figs 3.3(a) and (b)]. This means that trajectory T_0:

$$s\ =\ T_0(\hat{m}) \tag{3.4}$$

and trajectory T:

$$s\ =\ T(\hat{m}) \tag{3.5}$$

can be represented as solutions of the differential equation:

$$\frac{ds}{d\hat{m}}\ =\ \frac{\dot{B}[\phi(\hat{m}), \phi(s)]}{1-\dot{B}[\phi(\hat{m}), \phi(s)]} \tag{3.6}$$

obtained under initial conditions given by $\hat{m}=s=0$, and by $\hat{m}=\hat{m}_0$ and $s=s_0$ [where $\hat{m}_0+s_0=0$; eq(2.13)], respectively [cf. eq(2.28)]. As point $\dot{P}$ draws trajectory T_0 or T while staying on gradient G [Fig 3.1; cf. both Figs 3.3(a) and (b)], B associating with point $\dot{P}$ can be regarded as a monotonically increasing function of ξ or $\hat{m}+s$:

$$B\ =\ \hat{B}(\xi)\ =\ \hat{B}(\hat{m}+s) \tag{3.7}$$

and eq(3.6) can be rewritten as

$$\frac{ds}{d\hat{m}}\ =\ \frac{\hat{B}(\hat{m}+s)}{1-\hat{B}(\hat{m}+s)} \tag{3.6'}$$

It is possible to consider that both trajectory T_0 and T [eqs(3.4) and (3.5)] are projections on the ($\hat{m}$,s) plane of curves (called *characteristic curves*) constrained on the characteristic surface[eq(3.3)].

The projections on ($\hat{m}$,B) and (s,B) planes of the characteristic curve corresponding to trajectory T_0 (or T) can be represented as

$$B = B'(\hat{m}) \equiv \hat{B}[\hat{m} + T_0(\hat{m})] \quad [\text{or } \hat{B}[\hat{m} + T(\hat{m})]] \tag{3.8}$$

and

$$B = B''(s) \equiv \hat{B}[T_0^{-1}(s) + s] \quad [\text{or } \hat{B}[T^{-1}(s) + s]] \tag{3.9}$$

respectively. The expressions of trajectory T_0 (or T) in terms of projections $B'(\hat{m})$ and $B''(s)$ can be obtained by substituting $B'(\hat{m})$ and $B''(s)$ for $\hat{B}(\hat{m}+s)$ into eq(3.6') and executing the integration as

$$s \text{ (or } s - s_0) = \int_{0 \text{ (or } \hat{m}_0)}^{\hat{m}} \frac{B'(\hat{m})}{1 - B'(\hat{m})} d\hat{m} \tag{3.10}$$

and

$$\hat{m} \text{ (or } \hat{m} - \hat{m}_0) = \int_{0 \text{ (or } s_0)}^{s} \frac{1 - B''(s)}{B''(s)} ds \tag{3.11}$$

respectively. With respect to both eqs(3.10) and (3.11), the terms outside and inside the parentheses appearing in both the left-hand sides of the equations and at the lower limits of the integrals are concerned with trajectory T_0 and T, respectively. Similar expressions will be used hereafter for the similar equations.

When only the gradient in the liquid phase is applied (usual case), the characteristic surface is parallel to the s axis, represented as

$$B = B'(\hat{m}) \; [= \dot{B}(m, \rho^\circ)] = \dot{B}[\phi(\hat{m}), \rho^\circ] \tag{3.12}$$

rather than by eq(3.3) where ρ° stands for a positive constant. The projection on the ($\hat{m}$,B) plane of the characteristic curve can also be represented by eq(3.12), and trajectory T_0 or T can be represented concretely by eq(3.10).

When only the gradient in the solid phase is applied, the characteristic surface is parallel to the $\hat{m}$ axis, represented as

$$B = B''(s) \; [= \dot{B}(m^\circ, \rho)] = \dot{B}[m^\circ, \phi(s)] \tag{3.13}$$

rather than by eq(3.3) where m° stands for a positive constant. The projection on the (s, B) plane of the characteristic curve can also be represented by eq(3.13), and trajectory T_0 or T can be represented concretely by eq(3.11).

With the isocratic case, the characteristic surface is flat, parallel to the ($\hat{m}$,s) plane; this is represented as

$$B = \hat{B}(m^{\circ}, \rho^{\circ}) = B^{\circ} \tag{3.14}$$

Trajectory T_0 and T can be represented by eqs(2.8) and (2.11), respectively. These are solutions of eq(3.6') into which B° is substituted for $\hat{B}(\hat{m}+s)$ [i.e., eq(2.28)], obtained under initial conditions given by $\hat{m}=s=0$, and by $\hat{m}=\hat{m}_0$ and $s=s_0$, respectiverly.

Almost all the chromatographies can be characterized by one of the three characteristic curves drawn in Figs 3.2(a)-(c) giving trajectory T_0 as projection on the ($\hat{m}$,s) plane. The projections on ($\hat{m}$,B) and (s,B) planes are also drawn in Figs 3.2(a)-(c). The characteristic curve drawn in Fig 3.2(b) is intermediate between the two extremes drawn in Figs 3.2(a) and (c), respectively. Fig 3.2(a) corresponds to isocratic chromatography, whereas both Figs 3.2(b) and (c) correspond to gradient chromatography. In Fig 3.2(c), $B=0$ when $\hat{m}=s=0$, whereas, in Fig 3.2(b), B is almost, but not exactly, equal to zero when $\hat{m}=s=0$. In Fig 3.2(c), the characteristic curve is constructed of three straight lines: the first is superposed on the $\hat{m}$ axis, and the second and the third are parallel to B and s axes, respectively; the projection on the ($\hat{m}$,B) plane of the characteristic curve arises from the part parallel to the s axis present at $s=\infty$. Although Fig 3.2(c), in general, is realizable by using a step gradient, the case when it is realized by using a continuous concentration gradient is of interest (see the subsequent Chapter Ⅷ-X).

Further arguments on the characteristic surface[eqs(3.3), (3.12)-(3.14)] and the characteristic curve are performed in Appendix Ⅳ(A). It is recommended, however, to refer to Appendix Ⅳ(A) after attaining the subsequent Section(G).

(C) Usefulness of the ($\hat{m}$,s) Plane

The fact that the parameter g' is not involved in eq(3.4) or (3.5) means that trajectory T_0 or T with a nonlinear shape drawn on the ($\hat{m}$,s) plane[Fig 3.1; cf. both Figs 3.3 (a) and (b)] represents an assembly of trajectories obtained from a series of experiments carried out by applying gradients with different steepnesses g' but with similar shapes [as argued in Section(A)]. If trajectory T_0 or T with a nonlinear shape is mapped to the (V, L') plane, it will split into a number of trajectories each corresponding to each g' value (cf. Chapter Ⅶ Fig 7.7); this can be confirmed by substituting both eqs(2.5) and (2.6) into eq(3.4) or (3.5), generating the equation in which g' is involved as parameter. This is the reason why the ($\hat{m}$,s) plane is more useful; the argument developed on the basis of variable $\hat{m}$, s and ξ is more useful than that based on variable V, L' and Z, the former treating a series of similar experiments at the same time. Only with the isocratic case when trajectory T_0 or T is linear, the two arguments are identical because substituting both eqs(2.5) and (2.6) into eq(3.4) or (3.5) generates the same equation as before.

Provided that the flow-rate is constant independent of g', the rate of migration of

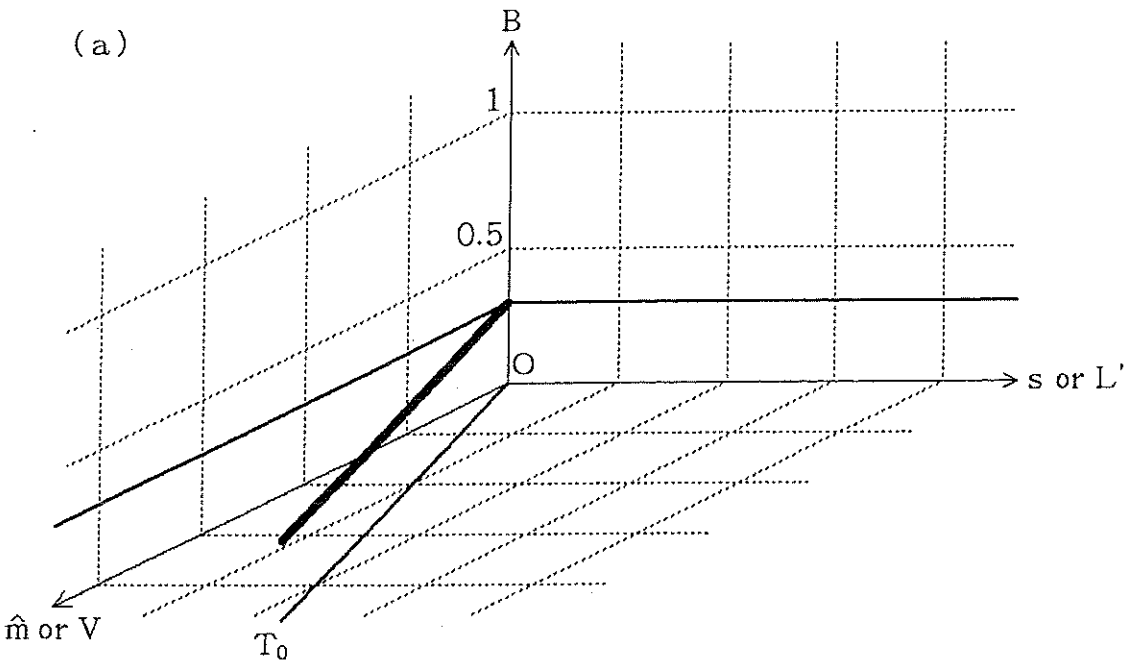


Fig 3.2. Three types of characteristic curve. The three projections of each are also drawn. The three projections and the corresponding characteristic curve in part(b) have been calculated on the basis of experimental data [see Fig 7.6 (middle curve), Fig 7.9 (middle curve) and Fig 7.10(a)].

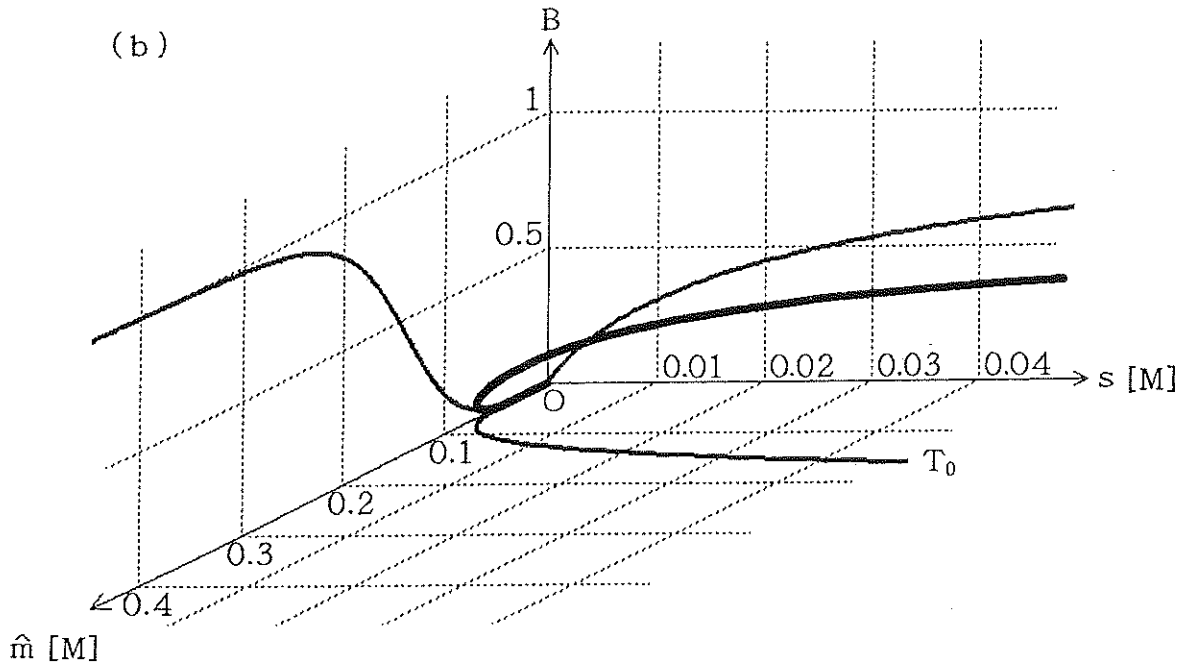


Fig 3.2. (b)

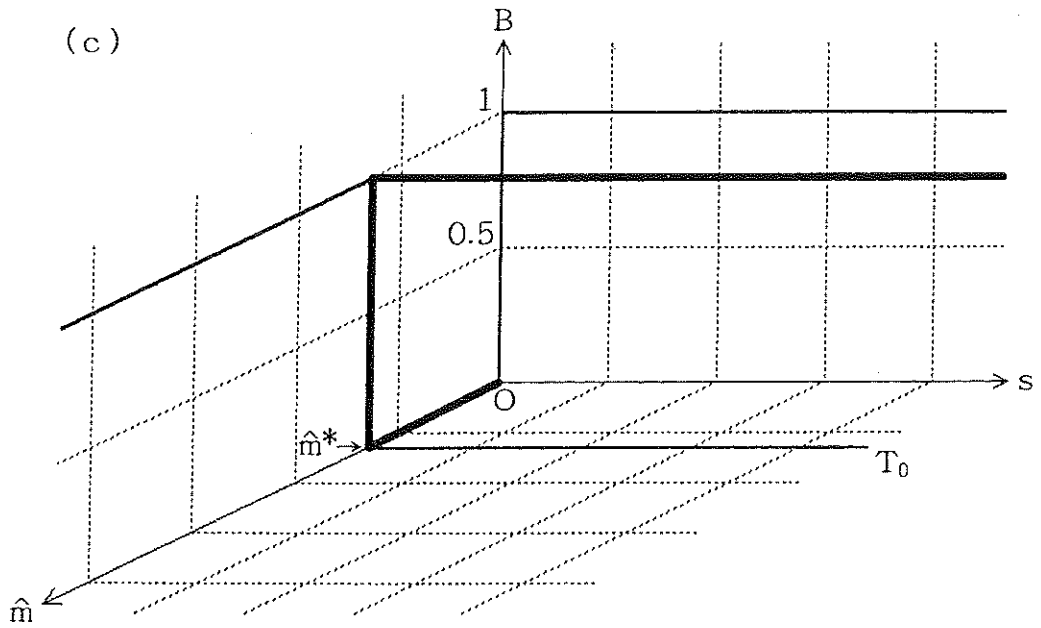


Fig 3.2. (c)

gradient G in either $\hat{m}$ or s direction and the rate of drawing trajectory T_0 or T on the $(\hat{m},s)$ plane are both proportional to g'. As gradient G and trajectory T_0 or T are both independent of the flow-rate, however, it is convenient to hypothesize in such a way that the flow-rate is inversely proportional to g', or that g' times the flow-rate is constant; the rate of migration of gradient G and the rate of drawing trajectory T_0 or T are both independent of g'.

(D) Expression of Gradient G in Terms of Projection $B'(\hat{m})$ or $B''(s)$

From both eqs(3.10) and (3.11), another expression of trajectory T_0 or T:

$$\xi = \hat{m}+s = \int_{0\ (\text{or}\ \hat{m}_0)}^{\hat{m}} \frac{d\hat{m}}{1-B'(\hat{m})} = \int_{0\ (\text{or}\ s_0)}^{s} \frac{ds}{B''(s)} \tag{3.15}$$

can be derived, where the first equality arises from eq(2.7). Eq(3.15) manifests that both $\hat{m}$ and s [as coordinates of point P on the $(\hat{m},s)$ plane] can be represented as functions of ξ or $\hat{m}+s$; this arises from the fact that point P always stays on gradient G. Writing $(\bar{m},\bar{s})$ for the coordinate of point P, gradient G can be represented as

$$\hat{m}+s\ (=\bar{m}+\bar{s}) = \int_{0\ (\text{or}\ \hat{m}_0)}^{\bar{m}} \frac{d\bar{m}}{1-B'(\bar{m})} = \int_{0\ (\text{or}\ s_0)}^{\bar{s}} \frac{d\bar{s}}{B''(\bar{s})} \tag{3.16}$$

[see both Figs 3.3(a) and (b)].

Eq(3.16), showing that both $\bar{m}$ and $\bar{s}$ are functions of $\hat{m}+s$, leads to

$$B'(\bar{m}) = B''(\bar{s}) = \hat{B}(\hat{m}+s) \tag{3.17}$$

Eq(3.16) also leads to

$$d\bar{m} = [1-B'(\bar{m})](d\hat{m}+ds) \tag{3.18}$$

and

$$d\bar{s} = B''(\bar{s})(d\hat{m}+ds) \tag{3.19}$$

or to

$$(\partial\bar{m}/\partial\hat{m})_s = (\partial\bar{m}/\partial s)_{\hat{m}} = 1-B'(\bar{m}) \tag{3.20}$$

and

$$(\partial\bar{s}/\partial\hat{m})_s = (\partial\bar{s}/\partial s)_{\hat{m}} = B''(\bar{s}) \tag{3.21}$$

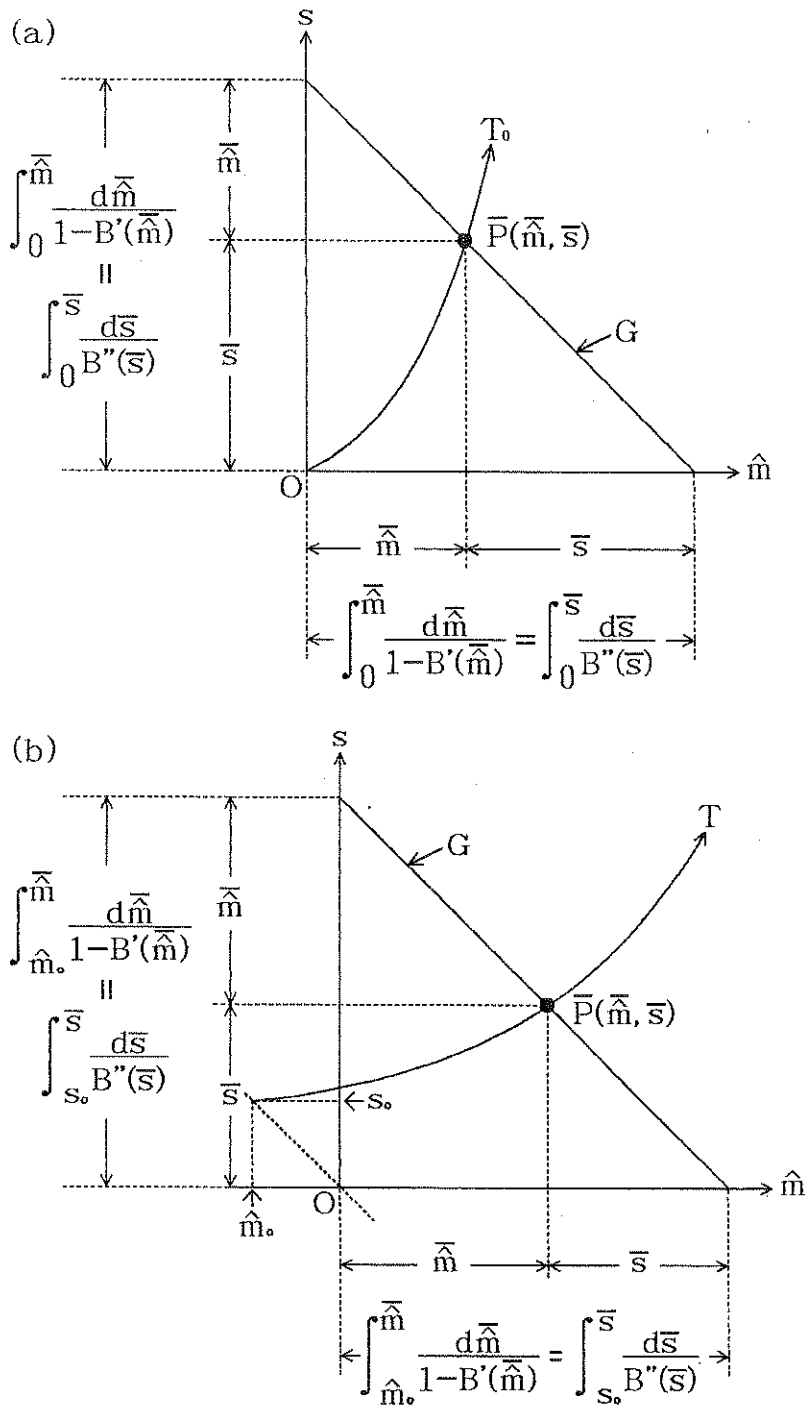


Fig 3.3. (a) Trajectory T_0 versus (b) Trajectory T.

(E) Capacity Ratio

Capacity ratio k can be defined as

$$k = (1-B)/B \tag{3.22}$$

or molecular partition, B, in the liquid phase can be represented by using k as

$$B = 1/(1+k) \tag{3.22'}$$

When B moves between 0 and 1, then k moves between ∞ and 0. Corresponding to $B'(\hat{m})$ and $B''(s)$

$$k'(\hat{m}) = \frac{1-B'(\hat{m})}{B'(\hat{m})} \tag{3.23}$$

and

$$k''(s) = \frac{1-B''(s)}{B''(s)} \tag{3.24}$$

are conceivable; $k'(\hat{m})$ and $k''(s)$ are monotonically decreasing functions of $\hat{m}$ and s, moving at most from ∞ to 0, respectively.

When both the gradient in the liquid phase and the gradient in the solid phase are applied at the same time, let us limit ourselves to the ideal case where k can be expressed as

$$k = \kappa'(\hat{m})\,\kappa''(s) \quad [= \kappa'\{\phi^{-1}(m)\}\,\kappa''\{\phi^{-1}(\rho)\}] \tag{3.25}$$

in which $\kappa'(\hat{m})$ and $\kappa''(s)$ are monotonically decreasing functions of $\hat{m}$ and s, moving at most from ∞ to 0, respectively. For the later purpose, let us introduce:

$$\tilde{B}'(\hat{m}) = \frac{1}{1+\kappa'(\hat{m})} \tag{3.26}$$

and

$$\tilde{B}'(s) = \frac{1}{1+\kappa''(s)} \tag{3.27}$$

When only the gradient in the liquid phase is applied, the function $\kappa''(s)$ can be replaced by a positive constant $\kappa^{\circ\prime\prime}$; eq(3.25) can be rewritten as

$$k = k'(\hat{m}) = \kappa^{\circ\prime\prime}\,\kappa'(\hat{m}) \tag{3.28}$$

When only the gradient in the solid phase is applied, the function $\kappa'(\hat{m})$ can be replaced by another positive constant $\kappa^{\circ\prime}$; eq(3.25) can be rewritten as

$$k = k''(s) = \kappa^{\circ\prime}\,\kappa''(s) \tag{3.29}$$

With the *isocratic* case, eq(3.25) becomes

$$k^{\circ}\ [=\ (1-B^{\circ})/B^{\circ}]\ =\ \kappa^{\circ\prime}\,\kappa^{\circ\prime\prime} \tag{3.30}$$

(F) Chromatogram as First Concept versus Abstract Flux

It would be possible to extend eq(2.23) to

$$\mathrm{div}_{\hat{m}}\left(\frac{1-B}{B}C\right)+\frac{\partial C}{\partial s}=0 \tag{3.31}$$

representing the abstract flux with gradient chromatography in CPV(OPV).

The Case When Only the Gradient in the Liquid Phase Is Applied. The relationship:

$$B\ =\ B'(\hat{m})\ =\ \frac{1}{1+k'(\hat{m})} \tag{3.32}$$

holds [see eqs(3.22'), (3.23) and (3.28)], and eq(3.31) has a general solution:

$$\begin{aligned} C\ &=\frac{1}{k'(\hat{m})}U\left(s-\int_0^{\hat{m}}\frac{d\hat{m}}{k'(\hat{m})}\right)\\ &=\frac{B'(\hat{m})}{1-B'(\hat{m})}U\left(s-\int_0^{\hat{m}}\frac{B'(\hat{m})}{1-B'(\hat{m})}d\hat{m}\right)\end{aligned} \tag{3.33}$$

in which U represents any function [see Appendix II(A)].

Let us consider the case when the initial MB(o) represented by eq(2.15) is completed by isocratic injection of the sample solution at the inlet of the column immediately before the injection of the concentration gradient. We assume that the initial concentration of gradient substance is present in the sample solution to be injected into the column, involving the case when the initial concentration is zero or when there is no gradient substance in the sample solution. [It is possible to consider that the case when the initial concentration of gradient substance is higher than that present in the sample solution represents the extreme case when the initial slope of the concentration gradient is infinitely steep. The case when the initial concentration of gradient substance is lower than that present in the sample solution is not considered here.] Because of the isocratic injection, molecular partition, B_o, in the liquid phase and the corresponding capacity ratio, $k_o\ [=(1-B_o)/B_o]$, taking place over the initial MB(o) should be uniform, equal to those taking place at the beginning of the concentration gradient, respectively. Initial condition to the differential equation, eq(3.31), can now be written as

$$\lim_{s\to 0} C = \frac{B'(\hat{m})}{1-B'(\hat{m})} U\left(-\int_0^{\hat{m}} \frac{B'(\hat{m})}{1-B'(\hat{m})} d\hat{m} \right)$$

$$= B_o F(-B_o \hat{m}) \left(= \frac{1}{1+k_o} F\left(-\frac{\hat{m}}{1+k_o} \right) \right) \qquad (3.34)$$

in which F(X) is defined to be zero when $X<0$ [Chapter II(C)]. This means that $\lim_{s\to 0} C = 0$ when $\hat{m}>0$, and that $\hat{m}$ appearing explicitly in eq(3.34) is smaller than, or at most equal to, zero. Further, when $\hat{m}\leqq 0$, then $B'(\hat{m})=B_o$. This is because the solvent to be injected into the column has a potential ability of bringing about partition B_o; this means that $B'(\hat{m})$ appearing explicitly in eq(3.34) represents B_o.

Under eq(3.34), eq(3.33) can be rewritten as

$$C = \frac{(1-B_o)B'(\hat{m})}{1-B'(\hat{m})} F\left((1-B_o)[\, s - \int_0^{\hat{m}} \frac{B'(\hat{m})}{1-B'(\hat{m})} d\hat{m} \,] \right)$$

$$\left(= \frac{k_o}{(1+k_o)k'(\hat{m})} F\left(\frac{k_o}{1+k_o} [\, s - \int_0^{\hat{m}} \frac{d\hat{m}}{k'(\hat{m})} \,] \right) \right) \qquad (3.35)$$

representing CGM1st.

Width, Δ_c, of CGM1st as a function of $\hat{m}$ [eq(3.35)] can be measured by the average of reciprocals of the product by $1-B_o$ of the derivative of the integral $\int^{\hat{m}} B'(\hat{m})d\hat{m}/[1-B'(\hat{m})]$ in function F; the average is taken for $\hat{m}$. [Let us say briefly that Δ_c can be measured by reciprocal of the product by $1-B_o$ of integrand $B'(\hat{m})/[1-B'(\hat{m})]$ for similar cases hereafter.] On the other hand, as s increases, the $\hat{m}$ coordinates over which CGM1st appears increase monotonically; they may tend to be constant. [In some instances, the precise meaning of this statement is that the $\hat{m}$ coordinates giving large enough C values compared to negligibly small ones under distribution of C increase monotonically with increase in s.] The corresponding $B'(\hat{m})$ and $B'(\hat{m})/[1-B'(\hat{m})]$ values increase monotonically to tend to unity and to approach infinity, respectively. This means that Δ_c decreases monotonically to tend to infinitesimal with increase in s.

With the isocratic case when $B'(\hat{m})=B_o=B^\circ$ and $k'(\hat{m})=k_o=k^\circ$, eq(3.34) coincides with eq(2.24), and eq(3.35) reduces to eq(2.20).

The Case When Only the Gradient in the Solid Phase Is Applied. The relationship:

$$B = B''(s) = \frac{1}{1+k''(s)} \qquad (3.36)$$

holds [see eqs(3.22'), (3.24) and (3.29)], and eq(3.31) has a general solution:

$$C = U\left(\int_0^s k''(s)ds - \hat{m} \right)$$

$$= U\left(\int_0^s \frac{1-B''(s)}{B''(s)} ds - \hat{m} \right) \tag{3.37}$$

[see Appendix II(A)].

We consider the case when the initial MB(o) represented by eq(2.15) is completed by isocratic injection at the inlet of the column. We assume that the solvent of the sample solution to be injected into the column is the same as the carrier liquid of chromatography, and, for the argument to be symmetric with that for the case when only the gradient in the liquid phase is applied, we also assume that the solid phase in the neighborhood of the inlet of the column where the initial MB(o) is formed is uniform bringing about constant B_o or k_o. Initial condition to eq(3.31) can now be written as

$$\lim_{s\to 0} C = U(-\hat{m})$$

$$= B_o F(-B_o \hat{m}) \quad \left(= \frac{1}{1+k_o} F\left(- \frac{\hat{m}}{1+k_o} \right) \right) \tag{3.38}$$

Under eq(3.38), eq(3.37) can be rewritten as

$$C = B_o F\left(B_o \left[\int_0^s \frac{1-B''(s)}{B''(s)} ds - \hat{m} \right] \right)$$

$$\left(= \frac{1}{1+k_o} F\left(\frac{1}{1+k_o} \left[\int_0^s k''(s)ds - \hat{m} \right] \right) \right) \tag{3.39}$$

representing CGM1st. The reciprocal of B_o in function F in eq(3.39) measures width, Δ_c, and determines the shape of CGM1st; this means that both width and shape of CGM1st [eq(3.39)] are constant, independent of s.

With the isocratic case when $B''(s)=B_o=B^o$ and $k''(s)=k_o=k^o$, eq(3.38) coincides with eq(2.24), and eq(3.39) reduces to eq(2.20).

The Case When Both the Gradient in the Liquid Phase and the Gradient in the Solid Phase Are Applied at the Same Time. The relationship:

$$B = \frac{1}{1+\kappa'(\hat{m})\kappa''(s)} \tag{3.40}$$

holds [see both eqs(3.22') and (3.25)], and eq(3.31) has a general solution:

$$C = \frac{1}{\kappa'(\hat{m})} U\left(\int_0^s \kappa''(s)ds - \int_0^{\hat{m}} \frac{d\hat{m}}{\kappa'(\hat{m})} \right) \tag{3.41}$$

[see Appendix II(A)].

Again, we consider the case when the initial MB(o) represented by eq(2.15) is completed by isocratic injection at the inlet of the column immediately before the injection of the concentration gradient. We assume that the initial concentration of gradient substance is present in the sample solution to be injected into the column, and that the solid phase where the initial MB(o) is formed is uniform. Denoting by κ_o' and κ_o'' the $\kappa'(\hat{m})$ and $\kappa''(s)$ values taking place uniformly over the initial MB(o), respectively, the relationship:

$$k_o\ [= (1-B_o)/B_o] = \kappa_o'\kappa_o'' \tag{3.42}$$

[cf. eq(3.30)] is fulfilled. The initial condition to eq(3.31) can be written as

$$\lim_{s\to 0} C = \frac{1}{\kappa'(\hat{m})} U\left(-\int_0^{\hat{m}} \frac{d\hat{m}}{\kappa'(\hat{m})} \right)$$

$$= B_o F(-B_o\hat{m}) \left(= \frac{1}{1+k_o} F\left(-\frac{\hat{m}}{1+k_o} \right) \right) \tag{3.43}$$

where $\kappa'(\hat{m})$ appearing explicitly in eq(3.43) represents κ_o'.

Under eq(3.43), eq(3.41) can be rewritten with reference to eq(3.42) as

$$C = \frac{1}{(1/\kappa_o' + \kappa_o'')\kappa'(\hat{m})} F\left(\frac{1}{1/\kappa_o' + \kappa_o''} \left[\int_0^s \kappa''(s)ds - \int_0^{\hat{m}} \frac{d\hat{m}}{\kappa'(\hat{m})} \right] \right) \tag{3.44}$$

representing CGM1st with width Δc measured by the reciprocal of the product by $1/(1/\kappa_o' + \kappa_o'')$ of integrand $1/\kappa'(\hat{m})$ in the second integral in function F i.e., by the product by $1/\kappa_o' + \kappa_o''$ of $\kappa'(\hat{m})$.

$\kappa'(\hat{m})$ and $\kappa''(s)$ decrease monotonically to tend to infinitesimal when $\hat{m}$ and s increase, respectively. On the other hand, when considering CGM1st to be a function of both $\hat{m}$ and s, the $\hat{m}$ coordinates over which CGM1st appears increase monotonically with increase in the s coordinates over whcich CGM1st appears; the $\hat{m}$ coorditates may tend to be constant. This means that Δc [decreasing with decrease of $\kappa'(\hat{m})$ (see above) or with increase in the $\hat{m}$ values over which CGM1st appears] decreases monotonically with increase in coordinate s (on the hypothetiocal column with infinite length) at which the monitoring is performed [see Chapter II(D)].

There are two cases. *First case*: When considering again that CGM1st is a function of both $\hat{m}$ and s, the functions $\kappa''(s)$ corresponding to the s coordinates over which

CGM1st appears decrease more rapidly than the functions $\kappa'(\hat{m})$ corresponding to the $\hat{m}$ coordinates over which CGM1st appears with increase in both $\hat{m}$ and s coordinates in such a way that the $\kappa'(\hat{m})$ values are still finite when the $\kappa''(s)$ values tend to infinitesimal. B tends to unity when $\kappa''(s)$ tends to infinitesimal [see both eqs(3.22') and (3.25)]; this means that the $\hat{m}$ coordinates over which CGM1st appears and the corresponding functions $\kappa'(\hat{m})$ with finite values tend to be constant. CGM1st with both constant finite width Δ_c and constant shape stays over these constant $\hat{m}$ coordinates. *Second case*: The functions $\kappa''(s)$ decrease less rapidly than the functions $\kappa'(\hat{m})$ with increase in both $\hat{m}$ and s in such a way that the $\kappa''(s)$ values are still finite when the $\kappa'(\hat{m})$ values tend to infinitesimal. For convenience' sake, the case when both $\kappa'(\hat{m})$ and $\kappa''(s)$ tend to infinitesimal at comparable rates is here regarded as an extreme of the second case. B now tends to unity when $\kappa'(\hat{m})$ tends to infinitesimal[eqs(3.22') and (3.25)] despite whether $\kappa''(s)$ tends to infinitesimal or not at the same time. CGM1st with infinitesimal Δ_c takes place.

When $\kappa''(s)=\kappa^{\circ\prime\prime}=\kappa_\circ''$ and eq(3.28) into which $\kappa_\circ''$ is substituted for $\kappa^{\circ\prime\prime}$ holds, then, due to eq(3.42), eq(3.44) reduces to eq(3.35). On the other hand, when $\kappa'(\hat{m})=\kappa^{\circ\prime}=\kappa_\circ'$ and eq(3.29) into which $\kappa_\circ'$ is substituted for $\kappa^{\circ\prime}$ holds, then eq(3.44) reduces to eq(3.39).

With the isocratic case when $\kappa'(\hat{m})=\kappa_\circ'=\kappa^{\circ\prime}$, $\kappa''(s)=\kappa_\circ''=\kappa^{\circ\prime\prime}$, $B_\circ=B^\circ$ and $k_\circ=k^\circ$, eq(3.43) coincides with eq(2.24), and eq(3.44) reduces to eq(2.20).

In Appendix Ⅲ(A), the arguments complementary to those developed above in CPV (OPV) are performed in OPV(CPV).

Some examples of the calculation of CGM1st[eqs(3.35), (3.39) and (3.44)] are shown for step gradients in Appendix Ⅳ(A). It is recommended, however, to refer to Appendix Ⅳ(A) after attaining the subsequent Section(G).

(G) Expression in Terms of Proper Time ξ : Molecular Band as Flux

Executing the coordinate transformations: $(\hat{m},s)\rightarrow(\xi,s)$ and $(\hat{m},s)\rightarrow(\xi,\hat{m})$, eq(3.6') can be rewritten as

$$ds/d\xi = \hat{B}(\xi) \tag{3.45}$$

and

$$d\hat{m}/d\xi = 1-\hat{B}(\xi) \tag{3.46}$$

or, with integration, as

$$s \text{ (or } s-s_\circ) = \int_0^\xi \hat{B}(\xi)d\xi \tag{3.47}$$

and

$$\hat{m} \ (\text{or } \hat{m}-\hat{m}_0) = \int_0^{\xi} [1-\hat{B}(\xi)]d\xi \tag{3.48}$$

respectively. It is possible to give ξ in eqs(3.45)-(3.48) the meaning of proper time. When the meaning of time is assigned to s, eq(3.45) or (3.47) represents contraction of time in CPV(OPV), and, when the meaning of time is assigned to $\hat{m}$, eq(3.46) or (3.48) represents contraction of time in OPV(CPV). [When interpreting eqs(3.47) and (3.48) to represent contraction of time, we usually consider that $\hat{m}_0=s_0=0$.] On the other hand, when the meaning of distance is assigned to s, eq(3.45) or (3.47) represents trajectory T_0 or T mapped to the (ξ, s) plane (OPV), and, when the meaning of distance is assigned to $\hat{m}$, eq(3.46) or (3.48) represents trajectory T_0 or T mapped to the $(\xi, \hat{m})$ plane (CPV).

Writing $(\bar{\xi}, \bar{s})$ and $(\bar{\xi}, \bar{\hat{m}})$ for coordinates of point $\bar{P}$ drawing trajectory T_0 or T on (ξ, s) and $(\xi, \hat{m})$ planes, then the corresponding gradient G can be represented by substituting ξ for $\hat{m}+s$ and $\bar{\xi}$ for $\bar{\hat{m}}+\bar{s}$ into eq(3.16) as

$$\xi \ (= \bar{\xi}) = \int_{0 \ (\text{or } s_0)}^{\bar{s}} \frac{d\bar{s}}{B''(\bar{s})} \tag{3.49}$$

(OPV) and

$$\xi \ (= \bar{\xi}) = \int_{0 \ (\text{or } \hat{m}_0)}^{\bar{\hat{m}}} \frac{d\bar{\hat{m}}}{1-B'(\bar{\hat{m}})} \tag{3.50}$$

(CPV), respectively. Eqs(3.49) and (3.50) are equivalent with eq(3.47) into which $\bar{s}$ is substituted for s, and eq(3.48) into which $\bar{\hat{m}}$ is substituted for $\hat{m}$:

$$\bar{s} \ (\text{or } \bar{s}-s_0) = \int_0^{\xi} \hat{B}(\xi)d\xi \tag{3.49'}$$

and

$$\bar{\hat{m}} \ (\text{or } \bar{\hat{m}}-\hat{m}_0) = \int_0^{\xi} [1-\hat{B}(\xi)]d\xi \tag{3.50'}$$

respectively.

Trajectory T_0 drawn in Figs 2.8(a), (d) and (g) correspond to the projections on the $(\hat{m}, s)$ plane of the three types of characteristic curve drawn in Figs 3.2(a)-(c), respectively. Figs 2.8(e) and (f) illustrate both trajectory T_0 and gradient G [drawn in Fig 2.8(d)] mapped to (ξ, s) and $(\xi, \hat{m})$ planes, respectively. Figs 2.8(g)-(i) correspond to Figs 2.8

(d)-(f), representing the extreme case when trajectory T_0 is constructed of two straight lines, respectively.

By using Appendix I eq(A1.1) in which $u=\hat{m}$, $v=s$, $x(u,v)=\xi(\hat{m},s)\equiv\hat{m}+s$[eq (2.7)], $y(u,v)=s$ and $z=\Omega$ or B, and with reference to eq(2.2), eq(3.31) can be transformed to

$$\mathrm{div}_s\,(B\Omega) + \partial\Omega/\partial\xi = 0 \tag{3.51}$$

On the other hand, by using Appendix I eq(A1.1) in which $x(u,v)=\hat{m}$ and $y(u,v)=\xi(\hat{m},s)\equiv\hat{m}+s$ instead, eq(3.31) can be transformed to

$$\mathrm{div}_{\hat{m}}\,[(1-B)\Omega] + \partial\Omega/\partial\xi = 0 \tag{3.52}$$

Similarly but with reference to eq(2.4) instead of eq(2.2), Appendix III(A) eq(A3.1) can also be transformed to either eq(3.51) or (3.52). Eqs(3.51) and (3.52), being extensions of eqs(2.33) and (2.34), represent MB(o) (as flux with density Ω migrating on the column at rate B; OPV) and MB(c) (as flux with density Ω migrating on the carrier liquid at rate 1 $-$B; CPV), respectively. We write down below the solutions of both eqs(3.51) and (3.52) obtained under the same circumstances as those where eqs(3.35), (3.39) and (3.44) are obtained as solutions of eq(3.31), or the same circumstances as those where eqs(A3.5), (A3.8) and (A3.12) are obtained as solutions of eq(A3.1) in Appendix III(A), respectively.

The Case When Only the Gradient in the Liquid Phase Is Applied. Eq(3.32) holds, and the solution of eq(3.51) (OPV) can be written as

$$\Omega = \frac{1-B_0}{1-B'(\xi-s)}F\left((1-B_0)\left[\xi-\int_0^{\xi-s}\frac{d\hat{m}}{1-B'(\hat{m})}\right]\right)$$

$$\left(= \frac{k_0[1+k'(\xi-s)]}{(1+k_0)k'(\xi-s)}F\left(\frac{k_0}{1+k_0}\left[\xi-\int_0^{\xi-s}\frac{1+k'(\hat{m})}{k'(\hat{m})}d\hat{m}\right]\right)\right) \tag{3.53}$$

which coincides with eq(2.15) initially when $\xi\to 0$, and the solution of eq(3.52) (CPV) can be written as

$$\Omega = \frac{1-B_0}{1-B'(\hat{m})}F\left((1-B_0)\left[\xi-\int_0^{\hat{m}}\frac{d\hat{m}}{1-B'(\hat{m})}\right]\right)$$

$$\left(= \frac{k_0[1+k'(\hat{m})]}{(1+k_0)k'(\hat{m})}F\left(\frac{k_0}{1+k_0}\left[\xi-\int_0^{\hat{m}}\frac{1+k'(\hat{m})}{k'(\hat{m})}d\hat{m}\right]\right)\right) \tag{3.54}$$

which coincides with eq(2.17) initially when $\xi\to 0$. Eq(3.54) can be obtained (a) by solving eq(3.52) directly by using the method similar to that applied in Appendix II(A), (b) by

substituting $B'(\hat{m})\Omega$ for C, and $\xi-\hat{m}$ for s into eq(3.35), or (c) by substituting $[1-B'(\hat{m})]\Omega$ for χ, and $\xi-\hat{m}$ for s into Appendix III(A) eq(A3.5). Eq(3.53) can be obtained (a) by substituting $B'(\xi-s)\Omega$ for C, and $\xi-s$ for $\hat{m}$ into eq(3.35), or (b) by substituting $[1-B'(\xi-s)]\Omega$ for χ, and $\xi-s$ for $\hat{m}$ into Appendix III(A) eq(A3.5). Eq (3.53) can be derived from eq(3.54) by substituting $\xi-s$ for $\hat{m}$, and eq(3.54) can be derived from eq(3.53) by substituting $\xi-\hat{m}$ for s. The mutual derivations between the two equations reflect the fact that MB(o)[eq(3.53)] and MB(c)[eq(3.54)] are projections on (s, Ω) and ($\hat{m}$, Ω) planes of FCB migrating along gradient G, respectively.

It can be concluded that width, Δ_o, of either MB(o)[eq(3.53)] or MB(c)[eq(3.54)] decreases monotonically to tend to infinitesimal with increase in ξ. This is because Δ_o in either eq(3.53) or (3.54) can be measured by the recoprocal of the product by $1-B_o$ of integrand $1/[1-B'(\hat{m})]$ in function F i.e., by $[1-B'(\hat{m})]/(1-B_o)$, and $1-B'(\hat{m})$ or $1-B'(\xi-s)$ decreases monotonically to tend to infinitesimal with increase in $\hat{m}$ or $\xi-s$; the $\hat{m}$ coordinates or the $\xi-s$ values over which MB appears, in general, increase with increase in ξ. The decrease of Δ_o taking place with increase in ξ is called *compression of band.* This can qualitatively be understood as being a result of the fact that the concentrations, m, of gradient substances over which the rear part of MB(o) appears are higher than those where the front part appears on the column (OPV), and that the relative rates, $B'(\hat{m})$ or $B'[\phi^{-1}(m)]$, of migration of the molecules that are present in the rear part are higher than those of the molecules that are present in the front part.

By comparing eq(3.35) with eq(3.54), it can be interpreted that the decrease of width, Δ_c, of the corresponding CGM1st taking place with increase in s[eq(3.35)] is a result of the enhancement of the two effects of compression of band and decrease of chromatographic dilatation. Thus, the decrease of Δ_c with increase in s takes place as a result of the decrease of the reciprocal of the integrand $B'(\hat{m})/[1-B'(\hat{m})]$ in function F in eq (3.35) with increase in $\hat{m}$ which takes place with increase in s. This i.e., the decrease of $[1-B'(\hat{m})]/B'(\hat{m})$ taking place with increase in $\hat{m}$ can be interpreted to arise from the decrease of $1/B'(\hat{m})$ (i.e., the decrease of chromatographic dilatation) enhanced by the decrease of $1-B'(\hat{m})$ [i.e., compression of band; eq(3.54)]. MB(c)[eq(3.54)] and the corresponding CGM1st[eq(3.35)] coincide with one another when Δ_o and Δ_c tend to infinitesimal at the same time with increase in ξ or s.

By comparing Appendix III(A) eq(A3.5) with eq(3.53), it can be interpreted that the constancy of width, Δ_χ, of the corresponding χGM1st is a result of the cancellation of the two effects of compression of band (to infinitesimal width) and increase of chromatographic dilatation (to infinite extent). Thus, the term s in function F in Appendix III(A) eq(A3.5) can be re-expressed as $s=\int_\delta[1-B''(s)]ds/[1-B''(s)]$, and the constancy of $[1-B''(s)]/[1-B''(s)]$ bringing about the constancy of Δ_χ can be interpreted to arise from the cancellation between the increase of $1/[1-B''(s)]$ (i.e., the increase of chromatographic dilatation) and the decrease of $1-B''(s)$ [i.e., compression of band; eq(3.53)] taking place with increase in s, respectively; the term $\int_{\hat{m}_0}^{\hat{m}} d\hat{m}/[1-B'(\hat{m})]$ in eq(3.53) can be

replaced by $\int \hat{\eta}\, ds/[1-B''(s)]$.

With the isocratic case when $B'(\hat{m})=B'(\xi-s)=B_o=B^o$ and $k'(\hat{m})=k'(\xi-s)=k_o=k^o$, eqs(3.53) and (3.54) coincide with eqs(2.16) and (2.18), respectively.

The Case When Only the Gradient in the Solid Phase Is Applied. Eq(3.36) holds, and the solution of eq(3.51) (OPV) can be written as

$$\Omega = \frac{B_o}{B''(s)} F\left(B_o\left[\int_0^s \frac{ds}{B''(s)} - \xi \right] \right)$$

$$\left(= \frac{1+k''(s)}{1+k_o} F\left(\frac{1}{1+k_o}\left[\int_0^s \{1+k''(s)\}ds - \xi \right] \right) \right) \qquad (3.55)$$

which coincides with eq(2.15) initially when $\xi \to 0$, and the solution of eq(3.52) (CPV) can be written as

$$\Omega = \frac{B_o}{B''(\xi-\hat{m})} F\left(B_o\left[\int_0^{\xi-\hat{m}} \frac{ds}{B''(s)} - \xi \right] \right)$$

$$\left(= \frac{1+k''(\xi-\hat{m})}{1+k_o} F\left(\frac{1}{1+k_o}\left[\int_0^{\xi-\hat{m}} \{1+k''(s)\}ds - \xi \right] \right) \right) \qquad (3.56)$$

which coincides with eq(2.17) initially when $\xi \to 0$. Eq(3.55) can be obtained (a) by solving eq(3.51) directly by using the method similar to that applied in Appendix II(A), (b) by substituting $[1-B''(s)]\Omega$ for χ, and $\xi-s$ for $\hat{m}$ into Appendix III(A) eq(A3.8), or (c) by substituting $B''(s)\Omega$ for C, and $\xi-s$ for $\hat{m}$ into eq(3.39). Eq(3.56) can be obtained (a) by substituting $[1-B''(\xi-\hat{m})]\Omega$ for χ, and $\xi-\hat{m}$ for s into Appendix III(A) eq (A3.8), or (b) by substituting $B''(\xi-\hat{m})\Omega$ for C, and $\xi-\hat{m}$ for s into eq(3.39). Eq (3.55) can be derived from eq(3.56) by substituting $\xi-s$ for $\hat{m}$, and eq(3.56) can be derived from eq(3.55) by substituting $\xi-\hat{m}$ for s. The mutual derivations between the two equations reflect the fact that MB(o)[eq(3.55)] and MB(c)[eq(3.56)] are projections on (s, Ω) and ($\hat{m}$, Ω) planes, respectively.

It can be concluded that width, Δ_Ω, of either MB(o)[eq(3.55)] or MB(c)[eq(3.56)] increases monotonically to tend to a finite width, and that the shape of either MB tends to be constant with increase in ξ. This is because Δ_Ω in either eq(3.55) or (3.56) can be measured by the reciprocal of the product by B_o of integrand $1/B''(s)$ in function F, and $B''(s)$ or $B''(\xi-\hat{m})$ increases monotonically to tend to unity with increase in s or $\xi-\hat{m}$; the s coordinates or the $\xi-\hat{m}$ values over which MB appears, in general, increase with increase in ξ. The shape of either MB(o) or MB(c) tends to be constant when Δ_Ω tends to be constant. Let us call the increase of Δ_Ω taking place with increase in ξ as

expansion of band. This can qualitatively be understood as being a result of the fact that the ρ values of the solid phase over which the front part of MB(o) appears are higher than those where the rear part appears on the column (OPV), and that the relative rates, $B''(s)$ or $B''[\phi^{-1}(\rho)]$, of migration of the molecules that are present in the front part are higher than those of the molecules that are present in the rear part.

By comparing eq(3.39) with eq(3.56), it can be interpreted that the constancy of width, Δ_c, of the corresponding CGM1st is a result of the cancellation of the two effects of expansion of band (to finite width) and decrease in chromatographic dilatation (to finite extent). Thus, the term $\hat{m}$ in function F in eq(3.39) can be re-expressed as $\hat{m} = \int_0^{\hat{m}} B'(\hat{m})d\hat{m}/B'(\hat{m})$, and the constancy of $B'(\hat{m})/B'(\hat{m})$ bringing about the constancy of Δ_c can be interpreted to arise from the cancellation between the decrease of $1/B'(\hat{m})$ (i.e., the decrease of chromatographic dilatation) and the increase of $B'(\hat{m})$ [i.e., expansion of band; eq(3.56)] taking place with increase in $\hat{m}$, respectively; the term $\int_0^{\xi-s} ds/B''(s)$ in eq(3.56) can be replaced by $\int_0^{\hat{m}} d\hat{m}/B'(\hat{m})$.

By comparing Appendix III(A) eq(A3.8) with eq(3.55), it can be interpreted that the increase (to approach infinity) of width, Δ_x, of the corresponding χGM1st taking place with increase in $\hat{m}$ [Appendix III(A) eq(A3.8)] is a result of the enhancement of the two effects of expansion of band and increase of chromatographic dilatation (to infinite extent). Thus, the increase of Δ_x with increase in $\hat{m}$ takes place as a result of the increase of the reciprocal of the integrand $[1-B''(s)]/B''(s)$ in function F in Appendix III(A) (A3.8) with increase in s which takes place with increase in $\hat{m}$. This i.e., the increase of $B''(s)/[1-B''(s)]$ taking place with increase in s can be interpreted to arise from the increase of $1/[1-B''(s)]$ (i.e., the increase of chromatographic dilatation) enhanced by the increase of $B''(s)$ [i.e., expansion of band; eq(3.55)].

With the isocratic case when $B''(s)=B''(\xi-\hat{m})=B_o=B^\circ$ and $k''(s)=k''(\xi-\hat{m})=k_o=k^\circ$, eqs(3.55) and (3.56) coincide with eqs(2.16) and (2.18), respectively.

The Case When Both the Gradient in the Liquid Phase and the Gradient in the Solid Phase Are Applied at the Same Time. Eq(3.40) holds, and the solution of eq(3.51) (OPV) can be written as

$$\Omega = \frac{1}{1/\kappa_o' + \kappa_o''}\left(\frac{1}{\kappa'(\xi-s)} + \kappa''(s)\right) F\left(\frac{1}{1/\kappa_o' + \kappa_o''}\left[\int_0^s \kappa''(s)ds - \int_0^{\xi-s} \frac{d\hat{m}}{\kappa'(\hat{m})}\right]\right) \tag{3.57}$$

which coincides with eq(2.15) initially when $\xi \to 0$, and the solution of eq(3.52) (CPV) can be written as

$$\Omega = \frac{1}{1/\kappa_o' + \kappa_o''}\left(\frac{1}{\kappa'(\hat{m})} + \kappa''(\xi-\hat{m})\right) F\left(\frac{1}{1/\kappa_o' + \kappa_o''}\left[\int_0^{\xi-\hat{m}} \kappa''(s)ds - \int_0^{\hat{m}} \frac{d\hat{m}}{\kappa'(\hat{m})}\right]\right) \tag{3.58}$$

which coincides with eq(2.17) initially when $\xi \to 0$. Eq(3.57) can be obtained (a) by substituting $B\Omega$ for C, and $\xi - s$ for $\hat{m}$ into eq(3.44), or (b) by substituting $(1-B)\Omega$ for χ, and $\xi - s$ for $\hat{m}$ into Appendix III(A) eq(A3.12); B is represented by eq(3.40). Eq(3.58) can be obtained (a) by substituting $B\Omega$ for C, and $\xi - \hat{m}$ for s into eq(3.44), or (b) by substituting $(1-B)\Omega$ for χ, and $\xi - \hat{m}$ for s into Appendix III(A) eq(A3.12). Eq(3.57) can be derived from eq(3.58) by substituting $\xi - s$ for $\hat{m}$, and eq(3.58) can be derived from eq(3.57) by substituting $\xi - \hat{m}$ for s. The mutual derivations between the two equations reflect the fact that MB(o)[eq(3.57)] and MB(c)[eq(3.58)] are projections on (s, Ω) and $(\hat{m}, \Omega)$ planes, respectively.

In function F in eq(3.57), the reciprocal of the product by $1/(1/\kappa_o' + \kappa_o'')$ of integrand $\kappa''(s)$ in the first integral and the reciprocal of the product by $1/(1/\kappa_o' + \kappa_o'')$ of integrand $1/\kappa'(\hat{m})$ in the second integral contribute to increasing and decreasing width, Δ_o, of MB(o) with a lapse of proper time ξ, respectively (OPV). The parallel takes place with eq(3.58) with respect to MB(c) (CPV). There can therefore be three modes of migration of MB(o) or MB(c): (a) that where only compression of band takes place, (b) that where only expansion of band takes place, and (c) that where both compression and expansion of band take place. In some instances with the last mode, compression and expansion of band are repeated alternately.

When B tends to unity with increase in s, Δ_c tends to either a constant finite value or infinitesimal [see Section(F)], and CGM1st[eq(3.44)] coincides with MB(c)[eq(3.58)]; this is because the term $1/\kappa'(\hat{m}) + \kappa''(\xi - \hat{m})$ in eq(3.58) can be rewritten as $1/[\kappa'(\hat{m})B]$, and when $s \gg \hat{m}$, then $s \approx \xi$ [see eq(2.7)]. This means that, with any mode of migration of MB(o) or MB(c), Δ_o tends to either a constant finite value or infinitesimal finally when B tends to unity with increase in ξ. In parallel with this process, width Δ_c of the corresponding CGM1st[eq(3.44)] decreases monotonically, and width Δ_χ of the corresponding χGM1st [Appendix III(A) eq(A3.12)] increases monotonically. When Δ_o tends to a constant finite value, then Δ_χ approaches infinity. [*Proof.* Δ_c also tends to a constant finite value (equal to the Δ_o value), representing the "first case" with the behavior of CGM1st [see Section(F)]; this corresponds to the "second case" with the behavior of χGM1st when Δ_χ approaches infinity [see Appendix III(A)]. *Q.E.D.*] On the other hand, when Δ_o tends to infinitesimal, then Δ_χ tends to a constant finite value. [*Proof.* Δ_c also tends to infinitesimal (similarly to Δ_o), representing the "second case" with the behavior of CGM1st[Section(F)]; this corresponds to the "first case" with the behavior of χGM1st when Δ_χ tends to a constant finite value[Appendix III(A)]. *Q.E.D.*] When Δ_o, Δ_c and Δ_χ tend to constant values, the shape of MB(c) or MB(o), the shape of CGM1st and the shape of χGM1st tend to be constant, respectively.

When $\kappa''(s) = \kappa^{o''} = \kappa_o''$ and eq(3.28) into which κ_o'' is substituted for $\kappa^{o''}$ holds, then, due to eq(3.42), eq(3.57) reduces to eq(3.53), and eq(3.58) reduces to eq(3.54). When $\kappa'(\hat{m}) = \kappa^{o'} = \kappa_o'$ and eq(3.29) into which κ_o' is substituted for $\kappa^{o'}$ holds, then eq(3.57) reduces to eq(3.55), and eq(3.58) reduces to eq(3.56).

With the isocratic case when $\kappa'(\hat{m}) = \kappa'(\xi - s) = \kappa_o' = \kappa^{o\prime}$, $\kappa''(s) = \kappa''(\xi - \hat{m}) = \kappa_o'' = \kappa^{o\prime\prime}$, $B_o = B^o$ and $k_o = k^o$, eqs(3.57) and (3.58) coincide with eqs(2.16) and (2.18), respectively.

Summary. Table 3.1 summarises the behaviors of Δ_a, Δ_c and Δ_x for the usual case when the migration of MB(o) on the column accelerates and when the migration of MB(c) on the carrier liquid decelerates. If the migration of MB(o) decelerates and the migration of MB(c) accelerates, then the concepts of solid phase, liquid phase, OPV, CPV, CPV (OPV), OPV(CPV), OPV[CPV(OPV)] and CPV[OPV(CPV)] are exchanged for the concepts of liquid phase, solid phase, CPV, OPV, OPV(CPV), CPV(OPV), CPV[OPV(CPV)] and OPV[CPV(OPV)], respectively. Table 3.2 corresponds to Table 3.1, summarizing the case when the migration of MB(o) decelerates and when the migration of MB(c) accelertates.

In Appendix IV(A), some examples of the calculations of CGM1st[eqs(3.35), (3.39) and (3.44)] and the corresponding MB(o) and MB(c)[eqs(3.53)-(3.58)] are shown for step gradients.

(H) Chromatogram as Second Concept versus Molecular Band as Flux

On the basis of the molecular flux represented by eq(3.51) or by its solution, eq (3.53), (3.55) or (3.57), CGM2nd (as a function of ξ obtained at a given position s; OPV) can be derived.

Thus, *when only the gradient in the liquid phase is applied*, CGM2nd can be obtained by combining eq(3.53) with the relationship, $C = B'(\xi - s)\Omega$, as

$$C = \frac{(1-B_o)B'(\xi-s)}{1-B'(\xi-s)} F\left((1-B_o)\left[\xi - \int_0^{\xi-s} \frac{d\hat{m}}{1-B'(\hat{m})} \right] \right)$$

$$\left(= \frac{(1-B_o)B'(\xi-s)}{1-B'(\xi-s)} F\left((1-B_o)\left[s - \int_0^{\xi-s} \frac{B'(\hat{m})}{1-B'(\hat{m})} d\hat{m} \right] \right) \right) \qquad (3.59)$$

Eq(3.59) can also be derived by substituting $\xi - s$ for $\hat{m}$ into eq(3.35), or, to the contrary, eq(3.35) can be derived by substituting $\hat{m} + s$ for ξ into eq(3.59) [see the right-hand side in parentheses in eq(3.59)]. With the isocratic case when $B'(\hat{m}) = B'(\xi - s) = B_o = B^o$, eq(3.59) reduces to eq(2.37).

When only the gradient in the solid phase is applied, CGM2nd can be obtained by combining eq(3.55) with the relationship, $C = B''(s)\Omega$, as

$$C = B_o F\left(B_o\left[\int_0^{s} \frac{ds}{B''(s)} - \xi \right] \right)$$

Table 3.1

The behaviors of Δ_Q, Δ_C and Δ_x for the usual case when the migration of MB(o) on the column accelerates and when the migration of MB(c) on the carrier liquid decelerates. "c.d." implies chromatographic dilatation. $\overset{\searrow}{=}$ and $\overset{\nearrow}{=}$ imply that the left-hand sides of the equations decrease and increase monotonically to approach the limiting values involving infinity, respectively.

Gradient	CPV	CPV(OPV)	OPV	OPV(CPV)
liquid	$\lim_{\xi\to\infty} \Delta_Q \overset{\searrow}{=} 0$	$\lim_{s\to\infty}$ c.d. $\overset{\searrow}{=} 1$ $\lim_{s\to\infty} \Delta_C \overset{\searrow}{=} 0$	$\lim_{\xi\to\infty} \Delta_Q \overset{\searrow}{=} 0$	$\lim_{\hat{m}\to\infty}$ c.d. $\overset{\nearrow}{=} \infty$ Δ_x = const
solid	$\lim_{\xi\to\infty} \Delta_Q \overset{\nearrow}{=}$ finite	$\lim_{s\to\infty}$ c.d. $\overset{\searrow}{=} 1$ Δ_C = const	$\lim_{\xi\to\infty} \Delta_Q \overset{\nearrow}{=}$ finite	$\lim_{\hat{m}\to\infty}$ c.d. $\overset{\nearrow}{=} \infty$ $\lim_{\hat{m}\to\infty} \Delta_x \overset{\nearrow}{=} \infty$
liquid and solid	$\lim_{\xi\to\infty} \Delta_Q = \begin{cases} 0 \\ \text{finite} \end{cases}$	$\lim_{s\to\infty}$ c.d. $\overset{\searrow}{=} 1$ $\lim_{s\to\infty} \Delta_C \overset{\searrow}{=} \begin{cases} 0 \\ \text{finite} \end{cases}$	$\lim_{\xi\to\infty} \Delta_Q = \begin{cases} 0 \\ \text{finite} \end{cases}$	$\lim_{\hat{m}\to\infty}$ c.d. $\overset{\nearrow}{=} \infty$ $\lim_{\hat{m}\to\infty} \Delta_z \overset{\nearrow}{=} \begin{cases} \text{finite} \\ \infty \end{cases}$

Table 3.2

The behaviors of Δ_α, Δ_c and Δ_x for the case when the migration of MB(o) on the column decelerates and when the migration of MB(c) on the carrier liquid accelerates. For the symbols c.d., $\searrow =$ and $\nearrow =$, see Table 3.1.

Gradient	CPV	CPV(OPV)	OPV	OPV(CPV)
liquid	$\lim_{\xi\to\infty} \Delta_\alpha \nearrow =$ finite	$\lim_{s\to\infty}$ c.d. $\nearrow = \infty$ $\lim_{s\to\infty} \Delta_c \nearrow = \infty$	$\lim_{\xi\to\infty} \Delta_\alpha \nearrow =$ finite	$\lim_{\hat{m}\to\infty}$ c.d. $\searrow = 1$ Δ_x = const
solid	$\lim_{\xi\to\infty} \Delta_\alpha \searrow = 0$	$\lim_{s\to\infty}$ c.d. $\nearrow = \infty$ Δ_c = const	$\lim_{\xi\to\infty} \Delta_\alpha \searrow = 0$	$\lim_{\hat{m}\to\infty}$ c.d. $\searrow = 1$ $\lim_{\hat{m}\to\infty} \Delta_x \searrow = 0$
liquid and solid	$\lim_{\xi\to\infty} \Delta_\alpha = \begin{cases} 0 \\ \text{finite} \end{cases}$	$\lim_{s\to\infty}$ c.d. $\nearrow = \infty$ $\lim_{s\to\infty} \Delta_c = \begin{cases} \text{finite} \\ \infty \end{cases}$	$\lim_{\xi\to\infty} \Delta_\alpha = \begin{cases} 0 \\ \text{finite} \end{cases}$	$\lim_{\hat{m}\to\infty}$ c.d. $\searrow = 1$ $\lim_{\hat{m}\to\infty} \Delta_x = \begin{cases} 0 \\ \text{finite} \end{cases}$

$$\left(= B_0 F\left(B_0\left[\int_0^s \frac{1-B''(s)}{B''(s)} ds + s - \xi \right] \right) \right) \qquad (3.60)$$

Eq(3.60) can also be derived by substituting $\xi - s$ for $\hat{m}$ into eq(3.39), or, to the contrary, eq(3.39) can be derived by substituting $\hat{m} + s$ for ξ into eq(3.60) [see the right-hand side in parentheses in eq(3.60)]. With the isocratic case when $B''(s) = B_0 = B^\circ$, eq (3.60) reduces to eq(2.37).

Finally, *when both the gradient in the liquid phase and the gradient in the solid phase are applied at the same time,* CGM2nd can be obtained by combining eq(3.57) with the relationship, $C = B\Omega = \Omega/[1 + \kappa'(\xi - s)\kappa''(s)]$, as

$$C = \frac{1}{(1/\kappa_0' + \kappa_0'')\kappa'(\xi - s)} F\left(\frac{1}{1/\kappa_0' + \kappa_0''} \left[\int_0^s \kappa''(s) ds - \int_0^{\xi - s} \frac{d\hat{m}}{\kappa'(\hat{m})} \right] \right) \qquad (3.61)$$

Eq(3.61) can also be derived by substituting $\xi - s$ for $\hat{m}$ into eq(3.44), or, to the contrary, eq(3.44) can be derived by substituting $\hat{m} + s$ for ξ into eq(3.61). With the isocratic case when $\kappa'(\hat{m}) = \kappa'(\xi - s) = \kappa_0' = \kappa^{0\prime}$ and $\kappa''(s) = \kappa_0'' = \kappa^{0\prime\prime}$, eq(3.61) reduces to eq(2.37) [cf. eq(3.30)].

From the mutual derivations between eqs(3.35) and (3.59), those between eqs(3.39) and (3.60), and those between eqs(3.44) and (3.61), it can be understood that the shape of distribution in C as a function of ξ (CGM2nd) is identical with the shape of distribution in C as a function of $\hat{m}$ (CGM1st); the ξ values over which CGM2nd[eq(3.59), (3.60) or (3.61)] appears are larger by a constant value of s (representing the dead volume of the column) than the $\hat{m}$ values over which CGM1st[eq(3.35), (3.39) or (3.44)] appears.

With gradient chromatography, however, CGM1st (based on the set of variables $\hat{m}$ and s) is conceptually more fundamental than CGM2nd (based on the set of variables ξ and s) in the following sense. Thus, due to the fundamental mechanism of chromatography, the rate of migration of a sample molecule at any instant is a function of a set of properties m and ρ of the environment, whereas the set (m, ρ) is related directly to the set $(\hat{m}, s)$ through both eqs(3.1) and (3.2). [Especially with the case of linear gradients when $\phi(\hat{m}) = \hat{m}$ and $\phi(s) = s$, m and ρ coincide with $\hat{m}$ and s, respectively; $m_{in} = 0$.] This means that the rate of migration of a sample molecule at any instant is determined directly by the set of time $\hat{m}$ and position s on the column[OPV(CPV) leading to χGM1st] or the set of time s and position $\hat{m}$ on the carrier liquid[CPV(OPV) leading to CGM1st].

On the other hand, time $\hat{m}$ or s is related to proper time ξ in a complicated manner with gradient chromatography. Thus, the rates, $\hat{B}(\xi)$, of migration of molecules in a slice of MB(o) or MB(c) are different between different stages of development of chromatography [for the definition of "slice", see Chapter II(C)]. Moreover, the rates $\hat{B}(\xi)$

are different between different slices at any stage of development. This means that contraction of time[eq(3.47) or (3.48)] takes place differently not only between different stages of development of chromatography in a slice of MB(o) or MB(c) but also between different slices of MB(o) or MB(c) at any stage of development.

With the isocratic case, however, contraction of time[eq(2.29) or (2.30)] takes place uniformly not only between different stages of development of chromatography in a slice of MB(o) or MB(c) but also between different slices of MB(o) or MB(c) at any stage of development. In other words, time $\hat{m}$ or s is proportional to proper time ξ always. This enables us to consider simply that proper time ξ is an expression of time $\hat{m}$ or s with a different scale. In fact, by using eqs(2.29) and (2.30), eqs(2.23) and (2.25) can be rewritten as

$$\mathrm{div}_{\hat{m}}\ [(1-B^{\circ})C] + \partial C/\partial \xi = 0 \tag{3.62}$$

and

$$\mathrm{div}_{s}\ (B^{\circ}\chi) + \partial \chi/\partial \xi = 0 \tag{3.63}$$

respectively. Due to eqs(2.2) and (2.4), eqs(3.62) and (3.63) are identical with eqs(2.34) and (2.33), respectively.

Fig 3.4 summarizes the relationships among the equations representing CGM1st, CGM2nd, χGM1st, χGM2nd, MB(o) and MB(c). The pictures reflected in OPV, CPV (OPV) and OPV[CPV(OPV)] are symmetric with those reflected in CPV, OPV(CPV) and CPV[OPV(CPV)], respectively, except for two points. Thus, (a) similarly to the isocratic case, the initial molecular distribution takes place over positive coordinate values in OPV and negative coordinate values in CPV(OPV), whereas it takes place over negative coordinate values in CPV and positive coordinate values in OPV(CPV) [see Chapter II(F); cf. Fig 2.9]. (b) Usually, the migration of MB(o) on the column accelerates (OPV) and the migration of CGM1st on the carrier liquid decelerates [CPV(OPV)], whereas the migration of MB(c) on the carrier liquid decelerates (CPV) and the migration of χGM1st on the column accelerates [OPV(CPV)].

Important Consideration. Eq(3.51) can be re-expressed [with reference to Appendix III (A) eq(A3.2)] as

$$(\partial \Omega/\partial \xi)_{s} + (\partial C/\partial s)_{\xi} = 0 \tag{3.51'}$$

Eq(3.51') shows that a quantity Q exists fulfilling both

$$(\partial Q/\partial \xi)_{s} = C \tag{3.64}$$

and

$$(\partial Q/\partial s)_{\xi} = -\Omega \tag{3.65}$$

where Q has a physical meaning of total amount of sample molecules loaded on the col-

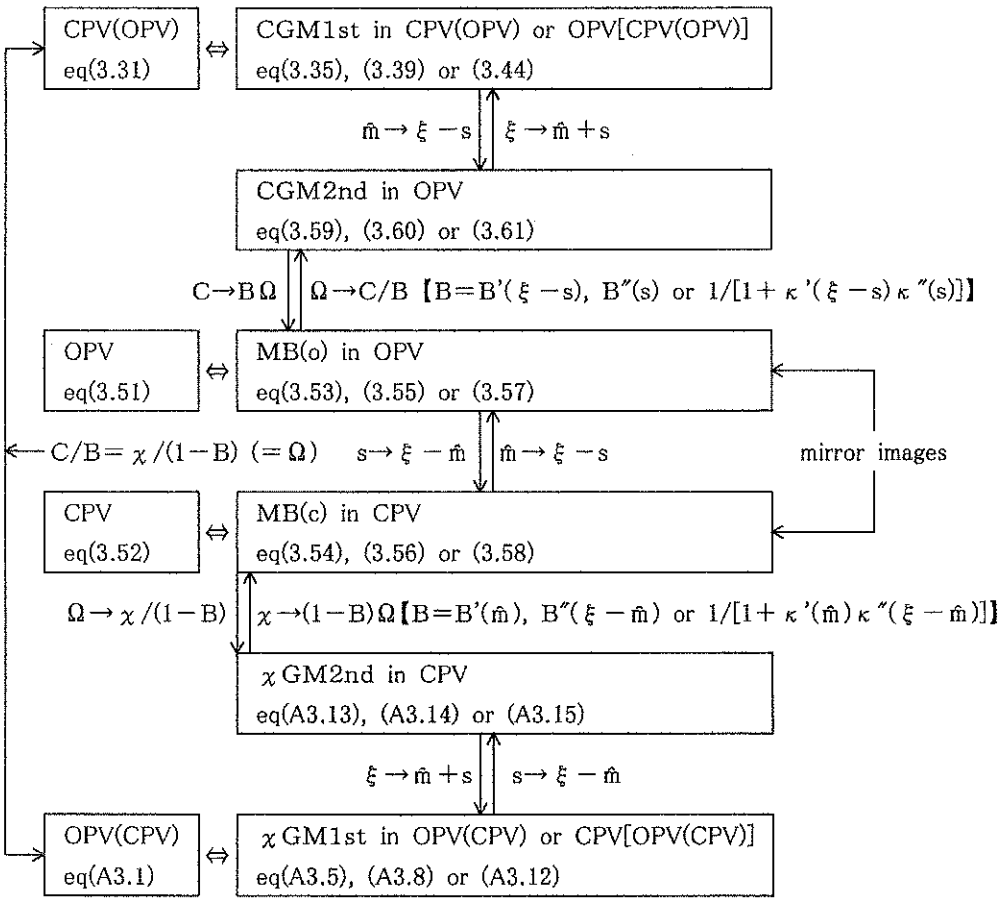


Fig 3.4. Relationships among the equations representing CGM1st, CGM2nd, χGM1st, χGM2nd, MB(o) and MB(c) with gradient chromatography.

umn. The pair of eqs(3.64) and (3.65) leads to

$$dQ = C d\xi - \Omega ds \tag{3.66}$$

As Q is constant ($dQ=0$), we obtain from eq(3.66):

$$C d\xi = \Omega ds \tag{3.67}$$

in which C is regarded as a function of ξ for a fixed value of s(CGM2nd), whereas Ω is regarded as a function of s for a fixed value of ξ [MB(o)]. Eq(3.67) shows that, when Ω[MB(o)] is conserved, then C(CGM2nd) is conserved and vice versa.

Appendix Ⅲ(B) eqs(A3.13)-(A3.15) represent the three kinds of χGM2nd corresponding to the three kinds of CGM2nd[eqs(3.59)-(3.61)], respectively. In parallel with the relationship between CGM1st and CGM2nd, χGM1st (based on the set of variables $\hat{m}$ and s) is conceptually more fundamental than χGM2nd (based on the set of variables ξ and $\hat{m}$) with gradient chromatography. Eq(3.52) can be re-expressed [with reference to Appendix Ⅲ(A) eq(A3.2)] as

$$(\partial \Omega / \partial \xi)_{\hat{m}} + (\partial \chi / \partial \hat{m})_{\xi} = 0 \tag{3.52'}$$

and, corresponding to eqs(3.64)-(3.67),

$$(\partial Q / \partial \xi)_{\hat{m}} = \chi \tag{3.68}$$

$$(\partial Q / \partial \hat{m})_{\xi} = -\Omega \tag{3.69}$$

$$dQ = \chi d\xi - \Omega d\hat{m} \tag{3.70}$$

and

$$\chi d\xi = \Omega d\hat{m} \tag{3.71}$$

are obtained. Eq(3.71) shows that, when Ω[MB(c)] is conserved, then χ(χGM2nd) is conserved and vice versa.

Both eqs(3.51') and (3.52') can be compared with the re-expression of either eq(3.31) or Appendix Ⅲ(A) eq(A3.1):

$$(\partial \chi / \partial \hat{m})_{s} + (\partial C / \partial s)_{\hat{m}} = 0 \tag{3.72}$$

and we now have

$$(\partial Q / \partial \hat{m})_{s} = C \tag{3.73}$$

$$(\partial Q / \partial s)_{\hat{m}} = -\chi \tag{3.74}$$

$$dQ = C d\hat{m} - \chi ds \tag{3.75}$$

and

$$C d\hat{m} = \chi ds \tag{3.76}$$

Eq(3.76) shows that, when χ (χGM1st) is conserved, then C(CGM1st) is conserved and vice versa.

Of course, eqs(3.67), (3.71) and (3.76) hold with isocratic chromatography. It should be noted, however, that it is only with ideal chromatography carried out in the absence of axial diffusion in the column that eqs(3.67), (3.71) and (3.76) hold precisely; these hold only approximately in the presence of axial diffusion (see the subsequent Chapter IV and V).

(I) The Case of Molecular Band with A Small Width

Chromatogran as First Concept. When both MB(o) and MB(c) have small widths, the corresponding FCB is peaked sharply. The projection of FCB on the ($\hat{m}$,s) plane is centered about point $\bar{P}$ on gradient G; point $\bar{P}$ draws trajectory T_0 on the ($\hat{m}$,s) plane following eq(3.6') [see Figs 3.1 and 3.3(a)]. In the corresponding abstract flux, B can be represented approximately as $\hat{B}(\hat{m}+s)$, and eq(3.31) can be rewritten as

$$\mathrm{div}_a \left(\frac{1-\hat{B}(\hat{m}+s)}{\hat{B}(\hat{m}+s)} C \right) + \frac{\partial C}{\partial s} = 0 \qquad (3.77)$$

in which function $\hat{B}(\hat{m}+s)$ fulfills either the equality between left- and right-hand sides of eq(3.17) combined with the equality between first and third terms in eq(3.16) (by using $\bar{\hat{m}}$ as intermediate parameter), or the equality between middle and right-hand side of eq (3.17) combined with the equality between first and last terms in eq(3.16) (by using $\bar{s}$ as intermediate parametetr); $\hat{m}_0=s_0=0$ in eq(3.16).

Eq(3.77) has a general solution:

$$C = B'(\bar{\hat{m}})F[-(\hat{m}-\bar{\hat{m}})] \qquad (3.78)$$

or

$$C = B''(\bar{s})F(s-\bar{s}) \qquad (3.78')$$

in which F represents any function provisionally; $\bar{\hat{m}}$ and $\bar{s}$ are defined implicitly as functions of $\hat{m}+s$ by the equality between first and third terms (where $\hat{m}_0=0$) and the equality between first and last terms (where $s_0=0$) in eq(3.16), respectively [see Appendix II(B)]. The identity between eqs(3.78) and (3.78') can be confirmed by using eq(3.17) and the equality between first and second (in parentheses) terms in eq(3.16).

Initially, point $\bar{P}$ stays at origin O(0,0) on the ($\hat{m}$,s) plane. With reference to both eq(3.17) and the relationship, $C=\hat{B}(\hat{m}+s)\Omega$, substituting $\bar{\hat{m}}=0$ and $\bar{s}=0$ into eqs (3.78) and (3.78') lead to eqs(2.17) and (2.15), respectively. This means that either eq (3.78) [combined with the equality between first and third terms in eq(3.16) where $\hat{m}_0=0$] or eq(3.78') [combined with the equality between first and last terms in eq(3.16) where $s_0=0$] represents CGM1st obtained when the initial MB(o) and MB(c) are represented by

eqs(2.15) and (2.17), respectively. With the isocratic case when $B'(\hat{m})=B''(s)=B^{\circ}$, both eqs(3.78) and (3.78') [combined with eq(3.16) where $B'(\hat{m})=B''(s)=B^{\circ}$] reduce to eq (2.20).

Appendix III(C) eqs(A3.16), (A3.17) and (A3.17') are concerned with χGM1st, corresponding to eqs(3.77), (3.78) and (3.78'), respectively.

With reference to Appendix III(A) eq(A3.2) into which $\hat{B}(\hat{m}+s)$ is substituted for B, and by using the relationship, $\partial \hat{B}(\hat{m}+s)/\partial \hat{m} = \partial \hat{B}(\hat{m}+s)/\partial s$, both eq(3.77) and Appendix III(C) eq(A3.16) can be re-expressed as

$$(\partial s/\partial \hat{m})_{\Omega} = -(\partial \Omega/\partial \hat{m})_{s}/(\partial \Omega/\partial s)_{\hat{m}} = \hat{B}(\hat{m}+s)/[1-\hat{B}(\hat{m}+s)] \qquad (3.79)$$

As will be mentioned in the subsequent subsection, the shape of either MB(o) or MB(c) is constant, and molecular density Ω in any slice of MB(o) or MB(c) is constant. Eq(3.79) therefore leads to eq(3.6').

Molecular Band as Flux. Eqs(3.51) and (3.52) can be rewritten as

$$\mathrm{div}_{s}\,[\hat{B}(\xi)\Omega] + \partial \Omega/\partial \xi = 0 \qquad (3.80)$$

and

$$\mathrm{div}_{\hat{m}}\,[[1-\hat{B}(\xi)]\Omega] + \partial \Omega/\partial \xi = 0 \qquad (3.81)$$

respectively, or both eq(3.77) and Appendix III(C) eq(A3.16) can be transformed to either eq(3.80) or (3.81). Eqs(3.80) and (3.81) have general solutions:

$$\Omega = F\left(s - \int_{0}^{\xi} \hat{B}(\xi)\mathrm{d}\xi \right) \qquad (3.82)$$

and

$$\Omega = F\left(-[\hat{m} - \int_{0}^{\xi} [1-\hat{B}(\xi)]\mathrm{d}\xi] \right) \qquad (3.83)$$

in which F represents any function, respectively [cf. Appendix II(A)]. Eq(3.83) can be derived from eq(3.82) by substituting $\xi - \hat{m}$ for s, and eq(3.82) can be derived from eq (3.83) by substituting $\xi - s$ for $\hat{m}$. It is possible to consider that eqs(3.82) and (3.83) represent solutions obtained under initial conditions given (when $\xi \to 0$) by eqs(2.15) and (2.17), respectively. Eqs(3.82) and (3.83) manifest that the shapes of MB(o) and MB(c) are constant, independent of ξ, respectively. With the isocratic case when $\hat{B}(\xi)=B^{\circ}$, eqs (3.82) and (3.83) reduce to eqs(2.16) and (2.18), respectively.

Eqs(3.80) and (3.81) can be re-expressed as

$$(\partial s/\partial \xi)_{\Omega} = -(\partial \Omega/\partial \xi)_{s}/(\partial \Omega/\partial s)_{\xi} = \hat{B}(\xi) \qquad (3.80')$$

and

$$(\partial \hat{m}/\partial \xi)_0 = -(\partial \Omega/\partial \xi)_0/(\partial \Omega/\partial \hat{m})_\xi = 1-\hat{B}(\xi) \qquad (3.81')$$

leading to eqs(3.45) and (3.46), respectively.

In Appendix Ⅳ(B), some examples of the calculations of CGM1st[eqs(3.78) or (3.78') combined with eq(3.16) in which $\hat{m}_0=s_0=0$, or eq(3.85)] and the corresponding MB(c)[eq (3.83)] are shown for step gradients.

Chromatogram as Second Concept. By combining eq(3.82) or (3.83) into which $\xi-s$ is substituted for $\hat{m}$ with $C=\hat{B}(\xi)\Omega$, CGM2nd (as a function of ξ for a given value of s):

$$C = \hat{B}(\xi)F\left(s - \int_0^{\xi} \hat{B}(\xi)d\xi\right) \qquad (3.84)$$

can be obtained. The equation derived by substituting $\hat{m}+s$ for ξ into eq(3.84):

$$C = \hat{B}(\hat{m}+s)F\left(s - \int_0^{\hat{m}+s} \hat{B}(\xi)d\xi\right)$$

$$= \hat{B}(\hat{m}+s)F\left(-[\hat{m} - \int_0^{\hat{m}+s} \{1-\hat{B}(\xi)\}d\xi]\right) \qquad (3.85)$$

is identical with either eq(3.78) [combined with the equality between first and third terms in eq(3.16) where $\hat{m}_0=0$] or eq(3.78') [combined with the equality between first and last terms in eq(3.16) where $s_0=0$], representing CGM1st. This is because, due to eq(3.17), the equality between first and last terms in eq(3.16) (where $s_0=0$) is equivalent with $\int_0^{\bar{t}} \hat{B}(\xi)d\xi = \bar{s}$; the equality between first and third terms in eq(3.16) (where $\hat{m}_0=0$) is equivalent with $\int_0^{\bar{t}} [1-\hat{B}(\xi)]d\xi = \bar{m}$. To the contrary, by substituting $\xi-s$ for $\hat{m}$ into eq(3.85), eq(3.84) can be derived. Eq(3.84) can also be represented as eq(3.78') combined with the equality between the first term (rewritten as ξ instead of $\hat{m}+s$) and the last term in eq(3.16) (where $s_0=0$). With the isocratic case when $\hat{B}(\xi)=B^0$, eq(3.84) reduces to eq(2.37).

The shape of distribution in C as a function of ξ [CGM2nd; eq(3.84)] is identical with the shape as a function of $\hat{m}$ [CGM1st; eq(3.85) i.e., either eq(3.78) or (3.78') combined with eq(3.16) in which $\hat{m}_0=s_0=0$]. The ξ values over which CGM2nd appears are larger by a constant value of s (representing the dead volume of the column) than the $\hat{m}$ values over which CGM1st appears.

Appendix Ⅲ(C) eqs(A3.18) and (A3.19) are concerned with χGM2nd and χGM1st, corresponding to eqs(3.84) and (3.85), respectively.

Fig 3.5 summarizes the relationships among the equations representing CGM1st,

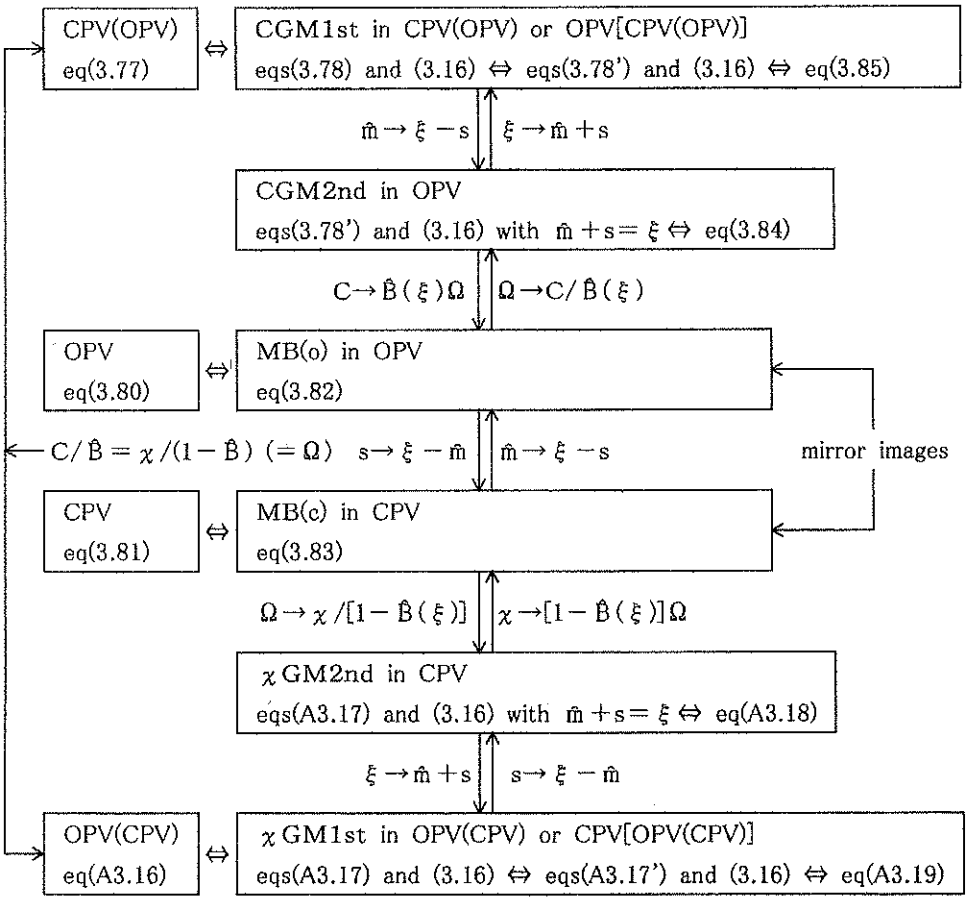


Fig 3.5. Relationships among the equations representing CGM1st, CGM2nd, χGM1st, χGM2nd, MB(o) and MB(c) with gradient chromatography when the width of MB is small.

CGM2nd, χGM1st, χGM2nd, MB(o) and MB(c). [Cf. both Figs 2.9 and 3.4.]

(J) Rewriting in Terms of Time η, Proper Time ξ, and Distance ζ

In addition to eqs(2.39)-(2.47), let us introduce the following symbols:

$$\left.\begin{array}{ll} v = B & [\text{when } (\eta,\zeta)=(\hat{m},s)] \\ v = 1-B & [\text{when } (\eta,\zeta)=(s,\hat{m})] \end{array}\right\} \tag{3.86}$$

$$\left.\begin{array}{ll} \hat{v}(\eta+\zeta) = \hat{B}(\hat{m}+s) & [\text{when } (\eta,\zeta)=(\hat{m},s)] \\ \hat{v}(\eta+\zeta) = 1-\hat{B}(\hat{m}+s) & [\text{when } (\eta,\zeta)=(s,\hat{m})] \end{array}\right\} \tag{3.87}$$

$$\left.\begin{array}{ll} v_o = B_o & [\text{when } (\eta,\zeta)=(\hat{m},s)] \\ v_o = 1-B_o & [\text{when } (\eta,\zeta)=(s,\hat{m})] \end{array}\right\} \tag{3.88}$$

$$\left.\begin{array}{ll} v'(\eta) = B'(\hat{m}) & [\text{when } (\eta,\zeta)=(\hat{m},s)] \\ v'(\eta) = 1-B''(s) & [\text{when } (\eta,\zeta)=(s,\hat{m})] \end{array}\right\} \tag{3.89}$$

$$\left.\begin{array}{ll} v''(\zeta) = B''(s) & [\text{when } (\eta,\zeta)=(\hat{m},s)] \\ v''(\zeta) = 1-B'(\hat{m}) & [\text{when } (\eta,\zeta)=(s,\hat{m})] \end{array}\right\} \tag{3.90}$$

$$\left.\begin{array}{ll} \hat{v}'(\eta) = \hat{B}'(\hat{m}) & [\text{when } (\eta,\zeta)=(\hat{m},s)] \\ \hat{v}'(\eta) = 1-\hat{B}'(s) & [\text{when } (\eta,\zeta)=(s,\hat{m})] \end{array}\right\} \tag{3.91}$$

$$\left.\begin{array}{ll} \hat{v}''(\zeta) = \hat{B}'(s) & [\text{when } (\eta,\zeta)=(\hat{m},s)] \\ \hat{v}''(\zeta) = 1-\hat{B}'(\hat{m}) & [\text{when } (\eta,\zeta)=(s,\hat{m})] \end{array}\right\} \tag{3.92}$$

$$\left.\begin{array}{ll} \dot{k} = k & [\text{when } (\eta,\zeta)=(\hat{m},s)] \\ \dot{k} = 1/k & [\text{when } (\eta,\zeta)=(s,\hat{m})] \end{array}\right\} \tag{3.93}$$

$$\left.\begin{array}{ll} \dot{k}^\circ = k^\circ & [\text{when } (\eta,\zeta)=(\hat{m},s)] \\ \dot{k}^\circ = 1/k^\circ & [\text{when } (\eta,\zeta)=(s,\hat{m})] \end{array}\right\} \tag{3.94}$$

$$\left.\begin{array}{ll} \dot{k}_\circ = k_\circ & [\text{when } (\eta,\zeta)=(\hat{m},s)] \\ \dot{k}_\circ = 1/k_\circ & [\text{when } (\eta,\zeta)=(s,\hat{m})] \end{array}\right\} \tag{3.95}$$

$$\left.\begin{array}{ll} \dot{k}'(\eta) = k'(\hat{m}) & [\text{when } (\eta,\zeta)=(\hat{m},s)] \\ \dot{k}'(\eta) = 1/k''(s) & [\text{when } (\eta,\zeta)=(s,\hat{m})] \end{array}\right\} \tag{3.96}$$

$$\left.\begin{array}{ll} \dot{k}''(\zeta) = k''(s) & [\text{when } (\eta,\zeta)=(\hat{m},s)] \\ \dot{k}''(\zeta) = 1/k'(\hat{m}) & [\text{when } (\eta,\zeta)=(s,\hat{m})] \end{array}\right\} \tag{3.97}$$

$$\left.\begin{array}{ll} \dot{\kappa}^{\circ\prime} = \kappa^{\circ\prime} & [\text{when } (\eta,\zeta)=(\hat{m},s)] \\ \dot{\kappa}^{\circ\prime} = 1/\kappa^{\circ\prime\prime} & [\text{when } (\eta,\zeta)=(s,\hat{m})] \end{array}\right\} \tag{3.98}$$

$$\left.\begin{array}{ll} \dot{\kappa}^{\circ\prime\prime} = \kappa^{\circ\prime\prime} & [\text{when } (\eta,\zeta)=(\hat{m},s)] \\ \dot{\kappa}^{\circ\prime\prime} = 1/\kappa^{\circ\prime} & [\text{when } (\eta,\zeta)=(s,\hat{m})] \end{array}\right\} \tag{3.99}$$

$$\left.\begin{aligned} \dot{\kappa}_{\circ}' &= \kappa_{\circ}' \quad [\text{when } (\eta,\zeta)=(\hat{m},s)] \\ \dot{\kappa}_{\circ}' &= 1/\kappa_{\circ}'' \quad [\text{when } (\eta,\zeta)=(s,\hat{m})] \end{aligned}\right\} \tag{3.100}$$

$$\left.\begin{aligned} \dot{\kappa}_{\circ}'' &= \kappa_{\circ}'' \quad [\text{when } (\eta,\zeta)=(\hat{m},s)] \\ \dot{\kappa}_{\circ}'' &= 1/\kappa_{\circ}' \quad [\text{when } (\eta,\zeta)=(s,\hat{m})] \end{aligned}\right\} \tag{3.101}$$

$$\left.\begin{aligned} \dot{\kappa}'(\eta) &= \kappa'(\hat{m}) \quad [\text{when } (\eta,\zeta)=(\hat{m},s)] \\ \dot{\kappa}'(\eta) &= 1/\kappa''(s) \quad [\text{when } (\eta,\zeta)=(s,\hat{m})] \end{aligned}\right\} \tag{3.102}$$

and

$$\left.\begin{aligned} \dot{\kappa}''(\zeta) &= \kappa''(s) \quad [\text{when } (\eta,\zeta)=(\hat{m},s)] \\ \dot{\kappa}''(\zeta) &= 1/\kappa'(\hat{m}) \quad [\text{when } (\eta,\zeta)=(s,\hat{m})] \end{aligned}\right\} \tag{3.103}$$

where v, $\dot{v}(\eta+\zeta)$, $v_{\circ}$, $v'(\eta)$, $v''(\zeta)$, $\dot{v}'(\eta)$ and $\dot{v}''(\zeta)$ are comprised between 0 and 1, and $\dot{k}$, $\dot{k}^{\circ}$, $\dot{k}_{\circ}$, $\dot{k}'(\eta)$, $\dot{k}''(\zeta)$, $\dot{\kappa}^{\circ'}$, $\dot{\kappa}^{\circ''}$, $\dot{\kappa}_{\circ}'$, $\dot{\kappa}_{\circ}''$, $\dot{\kappa}'(\eta)$ and $\dot{\kappa}''(\zeta)$ are comprised between 0 and ∞.

Eq(3.6'), both eqs(3.10) and (3.11), eq(3.15), both eqs(3.45) and (3.46), and both eqs (3.47) and (3.48), all representing trajectory $T_{\circ}$ or T, can be rewitten as

$$\frac{d\zeta}{d\eta} = \frac{\dot{v}(\eta+\zeta)}{1-\dot{v}(\eta+\zeta)} \tag{3.104}$$

either

$$\zeta \ (\text{or } \zeta-\zeta_{\circ}) = \int_{0\ (\text{or } \eta_{\circ})}^{\eta} \frac{v'(\eta)}{1-v'(\eta)}\,d\eta \tag{3.105}$$

or

$$\eta \ (\text{or } \eta-\eta_{\circ}) = \int_{0\ (\text{or } \zeta_{\circ})}^{\zeta} \frac{1-v''(\zeta)}{v''(\zeta)}\,d\zeta \tag{3.105'}$$

$$\xi = \eta+\zeta = \int_{0\ (\text{or } \eta_{\circ})}^{\eta} \frac{d\eta}{1-v'(\eta)} = \int_{0\ (\text{or } \zeta_{\circ})}^{\zeta} \frac{d\zeta}{v''(\zeta)} \tag{3.106}$$

$$d\zeta/d\xi = \dot{v}(\xi) \tag{3.107}$$

and

$$\zeta \ (\text{or } \zeta-\zeta_{\circ}) = \int_{0}^{\xi} \dot{v}(\xi)\,d\xi \tag{3.108}$$

respectively.

Both eqs(3.45) and (3.46) as interpreted to represent the relationship between time η and proper time ξ (contraction of time) can be rewritten as

$$d\eta/d\xi = 1-\hat{v}(\xi) \tag{3.109}$$

Both eqs(3.47) and (3.48), as interpreted to represent contraction of time, as

$$\eta \ (\text{or } \eta-\eta_0) = \int_0^{\xi} [1-\hat{v}(\xi)]d\xi \tag{3.110}$$

in which it usulally is considered that $\eta_0=0$.

Eqs(3.105), (3.105'), (3.106), (3.108) and (3.110) take place, conjugate to a closed circle of coordinate transformations:

$$\begin{array}{ccc} & (\xi,\zeta) & \\ \nearrow & & \searrow \\ (\eta,\xi) & \leftarrow & (\zeta,\eta) \end{array}$$

Thus, in eq(3.108), it is possible to consider that ξ is a function of ζ. It therefore is possible to consider that $\hat{v}$ is a function of ζ [$\hat{v}=v''(\zeta)$], and to write

$$\hat{v}(\xi) = \hat{v}[\xi(\zeta)] = v''(\zeta) \tag{3.111}$$

which leads to the equality between first and last terms in eq(3.106). By executing the coordinate transformation: $(\xi,\zeta)\rightarrow(\zeta,\eta)$, the equality between first and last terms in eq (3.106) becomes eq(3.105') in which it can be considered that ζ is a function of η. It therefore is possible to consider that v'' is a function of η [$v''=v'(\eta)$], and to write

$$v''(\zeta) = v''[\zeta(\eta)] = v'(\eta) \tag{3.112}$$

which leads to eq(3.105). By executing the coordinate transformation: $(\zeta,\eta)\rightarrow(\eta,\xi)$, eq (3.105) becomes the equality between first and third terms in eq(3.106) in which it can be considered that η is a function of ξ. It therefore is possible to consider that v' is a function of ξ [$v'=\hat{v}(\xi)$], and to write

$$v'(\eta) = v'[\eta(\xi)] = \hat{v}(\xi) \tag{3.113}$$

which leads to eq(3.110). By executing the coordinate transformation: $(\eta,\xi)\rightarrow(\xi,\zeta)$, eq (3.110) becomes eq(3.108).

Eq(3.16), both eqs(3.49) and (3.50), and both eqs(3.49') and (3.50'), all representing gradient G, can be rewritten as

$$\eta+\zeta \ (=\eta+\bar{\zeta}) = \int_{0\ (\text{or } \eta_0)}^{\bar{\eta}} \frac{d\bar{\eta}}{1-v'(\eta)} = \int_{0\ (\text{or } \zeta_0)}^{\bar{\zeta}} \frac{d\bar{\zeta}}{v''(\zeta)} \tag{3.114}$$

$$\xi \ (= \ \bar{\xi}) \ = \int_{0 \ (\text{or} \ \zeta_0)}^{\zeta} \frac{d\bar{\zeta}}{v''(\zeta)} \tag{3.115}$$

and

$$\zeta \ (\text{or} \ \bar{\zeta} - \zeta_0) \ = \int_{0}^{\xi} v(\xi) d\xi \tag{3.115'}$$

respectively.

Eq(3.17) can be rewritten as

$$v'(\eta) \ = \ v''(\zeta) \ = \ v(\eta + \zeta) \tag{3.116}$$

Both eqs(3.18) and (3.19) as either

$$d\eta \ = \ [1 - v'(\eta)](d\eta + d\zeta) \tag{3.117}$$

or

$$d\bar{\zeta} \ = \ v''(\bar{\zeta})(d\eta + d\zeta) \tag{3.117'}$$

Both eqs(3.20) and (3.21) as either

$$(\partial \eta / \partial \eta)_\zeta \ = \ (\partial \eta / \partial \zeta)_\eta \ = \ 1 - v'(\eta) \tag{3.118}$$

or

$$(\partial \bar{\zeta} / \partial \eta)_\zeta \ = \ (\partial \bar{\zeta} / \partial \zeta)_\eta \ = \ v''(\bar{\zeta}) \tag{3.118'}$$

Eqs(3.22) and (3.22') can be rewritten as

$$\dot{k} \ = \ (1 - v)/v \tag{3.119}$$

and

$$v \ = \ 1/(1 + \dot{k}) \tag{3.119'}$$

respectively. Both eqs(3.23) and (3.24) as either

$$\dot{k}'(\eta) \ = \ \frac{1 - v'(\eta)}{v'(\eta)} \tag{3.120}$$

or

$$\dot{k}''(\zeta) \ = \ \frac{1 - v''(\zeta)}{v''(\zeta)} \tag{3.120'}$$

Both eqs(3.32) and (3.36) as either

$$v = v'(\eta) = \frac{1}{1+\dot{k}'(\eta)} \tag{3.121}$$

or

$$v = v''(\zeta) = \frac{1}{1+\dot{k}''(\zeta)} \tag{3.121'}$$

Eq(3.40) as

$$v = \frac{1}{1+\dot{\kappa}'(\eta)\dot{\kappa}''(\zeta)} \tag{3.122}$$

Both eqs(3.26) and (3.27) as either

$$\dot{v}'(\eta) = \frac{1}{1+\dot{\kappa}'(\eta)} \tag{3.123}$$

or

$$\dot{v}''(\zeta) = \frac{1}{1+\dot{\kappa}''(\zeta)} \tag{3.123'}$$

Eq(3.25) as

$$\dot{k} = \dot{\kappa}'(\eta)\dot{\kappa}''(\zeta) \tag{3.124}$$

Both eqs(3.28) and (3.29) as either

$$\dot{k} = \dot{k}'(\eta) = \dot{\kappa}^{\circ\prime\prime}\dot{\kappa}'(\eta) \tag{3.125}$$

or

$$\dot{k} = \dot{k}''(\zeta) = \dot{\kappa}^{\circ\prime}\dot{\kappa}''(\zeta) \tag{3.125'}$$

Eqs(3.30) and (3.42) as

$$\dot{k}^{\circ}\ [= (1-v^{\circ})/v^{\circ}] = \dot{\kappa}^{\circ\prime}\dot{\kappa}^{\circ\prime\prime} \tag{3.126}$$

and

$$\dot{k}_{\circ}\ [= (1-v_{\circ})/v_{\circ}] = \dot{\kappa}_{\circ}'\dot{\kappa}_{\circ}'' \tag{3.127}$$

respectively.

Appendix Ⅲ(A) eq(A3.2) can be rewritten as

$$\Lambda = (1-v)\Omega \tag{3.128}$$

Both eq(3.31) and Appendix Ⅲ(A) eq(A3.1) can be rewritten as

$$\mathrm{div}_\zeta \left(\frac{v}{1-v} \Lambda \right) + \frac{\partial \Lambda}{\partial \eta} = 0 \tag{3.129}$$

Eqs(3.34), (3.38) and (3.43), and Appendix Ⅲ(A) eqs(A3.4), (A3.7) and (A3.11) as

$$\lim_{\eta \to 0} \Lambda = (1-v_o) f[(1-v_o)\zeta] \left(= \frac{\dot{k}_o}{1+\dot{k}_o} f\left(\frac{\dot{k}_o}{1+\dot{k}_o} \zeta \right) \right) \tag{3.130}$$

Both eq(3.35) and Appendix Ⅲ(A) eq(A3.8) as

$$\Lambda = \frac{v_o[1- v''(\zeta)]}{v''(\zeta)} f\left(v_o[\int_0^\zeta \frac{1- v''(\zeta)}{v''(\zeta)} d\zeta - \eta] \right)$$

$$\left(= \frac{\dot{k}''(\zeta)}{1+\dot{k}_o} f\left(\frac{1}{1+\dot{k}_o} [\int_0^\zeta \dot{k}''(\zeta) d\zeta - \eta] \right) \right) \tag{3.131}$$

Both eq(3.39) and Appendix Ⅲ(A) eq(A3.5) as

$$\Lambda = (1-v_o) f\left((1-v_o)[\zeta - \int_0^\eta \frac{v'(\eta)}{1-v'(\eta)} d\eta] \right)$$

$$\left(= \frac{\dot{k}_o}{1+\dot{k}_o} f\left(\frac{\dot{k}_o}{1+\dot{k}_o} [\zeta - \int_0^\eta \frac{d\eta}{\dot{k}'(\eta)}] \right) \right) \tag{3.132}$$

Both eq(3.44) and Appendix Ⅲ(A) eq(A3.12) as

$$\Lambda = \frac{\kappa''(\zeta)}{1/\kappa_o' + \kappa_o''} f\left(\frac{1}{1/\kappa_o' + \kappa_o''} [\int_0^\zeta \kappa''(\zeta) d\zeta - \int_0^\eta \frac{d\eta}{\kappa'(\eta)}] \right) \tag{3.133}$$

Both eqs(3.51) and (3.52) can be rewritten as

$$\mathrm{div}_\zeta (v\Omega) + \partial \Omega / \partial \xi = 0 \tag{3.134}$$

Both eqs(3.53) and (3.56) as

$$\Omega = \frac{1-v_o}{1-v'(\xi-\zeta)} f\left((1-v_o)[\xi - \int_0^{\xi-\zeta} \frac{d\eta}{1-v'(\eta)}] \right)$$

$$\left(= \frac{\dot{k}_o[1+\dot{k}'(\xi-\zeta)]}{(1+\dot{k}_o)\dot{k}'(\xi-\zeta)} f\left(\frac{\dot{k}_o}{1+\dot{k}_o} [\xi - \int_0^{\xi-\zeta} \frac{1+\dot{k}'(\eta)}{\dot{k}'(\eta)} d\eta] \right) \right) \tag{3.135}$$

Both eqs(3.54) and (3.55) as

$$\Omega = \frac{v_o}{v''(\zeta)} f\left(v_o[\int_0^{\zeta} \frac{d\zeta}{v''(\zeta)} - \xi] \right)$$

$$\left(= \frac{1+\dot{k}''(\zeta)}{1+\dot{k}_o} f\left(\frac{1}{1+\dot{k}_o}[\int_0^{\zeta} \{1+\dot{k}''(\zeta)\} d\zeta - \xi] \right) \right) \qquad (3.136)$$

Both eqs(3.57) and (3.58) as

$$\Omega = \frac{1}{1/\kappa_o' + \kappa_o''} \left(\frac{1}{\kappa'(\xi-\zeta)} + \kappa''(\zeta) \right) f\left(\frac{1}{1/\kappa_o' + \kappa_o''}[\int_0^{\zeta} \kappa''(\zeta) d\zeta - \int_0^{\xi-\zeta} \frac{d\eta}{\kappa'(\eta)}] \right) \qquad (3.137)$$

Both eq(3.59) and Appendix Ⅲ(B) eq(A3.14) can be rewritten as

$$\Lambda = \frac{v_o[1-v''(\xi-\eta)]}{v''(\xi-\eta)} f\left(v_o[\int_0^{\xi-\eta} \frac{d\zeta}{v''(\zeta)} - \xi] \right)$$

$$\left(= \frac{v_o[1-v''(\xi-\eta)]}{v''(\xi-\eta)} f\left(v_o[\int_0^{\xi-\eta} \frac{1-v''(\zeta)}{v''(\zeta)} d\zeta - \eta] \right) \right) \qquad (3.138)$$

Both eq(3.60) and Appendix Ⅲ(B) eq(A3.13) as

$$\Lambda = (1-v_o) f\left((1-v_o)[\xi - \int_0^{\eta} \frac{d\eta}{1-v'(\eta)}] \right)$$

$$\left(= (1-v_o) f\left((1-v_o)[\xi - \eta - \int_0^{\eta} \frac{v'(\eta)}{1-v'(\eta)} d\eta] \right) \right) \qquad (3.139)$$

Both eq(3.61) and Appendix Ⅲ(B) eq(A3.15) as

$$\Lambda = \frac{\kappa''(\xi-\eta)}{1/\kappa_o' + \kappa_o''} f\left(\frac{1}{1/\kappa_o' + \kappa_o''}[\int_0^{\xi-\eta} \kappa''(\zeta) d\zeta - \int_0^{\eta} \frac{d\eta}{\kappa'(\eta)}] \right) \qquad (3.140)$$

Exceptionally in eqs(3.138)-(3.140), η represents distance i.e., either the distance from origin O on the column (when $\eta = s$ and $v = 1-B$; OPV) or the distance from origin O on the carrier liquid (when $\eta = \hat{m}$ and $v = B$; CPV). By substituting ζ for η, $1-v'(\xi-\zeta)$ for $v''(\xi-\eta)$, $1-v'(\eta)$ for $v''(\zeta)$, $1-v''(\zeta)$ for $v'(\eta)$, $1-v_o$ for v_o, $1/\kappa'(\xi-$

ζ) for $\kappa''(\xi-\eta)$, $1/\kappa'(\eta)$ for $\kappa''(\zeta)$, $1/\kappa''(\zeta)$ for $\kappa'(\eta)$, $1/\kappa_o'$ for κ_o'', $1/\kappa_o''$ for κ_o', and f(−X) for f(X), then eqs(3.138)~(3.140) can be rewritten as

$$\Lambda = \frac{(1-v_o)v'(\xi-\zeta)}{1-v'(\xi-\zeta)} f\left((1-v_o)[\xi - \int_0^{\xi-\zeta} \frac{d\eta}{1-v'(\eta)}] \right) \tag{3.138'}$$

$$\Lambda = v_o f\left(v_o[\int_0^{\zeta} \frac{d\zeta}{v''(\zeta)} - \xi] \right) \tag{3.139'}$$

and

$$\Lambda = \frac{1}{(1/\kappa_o' + \kappa_o'')\kappa'(\xi-\zeta)} f\left(\frac{1}{1/\kappa_o' + \kappa_o''} [\int_0^{\zeta} \kappa''(\zeta)d\zeta - \int_0^{\xi-\zeta} \frac{d\eta}{\kappa'(\eta)}] \right) \tag{3.140'}$$

respectively.

Both eq(3.77) and Appendix Ⅲ(C) eq(A3.16) can be rewritten as

$$\mathrm{div}_\xi \left(\frac{\vartheta(\eta+\zeta)}{1-\vartheta(\eta+\zeta)} \Lambda \right) + \frac{\partial \Lambda}{\partial \eta} = 0 \tag{3.141}$$

Both eq(3.78) and Appendix Ⅲ(C) eq(A3.17') as

$$\Lambda = [1-v''(\bar{\zeta})]f(\zeta-\bar{\zeta}) \tag{3.142}$$

Both eq(3.78') and Appendix Ⅲ(C) eq(A3.17) as

$$\Lambda = [1-v'(\bar{\eta})]f[-(\eta-\bar{\eta})] \tag{3.142'}$$

Eq(3.79) as

$$(\partial\zeta/\partial\eta)_a = \vartheta(\eta+\zeta)/[1-\vartheta(\eta+\zeta)] \tag{3.141'}$$

Both eqs(3.80) and (3.81) as

$$\mathrm{div}_\xi [\vartheta(\xi)\Omega] + \partial\Omega/\partial\xi = 0 \tag{3.143}$$

Both eqs(3.82) and (3.83) as

$$\Omega = f\left(\zeta - \int_0^{\xi} \vartheta(\xi)d\xi \right) \tag{3.144}$$

Both eqs(3.80') and (3.81') as

$$(\partial\zeta/\partial\xi)_a = \vartheta(\xi) \tag{3.143'}$$

Both eqs(3.84) and Appendix Ⅲ(C) eq(A3.18) as

$$\Lambda = [1-\vartheta(\xi)]f\left(-[\eta - \int_0^{\xi} \{1-\vartheta(\xi)\}d\xi]\right) \tag{3.145}$$

Both eq(3.85) and Appendix Ⅲ(C) eq(A3.19) as

$$\Lambda = [1-\vartheta(\eta+\zeta)]f\left(-[\eta - \int_0^{\eta+\zeta} \{1-\vartheta(\xi)\}d\xi]\right)$$

$$= [1-\vartheta(\eta+\zeta)]\left(\zeta - \int_0^{\eta+\zeta} \vartheta(\xi)d\xi\right) \tag{3.146}$$

Exceptionally in eq(3.145), η represents distance i.e., either the distance from origin O on the column [when $\eta = s$ and $\vartheta(\xi) = 1-\hat{B}(\xi)$; OPV] or the distance from origin O on the carrier liquid [when $\eta = \hat{m}$ and $\vartheta(\xi) = \hat{B}(\xi)$; CPV]. By substituting ζ for η, $1-\vartheta(\xi)$ for $\vartheta(\xi)$, and f(−X) for f(X), then eq(3.145) can be rewritten as

$$\Lambda = \vartheta(\xi)f\left(\zeta - \int_0^{\xi} \vartheta(\xi)d\xi\right) \tag{3.145'}$$

Finally, both eqs(3.67) and (3.71) can be rewritten as

$$\Lambda d\xi = \Omega d\eta \tag{3.147}$$

in which η represents distance exceptionally again.

Chapter IV. Actual Isocratic Chromatography in the Presence of Axial Diffusion in the Column

(A) Axial Diffusion in the Column and Trajectory T_0

The argument in this Chapter is limited to quasi-static chromatography defined in Chapter I (A). Let us denote by B° both average C/Ω and average R_F taking place in MB(o) or MB(c), or both C/Ω and R_F taking place at the center of MB(o) or MB(c) if it is Gaussian in shape.

In the presence of axial diffusion in the column, we define trajectory T_0 only when MB(o) or MB(c) with a small width is formed initially at the inlet of the column (i.e., at origin O on the s or $\hat{m}$ coordinate axis) and when it spreads into a Gaussian distribution with its migration. Thus, trajectory T_0 is defined in this instance as trajectory drawn by the center of MB(o) or MB(c) on the $(\hat{m},s)$ plane. Trajectory T does not make appearance in the theory.

In the absence of axial diffusion in the column, molecular distribution C as a function of time $\hat{m}$ [CGM1st; OPV{CPV(OPV)}] or proper time ξ (CGM2nd; OPV) obtained at a given position s on the hypothetical column with infinite length (TPV) is identical with distribution C obtained by using a column with length s (EPV). In the presence of axial diffusion, the two distributions of C are identical only approximately due to border effects taking place at both ends (especially the outlet) of the actual column. It can be assumed, however, that the border effects are negligible because the two borders usually are partitioned off by filters; diffusion taking place in the column is continuous to diffusions taking place in the filters. These are continuous to those taking place in fine tubes connected to the filters.

It is only for convenience' sake that we take OPV, CPV(OPV) and OPV[CPV(OPV)] in this and the subsequent Chapter V. As far as isocratic chromatography is concerned, the quantities $\hat{m}$, s, ξ and $g'\Theta^\circ$ in any equation below can be replaced by V, L', Z and Θ° at the same time, respectively; the replacement will facilitate the intuitive understanding of the equation.

(B) Chromatogram as Second Concept

It would be possible to extend eq(2.33) to

$$\mathrm{div}_s\,(B^\circ\Omega - g'\Theta^\circ B^\circ \mathrm{grad}_s\,\Omega) + \partial\Omega/\partial\xi = 0 \qquad (4.1)$$

(OPV) in which $g'\Theta^\circ$ [with dimension of either marker concentration or wave length of absorption; see Chapter II (B)] represents the diffusion coefficient of sample molecules taking place in the liquid phase in the column, measured in the axial direction. The term $-g'\Theta^\circ B^\circ \mathrm{grad}_s\,\Omega$ in eq(4.1) manifests Fick's first law, where the factor B° is necessary because diffusion takes place only in the liquid phase (apparently). It should be noted that

chromatography is feasible in practice only when diffusion coefficient $g'\Theta^\circ$ is small enough for eq(3.67) to hold approximately. Eq(4.1) can be understood more intuitively if it is re-written as

$$\mathrm{div}_{L'}\ (B^\circ\Omega - \Theta^\circ B^\circ \mathrm{grad}_{L'}\ \Omega) + \partial\Omega/\partial Z = 0 \qquad (4.1')$$

in which Θ° (with dimensions of volume) now represents the diffusion coefficient.

When MB(o) represented by eq(2.15) is formed initially at the inlet of the column, the initial condition to eq(4.1) can be written as

$$\lim_{\xi \to 0} \Omega = F(s) \qquad (4.2)$$

Eqs(4.1) and (4.2) are identical with Appendix II(C) eqs(A2.17) and (A2.18), respectively, when r, t, Y, $\phi(t)$, $\phi(t)$ and Y_0 are substituted for s, ξ, Ω, B°, $g'\Theta^\circ B^\circ$ and F, respectively. Therefore, the solution of eq(4.1) obtained under condition given by eq(4.2) can be expressed by Appendix II(C) eq(A2.19) with substitutions as

$$\Omega = \int_{-\infty}^{\infty} F(s')G(s;\ B^\circ\xi + s',\ \sqrt{2g'\Theta^\circ B^\circ \xi})ds' \qquad (4.3)$$

representing MB(o) migrating on the column. When Θ° tends to infinitesimal, then eq(4.3) reduces to eq(2.16).

When MB(o) with a small width is formed initially, F(s) can be written as

$$F(s) = \delta(s) \qquad (4.4)$$

[cf. Appendix II(C) eq(A2.21)], and eq(4.3) reduces to

$$\Omega = G(s;\ B^\circ\xi,\ \sqrt{2g'\Theta^\circ B^\circ \xi}\ ) \qquad (4.5)$$

[cf. Appendix II(C) eq(A2.22)].

Let us calculate CGM2nd obtained when MB(o) with a small width is formed initially at the inlet of the column[eqs(4.2) and (4.4)]. This (i.e., distribution in C as a function of proper time ξ taking place at position s; OPV) can be calculated by combining eq(4.5) with eq(2.2) as

$$C = \frac{1}{\sqrt{4\pi g'\Theta^\circ \xi / B^\circ}} \exp\left(-\frac{(\xi - s/B^\circ)^2}{4g'\Theta^\circ \xi / B^\circ}\right) \qquad (4.6)$$

In eq(4.6), the term s/B° in the numerator in the exponential function represents proper time, $\hat{\xi}$, when the center of MB(o) passes through position s. Provided that $g'\Theta^\circ$ is small enough, however, the absolute value of the difference in proper times ξ taking

place when arbitrarily different slices of MB(o) pass through position s is much smaller than $\hat{\xi}$. Here, the slices of MB(o) with negligibly low density Ω are excluded from the argument, and it is assumed that s is large enough or that the column with large enough length is used (usual practice; EPV). (Unless the assumption holds, the consideration similar to that performed in Appendix V is necessary.) In eq(4.6), the term ξ (except that appearing in the numerator in the exponential function) can therefore be rewritten as

$$\xi \approx \hat{\xi} = s/B^{\circ} \tag{4.7}$$

Eq(4.6) (CGM2nd) can be rewritten approximately as

$$C = G[\xi\,;\ s/B^{\circ},\ \Delta^{\circ}(s;\ g')/B^{\circ}] \tag{4.8}$$

fulfilling

$$\lim_{s\to 0} C = \delta(\xi) \tag{4.9}$$

where

$$\Delta^{\circ}(s;\ g') = \sqrt{2g'\Theta^{\circ}s} \tag{4.10}$$

Both eqs(4.5) and (4.8) are almost compatible with eq(3.67) fulfilling:

$$\int_0^{\infty} Cd\xi \approx \int_{-\infty}^{\infty} Cd\xi \approx 1 = \int_{-\infty}^{\infty} \Omega ds \approx \int_0^{\infty} \Omega ds \tag{4.11}$$

It is possible to consider that $\Delta^{\circ}(s;\ g')$ [eq(4.10)] represents approximately the standard deviation, $\sqrt{2g'\Theta^{\circ}B^{\circ}\xi}$, of MB(o) [eq(4.5)]. In fact, the center, $\hat{s}$, of MB(o) can be represented as $B^{\circ}\xi$ [eq(4.5)], and when $g'\Theta^{\circ}$ is small enough, the difference in s values taking place in arbitrarily different slices of MB(o) is much smaller than the $\hat{s}$ value except for the slices with negligibly low density Ω; it is assumed that $\hat{s}$ is large enough or that the column with large enough length is used (see above). This means that the term $B^{\circ}\xi$ (i.e., $\hat{s}$) in standard deviation, $\sqrt{2g'\Theta^{\circ}B^{\circ}\xi}$, of MB(o) [eq(4.5)] can be replaced by s:

$$B^{\circ}\xi = \hat{s} \approx s \tag{4.12}$$

The variable s in the expression of $\Delta^{\circ}(s;\ g')$ as standard deviation of MB(o) [eq(4.10)] has a meaning of the coordinate at the center of MB(o) migrating on the column. The denominator, B°, of standard deviation, $\Delta^{\circ}(s;\ g')/B^{\circ}$, of CGM2nd[eq(4.8)] represents chromatographic dilatation. [The denominator, B°, of standard deviation of CGM1st[eq (4.15)] also represents chromatographic dilatation.]

For comparison with the argument on gradient chromatography which will be developed in the subsequent Chapter V(A), we here note that the relationship between left- and right-hand sides of either eq(4.7) or (4.12) can be rewritten as

$$\xi \ (= \hat{m} + s) \approx \frac{1-B^\circ}{B^\circ} s + s \tag{4.13}$$

Eq(4.13) can be interpreted to arise from the fact that marker concentration $\hat{m}$ [see Chapter II(B)] over which molecular distribution in Ω or C appears is almost uniform and that it is almost equal to marker concentration, $\hat{\mu} = (1-B^\circ)s/B^\circ$, taking place at the center of distribution in Ω or C. In fact, $\hat{m} = (1-B^\circ)s/B^\circ$ now represents trajectory T_0 drawn by the center of MB(o) and $\hat{m}$ can be replaced by $\hat{\mu}$.

Let us consider a convolution of eq(4.8):

$$C = \int_{-\infty}^{\infty} B^\circ F'(-B^\circ \xi')G[\xi;\ s/B^\circ + \xi',\ \Delta^\circ(s;\ g')/B^\circ]d\xi' \tag{4.14}$$

When Θ° tends to infinitesimal, then $\Delta^\circ(s;\ g')$ tends to infinitesimal[eq(4.10)], and eq (4.14) reduces to eq(2.37) in which F is replaced by function F'. For the interpretation on eq(4.14), see the subsequent Section(C).

(C) Derivation of Chromatogram as First Concept from Chromatogram as Second Concept

When MB(o) with a small width is formed initially at the inlet of the column[eqs(4.2) and (4.4)], CGM1st can be derived from CGM2nd[eq(4.8)] by substituting $\hat{m} + s$ for ξ [cf. Chapter II(F)]; this leads to

$$C = G\left(\hat{m};\ \frac{1-B^\circ}{B^\circ} s,\ \Delta^\circ(s;\ g')/B^\circ\right) \tag{4.15}$$

fulfilling

$$\lim_{s \to 0} C = \delta(\hat{m}) \tag{4.16}$$

Let us consider a convolution of eq(4.15):

$$C = \int_{-\infty}^{\infty} B^\circ F'(-B^\circ \hat{m}')G\left(\hat{m};\ \frac{1-B^\circ}{B^\circ} s + \hat{m}',\ \Delta^\circ(s;\ g')/B^\circ\right)d\hat{m}' \tag{4.17}$$

fulfilling

$$\lim_{s\to 0} C = B^{\circ}F'(-B^{\circ}\hat{m}) \tag{4.18}$$

Eq(4.18) represents a change in molecular density, C, of sample solution as a function of volume, $\hat{m}$, of injection, taking place immediately before the injection is effectuated at the inlet, s=0, of the column [OPV, EPV; cf. eq(2.24)]. Eq(4.17) represents CGM1st obtained under initial condition given by eq(4.18). When Θ° or $\Delta^{\circ}(s;\ g')$ tends to infinitesimal, eq(4.17) reduces to eq(2.20) in which function F is replaced by function F'. It should be noted that function F' appearing in both eqs(4.17) and (4.18), in general, is different from function F appearing in both eqs(4.2) and (4.3). F and F' coincide with one another either when both F and F' tend to a delta function[eq(4.4)] or in the absence of axial diffusion in the column when Θ° or $\Delta^{\circ}(s;\ g')$ tends to infinitesimal. It should also be noted that eq(4.14) represents CGM2nd obtained under initial condition given by eq(4.18) into which ξ is substituted for $\hat{m}$; eq(4.18) and eq(4.18) into which ξ is substituted for $\hat{m}$ are identical with one another [cf. Note 1 for eq(2.24) in Chapter II(E)].

Eqs(4.15) and (4.17) [cf. eq(4.10)] are identical with Appendix II(C) eqs(A2.22) and (A2.19), respectively, when r, r', t, Y, $\int_0^t \phi(t)dt$, $\sqrt{2\int_0^{t'} \phi(t)dt}$ and $Y_0(r')$ are substituted for $\hat{m}$, $\hat{m}'$, s, C, $(1-B^{\circ})s/B^{\circ}$, $\sqrt{2g'\Theta^{\circ}s}/B^{\circ}$ and $B^{\circ}F'(-B^{\circ}\hat{m}')$, respectively. Therefore, when considering both eqs(4.15) and (4.17) to represent abstract fluxes [CPV (OPV)], then the corresponding continuity equation can be expressed by using Appendix II(C) eq(A2.17) with substitutions; this leads to

$$\mathrm{div}_a\left(\frac{1-B^{\circ}}{B^{\circ}}C - \frac{g'\Theta^{\circ}}{B^{\circ 2}}\mathrm{grad}_a\ C\right) + \frac{\partial C}{\partial s} = 0 \tag{4.19}$$

which is an extension of eq(2.23).

Chapter V. Actual Gradient Chromatography in the Presence of Axial Diffusion in the Column

(A) Chromatogram as Second Concept

The argument in this Chapter is limited to quasi-static chromatography where diffusion coefficient Θ° or $g'\Theta^\circ$ can be replaced by a mean value taking place in the whole process of chromatography [see Chapter I (A)]. We consider the case when the migration of MB(o) is accelerated by any gradient, and, except when only the gradient in the solid phase is applied, we also limit ourselves to the case when MB(o) with a small width is formed initially at the inlet of the coplumn. As long as g' is fixed, the quantities $\hat{m}$, s, ξ, $g'\hat{\Theta}(\xi)$ and $g'\Theta(s)$ in any equation below can be replaced by V, L', Z, $\hat{\Theta}$ (as a function of Z) and Θ (as a function of L') at the same time, respectively. Let us denote by $\hat{B}(\xi)$ both average C/Ω and average R_F taking place at proper time ξ in MB(o) or MB(c), or both C/Ω and R_F taking place at the center of MB(o) or MB(c) if it is Gaussian in shape.

When the width of MB(o) is small enough, it would be possible to extend eq(3.80) to

$$\mathrm{div}_s\,[\hat{B}(\xi)\Omega - g'\hat{\Theta}(\xi)\hat{B}(\xi)\mathrm{grad}_s\,\Omega] + \partial\Omega/\partial\xi = 0 \qquad (5.1)$$

(OPV) in which $g'\hat{\Theta}(\xi)$ [with dimension of either marker concentration or wave length of absorption; see Chapter II (B)] or $\hat{\Theta}(\xi)$ (with dimensions of volume) represents a diffusion coefficient as a function of ξ [extension of diffusion coefficient $g'\Theta^\circ$ or Θ°; see eq(4.1) or (4.1')]. Molecular partitions, C/Ω or B, in the mobile phase taking place in different slices of MB(o) are different with gradient chromatography. In eq(5.1), however, C/Ω in any slice is replaced by average C/Ω or $\hat{B}(\xi)$, and the effect of non-uniform C/Ω is compensated by function $\hat{\Theta}(\xi)$. The derivation of the concrete form of function $\hat{\Theta}(\xi)$ or $\Theta(s)$[cf. eq(5.9)] will be performed in the subsequent Section(C). [Some comment on eq (5.1) is mentioned in the subsection entitled "Investigation of Pitt" in Appendix XI(B).]

When MB(o) with a small width is formed initially at the inlet of the column, the initial condition to eq(5.1) can be represented by both eqs(4.2) and (4.4) as

$$\lim_{\xi\to 0}\Omega = \delta(s) \qquad (5.2)$$

Under eq(5.2), eq(5.1) has a solution:

$$\Omega = G\left(s;\ \int_0^\xi \hat{B}(\xi)d\xi,\ \sqrt{2g'\int_0^\xi \hat{\Theta}(\xi)\hat{B}(\xi)d\xi}\right) \qquad (5.3)$$

representing MB(o) migrating on the column. [Eq(5.3) can be obtained by substituting s, ξ, Ω, $\hat{B}(\xi)$ and $g'\hat{\Theta}(\xi)\hat{B}(\xi)$ for r, t, Y, $\phi(t)$ and $\phi(t)$ into Appendix II(C) eq (A2.22), respectively. Cf. eq(5.1) with Appendix II(C) eq(A2.17).] With the isocratic case

when $\hat{B}(\xi)=B^{\circ}$ and $\hat{\Theta}(\xi)=\Theta^{\circ}$, eq(5.3) reduces to eq(4.5).

By combining eq(5.3) with the relationship, $C=\hat{B}(\xi)\Omega$ [cf. eq(2.2) or Appendix III eq(A3.2)], CGM2nd:

$$C = \frac{\hat{B}(\xi)}{\sqrt{4\pi g' \int_0^{\xi} \hat{\Theta}(\xi)\hat{B}(\xi)d\xi}} \exp\left[- \frac{\left(s - \int_0^{\xi} \hat{B}(\xi)d\xi \right)^2}{4g' \int_0^{\xi} \hat{\Theta}(\xi)\hat{B}(\xi)d\xi} \right] \quad (5.4)$$

can be calculated. Eq(5.4) can be compared with eq(4.6).

Eq(5.4) can be rewritten approximately as a Gauss function of ξ through the following three procedures. Thus, firstly, we rewrite the numerator outside the exponential function in the right-hand side of eq(5.4) as

$$\hat{B}(\xi) \approx \hat{B}(\hat{\xi}) = B''(s) \quad (5.5)$$

in which $\hat{\xi}$ represents proper time when the center of MB(o) passes through position s on the hypothetical column with infinite length (TPV); this is almost equal to proper time ξ when any slice of MB(o) passes through position s [cf. eq(4.7)], leading to the relationship between left-hand side and middle term in eq(5.5). On the other hand, $\hat{\xi}$ can be regarded as a function of s, leading to the equality between middle term and right-hand side in eq(5.5) [cf. eq(3.17)].

Secondly, we rewrite the term [ ] in the numerator inside the exponential function in eq(5.4) as

$$s - \int_0^{\xi} \hat{B}(\xi)d\xi \approx B''(s)\left(\int_0^{s} ds/B''(s) - \xi \right) \quad (5.6)$$

[*Proof of eq(5.6).* Eq(5.5) can be applied to $\hat{B}(\xi)$ in eq(5.6), leading to $\int_0^{\xi}\hat{B}(\xi)d\xi \approx \hat{B}(\hat{\xi})\xi = B''(s)\xi$. On the other hand, when regarding C as a function of s obtained for a given value of ξ, C represents a sharp peak, and the s value, $\hat{s}$, at the center of the peak is almost equal to that for any part of the peak, whereas $\hat{s}$ can be considered to be a function of ξ; this leads to $s=B''(\hat{s})s/B''(\hat{s}) = \hat{B}(\xi)\int_0^{\hat{s}} ds/B''(\hat{s}) \approx \hat{B}(\xi)\int_0^{s} ds/B''(s)$. By reconsidering C to be a function of ξ obtained for a given value of s, and applying eq(5.5) again, $s \approx B''(s)\int_0^{s} ds/B''(s)$ is obtained. This relationship and the previously obtained relationship, $\int_0^{\xi}\hat{B}(\xi)d\xi \approx B''(s)\xi$, lead to eq(5.6). *Q.E.D.*] By equalizing either side of eq(5.6) to zero, the equation representing trajectory T_0 can be obtained. Thus, equalizing to zero the left-hand side of eq(5.6) leads to eq(3.47) in which

$s_o=0$, whereas equalizing to zero the right-hand side of eq(5.6) leads to the equality between first an last terms in eq(3.15) in which $s_o=0$.

Lastly, when regarding C as a function of s obtained at a given proper time ξ (with respect to the center $s=\acute{s}$ of distribution C, being almost equal to the proper time with respect to any part of distribution C), then marker concentration $\hat{m}$ [Chapter II (B)] over which distribution C appears is almost uniform, almost equal to concentration, μ, at the center of distribution. As μ can be considered to be a function of s, ξ in function $\hat{\Theta}(\xi)$ in eq(5.4) can be represented approximately as

$$\xi = \hat{m} + s \approx \mu(s) + s \tag{5.7}$$

[cf. eq(4.13)]; this, with reference to eq(3.11), leads to:

$$d\xi \approx (d\mu/ds+1)ds = \left(\frac{1-B''(s)}{B''(s)} + 1\right)ds = ds/B''(s) \tag{5.8}$$

Let us define $\Theta(s)$ as

$$\Theta(s) \equiv \hat{\Theta}[\mu(s)+s] \approx \hat{\Theta}(\xi) \tag{5.9}$$

When regarding C as a function of ξ obtained for a given value of s, eq(5.5) can be applied to $\hat{B}(\xi)$ appearing in the integrals in the denoninators both inside and outside the exponential function in eq(5.4). With references to eqs(5.5), (5.8) and (5.9), and taking into account the fact that, at proper time $\xi=0$, distribution C (with infinitesimal width) is centered at the inlet, $s=0$, of the column, the integrals under consideration can be rewritten as

$$\int_0^{\xi} \hat{\Theta}(\xi)\hat{B}(\xi)d\xi \approx \int_0^{s} \Theta(s)B''(s)ds/B''(s) = \int_0^{s} \Theta(s)ds \tag{5.10}$$

By using eqs(5.5), (5.6) and (5.10), eq(5.4) (CGM2nd) can be rewritten as

$$C = G\left(\xi; \int_0^{s} ds/B''(s),\ \Delta(s;\ g')/B''(s)\right) \tag{5.11}$$

in which

$$\Delta(s;\ g') = \sqrt{2g'\int_0^{s} \Theta(s)ds} \tag{5.12}$$

Eq(5.11) fulfills eq(4.9). Both eqs(5.3) and (5.11) are almost compatible with eq(3.67) ful-

filling eq(4.11). With the isocratic case when $B''(s)=B^{\circ}$ and $\Theta(s)=\Theta^{\circ}$, eqs(5.11) and (5.12) reduce to eqs(4.8) and (4.10), respectively.

From eq(5.10) it is evident that $\Delta(s;\ g')$ [eq(5.12] represents approximately, the standard deviation, $\sqrt{2g'\int_{\hat{\xi}}\hat{\Theta}(\xi)\hat{B}(\xi)d\xi}$, of MB(o)[eq(5.3)]. The variable s in the espression of $\Delta(s;\ g')$ as standard deviation of MB(o)[eq(5.3)] has a meaning of the coordinate at the center of MB(o) migrating on the column. The denomonator, $B''(s)$, of standard deiation, $\Delta(s;\ g')/B''(s)$, of CGM2nd[eq(5.11)] represents chromatographic dilatation. [The denominator, $B''(s)$ or $B'[\mu(s)]$, of standard deviation of CGM1st[eq(5.14) or (5.14')] also represents chromatographic dilatation.]

The convolution of eq(5.11):

$$C=\int_{-\infty}^{\infty}B_{\circ}F'(-B_{\circ}\xi')G\left(\xi;\int_{0}^{s}ds/B''(s)+\xi',\ \Delta(s;\ g')/B''(s)\right)d\xi' \qquad (5.13)$$

reduces to eq(3.60) in which function F is replaced by function F' when $\Theta(s)$ or $\Delta(s;\ g')$ tends to infinitesimal [see eq(5.12)]. With the isocratic case when $B''(s)=B_{\circ}=B^{\circ}$ and $\Theta(s)=\Theta^{\circ}$, eq(5.13) reduces to eq(4.14). For the interpretation on eq(5.13), see the subsequent Section(B).

(B) Derivation of Chromatogram as First Concept from Chromatogram as Second Concept

When MB(o) with a small width is formed initially at the inlet of the column [eq(5.2], CGM1st can be be derived from CGM2nd[eq(5.11)] by substituting $\hat{m}+s$ for ξ [cf. Chapter Ⅲ(H)]; this leads to

$$C=G\left(\hat{m};\int_{0}^{s}\frac{1-B''(s)}{B''(s)}ds,\ \Delta(s;\ g')/B''(s)\right) \qquad (5.14)$$

fulfilling eq(4.16). [Some arguments on eq(5.14) or (5.14') in connection with eq(4.16) are performed in Appendix V.] As we consider the case when molecular partition in the liquid phase taking place in any slice of MB(o) is almost equal to that taking place at the center of MB(o), the relationship: $B''(s)=B'(\hat{m})\approx B'[\mu(s)]$ is fulfilled, and eq(5.14) can be rewritten as

$$C=G[\ \hat{m};\ \mu(s),\ \Delta(s;\ g')/B'\{\mu(s)\}\ ] \qquad (5.14')$$

in which

$$\hat{\mu}(s) = \int_0^s \frac{1-B''(s)}{B''(s)}\,ds \tag{5.15}$$

or

$$s = \int_0^{\hat{\mu}} \frac{B'(\hat{m})}{1-B'(\hat{m})}\,d\hat{m} \tag{5.15'}$$

Eq(5.15) or (5.15') into which $\hat{m}$ is substituted for $\hat{\mu}$ represents trajectory T_0 [cf. eqs (3.10) and (3.11)].

Let us consider a convolution of eq(5.14):

$$C = \int_{-\infty}^{\infty} B_0 F'(-B_0\hat{m}')G\left(\hat{m};\ \int_0^s \frac{1-B''(s)}{B''(s)}\,ds + \hat{m}',\ \Delta(s;\ g')/B''(s)\right)d\hat{m}' \tag{5.16}$$

fulfilling eq(4.18). Eq(5.16) appears to represent CGM1st obtained under initial condition given by eq(4.18). When $\Theta(s)$ or $\Delta(s;\ g')$ tends to infinitesimal, however, eq(5.16) reduces to eq(3.39) in which function F is replaced by function F'; F and F' coincide with one another at this limit. This means that eq(5.16) is valid only when the gradient in the solid phase is applied, representing CGM1st. With the isocratic case when $B''(s)=B_0=B^\circ$ and $\Theta(s)=\Theta^\circ$, eq(5.14) [or (5.14')] and eq(5.16) reduce to eqs(4.15) and (4.17), respectively. [Eq(5.13) represents CGM2nd corresponding to CGM1st represented by eq(5.16), obtained under initial condition given by eq(4.18) into which ξ is substituted for $\hat{m}$; eq (4.18) and eq(4.18) into which ξ is substituted for $\hat{m}$ are identical with one another.]

Eqs(5.14) and (5.16) [cf. eq(5.12)] are identical with Appendix II(C) eqs(A2.22) and (A2.19), respectively, when r, r', t, Y, $\int_0^t \phi(t)dt$, $\sqrt{2\int_0^t \phi(t)dt}$ and $Y_0(r')$ are substituted for $\hat{m}$, $\hat{m}'$, s, C, $\int_0^s [1-B''(s)]ds/B''(s)$, $\sqrt{2g'\int_0^s \Theta(s)ds}\,/B''(s)$ and $B^\circ F'(-B^\circ\hat{m}')$, respectively. Therefore, when considering both eqs(5.14) and (5.16) to represent abstract fluxes [CPV(OPV)], then the corresponding continuity equation can be expressed by using Appendix II(C) eq(A2.17) with substitution; this leads to

$$\mathrm{div}_{\hat{m}}\left(\frac{1-B''(s)}{B''(s)}C - g'\frac{d}{ds}\left\{\frac{1}{[B''(s)]^2}\int_0^s \Theta(s)ds\right\}\mathrm{grad}_{\hat{m}}\,C\right) + \frac{\partial C}{\partial s} = 0 \tag{5.17}$$

When only the gradient in the solid phase is applied, eq(5.17) is valid in general. When the gradient in the liquid phase is applied, eq(5.17) is valid only when MB(o) with a small

width is formed initially, despite whether or not the gradient in the solid phase is applied at the same time. The general argument for the case when the gradient in the liquid phase is applied is beyond the scope of the present treatment based on the partial differential equation of the type of Appendix II(C) eq(A2.17) or (A2.17'). With the isocratic case, eq(5.17) reduces to eq(4.19).

(C) Concrete Form of Function $\Theta(s)$ or $\Xi(s) \equiv \Theta(s)/\Theta^{\circ}$: Balance between Axial Diffusion and Compression/Expansion of Band

In general, axial diffusion in the column contributes to increasing standard deviation of MB(o) with its migration (OPV). On the other hand, with gradient chromatography, the migration of MB(o) accelerates only in condition that the rates of migration of different slices of MB(o) are different, provided that there is no axial diffusion. Thus, when only the gradient in the liquid phase is applied, the rate of migration of the slice decreases when going from rear to front of MB(o), inducing the decrease of standard deviation of MB(o) in the absence of axial diffusion [compression of band; see left part of Appendix IV (A) Fig A4.2(c)]. When only the gradient in the solid phase is applied, the reverse takes place i.e., the rate of migration of the slice increases when going from rear to front of MB(o), inducing the increase of standard deviation of MB(o) in the absence of axial diffusion [expansion of band; see left part of Appendix IV(A) Fig A4.3(c)]. It would be reasonable to consider that the rate of increase (or decrease) of standard deviation of MB(o) can be represented approximately as a sum of two quantities. The first quantity represents the rate of increase due to diffusion taking place, provided that there is no effect of the gradient. The second quantity represents the rate of decrease (with negative value) or the rate of increase (with positive value) taking place, provided that there is no axial diffusion in the column.

On the basis of these considerations, we calculate below the concrete form of function $\Delta(s; g')$ *as standard deviation of MB(o)*; $\Theta(s)$ or $\Xi(s) \equiv \Theta(s)/\Theta^{\circ}$ can be calculated by using eq(5.12). It should be noted, however, that the variable s in the expression of $\Delta(s; g')$ [eq(5.12)] or $\Delta^{\circ}(s; g')$ [eq(4.10)] indicates the coordinate at the center of MB (o) migrating on the column, while standard deviation $\Delta(s; g')$ or $\Delta^{\circ}(s; g')$, of MB(o) is extending over s values as current coordinates on the column. In order to avoid the confusion between the two meanings of s, let us consider that $\Delta(s; g')$ or $\Delta^{\circ}(s; g')$ represents standard deviation of the coresponding MB(c) taking place on the carrier liquid when the coordinate at the center of MB(o) on the column is s; standard deviation of MB(c) is equal to that of MB(o).

It is possible to consider that s is a function of proper time ξ, representing trajectory T_0 mapped to the (ξ, s) plane [eq(3.45) or eq(3.47) in whivh $s_0=0$]; s tends to zero when ξ tends to zero. $\Delta(s; g')$ therefore fulfills

$$\lim_{\xi \to 0} \Delta(s;\ g') = \lim_{s \to 0} \Delta(s;\ g') = 0 \tag{5.18}$$

$\Delta(s;\ g')$ can now be represented as a solution of the following differential equation obtained under initial condition given by eq(5.18):

$$\frac{d\Delta(s;\ g')}{d\xi} = \frac{d\Delta^{\circ}(s;\ g')}{d\xi} - \frac{B'[\mu(s)+\Delta(s;\ g')]-B'[\mu(s)-\Delta(s;\ g')]}{2} \tag{5.19}$$

in which $\mu(s)$ represents marker concentration[Chapter II(B)] at the center of MB(c) which corresponds to the center of MB(o), and $\mu(s)+\Delta(s;\ g')$ and $\mu(s)-\Delta(s;\ g')$ represent those at front and rear borders of twice the standard deviation of MB(c) which correspond to rear and front borders of twice the standard deviation of MB(o), respectively. $\mu(s)$ fulfills

$$\frac{d\mu}{ds} = \frac{1-B'[\mu(s)]}{B'[\mu(s)]} \tag{5.20}$$

which can be derived from eq(5.15').

The left-hand side and the first term of the right-hand side of eq(5.19) can be rewritten as

$$\frac{d\Delta(s;\ g')}{d\xi} = \frac{d\Delta(s;\ g')}{ds} \cdot \frac{ds}{d\xi} \tag{5.21}$$

and

$$\frac{d\Delta^{\circ}(s;\ g')}{d\xi} = \frac{d\Delta^{\circ}(s;\ g')}{ds} \cdot \frac{ds}{d\xi} \tag{5.22}$$

respectively, and eq(3.45) can be rewritten as

$$ds/d\xi = B'[\mu(s)] \tag{5.23}$$

By using eqs(5.21)-(5.23), eqs(5.19) can be rewritten as

$$\frac{d\Delta(s;\ g')}{ds} = \frac{d\Delta^{\circ}(s;\ g')}{ds} - \frac{B'[\mu(s)+\Delta(s;\ g')]-B'[\mu(s)-\Delta(s;\ g')]}{2B'[\mu(s)]} \tag{5.19'}$$

On the other hand, as

$$\frac{d\Delta^{\circ}(s;\ g')}{ds} = \sqrt{\frac{g'\Theta^{\circ}}{2}} \cdot \frac{1}{\sqrt{s}} \tag{5.24}$$

[see eq(4.10)] and

$$\frac{B'[\mu(s)+\Delta(s;\ g')]-B'[\mu(s)-\Delta(s;\ g')]}{2B'[\mu(s)]} \approx \frac{dB'[\mu(s)]/d\mu(s)}{B'[\mu(s)]}\Delta(s;\ g') \qquad (5.25)$$

then eq(5.19') becomes

$$\frac{d\Delta(s;\ g')}{ds} + \frac{dB'[\mu(s)]/d\mu(s)}{B'[\mu(s)]}\Delta(s;\ g') = \sqrt{\frac{g'\Theta^\circ}{2}}\cdot\frac{1}{\sqrt{s}} \qquad (5.26)$$

which is a linear differential equation of the first order with respect to $\Delta(s;\ g')$.

Under initial condition given by eq(5.18), eq(5.26) combined with eq(5.20) has a solution:

$$\Delta(s;\ g') = \sqrt{\frac{g'\Theta^\circ}{2}}\ [1-B'\{\mu(s)\}]\int_0^s \frac{ds}{[1-B'\{\mu(s)\}]\sqrt{s}} \qquad (5.27)$$

[see Appendix II(D)], determining function $\Delta(s;\ g')$ which can now be re-interpreted to represent standard deviation of MB(o). With the isocratic case when $B'[\mu(s)]=B^\circ$, eq (5.27) coincides with eq(4.10).

By substituting eq(5.27) into eq(5.12) and performing some calculations, function $\Xi(s)$ can be determined as

$$\Xi(s) \equiv \Theta(s)/\Theta^\circ$$

$$= \frac{1-B'[\mu(s)]}{2}\left(\int_0^s \frac{ds}{[1-B'\{\mu(s)\}]\sqrt{s}}\right)\cdot\left(\frac{1}{\sqrt{s}} - \frac{dB'}{d\mu}\cdot\frac{d\mu}{ds}\right.$$

$$\left.\cdot\int_0^s \frac{ds}{[1-B'\{\mu(s)\}]\sqrt{s}}\right) \qquad (5.28)$$

With the isocratic case when $B'[\mu(s)]=B^\circ$, eq(5.28) reduces to

$$\Xi(s) = 1 \qquad (5.29)$$

When interpreting function $\Delta(s;\ g')$ to represent part of standard deviation, $\Delta(s;\ g')/B'[\mu(s)]$, of CGM1st[eq(5.14')], the term $B'[\mu(s)]$ in eq(5.27) can be replaced by $B''(s)$ because molecular partition in the liquid phase taking place at the center of MB(o) is almost equal to that taking place in any slice of MB(o) [Section(B)]. Eq(5.27) can be re-written as

$$\Delta(s;\ g') = \sqrt{\frac{g'\Theta^{\circ}}{2}}\ [1-B''(s)]\int_0^s \frac{ds}{[1-B''(s)]\sqrt{s}} \qquad (5.27')$$

Eq(5.27') applies to $\Delta(s;\ g')$ in eq(5.14), whereas eq(5.27) applies to $\Delta(s;\ g')$ in eq (5.14').

When only the gradient in the liquid phase is applied, function $B'(\hat{m})$ or $k'(\hat{m})$ [see eq(3.32)] is given previously, and function $\hat{\mu}(s)$ can be calculated by using eq(5.15'). CGM1st can be represented concretely by eq(5.14') combined with both eqs(5.15') and (5.27). When only the gradient in the solid phase is applied, function $B''(s)$ or $k''(s)$ [see eq(3.36)] is given previously. CGM1st can be represented concretely by eq(5.14) or (5.16) combined with eq(5.27'). When both the gradient in the liquid phase and the gradient in the solid phase are applied at the same time, both functions $\kappa'(\hat{m})$ and $\kappa''(s)$, or function B [see eq(3.40)] is given previously. Function $\hat{\mu}(s)$ can be calculated as a solution, $\hat{m} = \hat{\mu}(s)$, of eq(3.6') into which B or $1/[1+\kappa'(\hat{m})\kappa''(s)]$ [eq(3.40)] is substituted for $\hat{B}(\hat{m}+s)$, obtained under initial condition given by $\hat{m}=s=0$; the solution, $\hat{m} = \hat{\mu}(s)$, can be re-expressed as eq(3.4). By substituting the solution, $\hat{m} = \hat{\mu}(s)$, into eq(3.40), B as a function of s can be obtained; this is $B''(s)$. CGM1st can be represented concretely by eq(5.14) combined with eq(5.27').

Chapter VI. Theory of Concentration Gradient Chromatography Combined with Competition Model

(A) Conclusion on the Theory of Concentration Gradient Chromatography

Below is summarized the conclusion for the usual case with gradient chromatography when only the gradient in the liquid phase (i.e., the concentration gradient) is applied and when MB(o) with a small width is formed initially at the inlet of the column.

Thus, CGM1st as a function of reduced elution volume, $\hat{m}$, obtained by using a column with reduced length, s, can be represented by eq(5.14') as

$$C = G[\hat{m};\ \mu(s),\ \sigma(s;\ g')] \tag{6.1}$$

in which s and $\hat{m}$ are represented by eqs(2.5) and (2.6) as

$$s = g'L' = gL \tag{6.2}$$

and

$$\hat{m} = g'V = gV^{\#} \tag{6.3}$$

respectively. The physical meanings of the symbols in both eqs(6.2) and (6.3) are: L'(with dimensions of volume)=total length of the column used, expressed as a sum of interstitial volumes in the column; L(with dimension of length)=total length of the column used; V (with dimensions of volume)=elution volume; $V^{\#}$(with dimension of length)=elution volume taking place, provided that the column with unit interstitial volume per unit length (i.e., the column with the parameter γ with unit value; see below) is used; g'(with dimension of concentration/volume)=mean slope or steepness of the concentration gradient applied; and g(with dimension of concentration/length)=mean slope or steepness of the concentration gradient applied, measured along the main axis of the column. L, $V^{\#}$ and g are related to L', V and g' by

$$L = L'/\gamma \tag{6.4}$$

$$V^{\#} = V/\gamma \tag{6.5}$$

and

$$g = \gamma g' \tag{6.6}$$

respectively, where γ (with dimensions of area) represents the mean value of the interstitial volume per unit length of the column or the effective area of the column section; this fluctuates microscopically along the main axis of the column, contributing to bringing about random heterogeneity of the flow of the carrier liquid which gives rise to axial molecular diffusion in the column [see Chapter I (A)]. It should be noted that the second definition of variable s and the first definition of variable $\hat{m}$ [see Chapter II (B)] are here used, and

that the concept of marker gradient is replaced by that of the mean slope of concentration gradient [see Chapter Ⅲ(A)]. It follows that both s and $\hat{m}$ have a dimension of concentration of gradient substance [see eqs(6.2) and (6.3)].

In eq(6.1), function $\mu(s)$ representing reduced elution volume at the center of CGM1st is defined implicitly by eq(5.15') as

$$s = \int_0^{\mu} \frac{B'(\hat{m})}{1-B'(\hat{m})} d\hat{m} \tag{6.7}$$

Function $\sigma(s; g')$ representing standard deviation of CGM1st is defined as

$$\sigma(s; g') = \Delta(s; g')/B'[\mu(s)] \tag{6.8}$$

in which $\Delta(s; g')$ is represented by eq(5.27) as

$$\Delta(s; g') = \sqrt{\frac{g'\Theta^{\circ}}{2}} [1-B'\{\mu(s)\}] \int_0^s \frac{ds}{[1-B'\{\mu(s)\}]\sqrt{s}} \tag{6.9}$$

Corresponding to eq(6.3), it is possible to consider

$$\mu = g'\dot{V} = g\dot{V}^{\#} \tag{6.10}$$

and

$$\sigma = g'\tau = g\tau^{\#} \tag{6.11}$$

where $\dot{V}$ (with dimensions of volume) represents elution volume at the center of CGM1st, and τ (also with dimensions of volume) represents standard deviation of CGM1st; $\dot{V}^{\#}$ and $\tau^{\#}$ (both with dimension of length) stand for $\dot{V}$ and τ taking place, provided that the column with unit interstitial volume per unit length is used, respectively. $\dot{V}^{\#}$ and $\tau^{\#}$ are related to $\dot{V}$ and τ by

$$\dot{V}^{\#} = \dot{V}/\gamma \tag{6.12}$$

and

$$\tau^{\#} = \tau/\gamma \tag{6.13}$$

respectively. The parameter θ° (with dimension of length) defined by

$$g'\Theta^{\circ} = g\theta^{\circ} \tag{6.14}$$

or

$$\theta^{\circ} = \Theta^{\circ}/\gamma \tag{6.15}$$

(where it should be recalled that Θ° has dimensions of volume) is related to height equivalent to a theoretical plate (denoted by $\hat{H}$) through

$$\hat{H} = 2\theta^{\circ} \tag{6.16}$$

at least when concentration gradient chromatography approaches isocratic chromatography with decrease in the g' value [cf. both Chapter I (A) and Appendix XI(A)].

Function $B'(\hat{m})$ which can be considered to be a given function when only the gradient in the liquid phase is applied [see Chapter V(C)] can be represented by eq(3.12) as

$$B'(\hat{m}) = \dot{B}(m) = \dot{B}[\phi(\hat{m})] \tag{6.17}$$

in which, for simplicity, $\dot{B}(m, \rho^{\circ})$ has been written as $\dot{B}(m)$. Eq(6.17) shows that the concrete expression of $B'(\hat{m})$ can be obtained when both functions $\phi(\hat{m})$ and $\dot{B}(m)$ are given.

Let us consider linear, concave and convex concentration gradients represented as

$$\phi(\hat{m}) = \hat{m} + m_{in} \tag{6.18}$$

$$\phi(\hat{m}) = \frac{e^{a\hat{m}/\bar{m}} - 1}{e^{a} - 1}\bar{m} + m_{in} \tag{6.19}$$

and

$$\phi(\hat{m}) = \left(1 - \frac{e^{a(1-\hat{m}/\bar{m})} - 1}{e^{a} - 1}\right)\bar{m} + m_{in} \tag{6.20}$$

respectively, where m_{in} stands for the initial concentration of the gradient. a represents a positive constant measuring concavity or convexity of the gradient, and, when a tends to zero, then both eqs(6.19) and (6.20) reduce to eq(6.18). $\bar{m}$ also represents a positive constant, and, when the concentration gradient is generated by mixing two buffers continuously in different ratios (usual practice), $\bar{m}$ can be expressed as

$$\bar{m} = m_f - m_{in} \tag{6.21}$$

in which m_{in} and m_f ($m_{in} < m_f$) stand for concentrations of so-called A (or initial) and B (or final) buffers, respectively. Denoting by V_T the total volume of the buffers, the mean slope, g', of concentration gradient can be defined as

$$g' = \bar{m}/V_T \tag{6.22}$$

Of course, another definition of g' is feasible. [For other types of concave and convex gradient, see the subsection entitled "Investigation of Jandera et al." in Appendix XI(B).]

Eqs(6.7)-(6.9) can now be rewritten as

$$s = \int_0^{\hat{\mu}} \frac{\dot{B}[\phi(\hat{m})]}{1-\dot{B}[\phi(\hat{m})]} d\hat{m} = \int_{m_{in}}^{\mu} \frac{\dot{B}(m)}{1-\dot{B}(m)} \cdot \frac{d\phi^{-1}}{dm} dm \qquad (6.7')$$

$$\sigma(s;\ g') = \Delta(s;\ g')/\dot{B}[\mu(s)] \qquad (6.8')$$

and

$$\Delta(s;\ g') = \sqrt{\frac{g'\Theta^{\circ}}{2}}\ [1-\dot{B}\{\mu(s)\}] \int_0^{s} \frac{ds}{[1-\dot{B}\{\mu(s)\}]\sqrt{s}} \qquad (6.9')$$

respectively, where μ represents the concentration of elution of gradient substance at the center or maximum of MB(o) or CGM1st, and ϕ^{-1} stands for the inverse function of ϕ.

A concrete expression of function $\dot{B}(m)$ will be given in the subsequent Section(B).

(B) Combination with Competition Model

Competition model offers the basis of the adsorption and desorption mechanism of a wide range of chromatographies (see the subsequent Chapter Ⅷ-X). The model states that adsorbing sites are arranged in some manner (usually with inter-site distances of the order of nm) on the surfaces of packed particles in the column; sample molecules with functional adsorption groups and gradient substances compete for adsorption on the sites of packed particles. In many instances, it can be deduced that a gradient substance occupies effectively almost one site when it is adsorbed, whereas a sample molecule covers plural sites. (For detail, see Chapter Ⅷ.)

On the basis of competition model, function $\dot{B}(m)$ (partition of sample molecules in the liquid phase) can be represented [by eq(8.51)] as

$$\dot{B}(m) = \frac{1}{1+q(\varphi m+1)^{-x'}} \qquad (6.23)$$

and the corresponding capacity ratio, $\dot{k}(m)$ [$=\{1-\dot{B}(m)\}/\dot{B}(m)$], can be written [by eq (8.52)] as

$$\dot{k}(m) = q(\varphi m+1)^{-x'} \qquad (6.23')$$

where q and φ are positive constants measuring the strengths of adsorption of sample molecule and gradient substance, respectively. x' is also a positive constant representing the number of gradient substances the adsorption of which on the adsorbent surface is impossible owing to the presence of an adsorbed sample molecule. [Provided that a gradient substance occupies exactly a single site when it is adsorbed, x' also represents the

number of sites on which the adsorption of gradient substance is impossible owing to the presence of an adsorbed sample molecule i.e., the number of sites covered by an adsorbed sample molecule.] x' therefore measures the size of the sample molecule. [For detail, see Chapter Ⅷ(B).]

When a linear concentration gradient is applied, eq(6.18) holds, and, by substituting eq(6.17) combined with both eqs(6.18) and (6.23) into eq(6.7), eq(6.7) can be integrated to give

$$s = \frac{1}{(x'+1)q\varphi}\left[\{\varphi(\mu + m_{in})+1\}^{x'+1} - (\varphi m_{in}+1)^{x'+1} \right] \tag{6.24}$$

or

$$\mu(s) = \left[\{ (x'+1)q\varphi s + (\varphi m_{in}+1)^{x'+1} \}^{1/(x'+1)} - 1 \right]/\varphi - m_{in} \tag{6.24'}$$

representing function $\mu(s)$ explicitly.

(C) Relationship with Appendix XI(B)

With linear concentration gradient, let us examine the case when $x' \gg 1$ i.e., the case of large molecule in size. In this instance, $x'+1 \approx x'$. Calculating the term $[\varphi(\mu + m_{in})+1]^{-x'}$ by using eq(6.24) or (6.24') into which x' is substituted for x'+1, substituting this term for $(\varphi m+1)^{-x'}$ into eq(6.23), and writing $B'[\mu(s)]$ for $\dot{B}(m)$ [with references to both eqs(6.17) and (6.18)] lead to

$$B'[\mu(s)] = \frac{s+R}{s+R+(x'\varphi)^{-1}} \tag{6.25}$$

and

$$1-B'[\mu(s)] = \frac{(x'\varphi)^{-1}}{s+R+(x'\varphi)^{-1}} \tag{6.25'}$$

where

$$R = \frac{(\varphi m_{in}+1)^{x'}}{x'q\varphi} \tag{6.26}$$

By substituting eq(6.25') into eq(6.9) and executing the integration,

$$\Delta(s;\ g') = \sqrt{2g'\Theta^{\circ}s}\ \frac{s/3+R+(x'\varphi)^{-1}}{s+R+(x'\varphi)^{-1}} \tag{6.27}$$

is obtained, and, with reference to eq(6.25), eq(6.8) can be rewritten as

$$\sigma(s;\ g') = \sqrt{2g'\Theta's}\ \frac{s/3+R+(x'\varphi)^{-1}}{s+R} \tag{6.28}$$

which, along with eq(6.28') below, can be compared with Appendix XI(B) eq(A11.64).

Again with linear concentration gradient, let us examine another case when $\varphi\ m \ll 1$. In this instance, eqs(6.23) and (6.23') can be rewritten as

$$\dot{B}(m) = \frac{1}{1+qe^{-x'\varphi\ m}} \tag{6.29}$$

and

$$\dot{k}(m) = qe^{-x'\varphi\ m} \tag{6.29'}$$

respectively. Eq(6.7) can be integrated to give

$$s = \frac{e^{x'\varphi\ m_{in}}(e^{x'\varphi\ \mu}-1)}{x'q\varphi} \tag{6.30}$$

or

$$\mu(s) = \frac{1}{x'\varphi}\ln\left(x'q\varphi e^{-x'\varphi\ m_{in}}\ s\ +\ 1\right) \tag{6.30'}$$

[instead of eqs(6.24) or (6.24')]. [*Note.* In eq(6.24), the terms $\varphi(\mu+m_{in})+1$ and $\varphi\ m_{in}+1$ can be replaced by $e^{\varphi(\mu+m_{in})}$ and $e^{\varphi\ m_{in}}$, respectively, since the relationsips $\varphi(\mu+m_{in})\ll 1$ and $\varphi\ m_{in}\ll 1$ now hold. This leads to eq(6.30) in which x' is replaced by x'+1. Here, we do not consider this equation, however.] Defining R as

$$R = \frac{e^{x'\varphi\ m_{in}}}{x'q\varphi} \tag{6.31}$$

[instead of eq(6.26)], eqs(6.25), (6.25'), (6.27) and (6.28) hold without any modification. [*Note.* From the argument done in the subsequent Chapter VIII(H), it will be understood that both cases when $x' \gg 1$ and $\varphi\ m \ll 1$ considered above correspond to the case when both sample molecule and gradient substance are adsorbed "weakly" on the adsorbent surface while performong the competition.]

Let us introduce the parameter:

$$p = [1-B'(0)]x'\varphi\ s\left(= \frac{k'(0)}{1+k'(0)}x'\varphi\ s\right) \tag{6.32}$$

[cf. eq(3.23)]. As $\mu(s)=0$ when $s=0$, $1-B'(0)$ can be written with reference to eq(6.25') as

$$1-B'(0) = \frac{1}{1+x'\varphi R} \tag{6.33}$$

and eq(6.32) becomes

$$p = \frac{s}{R+(x'\varphi)^{-1}} \tag{6.32'}$$

Eqs(6.27) and (6.28) can be rewritten respectively as

$$\Delta(s;\ g') = \sqrt{2g'\Theta s}\ \ \Gamma \tag{6.27'}$$

and

$$\sigma(s;\ g') = \sqrt{2g'\Theta s}\ \ \Gamma/B'[\mu(s)] \tag{6.28'}$$

[cf. eq(6.25)] in both of which

$$\Gamma = \frac{1+p/3}{1+p} \tag{6.34}$$

Eqs (6.28') and (6.34) can be compared with Appendix XI(B) eqs(A11.64) and (A11.87), respectively. [For the relationship between s and L', that between μ and $\dot{V}$, and that between σ and τ, see eqs(6.2), (6.10) and (6.11), respectively.]

(D) Relationship with Earlier Works

Over thirty years ago, dynamic investigation [see Chapter I (A)] of concentration gradient chromatography started in the laboratory of Prof.G.Bernardi on the basis of the experimental data of hydroxyapatite chromatography published in ref(6.1). The study is intimately connected to the study of competition model which was performed for the purpose of elucidating the adsorption and desorption mechanism taking place on the crystal surface of hydroxyapatite particles packed in the column (for detail, see the subsequent Chapter VIII). Paper(6.2) in which competition model was originally introduced in a specified form [accompanying the equation equivalent to eq(6.23); ref(6.2) eq(41)] is followed by the first paper(6.3) of dynamic investigation performed by using a very primitive method for the case of linear concentration gradient chromatography.

About thirty years ago, the parameter, s, playing a fundamental role in the present theory was originally introduced as product by slope, g' or g, of linear concentration gradient applied of length, L' or L, of the column[ref(6.4) eq(9)], underlying the fact that concentration of elution, μ [at the center or maximum of MB(o) or CGM1st], of gradient substance is determined by s [see ref(6.4)]. The parameter $\hat{m}$ playing the role symmetric with s did not make appearance in that epoch, hidden within the concept of concentra-

tion, m, of gradient substance. Further, the prototype of eq(6.7) which is valid only for the case of linear concentration gradient was derived in combination with competition model [ref(6.4) eq(12)], and, from this equation, the equation equivalent to eq(6.24) or (6.24') was derived[ref(6.4) eq(15)]. This can be rewritten by using the present notation as

$$s = \frac{1}{(x'+1)q\varphi}\left[(\varphi \mu + 1)^{x'+1} - (\varphi m_{in} + 1)^{x'+1} \right] \tag{6.35}$$

or

$$\mu(s) = \left[\left\{ (x'+1)q\varphi s + (\varphi m_{in} + 1)^{x'+1} \right\}^{1/(x'+1)} - 1 \right]/\varphi \tag{6.35'}$$

The prototype of eq(6.7) which holds independently of competition model but which is valid only for the case of linear concentration gradient was also derived[ref(6.5) eq(1)]; this can be rewritten by using the present notation as

$$s = \int_{m_{in}}^{\mu} \frac{\dot{B}(m)}{1-\dot{B}(m)}\, dm \tag{6.36}$$

Over twenty years ago, a semi-empirical continuity equation of linear concentration gradient chromatography in which account is taken of axial diffusion in the column was derived[ref(6.6) eq(17)]; this can be rewritten as

$$\mathrm{div}_m \left(\frac{1-\mathring{B}(m+s)}{\mathring{B}(m+s)} C - \frac{g'\Theta^*}{\mathring{B}(m+s)} \mathrm{grad}_m \frac{C}{\mathring{B}(m+s)} \right) + \frac{\partial C}{\partial s} = 0 \tag{6.37}$$

in which $\mathring{B}(m+s)$ corresponds to $\dot{B}(\dot{m}+s)$, and Θ^* is a positive constant, determined empirically for each slope, g', of the concentration gradient applied. The prototype of the present theory developed on the basis of eq(6.37) is sumarized in ref(6.7). The Gaussian expression of CGM1st obtained when MB(o) with a small width is formed initially at the inlet of the column was derived from the solution of eq(6.37). This[ref(6.7) eq(43)] can be rewritten as

$$C = G[m;\ \mu(s),\ \sigma^*(s;\ g')] \tag{6.38}$$

in which function $\mu(s)$ is defined implicitly by eq(6.36) [ref(6.7) eq(39)]. Function $\sigma^*(s;\ g')$, however, is semi-empirical, represented [by ref(6.7) eq(42)] as

$$\sigma^*(s;\ g') = \sqrt{2g'\Theta^* s}\ /\dot{B}[\mu(s)] \tag{6.39}$$

Eq(6.39) resembles eq(6.8) into which $\Delta^*(s;\ g')$ [eq(4.10)] is substituted for $\Delta(s;\ g')$. Whereas eq(6.35) or (6.35') [ref(6.7) eq(44)] can be derived from both eqs(6.23) and (6.36), the expression of $\sigma^*(s;\ g')$ combined with competition model [ref(6.7) eq(46)] i.e.,

$$\sigma'(s;\ g') = \sqrt{2g'\Theta^{*}s}\ [1+q\{\varphi\ \mu(s)+1\}^{-x'}] \qquad (6.40)$$

can be derived from both eqs(6.23) and (6.39). For each g' value applied to each experiment, the parameter Θ^{*} can be evaluated or the function $\sigma'(s;\ g')$ can be determine empirically [see refs(6.8, 6.9)].

Also over twenty years ago, the prototype of eq(5.17) was derived[ref(6.10) eq(7)]. This is valid only for the case of linear concentration gradient, and it can be rewritten as

$$\mathrm{div}_{m}\left[\frac{1-B''(s)}{B''(s)}C - g'\Theta^{*}\frac{d}{ds}\left\{\frac{s}{[B''(s)]^{2}}\right\}\mathrm{grad}_{m}\ C\right] + \frac{\partial C}{\partial s} = 0 \qquad (6.41)$$

Chapter Ⅶ. Experimental Verification of Dynamic Investigation

(A) Purpose

In Chapter Ⅵ, the conclusion on the theory of concentration gradient chromatography combined with competition model is summarized with regard to the usual case when MB(o) with a small width is formed initially at the inlet of the column. The purpose of this Chapter is to give experimental verifications of this conclusion. Our interest here is focused, however, on the verification of the dynamic theory of chromatography mentioned in Chapter Ⅵ(A), and competition model[eq(6.23) or (6.23')] only plays a role equivalent to any empirical expression of molecular partition $\acute{B}$ in the liquid phase as a function of concentration m of gradient substance. The experimental verification of the static theory of chromatography or the verification of competition model will be done in the subsequent Chapter Ⅷ.

All the experiments are carried out on hydroxyapatite(HA) columns by using lysozyme as a probe and applying three types of concentration gradient, linear[eq(6.18)], concave[eq (6.19)] and convex[eq(6.20)] gradients of potassium phosphate buffer at pH≈6.8 (i.e., an equimolar mixture of KH_2PO_4 and K_2HPO_4; called KP buffer). As far as the last gradient is concerned, only a slight convexity can be realized for a technical reason, however. According to competition model, competition takes place between lysozyme and potassium ion from the buffer for adsorption on the crystal surface of HA packed in the column, thus giving rise to eq(6.23) or (6.23') in which m represents molarity of potassium ions (for the role of potassium ion as active gradient substance, see the subsequent Chapter Ⅷ). The lysozyme molecules initially adsorbed at the inlet of the column forming a narrow MB(o) are driven out of the HA surface by potassium ions from concentration gradient, thus bringing about the development of the lysozyme molecules on the column.

(B) Materials and Methods

Both spherical HA particles (type S with diameters of about 5 μm) and HA packed SUS316 stainless-steel columns (KB columns) were prepared in Koken Co.Ltd., Tokyo. The scanning electron micrograph of type S HA particles almost identical with those used in the present work is presented in ref(7.1) Fig 1. The column internal diameter(ø) was 6 mm; lengths of 0.5, 1, 3 and 10 cm were prepared. The 3-cm column was used as either precolumn or main column. If a large overall column length was needed, it was provided by connecting 10-cm column in series by using fine tubes.

The HPLC experiments were carried out at room temperature(19-32℃) by connecting the column (or the column system) to an LC-9A pump system including a gradient controller (purchased from Shimadzu, Kyoto); the flow-rate was set to 0.5 ml/min always. The flow-rate was monitored in each experiment, and it was confirmed that the correct flow-rate was produced accompanying the error of at most 2%. In concentration gradient chromatography, 20-80 μg lysozyme dissolved in KP buffer was injected into the column (or

the column system) by using an injector located between the HPLC pump and the column inlet; the concentration of KP buffer was 1 mM and 1.5 mM with respect to phospate and potassium ions, respectively. The sample injection was followed by rinsing with KP buffer with the same concentration. During this process, virtually all the molecules (except denatured minor components) remained in the stationary phase (i.e., on the HA surface) at the inlet of the column forming a band [MB(o)] with a small width [which can be confirmed from ref(7.1) Fig 10(b')]. Material was then eluted by using a linear[eq(6.18)], a concave[eq(6.19)] or a convex[eq(6.20)] gradient of KP buffer. The sample elution was monitored by measuring the ultraviolet(UV) absorption at 280 nm in the flow cell (connected to the outlet of the column or the column system by using a fine tube). At the same time, the concentration gradient was monitored by measuring the refractive index in the special flow cell with a low angle (connected in series to the UV cell by using a fine tube the internal volume of which is negligibly small).

Three sets of experiments were designed. Each set involves three experiments carried out by using linear, concave and convex gradients, respectively. Among the three sets, the shapes of the gradient of the same type are similar, represented by a common function $\phi(\hat{m})$ [eq(6.18), (6.19) or (6.20)] but the steepness g' or g of the gradient are different from one another. Both initial concentration (molarity) m_{in} and final concentration (molarity) m_f of potassium ions [see eq(6.21)] are the same among all the experiments.

Experimentally, $\hat{\mu}$ [eq(6.7)] or $\hat{V}$ [eq(6.10)] was defined as $\hat{m}$ or V at which the maximum heigtht of chromatogram(CGM1st) or chromatographic peak appears. μ [eq(6.7')], therefore, stands for potassium molarity, m, of the KP buffer gradient at which the maximum height of chromatographic peak appears. σ [eq(6.8)] or τ [eq(6.11)] was defined as half-width at 0.6065 times the maximum height of chromatographic peak. $\hat{\mu}$ (or $\hat{V}$) and σ (or τ) are exactly equal to the first moment and the standard deviation of chromatographic peak, respectively, provided that the peak is precisely Gaussian in shape. Actually, the experimental peak was slightly asymmetric in shape with a small tailing [for instance, see ref(7.1) Fig 7(b) where the lysozyme chromatographic peak obtained for a similar experiment is illustrated.]

Lysozyme (from chicken egg white) used for all the experiments was purchased from P-L Biochemicals.

(C) Test of Concentration Gradient

The gradient controller [see Section(B)] is designed in such a way that the concentration gradient is generated by mixing the initial buffer (the A buffer with potassium concentration $m_{in}=0.0015$ M) with the final buffer [the B buffer with potassium concentration m_f; see eq(6.21)] in different ratios changing continuously with a lapse of time. When the flow-rate is set to 0.5 ml/min[Section(B)], the time, t_T, needed for potassium concentration to change from m_{in} to m_f can be set anyhow. Therefore, the total volume, V_T, of the

carrier liquid used for the development can also be set anyhow since $V_T = 0.5t_T$. All the experiments were carried out by fixing the parameter m_f to 0.375 M or by fixing the parameter $\bar{m}$ to 0.3735 M [see eq(6.21)], and steepness, g', of the potassium gradient was determined by setting the t_T or V_T value in each experiment [see eq(6.22)].

In Table 7.1, the values of the parameters t_T, V_T, g' and g that are to be used in the three sets of experiments [Section(B)] are summarized. In the first experiment in each set, the parameter a was set to zero in order for eq(6.18) to be realized, generating a linear potassium gradient. In the second and the third experiment, the parameter a was set to 3 in order for eqs(6.19) and (6.20) to be realized, generating concave and convex potassium gradients, respectively.

Nine curves (three of which are straight lines) drawn on the $(\bar{m}, m - m_{in})$ plane in Fig 7.1 are theoretical[eq(3.1)], representing the concentration gradients of potassium ions that are to be realized in the three sets of three experiments. These were calculated by using eq(6.18) [Figs 7.1(a), (d) and (g)], eq(6.19) [Figs 7.1(b), (e) and (h)] and eq(6.20) [Figs 7(c), (f) and (i)]; in both eqs(6.19) and (6.20), $\bar{m} = 0.3735$ M and $a = 3$ (see above). The g' and g values used in the first set[Figs 7.1(a), (b) and (c)], the second set[Figs 7.1(d), (e) and (f)] and the third set[Figs 7.1(g), (h) and (i)] can be found in Table 7.1. In each set, $\bar{m}$ can be represented in terms of V or V' by using eq(6.3) [cf. eq(6.6) in which $\gamma = 0.237$ cm^2; see Section(D)], and, in Fig 7.1, the curves are drawn also as functions of V or V'.

The points in Fig 7.1 are experimental plots. The points(○) were obtained in the absence of the column or the column system by estimating the $m - m_{in}$ values from the measurement of the refractive index in the flow cell set at the outlet of the pump system. The corresponding $\bar{m}$ values were determined in order for the extrapolation of the array of the experimental points(○) to pass through the origin of the $(\bar{m}, m - m_{in})$ plane. It can be seen in Fig 7.1 that the coincidence between theory and experiment is satisfactory; the gradient controller works well.

The points(△) were obtained in the presence of the column system with overall length of 33 cm; the measurement of the refractive index was performed at the outlet of the column system. The corresponding $\bar{m}$ values were determined in order for the array of the experimental points(△) to be superposed on the theoretical curve or the array of the experimental points(○) (taking place in the absence of the column system) except in the vicinity of the origin of the $(\bar{m}, m - m_{in})$ plane. It can de seen in Fig 7.1 that the superposition is done satisfactorily except in the vicinity of the origin. The deviation from the superposition in the vicinity of the origin taking place in the presence of the column, in general, increases with increase in steepness, g' or g, of the concentration gradient applied [cf. Figs 7.1(a), (d) and (g), Figs 7.1(b), (e) and (h), and Figs 7.1(c), (f) and (i), respectively].

The straight line and the arrays of two types of point(○ and △) drawn in Fig 7.2 were reproduced from Fig 7.1(g); these represent the theoretical curve (straight line) and

Table 7.1

The parameters t_T, V_T, g' and g in the three sets of experiments.

Parameter	Set			Comments
	First	Second	Third	
t_T (min)	597.6	298.8	149.4	
V_T (ml)	298.8	149.4	74.7	Calculated from $V_T = 0.5t_T$
g' (mM/ml)	1.25	2.5	5.0	Calculated from $g' = \bar{m}/V_T = 0.3735/V_T$ [see eq(6.22)]
g (mM/cm)	0.296	0.593	1.185	Calculated from $g = \gamma g' = 0.237g'$ [see eqs(6.14) and (6.15)]

Note. In each set, the steepness, g' or g, of the concentration gradient is defined to be equal to the slope of the linear potassium gradient of KP buffer used in the first experiment. Earlier(6.8, 6.9, 7.1), the slope of the linear KP gradient was expressed by using the parameter $g'_{(P)}(\phi=1$ cm) representing the increase of phosphate concentration (molarity) per unit volume of the carrier liquid taking place, provided that the internal column diameter, ϕ, is equal to 1 cm. $g'_{(P)}(\phi=1$ cm) is related to g' by $g'_{(P)}(\phi=1$ cm$) = 0.6^2g'/1.5=0.24g'$, where 0.6 represents ϕ of the column used (expressed in units of cm). Therefore, the $g'_{(P)}(\phi=1$ cm) values in the three sets are 0.3, 0.6 and 1.2 mM/ml, respectively. The parameter $g'_{(P)}(\phi=1$ cm) will often be used in the subsequent Chapter Ⅷ also.

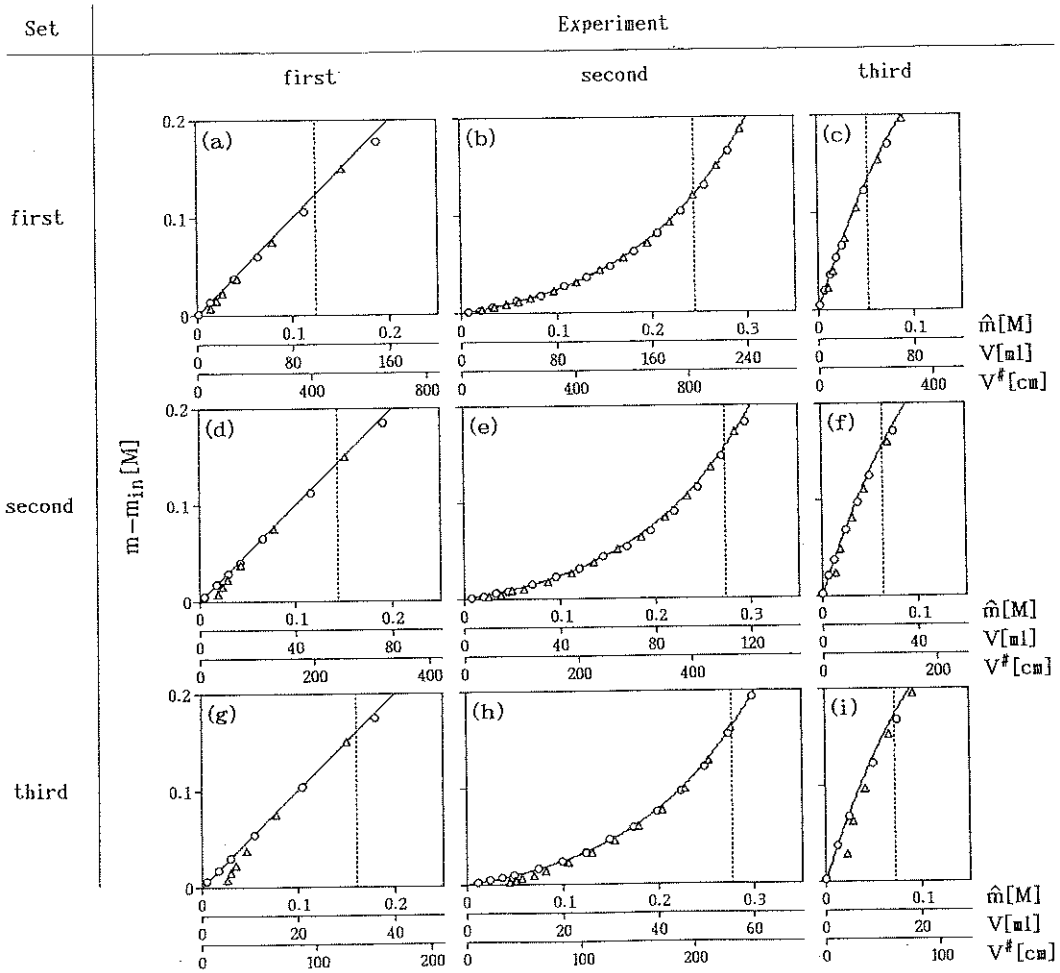


Fig 7.1. Curves (three of which are straight lies): theoretical curves representing the concentration gradients of potassium ions that should be realized in the three sets of three experiments. Points(○): experimental plots obtained in the absence of the column or the column system. Points(△): experimental plots obtained in the presence of the column system with overall length of 33 cm. The dotted vertical lines indicate the upper limits of $\hat{m}$, V or V^* that will actually be used for the elution of lysozyme under the respective experimental conditions.

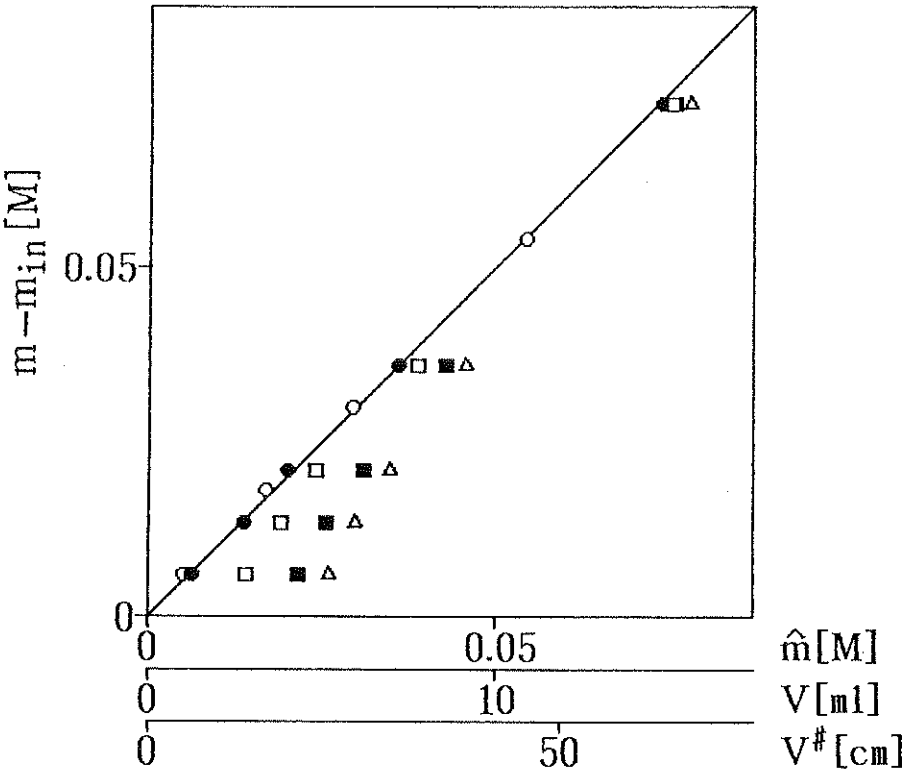


Fig 7.2. Straight line: theoretical curve (line) representing the linear concentration gradient of potasium ions. Points: experimental plots obtained in the absence(○) and the presences of the column (system) with overall length of 3 cm(●), 13 cm(□), 23 cm(■) and 33 cm(△). The theoretical curve and the experimental plots of both points(○ and △) were reproduced from Fig 7.1(g).

the experimental plots obtained in both the absence and the presence of the column system (with overall length of 33 cm), where a linear concentration gradient is applied. The points(●, □ and ■) in Fig 7.2 represent the corresponding experimental plots obtained in the presence of the column (systyem) with overall length of 3, 13 and 23 cm, respectively. It can be understood from Fig 7.2 that the deviation of the experimental plots from the theoretical curve taking place in the vicinity of the origin of the $(\hat{m}, m-m_{in})$ plane increases with increase in overall column length applied. The similar tendency can also be observed with nonlinear concentration gradients.

It can be assumed that the deviation of the experimental plots from the theoretical curve(Figs 7.1 and 7.2) arises from the demixing effect or the adsorption of potassium ions (from the concentration gradient) on the HA surface [see Chapter Ⅲ(A)]. This will hardly affect the chromatographic behavior of lysozyme since molecular partition in the mobile phase, $\hat{B}$, of lysozyme taking place when $m \lesssim 0.05$ M is negligibly small (cf. Fig 7.8), whereas the deviation under consideration occurs in this range of m(Figs 7.1 and 7.2). This means that, while the top region of the concentration gradient [in which $m \lesssim 0.05$ M] is passing through the inlet of the column, the lysozyme band [MB(o)] continues staying at the inlet. It is only when $m \gtrsim 0.05$ M that the migration of the lysozyme band begins.

(D) Determination of Interstitial Volume, γ, per Unit Length of the Column

The determination was done by using two methods. In the first method, two different proper elution volumes, Z, with respect to the points on the linear KP gradient at which $m=0.15$ M and $m=0.225$ M, respectively, were plotted as functions of overall length, L, of the column or the column system used; m is concerned with potassium ions. Three series of experiments were carried out in which the slopes of the potassium gradient applied were equal to the three g′ values used in the three sets of experiments argued in Section (C), respectively (see Table 7.1). With reference to Figs 7.1(a), (d) and (g), it can be confirmed that the behavior of the two points under consideration existing on any type of concentration gradient is unaffected by the adsorption of ions on the HA surface; the two points, both of them, migrate on the column at the R_F value equal to unity. All the six plots of Z versus L (obtained above in the three series of experiments) brought about linear arrays (with only slight fluctuations) of experimental points with slopes almost equal to one another. The mean slope, 0.2412 cm^2, of the six arrays can be considered to represent the γ value.

In the second method, two kinds of proper elution volume, Z, for the maximum height of the lysozyme peak obtained under two different isocratic conditions [where $m=0.6$ M and $m=0.675$ M] were plotted as functions of overall length, L, of the column or the column system, respectively. It can be assumed that lysozyme migrates at the R_F value equal to unity under these experimental conditions of high m values. [The assumption is

compatible with Fig 7.8 showing that $\dot{B}$ should be virtually equal to unity when $m \gtrsim 0.4$ M. Also cf. Appendix VI Fig A6.3.] The two plots obtained above brought about linear arrays (with only slight fluctuations) of experimental points with slopes equal to 0.2334 cm^2 and 0.2336 cm^2 (estimated by using the least square method), respectively. The mean slope, 0.2335 cm^2, can be considered to represent the γ value.

In this work, the average, 0.237 cm^2, of the two γ values obtained by using the two different methods will be used for all the calculations. [The measurement of γ was also done by using the pulse band of sucrose, generating the value of 0.2444 cm^2. It can be assumed that sucrose is hardly adsorbable on the HA surface during the development on the column since it has no electric charge [see ref(7.1); also cf. Chapter VIII(A)]. This value is close to the values obtained above. The γ value obtained from the sucrose experiment is not applied to the present work, however. The fact that the γ values obtained by using three different probes (inorganic ion, lysozyme and sucrose) with different molecular sizes are close to one another implies that there is virtually no gel filtration effect with HA chromatography; cf. Chapter I (A).]

The ratio of the void volume to the total packed volume of the HA particles in the column [$\approx \epsilon$; see eq(1.35)] can now be estimated to be $0.237/(0.6^2\pi/4)=0.838$; 0.6 cm stands for the internal diameter($\varnothing$) of the column.

(E) Concentration Gradient Chromatography

The points in Fig 7.3 are experimental plots of L versus μ for lysozyme, obtained for three different g' or g values indicated in Table 7.1; in part(a), (b) and (c), linear, concave and convex concentration gradients [shown in Figs 7.1(a), (d) and (g), Figs 7.1(b), (e) and (h), and Figs 7.1(c), (f) and (i)] were used, respectively. In any part of Fig 7.3, three arrays of experimental points occurring from left to right represent those that are obtained in the first, the second and the third experiment carried out by using different g' or g values, respectively (see Fig 7.3).

The points in Fig 7.4 were obtained by mapping the points in Fig 7.3 to the (μ,L) plane. The mapping of the points in Figs 7.3(a), (b) and (c) was carrird out by using eqs (6.18)-(6.20), or by using the theoretical curves drawn in Figs 7.1(a), (d) and (g), Figs 7.1(b), (e) and (h), and Figs 7.1(c), (f) and (i), respectively. The three groups of the three arrays of experimental points occurring in the middle, the right part and the left part of Fig 7.4 correspond to those appearing in Figs 7.3(a), (b) and (c), respectively. The three arrays of experimental points occurring from left to right in each group in Fig 7.4 correspond to those occurring in the same direction in each part of Fig 7.3.

The points in Figs 7.5(a), (b) and (c) were obtained by mapping the points in Figs 7.3(a), (b) and (c) to the (μ,s) plane by using eq(6.2), respectively.

The three arrays of experimental points occurring in the middle, the right part and the left part of Fig 7.6 were obtained by mapping to the (μ,s) plane the three groups of

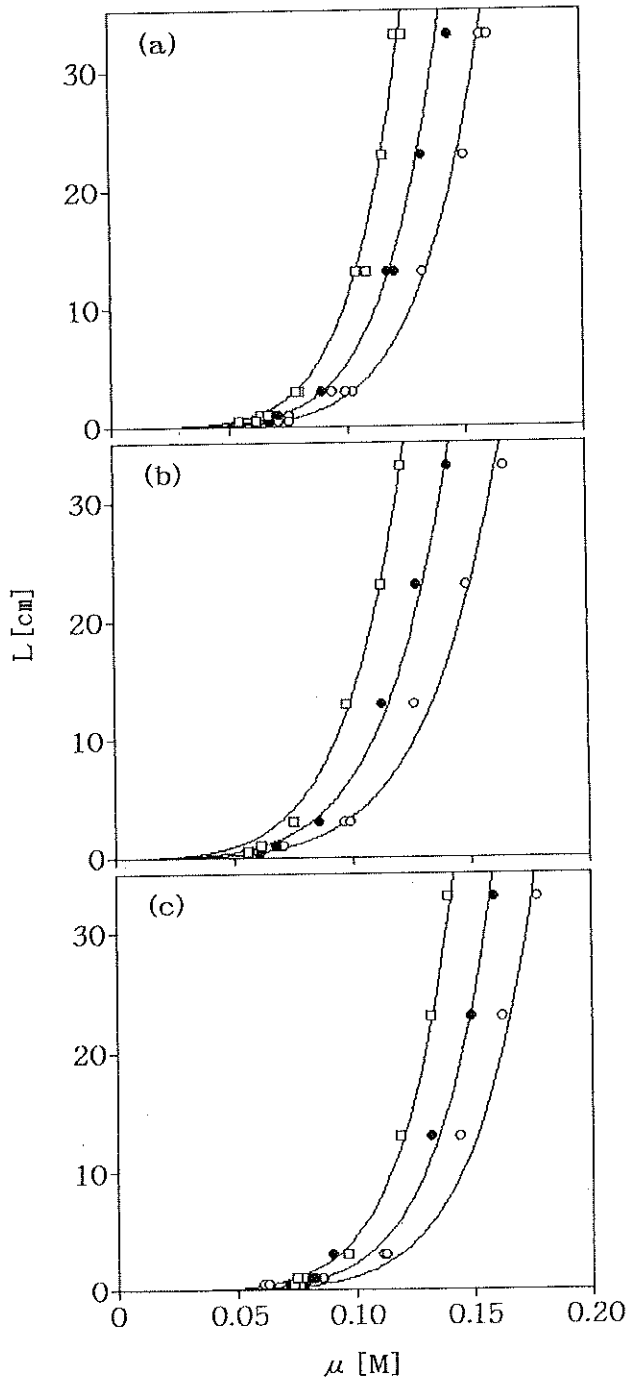


Fig 7.3. Points: experimental plots of L versus μ for lysozyme obtained when $\mathbf{g}=$ 0.296 mM/cm(□), 0.593 mM/cm(●) and 1.185 mM/cm(○). The concentration gradient applied is linear, concave and convex in (a), (b) and (c), respectively. Curves: theoretical curves calculated by using eq(6.7') combined with eq(6.2); function $\dot{B}$ is defined by eq (6.23).

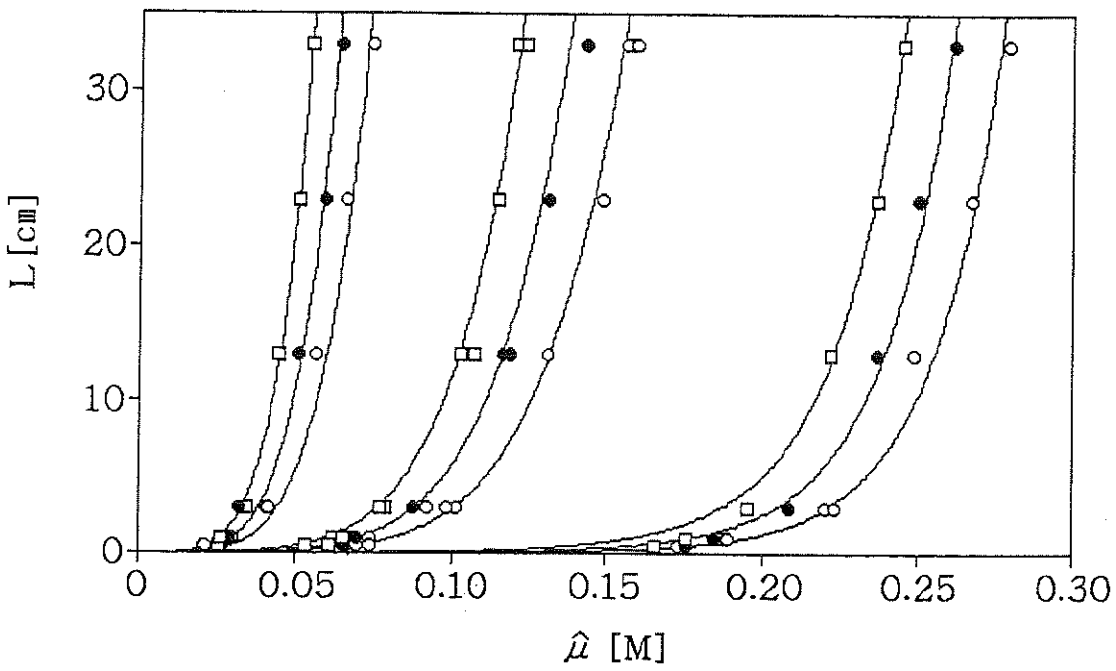


Fig 7.4. Points: experimental plots of L versus $\hat{\mu}$ for lysozyme obtained when g= 0.296 mM/cm(□), 0.593 mM/cm(●) and 1.185 mM/cm(○). The concentration gradient applied is linear, concave and convex for the three groups of the three arrays of experimental points occurring in the middle, the right part and the left part, respectively. Curves: theoretical curves calculated by using eq(6.7') combined with eq(6.2); function $\hat{B}$ is defined by eq(6.23).

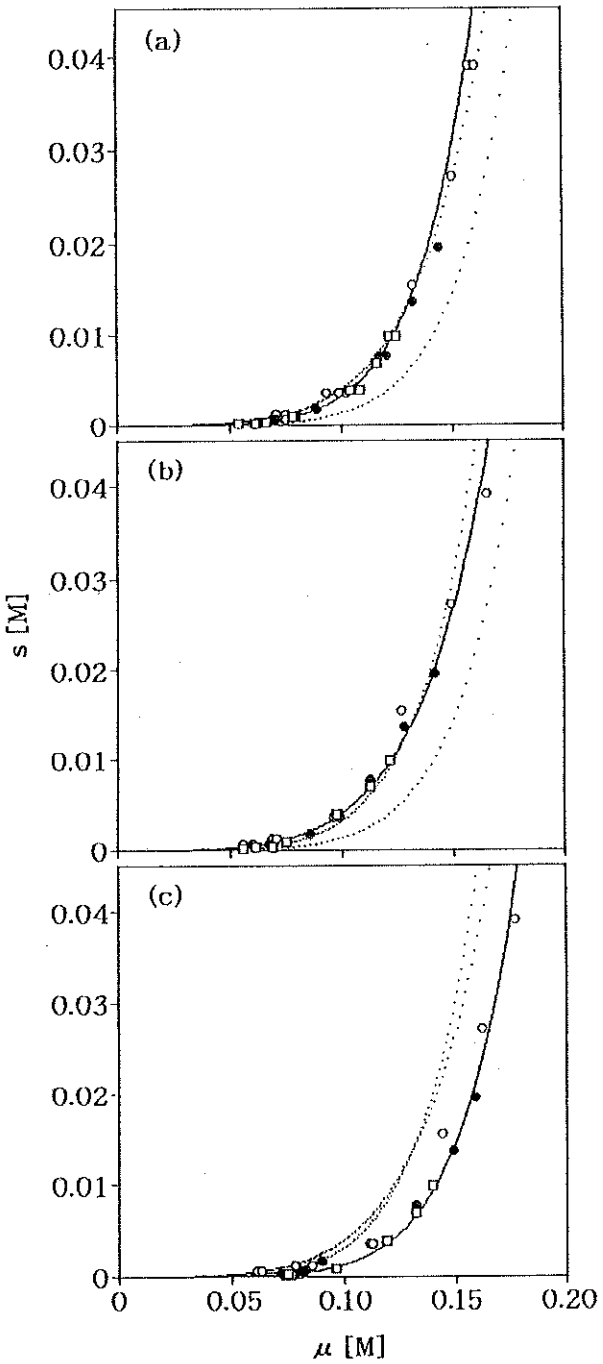


Fig 7.5. Points: experimental plots of s versus μ for lysozyme obtained when g= 0.296 mM/cm(□), 0.593 mM/cm(●) and 1.185 mM/cm(○). The concentration gradient applied is linear, concave and convex in (a), (b) and (c), respectively. Solid curves: theoretical curves calculated by using the equality between left- and right-hand sides of eq (6.7') where $\dot{B}$ is defined by eq(6.23). In each part, the theoretical curves appearing in the two other parts are also drawn as dotted curves.

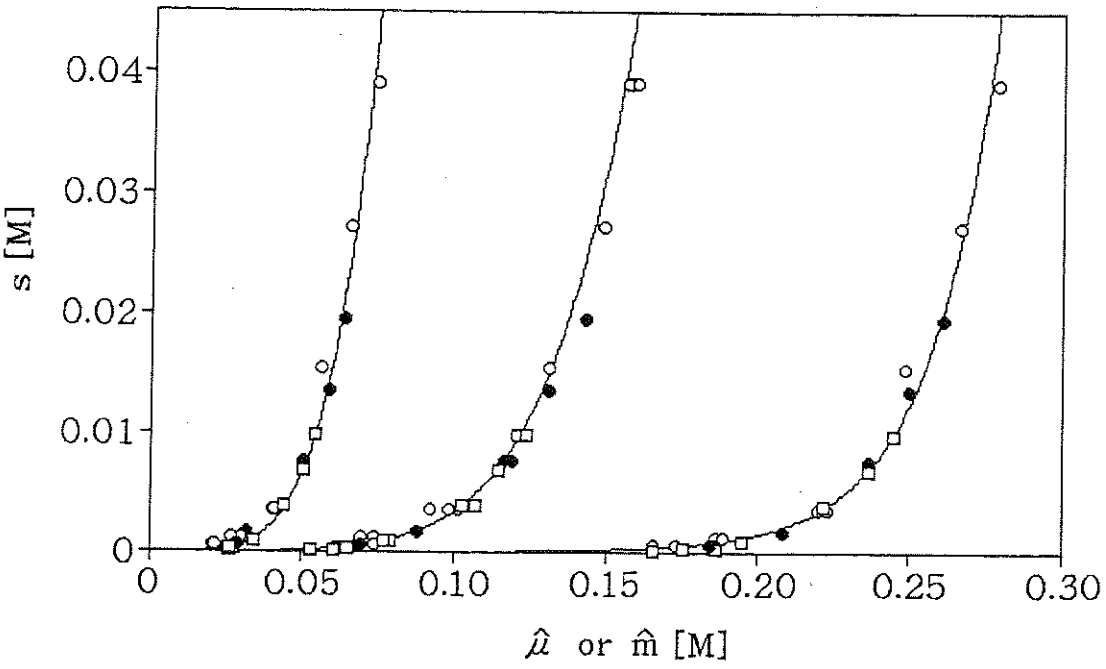


Fig 7.6. Points: experimental plots of s versus $\hat{\mu}$ for lysozyme obtained when g= 0.296 mM/cm(□), 0.593 mM/cm(●) and 1.185 mM/cm(○). The concentration gradient applied is linear, concave and convex for the three arrays of experimental points occurring in the middle, the right part and the left part, respectively. If the $\hat{m}$ axis is considered instead of the $\hat{\mu}$ axis, the three arrays of experimental plots represent three trajectories T_0 obtained with linear, concave and convex gradient elution modes, respectively. It can be considered that trajectories T_0 are the projections on the ($\hat{m}$,s) plane of three characteristic curves occurring in the ($\hat{m}$,s,B) space. Curves: theoretical curves calculated by using the equality between left-hand side and middle of eq(6.7') where $\dot{B}$ is defined by eq (6.23).

the three arrays of experimental points occurring in the middle, the right part and the left part of Fig 7.4, respectively. The three arrays of experimental points in Fig 7.6 can also be obtained by mapping the arrays in Figs 7.5(a), (b) and (c), respectively.

It is important to note that, on both (μ,L) (Fig 7.3) and ($\hat{\mu}$,L) (Fig 7.4) planes, the array of experimental points depends on the g' or g value applied, whereas, on both (μ,s) (Fig 7.5) and ($\hat{\mu}$,s) (Fig 7.6) planes, the array is independent of the g' or g value. It should also be noted that, by considering the $\hat{m}$ axis instead of the $\hat{\mu}$ axis, the three arrays of experimental points in Fig 7.6 represent three trajectories T_0 obtained with linear, concave and convex gradient elution modes, respectively.

The arrays of experimental points in Figs 7.7(a), (b) and (c) were obtained by mapping to the (L',$\dot{V}$) or (L',$\dot{V}^*$) plane the arrays occurring in the middle, the right part and the left part of Fig 7.4, respectively.

By consisering the V or V^* axis, instead of the $\dot{V}$ or $\dot{V}^*$ axis, it is possible to interpret that the three groups of the three arrays of experimental points in Figs 7.7(a), (b) and (c) represent three groups of three trajectories T_0, respectively. The three groups of trajectories T_0 in Figs 7.7(a), (b) and (c) are obtained with linear, concave and convex gradient elution modes, respectively. It is important to note that trajectory T_0 taking place on the (L',V) or (L,V^*) plane depends on the g' or g value applied (see Fig 7.7), whereas trajectory T_0 taking place on the ($\hat{m}$,s) plane is independent of the g' or g value (see Fig 7.6) in accordance with the argument done in Chapter III(C).

The solid curves in Fig 7.5 are theoretical, calculated by using the equality between left- and right-hand sides of eq(6.7') where function $\dot{B}$ is defined by eq(6.23). In each part of Fig 7.5, the theoretical curves appearing in the two other parts are also drawn as dotted curves. In order to obtain best fits with the experiment, the optimum values, 6.4, 9.82 and 25 M^{-1}, of the parameters x', ln q and φ [see eq(6.23)] have been used, respectively; these values will be used for all the calculations below.

The curves in Fig 7.6 are theoretical, calculated by using the equality between left-hand side and middle of eq(6.7') where function $\dot{B}$ is defined by eq(6.23).

The curves in Figs 7.3 and 7.4 were calculated by using eq(6.7') conbined with eq (6.2).

The curves in Fig 7.7 were calculated by using eq(6.7') combined with both eqs(6.2) and (6.10).

It can be seen in Figs 7.3-7.7 that the coincidence between theory and experiment is excellent.

The curve in Fig 7.8 is theoretical, calculated by using eq(6.23).

The three curves in Fig 7.9 (representing B' as a function of $\hat{m}$, respectively) were calculated by using eq(6.23) [into which $\dot{B}[\phi(\hat{m})]$ or $B'(\hat{m})$ is substituted for $\dot{B}(m)$]. For the calculation of the curves in the middle, the right part and the left part of Fig 7.9 (representing the curves for linear, concave and convex gradient elution modes), the functions $\phi(\hat{m})$ defined by eqs(6.18)-(6.20) have been used, respectively. Therefore, the

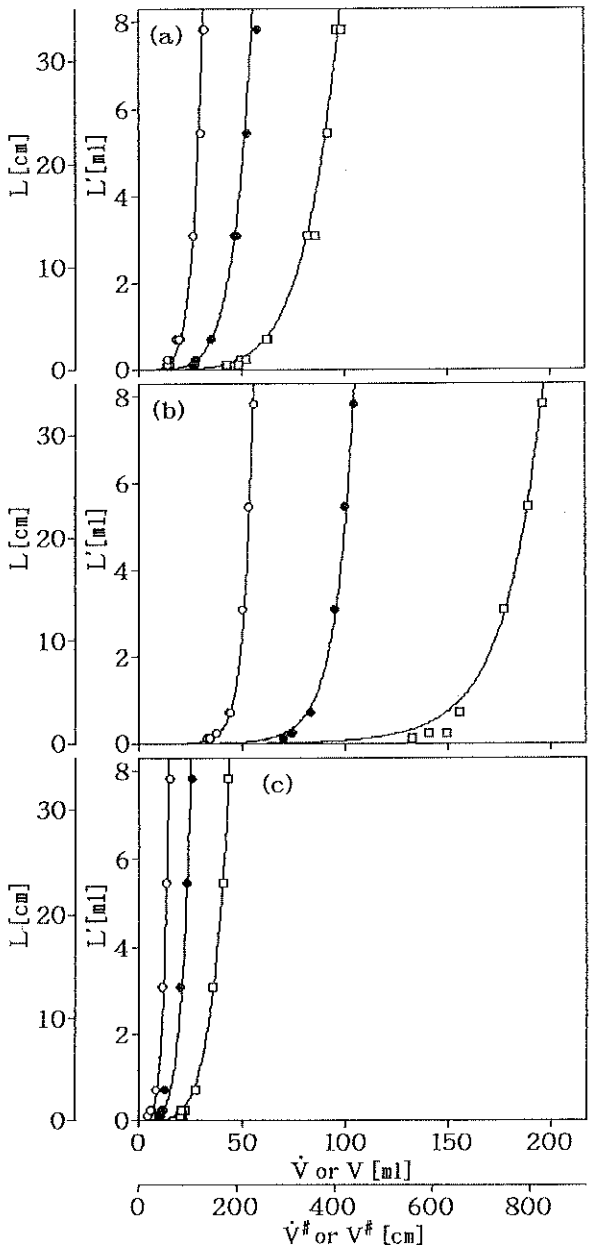


Fig 7.7. Points: experimental plots of L' or L versus $\dot{V}$ or $\dot{V}^{\#}$ for lysozyme obtained when g=0.296 mM/cm(□), 0.593 mM/cm(●) and 1.185 mM/cm(○). The concentration gradient applied is linear, concave and convex in (a), (b) and (c), respectively. If the V or $V^{\#}$ axis is considered instead of the $\dot{V}$ or $\dot{V}^{\#}$ axix, the three groups of the three arrays of experimental points in (a), (b) and (c) represent three groups of three trajectories T_0, respectively; the three groups of three trajectories T_0 are concerned with linear, concave and convex gradient elution modes, respectively. Curves: theoretical curves calculated by using eq(6.7') combined with both eqs(6.2) and (6.10); function $\dot{B}$ is defined by eq(6.23).

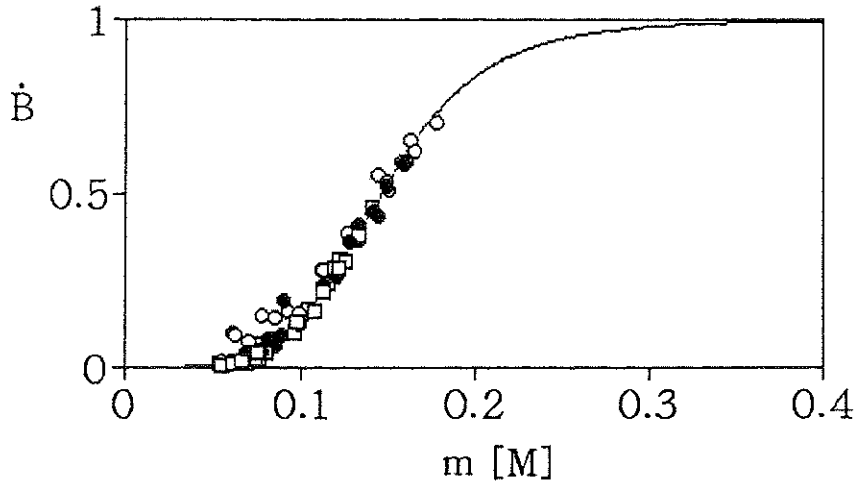


Fig 7.8. Curve: theoretical curve calculated by using eq(6.23). Points: experimental plots obtained by mapping all the points in Fig 7.9. The symbols are common to those used in Fig 7.9.

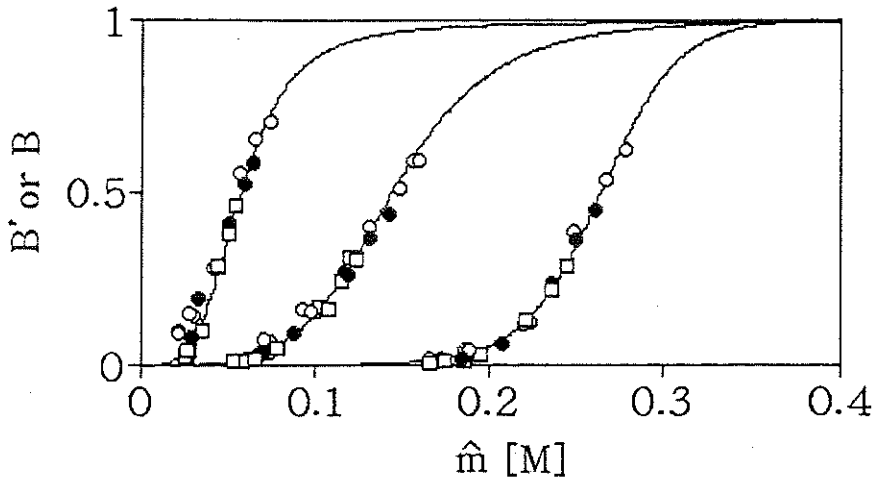


Fig 7.9. Curves: theoretical curve calculated by using eq(6.23) into which $\dot{B}[\phi(\hat{m})]$ or $B'(\hat{m})$ is substituted for $\dot{B}(m)$. The curves in the middle, the right part and the left part represent those for linear, concave and convex gradient elution modes, respectively. It can be considered that the three curves are the projections on the $(\hat{m},B)$ plane of three characteristic curves taking place in the $(\hat{m},s,B)$ space. Points: experimental plots obtained by mapping the points in Fig 7.6. The arrays of the experimental points in the middle, the right part and the left part correspond to those in the middle, the right part and the left part of Fig 7.6, respectively. The symbols are common to those used in Fig 7.6.

shape of the curve in the middle of Fig 7.9 [for the calculation of which eq(6.18) has been used] is identical with that of the curve drawn in Fig 7.8.

The solid curves in Figs 7.10(a)-(c) [representing B'' [see eq(3.9)] as a function of s, respectively] correspond to the curves in the middle, the right part and the left part of Fig 7.9, respectively. In each part of Fig 7.10, the theoretical curves appearing in the two other parts are also drawn as dotted curves. For the calculation of the curves in Fig 7.10, the fact that $B''(s)$ can be represented as $B'[T_0^{-1}(s)]$ [cf. eqs(3.4), (3.8) and (3.9)] has been used with reference to both eqs(3.10) and (3.11) in which $\hat{m}_0 = s_0 = 0$.

With reference to eqs(3.4), (3.8), (3.9) and (3.12), it is possible to consider that the three trajectories T_0 (Fig 7.6), the three curves(Fig 7.9) and the three solid curves[Figs 7.10(a), (b) and (c)] represent projections on $(\hat{m},s)$, $(\hat{m},B)$ and (s,B) planes of three characteristic curves taking place in the $(\hat{m},s,B)$ space, respectively. The characteristic curve drawn in Fig 3.2(b) represents that for linear concentration gradient chromatography, calculated by using the three projections drawn in Fig 7.6 (middle curve), Fig 7.9 (middle curve) and Fig 7.10(a), respectively. The three projections drawn in Fig 3.2(b) represent these projections.

The arrays of experimental points in the middle, the right part and the left part of Fig 7.9 were obtained by mapping to the $(\hat{m},B')$ plane those occurring in the middle, the right part and the left part of Fig 7.6 by the following way, respectively. Thus, by deviating the value of the parameter q or ln q (from the value used for the calculation of the theoretical curve in Fig 7.6), it is possible to superpose the theoretical curve on each experimental point in Fig 7.6. By using the deviated q value (in such a way that the superposition occurs), the B' value with respect to each experimental point in Fig 7.6 can be calculated through eq(6.23) into which $B'(\hat{m})$ is substituted for $\dot{B}(m)$. The position of any experimental point on the $(\hat{m},B')$ plane can thus be determined.

The arrays of experimental points in Figs 7.10(a)-(c) were obtained by mapping to the (s,B'') plane those occurring in the middle, the right part and the left part of Fig 7.9, respectively. The mapping was carried out by transforming the $\hat{m}$ value for each experimental point in Fig 7.9 to the s value by using the experimental plots in Fig 7.6.

Finally, the array of experimental points in Fig 7.8 was obtained by mapping to the $(m,\dot{B})$ plane all the three arrays of experimental points taking place on the $(\hat{m},B')$ plane (Fig 7.9); eqs(6.18)-(6.20) have been used for the mapping. As anticipated, the three arrays of experimental points realized on the $(\hat{m},B')$ plane(Fig 7.9) converge into a single array on the $(m,\dot{B})$ plane(Fig 7.8).

The argument below is concerned with standard deviation, σ or τ, of the chromatographic peak. The points in Fig 7.11 are experimental plots of σ versus L' or L obtained for the three g' or g values shown in Table 7.1; in part(a)-(c), linear, concave and convex concentration gradients are applied, respectively.

The points in Figs 7.12(a)-(c) were obtained by mapping to the (L',τ) or (L,τ^*) plane the experimental points in Figs 7.11(a)-(c), respectively.

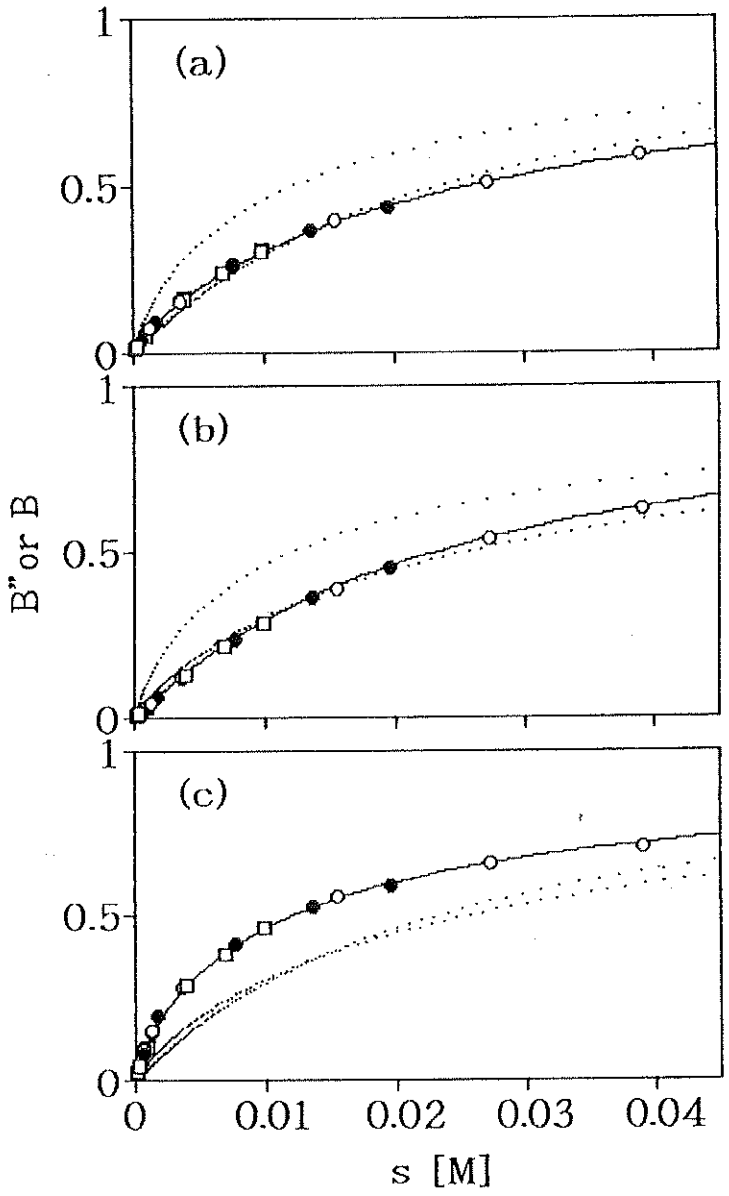


Fig 7.10. Solid curves: theoretical curves calculated by using the fact that $B''(s)$ can be represented as $B'[T_0^{-1}(s)]$. The solid curves in (a), (b) and (c) represent those for linear, concave and convex gradient elution modes, respectively. In each part, the theoretical curves appearing in the two other parts are also drawn as dotted curves. It can be considered that the three solid curves [in (a), (b) and (c)] are the projections on the (s,B) plane of three characteristic curves taking place in the ($\bar{m}$,s,B) space. Points: experimental plots obtained by mapping the points in Fig 7.9. The arrays of the points in (a), (b) and (c) correspond to those in the middle, the right part and the left part of Fig 7.9, respectively. The symbols are common to those used in both Figs 7.6 and 7.9.

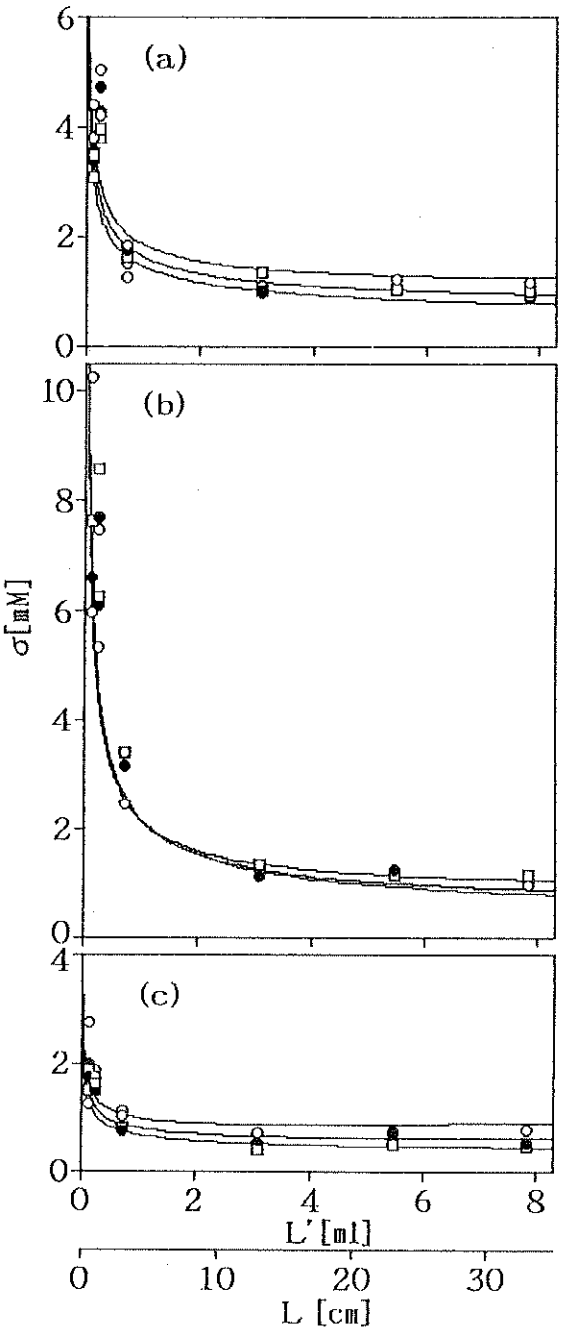


Fig 7.11. Points: experimental plots of σ versus L' or L for lysozyme obtained when g=0.296 mM/cm(□), 0.593 mM/cm(●) and 1.185 mM/cm(○). The concentration gradient applied is linear, concave and convex in (a), (b) and (c), respectively. Curves: theoretical curves calculated by using eq(6.8') with references to eqs(6.2), (6.7'), (6.9'), (6.18)-(6.20) and (6.23). [The prototype of the experimental plots can be found in ref(6.1) Fig 6.]

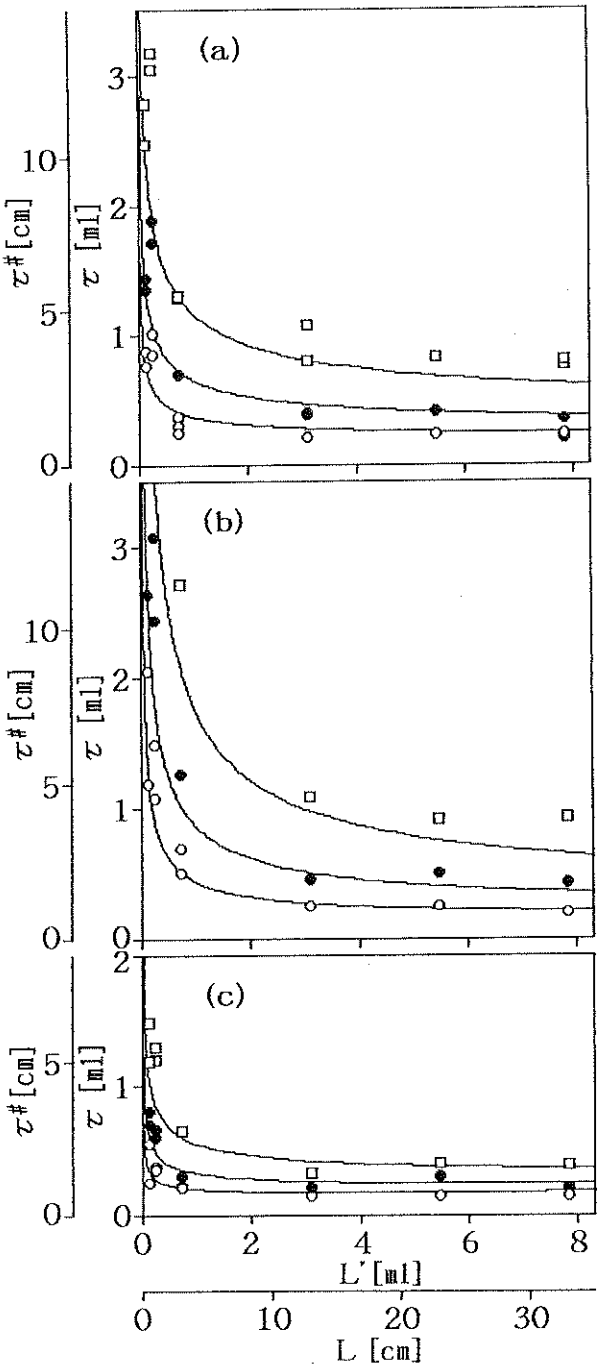


Fig 7.12. Points: experimental plots of τ or $\tau^{\#}$ versus L' or L for lysozyme obtained when g=0.296 mM/cm(□), 0.593 mM/cm(●) and 1.185 mM/cm(○). The concentration gradient applied is linear, concave and convex in (a), (b) and (c), respectively. Curves: theoretical curves calculated by using eq(6.8') combined with eq(6.11). [The prototype of the experimental plots can be found in ref(6.1)Fig 6.]

The curves in Fig 7.11 are theoretical, calculated by using eq(6.8') with references to eqs(6.2), (6.7'), (6.9'), (6.18)-(6.20) and (6.23). The curves in Fig 7.12 are also theoretical, calculated by using eq(6.8') combined with eq(6.11). [For the calculation of the curves drawn in both Figs 7.11 and 7.12, account is not taken of the leaking of the theoretical chromatogram to negative $\tilde{m}$ values taking place when s is extremely small (see Apendix V). It can be shown, however, that the leaking effect is negligible in practice as far as the curves under consideration are concerned.] In order to obtain best fits between theory and experiment in both Figs 7.11 and 7.12, the optimum value, 0.015 cm, of the parameter θ° or the optimum value, 0.00356 cm^3, of the parameter Θ° has been used [see eq(6.15)]. It can be seen in both Figs 7.11 and 7.12 that the coincidence between theory and experiment is fairly good. The experimental σ or τ tends to be slightly larger than the theoretical prediction when linear and concave gradients with the smallest g, 0.296 mM/cm, are applied, however [see Figs 7.11(a) and (b) as well as Figs 7.12(a) and (b)]. This problem will be argued in the subsequent Section(F).

In Appendix VI, another series of experiments carried out under much wider experimental conditions are analysed.

Good Separation Condition. In many instances, a good separation of the chromatographic peak from another peak can be attained when width σ of the peak under consideration is small; σ is represented in unit of the concentration of gradient substance. It can be understood from both Fig 7.11 and Appendix VI Fig A6.5 that, when g' or g is constant, then σ, in general, decreases rapidly with increase in L as long as L is small enough, but that σ increases slowly after the first rapid decrease. [In most cases in Fig 7.11 and in some cases in Appendix VI Fig A6.5, however, the minimum σ takes place outside the figure frame.] It can be considered that the first rapid decrease of σ arises as a result of the enhancement of the two effects of compression of band and decrease of chromatographic dilatation [see eq(3.35) and Appendix IV(A) Fig A4.2(c)]. The effect of axial diffusion in the column is small under these circumstances where B' is close to zero or where most of sample molecules stay on the adsorbent surface. On the other hand, the slow increase of σ taking place after the first rapid decrease can be considered to arise as a result of axial diffusion in the column. Both effects of compression of band and decrease of chromatographic dilatation are small under these circumstances where B' is close to unity or where most of sample molecules stay in the liquid phase.

It can also be understood from Appendix VI Fig A6.5 that σ, in general, decreases with decrease in g' or g, and that L giving σ the minimum value when g' or g is constant shifts to large values with decrease in g' or g. [In the range of the experimental conditions used in Fig 7.11, however, the rate of decreae of σ is very low, and the experimental σ is virtually independent of g' or g within the limits of the experimental error.] It can now be concluded that, as a general rule, a good separation condition can be attained by decreasing g' or g and increasing L moderately at the same time in order to have optimum L (but see the last paragraph in this Section).

By using both eqs(6.8) and (6.9), it can be predicted that optimum L giving σ the minimum value when g' or g is constant decreases as transition of B' from ≈ 0 to 1 taking place with increasing $\hat{m}$ becomes sharp, and that optimum L tends to infinitesimal when B' manifests a step transition [cf. Fig 3.2(c)]. This is evident because, once MB(o) adsorbed initially at the inlet of the column shifts from solid to liquid phase stepwise or completely, then it will only continue spreading, induced by axial diffusion taking place in the liquid phase. This means that the minimum (ideally the infinitesimal) σ can be brought about by using infinitesimal length, L, of the column since there is neither compression nor expansion of band when the molecules are staying only in the liquid or mobile phase. According to competition model, the transition of B' or $\dot{B}$ from ≈ 0 to 1 becomes sharp with increase in size x' of sample molecule; B' or $\dot{B}$ manifests a step transition when x' approaches infinity (see the subsequent Chapter Ⅷ). This means that optimum L giving σ the minimum value decreases with increase in size of sample molecule.

By using both eqs(6.8) and (6.9), it can also be predicted that, under a given experimental condition where both L and g' (or g) are fixed, σ decreases as transition of B' from ≈ 0 to 1 (taking place with increasing $\hat{m}$) becomes sharp; σ converges to a constant value when B' manifests a step transition. Therefore, according to competition model, σ can be predicted to decrease with increase in size x' of sample molecule, tending to a constant value when x' approaches infinity. [The aspect of the decrease of σ taking place with increase in x' calculated by using the old theory[Chapter Ⅵ(D)] is shown in ref(7.2) Fig 2.]

As for the mixture of molecules manifesting considerable differences in the sharpness of the transition of B' or $\dot{B}$ from ≈ 0 to 1 as a function of $\hat{m}$ or m (or, according to competition model, the mixture of molecules with considerable differences in size x'), it is imposible to consider the general optimum separation condition. This is because, the inverse of the order of elution may take place between different molecules when experimental conditions are changed [see the subsequent Chapter Ⅷ(D)].

(F) A Consideration

The experimental σ or τ of the lysozyme peak obtained by using the spherical HA packed column tends to be slightly larger than the theoretical prediction when linear and concave gradients with the smallest g (0.296 mM/cm) are applied [see Figs 7.11(a) and (b) as well as Figs 7.12(a) and (b)]. The parallel takes place with the plate-like HA packed column when a linear gradient with the smallest g (0.0387 mM/cm) is applied [see Appendix Ⅵ Figs A6.5 and A6.6]. It should be noted that, under these experimental conditions, the elution potassium concentration, μ, is the lowest on an average, being of the order of 0.1 M with the spherical HA packed column [see Figs 7.3(a) and (b)] and still lower with the plate-like HA packed column (see Appendix Ⅵ Fig A6.1). [A similar conclusion was attained for chromatography of cytochrome c carried out by using the spheri-

cal HA packed column.]

It is presumable that the deviation from the theoretical prediction arises from a secondary effect (probably with a kinetic mechanism; see below) which may or may not be specific to HA chromatography. Thus, under isocratic conditions with the spherical HA packed column, it was observed that standard deviation of the lysozyme peak tends to increase very rapidly (with an abnormal rate) with decrease in potassium concentration, m, of KP buffer when m is lower than about 0.1 M. Under these experimental conditions, molecular partition, $\dot{B}$, in the mobile phase occurring at the maximum height of MB(o) migrating on the column (which is numerically equal to the R_F value taking place at that position) is smaller than about 0.1 (see both Fig 7.8 and Appendix VI Fig A6.3). The observation leads to a prediction that the chromatographic peak with an abnormally large width will occur even under gradient conditions if a small g is applied since it induces a small μ (see above). Moreover, it can be suggested that the Θ° or θ° values estimated in both Section(E) and Appendix VI are also deviating toward values larger than the true values; this is because the sample molecule is staying in potassium concentration m lower than μ until it is eluted from the column.

Whether or not the abnormal increase in standard deviation of the chromatographic peak occurs in columns other than the HA column is not clear. In fact, the unpractical experimental data obtained by using extremely small $\dot{B}$ or R_F values (less than about 0.1) do not make appearance in public usually.

According to van Deemter et al. [or to the consideration performed in Chapter I (A)], the dependence of θ° [$=\dot{H}/2$; see eq(6.16)] on molecular partition, B°, in the mobile phase taking place with isocratic chromatography can be represented by Appendix XI (A) eq(A11.19') [or eq(1.33″)]; this has been derived on the basis of the first order kinetics introduced by Lapidus and Amundson[Appendix XI(A) eq(A11.5)] [or on the basis of the consideration performed in Chapter I (A)]. Let us examine whether or not the abnormal feature of HA chromatography can be explained by Appendix XI(A) eq(A11.19') [or eq (1.33″)]. With HA chromatography with competition mechanism(Chapter VIII), it appears to be reasonable to hypothesize that B° decreases to approach zero with decrease in m while increasing rate constant, ϕ_I, of adsorption infinitely and keeping rate constant, ϕ_{II}, of desorption constant; as a result, θ° would approach $\bar{\theta}^\circ$ [see Appendix XI(A) eq (A11.19'), or eq(1.33″)]. The hypothesis does not explain, however, the rapid increase in standard deviation of the lysozyme peak occurring with decrease in m with the isocratic case (see above). If B° decreases to approach zero while decreasing ϕ_{II} toward infinitesimal and keeping ϕ_I constant, then θ° increases to approach $\bar{\theta}^\circ + u/\phi_I$ [see Appendix XI(A) eq(A11.19'), or eq(1.33″)]. Although this hypothesis appears to be compatible with the increase in standard deviation of the lysozyme peak taking place more rapidly than that induced by the quasi-static mechanism, it does not explain satisfactorily the very rapid increase occurring especially when $m \lesssim 0.1$ M (see above). Moreover, the reason why this hypothesis should actually be realized cannot be found. It can be suggested that the

rapid increase in standard deviation is induced by a kinetic mechanism of higher order taking place when B° is small. Further, a possibility cannot be excluded that the dependence of Θ° on B° [or B; eq(1.33)] [which is neglected by replacing Θ° with a mean value in the present treatment; see the subsection entitled "Quasi-Static Chromatography versus Nonequilibrium Thermodynamics" in Chapter I (A)] interferes in the kinetic mechanism at least partially.

Chapter Ⅷ. Competition Model in Contrast with Hydroxyapatite Chromatography

(A) Background

Competition model which can be considered to offer the basis of the adsorption and desorption mechanism of a wide range of chromatographies [see the subsequent Section (D)-(H); Chapter Ⅸ and Ⅹ; and Appendix ⅪI(C), (D) and (F)] was originally introduced for the purpose of exploring the mechanism taking place on the crystal surfaces of hydroxyapatite(HA) particles packed in the column. The HA crystal with a chemical composition $Ca_{10}(PO_4)_6(OH)_2$ usually is considered to belong in the space group $P6_3/m$ characterized by primitive vectors $\mathbf{a}$, $\mathbf{b}$ and $\mathbf{c}$ with $\mathbf{a} \wedge \mathbf{b} = 120^\circ$, $\mathbf{a} \wedge \mathbf{c} = \mathbf{b} \wedge \mathbf{c} = 90^\circ$, $|\mathbf{a}| = |\mathbf{b}| = 0.942$ nm and $|\mathbf{c}| = 0.688$ nm(8.1, 8.2). HA chromatography, introduced over forty five years ago by Tiselius et al.(8.3) is a powerful technique for separation of proteins, nucleic acids and viruses in aqueous systems, and it often is carried out by using a concentration gradient of sodium or potassium phosphate buffer at pH≈6.8 [an equimolar mixture of NaH_2PO_4 and Na_2HPO_4 (called NaP buffer) or an equimolar mixture of KH_2PO_4 and K_2HPO_4 (called KP buffer; see Chapter Ⅶ)](7.1). The classical developments of HA chromatography are reviewed by Bernardi(8.4-8.6), and the recent developments are reviewed by Kawasaki (7.1).

Nearly forty years ago, Bernardi(8.7) carried out chromatography of DNA on the HA column by using a linear concentration gradient of KP buffer with phosphate elution molarity, μ, at the center of MB(o) slightly higher than 0.2 M. It was found out(8.7) that, when chromatography was done while keeping constant the ionic strength of the carrier liquid by applying a negative KCl gradient at the same time, elution phosphate molarity μ was essentially the same as in the absence of the negative KCl gradient. From these data, Bernardi(8.7) deduced that the adsorption of polynucleotides on HA takes place because of the electrostatic interaction between the negative phosphate groups of the nucleic acids and the positive calcium ions on the HA crystals. Increasing the molarity of the eluting phosphate buffer progressively reduces this interaction to zero, at which point desorption occurs(8.7). The decrease in the interaction appears to be due to a specific competition between the phosphate ions of the eluting buffer and the phosphates of polynucleotides for the calcium ions of HA, and not simply to increase of ionic strength [because μ is independent of the presence of the negative KCl gradient; see ref(8.7)].

Bernardi(8.7) also found out that μ for DNA was quasi-independent of molecular mass(M_w) when it was higher than about 10^5 Da, but that enzymatically degraded DNA (to M_w lower than 5×10^4 Da) were eluted at lower phosphate molarities. These results are supported by Wilson and Thomas(8.8) who showed that, when chromatographed by using a linear KP or NaP gradient, μ for DNA with more than about 100 nucleotide pairs (with $M_n \gtrsim 10^5$ Da) increased only slowly with increase in M_n, whereas μ for DNA with 17 to 100 nucleotide pairs (with M_n between 10^4 and 10^5 Da) decreased fairly rapidly with

decrease in M_n [see both Table I and Fig 2 in ref(8.8)]. On the other hand, low M_n substances like amino acids(8.3, 8.9) or oligonucleotides(8.10), in general, are not adsorbed or adsorbed only weakly on HA crystals except for some cases [8.11; cf. the subsequent Section(E)]. From the fact that μ for high M_n DNA is quasi-independent of M_n, Bernardi (8.7) deduced that the adsorption-elution phenomenon is fundamentally associated to one single property of the polynucleotides, namely, their linear charge density (i.e., the *intensive* property of the molecule).

The competition mechanism of HA chromatography (deduced above by Bernardi) can also be deduced from the quasi-independence of μ from M_n taking place with high M_n DNA. Thus, suppose that adsorbing sites are arranged on the crystal surface of HA (with a minimum inter-site distance of the order of magnitude of the size of the crystal unit cell; see above). Let x' be the number of phosphate ions (from the buffer) the adsorption of which on the HA surface is impossible owing to the presence of an adsorbed DNA molecule, and let x be the number of crystal adsorbing sites bonding with the adsorbed DNA. [If a phosphate ion (from the buffer) occupies a single crystal site when it is adsorbed, x' also represents the number of crystal sites on which the adsorption of phosphate ions is impossible owing to the presence of an adsorbed DNA molecule i.e., the number of crystal sites covered by an adsorbed DNA molecule. In this instance, $x \leqq x'$.] It should be noted that x' measures the size of the DNA molecule. It can now be considered that, if the competition mechanism takes place in fact, then μ should roughly be determined by the ratio x/x':

$$\mu \sim x/x' \tag{8.1}$$

or that μ should be quasi-independent of x' or M_n. Thus, when x' is constant, the strength of adsorption of DNA would increase with increasee in x, so that μ would increase with increase in x. On the other hand, when x is constant, then the larger the x' value, the more effectively the adsorption of DNA would be hindered and the desorption of DNA would be promoted by phosphate ions, respectively; this is because x' represents the degree or extent of receiving the effect of competition. μ therefore would decrease with increase in x'. It follows that μ would be determined by "density" x/x' (i.e., by the intensitive property of the molecule), and that μ is independent of M_n. [Further, μ would increase if phosphate ion is replaced by another anion larger in size but with the same electric charge as that of phosphate ion. Thus, for the anion (from the buffer), the degree or extent of receiving the effect of competition with sample molecules would increase with increase in its size. Arguing in the other direction, the inherent "force" of the anion driving sample molecules out of the HA surface would decrease with increase in size of the anion provided that its electric charge is constant. For the experimental proof of this hypothesis (along with the proof that μ decreases with increase in electric charge of competing ions), see the end of this Section.]

The reason why μ decreases with decrease in M_n when M_n is relatively low can be

understood as follows. Thus, the fact that extremely low M_m substances (like amino acids or oligonucleotides) are not adsorbed or adsorbed only weakly on the HA surface (even in the absence or in the presence of a small amount of competing ions) can be assumed to arise from the fact that only a small number (only one or even zero in typical cases) of functional groups per molecule are (is) available for the adsorption. In this instance, the absolute value of the energy of adsorption per molecule would be much smaller than that necessary to bring about fraction, $1-B$, of time spending in the adsorbed state close to unity. If concentration gradient chromatography is carried out, the μ values of these substances would be equal or close to zero. When considering a series of substances with M_m decreasing continuously to extremely small ones, the corresponding μ value would decrease to tend to zero or the vicinity of zero.

Additional experimental data implying the competition mechanism obtained by Kawasaki and Bernardi are illustrated in Fig 8.1 [reproduced from ref(6.1)]. Thus, chromatographies of cytochrome c ($M_m=1.25\times10^4$ Da), lysozyme ($M_m=1.43\times10^4$ Da), β-lactoglobulin A [$M_m=3.5\times10^4$ Da; cf. Chapter X(B)], collagen ($M_m=3\times10^5$ Da) and T_2 phage particle ($M_m\approx2.6\times10^8$ Da) were carried out on HA columns with several total lengths, L' or L, by using linear concentration gradients of KP buffer with two different slopes, g' or g, and Fig 8.1 shows the plots of phosphate elution molarity μ versus L. It can be seen in Fig 8.1 firstly that all the substances are eluted around $\mu=0.1$ M despite 10^4 times of difference between minimum and maximum values of M_m. This reinforces the data of the quasi-independence of μ from M_m obtained with high M_m DNA, implying the competition mechanism taking place even with substances other than polkynucleptides. Secondly, μ increases with increase in either L or g with protein molecules with M_m of the order of magnitude of 10^4 Da (cytochrome c, lysozyme and β-lactoglobulin A). When M_m increases to 3×10^5 Da (collagen), the dependence of μ on either L or g appears to decrease. [For this problem, cf. the legend for Fig 8.1. Later, a certain modification will be added to the interpretation on the collagen data, however [see Section(F)].] With T_2 phage particle with M_m about equal to 2.6×10^8 Da, μ is independent of both L and g (see Fig 8.1). [Similar data for lysozyme obtained later under different experimental conditions are illustrated in Fig 7.3, Fig 8.3(a) [reproduced from ref(6.9) or (7.1)], and Appendix VI Fig A6.1 [reproduced with modification from ref(6.8)]. Other similar data are published in ref (6.1) Fig 2, ref(6.8) Fig 4, and ref(6.9) Figs 5-9. It can be seen in ref(6.8) Fig 4 that μ for DNA ($M_m=1-5\times10^7$ Da) depends on both L and g fairly weakly.]

From the experimental analysis performed in Chapter VII, it can be understood that the increase of μ taking place with increase in L or g represents a natural conclusion predicted independently of whether the competition mechanism interferes or not. The decrease of the dependence of μ on either L or g taking place with increase in M_m, however, will be predicted quantitatively by using the competition model specified in the subsequent Section(B) and (C) [see Section(D)]. Both the quasi-independence of μ from M_m taking place with high M_m substances and the decrease of μ with decrease in M_m taking

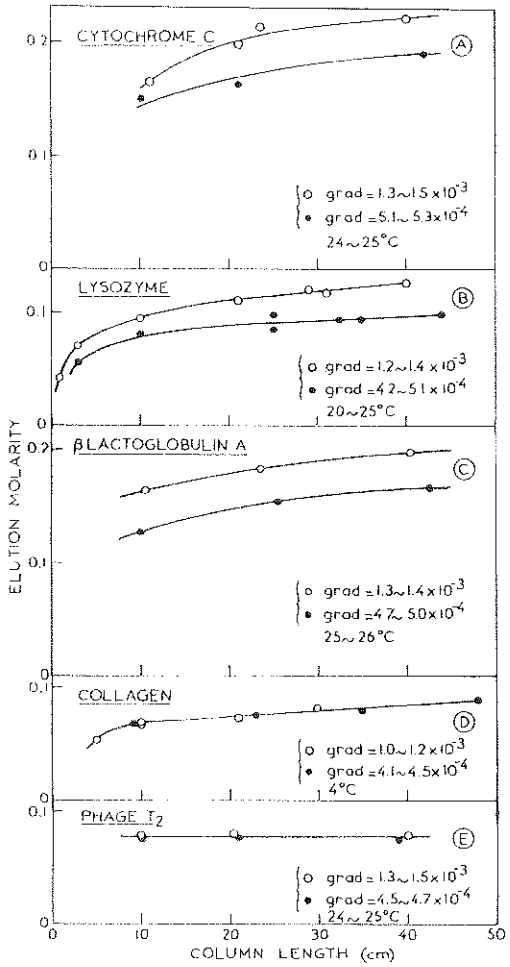


Fig 8.1. Plots of phosphate elution molarity, μ, versus total length, L, of the column for two different slopes, grad (M/ml), of the linear concentration gradient of KP buffer applied, obtained for HA chromatography for Ⓐ cytochrome c, Ⓑ lysozyme, Ⓒ β-lactoglobulin A, Ⓓ collagen, and Ⓔ T_2 phage particle; the symbol "grad" is identical with the symbol "$g'_{(P)}(\varnothing=1$ cm)" defined in Note in Table 7.1. [For the relationship between $g'_{(P)}(\varnothing=1$ cm) and g', also see Note in Table 7.1 where it should be noted that g' for potassium ion is 1.5 times as large as g' for phosphate ion.] The column internal diameter, $\varnothing$, is 1 cm always, and the HA particles used for the experiment are almost identical with those used in the experiments mentioned in Appendix VI. In part Ⓓ, it appears that μ for collagen depends only on L and that it is independent of grad. By carefully analyzing experiments carried out under condition of small enough sample loads for the effect of mutual interaction between collagen molecules to be eliminated almost completely, however, it can be shown that μ depends on both L and grad much slightly than the case of cytochrome c Ⓐ, lysozyme Ⓑ, or β-lactoglobulin A Ⓒ (cf. Fig 8.20). [Reproduced from ref(6.1) Fig 1.]

place with relatively low M_m substances will also be predicted quantitatively by using the specified competition model [see Section(B)-(D)].

It can be visualized(7.1) that adsorbing sites (called C sites) each constructed from two crystal calcium ions are arranged on the **a** (or **b**) surface of HA in a rectangular manner with an inter-site distance in the **b** (or **a**) direction equal to $|\mathbf{b}|$ $(=|\mathbf{a}|)=0.942$ nm and inter-site distance in the **c** direction equal to $|\mathbf{c}|/2=0.344$ nm. A phosphate ion (with a diameter of about 0.5 nm) from KP or NaP buffer and a phosphate group of nucleic acids can be adsorbed on a C site, respectively (consistently with the deduction of Bernardi; see above). According to the competition mechanism (see above), nucleic acids and phosphate ions from the buffer compete for adsorption on C sites. Except some cases, acidic proteins (with isoelectric point, pI, lower than 7) are also adsorbed mainly on C sites by using carboxyl groups (and/or phosphate groups in the case of phosphoproteins), and they compete for adsorption with phosphate ions. It can be suggested that the carboxyl group bonds to the position deviating slightly from that of the C site on the HA surface. In this instance also, let us say for the sake of simplicity that the carboxyl group bonds with the C site. On the **c** crystal surface of HA, other adsorbing sites (called P sites) are present, each constructed from six negatively charged oxygen atoms belonging to three crystal phosphates. P sites are arranged in a hexagonal manner with the minimum inter-site distance in both **a** and **b** directions equal to $|\mathbf{a}|=|\mathbf{b}|=0.942$ nm. Except some cases, basic proteins (with pI higher than 7) are adsorbed mainly on P sites by using ε-amino and/or guanidinyl groups, and they compete for adsorption with sodium ions (with a diameter of 0.19 nm) or potassium ions (with a diameter of 0.26 nm) from the buffer which are also adsorbed on P sites. [For detail on all the arguments above, see ref(7.1)]. A possibility cannot be excluded, however, that the two crystal surfaces of HA covered by an adsorbed acidic macromolecule and an adsorbed basic macromolecule constitute as a whole the surfaces represented by Miller indices higher than (100) [or (010)] and (001), respectively. If this is true, the effective arrangements of C and P sites on the active crystal surfaces would be deviating to some extent from those mentioned above.

It is experimentally confirmed that β-lactoglobulin A (pI=5.1-5.3) and collagen (although a basic pI can be deduced from its amino acid composition) are adsorbed mainly on C sites [see Section(F)], whereas cytochrome c (pI=9.8-10.6) and lysozyme (pI=10.5-11.0) are adsorbed mainly on P sites [see ref(7.1) and Section(E)-(G)]. Therefore, phosphate elution molarities, μ, for both cytochrome c and lysozyme(Fig 8.1) should be reinterpreted to represent potassium elution molarities of KP buffer expressed in unit 1.5 times as large as molarity; these are numerically equal to phosphate molarities.

Fig 8.2 [reproduced from ref(8.12)] illiustrates the plots of elution phosphate molarities μ (writen as $m_{elu(P)}$) versus logarithm of the parameter $s_{app(P)}$ [defined as being proportional to s $(=g'L'=gL)$; see eq(2.5) or (6.2), and cf. Fig 8.3(b)] obtained from a variety of linear concentration gradient HA chromatographies carried out by using competing ions with different sizes. Thus, in Fig 8.2(a), the sample applied is bovine serum albumin

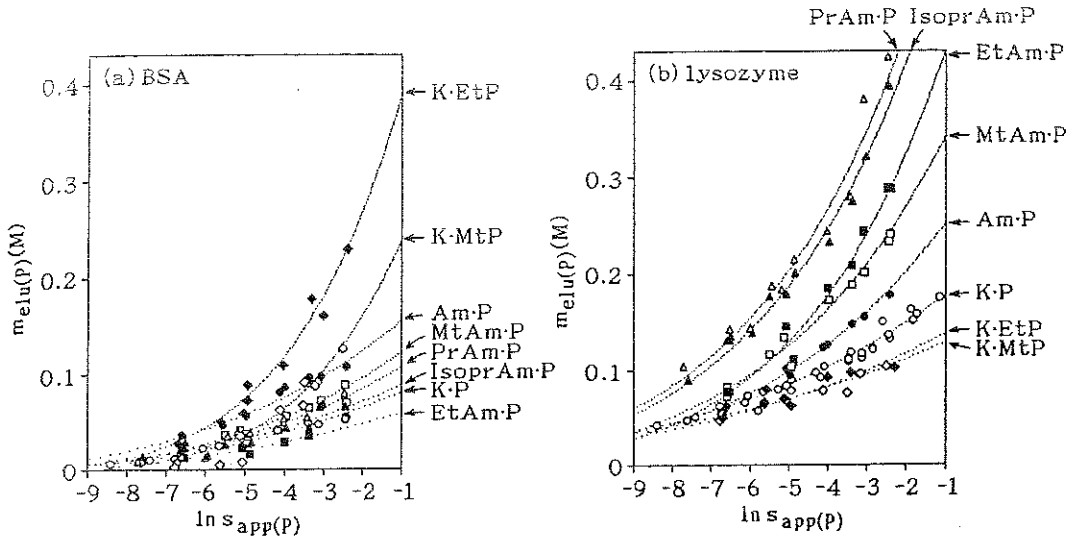


Fig 8.2. Plots of phosphate elution molarity μ (written as $m_{elu(P)}$) versus ln $s_{app(P)}$ for (a) bovine seumn albumin (BSA) and (b) lysozyme, obtained with HA columns by applying linear concentration gradients of eight types of buffer: KP(○), K·MtP(◇), K·EtP(◆), Am·P(●), MtAm·P(□), EtAm·P(■), PrAm·P(△), and IsoprAm·P(▲) buffer. The column internal diameter, ø, is 6 mm always, and the HA particles used for the experiment are almost identical with those used in the experiments in Fig 8.3. For detail, see text. [Reproduc-e d from ref(8.12) Fig 1.]

(with pI=4.7) which is experimentally confirmed to be adsorbed on C sites of HA(7.1), and linear concentration gradients of eight types of buffer were applied. These are KP buffer, two buffers (K·MtP and K·EtP buffers) obtained, respectively, by substituting methylphosphate and ethylphosphate ion for phosphate ion of KP buffer, and five buffers (Am·P, MtAm·P, EtAm·P, PrAm·P and IsoprAm·P buffers) obtained, respectively, by substituting ammonium, methylammonium, ethylammonium, propylammonium and isopropylammonium ion for potassium ion of KP buffer. For each buffer system, about ten or more experiments were performed while changing both total length, L' or L, of the column and slope, g' or g, of the concentration gradient applied (similarly to the case of Fig 8.1), thus generating about ten or more $s_{app(P)}$ values, or the corresponding experimental points [see Fig 8.2(a)]. It can be seen in Fig 8.12(a) that, when the cation contained in the buffer is potassium ion, the arrangement of the experimental points shifts considerably to high μ values with increase in size of the anion contained in the buffer i.e., in the order of phosphate, methylphosphate and ethylphosphate ion. On the other hand, the arrangement of the experimental points depends only slightly on the size of the cation contained in the buffer, and, when focusing our attention on the slight dependence, no correlation can be found between the position of the arrangement and the size of the cation [see Fig8.2(a)]. These data can be considered to manifest the fact that the competition takes place between bovine serum albumin and the anion from the buffer for adsorption on the HA surface, and that the inherent "force" of the anion driving the albumin molecule out of the HA surface decreases with increase in size of the anion.

In Fig 8.2(b), the sample applied is lysozyme (with pI=10.5-11.0) which is experimentally confirmed to be adsorbed on P sites of HA(7.1); linear concentration gradients of the eight types of buffer were also applied, and, for each buffer system, about ten or more experiments were performed while changing both L and g [as in Fig 8.2(a)]. It can be seen in Fig 8.2(b) that, when the anion contained in the buffer is phosphate ion, the arrangement of the experimental points shifts considerably to high μ values with increase in size of the cation contained in the buffer i.e., in the order of potassium, ammonium, methylammonium, ethylammonium, and propyl- or isopropylammonium ion. On the other hand, the arrangement of the experimental points depends only slightly on the size of the anion contained in the buffer [see Fig 8.2(b)]. These data can be considered to manifest the fact that the competition takes place between lysozyme and the cation from the buffer for adsorption on the HA surface, and that the inherent "force" of the cation driving the lysozyme molecule out of the HA surface decreases with increase in size of the cation. Similar experimental data were obtained for cytochrome c (pI=9.8-10.6) also(8.12). Phosphate elution molarities μ (where phosphate implies methylphosphte and ethylphosphate also) for lysozyme and cytochrome c should be re-interptreted to represent cation elution molarities expressed in unit 1.5 times as large as molarity.

It should be added that, elution molarities μ for basic proteins are of the same order of magnitude between the buffer systems containing univalent potassium (with a diame-

ter of 0.26 nm) and sodium (with a diameter of 0.19 nm) ions, respectively(7.1). Between the systems containing, respectively, divalent calcium (with a diameter of 0.20 nm) and magnesium (with a diameter of 0.13 nm) ions, μ for basic proteins are of the same order of magnitude again(7.1). μ in the divalent cation system, however, are generaly much lower than those in the univalent cation system(7.1). These data can also be considered to manifest the fact that the competition takes place between basic proteins and the cation from the buffer for adsorption on the HA surface. In this instance, the inherent "force" of the cation driving basic protein molecules out of the HA surface increases with increase in electric charge of the cation; the sizes of potassium, sodium, calcium and magnesium ions are of the same order of magnitude.

(B) Competition Model and the Calculation of Adsorption Isotherm

Over thirty years ago, a specified competition model was originally introduced by Kawasaki(6.2) who was working in the laboratory of Prod.G.Bernardi [cf. Chapter VI(D)]. The model states that adsprbing sites are arranged in some manner on the surfaces of packed particles in the column; sample molecules with functional adsorption groups and substances as a component of the concentration gradient (called gradient substances) compete for adsorption on the sites. In typical cases, a gradient substance occupies effectively only one site when it is adsorbed, whereas a sample molecule covers plural sites. The adsorption isotherm for each component of the sample mixture can be calculated by using competition model(6.2, 6.5, 8.13-8.17).

It can, in general, be assumed that both geometrical and energetical interactions take place (a) between sample molecule and gradient substance, (b) between sample molecule and "inactive" solvent components (involving water and other components coming in part from the concentration gradient) that do not interfere directly in the competition mechanism, (c) between gradient substance and "inactive" solvent components, (d) among sample molecules (involving all the components of the sample mixture), (e) among gradient substances, and (f) among "inactive" solvent components. In competition model, the geometrical interaction between sample molecule and gradient substance taking place on the adsorbent surface is emphasized in particular (in which the teminology "competition model" has its rise), and the geometrical interaction among gradient substances taking place on the adsorbent surface plays an important role of entropy effect [cf. the subsection entitled "Chemical Equilibrium Equation Model versus Competition Model" in Appendix XI(C)]. The presence of the "inactive" solvent components is neglected in appearance, and energy or free energy of adsorption of a substance simply implies the difference in energy or free energy levels of the total thermodynamic system taking place between the two states where the substance is adsorbed and it is in solution; the latter concept holds whether the "inactive" solvent components are present or not. The concept of the effective energetical interaction taking place among sample molecules on the adsorbent surface in the

presence of the "inactive" solvent components is replaced by the hypothetical concept of the energetical interaction taking place in the absence of the "inactive" solvent components. The energetical interactions between sample molecule and gradient substance taking place both on the adsorbent surface and in solution are neglected also (but see below), and the energetical interactions among gradient substances (taking place both on the adsorbent surface and in solution) and the geometrical interaction among gradient substances (taking place in the mobile phase) are incorpolated in the experimental parameter φ [eq (8.45); cf. the subsection entitled "Comparison with Competition Model" in Appendix XI (F)]; the energetical interaction implies the effective energetical interaction taking place in the presence of the "inactive" solvent substances. Especially with small sample loads when the density of sample molecules in a slice of the column is low (the case treated in this monograph), both geometrical and energetical interactions among sample molecules taking place both on the adsorbent surface and in solution are negligible in fact; only thermal energies are exchanged between molecules.

In competition model, the energetical interactions between sample molecule and gradient substance taking place both on the adsorbent surface and in solution are neglected (see above). When strong enough attractive interactions take place between a sample macromolecule and gradient substances in such a way that the macromolecule behaves in association with a number of gradient substances in the liquid phase, however, it would be possible to reconsider that the complex of macromolecule and gradient substances represents an element of the thermodymamic or statistical mechanical system in practice. In this instance, let us assume that the energy of association is low enough in comparison with the enerrgy of adsorption of the macromolecule on the adsorbent surface (although the former is high enough for the association to be realized in practice). This would mean that, when the complex is adsorbed on the adsorbent surface, a portion of competing substances (the number of which is denoted by x'') are released from the local surface of the macromolecule in order for the macromolecule to keep in direct contact with the adsorbent surface (through the local surface). This would mean that the competition between the complex and gradient substances for adsorption on the adsorbent surface takes place while releasing x'' gradient substances, and that the number x' of gradient substances (from the bulk solution) the adsorption of which is impossible owing to the presence of the adsorbed complex is apparently replaced by the number $x'-x''$. On the other hand, when the complex is desorbed, the maximum possible number of gradient substances (from the bulk solution) that can be adsorbed on the adsorbent surface where the complex was present before desorption is equal to x'. As x'' gradient substances (from the bulk solution) are added to the complex when it is desorbed, however, it would be apparent that the maximum possible number of gradient substances that can be adsorbed on the adsorbent surface where the complex was present before desorption is equal to $x'-x''$. In conclusion, the parameter x' appearing in competition model would actually be representing $x'-x''$ provided that $x'>x''$. *

---

* [*Note*. Here it is assumed that the x'' value virtually is kept constant during the chromatographic process].

With small sample loads when the density of sample molecules in a slice of the column is low and when both geometrical and energetical interactions among sample molecules taking place both on the adsorbent surface and in solution are negligible, it is sufficient to consider a two-component system of gradient substance [hereafter also called as competing substance; denoted by subscript (0)] and the component under consideration of the sample mixture [hereafter called simply as sample molecule; denoted by subscript (1)]. Adsorption isotherm for sample molecule can now be represented as a relationship among three quantities: (a) density of sample molecules on the adsorbent surface, (b) activity or concentration of sample molecules in solution, and (c) activity or concentration of competing substances in solution. The calculation of adsorption isotherm will be performed below by using a simplified form of the general method developed in refs(8.15-8.17) under assumption that a competing substance occupies a single site of the adsorbent when it is adsorbed. If it occupies plural sites, the interpretation on the parameter x' should be modified in some processes of the calculation.

Thus, assuming that a sample molecule can take a number of different configurations when it is adsorbed on the adsorbent surface or that the molecule can be adsorbed by using a number of different local molecular surfaces each of which can face the adsorbent surface, partition function, Ξ, for the grand canonical two-component adsorbed system can be written as

$$\Xi = \sum_{n'_{(0)}+n'_{(1)} \leqq M} \exp\left(\sum_{\rho=0}^{1} n'_{(\rho)} \mu_{(\rho)}/kT \right) Z \tag{8.2}$$

in which

$$Z = \omega[\mathbf{n}'] e^{n'_{(0)} \varepsilon /kT} \left(\sum_{j=1}^{\nu} e^{E_j/kT} \right)^{n'_{(1)}} \tag{8.3}$$

and

$$\mathbf{n}' = (n'_{(0)}, n'_{(1)}) \tag{8.4}$$

The physical meanings of the symbols in eqs(8.2)-(8.4) are: $n'_{(\rho)}$=total number of competing substances (when $\rho=0$) or sample molecules (when $\rho=1$) on the adsorbent surface, comprised between 0 and M; M=upper limit of the $n'_{(0)}+n'_{(1)}$ value which depends on the ratio between $n'_{(0)}$ and $n'_{(1)}$; $\mu_{(\rho)}$=chemical potential for component ρ; $-\varepsilon$ ($\varepsilon > 0$)=effective adsorption energy of a competing substance on an adsorbing site, or the difference in effective energy levels of the total thermodynamic system taking place between the two states where competing substance is adsorbed and it is in solution (for "effective-

ness" see below); j=a configuration of sample molecule on the adsorbent surface; ν =total number of possible configurations of sample molecule on the adsorbent surface; $-E_j$ ($E_j>0$)=adsorption energy of a sample molecule on adsorbing sites taking place when the j th configuration is being realized, or the difference in energy levels of the total thermodynamic system taking place between the two states where sample molecule is adsorbed (in the j th configuration) and it is in solution; k=Boltzmann constant; T=absolute temperature; and $\omega[\mathbf{n}']$=total number of microscopic states on the adsorbent surface taking place when the total numbers of competing substances and sample molecules are $n'_{(0)}$ and $n'_{(1)}$, respectively. This depends on both location and orientation of all the substances (competing substances+sample molecules) on the adsorbent surface. [*Note 1.* The symbol k represents the Boltzmann constant whenever it appears in the form of kT. In this instance, let us reconsider that "kT" represents a symbol rather than a product of k by T. Otherwise, k represents capacity ratio. An exception of this rule takes place, however, in the subsection entitled "Analysis of Figs 10.10, 10.11 and 10.13 for Polyphosphates" in Chapter X(C). *Note 2.* With HA chromatography, it can, in general, be assumed that a protein molecule can be adsorbed on both C and P sites by using carboxyl (and/or phosphate) groups, and ε-amino and/or guanidinyl ghroups, respectively. It can, however, be assumed that a Boltzmann distribution takes place between the two types of adsorption and that, in many instances, the Boltzmann distribution is biased toward one of the two extremes: acidic molecules are adsorbed mainly on C sites whereas basic molecules are adsorbed mainly on P sites [see Section(A)]. Eqs(8.2)-(8.4) are valid only for the case when the Boltzmann distribution is biased toward one of the two extremes.]

The term $\sum_{j=1}^{\nu} e^{E_j/kT}$ in eq(8.3) can be rewritten as

$$\sum_{j=1}^{\nu} e^{E_j/kT} = \tau e^{E/kT} = e^{(E+kT\ln\tau)/kT} \tag{8.5}$$

in which

$$E = \sum_{j=1}^{\nu} \gamma_j E_j \tag{8.6}$$

$$\ln\tau = -\sum_{j=1}^{\nu} \gamma_j \ln\gamma_j \tag{8.7}$$

and

$$\gamma_j = e^{E_j/kT} / \sum_{j'=1}^{\nu} e^{E_{j'}/kT} \tag{8.8}$$

γ_j [eq(8.8)] represents the probability of occurrence of the j th configuration, manifesting a Boltzmann distribution. E [eq(8.6)] and $\ln\tau$ [eq(8.7)] represent expectation values of $E_{j'}$ and $\ln(1/\gamma_{j'})$, respectively. τ therefore represents the effective number of adsorption configurations which a sample molecule can take on the adsorbent surface, provided that the molecular conformation does not change between adsorbed and solution states. If the conformation change takes place between the two states, the interpretation on τ should be modified. $-(E+kT\ln\tau)$ [eq(8.5)] represents free energy of adsorption per molecule. Absolute value of free energy of adsorption (abbreviated as AVFA) per molecule, $E+kT\ln\tau$, will be written as J in the subsequent Chapter IX and X. [*Note.* In the argument above, it tacitly is assumed that x' [cf. eq(8.20)] is constant, independent of the molecular configuration on the adsorbent surface, or the average of x' is considered when x' depends on the configuration actually.]

The term $\omega[\mathbf{n}']$ in in eq(8.3) can be represented as

$$\omega[\mathbf{n}'] = \frac{1}{n'_{(\omega)}!n'_{(\omega)}!} \prod_{I=1}^{n'_{(\omega)}+n'_{(\omega)}} \{\phi_{(\rho)}[\mathbf{n}'']\}_I \tag{8.9}$$

in which ρ fluctuates arbitrarily between 0 and 1 with increase in I, and $\phi_{(\rho)}[\mathbf{n}'']$ represents the increment in times of the total number of both location and orientation of all the sbstances (competing substances+sample molecules) on the adsorbent surface taking place when the $n''_{(\omega)}$ th competing substance is added (provided that $n''_{(\omega)}-1$ competing substances and $n''_{(\omega)}$ sample molecules were present on the adsorbent surface before addition; the case when $\rho=0$), or when the $n''_{(\omega)}$ th sample molecule is added (provided that $n''_{(\omega)}$ competing substances and $n''_{(\omega)}-1$ sample molecules were present before addition; the case when $\rho=1$); it was provisionally hypothesized that all the competing substances and all the sample molecules were discernible from one another, respectively. $\phi_{(\omega)}[1,0]$ and $\phi_{(\omega)}[0,1]$ represent, however, the number of both location and orientation of a competing substance and that of a sample molecule taking place in the absence of any substance, respectively; these can be written as

$$\phi_{(\omega)}[1,\ 0] = \phi_{(\omega)}[0,\ 1] = n_o z \tag{8.10}$$

in which n_o represents the total number of adsorbing sites on the adsorbent surface, and z represents the coordination number of the sites. Here, it is assumed that both compet-

ing substance and sample molecule are asymmetric in shape. When these are symmetric, the z value reduces apparently. $\phi_{(\rho)}[\mathbf{n}'']$ decreases monotonically with increase in either $n''_{(\omega)}$ or $n''_{(\mu)}$ unless a certain type of phase transition takes place in the adsorbed phase, tending to zero when $n''_{(\omega)}+n''_{(\mu)}$ tends to $M+1$. $\omega[\mathbf{n}']$ is a state quantity. Thus, for a serial increase of I: 1, 2,..., $n'_{(\omega)}+n'_{(\mu)}$, there are a number of ways of variation of the corresponding set $\mathbf{n}''$ or $(n''_{(\omega)},n''_{(\mu)})$. The $\omega[\mathbf{n}']$ value is uniquely determined by the final set $(n'_{(\omega)},n'_{(\mu)})$ whatever may be the way through which the final set is attained.

Let us introduce

$$p_{(\rho)}[\mathbf{n}''] = \phi_{(\rho)}[\mathbf{n}'']/(n_0 z) \tag{8.11}$$

fulfilling

$$\left.\begin{aligned} \lim_{n''_{(\omega)}+n''_{(\mu)}\to 1} p_{(\rho)}[\mathbf{n}''] &= 1 \\ \lim_{n''_{(\omega)}+n''_{(\mu)}\to M+1} p_{(\rho)}[\mathbf{n}''] &= 0 \end{aligned}\right\} \tag{8.12}$$

where ρ represents either 0 or 1. Provided that the type of phase in the adsorbed system is constant, $p_{(\rho)}[\mathbf{n}'']$ decreases monotonically with increase in either $n''_{(\omega)}$ or $n''_{(\mu)}$, and it represents the probability that, when the $n''_{(\omega)}$ th competing substance is added at random to the adsorbent surface on which $n''_{(\omega)}-1$ competing substances and $n''_{(\mu)}$ sample molecules are adsorbed already, it is adsorbed successfully on the surface without being sterically hindered by already adsorbed substances (the case when $\rho=0$), or the probability that when the $n''_{(\mu)}$ th sample molecule is added at random to the adsorbent surface on which $n''_{(\omega)}$ competing substances and $n''_{(\mu)}-1$ sample molecules are adsorbed already, it is adsorbed successfully on the surface (the case when $\rho=1$). The randomness means that taking place within the limits that are compatible with the type of phase in the adsorbed system, and the Bragg-Williams random mixing approximation is used in the consideration.

With high M_n sample molecules with asymmetric (e.g., elongate) shapes, at least two types of phase would be conceivable in their adsorbed state: partially superposed phase (on one another) and non-superposed phase. Especially when the molecules are elongate in shape, taking into account the balance between energy and entropy effects, it would be the non-superposed phase that can be realized actually where the molecules are adsorbed with their main axes in parallel with one another. Still the presences of some sub-phases would be conceivable in the non-superposed phase. When the density of sample molecules is low, however, it would be reasonable to assume that the type of phase with respect to sample molecules taking place on the adsorbent surface is virtually constant. On the other hand, competing substances (with low M_n) are more or less symmetric in shape usually, implying that the phase transition such as affecting the $p_{(\rho)}$ value hardly takes place on the adsorbent surface even when their density is high. Hereafter, we assume that either $p_{(\omega)}$ or $p_{(\mu)}$ represents the probability.

Again introducing

$$\{y_{(\rho)}[\mathbf{n}'']\}_I = \frac{\{p_{(\rho)}[\mathbf{n}'']\}_I}{1-\frac{I-1}{M}} \tag{8.13}$$

($\rho = 0, 1$), eq(8.9) can be rewritten as

$$\omega[\mathbf{n}'] = \frac{(n_0 z)^{n'_{(0)}+n'_{(1)}}}{n'_{(0)}!n'_{(1)}!} \prod_{I=1}^{n'_{(0)}+n'_{(1)}} \{p_{(\rho)}[\mathbf{n}'']\}_I$$

$$= \left(\frac{n_0 z}{M}\right)^{n'_{(0)}+n'_{(1)}} \frac{M!}{n'_{(0)}!n'_{(1)}!(M-n'_{(0)}-n'_{(1)})!} \exp\left(\sum_{I=1}^{n'_{(0)}+n'_{(1)}} \{\ln y_{(\rho)}[\mathbf{n}'']\}_I\right) \tag{8.9'}$$

As $\omega[\mathbf{n}']$ is a state quantity, $\sum_{I=1}^{n'_{(0)}+n'_{(1)}} \{\ln y_{(\rho)}[\mathbf{n}'']\}_I$ is also a state quantity from which it follows:

$$\sum_{I=1}^{n'_{(0)}+n'_{(1)}} \{\ln y_{(\rho)}[\mathbf{n}'']\}_I = \sum_{\rho=0}^{1} \sum_{n''_{(\rho)}=1}^{n'_{(\rho)}} \ln y_{(\rho)}[\mathbf{n}''] \tag{8.14}$$

Eq(8.3) can be rewritten by using eqs(8.5), (8.9') and (8.14) as

$$Z = \frac{M!}{n'_{(0)}!n'_{(1)}!(M-n'_{(0)}-n'_{(1)})!} A_{(0)}^{n'_{(0)}} A_{(1)}^{n'_{(1)}} \tag{8.3'}$$

in which

$$A_{(0)} = \frac{n_0 z}{M} \exp\left(\frac{1}{n'_{(0)}} \sum_{n''_{(0)}=1}^{n'_{(0)}} \ln y_{(0)}[\mathbf{n}'']\right) e^{\varepsilon/kT} \tag{8.15}$$

and

$$A_{(1)} = \frac{n_0 z}{M} \exp\left(\frac{1}{n'_{(1)}} \sum_{n''_{(1)}=1}^{n'_{(1)}} \ln y_{(1)}[\mathbf{n}'']\right) e^{(E+kT\ln\tau)/kT} \tag{8.16}$$

In a grand canonical system, the probability of occurrences of the $n'_{(\rho)}$ values manifests a sharp distribution around the expectation value $n_{(\rho)}$. In both eqs(8.15) and (8.16),

it is possible to execute the approximation:

$$\frac{1}{n'_{(\rho)}} \sum_{n''_{(\rho)}=1}^{n'_{(\rho)}} \ln y_{(\rho)}[\mathbf{n}''] \approx \ln y_{(\rho)}[\mathbf{n}] \equiv \ln y_{(\rho)}(\boldsymbol{\theta}) \tag{8.17}$$

($\rho = 0, 1$); a justification of eq(8.17) is given in Appendix Ⅶ. 【It is recommended, however, to see Appendix Ⅶ after attaining eq(8.2').】 In eq(8.17), $\boldsymbol{\theta}$ is defined as

$$\boldsymbol{\theta} = (\theta_{(0)}, \theta_{(1)}) \tag{8.18}$$

in which

$$\theta_{(0)} = n_{(0)}/n_0 \tag{8.19}$$

and

$$\theta_{(1)} = x' n_{(1)}/n_0 \tag{8.20}$$

$\theta_{(0)}$ [eq(8.19)] represents the density of competing substances on the adsorbent surface. x' [eq(8.20)] is identical with x' appearing in eq(8.1), representing the number of adsorbing sites on which the adsorption of competing substances is impossible owing to the presence of an adsorbed sample molecule. Here, we assume that this is virtually equal to the number of sites on which the adsorption of other sample molecules is impossible owing to the presence of the adsorbed molecule under consideration. Under this assumption, $\theta_{(1)}$ [eq(8.20)] represents the density of sample molecules on the adsorbent surface. Let us write as $f[\mathbf{n}]$ and $f(\boldsymbol{\theta})$ when f is regarded as functions of $\mathbf{n}$ and $\boldsymbol{\theta}$, respectively [see eq (8.17)].

By using eq(8.17) and another approximation:

$$y_{(\rho)}(\boldsymbol{\theta}) = \frac{p_{(\rho)}(\boldsymbol{\theta})}{1 - \dfrac{n_{(0)}+n_{(1)}-1}{M}} \approx \frac{p_{(\rho)}(\boldsymbol{\theta})}{1 - \dfrac{n_{(0)}+n_{(1)}}{M}} \tag{8.21}$$

($\rho = 0, 1$), eqs(8.15) and (8.16) can be rewritten as

$$A_{(0)} = \frac{n_0 z}{M} \cdot \frac{p_{(0)}(\boldsymbol{\theta})}{1 - \dfrac{n_{(0)}+n_{(1)}}{M}} e^{\varepsilon/kT} \tag{8.15'}$$

and

$$A_{(1)} = \frac{n_0 z}{M} \cdot \frac{p_{(1)}(\boldsymbol{\theta})}{1 - \dfrac{n_{(0)}+n_{(1)}}{M}} e^{(E+kT\ln\tau)/kT} \tag{8.16'}$$

respectively; $p_{(\rho)}(\boldsymbol{\theta})$ represents the probability that a comperting substance (when $\rho=0$) or a sample molecule (when $\rho=1$) is adsorbed successfully by its addition on the adsorbent surface where competing substances and sample molecules are adsorbed already in density $\theta_{(0)}$ and $\theta_{(1)}$, respectively. Ξ [eq(8.2)] can now be calculated by using eqs(8.3'), (8.15') and (8.16') as

$$\Xi = \sum_{n'_{(0)}+n'_{(1)} \leqq M} \frac{M!}{n'_{(0)}!n'_{(1)}!(M-n'_{(0)}-n'_{(1)})!} \prod_{\rho=0}^{1} (e^{\mu_{(\rho)}/kT} A_{(\rho)})^{n'_{(\rho)}}$$

$$= \left(1 + \sum_{\rho=0}^{1} e^{\mu_{(\rho)}/kT} A_{(\rho)} \right)^{M} \qquad (8.2')$$

The probability that $n'_{(0)}$ competing substances or $n'_{(1)}$ sample molecules are adsorbed on the adsorbent surface can be represented as $e^{n'_{(\rho)}\mu_{(\rho)}/kT} Z/\Xi$ (where $\rho=0$ or 1). The expectation value, $n_{(\rho)}$, of $n'_{(\rho)}$ can be calculated by using eq(8.2') as

$$n_{(\rho)} = \sum_{n'_{(0)}+n'_{(1)} \leqq M} n'_{(\rho)} e^{n'_{(\rho)}\mu_{(\rho)}/kT} Z/\Xi$$

$$= kT \partial \ln \Xi / \partial \mu_{(\rho)}$$

$$= \frac{M \lambda_{(\rho)} A_{(\rho)}}{1 + \sum_{\rho'=0}^{1} \lambda_{(\rho')} A_{(\rho')}} \qquad (8.22)$$

in which

$$\lambda_{(\rho)} = e^{\mu_{(\rho)}/kT} \qquad (8.23)$$

represents absolute activity. Eq(8.22) for $\rho=0$ and $\rho=1$ can be rewritten as

$$\frac{\frac{\lambda_{(0)}z}{\theta_{(0)}}\cdot\frac{p_{(0)}(\boldsymbol{\theta})}{1-\frac{n_{(0)}+n_{(1)}}{M}}e^{\varepsilon/kT}}{1+\sum_{\rho'=0}^{1}\lambda_{(\rho')}A_{(\rho')}}=1 \tag{8.24}$$

and

$$\frac{\frac{\lambda_{(1)}x'z}{\theta_{(1)}}\cdot\frac{p_{(0)}(\boldsymbol{\theta})}{1-\frac{n_{(0)}+n_{(1)}}{M}}e^{(E+kT\ln\tau)/kT}}{1+\sum_{\rho'=0}^{1}\lambda_{(\rho')}A_{(\rho')}}=1 \tag{8.25}$$

respectively, and dividing eq(8.24) by eq(8.25) leads to

$$\lambda_{(0)}zp_{(0)}(\boldsymbol{\theta})e^{\varepsilon/kT}/\theta_{(0)}=\lambda_{(1)}x'zp_{(1)}(\boldsymbol{\theta})e^{(E+kT\ln\tau)/kT}/\theta_{(1)}=\text{constant} \tag{8.26}$$

The constant in eq(8.26) can be determined to be unity by substituting eq(8.26) into either eq(8.24) or (8.25). Eq(8.26) becomes

$$\lambda_{(0)}=\frac{\theta_{(0)}}{zp_{(0)}(\boldsymbol{\theta})}e^{-\varepsilon/kT} \tag{8.27}$$

and

$$\lambda_{(1)}=\frac{\theta_{(1)}}{x'zp_{(1)}(\boldsymbol{\theta})}e^{-(E+kT\ln\tau)/kT} \tag{8.28}$$

$\lambda_{(0)}$ and $\lambda_{(1)}$ are approximately proportional to concentrations in solution, m and C, of competing substance and sample molecule, respectively. What we should do next is to represent the adsorption isotherm for sample molecule as a relationship among $\theta_{(1)}$, $\lambda_{(1)}$ and $\lambda_{(0)}$ [or Λ; cf. eq(8.40)] by eliminating $\theta_{(0)}$ between eqs(8.27) and (8.28). For this purpose, it is necessary to represent both $p_{(0)}(\boldsymbol{\theta})$ and $p_{(1)}(\boldsymbol{\theta})$ in concrete forms.

Due to the assumption, a competing substance occupies a single site when it is adsorbed on the adsorbent surface; this means that $p_{(0)}(\boldsymbol{\theta})$ [eq(8.27)] can be represented as

$$p_{(0)}(\boldsymbol{\theta})=1-\theta_{(0)}-\theta_{(1)} \tag{8.29}$$

Below is given the proof that $p_{(1)}(\boldsymbol{\theta})$ [eq(8.28)] can be represented as

$$p_{(i)}(\boldsymbol{\theta}) = \left(\frac{1-\theta_{(0)}-\theta_{(i)}}{1-\theta_{(i)}} \right)^{x'} p_{(i)}(0, \theta_{(i)}) \tag{8.30}$$

in which $p_{(i)}(0, \theta_{(i)})$ represents the probability that a sample molecule is adsorbed successfully by its addition on the adsorbent surface occupied already by other sample molecules in density $\theta_{(i)}$ in the absence of competing substance.

Prrof. $\prod_{l=1}^{n(0)+n(1)} \{p_{(\rho)}[\mathbf{n}'']\}_l$ or $\sum_{l=1}^{n(0)+n(1)} \{\ln p_{(\rho)}[\mathbf{n}'']\}_l$ is a state quantity because $\omega[\mathbf{n}]$ is a state quantity [see eq(8.9')]; this means that

$$\sum_{l=1}^{n_{(0)}+n_{(1)}} \{\ln p_{(\rho)}[\mathbf{n}'']\}_l = \sum_{\rho=0}^{1} \sum_{n''_{(\rho)}=1}^{n_{(\rho)}} \ln p_{(\rho)}[\mathbf{n}''] \tag{8.31}$$

[cf. eq(8.14)]. On the other hand, for an arbitrary function $f(n_{(0)},n_{(1)})$, the relationship:

$$f(n_{(0)},n_{(1)}) = \sum_{\rho=0}^{1} \int^{n_{(\rho)}} (\partial f / \partial n''_{(\rho)}) dn''_{(\rho)} \tag{8.32}$$

is fulfilled. By considering $\sum_{l=1}^{n(0)+n(1)} \{\ln p_{(\rho)}[\mathbf{n}'']\}_l$ for $f(n_{(0)},n_{(1)})$ and replacing the integral by the sum

$$\frac{\partial \sum_{l=1}^{n_{(0)}+n_{(1)}} \{\ln p_{(\rho)}[\mathbf{n}'']\}_l}{\partial n_{(i)}} = \ln p_{(i)}[\mathbf{n}] \equiv \ln p_{(i)}(\boldsymbol{\theta}) \tag{8.33}$$

is obtained, and, by using both eqs(8.9') and (8.33)

$$e^{\partial \ln \omega[\mathbf{n}] / \partial n_{(i)}} = x'zp_{(i)}(\boldsymbol{\theta}) / \theta_{(i)} \tag{8.34}$$

can be derived, where Stirling's approximation ($\ln N! \approx N\ln N - N$; $N \gg 1$) has been used. On the other hand, $\omega[0,n_{(i)}]$ can be represented as

$$\omega[0,n_{(i)}] = \frac{(n_e z)^{n_{(i)}}}{n_{(i)}!} \prod_{n''_{(i)}=1}^{n_{(i)}} p_{(i)}[0,n''_{(i)}] \tag{8.35}$$

and we have

$$\frac{d\sum_{n''_{(i)}=1}^{n_{(i)}} \ln p_{(i)}[0,n''_{(i)}]}{dn_{(i)}} = \ln p_{(i)}[0,n_{(i)}] \equiv \ln p_{(i)}(0,\theta_{(i)}) \tag{8.36}$$

By using both eqs(8.35) and (8.36)

$$e^{d\ln\omega[0,n_{(i)}]/dn_{(i)}} = x'zp_{(i)}(0,\theta_{(i)})/\theta_{(i)} \tag{8.37}$$

can be derived. As a competing substance occupies a single site when it is adsorbed, $\omega[\mathbf{n}]$ can be represented as

$$\omega[\mathbf{n}] = \omega[0,n_{(i)}]\frac{(n_s - x'n_{(i)})!}{n_{(\omega)}!(n_s - n_{(\omega)} - x'n_{(i)})!} \tag{8.38}$$

With reference to both eqs(8.19) and (8.20), and by using Stirling's approximation, eqs (8.34), (8.37) and (8.38) lead to

$$\frac{p_{(i)}(\boldsymbol{\theta})}{p_{(i)}(0,\theta_{(i)})} = \exp\left(\frac{\partial \ln\{\omega[\mathbf{n}]/\omega[0,n_{(i)}]\}}{\partial n_{(i)}}\right) = \left(\frac{1-\theta_{(\omega)}-\theta_{(i)}}{1-\theta_{(i)}}\right)^{x'} \tag{8.39}$$

or eq(8.30). *Q.E.D.*

By using both eqs(8.29) and (8.30), and introducing the parameter:

$$\Lambda = \lambda_{(\omega)} z e^{\varepsilon/kT} \tag{8.40}$$

representing the "force" of competing substances to drive sample molecule out of the adsorbent surface, eqs(8.27) and (8.28) can be rewritten as

$$\Lambda = \frac{\theta_{(\omega)}}{1-\theta_{(\omega)}-\theta_{(i)}} \tag{8.27'}$$

and

$$\lambda_{(i)} = \frac{\theta_{(i)}}{x'zp_{(i)}(0,\theta_{(i)})} e^{-(E+kT\ln\tau)/kT}\left(\frac{1-\theta_{(i)}}{1-\theta_{(\omega)}-\theta_{(i)}}\right)^{x'} \tag{8.28'}$$

respectively. By eliminating $\theta_{(\omega)}$ between eqs(8.27') and (8.28'), the adsorption isotherm for sample molecule:

$$\lambda_{(i)} = \frac{\theta_{(i)}}{x'zp_{(i)}(0,\theta_{(i)})} e^{-(E+kT\ln\tau)/kT}(\Lambda+1)^{x'} \tag{8.41}$$

can be derived. The other equation obtained by eliminating $\theta_{(\omega)}$ between eqs(8.27') and (8.28') represents the adsorption isotherm for competing substance. We here treat, however, the case when concentration m in solution of competing substances is high enough for the majority of them to be in solution or the liquid phase in the two phase system; the presence of sample molecules hardly affects the activity or concentration of competing substances in the liquid phase [see Chapter III(A)].

When the density of sample molecules in the slice of the column is low, the density $\theta_{(\omega)}$ on the adsorbent surface is low, and $p_{(\omega)}(0, \theta_{(\omega)})$ is almost equal to unity:

$$p_{(\omega)}(0, \theta_{(\omega)}) \approx 1 \tag{8.42}$$

Molecular concentration C in solution is also low, and $\lambda_{(\omega)}$ is almost proportional to C:

$$\lambda_{(\omega)} \approx \Gamma C \tag{8.43}$$

with a proportionality constant Γ. Further writing

$$\Lambda = \varphi m \tag{8.44}$$

in which

$$\varphi = \lambda_{(\omega)} z e^{\varepsilon/kT}/m \tag{8.45}$$

measures the strength of adsorption of competing substance, or the inherent "force" of competing substance to drive sample molecule out of the adsorbent surface, eq(8.41) can be re-expressed approximately as

$$\theta_{(\omega)} = \Gamma x' z e^{(E+kT\ln\tau)/kT} (\varphi m+1)^{-x'} C \tag{8.41'}$$

representing a linear adsorption isotherm. Thus, eq(8.41') manifests that $\theta_{(\omega)}$ is a linear function of C with a slope decreasing monotonically with increase in m, provided that φ is approximately constant.

If competing substance can take several configurations on the adsorbent surface, ε involves the entropy effect. To the contrary, if competing substance is symmetric in shape, the ε value reduces; this may bring about the situation equivalent to that where z is equal to unity in eq(8.40) or (8.45) [cf. the explanation of eq(8.10)]. [In the earlier papers(6.2, 6.4, 6.5, 8.13, 8.14), it is assumed that $z=1$ in the corresponding equation.] The parameter ε may also imply the effect of energetical interaction among competing substances taking place on the adsorbent surface. It can be assumed, however, that the effect under consideration is much reduced in the presence of the solvent because the effect of interaction between competing substance and solvent should be subtracted.

For the estimation of φ [eq(8.45)], it appears to be possible to use the activity coefficient data showing the dependence of activity on concentration in aqueous solution published in the literature. It is questionable, however, if these data for bulk solutions are

applicable to phenomena taking place in the vicinity of the adsorbent surface. Going back to the methodology in which the presence of the solvent is neglected, and bearing in mind all the arguments performed above, we hereafter assume simply that φ is constant; a lot of secondary efects might dissipate in the approximation of constant φ [cf. the subsections entitled "Analysis of Fig 9.1" and "Analysis of Fig 9.2" respectively in Chapter IX(C), and the subsection entitled "Comparison with Competition Model" in Appendix XI(F)].

The assumption used above that a competing substance occupies a single site when it is adsorbed on the adsorbent surface reduces the calculation drastically. Under this assumption, the meaning of the parameter x' as *number of adsorbing sites* on which the adsorption of competing substances is impossible owing to the presence of an adsorbed sample molecule can be replaced by the meaning as *number of competing substances* the adsorption of which is impossible owing to the presence of an adsorbed sample molecule. If a competing substance occupies plural sites when it is adsorbed, only the second meaning can be given to x' approximately.

(C) $\dot{B}(m)$ or $\dot{k}(m)$

Let us calculate partition of sample molecules in the liquid phase as a function of concentration, m, of competing substances in the liquid phase:

$$\dot{B}(m) = C/\Omega \tag{8.46}$$

or the corresponding capacity ratio $\dot{k}(m)$ $[=\{1-\dot{B}(m)\}/\dot{B}(m)]$. [We here consider that $\dot{B}(m)$ represents either B°_{1} or B°; $B^{\circ}_{1} \approx B^{\circ}$ [eq(1.57)]. Cf. the subsection entitled "Perspective" in Chapter I (B).] In eq(8.46), Ω can be represented by its definition as

$$\Omega = N/U \tag{8.47}$$

in which N stands for the total number of sample molecules in the two phase system as model of the slice of the column, and U for the total interstitial volume of that system. N $(=n_{(l)}+CU)$ can be represented by using eq(8.20) as

$$N = n_{\circ}\theta_{(l)}/x' + CU \tag{8.48}$$

By using eqs(8.41'), (8.47) and (8.48), and introducing the parameter:

$$q = \beta e^{(E+kT\ln\tau)/kT} \tag{8.49}$$

in which

$$\beta = \Gamma n_{\circ} z/U \tag{8.50}$$

$\dot{B}(m)$ [eq(8.46)] can be calculated as

$$\dot{B}(m) = \frac{1}{1+q(\varphi m+1)^{-x'}} \qquad (8.51)$$

or $\dot{k}(m)$ can be represented as

$$\dot{k}(m) = q(\varphi m+1)^{-x'} \qquad (8.52)$$

[The prototype of eq(8.51) or (8.52) can be found in ref(6.2) eq(41).]

The parameter β [eq(8.50)] is proportional to the ratio of the effective total area, $n_s z$, of the adsorbent surfaces (i.e., the size of the solid phase) to the total interstitial volume U (i.e., the size of the liquid phase), representing the property of the column, and the parameter q [eq(8.49)] measures the strength of adsorption of sample molecule. If AVFA per molecule, $E+kT\ln\tau$, is equal to zero, then $q=\beta$ [see eq(8.49)]. On the other hand, $\dot{B}=1/(1+\beta)$ when both $q=\beta$ and $m=0$, whereas, due to its physical meaning, molecular partition $\dot{B}$ in the liquid phase taking place when $E+kT\ln\tau=0$ should be close to unity even in the absence ($m=0$) of competing substance; this means that $\beta \ll 1$. $\dot{B}$ is exactly equal to unity if $q=0$ [eq(8.51)] or $E+kT\ln\tau=-\infty$ [eq(8.49)] i.e., if a strong repulsive interaction takes place between sample molecule and the surface of the particles packed in the column; $E+kT\ln\tau$ can be defined to have a negative value in the presence of repulsive interaction. Usually, the concentration gradient technique is used only when q is large enough for $\dot{B}$ to be close to zero in the presence of the initial concentration, m_{in}, of gradient substances; m_{in} is often equal or close to zero. In the develpoment process of chromatography, $\dot{B}$ increases from ≈ 0 toward 1 with increase in m from m_{in} around MB(o) or MB(c).

Let us consider a series of "homologous" molecules with different "sizes" x' among which the quantity, $(E+kT\ln\tau)/x'$, is kept constant while fulfilling the approximation:

$$(E+kT\ln\tau)/x' \approx (x\varepsilon+kT\ln\tau)/x' \approx (x/x')\varepsilon \approx \text{constant} \qquad (8.53)$$

In eq(8.53), $-\varepsilon$ ($\varepsilon>0$) represents the adsorption energy of a functional group of sample molecule on a site of the adsorbent, and x is identical with x appearing in eq(8.1) i.e., it represents the number of adsorbing sites bonding with the adsorbed sample molecule, or the number of functional groups per molecule used for adsorption. On the surface of adsorbed sample molecule, there, in general, also exist free functional groups that cannot be used for adsorption. The approximate equality between first and second terms in eq(8.53) (i.e., the relationship: $E\approx x\varepsilon$) arises from the possbility that a weak energetical interaction (attractive or repulsive) may take place between sample molecule and the adsorbent surface beside the interaction between functional groups and adsorbing sites [cf. ref(7.1)]. The approximate equality between second and third terms in eq(8.53) (i.e., the relationship: $x\varepsilon \gg kT\ln\tau$) arises from the consideration performed above that q or $x\varepsilon + kT\ln\tau$ is large enough for $\dot{B}$ (at $m=m_{in}$) to be close to zero usually. Thus, for this to

occur, it would be the energy term, $x\varepsilon$, rather than the entropy term, $kT\ln\tau$, that can increase. It would be difficult for a magnitude comparable to that of $x\varepsilon$ to be generated by the term $kT\ln\tau$ when $x\varepsilon + kT\ln\tau$ is large, thus leading to the conclusion that $x\varepsilon \gg kT\ln\tau$ [cf. the argument with respect to eq(8.58)]. We argue below how the shape of function $\dot{B}(m)$ changes with increase in x' when eq(8.53) holds. For this purpose, it is convenient to rewrite eq(8.51) as

$$\dot{B}(m) = 1/(1+\beta Y^{-x'}) \tag{8.51'}$$

in which

$$Y = \exp\left(-\frac{E+kT\ln\tau}{x'kT}\right)(\varphi m+1) \tag{8.54}$$

When x' increases to approach infinity while keeping $(E+kT\ln\tau)/x'$ constant, then eq (8.51') tends to

$$\left.\begin{aligned} \dot{B}(m) &= 0 \quad (\text{when } Y<1 \text{ or } m<m^*) \\ \dot{B}(m) &= 1/(1+\beta) \quad (\text{when } Y=1 \text{ or } m=m^*) \\ \dot{B}(m) &= 1 \quad (\text{when } Y>1 \text{ or } m>m^*) \end{aligned}\right\} \tag{8.55}$$

representing the Heaviside-type step function, where

$$m^* = \left[\exp\left\{\frac{E+kT\ln\tau}{x'kT}\right\} - 1\right]/\varphi \approx [\exp((x/x')\varepsilon/kT)-1]/\varphi \approx (x/x')\varepsilon/(\varphi kT) \tag{8.56}$$

stands for the critical value of m at which the step transition of $\dot{B}$ from 0 to 1 takes place. The approximate equation between third and last terms in eq(8.56) holds provided that $(x/x')\varepsilon/(\varphi kT)$ is small. It can now be understood that the sigmoidal shape of function $\dot{B}(m)$ (manifesting the gradual transition of $\dot{B}$ from ≈ 0 to 1 taking place with increase in m) sharpens with increase in molecular size x' of the homologous series; the transition of $\dot{B}$ takes place stepwise when x' approaches infinity.

(D) Quantitative Test of Competition Model

Whether or not the following three points obtained experimentally on HA columns [cf. Section(A)] can be explained quantitatively by competition model is tested: (a) quasi-independence of elutution molarity μ on M_m taking place when M_m is high, (b) decrease of μ with decrease in M_m taking place when M_m is relatively low, and (c) decrease with increase in M_m of the dependence of μ on both length L of the column and slope g of the linear concentration (molarity) gradient applied. At the same time, the experimental

parameters involved in competition model are evaluated by comparing the result derived from the model with the experimental result in order to have a best fit between them. Whether reasonable values are obtained or not is involved in the test.

Thus, let us recall a series of chromatographies of lysozyme carrieed out on HA columns with several total lengths L by using linear concentration gradients of KP buffer with different slopes g [Fig 8.3; reproduced from ref(6.9) or (7.1)]. The points in Fig 8.3 (a) are experimental plots of $m_{elu(P)}$ versus L for four different g values where $m_{elu(P)}$ stands for elution phosphate molarity of KP buffer at which the maximum height of the chromatographic peak (chromatogram) appears. [Fig 8.3 represents the same type of diagram as those drawn in Fig 7.3, Fig 8.1 and Appendix VI Fig A6.1.] The HA particles used for the experiment in Fig 8.3 are almost identical with those used in the experiments mentioned in Chapter VII. It should be recalled [Section(A)] that lysozyme is adsorbed mainly on P sites by using ε-amino and/or guanidinyl groups, and that it competes for adsorption with potassium ions from KP buffer which are also adsorbed on P sites. Therefore, μ represents elution molarity $m_{elu(K^+)}$ with respect to potassium ions, which is 1.5 times as high as $m_{elu(P)}$. It can be seen in Fig 8.3(a) that $m_{elu(P)}$ increases with increase in L and g when g and L are constant, respectively. The dependence of $m_{elu(P)}$ on L differs when g applied is different, giving four arrangements of the experimental points corresponding to the four values of g [in parallel with the diagrams in Fig 7.3, Fig 8.1 and Appendix VI Fig A6.1; see Fig 8.3(a)].

The points in Fig 8.3(b) are plots of $m_{elu(P)}$ versus ln $s_{app(P)}$ instead of L for the experimental points in Fig 8.3(a) where $s_{app(P)}$ [$=g'_{(P)}(\varnothing=1\ cm)\cdot L$] represents the experimental parameter related to s by $s=0.970s_{app(P)}$ (cf. Note in Table 7.1); s is defined by eq (6.2) as $s=gL$ in which g is concerned with competing potassium ions. [Fig 8.3(b) represents the same type of diagram as those drawn in Fig 7.5, Fig 7.6 and Appendix VI Fig A6.2.] It can be seen in Fig 8.3(b) that the four arangements of the experimental points on the (L, $m_{elu(P)}$) plane [Fig 8.3(a)] converge into a single arrangement when mapped to the (ln $s_{app(P)}$, $m_{elu(P)}$) plane (in parallel with the diagrams in Fig 7.5, Fig 7.6 and Appendix VI Fig A6.2). It can be considered that the arrangement of the experimental points in Fig 8.3(b) represents trajectory T_0. In fact, as in Appendix VI Fig A6.2, in Fig 8.3(b) also, $m_{elu(P)}$ or μ can be replaced by $\hat{\mu}$ or $\hat{m}$ in practice since m_{in} (with a small value of 1 mM with respect to phosphate ions) is negligible in eq(6.18). Moreover, replacing the ln $s_{app(P)}$ axis in Fig 8.3(b) by the ln s axis only brings about a slight shift of the total arrangement of the experimental points. The convergence of the experimental points [Fig 8.3 (a)] into a single arrangement [Fig 8.3(b)] takes place independently of the adsorption and desorption mechanism i.e., of competition model (see Chapter VII).

The experimental plots in Fig 8.3(b) are done, however, for the purpose of testing competition model, and it is for this purpose that the logarithm of $s_{app(P)}$ is taken as abscissa. First, taking the logarithm brings about a quasi-linear arrangement of the experimental points, which facilitates the comparison with the theoretical curve. Second, variable

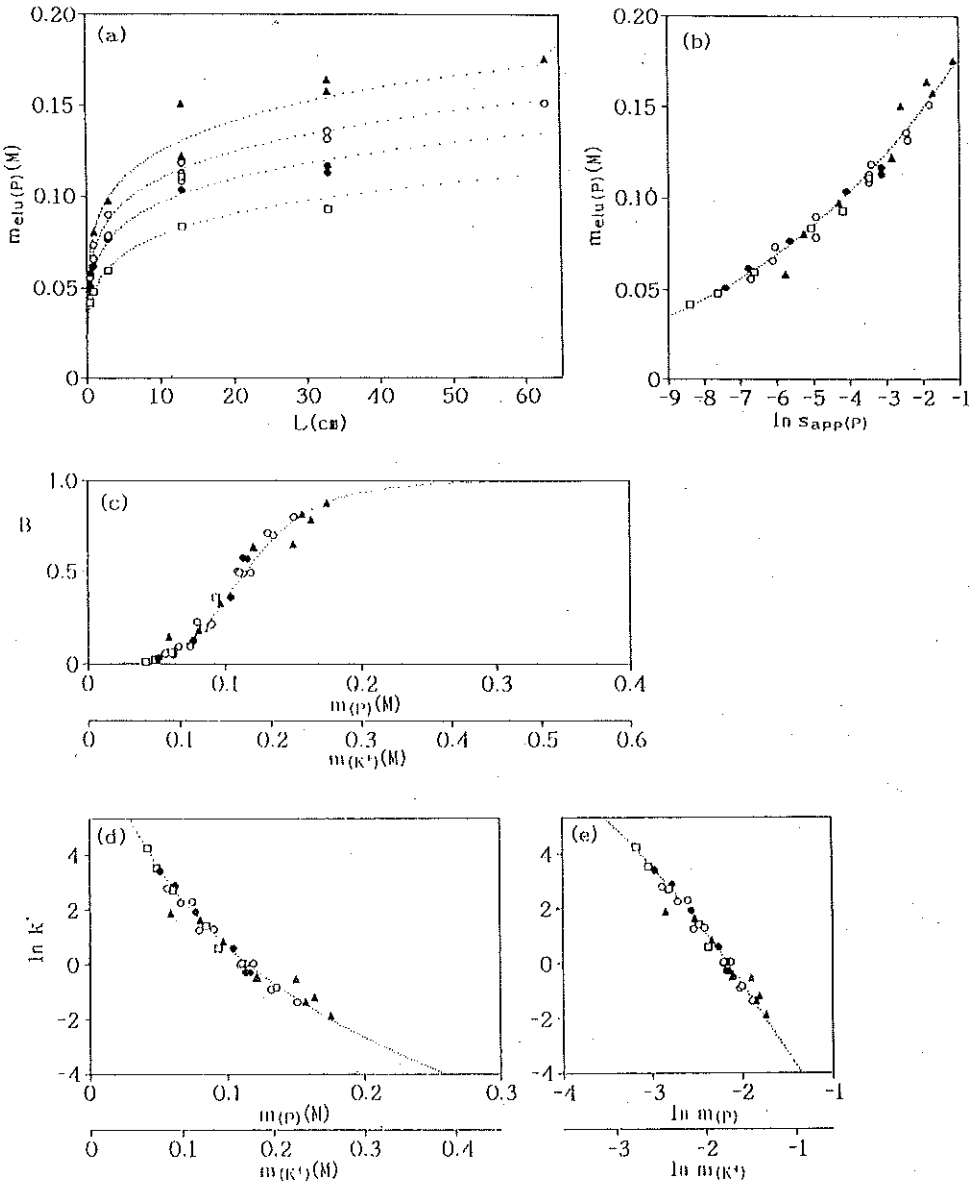


Fig 8.3. HPLC analysis of chicken lysozyme, carried out on HA columns with different lengths L by using linear concentration gradients of KP buffer with four different slopes; the column internal diameter, ø, is 6 mm always. The HA particles used for the experiment are almost identical with those used in the experiments mentioned in Chapter Ⅶ. Points in (a)-(e): experimental plots of (a) $m_{elu(P)}$ versus L, (b) $m_{elu(P)}$ versus ln $s_{app(P)}$, (c) B i.e., $\dot{B}$ versus $m_{(P)}$ or $m_{(K^+)}$, (d) ln k' i.e., ln $\dot{k}$ versus $m_{(P)}$ or $m_{(K^+)}$, and (e) ln k' i.e., ln $\dot{k}$ versus ln $m_{(P)}$ or ln $m_{(K^+)}$ for four different $g'_{(P)}$(ø=1 cm) values: 5.0(▲), 2.5(○), 1.25 (●), and 0.45(□) mM/ml [cf. Note in Table 7.1]; $m_{in(P)}$=1 mM and T=21.0-29.7 ℃. Curves in (a)-(e): theoretical curves. For detail, see text. [Reproduced directly from ref (7.1) Fig17; the original diagrams can be found in ref(6.9).]

$s_{app(P)}$ can in general be defined without any knowledge about both the magnitude of the interstitial volume of the column and the type (C or P) of crystal site on which the adsorption takes place; $s_{app(P)}$ can be converted to s at any time when the exact knowledge is available.

The curve in Fig 8.3(b) is theoretical, calculated by using eq(6.24) or (6.24') in which $m_{in}=1.5$ mM, $\mu = \mu - m_{in} = 1.5m_{elu(P)} - m_{in}$ mM, and $s=0.970s_{app(P)}$. For the other parameters, optimum values of φ =25 M^{-1}, x'=5.7 and ln q=9.5 were used in order to have a best fit with the experiment. It can be seen in Fig 8.3(b) that the coincidence of the theoretical curve with the experimental plots is excellent, explaining a slight displacement from the linearity of the arrangement of the experimental points. [Both x' and ln q values used above are slightly different from the corresponding values, 6.4 and 9.82, used in Chapter Ⅶ, respectively. The differences are within the limits of the experimental error. Thus capacity ratio $\hat{k}(m)$ [eq(8.52)] can roughly be represented as $qe^{-x'\varphi m}$, and it is possible to consider that the fundamental shape of the theoretical curve is determined by the product of x' by φ with a modification by q; this makes it difficult to obtain exact evaluations of the individual parameters, x' and φ, by comparing the theoretical curve with the experimental plots. In ref(6.9) Appendix Ⅰ, it was estimated that the ranges between upper and lower limits of possible values of φ and q, respectively, extend much more widely than that of x', (x', φ, ln $q_{app(P)}$) ranging between (8, 10 M^{-1}, 7.9) and (4, ∞ M^{-1}, ∞) where $q_{app(P)}=0.970q$. In Fig 8.3(b), φ is assumed to be 25 M^{-1} for two reasons. The first is that the φ value of the order of magnitude of 10 M^{-1} is implied from the chromatographic experiment of poly-L-lysine(8.18) [see the subsequent Section(E)]. The second can be found in ref(6.9) Appendix Ⅰ Fig 15.]

The lysozyme molecule can be represented approximately by a prolate spheroid of 4.5 ×3×3 nm(8.19). Fig 8.4 [reproduced from ref(6.4)] illustrates schematically a lysozyme molecule adsorbed on P sites of HA, where it is assumed that the crystal surface over which the adsorption of lysozyme occurs constitutes a (001) surface as a whole [see Section(A)]. It is reasonable to consider that a competing potassium ion (with a diameter of 0.26 nm) occupies a single P site when it is adsorbed since the minimum inter-site distance between P sites on the (001) surface is 0.942 nm [Section(A)]. This implies that x' represents the number of P sites on which the adsorption of potassium ions is impossible owing to the presence of a lysozyme molecule. The x' values, 4-8, estimated above for lysozyme therefore are very reasonable (see Fig 8.4). These are reasonable even if the crystal surface covered by the molecule is characterized by Miller indices higher than (001). In this instance, the effective arrangement of sites would deviate to some extent [see Section(A)]. Only a slight change of the x' value can be anticipated, however.

In ref(8.18), under several assumptions, the absolute value, ε, of the energy of adsorption of an ε-amino group on a P site was estimated to be 8.4-9.2 kJ/mol, implying at the same time that the values of φ [eq(8.45)] and β [eq(8.50)] would be of the order

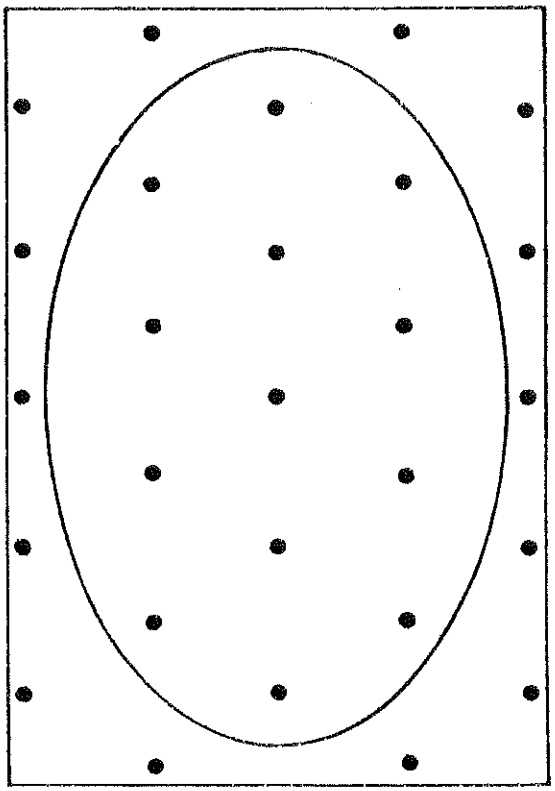


Fig 8.4. Schematic representation of lysozyme adsorbed on P sites of HA. It is assumed that lysozyme is represented by a prolate spheroid of dimensions 4.5×3×3 nm and that P sites are arranged hexagonally with the minimum inter-site distance of 0.942 nm. [Reproduced from ref(6.4) Fig 3.]

of magnitude of 10 M^{-1} and 10^{-2}, respectively [for detail, see the subsequent Section(E)]. Therefore, if we use the values, $\varphi = 25\ M^{-1}$ and $\ln q = 9.5$, that can be estimated from Fig 8.3(b) and if it is assumed that the energy of adsorption for guanidinyl group is the same as that for ε-amino group, then it can be calculated for lysozyme that $x\varepsilon/kT \approx (E + kT\ln\tau)/kT = \ln q - \ln\beta \approx 14.1$ [see both eqs(8.49) and (8.53)] and that $x = 3.8$-4.2; $kT = 2.48$ kJ/mol at 25℃. This means that 3.8 to 4.2 basic groups out of the total of 18 per molecule are used for bonding with P sites. The x value would still be modified if a weak energetical interaction (attractive or repulsive) takes place between lysozyme molecule and HA surface beside the interaction between basic functional groups and P sites.

The four curves in Fig 8.3(a) were obtained by mapping the theoretical curve drawn in Fig 8.3(b) to the (L, $m_{el(P)}$) plane when the four g or $g'_{(P)}$($\varnothing = 1$ cm) values are given, respectively.

The points and the curve in Fig 8.3(c) were obtained by mapping the points and the curve in Fig 8.3(b) to the ($m_{(P)}$, $\dot{B}$) plane, respectively, where the symbol B is used instead of $\dot{B}$, and the $m_{(K^+)}$ ($= 1.5m_{(P)}$) axis is added; $m_{(K^+)}$ represents the potassium molarity of KP buffer (cf. Fig 7.8, Fig 7.9 and Appendix VI Fig A6.3). The mapping of the theoretical curve can be achieved by simply substituting the numerical values of the parameters x', φ and q ($= q_{app(P)}/0.970$) into eq(8.51). The method for the mapping of the experimental points was mentioned in Chapter VII(E). As $m_{(K^+)} \approx \hat{m}$, it can be considered that the experimental points and the theoretical curve in Fig 8.3(b) correspond to the projection on the ($\hat{m}$,s) plane of the characteristic curve present in the ($\hat{m}$,s,B) space. Similarly, the experimental points and the theoretical curve in Fig 8.3(c) correspond to the projection on the ($\hat{m}$,B) plane of the characteristic curve. (Cf. Fig 3.2).

Fig 8.5 illustrates theoretical curves, $\dot{B}(m)$, for lysozyme ($x' = 5.7$) and for four hypothetical molecules that are "homologous" to lysozyme with $x' = 1.47$, 15.0, 50.0 and ∞, respectively; for all the molecules, $(E + kT\ln\tau)/(x'kT) = (\ln q - \ln\beta)/x' = (9.5 + 4.6)/5.7 = 2.474$ [see both eqs(8.49) and (8.53)] with the assumptions of $\beta = 10^{-2}$ and $\varphi = 25\ M^{-1}$. In Fig 8.5, the curves for finite x' values have been calculated by using both eqs(8.51') and (8.54), whereas the curve for the infinite x' value (being an assembly of two open straight half-lines and a point; see below) has been calculated by using both eqs(8.55) and (8.56). The curve for lysozyme ($x' = 5.7$) is identical with the theoretical curve drawnin Fig 8.3(c), and all the curves cross at point [m^*, $1/(1+\beta)$] = (0.435, 0.990); this is represented by a filled-circle (see Fig 8.5). The curve for $x' = \infty$ is constructed of this point and two open straight half-lines parallel to the m axis, manifesting a step transitionof $\dot{B}$ from 0 to 1 taking place at $m = m^*$ (see Fig 8.5). The minimum x' value, 1.47, corresponding to one of the curves drawn in Fig 8.5 has been calculated as value taking place, provided that $E + kT\ln\tau = \varepsilon = 9$ kJ/mol. This is the value taking place, provided that the molecule is adsorbed by using only one ε-amino or guanidinyl group and that the entropy factor $kT\ln\tau$ is negligible. It can be seen in Fig 8.5 that, as x' decreases, the transition of $\dot{B}$ toward unity (taking place with increse in m) becomes less sharp and that the m values

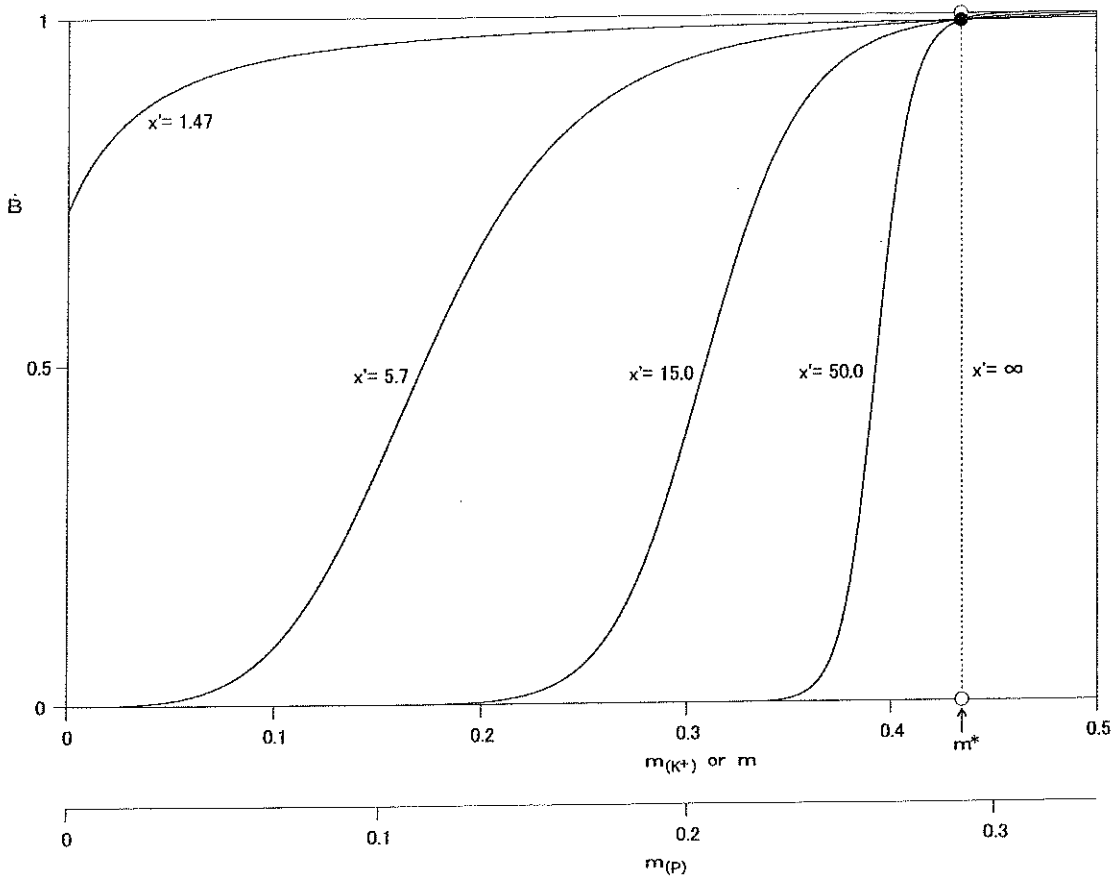


Fig 8.5. Functions $\dot{B}(m)$ for lysozyme ($x'=5.7$) and for four hypothetical molecules that are "homologous" to lysozyme with $x'=1.47$, 15.0, 50.0 and ∞, respectively, where $m=m_{(K^+)}=1.5m_{(P)}$. All the curves cross at point $(m, \dot{B})=[m^*, 1/(1+\beta)]=(0.435, 0.990)$ represented by a filled circle. The prototype of this diagram can be found in both ref(6.2) Fig 7 and ref(8.13) Appendix II Fig A5. In these diagrams, however, the values of the parameter x' are overestimated. For detail, see text.

over which the transition occurs shift to lower values; the $\dot{B}$ value at $m=0$, being almost equal to zero when x' is large enough, increases with decrease in x'. [The prototype of Fig 8.5 can be found in ref(6.2) Fig 7 and ref(8.13) Appendix II Fig A5. In these diagrams (drawn on the basis of the consideration done in the early stage ofdevelopment of the theory), much too large x' and x values are assumed and a much toosmall φ value is assumed implicitly. Nevertheless, these diagrams explain satisfactorily the situation virtually equivalent to that explained by Fig 8.5. This arises from the fact that the fundamental shape of the curve $\dot{B}(m)$ is determined by the product of x' by φ; it depends on the individual x' and φ values only slightly when once the value of $x'\varphi$ is given. This is intimately related to the fact that the fundamental shape of the theoretical curve drawn in Fig 8.3(b) is determined by the product of x' by φ (see above).]

In the absence of competing ions when $m=0$, eq(8.51) can be rewritten by using eq (8.49) as

$$\dot{B}(m=0) = 1/(1+\beta e^{(E+kT\ln\tau)/kT}) \tag{8.57}$$

Eq(8.57) is independent of x', and it holds independently of the competition mechanism. Fig 8.6 illustrates $\dot{B}(m=0)$ as a function of AVFA per molecule, $E+kT\ln\tau$; it is assumed that $\beta=10^{-2}$. It can be seen in Fig 8.6 that $\dot{B}(m=0)$, equal to $1/(1+\beta)=0.990$ when $E+kT\ln\tau=0$, decreases with increase in $E+kT\ln\tau$; $\dot{B}(m=0)$ is almost equal to zero when $E+kT\ln\tau \gtrsim 25$ kJ/mol. This means that, when $E+kT\ln\tau \approx x\varepsilon \geqq 27$ kJ/mol or when three or more than three ε-amino or guanidinyl groups are available, then the molecule can be retained almost completeyely on the HA column in the absence of competing ions. When $E+kT\ln\tau \approx \varepsilon = 9$ kJ/mol or when only one functional group is available, then the molecule spends only about 30% of the total time on the HA surface, or it migrates on the column at a relative rate, R_F, of about 0.7 in the absence of competing ions (see both Figs 8.5 and 8.6). [For the argument similar to the above for the case when acidic (i.e., phosphate or carboxyl) functional groups are used for the adsorption, see the subsequent Section(E).]

The curves drawn in Fig 8.7 correspond to those drawn in Fig 8.5, representing $m_{elu(P)}$ as functions of $\ln s_{app(P)}$. In Fig 8.7, the curves for finite x' were calculated by using eq (6.24) or (6.24') where $\mu = \mu - m_{in} = 1.5m_{elu(P)} - m_{in}$, $m_{in}=1.5$ mM and $s=0.970s_{app(P)}$; the curve for infinite x' can be represented as $m_{elu(P)}=(2/3)m^*=0.290$ M. The curve for $x'=5.7$ in Fig 8.7 is identical with the theoretical curve drawn in Fig 8.3(b). The curves drawn in Fig 8.7 and those drawn in Fig 8.5 correspond to the projections on $(\hat{m},s)$ and $(\hat{m},B)$ planes of a series of characteristic curves present in the $(\hat{m},s,B)$ space, respectively, manifesting that the characteristic curve of the type drawn in Fig 3.2(b) converges to that drawn in Fig 3.2(c) when x' increases to approach infinity. [It should be recalled that the curve for $x'=\infty$ explains the experiment of T_2 phage particle; see Fig 8.1Ⓔ.] The usual experimental conditions are involved in the diagram of Fig 8.3(b) or 8.7, and Fig 8.7 explains the following aspects. Thus, under a given experimental condition where

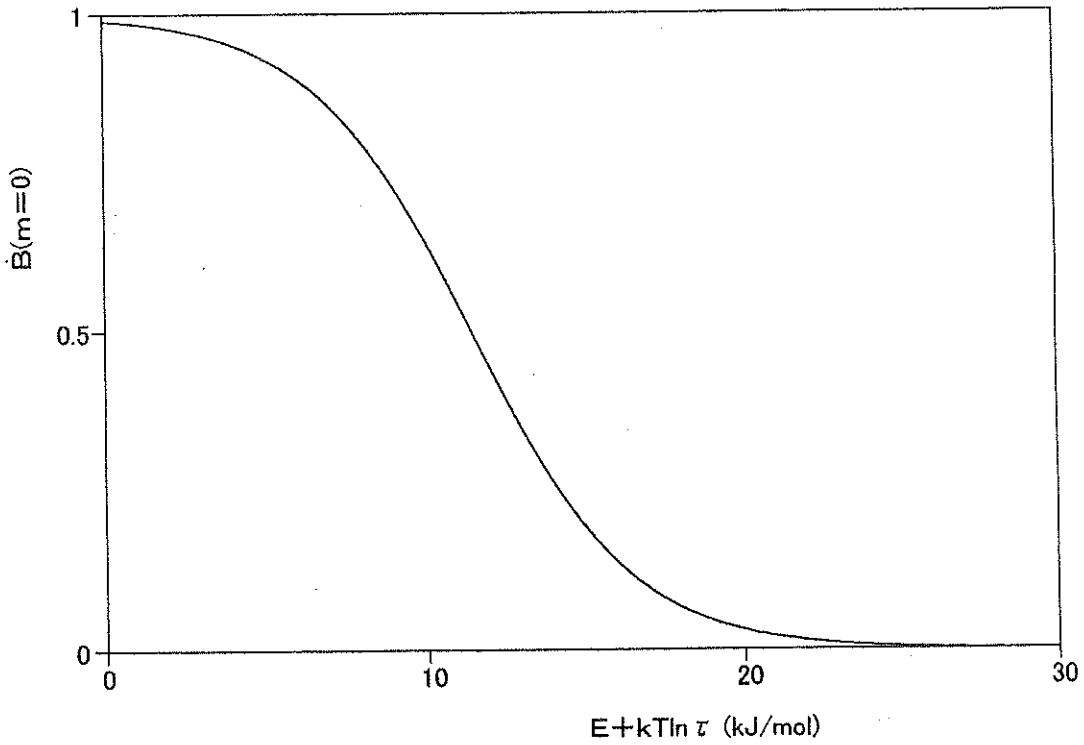


Fig 8.6. $\dot{B}(m=0)$ as a function of $E+kT\ln\tau$. The prototype of this diagram can be found in ref(6.2) Fig 5. For detail, see text.

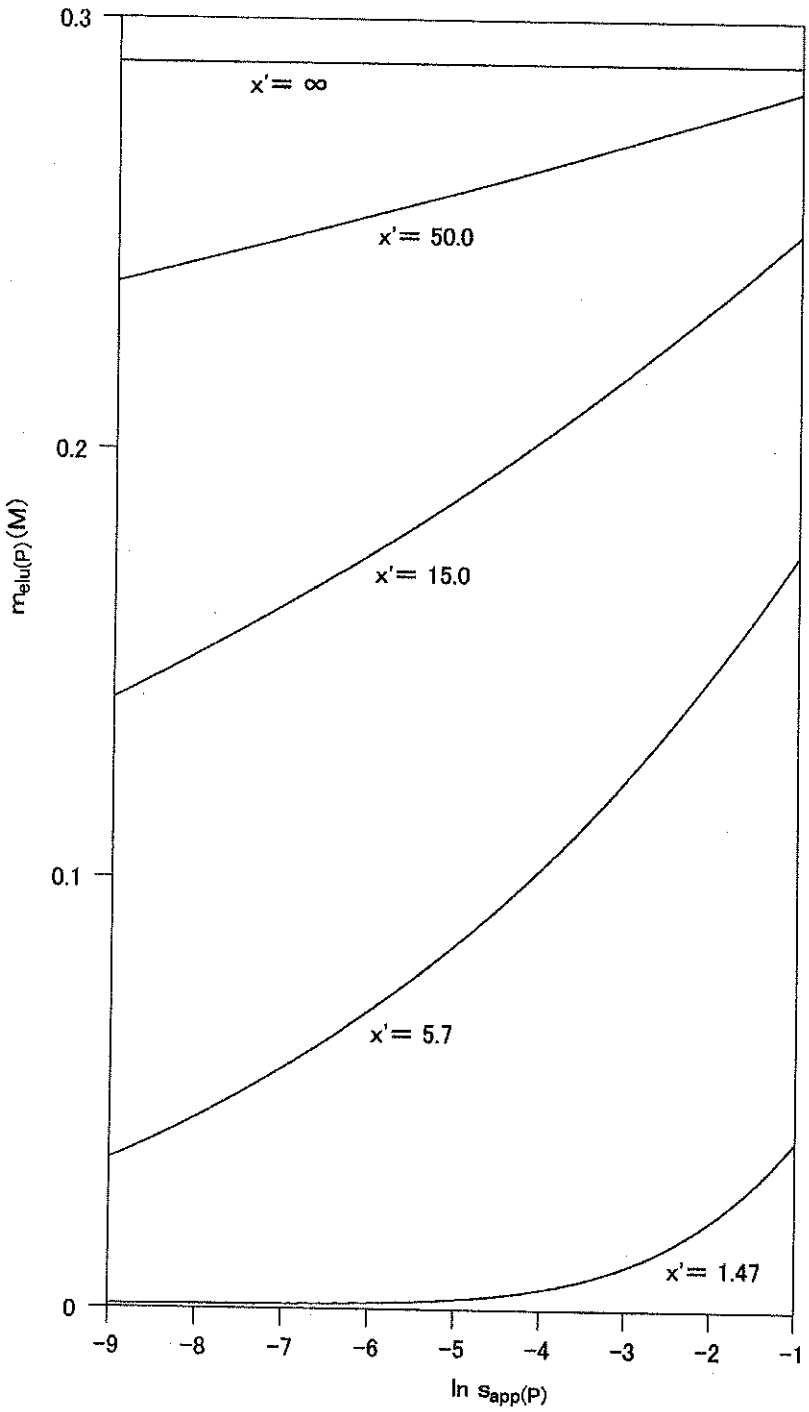


Fig 8.7. $m_{elu(P)}$ as functions of ln $s_{app(P)}$ for lysozyme ($x'=5.7$) and for four hypothetical molecules that are "homologous" to lysozyme with $x'=1.47$, 15.0, 50.0 and ∞, respectively (cf. Fig 8.5). The curve for $x'=5.7$ is identical with the theoretical curve drawn in Fig 8.3(b). For detail, see text.

$s_{app(P)}$ (i.e., both L and g) is given, $m_{elu(P)}$ decreases considerably with decrease in x' if x' is relatively small, whereas $m_{elu(P)}$ is almost independent of x' if x' is large enough. The dependence of $m_{elu(P)}$ on $s_{app(P)}$ (i.e., on either L or g) decreases with increase in x'; $m_{elu(P)}$ is independent of $s_{app(P)}$ (i.e., of both L and g) when $x'=\infty$. By replacing x' and $m_{elu(P)}$ by M_m and μ, respectively, all these aspects are what we desired to test, giving a quantitative verification of competition model. It can also be anticipated from Fig 8.7 that, under unusual experimental conditions where $s_{app(P)}$ takes very large values (beyond the range appearing in Fig 8.7), theoretical curves for different x' values will cross one another, giving rise to the inversion of $m_{elu(P)}$ or μ values between them. In many instances, however, it would be difficult to perform the chromatographic experiment in practice under these conditions, disturbed by strong demixing effects (cf. Fig 7.1). The inversion of μ, in general, takes place under usual experimental conditions between molecule with large AVFA ($E+kT\ln\tau$) and small x' and molecule with small AVFA and large x'.

For experimental analyses for substances other than lysozyme, see refs(6.8, 6.9).

(E) Importance of the Term, $\sum_{j=1}^{\nu} e^{E_j/kT}$, in Partition Function Ξ versus Energy, $-\varepsilon$, of Adsorption per Functional Group of Macromolecule

Adsorption Energy of Phosphate Group on A C Site. Earlier(8.20), the chromatogram of a mixture of AMP, ADP, ATP and adenosine tetraphosphate obtained by Bernardi(8.11) on an HA column by using a linear concentration gradient of KP buffer [Fig 8.8; reproduced from ref(8.20)] was analysed by using eq(6.24) or (6.24') [to be precise, its old type, eq(6.35) or (6.35')] in the following background. Thus, it was shown by Krane and Glimcher(8.21) that various nucleoside tri- and diphosphates as well as inorganic pyrophosphate are adsorbed on apatite crystals, and that the terminal phosphorus atom of the bound nucleotide is transferred, after incubation for several minutes, to a crystal surface phosphate with the formation of pyrophosphate on the crystal and the respective di- and monophosphates. By combining this finding with the comparative study of the crystallographic structure of HA with that of octacalcium phosphate [which leads to the model of the surface structure of HA [Section(A)]; see ref(8.20)], Taves and Reedy(8.22) proposed that tripolyphosphate is likely to be adsorbed on the **a** i.e., (100) [or **b** i.e., (010)] surface of HA with its long axis parallel to the **c** axis of the crystal, and that the three phosphate groups of the molecule occupy three successive hydroxyl positions of HA [separated by $|\mathbf{c}|/2=0.344$ nm]; hydroxyl positions mean the positions at which hydroxyl ions should be present, provided that the positions are situated in the interior of the crystal.

Kawasaki(8.20) considered that a hydroxyl position on the crystal surface (which is inserted between two crystal calcium ions) corresponds to a chromatographic C site, or that a C site is constructed from two calcium ions [cf. Section(A)]; this is firmly supported by HA chromatography carried out by Bernardi (Fig 8.8). Fig 8.8 manifests that AMP

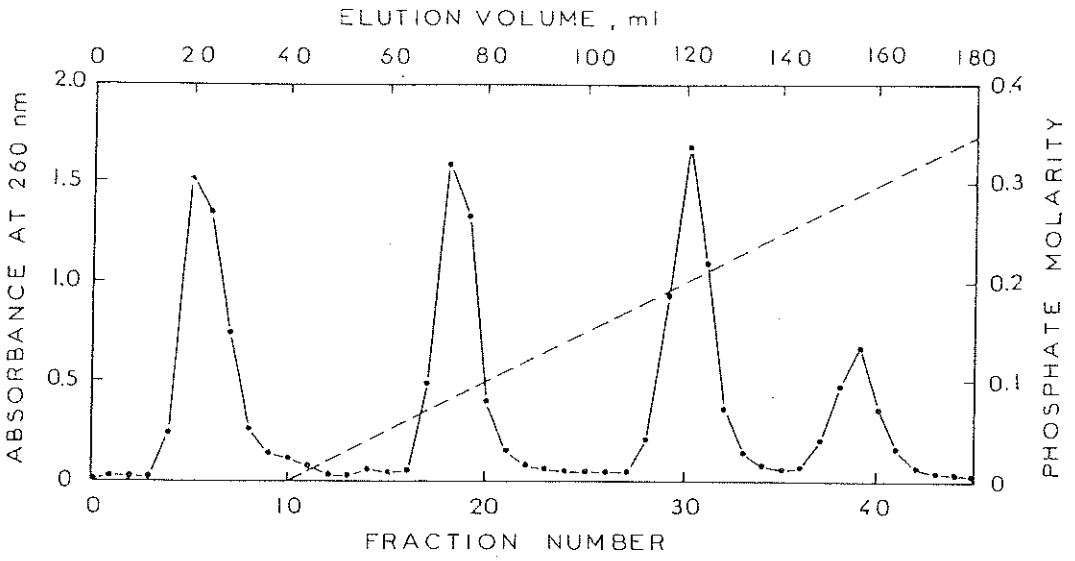


Fig 8.8. Experimental chromatogram at room temperature of a mixture of AMP, ADP, ATP and adenosine tetraphosphate obtained on a 10×1 cm HA column. The HA particles used for the experiment are almost identical with those used in the experiments mentioned in Appendix VI. A linear concentration gradient of KP buffer with a slope of $g'_{(P)}(\varnothing=1\ \text{cm}) = 2.5$ mM/ml was applied for the elution [cf. Note in Table 7.1]. The four chromatographic peaks represent those of AMP, ADP, ATP and adenosine teteraphosphate from left to right, respectively. For detail, see text. [Reproduced directly from ref(8.20) Fig 3; the original diagram can be found in ref(8.11).]

[along with other nucleoside monophosphates; see ref(8.11)] are eluted isocratically by 1 mM phosphate of KP buffer with some retardation; ADP, ATP and adenosine tetraphosphate are eluted at increasing higher characteristic phosphate molarities (0.08 M, 0.20M and 0.29 M, respectively) with a quasi-linear relationship between the number of phosphate groups and the molarity (Fig 8.8). This would indicate that the nucleoside phosphates are adsorbed via the phosphate groups (on C sites) and that the interval between the neighboring phosphate groups on the polyphosphate chain fits satisfactorily with that between C sites on the crystal surface. Bernardi(8.11) reported that the chromatography of the mixture of AMP, ADP, ATP and adenosine tetraphosphate gave yields of 133%, 113 %, 113% and 50%, respectively, with an overall recovery of 102%. It can be suggested that this may be due, at least partially, to the fact that the terminal phosphorus of the bound nucleoside di-, tri- and tetraphosphates was partially transferred to a crystal surface phosphate with the formation of pyrophosphate on the crystal and the respective nucleoside mono-, di- and triphosphate.

Fig 8.8 was analysed by Kawasaki(12.20) by using eq(6.35) or (6.35') under assumption that the x' value of nucleoside polyphosphate increases by unity when a single univalent phosphate is inserted in the polyphosphate chain of the molecule, but that the entropy factor, $kT\ln\tau$, does not change by the insertion. By comparing the theory with the experiment (Fig 8.8), it was estimated(8.20) that the absolute value, ε, of the energy of adsorption of a univalent phosphate group on a C site is 0.9-1 kcal/mol (3.8-4.2 kJ/mol), and that $\varphi = 4.6\text{-}6.7\ M^{-1}$. [It should be noted that these φ values are concerned with the equimolar mixture of $H_2PO_4^-$ and HPO_4^{2-} that can be adsorbed on C site; these are about 1/5 the φ value ($25\ M^{-1}$) assumed for potassium ion that can be adsorbed on P site.]

From Fig 8.8 it can also be estimated(8.20) that $\dot{B}$ (at $m_{(P)}=1$ mM) for AMP and that for ADP are equl to 0.2-2.3 and 0.06-0.07, respectively (although only low precisions can be anticipated in these estimations). Assuming that $\beta = 10^{-2}$ for C site as well and that $\dot{B}(m_{(P)}=1\ mM) \approx \dot{B}(m=0)$, it can now be calculated by using eq(8.57) that $E+kT\ln\tau$ for AMP = 13.5-14.9 kJ/mol and that $E+kT\ln\tau$ for ADP = 17.8-18.2 kJ/mol. It is important to note that the latter value coincides almost perfectly with the sum of the former value and the ε value (about 4 kJ/mol) for univalent phosphate estimated in the preceding paragraph: 17.5-18.9 kJ/mol. Neglecting the entropy term $kT\ln\tau$, it can be considered that the $E+kT\ln\tau$ value for AMP (13.5-14.9 kJ/mol) reptresents approximately the absolute value, ε, of the energy of adsorption of a divalent phosphate group on a C site; ε for divalent phosphate is about 3.5 times as large as that for univalent phosphate.

Among low M_n substances, nucleoside polyphosphates examined above are the exceptional ones that are retained on the HA column and that are eluted at phosphate molarities comparable to those for high M_n substances like DNA, typical proteins etc. [cf. Section(A)]. The exceptional behavior of nucleoside polyphosphates can be considered to arise for two reasons. The first is that a divalent phosphate group with a high ε value is participating in the adsorption. The second is that a complete fit is brought about between

the arrangement of adsorption groups on the molecule and the arrangement of adsorbing sites on the adsorbent. In connection, the following remark of Bernardi(8.6) should be added: "The very high eluting (phosphate) molarities required by phosphoproteins in comparison with nucleic acids may be due, in part at least, to the monoesterified (i.e., divalent) phosphate groups in contrast to the diesterified (i.e., univalent) groups of nucleic acids. Another consideration is that phosphoproteins have runs of phosphorylserines, which form areas of very high density of groups able to interact with HA."

With regard to chromatography of oligonucleotide with only univalent phosphate groups except the terminal divalent phosphate, if only univalent phosphates are available for bonding with C sites (because of a certain stereochemical hindrance perhaps), then it can be estimated from Fig 8.6 that at least six phosphates should be used for bonding in order for the molecule to be retained almost completely on the HA column in the absence of competing ions. [$\varepsilon \approx 4$ kJ/mol, and the minimum $E+kT\ln\tau$ value necessary for almost complete retention to take place$\approx$25 kJ/mol; this leads to $25/4 \approx 6$.]

Adsorption Energy of ε-amino group on A P Site. Earlier(8.18, 8.23), the chromatogram of poly-L-lysine (with M_n ranging between 1.5×10^3 and 8×10^3 Da i.e., with degree of polymerization of about 7 to 38) obtained by Bernardi(8.5) on an HA column by using a linear concentration gradient of NaP buffer [Fig 8.9; reproduced from ref(8.18)] was analysed by using the method used above for the analysis of the nucleoside(poly)phosphate mixture with several additional assumptions. The chromatogram contains a sharp peak (peak No.1) appearing before the concentration gradient begins and a series of eight peaks (peak Nos.2 to 9) that are eluted at different sodium molarities between 0.25 and 0.9 M (see Fig 8.9). The intervals between the latter neighboring peaks are roughly constant, and the heights of peaks decrease gradually on the right-hand side of the chromatogram (Fig 8.9). It can be assumed(8.18) that the poly-L-lysine molecule with a highly-stretched conformation(8.24) is adsorbed on P sites of HA by using ε-amino groups of side-chains, and that the discrete distribution of peaks represents a reflection of a stepwise variation in number of ε-amino groups per molecule that bond with P sites. The gradual decrease of the heights of the chromatogram (as in a binomial distribution) reflects a statistical property with respect to the distribution of the polypeptide-chain-lengths of the poly-L-lysine sample[8.18; see Fig 8.9]. In the first peak (peak No.1) are involved the components small in size with the absolute value of total energy of adsorption per molecule too small to be retained on the column(8.18).

It can be considered(8.18) that, along the highly-stretched chain of poly-L-lysine, there are two arrays of ε-amino groups of the side-chains arranged with a minimum inter-distance of 0.723 nm. As a possible adsorption configuration of poly-L-lysine on the HA surface, it was proposed(8.18) that every four ε-amino groups on one of the two arrays of these groups (i.e., every eight ε-amino groups of the whole molecule) bond with every three P sites on an array of P sites arranged with a minimum inter-distance of 0.942 nm on the HA surface; it is assumed that the crystal surface on which a poly-L-

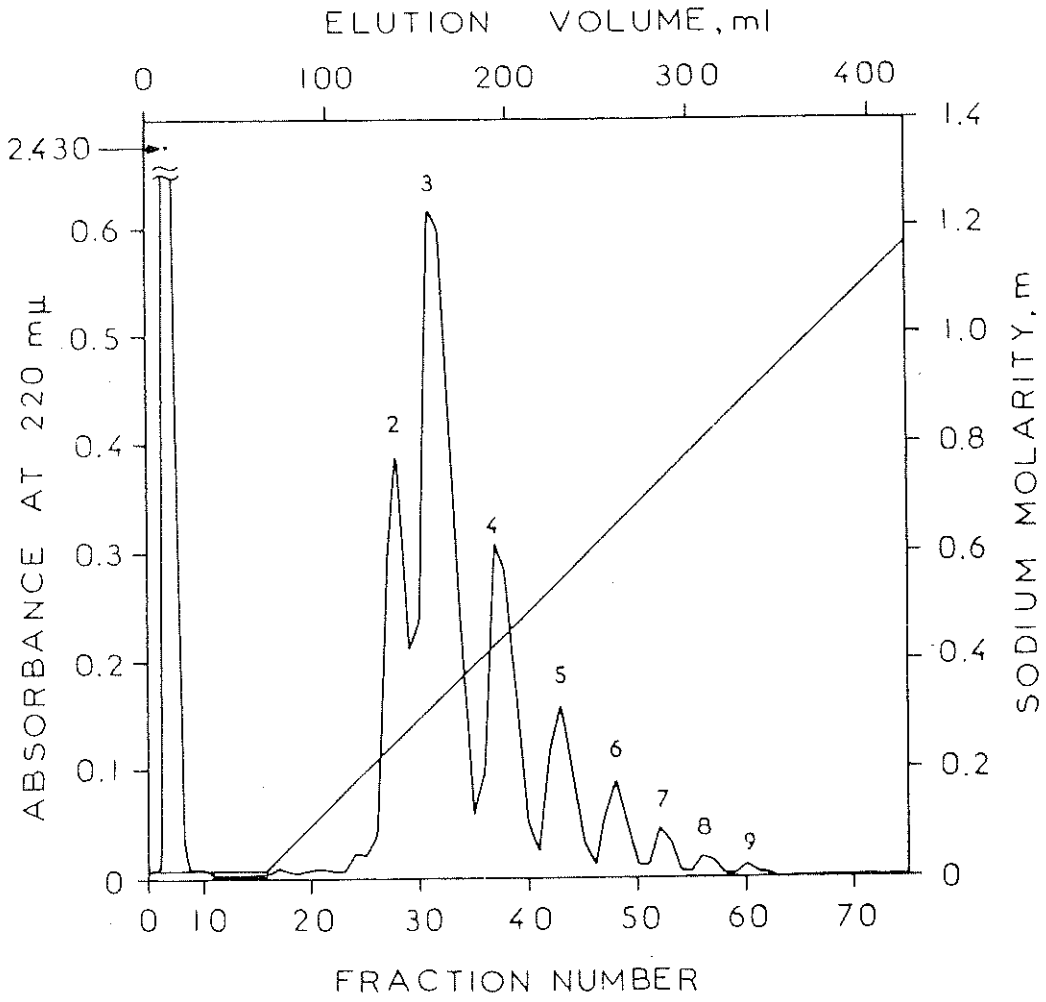


Fig 8.9. Experimental chromatogram at room temperature of a synthetic heterogeneous poly-L-lysine·HBr sample with M_n ranging between 1.5×10^3 and 8×10^3 Da (degrees of polymerization 7-38), obtained on a 22×1 cm HA column. The HA particles used for the experiment are almost identical with those used in the experiments mentioned in Appendix VI. A linear concentration gradient of NaP buffer with a slope of $g'_{(P)}(\sigma=1\text{ cm})=2.2$ mM/ml was applied for the elution [cf. Note in Table 7.1]. For detail, see text. [Reproduced directly from ref(8.18) Fig 1; the original diagram can be found in ref(8.5).]

lysine molecule is adsorbed is constructing as a whole a (001) surface. It follows that the molecules involved in peak No.1 should be adsorbed by using only one ε-amino group; the molecules involved in peaks No.2 to 9 (eluted between 0.25 and 0.9 M of the sodium gradient) should be adsorbed by using two to nine ε-amino groups, resectively (see Fig 8.9). This means that the minimum degree of polymerization of molecules in the mixture is less than or equal to eight, and that the maximum degree of polymerization is 72. Taking into account the accuracy of the measurement of M_m, this result of the calculation can be considered to be compatible with the estimation that the degree of polymerization extends between 7 and 38 (see above). This is because the total area of the five peaks (peak No.5 to 9) eluted at highest sodium molarities occupies only a minor proportion of the area of the total chromatogram(8.18; see Fig 8.9).

On the basis of the above consideration plus several additional assumptions, it was estimated(8.18) by using eqs(6.35) and (6.35') that the absolute value, ε, of energy of adsorption of an ε-amino group on a P site is 2-2.2 kcal/mol (8.4-9.2 kJ/mol), implying at the same time that the values of φ and β would be of the order of magnitude of 10 M^{-1} and 10^{-2}, respectively [cf. ref(8.23)]. It follows that the absolute value of adsorption energy taking place when two ε-amino groups are used (about 18 kJ/mol) is the same as that for ADP (17.8-18.2 kJ/mol); ADP can be eluted only by applying the concentration gradient of KP buffer (see Fig 8.8). Therefore, the conclusion that poly-L-lysine molecules adsorbed by using only one ε-amino group are eluted before the concentration gradient of NaP buffer is applied but that the molecules adsorbed by using two or more than two ε-amino groups can be eluted only by applying the concentration gradient of NaP buffer is very reasonable (cf. Fig 8.6).

Adsorption Energy of Carboxyl Group on A C Site. Earlier(8.25), the multi-peak chromatograms of collagen obtained by Kawasaki and Bernardi(8.26) on HA columns by using linear concentration gradients of NaP buffer [drawn in Fig 8.14 which will be considered in detail in the subsequent Section(F)] were analysed, and it was estimated that the absolute value, ε, of energy of adsorption of a carboxyl group on a C site is 0.7 kcal/mol (2.9 kJ/mol). This means that at least 25/2.9 i.e., eight to nine carboxyl groups should be used for bonding with C sites in order for the acidic protein molecule to be retained almost completely on the HA column in the absence of competing ions, provided that $\beta = 10^{-2}$ (cf. Fig 8.6). The number of carboxyl groups necessary for the acidic protein molecule to be adsorbed by using the energy comparable to that used for the adsorption of ADP is about six ($\approx$18/2.9; see Fig 8.6). The estimation of the adsorption energy of a carboxyl group, however, was done by combining the chromatographic theory with microheterogeneous collagen model [for detail, see the subsequent Section(F)].

The ε, β and φ values estimated for HA chromatography can be compared with the corresponding values that can be estimated for both reversed-phase(Chapter IX) and ion-exchange(Chapter X) chromatographies.

Importance of the Term, $\sum_{j=1}^{\nu} e^{E_j/kT}$, in Partition Function Ξ. It would be possible to represent the protein molecule (in native state) by using a rigid molecular model on the surface of which charged adsorption groups are arranged with slight flexibilities. [Usually, all the charged groups contained in the protein are present on the molecular surface, and, around neutral pH, these involve ε-amino, guanidinyl and carboxyl groups. The divalent phosphate group is added with phosphoprotein. The imidazole group has no effective charge as far as HA chromatography is concerned(8.27).] The term $\Sigma_{j=1}^{\nu} e^{E_j/kT}$ in partition function Ξ [eq(8.5)] shows that the molecule, in general, can take a number of different adsorption configurations on the adsorbent surface. In other words, the molecule can be adsorbed by using a number of different local surfaces each of which can face the adsorbent surface. Eq(8.8) shows that a Boltzmann distribution is realized among the configurations and that the energetically most stable adsorption configuration takes place in the highest probability. Thus, with the "basic" protein molecule adsorbed by using basic groups on P sites of HA, assigning to ε the value of 8.4-9.2 kJ/mol, it can be calculated that $e^{\varepsilon/kT}=30$-41 at 25℃. This means that the probability that the "basic" protein molecule is adsorbed in the energetically most stable configuration by using the maximum possible number of basic groups is about 30~41 times as high as the probability that it is adsorbed in the other configutations, provided that there is only one most stable configuration. With the "acidic" molecule adsorbed by using carboxyl groups on C sites, assigning to ε the value of 2.9 kJ/mol, it can be calculated that $e^{\varepsilon/kT}=3.2$ at 25℃ [and that $e^{\varepsilon/kT}=3.6$ at 4℃; cf. Fig 8.18(d)]. This means that the probability that the "acidic" protein molecule is adsorbed in the energetically most stable configuration by using the maximum possible number of carboxyl groups is about 3.2-3.6 times as high as the probability that it is adsorbed in the other configurations, provided that there is only one most stable configuration. In other words, it in general is the *local* molecular surface, and not the total molecular surface, that can be recognized by the crystal surface of HA. Consistently with this statement, with HA chromatography, the correlation between pI (reflecting the property of the total molecular surface) and μ is very weak among the "acidic" and "basic" globular proteins, respectively (i.e., among the proteins obeying the same adsorption and desorption mechanism). See Fig 8.10 [reproduced from ref(6.9)].

Ion-Exchange and Reversed-Phase Chromatograohies in Contrast to HA Chromatography. Figs 8.11(a) and 8.12 illustrate the plots of pI versus retention time for several globular proteins, obtained for anion- and cation-exchange chromatographies carried out by using a linear concentration gradient of NaCl, respectively (for detail, see the legends for the diagrams). In either Fig 8.11(a) or 8.12, a strong correlation can be found between pI and retention time in contrast to the case of HA chromatography when a weak correlation between μ and pI takes place among the proteins obeying the same adsorption and desorption mechanism (Fig 8.10); retention time and elution concentration (molarity) μ

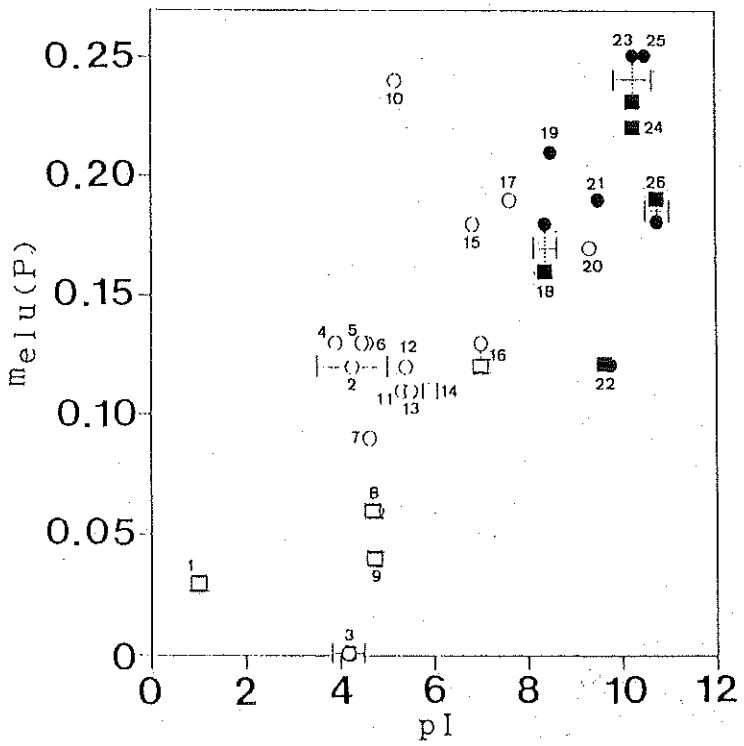


Fig 8.10. Plots of $m_{elu(P)}$ i.e., μ versus pI for 26 proteins [1, pepsin; 2, Lima bean trypsin inhibitor; 3, ovamucoid; 4, pepsinogen; 5, soybean trypsin inhibitor; 6, α-lactalbumin; 7, ovalbumin; 8, bovine serum albumin; 9, deoxyribonuclease I; 10, β-lactoglobulin A; 11, carbonic anhydrase B; 12, catalase (bovine liver); 13, insulin; 14, snail acid deoxyribonuclease; 15, conalbumin; 16, myoglobin; 17, hemoglobin (horse); 18, α-chymotrypsin; 19, γ-chymotrypsin; 20, trypsinogen; 21, chymotrypsinogen; 22, ribonuclease A; 23, cytochrome c; 24, spleen acid deoxyribonuclease; 25, papaya lysozyme; 26, lysosyme (chicken)], obtained for HA chromatography by using linear concentration gradients of either KP or NaP buffer, where $\varnothing = 1$ cm, L = 18-23 cm, and $g'_{(P)}(\varnothing = 1 \text{ cm}) = 2.4\text{-}2.5$ mM/ml [cf. Note in Table 7.1]; $m_{elu(P)}$ is almost independent of the type of cation (potassium or sodium). The HA particles used for the experiment are almost identical with those used in the experiments mentioned in Appendix VI. The molecules corresponding to points ○ and □ behave as "acidic" molecules, whereas those corresponding to points ● and ■ behave as "basic" molecules on the HA column [see Section(A)]; □ and ■ are for the KP buffer system, and ○ and ● are for the NaP buffer system. [Reproduced from ref(6.9) Fig 2. Similar data are presented in ref(7.1) Fig 12 for several types of HA particle.]

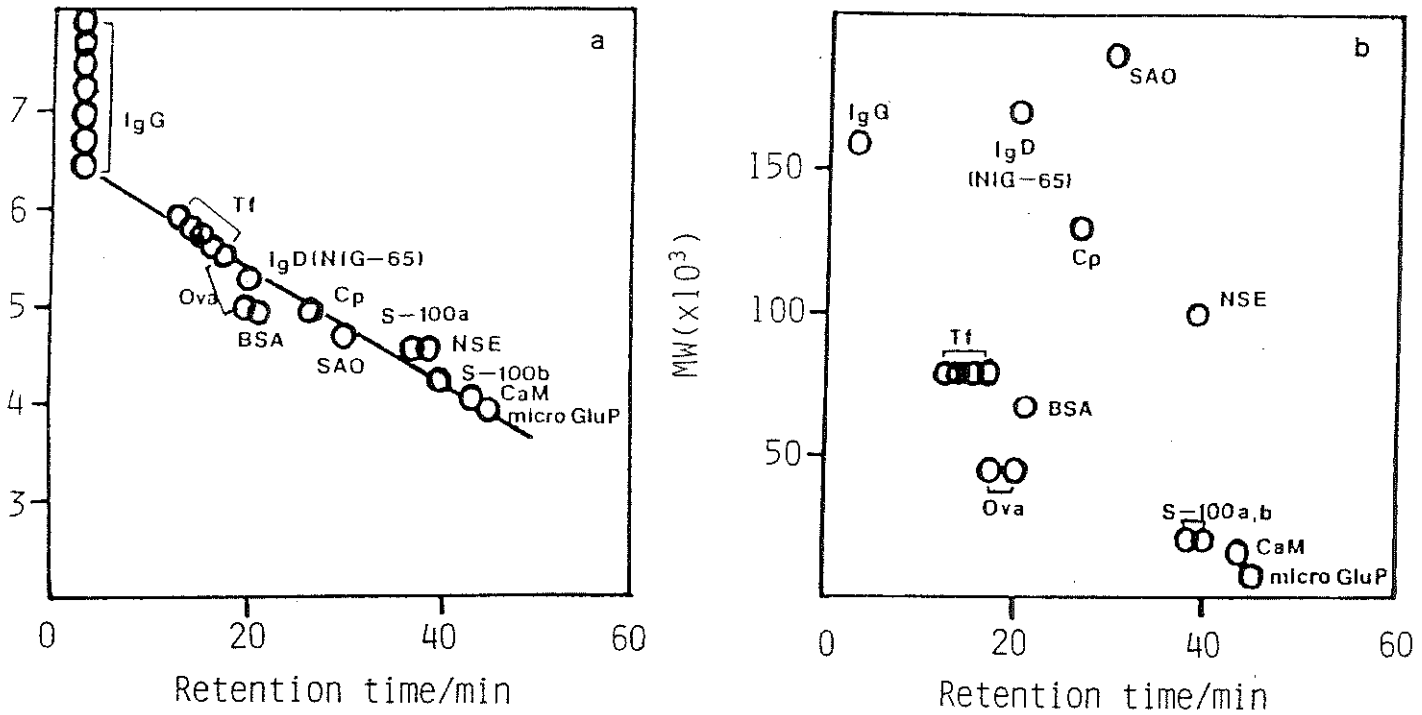


Fig 8.11. (a) Plots of pI versus retention time (in the usual sense) and (b) plots of pI versus M_n (written as MW), obtained for several proteins on a DEAE anion-exchange column system (constructed of 1×0.46 cm precolumn and 7.5×0.78 cm main column). A linear NaCl gradient (from 0 to 0.4 M) was applied in the presence of 50 mM Tris-HCl buffer at pH 7.5. [With linear concentration gradient, retention time and elution concentration (or molarity) μ can be regarded as linear functions of one another.] The pI values were measured by two-dimensional electrophoresis in the absence of denaturing agents. Abbreviations: Tf=transferrin, Ova=ovalbumin, BSA=bovine serum albumin, Cp=ceruloplasmin, SAO=serum amine oxidase, NSE=neuron-specific enolase, CaM=calmodulin, micro GluP=micro glutamic acid-rich protein. [Reproduced from ref(8.28) Fig 2.]

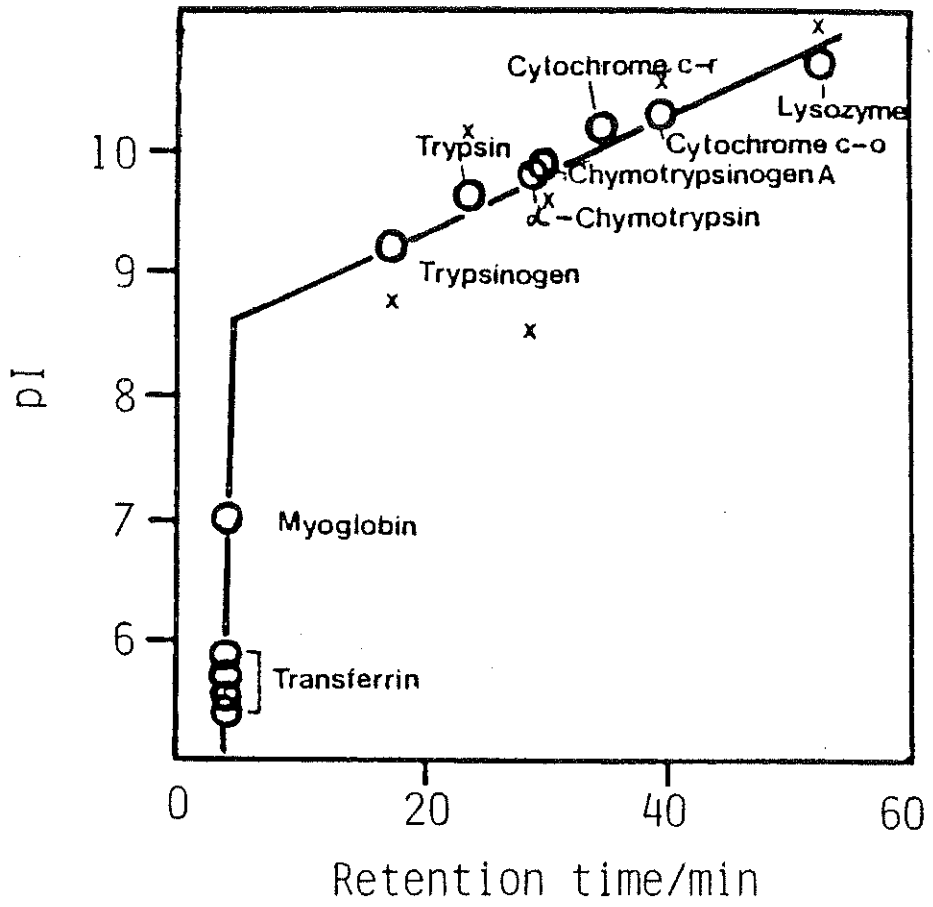


Fig 8.12. (a) Plots of pI versus retention time (in the usual sense), obtained for several proteins on a sulfopropyl cation-exchange column system (constructed of 1×0.46 cm precolumn and 7.5×0.78 cm main column). A linear NaCl gradient (from 0 to 0.4 M) was applied in the presence of 20 mM sodium phosphate buffer at pH 6.0. [Retention time and elution concentration (or molarity) μ can be regarded as linear functions of one another; see the legend of Fig 8.11.] The pI values were measured by two-dimensional electrophoresis in the absence of denaturing agents, or estimated from amino acid composition by using the micro-computer method with respect to some basic proteins. The × marks were plotted by employing the pI values in some literatures. [Reproduced from ref(8.28) Fig 5.]

are linear functions of one another when a linear concentration gradient is applied. With ion-exchange chromatography, the geometrical arrangement of the adsorbing sites (called ion-exchangers) on the adsorbent surface would fluctuate microscopically to a considerable extent among different loci in the column, as the adsorbing sites are part of an organic substrate with a more or less flexible stereochemical structure. This implies that the energetically most stable configuration of a protein molecule adsorbed on the organic substrate varies among different loci in the column and that the charges on the total molecular surface (reflecting pI as a whole) are used fairly uniformly for bonding with ion-exchangers throughout a development on the column. [Of course, this does not mean that all the charges on the molecular surface are used for the adsorption at the same time at a given moment in the development process.]

Fig 8.11(b) illustrates the plots of M_m (written as MW) versus retention time for anion-exchange chromatography, showing that there is virtually no correlation between M_m and retention time. This can be interpreted to correspond to the fact that, with HA chromatography, all the substances with M_m ranging between 10^4 and 10^8 Da are eluted around the same phosphate molarity ($\mu \approx 0.1$ M) of KP buffer (see Fig 8.1). This implies that, even with ion-exchange chromatography, eq(8.1) is valid, and that competition model applies. (Cf. the subsequent Chapter X.)

With reversed-phase chromatography also, the adsorption sites can be considered to be part of an organic substrate with a flexible strucure. It can further be assumed that the tertiary structure of the protein molecule is destroyed to a considerable extent in the environment where reversed-phase chromatography is performed. These imply that the hydrophobic structures appearing on the molecular surface of protein or peptide are used fairly uniformly for the reaction with the adsorbent. Either Fig 8.13(a) or (b) illustrates the plots of retention time versus hydrophobicity, $\ln (1 + \sum_j D'_j n_{ij})$, for a number of peptides, obtaind for reversed-phase chromatography on a C_{18} column carried out by using a linear acetonitrile gradient (for detail, see the legend for the diagrams). As anticipated, a fairly strong correlation can be found between retention time and hydrophobicity (see Fig 8.13). A stronger correlation might be obtained if the parameter $\ln (1 + \sum_j D'_j n_{ij})$ is improved. (Cf. the subsequent Chapter IX.)

The argument relevant to those performed in this subsection will be continued in the subsequent Section(G) and (H).

(F) Microheterogeneous Models of Collagen and Myosin

Collagen is a structural protein involved in a wide range of vertebrate and invertebrate species(8.30). Calf-skin collagen mainly investigated in this Section belongs in type I out of a considerable number of collagens that can be distinguished genetically in higher animals(cf. Fig 8.15). Type I collagen moleule, with M_m slightly less than 3×10^5 Da, can be represented by a rod of 300×1.5 nm(8.31). This is made up of three peptide

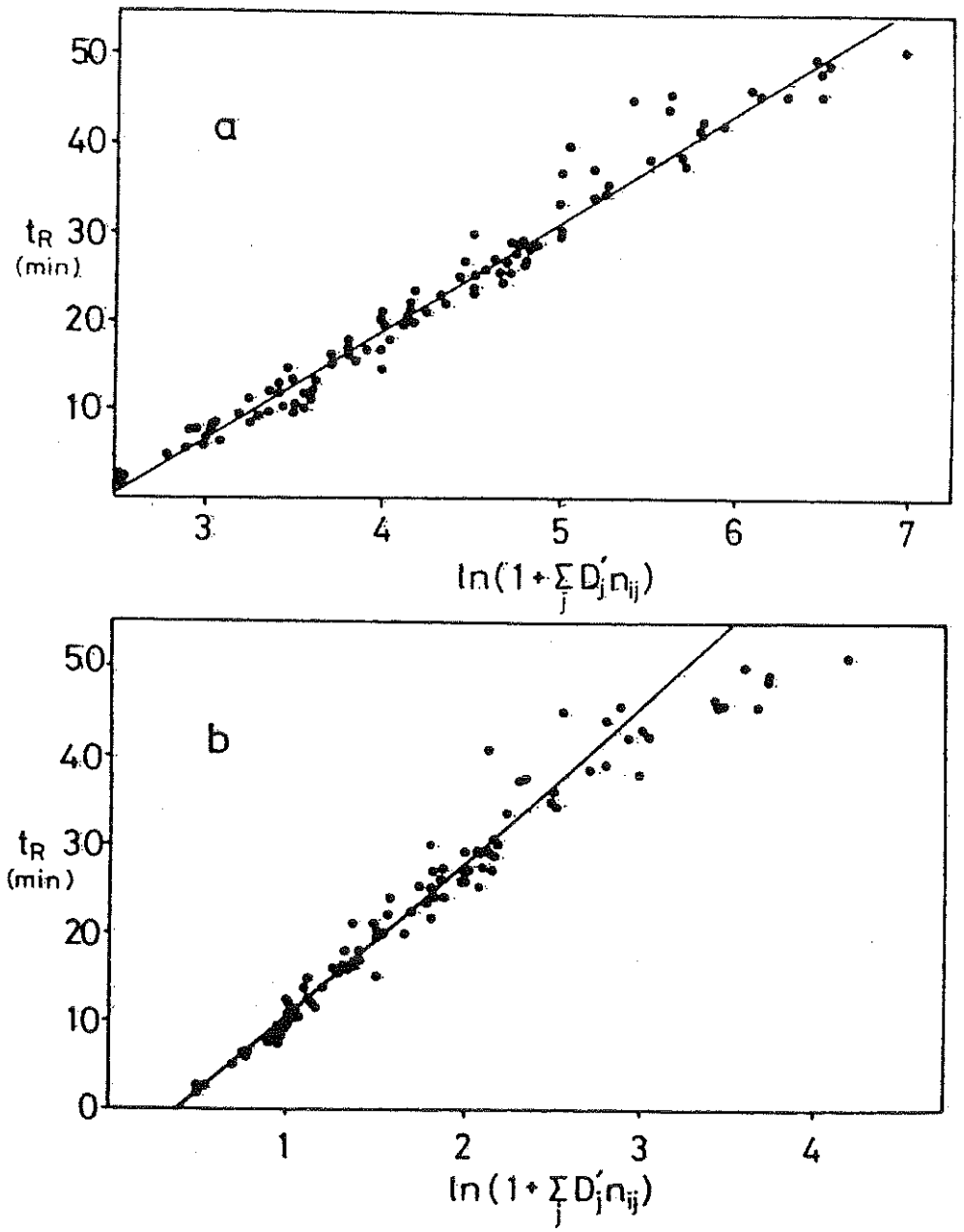


Fig 8.13. Plots of retention time (in the usual sense; written as t_R) versus molecular hydrophobicity ln $(1+\sum_j D_j' n_{ij})$, obtained for a number of peptides on a C_{18} column (30 × 0.4 cm). A linear acetonitrile(ACN) gradient (in which 0.07% trifluoroacetic acid is contained) was applied in the presence of 0.1% trifluoroacetic acid at pH 2. [Retention time and elution concentration (or volume fraction) μ of ACN can be regarded as linear functions of one another; see the legend of Fig 8.11.] For both parameters D_j' and n_{ij}, see ref (8.29); the definitions of D_j' in part(a) and (b) are different. [Reproduced from ref(8.29) Fig 2.]

chains (called α chains) consisting of slighly more than 1000 amino (and imino) residues, respectively. Two of the α chains (α_1 chains) are identical and the other (α_2 chain) has a slightly different amino acid composition (and sequence) (8.32-8.35). The three α chains together form a triple helix and a rod-like external shape (see above), the N and C terminals appearing at the same ends of the rod(8.30). Collagen partially involves molecules in which α chains are cross-linked by a covalent bond(8.30-8.32, 8.35; cf. Appendix IX). Cross-links are formed between not only α chains belonging in a single collagen molecule but also those belonging in different molecules. In the latter case, collagen"polymers" are produced (cf. Appendix IX). These are hardly extractable under the condi-tion where "monomer" molecules usually are extracted(8.36, 8.37); a slight amount of "polymers" that are contaminating the "monomer" preparation can be eliminated by treatment with protease at the same time with the elimination of the intramolecular cross-links[8.36, 8.37; cf. Figs 8.15(b) and (c)]. The collagen sample used in the experiments in Figs 8.14, 8.16 and 8.17 was prepared by using the method of ref(8.36). To only some of hydroxylysyl residues (out of 3000 total residues per molecule) are attached carbohydrates in the form of galactosyl-hydroxylysine and glucosylgalactosylhydroxylysine(8.30, 8.32, 8.35). The greater parts of both α_1 and α_2 chains consist of repetitions of triplet structures of Gly-X-Y where X and Y can be amino and imino acid residues(8.32, 8.35, 8.38-8.40). Thus, glysine occupies almost one-third of the total residues of an α chain; prolline and hydroxyproline occupy one-fifth to a quarter [also see ref(8.34)]. Therefore, X and Y positions are often occupied by imino acid residues. Both aspartic and glutamic acid residues with carboxyl groups occupy about 7% of the total residues; about 230 acidic residues are involved in a intact collagen molecule. The carboxyl groups are all free and titratable(8.41).

It can be assumed that collagen [although a basic pI can be deduced from its amino acid composition(8.32-8.35)] is adsorbed on C sites of HA by using carboxyl groups since the elution of collagen from the HA column is achieved almost independently of the molarity of KCl or NaCl co-existing in KP or NaP buffer [8.25; cf. ref(7.1)].

When chromatographed on HA columns under high-resolution conditions by using a shallow linear concentration gradient of NaP buffer [see the subsection entitled "Good Separation Condition" in Chapter Ⅶ(E)], type I collagen (called simply as collagen hereafter) gives multi-peak chromatograms involving about ten peaks eluted between 0.04 and 0.12 M with respect to phosphate [see Fig 8.14; reproduced from ref(8.25)]. Similar chromatograms were obtained more recently [see Figs 8.15(a)-(c); reproduced from ref(8.42)]. It can be seen in Fig 8.14 as well as in Figs 8.15(a)-(c) that the intervals between the neighboring peaks are roughly constant and that the heights of peaks decrease gradually on the right-hand side of the chromatogram (similary to the case with poly-L-lysine; Fig 8.9); some components appear to be accumulated near the left border of the chromatogram. It was confirmed(8.26) that rechromatography of the different parts of the chromatogram (carried out under the same experimental condition) gives patterns with narrow widths eluted at phosphate molarities almost equal to those where the fractions appeared

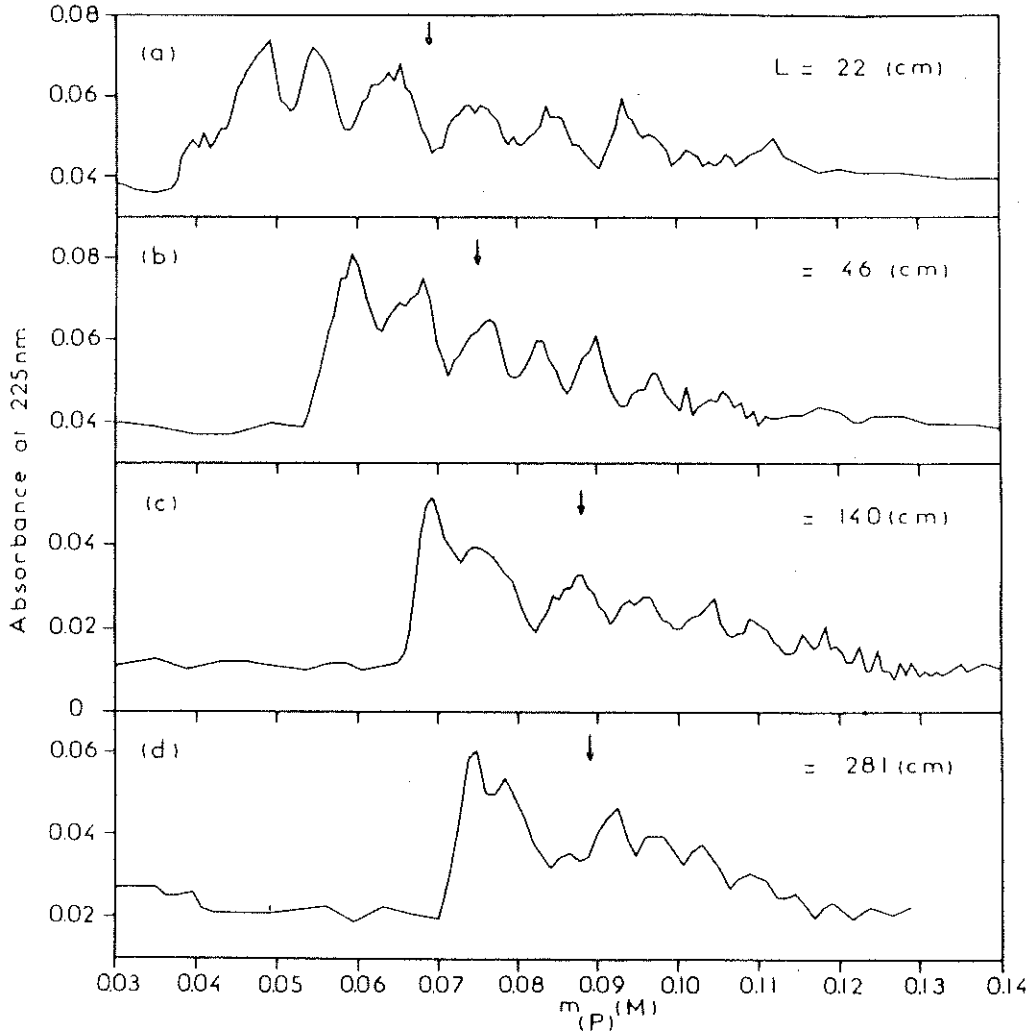


Fig 8.14. Experimental chromatograms of calf-skin type I collagen at 4℃ represented as functions of $m_{(P)}$ in NaP buffer, obtained on HA columns (ϕ=0.5 cm) with four different total lengths L by using a linear concentration gradient of NaP buffer with a slope $g'_{(P)}(\phi=1\text{ cm})=0.0375$ mM/ml [cf. Note in Table 7.1]. Both 0.15 M NaCl and 1 M urea are present in NaP buffer always. The concentration of urea, 1 M, is far below that causing denaturation of collagen(8.27). It was later confirmed that essentially the same chromatogram can be obtained in the absence of urea. The arrow shows the position of the center of gravity of the total chromatogram. The HA particles used for the experiment are almost identical with those used in the experiments mentioned in Appendix VI. [Reproduced directly from ref(8.25) Appendix I Fig A3; the original diagrams can be found in ref (8.26).]

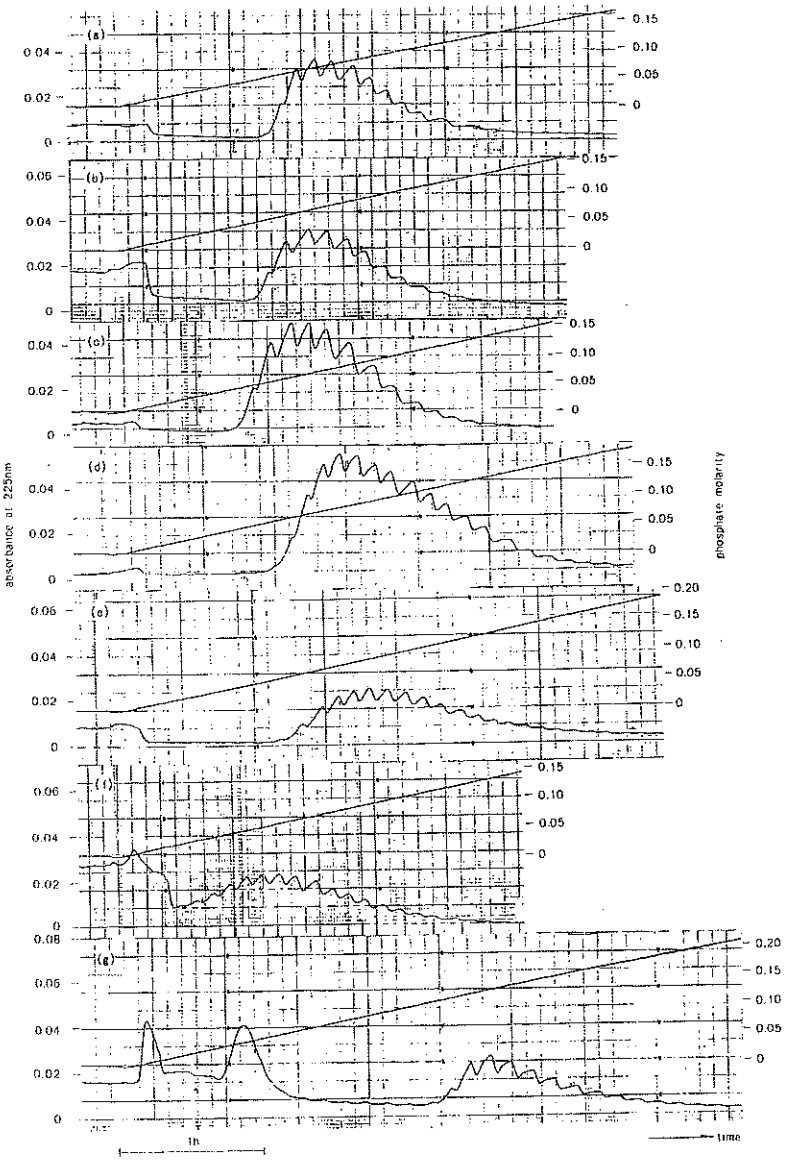


Fig 8.15. Experimental chromatograms at 4℃ of (a) type I collagen extracted by acetic acid from calf skin, (b) type I collagen extracted by acetic acid from calf skin and treated with pepsin, (c) type I collagen extracted by pepsin from calf skin, (d) type II collagen from bovine articular cartilage, (e) type III collagen from human placenta, (f) type IV collagen from human placenta, and (g) type V collagen from human placenta, obtained by using the HPLC column system packed with HA particles almost identical with those used in the experiments in Fig 8.14 or those used in the experiments mentioned in Appendix VI. For all the experiments, the column system ($\phi = 0.6$ cm) with total length L = 13cm was used, and a linear concentration gradient of NaP buffer with a slope $g'_{(P)}(\phi = 1$ cm$) = 0.225$ mM/ml [cf. Note in Table 7.1] was applied; both 0.15 M NaCl and 1 M urea are present in the NaP buffer always. [Reproduced from ref(8.42) Fig 14.]

in the first chromatogram [see both Figs 8.16 and 8.17; reproduced from ref(8.26), respectively]. The chromatograms drawn in both Figs 8.16 and 8.17 were obtained by using the NaP gradient steeper than that used in Fig 8.14, bringing about lower resolutions [see the subsection entitled "Good Separation Condition" in Chapter Ⅶ(E)]. When the fraction corresponding to a single peak in the multi-peak chromatogram obtained under high-resolution condition was rechromatographed under the same experimental condition, the chromatogram consisting of only one peak was not obtained. Instead, a chromatogram with a small total width consisting of some peaks arised around the position of the fraction in the first chromatogram; the intervals between the neighboring peaks in the second chromatogram were almost equal to those taking place in the first chromatogram. (The interpretation of this phenomenon will be given later.) Amino acid analysis, measurements of the intrinsic viscosity and the optical rotatory dispersion, and electron-microscopical observations of segment-long-spacing fibers for different chromatographic fractions were performed, but no differences were detected so far(8.25).

Kawasaki and Bernardi(8.26) considered that the multi-peak collagen chromatogram (Fig 8.14) arose not as a result of the occurrence of several (about ten) molecular species each of which corresponds to a peak, but rather as a result of different particular distributions of functional carboxyl groups on the macromolecules, so that one peak may corresponds to several components. Kawasaki(8.25, 8.43, 8.44) deduced the existence of a statistical assembly of a large number of molecular species behind the multi-peak chromatogram by considering (a) that the discrete distribution of peaks is a reflection of a stepwise variation in number (taking almost only integral values) of carboxyl groups per molecule that bond with C sites, (b) that the gradual decrease of the heights of the peaks taking place on the right-hand side of the chromatogram is a reflection of the statistical property regarding a variety of arrangements of carboxyl groups taking place on the molecular surfaces of a number of different species, respectively, and (c) that the accumulation of some components near the left border of the chromatogram arises as a result of the Boltzmann distribution of the adsorption configuration of a molecule [see eq(8.8)]. It can be assumed(8.25, 8.43, 8.44) that the collagen molecule with a rod-like shape is adsorbed by using the lateral surface (with overwhelmingly high probabilities) and that the adsorption configuration is virtually limited within the rotation of the rod around the main axis.

Kawasaki(8.25, 8.43, 8.44) proposed a microheterogeneous collagen model. This states that the primary structures of the three α $(=2\alpha_1+\alpha_2)$ peptides constructing the collagen whole molecule are fluctuating around the mean structures; the probabilities that aspartic and glutamic acid residues (with carboxyl groups) are present at "correct" positions on the α peptides are less than unity, respectively. Here, the "correct" positions are defined as positions or sequence numbers where it was concluded by using the organochemical method that the amino acid residues under consideration should be present. In Appendix Ⅷ(A) [the origin of which can be found in ref(8.25) Appendix Ⅲ], the method-

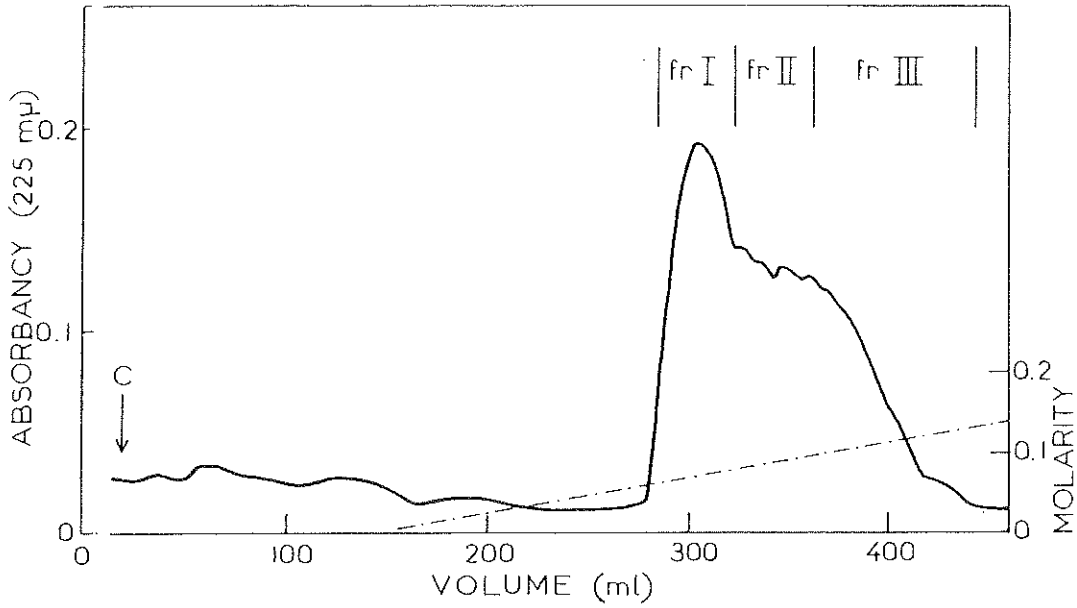


Fig 8.16. Experimental chromatogram of calf-skin type I collagen at 4℃, obtained on a 35×1 cm HA column by using a linear concentration gradient of NaP buffer with a slope $g'_{(P)}(\phi=1\ cm)=0.45$ mM/ml [cf. Note in Table 7.1]; both 0.15 M NaCl and 1 M urea are present in the NaP buffer always. The HA particles used for the experiment are identical with those used in the experiments in Fig 8.14. The chromatographic resolution is lower than that obtained in Fig 8.14 because the concentration gradient with a steeper slope is applied. [Reproduced from ref(8.26) Fig 3.]

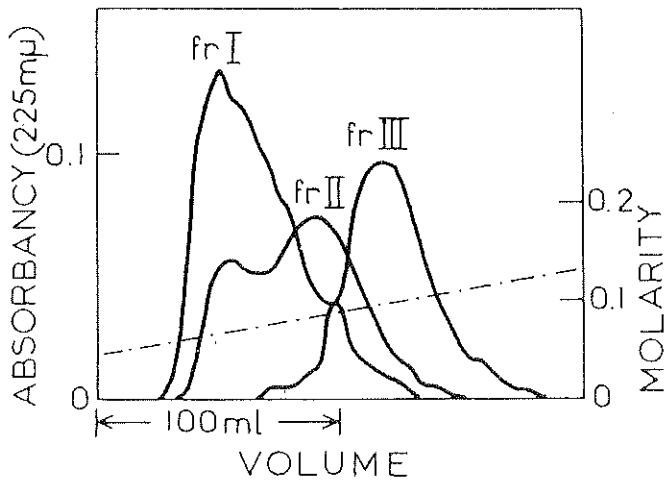


Fig 8.17. Rechromatographies of fractions I-III from the diagram presented in Fig 8.16. The experimental conditions are identical with those used in Fig 8.16. [Reproduced from ref(8.26) Fig 4.]

ology for the "determination" of the collagen primary structure is reconsidered with a conclusion that it in principle is the most-frequently-occurring primary structure that can be determined or *picked up* by using the organochemical method (unless it a priori can be assumed that the primary structure should be unequivocal). Therefore, microheterogeneous collagen model is not incompatible with the fact that the primary structure of the α chains are "determinable" by using the organochemical method. On the basis of the central dogma of biology, it in general is admitted that the primary structure of a protein is highly unequivocal (except for the variation taking place as a result of posttranslational modifications; see below). It should be pointed out(8.25), however, that, even though the primary structures of a number of globular proteins which respectively induce the corresponding intricate tertiary structures are highly unequivocal (consistently with theteleological necessity), the unequivocal arrangement of amino acid residues is not required for the simple triple-helical structure of collagen to be maintained; especially with amino acid residues other than glycil and imino acid residues, we find no reasons why they should be present at "correct" positions in high probabilities [for detail, see Appendix Ⅷ(B)]. It should also be pointed out that collagen is biosynthesized in an overwhelmingly large amount in comparison with globular proteins; this suggests a certain difference of the production mechanism between collagen and globular proteins. [It can be concluded[Appendix Ⅷ(C)] that the heterogeneous collagen chromatograms(Figs 8.14 and 8.15) cannot satisfactorily be explained in terms of posttranslational modifications nor of deaminations of asparginyl and/or glutaminyl residues if they take place spontaneously. This is because the maximum possible degree of molecular heterogeneity that can arise from these mechanisms is much too small to explain the experimental chromatograms.] In Appendix Ⅷ(B) [the origin of which can also be found in ref(8.25) Appendix Ⅲ], the collagen biosynthesis is outlined briefly, and it is suggested that the equivocal primary structures of the α chains may arise at a translational level of biosynthesis due to the lack of the proofreading mechanism or to the extremly weak such mechanism compared to that taking place with globular proteins. In Appendix Ⅸ, the experiment of Yamauchi et al. manifesting a heterogeneity of the collagen primary structure is presented. Unfortunately, the microheterogeneous concept such as considered above is out of the current of the modern biology perhaps because of an *apparent* inconsistency with a number of circumstantial evidences obned by biologists so far.

In refs(8.25, 8.43, 8.44), attempt was made to reproduce the multi-peak collagen chromatograms(Fig 8.14) theoretically by using microheterogeneous model, and the absolute value, ε, of energy of adsorption of a carboxyl group on a C site was estimated through this process. Below is followed the treatment performed in refs(8.25, 8.43, 8.44) with modifications some of which are based on new knowledges about the surface structure of the HA particles used. Thus, neglecting the mutual interactions among sample (collagen) molecules which may take place in the present case (see below), elution phosphate molarity, μ, for any component of the mixture can be represented by eq(6.24') or (6.35'). This

means that, when x' is constant, then μ is determined by the quantity q, or the quantity:

$$\phi = x + (kT/\varepsilon)\ln\tau \tag{8.58}$$

[see both eqs(8.49) and (8.53)] where x is represented as

$$x = \sum_{j=1}^{\nu} x_j e^{x_j \varepsilon / kT} \Big/ \sum_{j=1}^{\nu} e^{x_j \varepsilon / kT} \tag{8.59}$$

Eq(8.59) arises from eq(8.8) in which $E_j = x_j \varepsilon$; x_j represents the number of carboxyl groups bonding with C sites when the j th adsorption configuration is being realized. $\ln\tau$ [eq(8,58)] is represented by eq(8.7) where γ_j is defined by eq(8.8) in which $E_j = x_j \varepsilon$. It should be noted that

$$\lim_{\varepsilon \to \infty} \phi = \lim_{\varepsilon \to \infty} x = \max_{j=1}^{\nu} x_j \tag{8.60}$$

What we should do now is to calculate the distribution of ϕ [written as $D(\phi)$]. $D(\phi)$ can be transformed to the distribution of μ (without considerable deformation of the distribution aspect), and this latter represents the theoretical collagen chromatogram if the effect of the axial molecular diffusion in the column is added.

Preliminarily, let us examine the model that 230 carboxyl groups are arranged at random on the lateral surface of each molecular species of the mixture and that each carboxyl group (if it is present near a C site on the HA surface) can move freely within the effective area around its mean position on the molecular surface without considerable loss of energy in order to bond with the C site. We assume that the carboxyl group can also move slightly in the perpendicular direction relative to the molecular surface (to be precise, the mean molecular surface). Of all the carboxyl groups that are present on the lateral molecular surface, only those existing within the local region of the surface facing the HA surface would be able to bond with C sites; this region is elongate, parallel to the main axis of the molecule. Let us denote by h_1 the total width of this region, and by ℓ the circumferential distance around the main axis of the molecule on the molecular surface; ℓ can be estimated to be 4.71 nm by replacing the collagen rod by a cylinder with a diameter of 1.5 nm. The probability, p_1, that, in a given adsorption configuration, a carboxyl group can be found within the local region of the molecular surface facing the HA surface can be represented as

$$p_1 = h_1/\ell \tag{8.61}$$

On the other hand, let us denote by d the *effective* inter-distance between C sites measured along the main axis of the adsorbed collagen molecule, and by h_2 the diameter of

the effective area on the molecular surface where a carboxyl group can move freely (around its main position; see above), measured along the main axis of the adsorbed molecule. The probability, p_2, that, in a given adsorption configuration, a carboxyl group which is present within the local region (with width h_1) facing the HA surface bonds with a C site can be represented as

$$\left.\begin{aligned} p_2 &= h_2/d \quad (\text{if } h_2 < d) \\ p_2 &= 1 \quad\quad (\text{if } h_2 \geqq d) \end{aligned}\right\} \tag{8.62}$$

Therefore, the probability, ϕ, that, in a given adsorption configuration, a given carboxyl group existing on the total molecular surface bonds with a C site can be represented as $\phi = p_1 p_2$, or as

$$\left.\begin{aligned} \phi &= h_1 h_2/(\ell\, d) \quad (\text{if } h_2 < d) \\ \phi &= h_1/\ell \quad\quad\quad (\text{if } h_2 \geqq d) \end{aligned}\right\} \tag{8.63}$$

Taking into account the fact that the carboxyl group is attached to the end of the flexible side-chain of either aspartic or glutamic acid residue, it is reasonable to consider that both h_1 and h_2 are of the order of magnitude of several times 0.1 nm.

The distribution $D(\phi)$, which depends on both ε and ϕ, can now be calculated (8.25, 8.43, 8.44). The calculation shows that, provided that $\varepsilon \to \infty$, then $D(\phi)$ manifests a completely-discrete distribution appearing only when ϕ [$=x$; see eq(8.60)] takes integral values. The heights of the distribution peaks decrease gradually on both sides of the peak with the maximum height (like in a binomial distribution) and, especilally when $1/\phi$ is of the order of magnitude of ten, then the total number of distribution peaks (with finite heights in practice) is of the order of ten in parallel with the fact that the total number of peaks in the experimental chromatogram is of the order of ten(Figs 8.14 and 8.15). Further, provided that the second equality holds in eqs(8.63) where $\ell = 4.71$ nm, the value of the order of magnitude of ten for $1/\phi$ leads to the reasonable value of the order of magnitude of several times 0.1 nm for the parameter h_1. Fig 8.18(a) illustrates a typical example of the calculation obtained assuming that $\varepsilon \to \infty$ and that $1/\phi = 18$.

Figs 8.18(b)-(f) show that, when ε decreases to take finite values, then the discrete distribution of peaks smears slowly. Some components are accumulated gradually near the left border of distribution $D(\phi)$ with decrease in ε [Figs 8.18(b)-(e)], and almost only the accumulation part of the total chromatogram survives finally[Fig 8.18(f)]. Especially when the value of the Boltzmann factor $e^{\varepsilon/kT}$ is about 3.6 or when ε is about 2.9 kJ/mol[Fig 8.18(d)], the total shape of distribution $D(\phi)$ is very similar to the shapes of the experimental collagen chromatograms(Figs 8.14 and 8.15); $kT = 2.30$ kJ/mol at 4℃.

In refs(8.25, 8.43), the preliminary random collagen model was improved to the model that each of 230 carboxyl groups is present at each "correct" position on the lateral molecular surface in probability, π, less than unity and that the carboxyl group is present

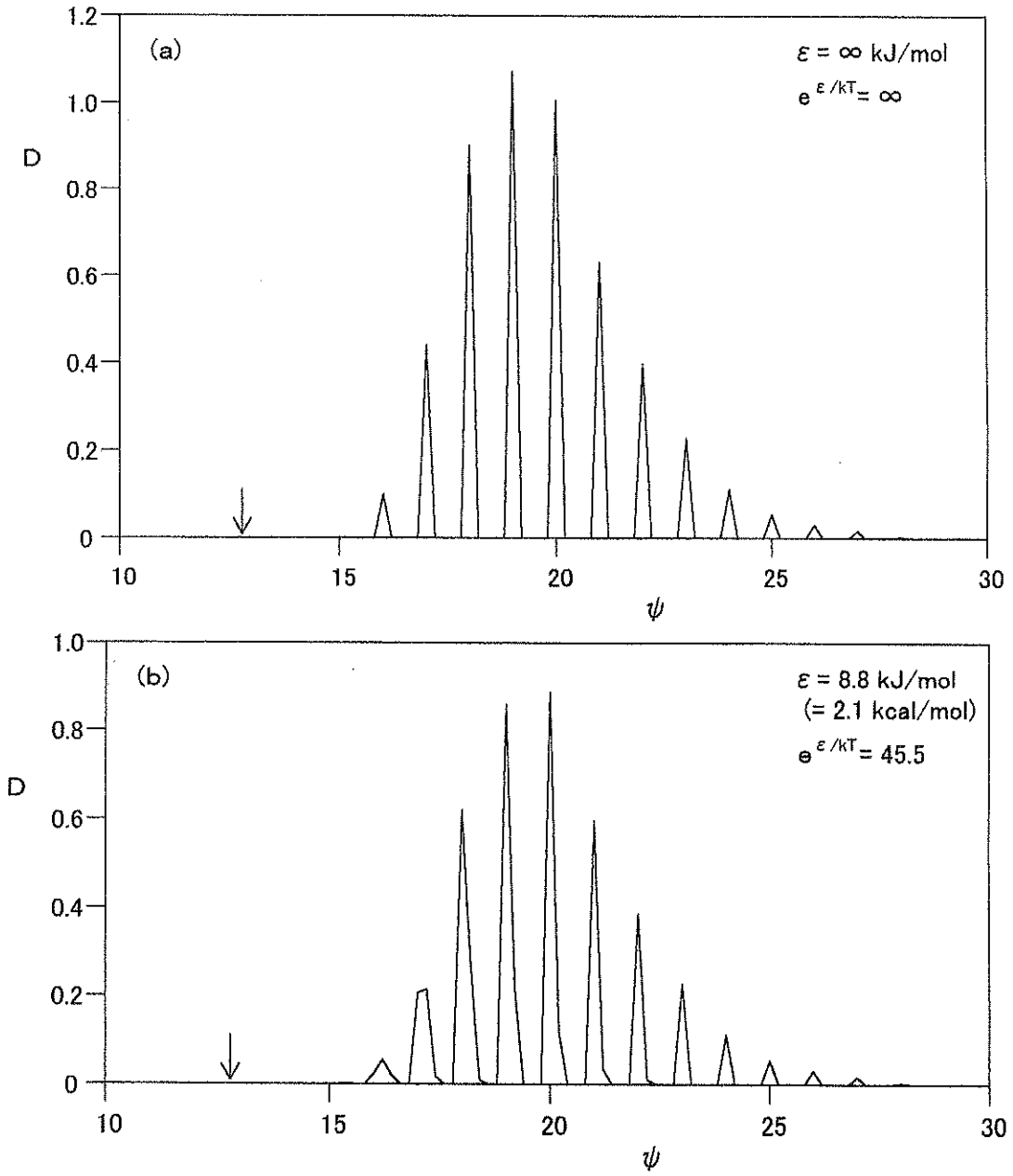


Fig 8.18. Functions $D(\phi)$ for several values of ε, obtained by assuming that 230 carboxyl groups are partitioned at random among 18 elementary domains on the side surface of each collagen molecule; kT=2.30 kJ/mol at 4℃. The current ϕ values were divided into elements of 0.2 in size, and the probability $D(\phi)$ that ϕ is between $\phi-0.1$ and $\phi+0.1$ was estimated by using the Monte Carlo method with 5000 trials. For detail, cf. both Appendix X and the legend for Fig 8.19. The ε values assumed in (b) and (c) are equal to the absolute values of the adsorption energy of ε-amino group on a P site and the adsorption energy of univalent phosphate group on a C site, respectively. The arrow drawn in each diagram indicates the value of 230/18=12.8. [The prototype of the diagrams can be found in ref(8.44) Fig 1.]

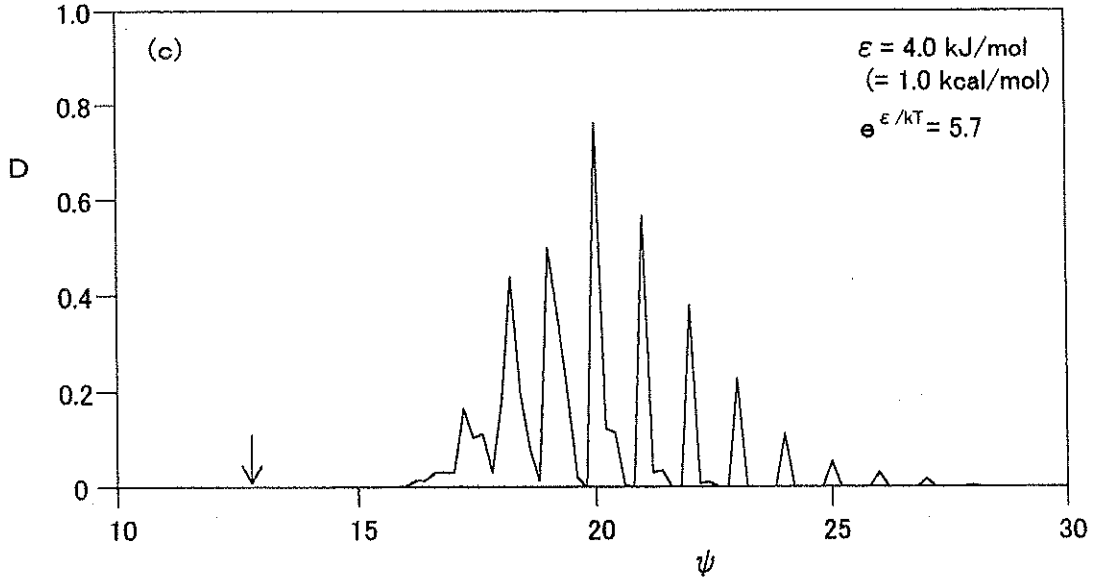


Fig 8.18. (c)

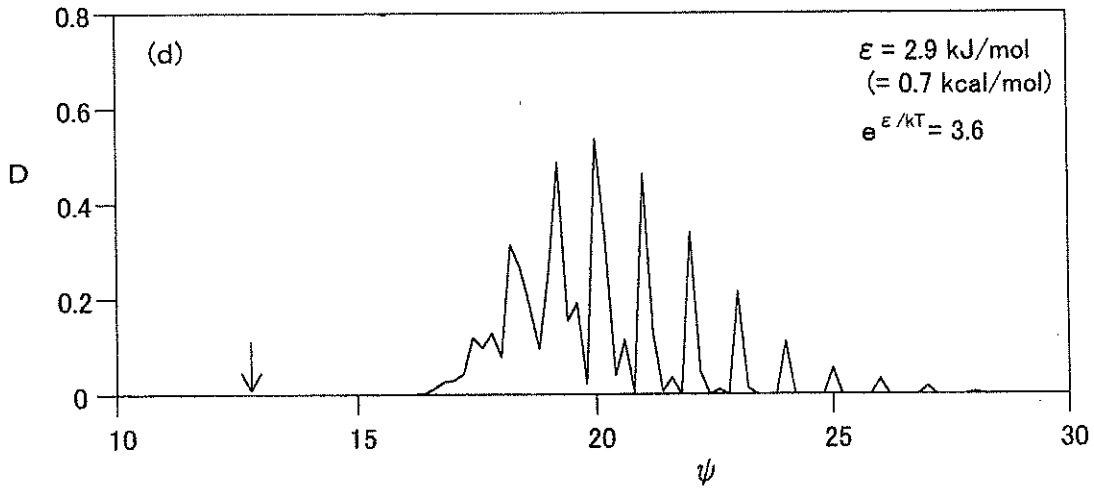


Fig 8.18. (d)

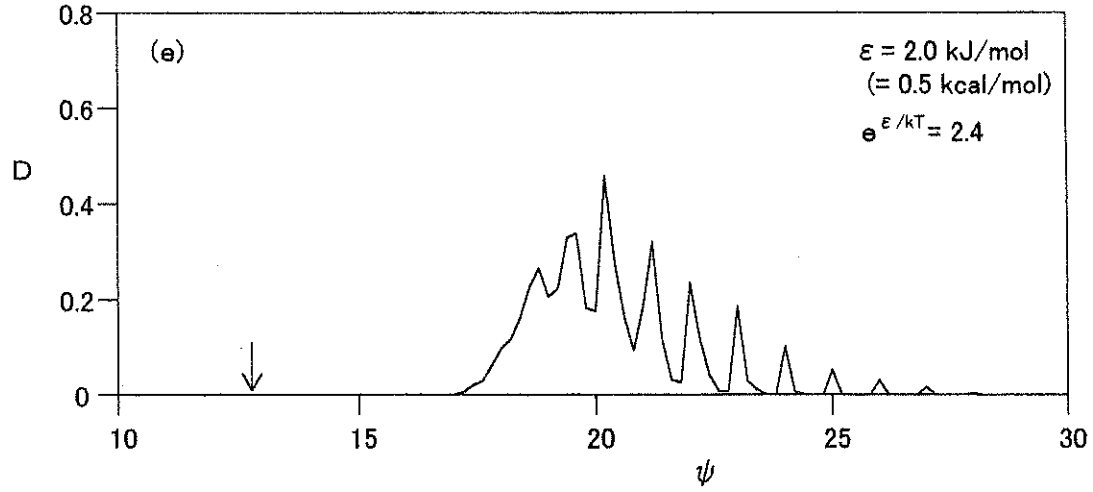


Fig 8.18. (e)

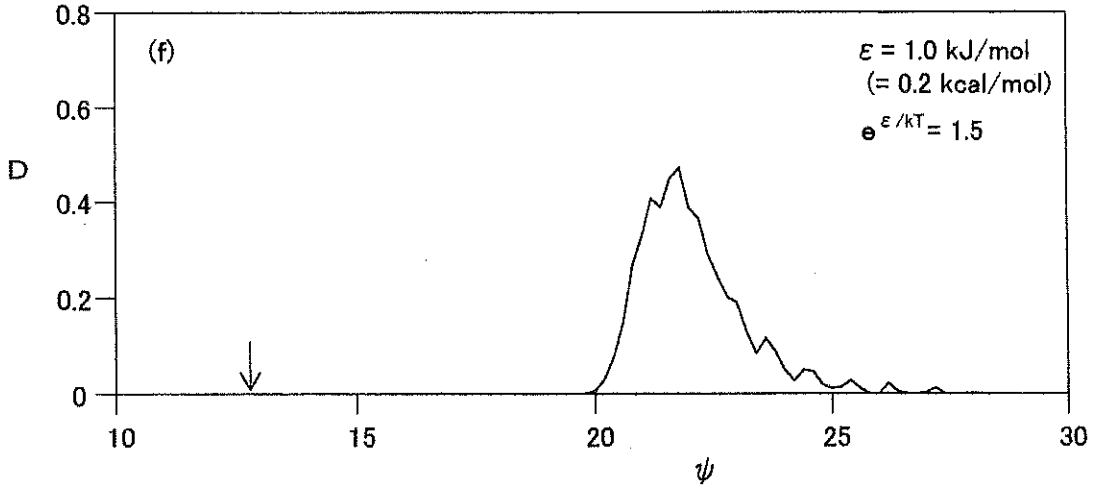


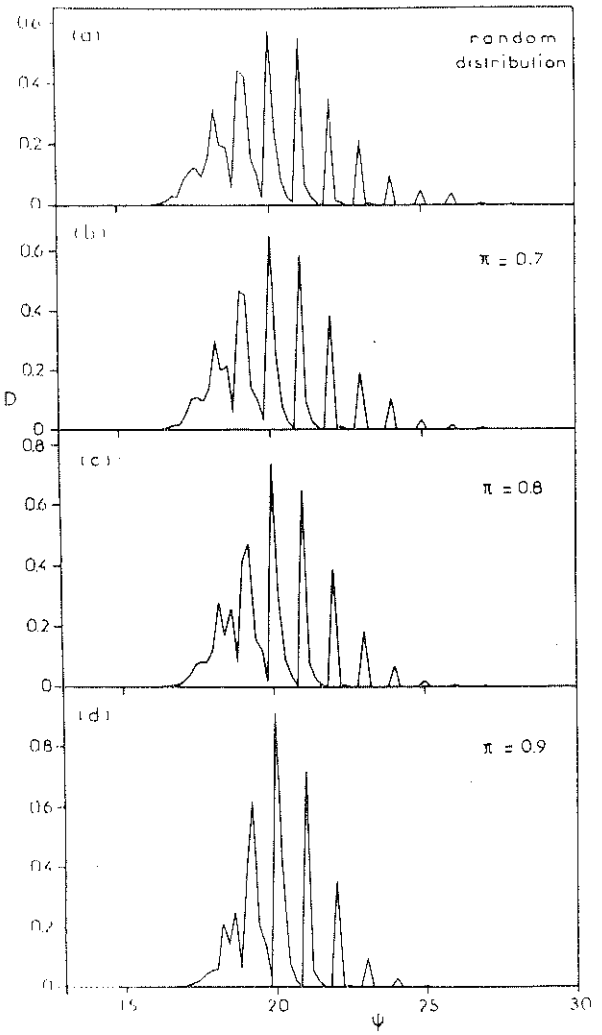
Fig 8.18. (f)

at any other position on the lateral molecular surface in probability $1-\pi$. As "correct" position, the statistically most probable position was assumed [see Appendix X(A)]; this assumption would be reasonable because 230 is a large number. The improved model would coincide approximately with microheterogeneous collagen model if to π is assigned the meaning of the probability that aspartic and glutamic acid residues (with carboxyl groups) are present at "correct" positions on the α peptide chains. This is because, provided that the equivocal primary structures of the α peptide chains arise at a translational level of biosynthesis[Appendix Ⅷ(B)], the total number of both aspartic and glutamic acid residues per molecule would be kept virtually constant among different molecular species since, again, the average, 230, of the total number of these residues is large [see Appendix X(B)]. It can be shown(8.25, 8.34) that, when $\pi \lesssim 0.5$, distribution $D(\phi)$ is quasi-independent of π, almost identical with the distribution obtained by using the preliminary random model. Fig 8.19 shows that, when $0.7 \lesssim \pi \lesssim 0.8$, the width of distribution $D(\phi)$ decreases slowly with increase in π and that, when $\pi \gtrsim 0.8$, the rate of decrease accelerates considerably; it is assumed: $\nu\,(=1/\phi)=18$ and $\varepsilon = 2.9$ kJ/mol ($e^{\varepsilon'/kT}=3.6$). For detail on the calculation, see Appendix X(A) with reference to Appendix X(B).

If x', φ and β are given, then, by using eqs(6.35'), (8.49), (8.53) and (8.58), distribution $D(\phi)$ can be transformed to the distribution of μ obtained under any experimental condition where both s ($=gL$) and m_{is} are given. Further, by using the theory of concentration gradient chromatography(Chapter VI), the distribution of μ can be transformed to the theoretical collagen chromatogram in which account is taken of the effect of axial diffusion in the column. As the parameter ε is involved in the equations representing the contribution of each component of the mixture to the total chromatogram [i.e., as ε is involved in the term q in eq(6.35')], then it must be possible that the ε value be estimated by comparing the theoretical chromatogram with the experimental chromatogram especially with an effort to obtain best fits of the intervals of successive peaks between theoretical and experimental chromatograms. It should be emphasized that the ε value estimated by using this method is independent of the value estimated from the degree of accumulation of some components near the left border of distribution $D(\phi)$ (see Fig 8.18). If the two ε values coincide with one another, the microheterogeneous interpretation of the collagen chromatograms(Figs 8.14 and 8.15) is very reliable.

In ref(8.25), attempt was made to calculate a series of theoretical chromatograms corresponding to a series of experimental chromatograms(Fig 8.14) by using the improved collagen model in which three parameters ν $(=1/\phi)$, ε and π are involved. For the calculation, however, instead of eq(6.1) combined with both eq(6.24') and the pair of eqs (6.8) and (6.9), eq(6.38) combined with both eqs(6.35') and (6.40) (old type of the present theory) was used. Eqs(6.24'), (6.8) and (6.9) are equivalent with eqs(6.35'), (6.8') and (6.9'), respectively. Therefore, it can essentially be restated that eq(6.40) was used instead of the pair of eqs(6.8') and (6.9') for the calculation. As far as the present problem is concerned, it can be considered that the replacement of the pair of eqs(6.8') and (6.9')

Fig 8.19. Functions $D(\phi)$ for random [part(a)] and semi-random [part(b)-(d)] distributions of X (=230) carboxyl groups on the side surface (abstract surface) of each collagen molecule that consists of ν (=18) elementary domains (see Appendix X Fig A10.1). It is assumed that ε =0.7 kcal/mol (=2.9 kJ/mol); kT=2.30 kJ/mol at 4℃. The calculation was performed by using the Monte Carlo method with 5000 trials; the current ϕ values were divided into elements of 0.2 in size, and the probability that ϕ is between $\phi'-0.1$ and $\phi'+0.1$ was estimated, where ϕ'=J, J+0.2, J+0.4,..., and J represents an integer with a small enough value. The curves $D(\phi)$ were drawn by connecting the probabilities occurring in respective elements. If elements smaller than 0.2 in size are used, substructures appear in the curves. Due to axial diffusion taking place in the column, however, these substructures will not appear in the final chromatogram. For the calculations of the diagrams in (b)-(d), the set $(x_1,x_2,...,x_\nu)$ was assigned to each collagen molecule by using Appendix X Fig A10.1. Thus, by using a uniform series of real random numbers comprised between 0 and 1 produced by the computer, a real number, p, was assigned to every elementary surface under the thick folded line ζ_j in Appendix X Fig A10.1. If $p \leqq \pi$, a carboxyl group was assumed to enter this elementary surface. If $p > \pi$, the real number p was produced again. The number was transformed into an integer j' comprised between 1 and ν. It was assumed that the carboxyl group enters an elementary surface that belongs in both the j' th elementary domain and the elementary surfaces above the thick folded line in Appendix X Fig A10.1. After the trials for all the X elementary surfaces that are present under the thick folded line ζ_j, the total number of carboxyl groups was estimated for every elementary domain or every vertical column of elementary surfaces. This represents the value of x_j. [Reproduced from ref(8.25) Fig 3.] Note that the diagram drawn in (a) should be identical with that drawn in Fig 8.18(d). A slight difference arises between the two diagrams, however, because of the difference of serial random numbers produced by the computer in the respective calculations.



by eq(6.40) is a good approximation in order to simplify the calculation. In fact, the calculation under consideration is only concerned with the width or standard deviation of the chromatographic peak with respect to each molecular species constructing a microheterogeneous mixture or the total chromatogram as a whole, and the calculation is done for a single value of the parameter g'; the value of either $g'\Theta^{\circ}$ [eq(6.9')] or $g'\Theta^{*}$ [eq(6.40)] can be chosen freely in order to obtain a good fit with experiment. Both in the pair of eqs(6.8') and (6.9') and in eq(6.40), the parameter q which characterizes each molecular species in the mixture is involved. [In the pair of eqs(6.8') and (6.9'), the parameter q is involved implicitly through function μ(s)[eq(6.35')], whereas, in eq(6.40), q is involved both explicitly and implicitly.] Therefore, there should arise a difference between the dependence of standard deviation of the chromatographic peak on the type of molecule calculated from the pair of eqs(6.8') and (6.9') and that calculated from eq(6.40). It can be shown, however, that the dependence of standard deviation of the chromatographic peak on the type of molecule, in general, takes place only slightly (except under extreme experimental conditions), and that only a slight difference arises between the results of the calculation obtained from the two methods.

In order to evaluate the parameter x' involved in both eqs(6.35') and (6.40), the experimental ln $s_{app(P)}$ versus $m_{elu(P)}$ ($\equiv \mu$) plots [corresponding to those presented in Fig 8.3 (b) for lysozyme] were performed for the maximum height of the total collagen chromatogram[Fig 8.20; reproduced from ref(7.2) Appendix II]. Assuming that $\varphi = 6.7\ M^{-1}$ [see the subsection entitled "Adsorption Energy of Phosphate Group on A C Site" in Section(E)], it can be estimated from Fig 8.20 that $x' = 40$ and that ln $q = 14.95$ [see the legend for Fig 8.20; cf. ref(7.2) Appendix II]. It should be noted that the parameter x' is common to all the molecular species of collagen and that the parameter q estimated above is only for the species contained in the maximum height of the total chromatogram. The parameter q for an arbitrary molecular species is related to the parameter ε through both eqs (8.49) and (8.53) with interventions of both eqs(8.58) and (8.59). Therefore, for the calculation of the theoretical chromatograms, it also is necessary that the value of the parameter β [involved in eq(8.49)] be given. With reference to the analysis of the poly-L-lysine chromatogram performed in the subsection entitled "Adsorption Energy of ε-amino group on A P Site" in Section(E), it was assumed that $\beta = 2 \times 10^{-3}$. It can be confirmed, however, that the theoretical chromatogram hardly depends on the exact value of β.

Fig 8.21 [reproduced from ref(8.25)] illustrates best theoretical chromatograms (corresponding the the experimental chromatograms presented in Fig 8.14) obtained assuming: $\nu\,(=1/\phi) = 18$, $\varepsilon = 2.9$ kJ/mol ($e^{\varepsilon/kT} = 3.6$) and $\pi = 0.8$ with good fits with the experiment; these values of ν, ε and π are consistent with the ln q value of 14.95 estimated for the molecular species contained in the maximum height of the total collagen chromatogram. It should be emphasized that the optimum ε value of 2.9 kJ/mol estimated from the degree of accumulation of some components near the left border of distribution $D(\phi)$ [Fig 8.18; cf. Fig 8.19(c)] automatically brings about good fits of the intervals of succes-

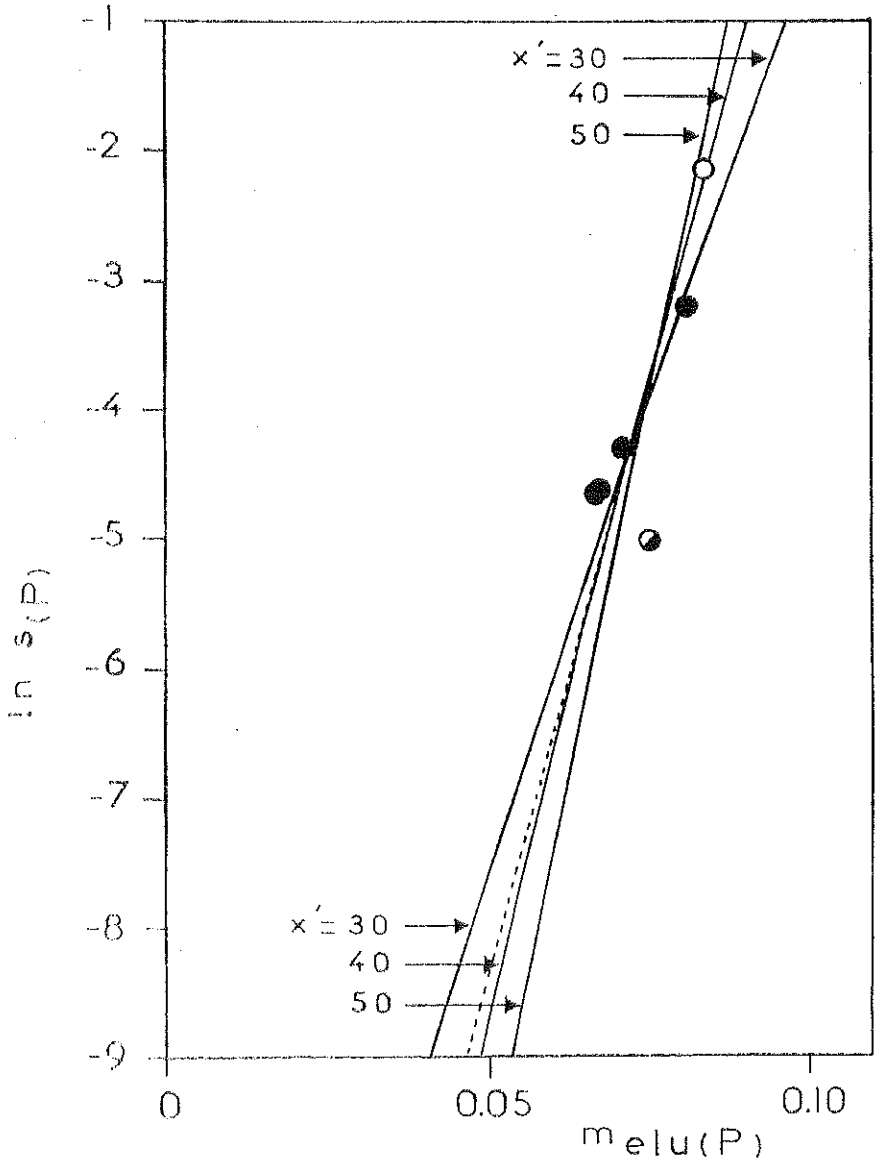


Fig 8.20. The points are experimental plots of ln $s_{app(P)}$ (written as ln $s_{(P)}$) versus elution phosphate molarity $m_{elu(P)}$ at the maximum height of the collagen chromatogram; these were obtained for the case of small enough sample loads when the effect of mutual interaction between collagen molecules is almost compleltely negligible. The dotted straight line is the regression line of $m_{elu(P)}$ on ln $s_{app(P)}$ for these experimental points. The three solid curves (being almost straight lines) are theoretical, calculated for three x' values by using eq(6.35') in which $\mu = m_{elu(P)}$ and $m_{in(P)} = 1$ mM, respectively; it is assumed that $\varphi = 6.7$ M^{-1}. For each x' value, the ln q value was chosen in order for the theoretical curve to coincide best with the regression line. It can be seen that a best fit between the theoretical curve and the regression line is obtained when x'=40 and ln q=14.95. [Reproduced from ref(7.2) Appendix II Fig A3, or ref(6.4) Fig 5(c).]

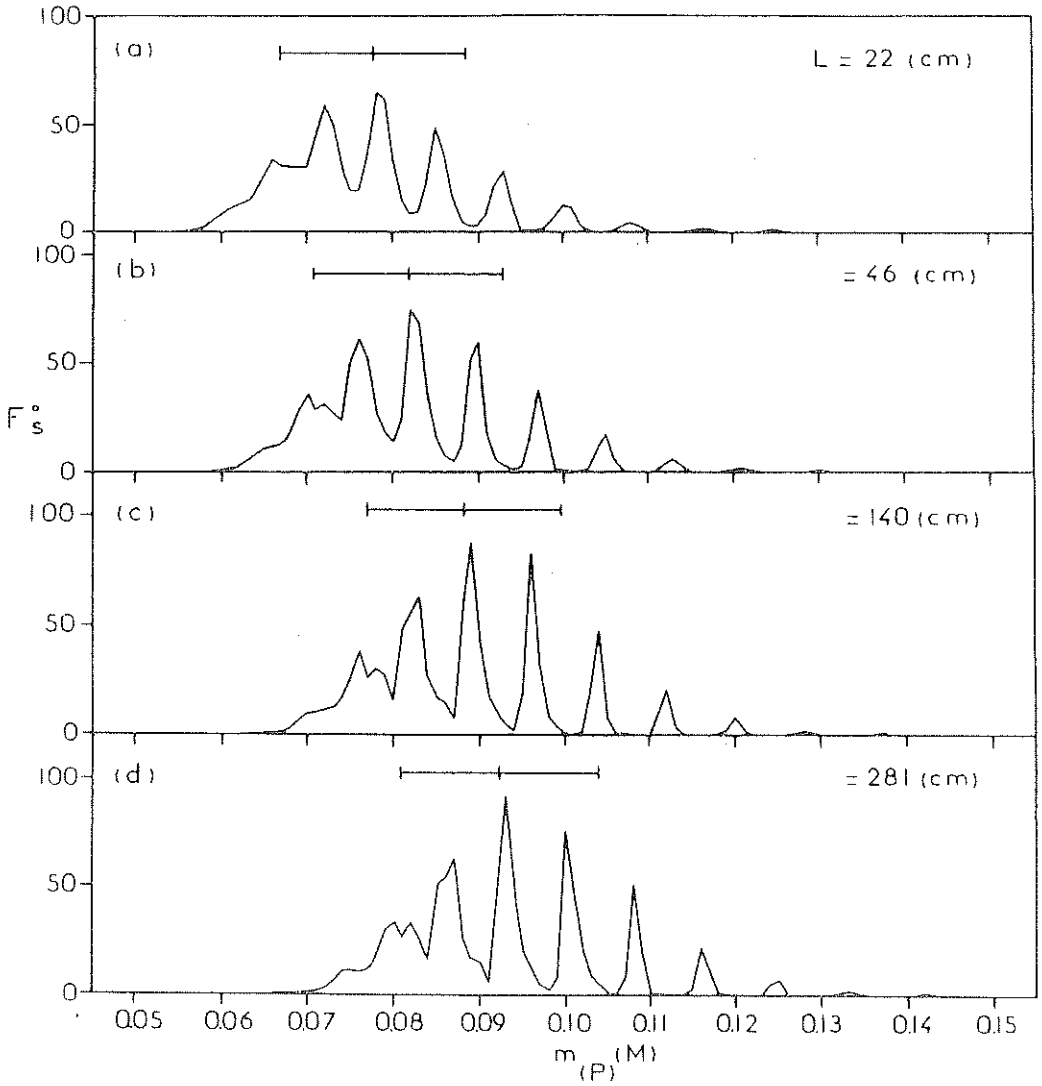


Fig 8.21. Theoretical collagen chromatograms in the absence of mutual molecular interactions, calculated by using eq(6.38) combineed with both eqs(6.35') and (6.40). Molecular density C is written as F_s°, and both the center of gravity and twice the standard deviation are shown for each chromatogram. The microheterogeneous model with $\varepsilon = 0.7$ kcal/mol (=2.9kJ/mol) and $\pi = 0.8$ (kT=2.30 kJ/mol at 4℃) was used, and the experimental conditions in (a)-(d) are the same as those for the experimental chromatograms drawn in Figs 8.14(a)-(d), respectively. For the calculation, the diffusion parameter Θ^* [eq(6.40)] is assumed to be $\Theta^* = \gamma\,\theta^*$ in which $\theta^* = 0.3$ cm and $\gamma = 0.8 \times 3.14 \times \varnothing^2/4 = 0.8 \times 3.14 \times 0.5^2/4 = 0.157$ cm^2; 0.8 represents the ratio of the void volume to the total packed volume of the HA crystals in the column estimated in ref(8.4) [cf. Chapter Ⅶ(D)]; the conversion of $g'_{\infty}(\varnothing = 1$ cm) to g' [cf. eqs(6.2), (6.35') and (6.40)] was done by using this γ value. [Reproduced from ref(8.25) Fig 5.]

sive peaks between theoretical(Fig 8.21) and experimental(Fig 8.14) chromatograms. Arguing in the other direction, the optimum ε value obtained with an effort to obtain best fits of the intervals of successive peaks between theoretical and experimental chromatograms automatically brings about the best degree of accumulation of some components near the left border of distribution $D(\phi)$ or the theoretical chromatogram.

When ε is given, there are two ways of reguration of the total number of peaks in the theoreical chromatogram; the peaks mean those with finite heights in practice. In the first way, the total number of peaks can be decreased by increasing ν while keeping π constant. This procedure, however, brings about a concomitant decrease of the ϕ or $m_{(P)}$ values over which the peaks appear, and the distribution of pealks shifts to low ϕ or $m_{(P)}$ values at a rate higher than the rate of decrease in the total number of peaks [cf. ref (8.43) Fig 1]. In the second way, the total number of peaks can be decreased by increasing π while keeping ν constant. This procedure does not bring about a shift of the ϕ or $m_{(P)}$ values over which the peaks appear (see Fig 8.19). These considerations lead to the conclusion that the balance between the ϕ or $m_{(P)}$ values over which the peaks appear (i.e., the position of the total chromatogram) and the total number of peaks (i.e., the width of the total chromatogram) depends on the combinations of the values of the two parameters ν and π, and the optimum combination of $\nu=18$ and $\pi=0.8$ was attained finally. It can be considered that the value, 0.8, of π is high enough for the "determination" of the primary structures of the α peptides to be feasible [see Appendix Ⅷ(A)].

Microheterogeneous collagen model now is highly relaiable from three criteria. (a) The same value, 2.9 kJ/mol, of the parameter ε can be obtained from both the degree of accumulation of some components near the left border of the chromatogram and the intervals of successive peaks in the chromatogram. (b) The value, 18, of the parameter ν leads to the value, 0.26 nm, of the parameter h_1 by using the second equality in eq (8.63) in which $\ell=4.71$ nm. As will be mentioned later, it is reasonable to consider that it is the second equality rather than the first equality that is preferred in eq(8.63), and that collagen is adsorbed on effectively only one array of C sites with its main axis parallel to the array. In this instance, h_1 represents the diameter itself of the distance where a carboxyl group can move freely (around its mean position on the molecular surface), measured circumferentially around the main axis of the molecule. As carboxyl group is attached to the end of the flexible side-chain of either aspartic or glutamic acid residue, the value of 0.26 nm assigned to the parameter h_1 is very reasonable. And (c) the optimum value, 2.9 kJ/mol, of the parameter ε assigned to carboxyl group is of the same order of magnitude as the value, 3.8-4.2 kJ/mol, deduced for univalent phospate group and the value, 8.4-9.2 kJ/mol, deduced for ε-anino group [see Section(E)]. [*Note.* I have experiences that a single peak in the multi-peak chromatogram of calf-skin type I collagen splitted into several sub-peaks when chromatography of the type presented in Fig 8.15 was carried out by using a linear NaP gradient with a slope $g'_{(P)}(\varnothing=1$ cm) several times as shallow as that applied in Fig 8.15. In view of this experiment, it is probable that some notches

or sub-structures appearing in some peaks in the chromatograms presented in Fig 8.14 [as well as those appearing in the chromatograms presented in ref(8.26) Figs 7 and 8] are not artifacts but are real sub-peaks at least partially. It can be assumed that these sub-peaks (belonging in a peak) represent molecular species with almost constant values of x but with different values of $(kT/\varepsilon)\ln\tau$ [see eq(8.58)], and that the sub-peaks correspond to the sub-structures appearing in the distribution curve $D(\phi)$ when elements smaller than 0.2 in size are used for the calculation (see the legend for Fig 8.19). In ref(8.23), the argument related to this problem is performed for the multi-peak chromatogram of poly-L-lysine(Fig 8.9).]

Until now all the arguments were performed assuming that the mutual interaction taking place between collagen molecules is negligible. It can be deduced(8.25), however, that the apparently repulsive energetical interaction interferes between collagen molecules adsorbed on the HA surface along with the geometrical interaction. Fig 8.22 [reproduced from ref(8.25)] illustrates a series of theoretrical collagen chromatograms (corresponding to the experimental chromatograms in Fig 8.14) calculated taking into account these interactions. For the calculation, it was assumed that the apparently repulsive interaction energy for one collagen molecule with another is 3 kcal/mol (13 kJ/mol) when these make maximum contact in parallel with one another on the HA surface. The overload theory of chromatography(7.1, 8.15-8.17, 8.45-8.51), however, is at the stage of development much behind that of the present theory which is valid only in the absence of the molecular interaction, and it is out of the scope of this monograph. It can be expected that much better theoretical chromatograms will be calculable by improving the overload theory.

It can be considered that the x' value of 40 that has been estimated from Fig 8.20 is apparently much smaller than the true x' value. For the purpose of estimating the true x' value, let us consider the ideal monocrystal HA with a large enough size and let us examine two hypothetical cases when collagen is adsorbed with its main axis parallel to the **b** (or **a**) direction on the (100) [or (010)] surface(Case 1) and when it is adsorbed with its main axis parallel to the **c** direction on the same surface(Case 2). In Case 1, the interdistance, d, between C sites along the main axis of the adsorbed collagen molecule is equal to $|\mathbf{b}|$ $(=|\mathbf{a}|)$ or 0.942 nm, and the interdistance between arrays of C sites parallel to the main axis of the molecule is equal to $|\mathbf{c}|/2$ or 0.344 nm [see Section(A)]. It can be estimated that the number of arrays of C sites on which the adsorption of phosphate ions from the buffer (with a diameter of about 0.5 nm) is impossible due to the presence of the adsorbed collagen molecule (with a diameter of 1.5 nm) is 2 to 4, from which it follows that x' is of the order of magnitude of $(300/0.942)\times 2$ to $(300/0.942)\times 4$, or 640 to 1270. In Case 2, d is equal to $|\mathbf{c}|/2$ or 0.344 nm, and the interdistance between arrays of C sites parallel to the main axis of the adsorbed collagen molecule is $|\mathbf{b}|$ $(=|\mathbf{a}|)$ or 0.942 nm [see Section(A)]. It now is reasonable to consider that only one array of C sites is covered by the molecule and that x' is of the order of magnitude of 300/0.344 or 870. All these x' values are much larger than 40.

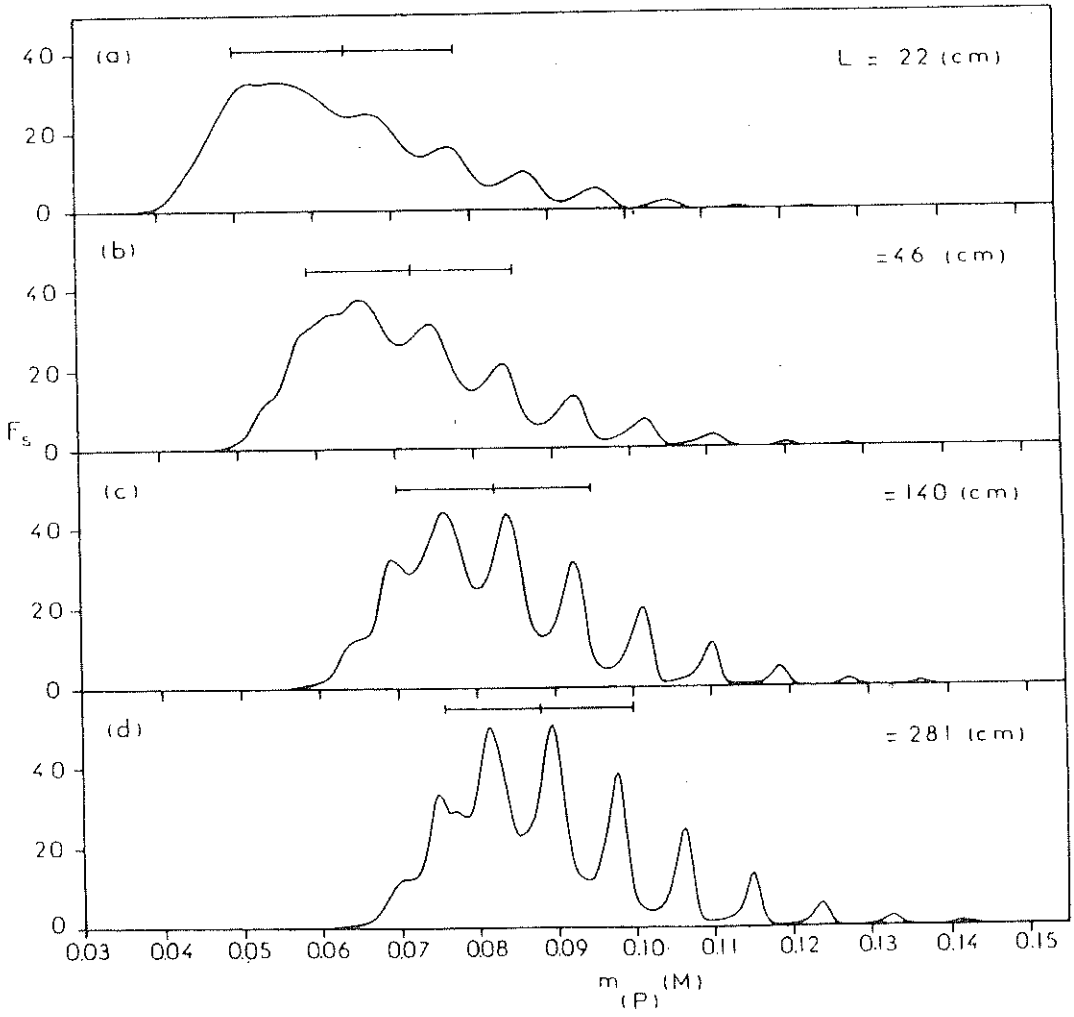


Fig 8.22. Theoretical collagen chromatograms, calculated by taking into account the mutual molecular interaction. Molecular density C is written as F_s, and both the center of gravity and twice the standard deviation are shown for each chromatogram. The same microheterogeneous model as that used in Fig 8.21 was applied with the additional assumption that the apparently repulsive energetical interaction takes place between collagen molecules adsorbed in parallel with one another on the HA surface and that the absolute value of the interaction energy is 3 kcal/mol (13 kJ/mol) when the molecules make maximum contact [for detail, see ref(8.25)]. The experimental conditions in (a)-(d) are the same as those applied in part (a)-(d) of both Figs 8.14 and 8.21, respectively. [Reproduced from ref(8.25) Fig 8.]

In parallel with the suggestion obtained for reversed-phase chromatography(8.52) that phosphate ions may form ion pairs with cation groups on peptides, it is highly probable that the drastically small x' value (estimated from Fig 8.20) arises as a result of strong attractive interactions taking place between collagen molecule and competing phosphate ions from the NaP buffer. In this instance, it can be considered that it is the value of $x'-x''$ rather than the value of x' that has been estimated from Fig 8.12. Still all the arguments with respect to microheterogeneous collagen model is valid since the arguments hold only by replacing x' by $x'-x''$ [see Section(B)]. 〖*Note 1.* The fact (see above) that the ν, ε and π values estimated for the calculation of Fig 8.21 are consistent with the ln q value estimated for the molecular species contained in the maximum height of the total chromatogram (see Fig 8.20) is compatible with the situation where the energy of association of the complex of collagen molecule and competing phosphate ions is much lower than the enerrgy of adsorption of collagen molecule on the adsorbent surface [see Section(B)]. *Note 2.* It might be possible that associations of phospate and calcium ions [$Ca_9(PO_4)_6$; called Posner's clusters] be produced in the vicinity of the **a** (or **b**) surface of HA, which may participate in the crystal growth mechanism of HA (8.53, 8.54). Provided that Posner's clusters are stable enough for them to be regarded as competing ions, it might be possible that an apparently small x' value be obtained since the number of clusters the adsorption of which on the HA surface is impossible due to the presence of the adsorbed collagen molecule is smaller than the corresponding number for individual phosphate ions. Quantitatively, however, the cluster hypothesis is insufficient to explain the drastical decrease of the x' value (such as estimated above). More fundamentally, the idea itself of regarding Posner's clusters as competing ions is questionable. In the present theory, the effect of the mutual energetical interactions among competing phosphate ions, if it is important, is incorpolated in the parameter φ [see eq(8.45)].〗

It is unlikely that collagen be adsorbed on the HA surface by utilizing only a part of the rod, thus reducing the x' value drastically. In fact, from the value, 14.95, of ln q estimated for the molecular species contained in the maximum height of the total collagen chromatogram (see Fig 8.20), it can be calculated by using eq(8.49) that $E+kT\ln\tau=49$ kJ/mol (where it has been assumed that $kT=2.30$ kJ/mol and that $\beta=2\times10^{-3}$; see above). This means that, if only half the total length of the rod is utilized for the adsorption, the energy of about 25 kJ/mol is lost compared to the case when the total length is utilized. As this is a large loss, it is difficult to consider that the loss of energy can be compensated by the gain of entropy if this latter can be generated only when collagen is adsorbed by utilizing a part of the rod (through a certain mechanism).

The HA particles used for chromatographies presented in Figs 8.14-8.17 and 8.20 are polycrystals with a plate-like total shape with a thickness of the order of 1 μm and a diameter of the flat surface of the order of several times 10 μm (the same type of particle as that used in the experiments presented in Appendix VI). The scanning electron micrograph of the surface structure of this type of particle is published in ref(7.1) Fig 9(c)

where it can be seen that the surface is irregular and rugged. From ref(7.1) Fig 9(c), it is likely that the size of the crystallites is much smaller than the total length, 300 nm, of the collagen rod (perhaps being of the order of magnitude of 10 nm as deduced from the general habit of the HA polycrystal), and it can be suggested that the adsorbed collagen rod should be bending to some extent in order for almost all the length of the rod to be utilized for the contact with the HA surface. Multi-peak chromatograms quite similar to those presented in Figs 8.14 and 8.15 can be obtained by using another type of HA particle with a spherical total shape with a diameter of about 5 μm (the same type as that used in the experiments presented in Chapter Ⅶ); these particles were prepared by aggregating smaller polycrystal particles, respectively. The scanning electron micrograph of the surface structure of the spherical HA particle is published in ref(7.1) Fig 9(b) where it can be seen that the surface is irregular again but that the irregularity is quite different in aspect from that taking place on the surface of the plate-like particle. The fact that the chromatograms quite similar to one another are obtained by using HA particles with different surface irregularities strongly suggests that almost all the length of the rod is utilized for the adsorption. In fact, if only a minor part of the rod were utilized, it would be owing to the irregularity itself of the crystal surface structure, and a drastical difference can be anticipated to arise in shapes of the chromatograms between HA particles with different surface irregularities. The suggestion obtained above that almost all the length of the rod should be utilized for the adsorption is consistent with the thermodynamic consideration done in the preceding paragraph.

It can now be visualized that collagen is adsorbed by using almost all the length of the rod over a considerable number of crystallites or monocrystalline domains taking place on the polycrystal surface of HA. From the fact that the collagen chromatograms quite similar to one another are obtained by using HA particles with different surface irregularities (which imply different modes of existence of crystallites), it is highly probable that the exact arrangement of C sites on the HA surface is not important for the adsorption mechanism of the collagen molecule. In other words, it is highly probable that almost all the carboxyl groups that are present within the width h_1 of the molecular surface facing the HA surface can bond with C sites or that the second equality in eq(8.62) or (8.63) holds practically with $h_2 \gtrsim d$. By using the second equalty in eq(8.63), it can be estimated that $h_1 = 0.26$ nm (see above). From the fact that the carboxyl group is attached to the end of the flexible side chain of either glutamic or aspartic acid residue, it would be reasonable to consider that this value of h_1 is close to the lower limit rather than the upper limit of the possible distance over which the carboxyl group can move freely around its mean position. This strongly suggests that the collagen rod is adsorbed on effectively only one array of C sites with its main axis parallel to the array. This is because, if the molecule were adsorbed over plural arrays of C sites, h_1 would represent by its definition [cf. eq(8.61)] a quantity larger than the distance over which the carboxyl group can move freely around its mean position. This would mean that the distance over which the car-

boxyl group can move freely around its mean position should still be smaller than the lower limit close to 0.26 nm. When recalling the hypothesis performed above for the ideal monocrystal HA, the consideration that the collagen rod is adsorbed on effectively only one array of C sites with its main axis parallel to the array implies that the crystallites are orienting around a single direction in the polycrystal with a fluctuation (consistently with the general habit of the HA crystal) and that the collagen rod is adsorbed with its main axis quasi-parallel to the **c** axes of the respective crystallites. Thus, the situation similar to Case 2 with the ideal monocrystal HA would takes place; in this ideal case, the inter-site distance of C sites along the main axis of the adsorbed rod is the smallest possible of 0.344 nm [which would make it be possible for the second equality in eq(8.62) or (8.63) to hold] and the interdistance between arrays of C sites parallel to the main axis of the adsorbed collagen molecule is the largest possible of 0.942 nm (which would make it be possible for the collagen rod to be adsorbed on only one array of C sites). It can therefore be suggested that the effective inter-site distance of C sites along the main axis of the adsorbed rod actually is close to 0.344 nm and that the the interdistance between effective arrays of C sites parallel to the main axis of the adsorbed collagen molecule is close to 0.942 nm. It can also be suggested that the value of the parameter h_2 is also close to 0.344 nm (not being much larger than 0.344 nm); this is because it can be assumed that the carboxyl graup can move almost isotropically around its mean position on the collagen surface. Finally, it can be assumed that the **c** surface hardly appears on the crystallite surface over which the collagen rod is adsorbed since the elution of collagen from the HA column is achieved almost independently of the molarity of KCl or NaCl co-existing in KP or NaP buffer (see above). This is consistent with the situation where the crystallites are orienting around a single direction in the polycrystal with a fluctuation.

Rechromatography of a single peak in the multi-peak collagen chromatogram does not give a chromatogram consisting of only one peak. Instead, a chromatogram with a small total width consisting of some peaks arises around the position of the fraction in the first chromatogram (see above). It is probable that the presence of some peaks in the second chromatogram is brought about, affected by a slight fluctuation of the ϕ [eq(8.58)] value with respect to any given molecule taking place from position to position on the column because of the illegurarity of the mode of presence of crystallites on the polycrystal HA surface. Thus, if $h_2 \gg d$ (where d now represents the effective inter-site distance of C sites along the main axis of the adsorbed collagen rod), then the second equality in eq (8.62) or (8.63) would hold very precisely, and the first equality would not be realized at all. In this instance, the fluctuation of the ϕ value would not take place at all. It can be deduced, however, that the relationship, $h_2 \approx d$, holds actually (see above). This would mean that, although it is the second equality that is dominant in eq(8.62) or (8.63), the first equality also contributes to bringing about a slight fluctuation of the ϕ value. The fluctuation of ϕ would bring about a shallowing of the split between neighboring peaks in the multi-peak chromatogram. At the same time, some components which should belong in

a peak under consideration in the total chromatogram in the absence of the fluctuation of ϕ would invade neighboring peaks and vice versa in the presence of the fluctuation. Re-chromatography of a single peak in the total chromatogram contaminated by components of invasion would give a chromatogram consisting of some peaks instead of a single peak. The fluctuation of ϕ might also be induced if a lag of time arises between occurrences of different adsorption configurations of a molecule due to the presence of RMT [of which account is not taken in the present theory; cf. Chapter I (A)].

Figs 8.15(d)-(g) [reproduced from ref(8.42)] illustrate chromatograms obtained on an HA column system by using a linear concentration gradient of NaP buffer for other types of collagen [type II collagen from bovine articular cartilage(d), type III collagen from human placenta(e), type IV collagen from human placenta(f), and type V collagen from human placenta(g)] giving multi-peak chromatograms similar to those obtained for type I collagen from calf-skin [Figs 8.15(a)-(c)], respectively.

Figs 8.23(a) and (b) [reproduced from ref(8.42)] illustrate chromatograms for myosin ($M_w \approx 4.8 \times 10^5$ Da) from chicken pectoral muscle, obtained on an HA column system by using linear concentration gradients of KP buffer with relatively steep and shallow slopes, respectively. It can be assumed that myosin is adsorbed on C sites since the elution of myosin from the HA column is achieved almost independently of the molarity of KCl co-existing in KP buffer. It can be seen in Fig 8.23(b) that a multi-peak chromatogram is obtained under high-resolution condition of shallow concentration gradient in parallel with the case of collagen [cf. Figs 8.23(a) and (b) with Figs 8.16 and 8.14, respectively]. Myosin resembles collagen in that its molecular conformation is relatively simple in part and that it is biosynthesized in an overwhelmingly large amount in comparison with globular proteins. It is highly probable that myosin is microheterogeneous like collagen.

(G) Some Considerations on the Adsorption of Globular Proteins on the Hydroxyapatite Surface

Earlier(7.1), the resemblance of HA chromatography to affinity chromatography was emphasized by considering that the geometrical arrangement of atoms on the local surface of sample molecule can be discriminated by the regular stereochemical structure of the crystal surface of HA. In fact, the concept would apply to the case of nucleoside polyphosphates(Fig 8.8) as well as the case of poly-L-lysine with highly-stretched conformation. (Strong repulsive electrostatic interactions can be anticipated to take place between functional ε-amino groups arranged on the poly-L-lysine polypeptide chain while restricting to a large extent the positions of these groups relative to one another; Fig 8.9). With regard to collagen, however, it can be considered that the exact arrangement of C sites on the adsorbent surface is not important for the adsorption mechanism; this is due to the fact that the diameter of the distance where a functional carboxyl group can move freely around its mean position on the molecular surface is large enough [see Section(F)].

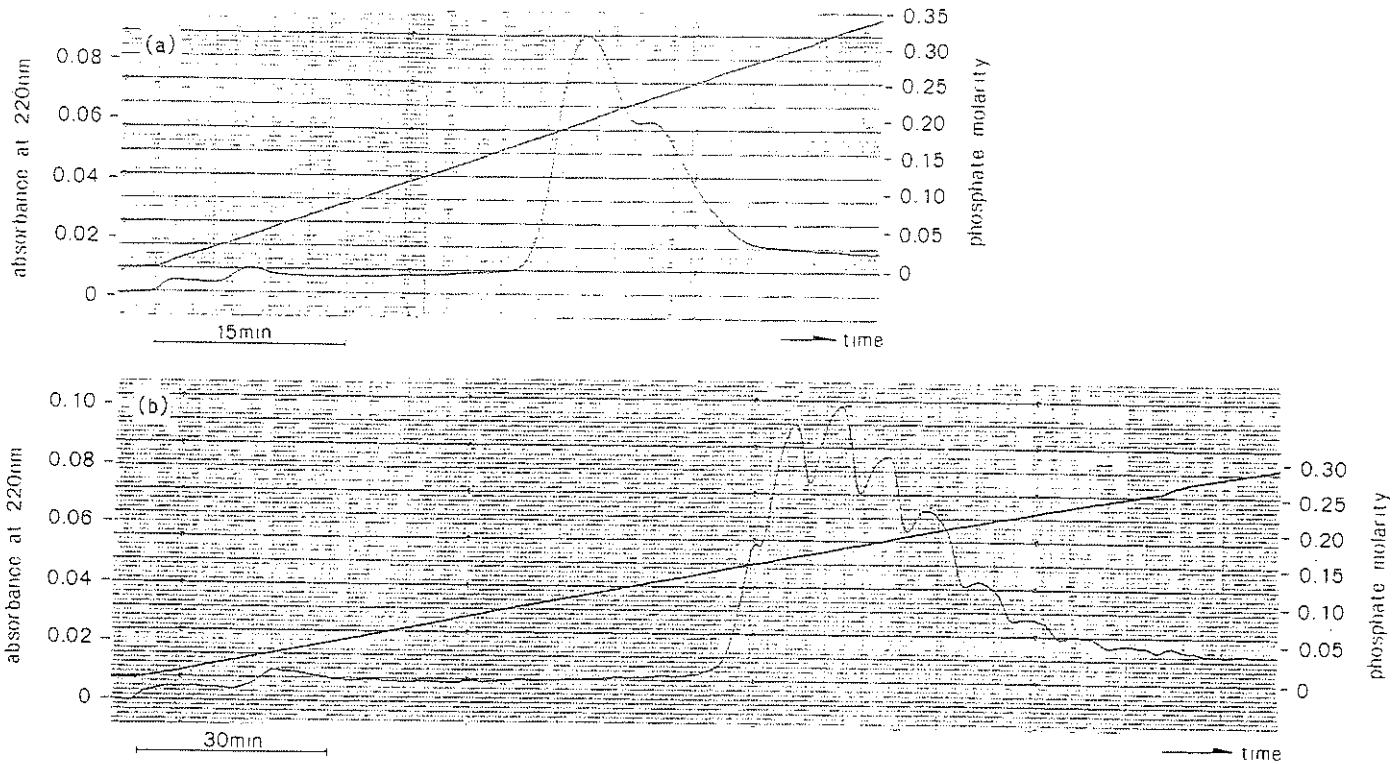


Fig 8.23. Experimental chromatograms at 4℃ of myosin from chicken pectoral muscle, obtained by using the HPLC column system packed with HA particles identical with those used in the experiments in Fig 8.15. The column system (σ=0.6 cm) with total length L=13 cm was used, and in (a) and (b), linear concentration gradients of KP buffer with slopes $g'_{(P)}(\sigma=1\text{ cm})=1.25$ mM/ml and 0.225 mM/ml [cf. Note in Table 7.1] were applied, respectively; 0.5 M KCl is present in the KP buffer always. [Reproduced from ref (8.42) Fig 12.]

By analogy, it can be suggested that the diameter of the distance where a functional adsorption group can move freely around its mean position on the molecular surface is large enough with native globular proteins also. The weak correlation between pI and $m_{elu(P)}$ taking place respectively among the acidic and the basic globular proteins(Fig 8.10) therefore may be a reflection of the weak correlation taking place between pI and the total number of adsorption groups that are present within the local molecular surface facing the HA surface. It can be seen in ref(7.1) Fig 12 that the constellations in the $m_{elu(P)}$ versus pI plots for globular proteins for six types of HA particle with different surface irregularities are almost identical with one another. This may support the suggestion that the exact arrangement of adsorbing sites is not important for the adsorption mechanism of globular proteins either.

It should be noted, however, that the size of globular proteins (with M_n of the order of 10^4 to 10^5 Da) usually is in the range of 3 to 10 nm being much smaller than the length of collagen rod (300 nm). It would therefore be possible that globular proteins are adsorbed on a crystallite or monocryslalline domain (perhaps of the order of magnitude of 10 nm) on the polycrystal HA surface where a regular arrangement of adsorbing sites can be anticipated [as assumed in the analyses of both nucleoside polyphosphates and poly-L-Lysine; see Section(E)]. Moreover, as far as the adsorption of basic proteins on the **c** crystal surface is concerned, the minimum possible inter-site distance of 0.942 nm on the adsorbent surface can be assumed to be much larger than the diameter of the distance where a functional adsorption group can move freely around its mean position on the molecular surface [the order of 0.26 to 0.344 nm by analogy with the analysis of the collagen data; Section(F)]. In conclusion, it would be reasonable to assume that the weak correlation between pI and $m_{elu(P)}$ taking place with native globular proteins(Fig 8.10), in general, arises from the amalgam of two mechanisms: (a) the weak correlation between pI and the total number of adsorption groups that are present within the local moleculr surface facing the HA surface, and (b) the fit between the geometrical arrangement of atoms on the local moleculr surface facing the HA surface and the regular stereochemical structure of the crystal surface of HA, which occurs independently of the pI value. [In connection, the fit between the geometrical arrangement of charged groups on the local molecular surface and that of ion-exhangers on the adsorbent surface is suggested to take place instantaneously (but differently from an instant to another) with ion-exchange chromatography, thus giving rise to a strong correlation between pI and retention time. The similar mechanism might occur partially with reversed-phase chromatography also, where both charged groups on the molecular surface and ion-exchangers on the adsorbent surface are replaced by hydrophobic structures. See the subsection entitled "Ion-Exchange and Reversed-Phase Chromatographies in Contrast to HA Chromatography" in Section(E).]

Recently, chromatographies of twenty native globular proteins with pI ranging between 1 and 11 were carried out by using a linear concentration gradient of KP buffer on columns packed with four types of calcium phosphate, respectively(8.55). These are HA

[$Ca_{10}(PO_4)_6(OH)_2$], dicalcium phosphate dihydrate or brushite ($CaHPO_4 \cdot 2H_2O$), octacalcium phosphate [$Ca_8H_2(PO_4)_6 \cdot 5H_2O$], and β-tricalcium phosphate [$Ca_3(PO_4)_2$]. The $m_{elu(P)}$ versus pI plots were compared among them, and it was found out that the constellations of the plots were almost identical with one another with respect to either acidic or basic proteins except for slight differences [see Fig 8.24; reproduced with slight modifications from ref (8.55)]. As it can be anticipated that the arrangement of adsorbing sites on the crystal surface is different among different types of calcium phosphate, it can be suggested from these experiments that the exact arrangement of adsorbing sites is not important for the adsorption mechanism of globular proteins. At pH≈6.8 where all the experiments were carried out, however, HA is the most stable thermodynamically. Therefore, a possibility cannot be excluded that the surfaces of calcium phosphates other than HA are submitted to phase transition toward the HA structure at pH≈6.8. If this is true, then, whatever type of calcium phosphate may be used for the experiment, the adsorption of globular proteins would take place on the crystal surface with a HA structure, thus giving rise to constellations of the $m_{elu(P)}$ versus pI plots that are almost identical with that taking place with HA. [For further investigations on relevant problems, see ref(8.56).]

(H) Relationships with Reversed-Phase and Ion-Exchange Chromatogarphies

With many reversed-phase chromatographies, the log $\dot{k}$ versus m plots give a straight regression line with a negative slope (see the subsequent Chapter IX), whereas a straight regression line with a negative slope is obtained in the log $\dot{k}$ versus log m plots with many ion-exchange chromatographies (see the subsequent Chapter X). We show below that both plots can be explained by using competition model in a united manner.

Thus, the strength of adsorption of competing substance on the adsorbent surface [representing the inherent "force" of competing substance to drive sample molecule out of the adsorbent surface; see Section(B)] can be measured by the parameter φ [eq(8.45)]. Let us first consider the case when competing substance is adsorbed weakly on the adsorbent surface with a small value of φ while fulfilling the relationship $\varphi m \ll 1$ in the range of m values where chromatography is feasible in practice. In this instance, the relationship:

$$\varphi m + 1 \approx e^{\varphi m} \tag{8.64}$$

holds, and eq(8.52) can be rewritten as

$$\ln \dot{k}(m) \approx -x'\varphi m + \ln q \tag{8.65}$$

indicating that $\ln \dot{k}$ decreases linearly with increase in m. In order for sample molecule to be eluted from the column within the range of m values under consideration, it, in general, is necessary that $(E+kT\ln\tau)/x'$ [$\approx(x/x')\varepsilon$] [see eq(8.53)] be small since φ (for the physical meaning of which see above) is small. The small value of $(E+kT\ln\tau)/x'$ [$\approx(x/x')\varepsilon$] occurs either when $E+kT\ln\tau$ ($\approx x\varepsilon$) is small or when x' is large. E+

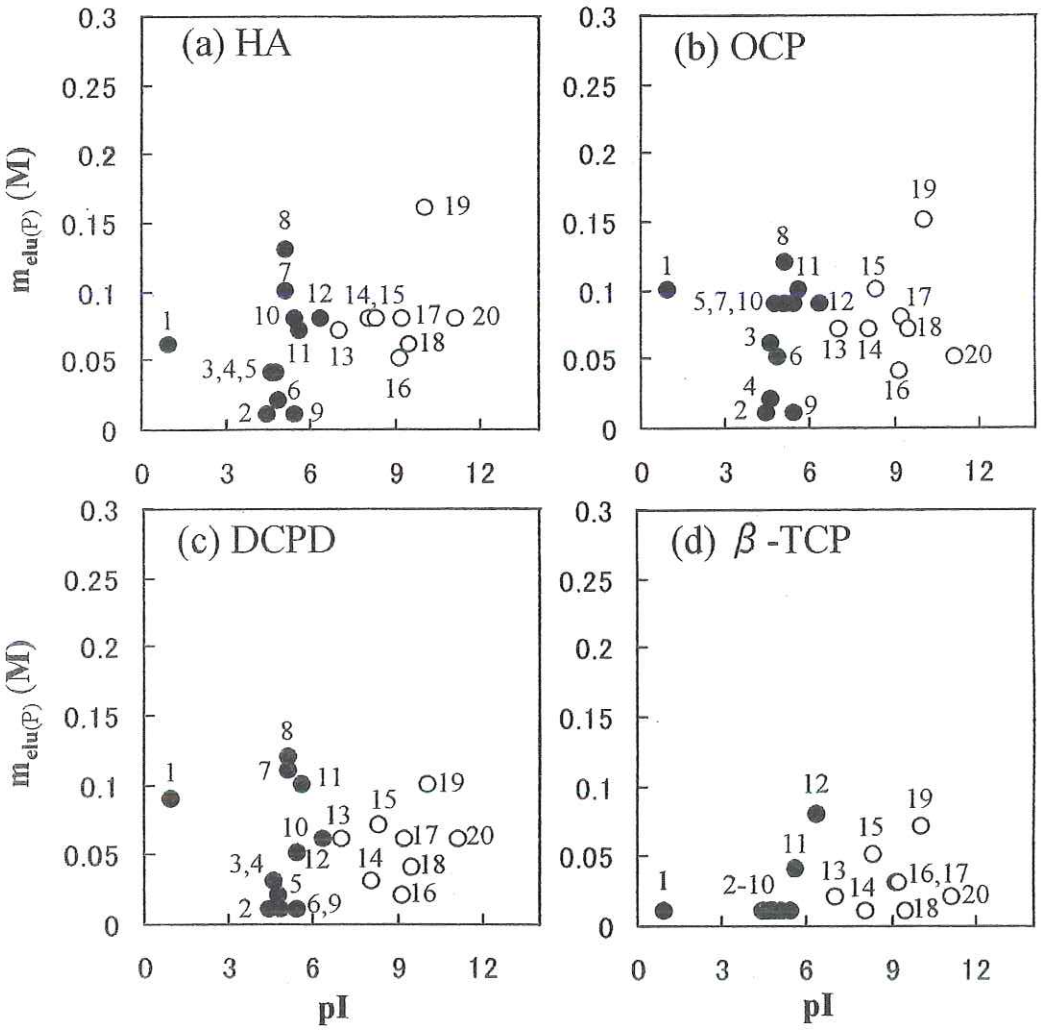


Fig 8.24. Plots of $m_{elu(P)}$ versus pI for (a) HA (synthesized by hydrolysis of α-tricalcium phosphate), (b) octacalcium phosphate (OCP), (c) dicalcium phosphate dihydrate or brushite (DCPD), and (d) β-tricalcium phosphate (β-TCP) for 20 proteins [1, pepsin (porcine stomach mucosa); 2, lactalbumin (bovine milk); 3, trypsin inhibitor (soybean); 4, ovalbumin (chicken egg serum); 5, albumin (bovine serum); 6, α-amylase (porcine); 7, β-lactoglobulin A (bovine milk); 8, β-lactoglobulin B (bovine milk); 9, insulin (bovine pancreas); 10, holo-transferrin (bovine); 11, catalase (bovine liver); 12, conalbumin (chicken egg white); 13, hemoglobin (bovine); 14, myoglobin (horse skeltal muscle); 15, γ-chymotrypsin (bovine pancreas); 16, papain (papaya latex); 17, trypsinogen (bovine pancreas); 18, ribonuclease A (bovine pancreas); 19, cytochrome c (horse heart); 20, lysozyme (chicken egg white)]. These were obtained at room temperature on 25×0.4 cm columns by using a linear concentration gradient of KP buffer with slope $g'_{(P)}(\phi=1\ cm)=0.784$ mM/ml; $m_{ia(P)}=$ 10 mM. ● indicates acidic proteins, and ○ indicates neutral or basic proteins. [Reproduced with slight modifications from ref(8.55) Fig 1.]

$kT\ln\tau$ or q [eq(8.49)] measures the strength of adsorption of sample molecule on the adsorbent surface, and it is only apparent that the strength of adsorption also depends on x', inversely proportional to x' [cf. Section(A)]. Therefore, when eq(8.64) or (8.65) holds, let us say that both sample molecule and competing substance are adsorbed "weakly" on the adsorbent surface while performing the competition. Only for the sake of simplicity, we hereafter use this expression even when the elution of molecules from the column takes place at considerable high values, m_{elu} or μ, of m.

Let us consider the other extreme case when competing substance is adsorbed strongly on the adsorbent surface with a large value of φ while fulfilling the relationship $\varphi m \gg 1$ in the range of m values where chromatography is feasible in practice (except the m value close to zero). In this instance, the relationship:

$$\varphi m + 1 \approx \varphi m \tag{8.66}$$

holds, and eq(8.52) can be rewritten as

$$\ln \dot{k}(m) \approx -x'\ln m + \ln q - x'\ln\varphi \tag{8.67}$$

indicating that $\ln \dot{k}$ decreases linearly with increase in $\ln m$. In order for sample molecule to be eluted from the column within the range of m values under consideration (not close to zero), it is necessary that $(E+kT\ln\tau)/x'$ [$\approx(x/x')\varepsilon$] be large since φ is large. When eq(8.66) or (8.67) holds, let us say that both sample molecule and competing substance are adsorbed "strongly" on the adsorbent surface while performing the competition.

It is possible to explain the adsorption and desorption mechanisms of both reversed-phase and ion-exchange chromatographies by using competition model. Thus, with reversed-phase chromatography, it can be assumed that competing substance corresponds to the less polar component in the binary carrier liquid system (like acetonitrile in the acetonitrile/H_2O system) and that both sample molecule and the less polar component from the carrier liquid are adsorbed "weakly" on sites [like octadecyl(C_{18}) groups] arranged on the adsorbent surface while performing the competition (for detail, see Chapter IX). With ion-exchange chromatography, it can be assumed that competing substance corresponds to either cation or anion from the buffer or the carrier liquid, and that both sample molecule and ion (cation or anion) are adsorbed "strongly" on sites (called cation- or anion-exchangers) arranged on the adsorbent surface while performing the competition (for detail, see Chapter X).

Figs 8.3(d) and (e) represent $\ln \dot{k}$ versus m, and $\ln \dot{k}$ versus $\ln m$ plots for lysozyme obtained with HA chromatography (where the symbol k' is used instead of $\dot{k}$), respectively. It can be seen in Figs 8.3(d) and (e) that the arrangements of the experimental points on (m, $\ln \dot{k}$) and ($\ln m$, $\ln \dot{k}$) planes deviate from linearity slightly, being concave and convex, respectively. This indicates that the adsorptions of lyzozyme and competing potassium ion on P sites of HA are neither extremely "weak" nor extremely "strong"; it is eq(8.52), rather than eq(8.65) or (8.67), that coincides best with the ex-

periment. [For similar plots for other substances with HA chromatography, see ref(6.9) Fig 10.]

Chapter IX. Reversed-Phase Chromatography versus Competition Model

(A) Background

In 1965-1970, on the basis of several experiments, it was established that the fundamental adsorption and desorption mechanism of HA chromatography is brought about by a competition between sample molecule and gradient substance for adsorption on the crystal surfaces of HA particles packed in the column[6.1-6.3, 12.7; see Chapter VIII(A)]. This led to competition model with a specified form[6.2; see Chapter VIII(B)]. It is with a delay of over ten years that investigations on the adsorption and desorption mecahnism of both reversed-phase and ion-exchange chromatographies were performed vigorously by a number of authors. In a considerable number of these investigations, the interest was focused on the fact that, when the concentration gradient mode is applied, the chromatographic behavior of high M_m substances (e.g., those with M_m higher than 10^4 to 10^5 Da) is apparently quite different from the behavior of low M_m substances (e.g., those with M_m lower than 10^4 to 10^5 Da). Thus, only with high M_m substances, it is apparent that the molecules are initially adsorbed completely at the inlet of the column, that desorption takes place suddenly when the concentration of the gradient substance reaches some critical value, and that, once desorption takes place, the molecules migrate on the column without being re-adsorbed to the packed particles at all ("on-off" mechanism). [This means that, under isocratic condition, a high M_m substance can migtrate on the column at a relative rate, R_F, higher than zero and lower than unity only when the gradient substance is present in concentration close to the critical value; the terminology "gradient substance" is used even in the absence of concentration gradient i.e., under isocratic condition.] In contrast, low M_m substances obey the conventional "partition" mechanism taking place between stationary and mobile phases.

It should be recalled that the interest in focus in these investigations already is taken in the early stage of the study of HA chromatography[6.1-6.3; see Chapter VIII(A)]. Thus, in refs(6.1-6.3), it was demonstrated that the "on-off" mechanism should occur when the transition from ≈ 0 to 1 of molecular partition, B, in the mobile phase takes place rapidly (or sharply) enough with increase in concentration, m, of the gradient substance, whereas the "partition" mechanism should occur when the transition of B takes place slowly enough; the transition of B should be sharpened with increase in size x' or M_m of the sample molecule under investigation if the competition mecahism takes place in fact [see ref(6.2) Fig 7; cf. Fig 8.5 with reference to Fig 3.2]. This means that the competition mechanism gives rise to "on-off" and "partition" mechanisms with high enough and low enough M_m substances, respectively. It is to be regretted that all the investigations on reversed-phase and ion-exchange chromatographies were performed without any reference to the eralier study of HA chromatography.

In this Chapter, important experiments of reversed-phase chromatographies carried out

by several authors for the purpose of elucidating the adsorption and desorption mechanism are presented. These are examined on the basis of competition model apart from the interpretations of the authors. In Appendix XI(C)-(F), the theoretical bases of the interpretations of the authors are summarized along with classical theories of the adsorption and desorption mechanism, and these are compared with the interpretation based on competition model. In Section(B), only brief considerations are given, and quantitative analyses of experiments will be performed in Section(C)-(F). Ion-exchange chromatography will be treated in the subsequent Chapter X.

(B) General Aspect of Reversed-Phase Chromatography

Lochmüller and McGranaghan(9.1) carried out isocratic chromatographics of several quasi-monodisperse polystyrene samples (with M_m between 6×10^2 and 2.8×10^6 Da) on two columns packed with C_8-bonded partcles (30 nm pore) and C_{18}-bonded particles (10 nm pore), respectively; two types of binary mobile phase system: tetrahydrofuran(THF; good solvent)/water(H_2O; poor solvent) and methylene chloride($MeCl_2$; good solvent)/acetoniyrile (ACN; poor solvent) with several volume fraction ratios were used. Figs 9.1 and 9.2 [reproduced from ref(9.1)] illustrate the plots of $\log_{10} k$ (written as log k') versus volume fraction of good solvent (here denoted by m; $0\leqq m\leqq 1$) obtained from the experiments. The diagrams are characterized by three points: (a) $\log_{10} k$, in general, decreases linearly with increase in m. (b) The absolute value, $-d\log_{10} k/dm$ (denoted by S), of the negative slope of $\log_{10} k$ as a function of m increases monotonically with increase in M_m of polystyrene. And (c) the m value that corresponds to $\log_{10} k=0$ or $k=1$ shifts to high values with increase in M_m in such a way that the rate of shift decreases with increase in M_m; the m value that corresponds to $k=1$ appears to become quasi-independent of M_m when M_m is high enough (see both Figs 9.1 and 9.2). [In ref(9.1), the symbol "log" is used instead of the symbol "$\log_{10}$". Here and hereafter, we would like to interpret that the symbol "log" appearing in any chromatographic literature represents "$\log_{10}$" and not the natural logarithm "ln" in accordance with the conventional rule. Exceptionally in my earlier papers(6.4, 6.5, 8.13, 8.14), however, the symbol "log" is used to represent "ln". In this monograph, the symbol "log" is used when the basis of the logarithm is not defined.]

From these experimental data, it is probable that both polystyrene and good solvent molecule (THF or $MeCl_2$) are adsorbed "weakly" [see Chapter VIII(H)] on the C_8 or C_{18} surface while performing the competition. In fact, if this is the situation, then eq(8.65) in which (ln 10)S is substituted for $x'\varphi$ should be fulfilled; this predicts both points(a) and (b) since x' should mesure M_m. Further, it is reasonable to assume that the assembly of polystyrene molecules with different x' or M_m represents approximately an assembly of "homologous" molecules fulfilling eq(8.53), while both Figs 9.1 and 9.2 are quite parallel to Fig 8.5 representing the behavior of a series of "homologous" molecules. This behavior is compatible with point(c) because that $k=1$ means that $B\equiv 1/(1+k)=1/2$. This implies

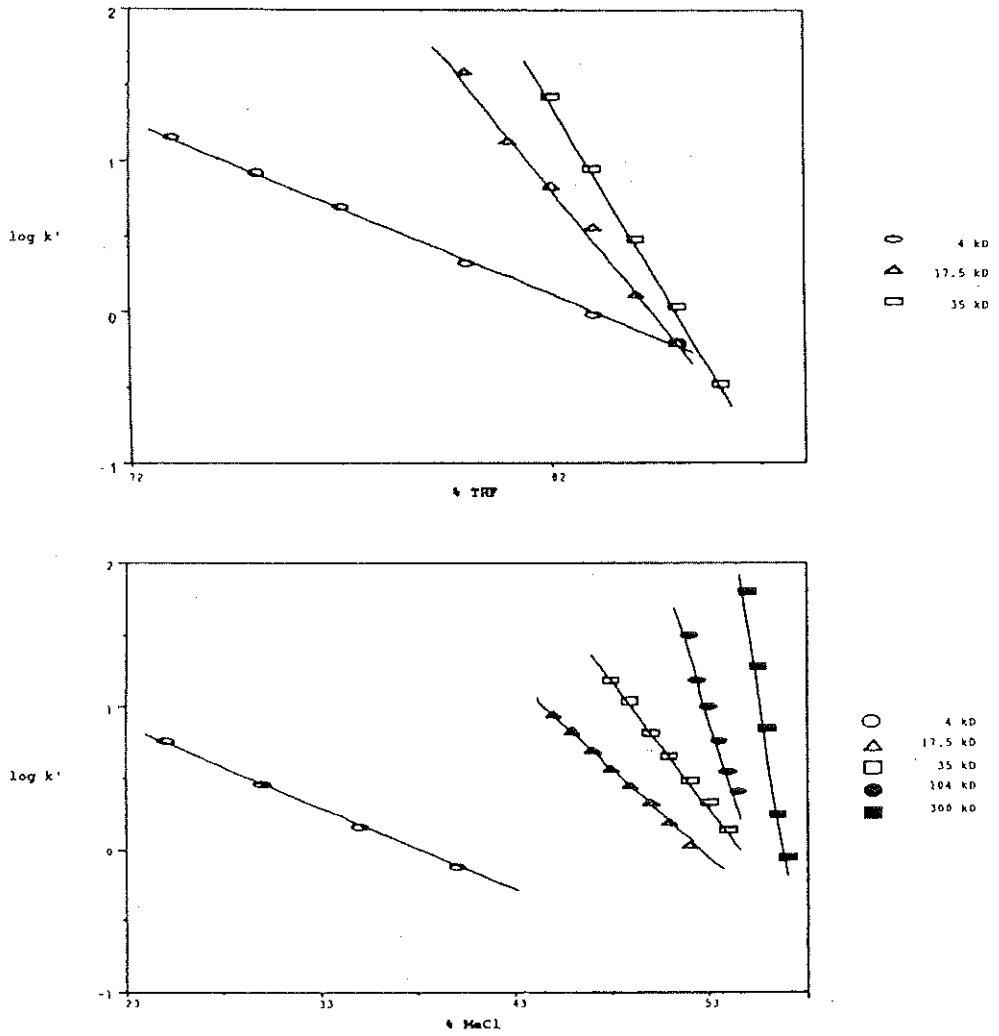


Fig 9.1. Plots of log k' i.e., $\log_{10}$ k versus volume fraction, m ($0 \leqq m \leqq 1$; the $100\times$ m values are shown in the diagram), of good solvent for polystyrenes with different M_n. These were eluted isocratically from a C_8 (30 nm pore) column by using THF/H_2O (top) and $MeCl_2$/ACN (bottom) mobile phase systems with different m values; left- and right-hand sides of the slash represent good and poor solvents, respectively. The regression line for the almost linear arrangement of the plots for polystyrenes with any M_n can be represented by eq(9.11) or (9.11'), where, by the direct surveying of the diagram, the (M_n; S,W; $\hat{S}$,$\hat{W}$) values for the three regression lines for the THF/H_2O system (top) can be estimated to be (4×10^3 Da; 11.41, 9.464; 26.27, 21.79), (1.75×10^4 Da; 35.00, 29.508; 80.59, 67.95), and (3.5×10^4 Da; 48.18, 40.913; 110.94, 94.21). The corresponding values for the five regression lines for the $MeCl_2$/ACN system (bottom) can be estimated to be (4×10^3 Da; 5.17, 1.939; 11.90, 4.46), (1.75×10^4 Da; 12.16, 6.417; 28.00, 14.78), (3.5×10^4 Da; 17.54, 9.609; 40.39, 22.13), (1.04×10^5 Da; 47.15, 25.96; 108.57, 59.78), and (3×10^5 Da; 90.50, 51.76; 208.39, 119.18). [Reproduced from ref(9.1) Fig 5.]

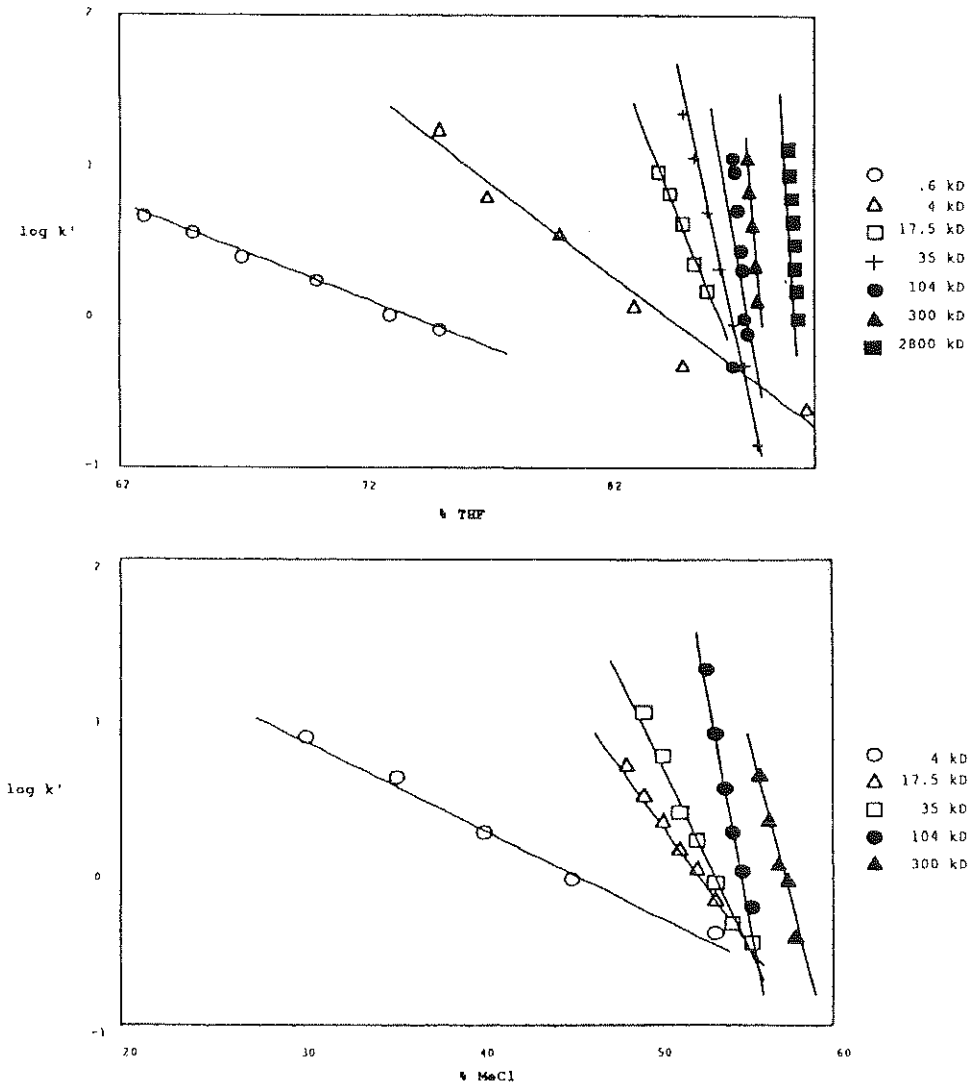


Fig 9.2. As Fig 9.1 for a C_{18} (10 nm pore) column. The plots for polystyrenes with M_m of 1.04×10^5, 3×10^5, $2.8\times10_6$ Da for the THF/H_2O system (top) and those for polystyrenes with M_m of 3×10^6 Da for the $MeCl_2$/ACN system (bottom) were eliminated from the object of experimental analysis for the reason mentioned in the text. By the direct surveying of the diagram, (M_m;S,W; $\hat{S}$,$\hat{W}$) values for the four other regression lines for the THF/H_2O system (top) can be estimted to be (6×10^2 Da; 6.42, 4.739; 14.78, 10.91), (4×10^3 Da; 12.52, 10.525; 28.83, 24.23), (1.75×10^4 Da; 43.00, 37.069; 99.01, 85.36), and (3.5×10^4 Da; 78.57, 68.218; 180.92, 157.08). Those for the four other regression lines for the $MeCl_2$/ACN system (bottom) can be estimated to be (4×10^3 Da; 5.50, 2.504; 12.66, 5.77), (1.75×10^4 Da; 14.90, 7.900; 34.31, 18.19), (3.5×10^4 Da; 23.44, 12.671; 53.97, 29.18), and (1.04×10^5 Da, 67.20, 37.337; 154.73, 85.97), where it has been assumed that the numeral figures calibrating the abscissa of the bottom diagram are attached to the dimly drawn protuberances on the abscissa. [Reproduced from ref(9.1) Fig 3.]

again that the competition mechanism takes place with reversed-phase chromatography. Further analyses of both Figs 9.1 and 9.2 will be performed in the subsequent Section(C).

In Fig 9.3 [reproduced from ref(9.1)] is presented a chromatogrm of a nominally monodisperse polystyrene standard ($M_n = 2 \times 10^3$ Da; weight average M_w/number average M_n = 1.06) obtained on a C_{18} column by using a linear concentration gradient of THF in the binary THF/H_2O system. It can be seen in Fig 9.3 that partial separations among different oligomers occur especially in the left part of the chromatogram in which it can be assumed that the components with relatively low M_n are involved. The chromatogram in Fig 9.3 is quite similar in aspect to those of poly-L-glutamate ($M_n = 1.36 \times 10^4$ Da) and poly-L-arginine ($M_n = 2.4 \times 10^4$ Da) obtained on an HA column by using linear concentration gradients of KP or KCl [see Figs 9.4 and 9.5 reproduced from ref(7.1), respectively; cf. Fig 8.9]. This also suggests that the adsorption and desorption mechanism taking place with reversed-phase chromatography is similar to that taking place with HA chromatography.

Alhedai et al.(9.2) carried out isocratic chromatographies of quasi-monodisperse polystyrene samples (with M_n between 2×10^3 and 10^6 Da) on two columns packed with C_{18}-bonded particles with 30 and 10 nm pore size, respectively; the binary $MeCl_2$/methanol (MtOH) mobile phase system with several volume fraction ratios were used. Although the ln k versus m plots obtained from these experiments [ref(9.2) Figs 1-4 in which ln k and m are written as ln k' and ϕ, respectively] are fluctuating to some extent, the tendency quite parallel to that shown in both Figs 9.1 and 9.2 can be found. In ref(9.2) Figs 1-4, however, the total arrangement of the plots, in general, are slightly concave in shape [as in Fig 8.3(d) with HA chromatography], suggesting that the value of the term φ m now is not completely negligible compared with unity [see both eqs(8.64) and (8.65)].

By using best regression fits for the quasi-linear arrangements of the plots, Alhedai et al.(9.2) estimated that the absolute value, $-d\ln k/dm$ [denoted by $\hat{S}$; $\hat{S} = (\ln 10)S$], of the negative slope of the regression line can be represented as a function of M_n of the sample applied as $\hat{S} = 0.0439M_n^{0.586}$ and $\hat{S} = 0.0152M_n^{0.730}$ for 30 and 10 nm pore C_{18} columns, respectively. [In ref(9.2), the relationships: $\hat{S} = 0.668P^{0.586}$ and $\hat{S} = 0.452P^{0.730}$ were obtained, respectively, where P stands for the degree of polymerization of polystyrene. These can be transformed to the relationships above by using $M_n = 104.14P$; cf. both eqs (9.14) and (9.14').] Alhedai et al.(9.2) mention, however, that the power of M_n appears to increase slightly if the upper limit of M_n used for the analysis is increased considerably beyond the scope argued above. Further, by analysing the polystyrene data obtained by Lochmüller and McGranaghan[Fig(9.1)], Alhedai et al.(9.2) estimated that S or $\hat{S}$ for the C_8 column (with 30 nm pore) can be represented as $\hat{S} = 1.03P^{0.669}$ and $\hat{S} = 0.472P^{0.654}$ in the presences of THF/H_2O and $MeCl_2$/ACN mobile phase sysyems, which leads to $\hat{S} = 0.0460M_n^{0.669}$ and $\hat{S} = 0.0226M_n^{0.654}$, respectively. [The proportionality constants in the right-hand sides of both of these equations, however, are deviating from possible true values considerably [cf. Fig 9.10(b)]. If the proportionality constants are multiplied by ln

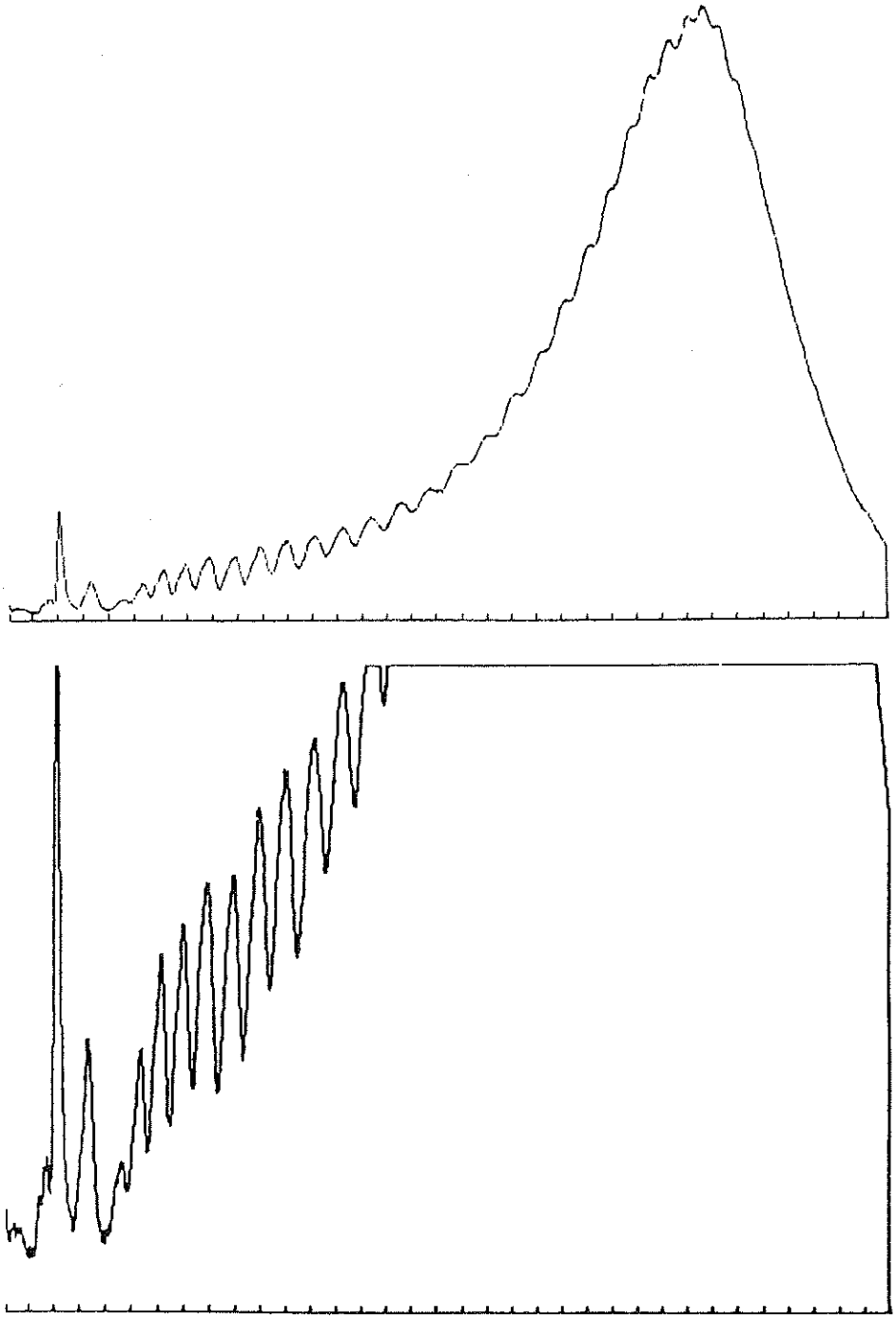


Fig 9.3. Chromatogram of a nominally monodisperse polystyrene standard ($M_n = 2 \times 10^3$ Da; weight average M_w/number average M_n = 1.06) obtained on a C_{18} column by using a linear concentration gradient of THF in the binary THF/H_2O system. The full scale of the bottom diagram is 0.3 times as large as that of the top. [Reproduced from ref (9.1) Fig 8.]

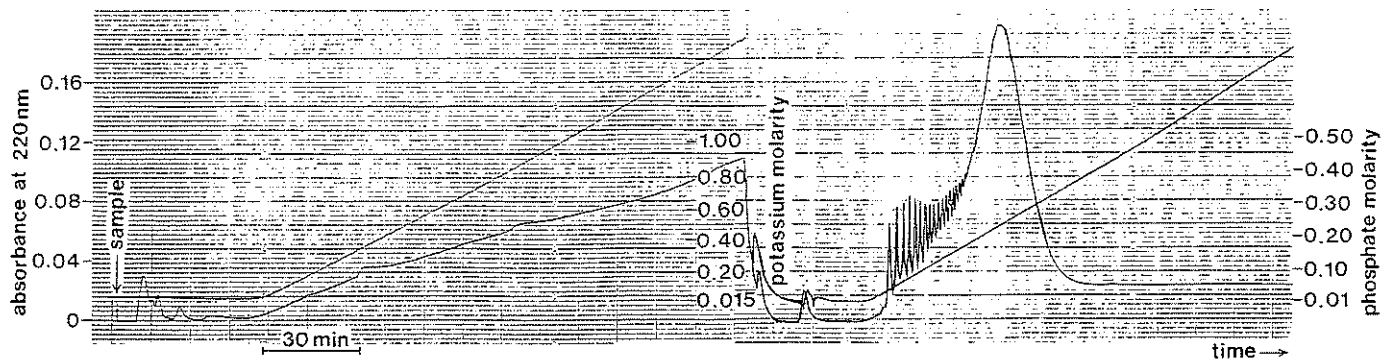


Fig 9.4. Double gradient chromatogram of poly-L-glutamate ($M_n = 1.36 \times 10^4$ Da) obtained on an HA column first by applying a linear KCl gradient (left part of the diagram) and second by applying a linear KP gradient (right part of the diagram). The fact that the molecules are eluted by the second gradient manifests that they are adsorbed on crystal C sites while performing the competition with phosphate ions from the KP buffer for adsorption; see Chapter Ⅷ(A). [For detail, see ref(7.1). Reproduced from ref(7.1) Fig 4.]

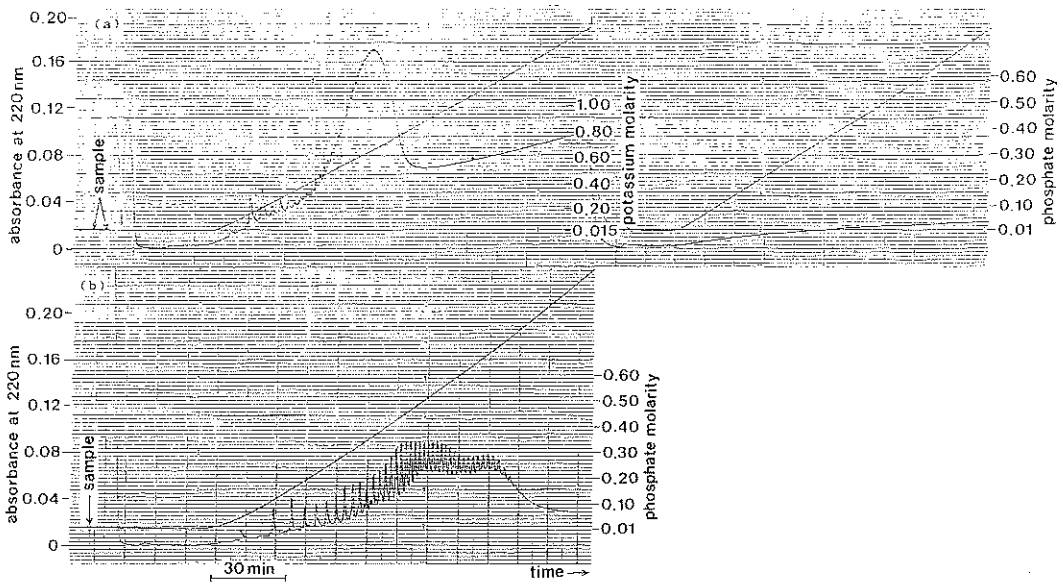


Fig 9.5. (a) Double gradient chromatogram of poly-L-arginine ($M_n = 2.4 \times 10^4$ Da) obtained on an HA column in the same way as in Fig 9.4. The fact that the molecules are eluted by the first gradient manifests that they are adsorbed on crystal P sites while performing the competition with potassium ions from the KCl solution for adsorption; see Chapter Ⅷ(A). [For detail, see ref(7.1).] (b) Single KP gradient chromatogram for the same sample obtained on the same column. The difference in shape of the chromatograms between (a) and (b) perhaps arises from the secondary effect of the interaction of poly-L-arginine with solvent. [Reproduced from ref(7.1) Fig 6.]

10, $\hat{S} = 0.106 M_m^{0.669}$ and $\hat{S} = 0.0521 M_m^{0.654}$ are obtained, respectively; these are reasonable conclusions.] For other arguments performed in ref(9.2), see Appendix XI(F).

In the above analyses, $\hat{S}$ always is proportional to $M_m^{0.667}$ or $M_m^{2/3}$ approximately. This would mean that the molecular conformation of polystyrene taking place on the C_8 or C_{18} surface is not planar or stretched. It would be reasonable to assume that the molecular conformation is three-dimensional in such a way that the effective volume occupied by the conformation is proportional to M_m, and that the effective area of the adsorbent surface occupied by the molecule is proportional to the projection of the three-dimensional conformation, which is proportional to the 2/3 power of the volume occupied by the conformation. According to competition model, the area of the adsorbent surface occupied by the molecule should be proportional to x' or $\hat{S}$. As a result, $\hat{S}$ should be proportional to $M_m^{2/3}$. [*Note 1.* Alhedai et al.(9.2) mention that $\hat{S}$ is approximately proportional to the 0.472 to 0.517 power of M_m if the estimation is done by using the "gradient elutiuon measurement method based on the LSS gradient hypothesis" instead of the isocratic elution meaurement method used above. In the former method, the linear concentration gradient elution data are used for the analysis on the basis of the hypothesis that the ideal LSS gradient should be formed [for the LSS gradient, see Appendix XI(B); cf. Chapter X (A) Figs 10.3-10.5]. If this is not the actual situation, however, the power of M_m estimated by using this method would deviate from the true value. Alhedai et al.(9.2) point out that the somewhat small estimation of the power of M_m arises as a result of this type of artifact. On the other hand, by using the same method, the Snyder's group[9.3; cf. refs (9.4, 9.5)] showed that S or $\hat{S}$ is proportional to 0.5 power of M_m for reversed-phase chromatography of polystyrene carried out on a C_{18} column (with 15 nm pore) in the presence of the THF/H_2O mobile phase system. *Note 2.* It is possible that solvent molecules are entrapped in the three-dimensional conformation of polystyrene both in solution and on the C_8 or C_{18} surface, and that the compound apparently behaves as an element of the thrmodynamic or statistical mechanical system [cf.Appendix XI(F)]. *Note 3.* With HA chromatography of DNA or proteins carried out by using the KP gradient, concentration, μ, of KP buffer at which the molecular elution takes place decreases drastically when the molecule is denatured. This can be deduced(7.1, 8.4, 8.6, 8.7, 8.27) to arise from the fact that the charged groups that are available for interaction with adsorbing sites of HA in rigid, ordered structure drastically decrease in number on the "outer surface" of randomly-coiled molecules. Further, a possibility cannot be excluded that the decrease of μ is also brought about by the swelling of the molecular volume taking place in the denatured state; this would increase x' or decrease the x/x' value [cf. eq(8.1)]. The randomly-coiled conformation is three-dimensional as opposed to the highly-stretched conformation of relatively low M_m (1.5×10^3 to 8×10^3 Da) poly-L-lysine [see Chapter VIII(E) with reference to Fig 8.9]. The important problem with regard to the conformation of macromolecules with flexible structures taking place on the adsorbent surface is argued in ref(9.3) Appendices I and II. Cf. the last paragraph in the subsection entitled "Further Considera-

tion" in the subsequent Section(C).]

Terabe(9.6) carried out isocratic chromatographies of benzene (M_m=78 Da) and four peptides or proteins [(Gly^4,Phe^5)-LH-RH ($M_m=1.1\times10^3$ Da; LH-RH means lutcinizing hormone releasing hormone), ACTH-(1-26)-NH_2 ($M_m=3.1\times10^3$ Da; ACTH means adrenocorticotropic hormone), insulin ($M_m=5.8\times10^3$ Da) and cytochrome c ($M_m=1.25\times10^4$ Da)] on a C_{18} column in the presence of the ACN/0.005 M phosphate buffer (pH 3.0) mobile phase system (containing 0.1 M sodium sulphate) while changing volume fraction, m, of ACN. Fig 9.6 [reproduced from ref(9.6)] illustrates the plots of $\log_{10}$ k (written as log k') versus m obtained from the experiments. Fig 9.6 is quite parallel to both Figs 9.1 and 9.2 showing (a) that $\log_{10}$ k decreases linearly with increase in m, and (b) that S increases monotonically with increase in M_m of the sample applied. The analysis of Fig 9.6 will be performed in the subsequent Section(D).

Koyama et al.(9.7) carried out isocratic chromatographies of C_6-phenone and three proteins (ribonuclease A, lysozyme and ovalbumin) on a C_8 (30nm pore) column in the presence of the ACN/H_2O mobile phase system (containing 0.1% trifluoroacetic acid) while changing the m value of ACN. Again the $\log_{10}$ k versus m plots quite parallel to those in Figs 9.1, 9.2 and 9.6 were obtained from the experiments showing (a) that $\log_{10}$ k decreases linearly with increase in m, and (b) that the S values for the high M_m substances (proteins) are about ten times as high as that for the low M_m substance (C_6-phenone) [see Fig 9.7 [reproduced from ref(9.7)] in which $\log_{10}$ k is written as log k'.]

In addition, Koyama et al.(9.7) carried out linear concentration gradient chromatographies of low M_m substances (C_4-phenone, C_5-phenone, C_6-phenone, Lys-bradykinin and Met-Lys-bradykinin) and high M_m substances (ribonuclease A, cytochrome c, lysozyme, bovine serum albumin, myoglobin and ovalbumin) on the C_8 columns with four different total lengths comprised between 1 and 25 cm. For all the experiments, the same ACN gradient was used by increasing the volume fraction, m, of ACN from 0.15 to 0.60 linearly in a constant duration of time (in the usual sense) under condition of constant flow-rate. Fig 9.8 [reproduced from ref(9.7)] illustrates the experimental plots of retention time (represented in an arbitrary unit; written as ratio of retention time) versus length of the column for each substance applied, where it can be seen that retention time, in general, increases with increase in length of the column drawing a vonvex curve, and that the increase of retention time occurs more rapidly with low M_m substances (part A) than with high M_m substances (part B).

Volume fraction μ (proportional to $\bar{\mu}$) of ACN at which the sample molecule [to be precise the center of MB(o)] is eluted is proportional to retention time minus dead time (corresponding to dead volume) of the column, provided that, at time 0, both the beginning of the ACN gradient and the initial MB(o) with a small width stayed at the inlet of the column; time, dead time, and time minus dead time correspond to Z, L' and V (=Z −L'), respectively. On the other hand, slope g' (with dimension of volume fraction/volume) or g (with dimension of volume fraction/length) of the ACN gradient is constant a-

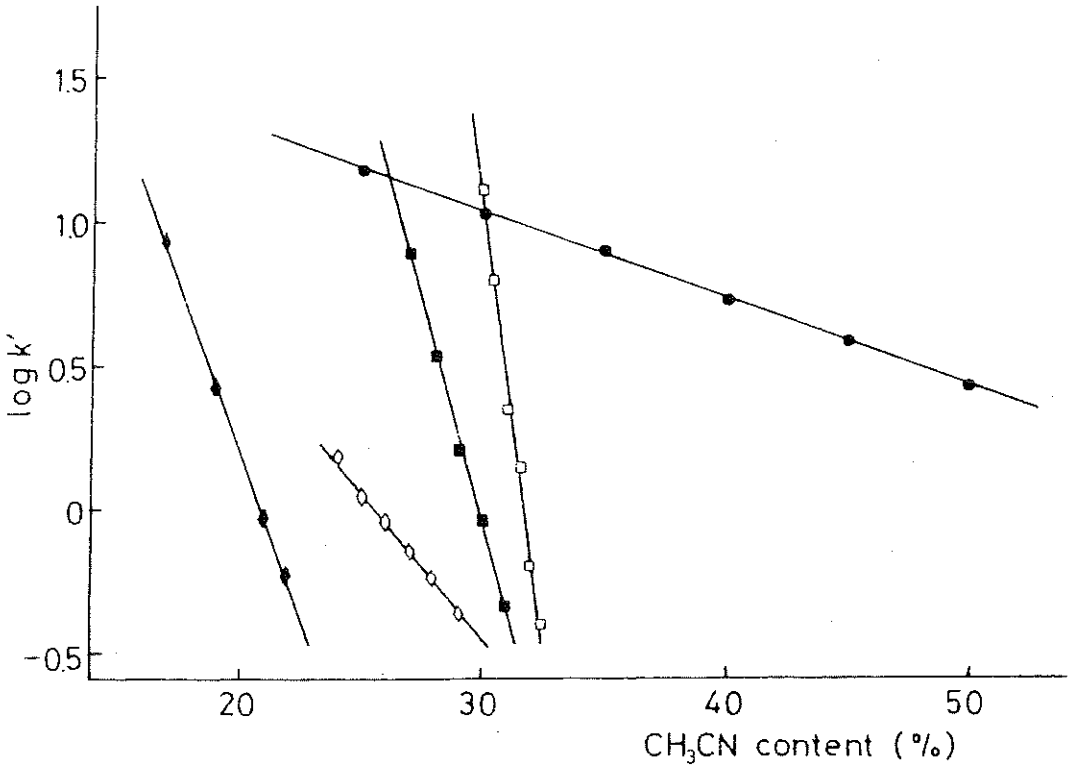


Fig 9.6. Plots of log k' i.e., $\log_{10}$ k versus volume fraction, m ($0 \leqq m \leqq 1$; the $100\times$ m values are shown in the diagram), of ACN for benzene(●) and for peptides (or proteins): (Gly^4,Phe^5)-LH-RH(◇), ACTH-(1-26)-NH_2(◆), insulin(■), and cytochrome c(□), obtained for isocratic chromatography carried out on a C_{18} column by using ACN/0.005 M phosphate buffer (pH 3.0) mobile phase systems with different m values (containing 0.1 M sodium sulphate). The regression line for the almost linear arrangement of the plots for any substance can be represented by eq(9.11) or (9.11'), where, by the direct surveying of the diagram, the (M_n;S,W; $\hat{S}$,$\hat{W}$) values can be estimated to be (78 Da; 3.0, 1.921; 6.91, 4.42) for benzene, (1.1×10^3 Da; 10.3, 2.639; 23.7, 6.08) for (Gly^4,Phe^5)-LH-RH, (3.1×10^3Da; 22.4, 4.667; 51.6, 10.75) for ACTH-(1-26)-NH_2, (5.8×10^3 Da; 29.4, 8.783; 67.7, 20.22) for insulin, and (1.25×10^4 Da; 63.4, 20.049; 146.0, 46.16) for cytochrome c. [Reproduced from ref(9.6) Fig 5.]

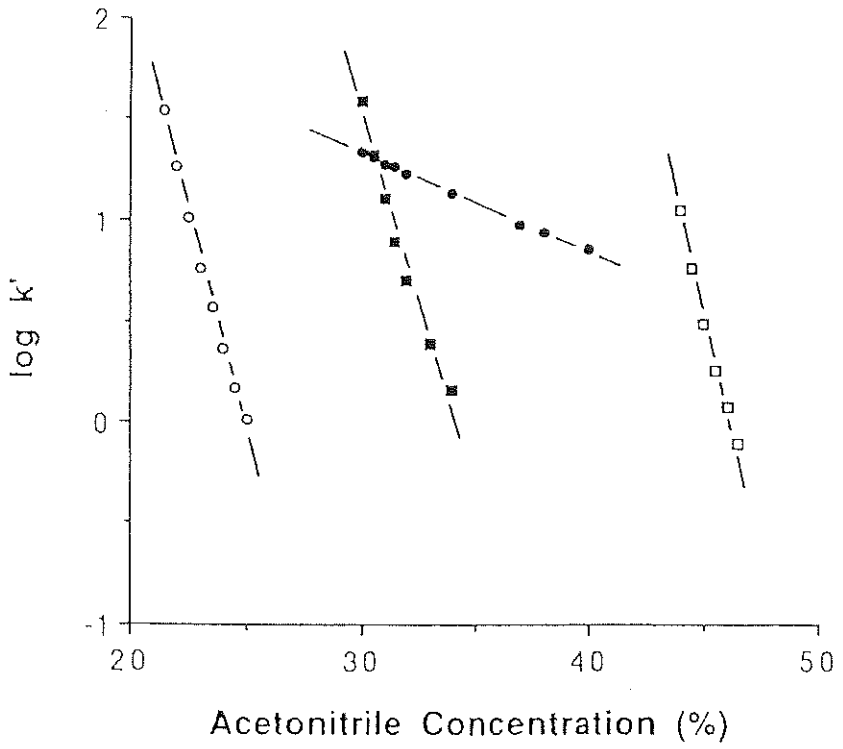


Fig 9.7. Plots of log k' i.e., $\log_{10}$ k versus volume fraction, m ($0 \leqq m \leqq 1$; the $100\times$ m values are shown in the diagram), of ACN for C_6-phenone(●), ribonuclease A(○), lysozyme(■), and ovalbumin(□), obtained for isocratic chromatography carried out on a C_8 (30 nm pore) column by using ACN/H_2O mobile systems with different m values (containing 0.1% trifluoroacetic acid). [Reproduced from ref(9.7) Fig 5.]

mong all the experiments in Fig 9.8. This means that the arrangement of the experimental points for any substance plotted in Fig 9.8 corresponds to that for any g' or g value plotted in Fig 7.3(a) (or Fig 7.4 middle part), Fig 8.1, Fig 8.3(a), or Appendix VI Fig A6.1 (except for the fact that, in Fig 9.8, retention time is taken instead of retention time minus dead time); it should be recalled that $\mu \approx \hat{\mu}$. The fact that the g' or g value of the ACN gradient is constant also means that time, dead time, and time minus dead time correspond to ξ, s and $\hat{m}$ $(= \xi - s)$, respectively, from which it follows that the arrangement of the experimental points for any substance plotted in Fig 9.8 corresponds to trajectory T_0 drawn in in Fig 7.6 (the middle curve), Fig 8.3(b), or Appendix VI Fig A6.2 (except for the fact that, in Fig 9.8, retention time is taken instead of retention time minus dead time; cf. the following second paragraph).

With HA chromatography, μ or $\hat{\mu}$ increases with increase in not only length L' or L of the column but also slope g' or g of the KP gradient applied [Fig 7.3(a) (or Fig 7.4 middle part), Fig 8.1, Fig 8.3(a), and Appendix VI Fig A6.1], and the dependence of μ or $\hat{\mu}$ on either L' (or L) or g' (or g) desreases with increase in M_m or x' [see both Figs 8.1 and 8.7; in Fig 8.7, $s_{app(P)}$ is proportional to both L' (or L) and g' (or g)]. The decrease of the dependence of μ or $\hat{\mu}$ on s [i.e., on either L' (or L) or g' (or g)] taking place with increasein M_m or x' can be explained by the competition mechanism [Chapter VIII(D)]. Therefore, the fact that the increase of retention time with increase in the total length of the column occurs more rapidly with low M_m substances than with high M_m substances (Fig 9.8) implies again that the competition mechanism takes place with reversed-phase chromatography.

Fig 9.8 is consistent with Fig 9.7 manifesting that S increases with increase in M_m. Thus, the arrangement of the experimental points for any substance plotted in Fig 9.8 corresponds directly to trajectory T_0 mapped to the (ξ, s) plane shown in Fig 2.8(e); this can be re-mapped to the $(\hat{m}, s)$ plane shown in either Fig 2.8(d) or 3.2(b). On the other hand, the arrangement of the experimental points for any substance plotted in Fig 9.7 can be mapped to the $[m, B \equiv 1/(1+k)]$ plane i.e., the $(\hat{m}, B)$ plane shown in Fig 3.2(b). Trajectory T_0 drawn on the $(\hat{m}, s)$ plane and the curve drawn on the $(\hat{m}, B)$ plane are projections of a characteristic curve taking place in the $(\hat{m}, s, B)$ space, respectively [Fig 3.2(b)]; the two projections drawn in Fig 3.2(b) approach those drawn in Fig 3.2(c) with increase in x' or M_m, respectively. It can be seen in Fig 3.2(c) that trajectory T_0 is parallel to the s axis; this means that retention time minus dead time is independent of total length of the column used. On the other hand, it can be seen in Fig 3.2(c) that the transition of B from 0 to 1 occurs stepwise with increase in $\hat{m}$; this means that $S = \infty$.

Fig 9.9 [reproduced from ref(9.7)] illustrates the experimental plots of the width of the chromatogram (represented in an arbitrary unit; written as ratio of bandwidth) versus length of the column for each of low M_m substances (C_4-phenone, C_5-phenone and C_6-phenone; part A) and each of high M_m substances (ribonuclease A, lysozyme, bovine serum albumin, myoglobin and ovalbumin; part B), obtained for linear concentration gradient

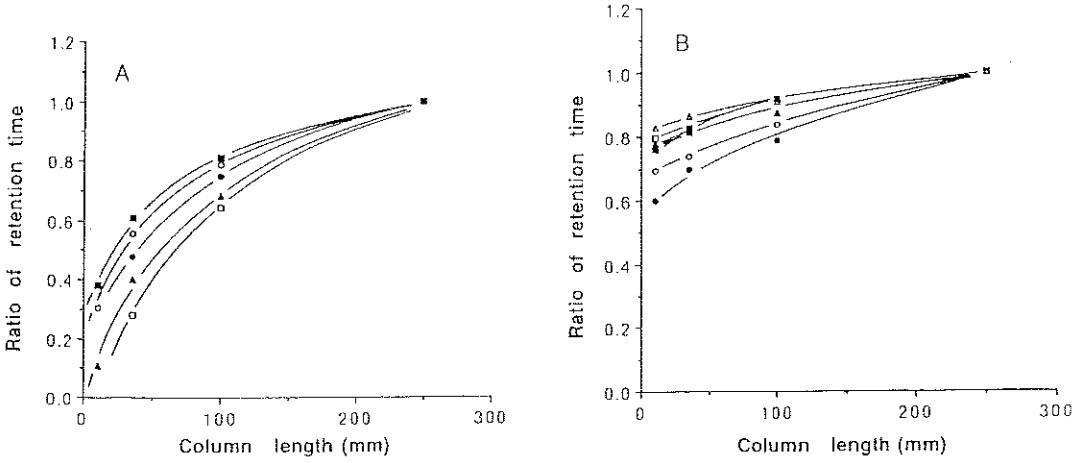


Fig 9.8. Plots of ratio of retention time (i.e., retention time represented in an arbitrary unit) versus column length with linear concentration gradient chromatography carried out on a C_8 (30 nm pore) column by increasing volume fraction, m, of ACN from 0.15 to 0.60 in 15 min in the ACN/H_2O mobile system (containing 0.1 % trifluoroacetic acid) for (A) low M_m substances: C_4-phenone(●), C_5-phenone(○), C_6-phenone(■), Lys-bradykinin(□), and Met-Lys-bradikinin(▲), and (B) high M_m substances or proteins: ribonuclease A (●), cytochrome c(○), lysozyme(■), bovine serum albumin(□), myoglobin(▲), and ovalbumin(△). [Reproduced from ref(9.7) Fig 1.]

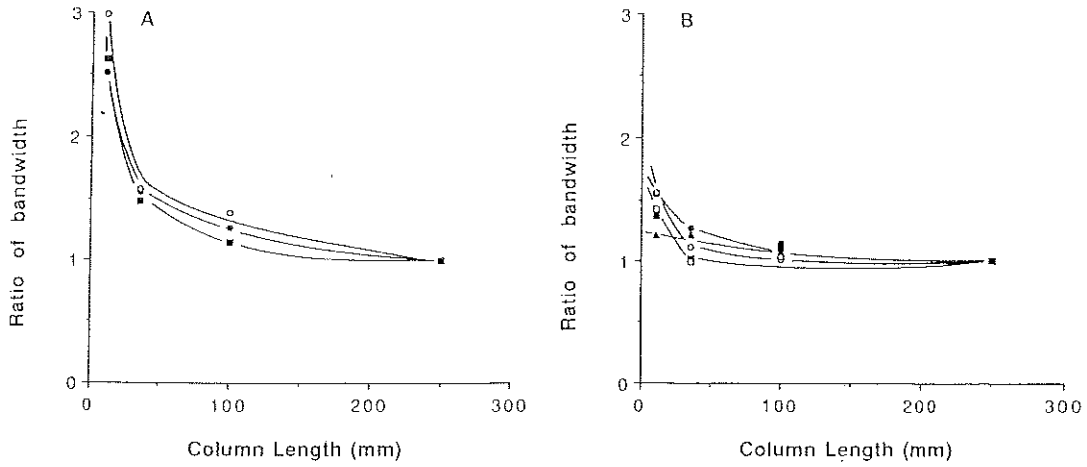


Fig 9.9. Plots of ratio of bandwidth (i.e., the width of chromatographic peak represented in an arbitrary unit) versus column length with linear concentration gradient chromatograohy carried out on a C_8 (30 nm pore) column under the same experimental condition as that applied in Fig 9.8 for (A) low M_m substances: C_4-phenone(●), C_5-phenone (○), C_6-phenone(■), and (B) high M_m substances or proteins: ribonuclease A(●), lysozyme(○), bovine serum albumin(■), myoglobin(△), and ovalbumin(▲). [Reproduced from ref(9.7) Fig 2.]

chromatographies carried out on the C_8 columns under the same experimental conditions as those used in Fig 9.8. Koyama et al.(9.7) points out that, whereas the width of the chromatograms for the low M_m substances decreases with increase in length of the column from 1 to 25 cm (Fig 9.9 part A), that for high M_m substances remains almost constant when length of the column exceeds 3.5 cm (after the first decrease taking place when length of the column is increased from 1 to 3.5 cm; see Fig 9.9 part B). The arrangement of the experimental points for any substance plotted in Fig 9.9 corresponds to that for any g' or g value plotted in Fig 7.11(a), Fig 7.12(a), Appendix VI Fig A6.5, or Appendix VI Fig A6.6. From the general theory of concentration gradient chromatography [which is independent of whether the competition mechanism takes place or not; see eqs (6.2), (6.8) and (6.9)], it can be anticipated that the width of the reversed-phase chromatogram (Fig 9.9) will increase gradually with increase in length of the column after the first rapid decrease if length of the column is increased beyond the frame of the diagram, and that the length giving the chromatogram the minimum width will shift to smaller lenghts with increase in the sharpness of the transition of B (from ≈ 0 to 1) taking place with increase in ACN volume fraction m. Therefore, provided that the competition mechanism takes place in fact, the shift of the optimal column length to smaller lengths should occur with increase in x' or M_m of the sample applied [see the subsection entitled "Good Separation Condition" in Chapter VII(E)]. Fig 9.9 appears to be compatible in aspect with the assumption that the optimal column length shifts to lower lengths with increase in M_m. This implies once more that the competition mechanism takes place with reversed-phase chromatography; Figs 9.7-9.9 are consistent with one another.

The data obtained by Geng and Regnier(9.8) are exceptional, who carried out isocratic chromatographies of seven proteins with M_m between 3.3×10^3 and 4.4×10^4 Da (glucagon, insulin, cytochrome c, ribonuclease A, lysozyme, trypsin inhibitor and ovalbumin) on a C_8 column in the presence of the 2-propanol/formic acid aqueous solution mobile phase system while changing volume fraction, m, of 2-propanol. From these experiments, linear arrangements (with negative slopes) of the $\log_{10}$ k versus $\log_{10}$ m plots (and not the $\log_{10}$ k versus m plots) were obtained for all the proteins examined, just as with ion-exchange chromatography which will be argued in the subsequent Chapter X. When regarding these data, we are obliged to assume that, exceptionally in these experiments, both protein and 2-propanol are adsorbed "strongly" on the C_8 surface while performing the competition [cf. both Chapter X and Appendix XI(C)].

Important experiments of polystyrenes with relatively low M_m carried out by Larmann et al.(9.4) will be analyzed in the subsequent Section(E). Important experiments for other types of substance than those exmined above (with relatively low M_m) were performed by several authors [for instances, see refs(9.9-9.14)]. The data obtained by Jandera(9.13, 9.14) will be analyzed in the subsequent Section(F).

(C) Analysis of the Experiment of Lochmüller and McGranaghan

Theoretical Preparation. In eq(8.65) i.e.,

$$\ln k = -x'_{\varphi} m + \ln q \tag{9.1}$$

the term ln q can be represented by eq(8.49) as

$$\ln q = J/kT + \ln \beta \tag{9.2}$$

in which

$$J = E + kT\ln \tau \tag{9.3}$$

represents the AVFA per molecule.

Let us consider an assembly of "homologous" molecules characterized by eq(8.53) as J/x'=constant, or as

$$J/(x'_{\varphi} kT) = \gamma \tag{9.4}$$

in which γ represents a positive constant. Eq(9.2) can now be rewritten as

$$\ln q = \gamma x'_{\varphi} + \ln \beta \tag{9.5}$$

where it can be considered that ln q is a function of x'_{φ} representing the "relative molecular size" of a member of the "homologous" molecules. Eq(9.5) fulfills

$$\lim_{x'_{\varphi} \to 0} \ln q = \ln \beta \tag{9.6}$$

Eq(9.1) can be rewritten as

$$\ln k = -x'_{\varphi} m + \gamma x'_{\varphi} + \ln \beta \tag{9.7}$$

where it can be considered that ln k is a function of m, and that x'_{φ} is a parameter. When considering ln k to be a function of x'_{φ} and m to be a parameter, it is convenient to rewrite eq(9.7) as

$$\ln k = (\gamma - m)x'_{\varphi} + \ln \beta \tag{9.7'}$$

Eq(9.7') fulfills

$$\lim_{x'_{\varphi} \to 0} \ln k = \ln \beta \tag{9.8}$$

independent of the m value.

When x'_{φ} can be represented as a function of M_m or P as

$$x'_{\varphi} = f_{Mm}(M_m) \; [= f_P(P)] \tag{9.9}$$

fulfilling

$$\lim_{M_m \to 0} f_{Mm}(M_m) \; [= \lim_{P \to 0} f_P(P)] \; = \; 0 \tag{9.10}$$

then eqs(9.5)-(9.7), (9.7') and (9.8) can be rewritten as

$$\ln q \; = \; \gamma f_{Mm}(M_m) \; + \; \ln \beta \tag{9.5a}$$

$$\lim_{M_m \to 0} \ln q \; = \; \ln \beta \tag{9.6a}$$

$$\ln k \; = \; -f_{Mm}(M_m)m \; + \; \gamma f_{Mm}(M_m) \; + \; \ln \beta \tag{9.7a}$$

$$\ln k \; = \; (\gamma - m) f_{Mm}(M_m) \; + \; \ln \beta \tag{9.7'a}$$

and

$$\lim_{M_m \to 0} \ln k \; = \; \ln \beta \tag{9.8a}$$

respectively; eq(9.8a) holds independent of m, and M_m and $f_{Mm}(M_m)$ can be replaced by P and $f_P(P)$, respectively. It should be noted that eq(9.10) gives a necessary condition for eq(9.4) to be justified. [f_{Mm} and f_P are symbols. In eq(9.10), do not misunderstand as if the subscripts M_m and P as parts of the symbols tend to zero when M_m and P as variables tend to zero, respectively.]

Analysis of Fig 9.1. This is concerned with chromatpgraphies of polystyrenes with different M_m carried out on a C_8 (30 nm pore) column in the presences of THF/H_2O and $MeCl_2$/ACN mobile phase systems. In Fig 9.1, the regression line for the arrangement of the experimental points for the sample with any M_m can be represented as

$$\log_{10} k \; = \; -Sm \; + \; W \tag{9.11}$$

or

$$\ln k \; = \; -\hat{S}m \; + \; \hat{W} \tag{9.11'}$$

in which $\hat{S} = (\ln 10)S$ and $\hat{W} = (\ln 10)W$. The M_m, S, W, $\hat{S}$ and $\hat{W}$ values for the respective regression lines (estimated by the direct surveying of the diagram) are presented in the legend for Fig 9.1. It would be reasonable to assume that the assembly of polystyrenes with different M_m represent an assembly of "homologous" molecules fulfilling eq (9.4). Under this assumption, $\hat{S}$ and $\hat{W}$ stand for $f_{Mm}(M_m)$ and $\gamma f_{Mm}(M_m) + \ln \beta$, respectively [see eq(9.7a)].

The points(○ and □) in Fig 9.10(a) represent the plots of $\hat{S}$ (estimated from Fig 9.1) versus M_m for THF/H_2O and $MeCl_2$/ACN mobile phase systems, respectively. When the two plots are mapped to the $(M_m^{2/3}, \hat{S})$ plane, two almost linear arrangements of the experimental points the extrapolations of which can, respectively, be assumed to pass through the origin are obtained [Fig 9.10(b)]; eq(9.10) or (9.4) can be justified only when the extrapolation of the arrangement of the experimentl points passes through the origin. For either THF/H_2O or $MeCl_2$/ACN mobile phase system, the arrangenent of the experimental points on the $(M_m^{2/3}, \hat{S})$ plane can now be represented as

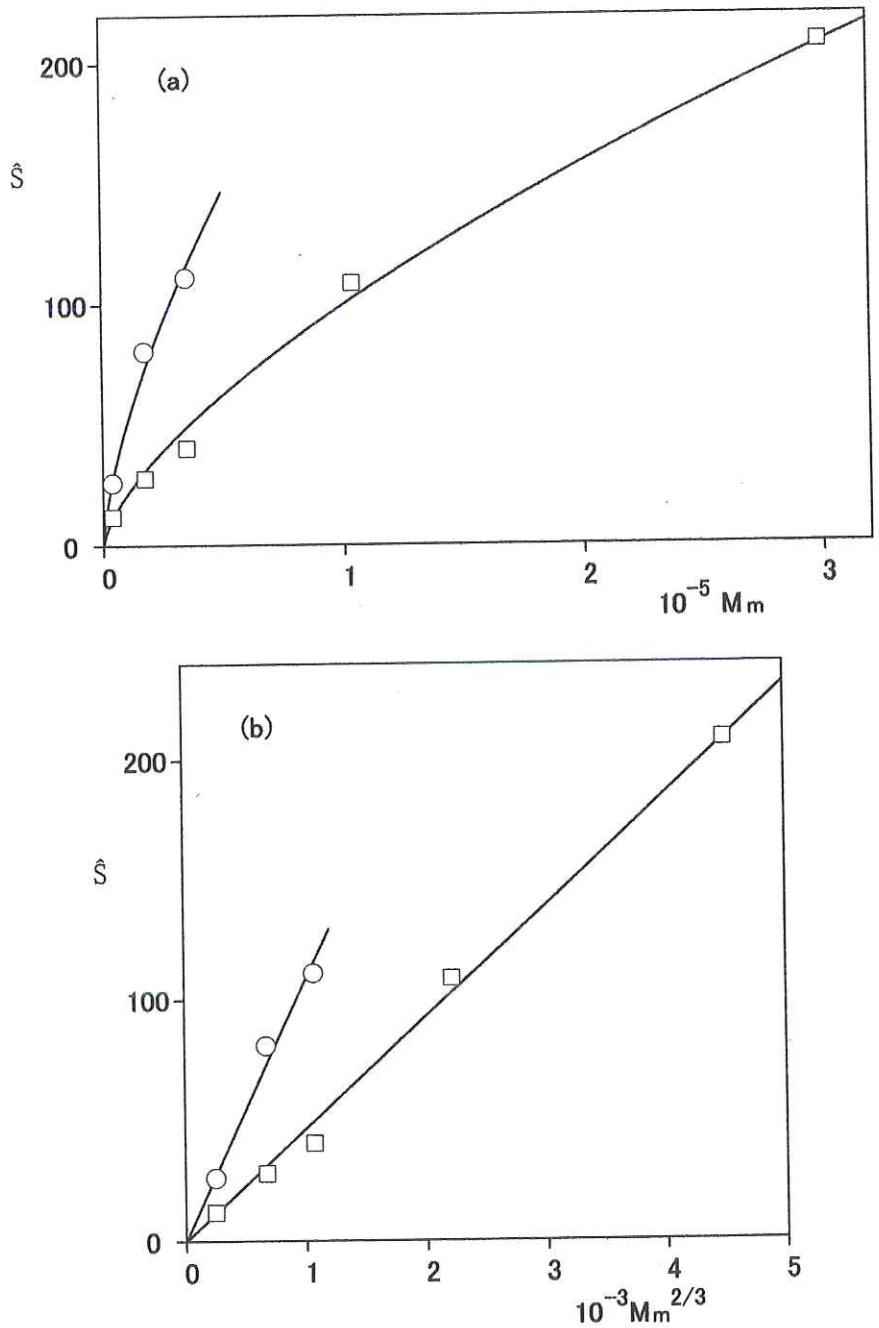


Fig 9.10. (a) Points(○ and □): experimental plots of $\hat{S}$ (obtained from Fig 9.1) versus M_m for C_8 (30 nm pore) column THF/H_2O and $MeCl_2$/ACN mobile phase systems, respectively. [The plots for the points(○) correspond to those presented in ref(9.1) Fig 6.] Curves: regression curves corresponding to the regression lines drawn in (b). (b) Points(○ and □): experimental plots of $\hat{S}$ versus $M_m^{2/3}$ for the corresponding points in (a). Straight lines: regression lines (passing through the origin) of $M_m^{2/3}$ on $\hat{S}$ for points (○ and □).

$$\hat{S} = \omega_{Mm} M_m^{2/3} \tag{9.12}$$

or function $f_{Mm}(M_m)$ [eq(9.9)] can be written as

$$f_{Mm}(M_m) = \omega_{Mm} M_m^{2/3} \; [= \omega_P P^{2/3}] \tag{9.13}$$

where ω_{Mm} and ω_P are positive constants. These can be expressed by using eq(9.9) as

$$\omega_{Mm} = x'\varphi / M_m^{2/3} \tag{9.14}$$

and

$$\omega_P = x'\varphi / P^{2/3} \tag{9.14'}$$

representing the "relative sizes" per unit M_m and per monomer unit taking place on the adsorbent surface, respectively; the 2/3 power of either M_m or P is considered because the molecular size is measured on the two-dimensional adsorbent surface (through the competition mechanism). ω_{Mm} and ω_P are related to one another as $\omega_P = (M_m/P)^{2/3} \omega_{Mm} = 104.14^{2/3} \omega_{Mm} = 22.23 \omega_{Mm}$ where 104.14 (Da) represents the M_m of styrene being equal to that of the monomer unit of polystyrene.

The two straight lines drawn in Fig 9.10(b) are the regression lines (passing through the origin) of $M_m^{2/3}$ on $\hat{S}$ [eq(9.12)] calculated by using the least square method for the two arrangements of the experimental points(○ and □), respectively. [Hereafter, all the regression lines considered originally in this monograph will be calculated by using the least square method.] As the slopes of the regression lines, the parameters ω_{Mm} for THF/H_2O and $MeCl_2$/ACN mobile phase systems can be evaluated to be 0.108 and 0.0463, respectively [see eq(9.12)]. The two curves passing through the origin drawn in Fig 9.10(a) correspond to the two regression lines drawn in Fig 9.10(b).

Eqs(9.5a), (9.7a) and (9.7'a) can now be represented as

$$\ln q = \gamma \omega_{Mm} M_m^{2/3} + \ln \beta \tag{9.5b}$$

$$\ln k = \ln \beta + \gamma \omega_{Mm} M_m^{2/3} - \omega_{Mm} m M_m^{2/3} \tag{9.7b}$$

and

$$\ln k = (\gamma - m) \omega_{Mm} M_m^{2/3} + \ln \beta \tag{9.7'b}$$

respectively; M_m and ω_{Mm} can be replaced by P and ω_P, respectively.

From eq(9.5b) [with references to both eqs(9.1) and (9.11')], it can be anticipated that the experimental plots of $\hat{W}$ versus $M_m^{2/3}$ will give a linear arrangement represented as

$$\hat{W} = \Phi_{Mm} M_m^{2/3} + \Phi' \tag{9.15}$$

in which

$$\hat{W} = \ln q \tag{9.16}$$

$$\Phi_{Mm} = \gamma\,\omega_{Mm} \tag{9.17}$$

and

$$\Phi' = \ln\beta \tag{9.18}$$

The points(○ and □) in Fig 9.11(a) represent the plots of $\hat{W}$ (estimated from Fig 9.1) versus M_m for THF/H_2O and $MeCl_2$/ACN mobile phase systems, respectively. When the two plots are mapped to the ($M_m^{2/3}$,$\hat{W}$) plane, two almost linear arrangements of the experimental points are obtained in fact [Fig 9.11(b)].

One of the two straight lines (with the smaller slope) drawn in Fig 9.11(b) is the regression line of $M_m^{2/3}$ on $\hat{W}$ with respect to the five points(□) for the $MeCl_2$/ACN system. As the slope, Φ_{Mm}, of the regression line, $\gamma\,\omega_{Mm}$ can be evaluated to be 0.0275, or the parameter γ can be evaluated to be $0.0275/\omega_{Mm}=0.0275/0.0463=0.594$ [see eq(9.17)]. On the other hand, as the intersection, Φ', with the $\hat{W}$ axis of the regression line, $\ln\beta$ can be evaluated to be -3.84, or the parameter β can be evaluated to be 2.15×10^{-2} [see eq(9.18)]. As anticipated [see Chapter Ⅷ(C)], the value of the parameter β [see eq (8.50)] is much smaller than unity in fact. This, along with the fact that almost linear arrangements of the experimental points are obtained on the ($M_m^{2/3}$,$\hat{W}$) plane [Fig 9.11(b)], strongly supports the competition model with reversed-phase chromatography. The other straight line (with the larger slope) drawn in Fig 9.11(b) is the regression line (defined so as to intersect the $\hat{W}$ axis at -3.84) of $M_m^{2/3}$ on $\hat{W}$ with respect to the three points(○) for the THF/H_2O system. [Here, the evaluation of $\ln\beta$ through the regression line for only three experimental points(○) has been avoided, and it simply is assumed that the $\ln\beta$ value for the THF/H_2O system is the same as the value for the $MeCl_2$/ACN system.] As the slope, Φ_{Mm}, of the regression line, $\gamma\,\omega_{Mm}$ can be evaluated to be 0.0958, or the parameter γ can be evaluated to be $0.0958/0.108=0.887$ [see eq(9.17)]. The two curves drawn in Fig 9.11(a) correspond to the two regression lines drawn in Fig 9.11(b).

Let us pay attention to eq(9.7'b) from which it can be anticipated that, when m is constant, the experimental plots of ln k versus $M_m^{2/3}$ will give a linear arrangement represented as

$$\ln k = \Psi_{Mm}M_m^{2/3} + \Psi' \tag{9.19}$$

in which

$$\Psi_{Mm} = (\gamma - m)\,\omega_{Mm} \tag{9.20}$$

and

$$\Psi' = \ln\beta \tag{9.21}$$

Further, $\Psi_{Mm}/\omega_{Mm}+m$ will give a constant value independent of m, representing γ:

$$\gamma = \Psi_{Mm}/\omega_{Mm} + m \tag{9.20'}$$

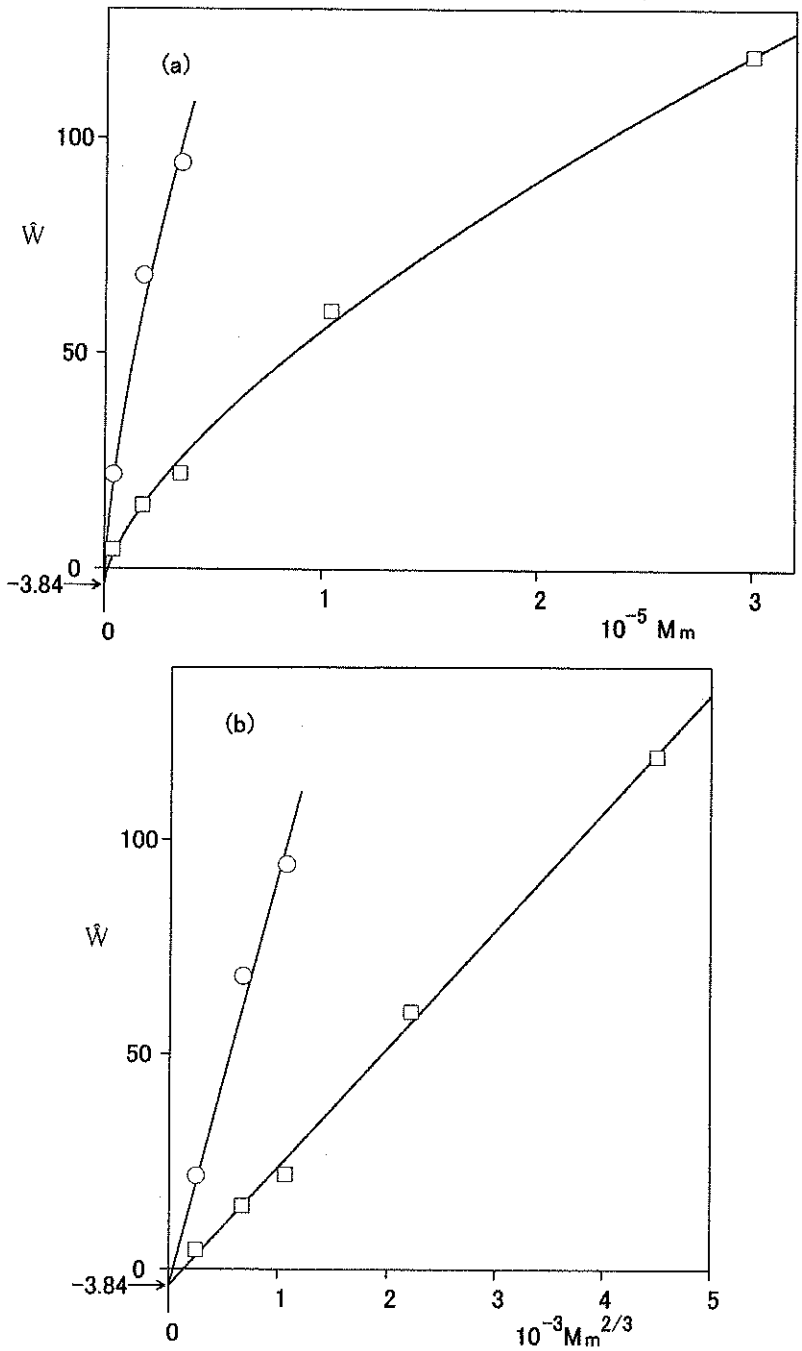


Fig 9.11. (a) Points(○ and □): experimental plots of $\hat{W}$ (obtained from Fig 9.1) versus M_m for C_8 (30 nm pore) column THF/H_2O and $MeCl_2$/ACN mobile phase systems, respectively. Curves: regression curves corresponding to the regression lines drawn in (b). (b) Points(○ and □): experimental plots of $\hat{W}$ versus $M_m^{2/3}$ for the corresponding points in (a). Straight line with the smaller slope: regression line of $M_m^{2/3}$ on $\hat{W}$ for the five points(□). Straight line with the larger slope: regression line (defined so as to intersect the $\hat{W}$ axis at -3.84) of $M_m^{2/3}$ on $\hat{W}$ for the three points(○).

Therefore, when m tends to infinitesimal, then Ψ_{Mm} will coincide with $\gamma\,\omega_{Mm}$ i.e., the slope of the linear arrangement of the experimental points taking place on the $(M_m^{2/3},\hat{W})$ plane [Fig 9.11(b)]. It can also be anticipated that the intersection, Ψ', with the ln k axis of the extrapolation of the arrangement of the experimental points (obtained for any value of m) will give the value of $\ln\beta$ [see eq(9.21)].

In Fig 9.12, the six arrangements of six types of point, respectively, represent the plots of ln k versus $M_m^{2/3}$ for six constant m values (between 0 and 0.5), obtained for five polystyrene samples with different M_m in the $MeCl_2$/ACN system (Fig 9.1 bottom). For the plots, the ordinates corresponding to each of the five polystyrene samples have been calculated for the six m values by using eq(9.11') in which both parameters $\hat{S}$ and $\hat{W}$ are characteristic of each sample; these are presented in the legend for Fig 9.1. As anticipated, it can be seen in Fig 9.12 that all the six arrangements of the experimental points are almost linear; the arrangement of the five points for m=0 is identical with that taking place on the $(M_m^{2/3},\hat{W})$ plane [i.e., one of the two arrangements illustrated in Fig 9.11(b)]. It can also be seen in Fig 9.12 that the extrapolations of the six arrangementsof the experimental points intersect the ln k axis almost at the same position.

The six straight lines drawn in Fig 9.12 are the regression lines of $M_m^{2/3}$ on ln k [represented by eq(9.19)] for the six arrangements of the experimental points. Both Ψ_{Mm} and Ψ' values for each of the six regression lines are presented in the legend for Fig 9.12; the regression line for m=0 is identical with that taking place on the $(M_m^{2/3},\hat{W})$ plane [i.e., one of the two regression lines drawn in Fig 9.11(b)]. It can be seen in Fig 9.12 that the intersections, Ψ', of the regression lines with the ln k axis are virtually constant in fact; Ψ' increases slightly from -3.84 to -2.25 with increase in m from 0 to 0.5 (see the legend for Fig 9.12). On the other hand, by using eq(9.20') [in which $\omega_{Mm}=0.0463$; see Fig 9.10(b)], it can be shown that the γ value estimated from Fig 9.12 is also almost independent of m, decreasing slightly with increase in m (i.e., when m=0, 0.1, 0.2, 0.3, 0.4 and 0.5, then $\gamma=0.594$, 0.590, 0.589, 0.587, 0.584 and 0.582, respectively).

It might be possible that the slight dependencies of both parameters Ψ' and γ on the m value arise from minor secondary mechanisms other than those of which account is taken in competition model, bringing about a slight dependence of the parameter φ on m [cf. Appendix XI(F) eq(A11.153) or (A11.153')]. It might be possible that both $\ln\beta$ [$=\Psi'$] and γ values obtained in the absence of competing substance when m=0 are the closest to the true vlues. A possibility cannot be excluded, however, that the slight dependences of both Ψ' and γ on m arise from a systematic experimental error.

Cf. Table 9.1 for all the arguments performed in this subsection.

Analysis of Fig 9.2. This is concerned with chromatpgraphies of polystyrenes with different M_m carried out on a C_{18} (10 nm pore) column in the presences of THF/H_2O and $MeCl_2$/ACN mobile phase systems. In Fig 9.2, however, the data for the 1.04×10^5, 3×10^5 and 2.8×10^6 Da polystyrenes in the THF/H_2O system, and those for the 3×10^5 Da

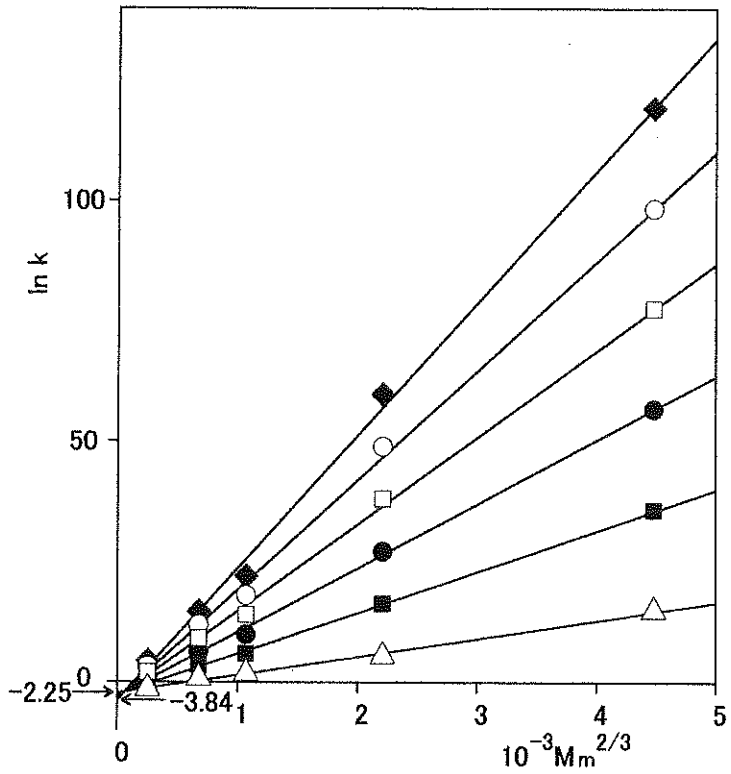


Fig 9.12. Points: plots of ln k versus $M_m^{2/3}$ for six constant m values [0(◆), 0.1 (○), 0.2(□), 0.3(●), 0.4(■), and 0.5(△)], obtained for five polystyrene samples with different M_m in the $MeCl_2$/ACN system (Fig 9.1 bottom). For the plots, the ordinates corresponding to each of the five polystyrene samples have been calculated for the six m values by using eq(9.11') in which both parameters $\hat{S}$ and $\hat{W}$ are characteristic of each sample; these are presented in the legend for Fig 9.1. The results of the calculations are as follow. For the sample with $M_m=4\times10^3$ Da or $M_m^{2/3}=252$, (m, ln k) = (0, 4.46), (0.1, 3.27), (0.2, 2.08), (0.3, 0.89), (0.4, −0.30) and (0.5, −1.49); for the sample with $M_m=1.75\times10^4$ Da or $M_m^{2/3}=$ 674, (m, ln k) = (0, 14.78), (0.1, 11.98), (0.2, 9.18), (0.3, 6.38), (0.4, 3.58) and (0.5, 0.78); for the sample with $M_m=3.5\times10^4$ Da or $M_m^{2/3}=$ 1070, (m, ln k) = (0, 22.13), (0.1, 18.09), (0.2, 14.05), (0.3, 10.01), (0.4, 5.97) and (0.5, 1.94); for the sample with $M_m=1.04\times10^5$ Da or $M_m^{2/3}=2212$, (m, ln k) = (0, 59.78), (0.1, 48.92), (0.2, 38.07), (0.3, 27.21), (0.4, 16.35) and (0.5, 5.50); and for the sample with $M_m=3\times10^5$ Da or $M_m^{2/3}=4481$, (m, ln k) = (0, 119.18), (0.1, 98.34), (0.2, 77.50), (0.3, 56.66), (0.4, 35.82) and (0.5, 14.99). Straight lines: regression lines of $M_m^{2/3}$ on ln k [eq(9.19)] for the arrangements of the experimental points, where (Ψ_{Mm}, Ψ') = (0.0275, −3.84) for m=0; (0.0227, −3.52) for m=0.1; (0.0180, −3.21) for m=0.2; (0.0133, −2.89) for m=0.3; (0.00852, −2.57) for m=0.4; and (0.00378, −2.25) for m=0.5.

polystyrene in the $MeCl_2$/ACN system are not used for the analysis. This is because the data for the 3×10^5 Da molecule in the $MeCl_2$/ACN system is abnormal in that the S value is smaller than that for the 1.04×10^5 Da molecule (see Fig 9.2 bottom). Lochmüller and McGranaghan(9.1) suggested that this arose from the pore exclusion (or gel filtration) effect [see Chapter I (A)] taking place only when M_m is extremely high. Both the arrangement of the experimental points and the corresponding regression line for the 1.04×10^5 Da molecule in the THF/H_2O system (Fig 9.2 top) are also abnormal for unknown reason. Further, it can be shown that the experimental $\hat{S}$ versus $M_m^{2/3}$ plots [cf. Fig 9.13 (b)] for both 3×10^5 and 2.8×10^6 Da molecules in the THF/H_2O system (Fig 9.2 top) deviate considerably from linearity toward low $\hat{S}$ values. This suggests that the pore exclusion also takes place in the THF/H_2O system when M_m is very high. The M_m, S, W, $\hat{S}$ and $\hat{W}$ values for the respective regression lines [eq(9.11) or (9.11'); estimated by the direct surveying of the diagram] are shown in the legend for Fig 9.2.

Fig 9.13 corresponds to Fig 9.10; the points(○ and □) in Fig 9.13(a) represent the plots of $\hat{S}$ (estimated from Fig 9.2) versus M_m for THF/H_2O and $MeCl_2$/ACN mobile phase systems, respectively. When the two plots are mapped to the $(M_m^{2/3}, \hat{S})$ plane, two approximately linear arrangements of the experimental points the extrpolation of which can, respectively, be assumed to pass through the origin are obtained [Fig 9.13(b)]. For either THF/H_2O or $MeCl_2$/ACN mobile phase system, the arrangenent of the experimental points on the $(M_m^{2/3}, \hat{S})$ plane can be represented by eq(9.12), or function $f_{Mm}(M_m)$ can be expressed by eq(9.13).

The two straight lines drawn in Fig 9.13(b) are the regression lines (passing through the origin) of $M_m^{2/3}$ on $\hat{S}$ [eq(9.12)] calculated for the two arrangements of the experimental points(○ and □), respectively. As the slopes of the regression lines, the parameters ω_{Mm} for THF/H_2O and $MeCl_2$/ACN mobile phase systems can be evaluated to be 0.161 and 0.0648, respectively [see eq(9.12)]. The two curves passing through the origin drawn in Fig 9.13(a) correspond to the two regression lines drawn in Fig 9.13(b).

Fig 9.14 corresponds to Fig 9.11; the points(○ and □) in Fig 9.14(a) represent the plots of $\hat{W}$ (estimated from Fig 9.2) versus M_m for THF/H_2O and $MeCl_2$/ACN mobile phase systems, respectively. When the two plots are mapped to the $(M_m^{2/3}, \hat{W})$ plane, two approximately linear arrangements of the experimental points with positive slopes are obtained [Fig 9.14(b)].

Two straight lines drawn in Fig 9.14(b) are the regression lines of $M_m^{2/3}$ on $\hat{W}$ with respect to the four points (○) and the four points(□) for THF/H_2O and $MeCl_2$/ACN systems, respectively. As the slopes, Φ_{Mm}, of the regression lines, $\gamma\,\omega_{Mm}$ for THF/H_2O and $MeCl_2$/ACN systems can be evaluated to be 0.148 and 0.0415, respectively. Correspondingly, the parameter γ can be evaluated to be $0.148/\omega_{Mm}=0.148/0.161=0.919$, and $0.0415/\omega_{Mm}=0.0415/0.0648=0.640$, respectively [see eq(9.17)]. On the other hand, as the intersection, Φ', with the $\hat{W}$ axis of the regression line, $\ln\beta$ for the THF/H_2O system can be evaluated to be -7.34, or the parameter β for that system can be evaluated

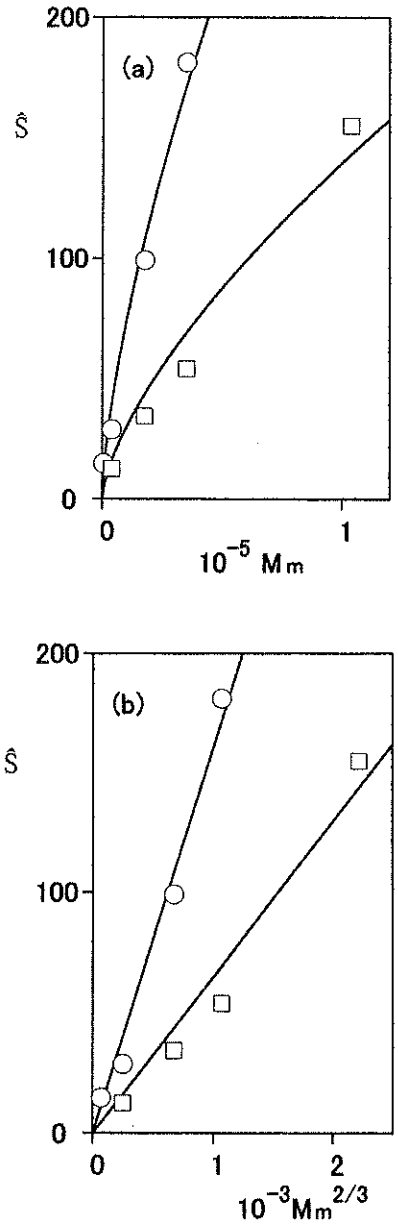


Fig 9.13. (a) Points(○ and □): experimental plots of $\hat{S}$ (obtained from Fig 9.2) versus M_m for C_{18} (10 nm pore) column THF/H_2O and $MeCl_2$/ACN mobile phase systems, reaspectively; the data for 1.04×10^5 Da, 3×10^5 Da and 2.6×10^6 Da polystyrenes in the THF/H_2O system and those for the 3×10^6 Da polystyrene in the $MeCl_2$/ACN system were eliminated. [The plots for the points(□) correspond to some parts of the plots presented in ref(9.1) Fig 4.] Curves: regression curves corresponding to the regression lines drawn in (b). (b) Points(○ and □): experimental plots of $\hat{S}$ versus $M_m^{2/3}$ for the corresponding points in (a). Straight lines: regression lines (passing through the origin) of $M_m^{2/3}$ on $\hat{S}$ for points(○ and □).

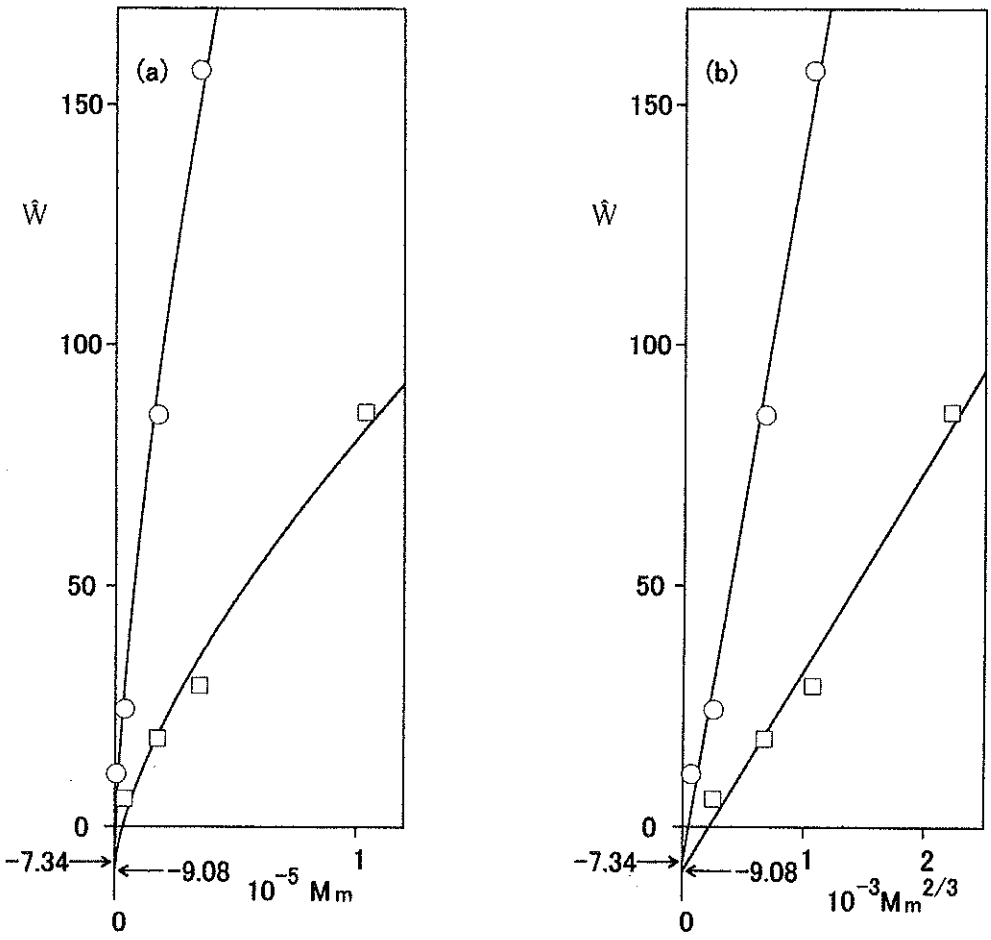


Fig 9.14. (a) Points(○ and □): experimental plots of $\hat{W}$ (obtained from Fig 9.2) versus M_m for C_{18} (10 nm pore) column THF/H_2O and $MeCl_2$/ACN mobile phase systems, respectively. Curves: regression curves corresponding to the regression lines drawn in (b). (b) Points(○ and □): experimental plots of $\hat{W}$ versus $M_m^{2/3}$ for the corresponding points in (a). Straight lines: regression lines of $M_m^{2/3}$ on $\hat{W}$ for points(○ and □).

to be 6.49×10^{-4}; $\ln\beta$ for the $MeCl_2$/ACN system can be evaluated to be -9.08, or the parameter β for that system can be evaluated to be 1.14×10^{-4} [see eq(9.18)]. As anticipated, the values of the parameter β estimated for the two systems are of the same order of magnitude, being much smaller than unity in fact. The two curves drawn in Fig 9.14(a) correspond to the two regression lines drawn in Fig 9.14(b)

Both Figs 9.15 and 9.16 correspond to Fig 9.12. Thus, in Fig 9.15, the five arrangements of five types of point, respectively, represent the plots of ln k versus $M_m^{2/3}$ for five constant m values (between 0 and 0.8), obtained for four polystyrene samples with different M_m in the THF/H_2O system (Fig 9.2 top). In Fig 9.16, the six arrangements of six types of point, respectively, represent the plots of ln k versus $M_m^{2/3}$ for six constant m values (between 0 and 0.5), obtained for four polystyrene samples with different M_m in the $MeCl_2$/ACN system (Fig 9.2 bottom). For the plots, the ordinates corresponding to each of the polystyrene samples have been calculated for the respective m values by using eq(9.11') in which both parameters $\hat{S}$ and $\hat{W}$ are characteristic of each sample; these are presented in the legend for Fig 9.2. It can be seen in both Figs 9.15 and 9.16 that all the arrangements of the experimental points are almost linear; the arrangements of the points for m=0 in both Figs 9.15 and 9.16 are identical with those taking place on the $(M_m^{2/3},\hat{W})$ plane [illustrated in Fig 9.14(b)].

The five straight lines drawn in Fig 9.15 and the six straight lines drawn in Fig 9.16 are the regression lines of $M_m^{2/3}$ on ln k [represented by eq(9.19)] for the arrangements of the experimental points. Both Ψ_{Mm} and Ψ' values for each of the regression lines are presented in the legends for Figs 9.15 and 9.16; the regression lines for m=0 are identical with those taking place on the $(M_m^{2/3},\hat{W})$ plane [illustrated in Fig 9.14(b)]. It can be seen in both Figs 9.15 and 9.16 that the intersection, Ψ', of the regression line with the ln k axis increases slightly but more rapidly than that taking place with the C_8 30 nm pore column $MeCl_2$/ACN system (Fig 9.12) with increase in m. [In Fig 9.15 (C_{18} 10 nm pore column THF/H_2O system), Ψ' increases from -7.34 to -2.11 with increase in m from 0 to 0.8, and, in Fig 9.16 (C_{18} 10 nm pore column $MeCl_2$/ACN system), Ψ' increases from -9.08 to -2.16 with increase in m from 0 to 0.5.] On the other hand, by using eq(9.20'), it can be shown that the γ values estimated from Figs 9.15 and 9.16 are almost independent of m, decreasing slightly with increase in m. [In Fig 9.15 [$\omega_{Mm}=0.161$; see Fig 9.13(b)], when m=0, 0.2, 0.4, 0.6 and 0.8, then $\gamma=0.919$, 0.908, 0.901, 0.891 and 0.881, respectively, and, in Fig 9.16 [$\omega_{Mm}=0.0648$; see Fig 9.13(b)], when m=0, 0.1, 0.2, 0.3, 0.4 and 0.5, then $\gamma=0.640$, 0.628, 0.614, 0.601, 0.587 and 0.573, respectively.]

It might be possible that the minor secondary mechanisms are more important with the C_{18} (10 nm pore) column than with the C_8 (30 nm pore) column because the dependences of both Φ' and γ on m occur to larger extents with the former column (cf. both Figs 9.15 and 9.16 with Fig 9.12). It might be possible that both $\ln\beta$ [$=\Psi'$] and γ values obtained in the absence of competing substance when m=0 are the closest to the

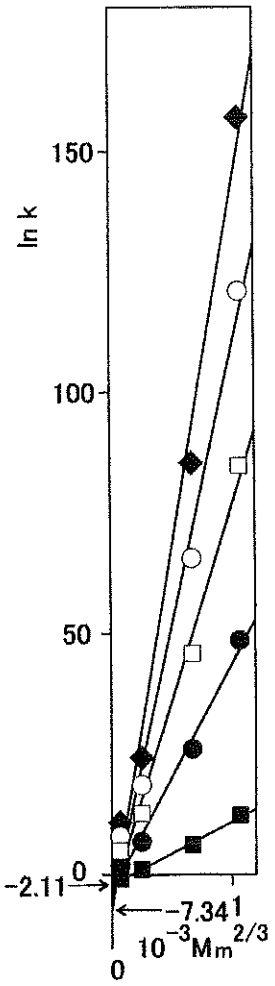


Fig 9.15. Points: plots of ln k versus $M_m^{2/3}$ for five constant m values [0(◆), 0.2 (○), 0.4(□), 0.6(●), and 0.8(■)], obtained for four polystyrene samples with different M_m in the THF/H_2O system (Fig 9.2 top). For the plots, the ordinates corresponding to each of the four polystyrene samples have been calculated for the five m values by using eq(9.11') in which both parameters $\hat{S}$ and $\hat{W}$ are characteristic of each sample; these are presented in the legend for Fig 9.2. The results of the calculations are as follow. For the sample with $M_m = 6\times10^2$ Da or $M_m^{2/3} = 71$, (m, ln k) = (0, 10.91), (0.2, 7.95), (0.4, 5.00), (0.6, 2.04) and (0.8, −0.91); for the sample with $M_m = 4\times10^3$ Da or $M_m^{2/3} = 252$, (m, ln k) = (0, 24.23), (0.2, 18.46), (0.4, 12.70), (0.6, 6.93) and (0.8, 1.17); for the sample with $M_m = 1.75\times10^4$ Da or $M_m^{2/3} = 674$, (m, ln k) = (0, 85.36), (0.2, 65.56), (0.4,45.76), (0.6, 25.95) and (0.8, 6.15); and for the sample with $M_m = 3.5\times10^4$ Da or $M_m^{2/3} = 1070$, (m, ln k) = (0, 157.08), (0.2, 120.90), (0.4, 84.71), (0.6, 48.53) and (0.8, 12.34). Straight lines: regression lines of $M_m^{2/3}$ on ln k [eq(9.19)] for the arrangements of the experimental points, where $(\Psi_{Mm}, \Psi') = (0.148, -7.34)$ for m=0; (0.114, −6.04) for m=0.2; (0.0806, −4.73) for m=0.4; (0.0469, −3.43) for m=0.6; and (0.0131, −2.11) for m=0.8.

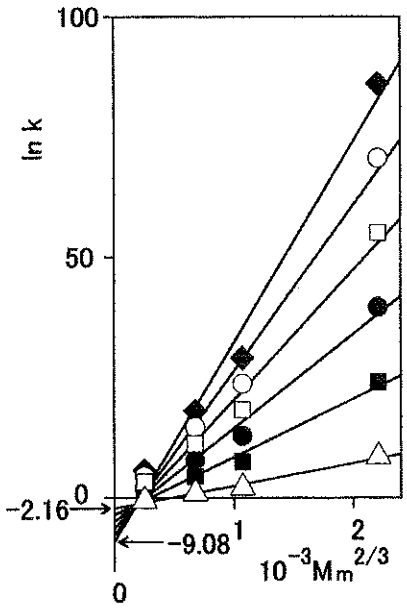


Fig 9.16. Points: plots of ln k versus $M_m^{2/3}$ for six constant m values [0(◆), 0.1 (○), 0.2(□), 0.3(●), 0.4(■), and 0.5(△)], obtained for four polystyrene samples with different M_m in the $MeCl_2$/ACN system (Fig 9.2 bottom). For the plots, the ordinates corresponding to each of the four polystyrene samples have been calculated for the six m values by using eq(9.11') in which both parameters $\hat{S}$ and $\hat{W}$ are characteristic of each sample; these are presented in the legend for Fig 9.2. The results of the calculations are as follow. For the sample with $M_m = 4\times10^3$ Da or $M_m^{2/3} = 252$, (m, ln k) = (0, 5.77), (0.1, 4.50), (0.2, 3.24), (0.3, 1.97), (0.4, 0.71) and (0.5, −0.56); for the sample with $M_m = 1.75\times10^4$ Da or $M_m^{2/3} = 674$, (m, ln k) = (0, 18.19), (0.1, 14.76), (0.2, 11.33), (0.3, 7.90), (0.4, 4.47) and (0.5, 1.04); for the sample with $M_m = 3.5\times10^4$ Da or $M_m^{2/3} = 1070$, (m, ln k) = (0, 29.18), (0.1, 23.78), (0.2, 18.39), (0.3, 12.99), (0.4, 7.59) and (0.5, 2.20); and for the sample with $M_m = 1.04\times10^5$ Da or $M_m^{2/3} = 2212$, (m, ln k) = (0, 85.97), (0.1, 70.50), (0.2, 55.02), (0.3, 39.55), (0.4, 24.08) and (0.5, 8.61). Straight lines: regression lines of $M_m^{2/3}$ on ln k [eq(9.19)] for the arrangements of the experimental points, where $(\Psi_{M_m}, \Psi') = (0.0415, -9.08)$ for m=0; (0.0342, −7.70) for m=0.1; (0.0268, −6.31) for m=0.2; (0.0195, −4.93) for m=0.3; (0.0121, −3.54) for m=0.4; and (0.00472, −2.16) for m=0.5.

true vlues. A possibility cannot be excluded, however, that these dependencies arise from systematic experimental errors.

Cf. Table 9.1 for all the arguments performed in this subsection.

Summary of the Important Results Obtained from the Analyses of Both Figs 9.1 and 9.2. These are summarized in Table 9.1 (where all the columns are numbered in connection with the numberings made in Tables 9.4, 9.7-9.12). Let us first pay attention to Table 9.1 column<8a>, where the β values estimated for both C_8 (30 nm pore) and C_{18} (10 nm pore) columns are presented; these can be compared with the corresponding value of the order of magnitude of 10^{-2} deduced for the HA column [see Chapter Ⅷ(E)]. It can be seen in Table 9.1 column<8a> that the β value estimated for the C_8 (30 nm pore) column is about 30 [i.e., $2.15\times10^{-2}/(6.49\times10^{-4})$] to 190 [i.e., $2.15\times10^{-2}/(1.14\times10^{-4})$] times as large as those estimated for the C_{18} (10 nm pore) column. This implies that the ratio of the effective total area of the adsorbent surface to the total interstitial volume in a slice of the C_8 (30 nm pore) column is 30 to 190 times as large as that for theC_{18} (10 nm pore) column [see eq(8.50) for the physical meaning of β]. Especially with concentration gradient chromatography with small sample loads (when the mutual interaction between sample molecules is negligible), however, it can be considered that such a large difference of the β values does not bring about a considerable difference in properties of the column (from a practical point of view). With HA chromatography, this consideration can be confirmed directly from Figs 9, 10, 12 and 13 in ref(7.1), where the chromatographic behaviors of several proteins on the columns packed with HA particles with extremely different external crystal shapes are compared; only slight differences were observed.

It can be seen in Table 9.1 column<1a> or <1> that the "relative size" per unit M_m, $x'\varphi/M_m^{2/3}$, or the "relative size" per monomer unit $x'\varphi/P^{2/3}$, taking place on the adsorbent surface with the THF/H_2O system is more than twice as large as that with the $MeCl_2$/ACN system with both C_8 (30 nm pore) and C_{18} (10 nm pore) columns. On the other hand, $x'\varphi/M_m^{2/3}$ or $x'\varphi/P^{2/3}$ for the C_{18} (10 nm pore) column is less than 1.5 times as large as that for the C_8 (30 nm pore) column with both THF/H_2O and $MeCl_2$/ACN systems (Table 9.1 column<1a> or <1>).

The quantities $J/M_m^{2/3}$ and $J/P^{2/3}$ represent the AVFA per unit M_m and the AVFA per monomer unit, respectively; the free energy of adsorption can be assumed to be equal to the energy of adsorption approximately. It can be seen in Table 9.1 column<5a> and <5> that $J/M_m^{2/3}$ or $J/P^{2/3}$ for the THF/H_2O system is about 3.5 times as large as that for the $MeCl_2$/ACN system with both C_8 (30 nm pore) and C_{18} (10 nm pore) columns. On the other hand, $J/M_m^{2/3}$ or $J/P^{2/3}$ for the C_{18} (10 nm pore) column is about 1.5 times as large as that for the C_8 (30 nm pore) column with both THF/H_2O and $MeCl_2$/ACN systems (Table 9.1 coumn<5a> and <5>). All the $J/P^{2/3}$ values (ranging between 1.51 and 8.13 kJ/mol; Table 9.1 column<5>) are comparable with the absolute value of energy of adsorption for a univalent phosphate group on a C site (3.8-4.2 kJ/mol), that for an ε-amino group on a P site (8.4-9.2 kJ/mol), and that for a carboxyl group on a C site (2.9 kJ/

Table 9.1

Summary of the analysis of the experiments of high M_m polystyrenes in THF/H_2O and $MeCl_2$/ACN mobile phase systems on C_8 and C_{18} columns carried out by Lochmüler and and McGranaghan(Figs 9.1 and 9.2). The value of kT at 25℃ (2.48 kJ/mol) is used for the analysis.

	⟨1a⟩	⟨1⟩	⟨4a⟩	⟨4⟩	
Column and Mobile Phase System	$\omega_{Mm} = x'\varphi/M_{Mm}^{2/3}$	$\omega_P = x'\varphi/P^{2/3} = 22.13\,\omega_{Mm}$	$\Phi_{Mm} = \gamma\,\omega_{Mm} = J/(M_{Mm}^{2/3}kT)$	$\Phi_P = \gamma\,\omega_P = J/(P^{2/3}kT) = 22.13\,\Phi_{Mm}$	
C_8 (30nm) THF/H_2O Fig 9.1 top	0.108	2.39	0.0958	2.12	⇒
C_8 (30nm) $MeCl_2$/ACN Fig 9.1 bottom	0.0463	1.02	0.0275	0.609	⇒
C_{18} (10nm) THF/H_2O Fig 9.2 top	0.161	3.56	0.148	3.28	⇒
C_{18} (10nm) $MeCl_2$/ACN Fig 9.2 bottom	0.0648	1.43	0.0415	0.918	⇒

	⟨5a⟩	⟨5⟩	⟨6⟩	⟨7⟩	
	$\gamma\ \omega_{Mm}kT = J/M_{Mm}^{2/3}$ (kJ/mol)	$\gamma\ \omega_P kT = J/P^{2/3}$ (kJ/mol)	$\gamma = \gamma\ \omega_{Mm}/\omega_{Mm} = \gamma\ \omega_P/\omega_P$	$\gamma\ kT = J/(x'\varphi)$	
⇒	0.238	5.26	0.887	2.20	⇒
⇒	0.0682	1.51	0.594	1.47	⇒
⇒	0.367	8.13	0.919	2.28	⇒
⇒	0.103	2.28	0.640	1.59	⇒

	⟨8⟩	⟨8a⟩	⟨12⟩	⟨13a⟩	⟨13⟩
	$\Phi' = \ln\ \beta$	$\exp(\ln\ \beta) = \beta$	φ	$x'/M_{Mm}^{2/3}$	$x'/P^{2/3}$
⇒	(-3.84)	(2.15×10^{-2})	$\lesssim 0.56$	$\gtrsim 0.19$	$\gtrsim 4.3$
⇒	-3.84	2.15×10^{-2}	$\lesssim 0.83$	$\gtrsim 0.056$	$\gtrsim 1.2$
⇒	-7.34	6.49×10^{-4}	$\lesssim 0.56$	$\gtrsim 0.29$	$\gtrsim 6.4$
⇒	-9.08	1.14×10^{-4}	$\lesssim 0.83$	$\gtrsim 0.078$	$\gtrsim 1.7$

(cont.) **Table 9.1**

mol) of HA, respectively [see Chapter Ⅷ(E)]. [*Note.* As for low M_m (1.5×10^3 to 8×10^3 Da) poly-L-lysine with a highly-stretched conformation on the HA surface, it can be assumed that, of all the fuctional groups that are present on the local molecularar surface facing the adsorbent surface, only some number can react with the adsorbing sites arranged discretely on the surface; it is necessary that the functinal group be superposed precicely enough on the crystal adsorbing site for the chemical bond to be formed [see the subsection entitled "Adsorption Energy of ε-Amino Group on A P Site" in Chapter Ⅷ(E)]. As for the collagen molecule on the HA surface, however, it can be assumed that virtually all the fuctional groups that are present on the local molecar surface facing the adsorbent surface can react with the adsorbing sites [Chapter Ⅷ(F)]. With reversed-phase chromatography, we have no knowledge about how many functional groups that are present on the local molecular surface facing the adsorbent surface are superposable well on adsorbing sites (i.e., C_8 or C_{18} structures); $J/P^{2/3}$ only represents the average of the ΛVFΛ assigned to a monomer unit that is present on the molecular surface facing the adsorbent surface. It, however, is reasonable to consider that, on the reversed-phase surface, the geometrical arrangement of the flexible C_8 or C_{18} structures can fluctuate to a considerable extent around the mean arrangement in order for a large number of functional groups that are present on the molecular surface facing the adsorbent surface to be superposed well on the structures [cf. the subsection entitled "Ion-Exchange and Reversed-Phase Chromatographies in Contrast to HA Chromatography" in Chapter Ⅷ(E)]. Further both C_8 and C_{18} structures are large in size. These suggest that the situation takes place as if C_8 or C_{18} structures cover continuously over the total adsorbent surface, and that a very large proportion of functional groups that are present on the molecular surface facing the adsorbent surface are participating in the reaction with C_8 or C_{18} structures actually.]

In the fundamental equation, eq(9.1), both parameters x' and φ are present while forming a product, so that it is impossible to estimate the individual x' and φ values. In order for eq(9.1) to hold precisely or for a precisely linear arrangement of the experimental log k versus m plots to be obtained, however, it is necessary that the term φ m be negligibly small compared with unity [see Chapter Ⅷ(H)]. Let us assume that the upper limit, $(\varphi\ m)_{u.l.}$, of the φ m value that brings about *practically* linear arrangements of the experimental points is 0.5. It can be seen in both Figs 9.1 and 9.2 that the maximum m value used for the experiment is lower than 0.9 and 0.6 with THF/H_2O and $MeCl_2$/ACN systems, respectively. The upper limits of the possible φ values for THF/H_2O and $MeCl_2$/ACN systems can be estimated to be $0.5/0.9=0.56$ and $0.5/0.6=0.83$, respectively (Table 9.1 column<12>). By using the values presented in Table 9.1 column <1a> and <1>, the lower limits of $x'/M_m^{2/3}$ and $x'/P^{2/3}$ can be evaluated, respectively; these are presented in Table 9.1 column<13a> and <13>. [*Note.* In the ln k versus $m_{(K^+)}$ plots for lysozyme with HA chromatography [Fig 8.3(d)], $m_{(K^+)}$ is comprised between 0.05 and 0.3 M, from which it can be estimated that the range of the φ $m_{(K^+)}$ values used for the experiment is between 1.25 and 7.5 since $\varphi = 25\ M^{-1}$. In this instance, the arrangement of the experi-

mental points on the ($m_{(K)}$, ln k) plane is slightly convave in shape; seeFig 8.3(d).]

Further Consideration. It would be reasonable to assume that, on the C_8 or C_{18} surface, an adsorbing site (a C_8 or C_{18} structure) is present per area of the order of magnitude of nm^2, and that a competing substance (THF or $MeCl_2$) occupies approximately a single site when it is adsorbed. Under this assumption, the parameter x' has a meaning of the area (expressed in units of nm^2) of the adsorbent surface occupied by an adsorbed polystyrene molecule. Further, it would be reasonable to assume that x' is of the order of magnitude of the area, $\pi (R_e)_{sd}^2$, of the great circle of the equivalent sphere of polystyrene adsorbed on the C_8 or C_{18} surface, where $(R_e)_{sd}$ stands for the radius of the equivalent sphere. By using the values presented in Table 9.1 column<13a>, it can be estimated that

$$\pi (R_e)_{sd}^2/M_m^{2/3} \gtrsim 0.19 \text{ to } 0.29 \tag{9.22}$$

for the THF/H_2O system, and that

$$\pi (R_e)_{sd}^2/M_m^{2/3} \gtrsim 0.056 \text{ to } 0.078 \tag{9.22'}$$

for the $MeCl_2$/ACN system. Eq(9.22) or (9.22') can be compared with the case of lysozyme adsorbed on the HA surface. Thus, lysozyme with M_m of 1.43×10^4 Da can be represented approximately by a prolate spheroid of $4.5\times3\times3$ nm (see Fig 8.4). Denoting by A the area (expressed in units of nm^2) of the HA surface occupied by an adsorbed lysozyme molecule, it can be estimated that $A/M_m^{2/3}\approx\pi\times(4.5/2)\times(3/2)/(1.43\times10^4)^{2/3}=10.6/591=0.018$ (where it has been assumed that the molecule is adsorbed in such a way that x' is maximized). This means that the lower limits of the $\pi (R_e)_{sd}^2/M_m^{2/3}$ values for polystyrene in THF/H_2O and $MeCl_2$/ACN systems are 11 to 16 times [see eq(9.22)] and 3 to 4 times [see eq(9.22')] as large as the $A/M_m^{2/3}$ value for lysozyme, respectively. This is a reasonable conclusion because the molecular conformation of lysozyme in the native state is very compact.

A study on the conformation of polystyrene dissolved in THF (at 23℃) was performed by Boni et al.(9.15). The five points in Fig 9.17(a) represent the $\log_{10}(4\pi R_e^3/3)$ versus $\log_{10}M_m$ plots (where R_e stands for the radius of the equivalent hydrodynamic sphere of polystyrene in solution) obtained by combining ref(9.15) eq(7) with the five data for polystyrene dissolved in THF [presented in ref(9.15) Table I], where it can be seen that the arrangement of the experimental points is almost linear. The straight line drawn in Fig 9.17(a) is the regression line of $\log_{10}M_m$ on $\log_{10}(4\pi R_e^3/3)$ for the five experimental points; this can be represented as

$$\log_{10}(4\pi R_e^3/3) = 1.76\log_{10}M_m - 5.33 \tag{9.23}$$

or

$$4\pi R_e^3/3 = 4.68\times10^{-6} M_m^{1.76} \tag{9.23'}$$

The five points and the curve [eq(9.23')] presented in Fig 9.17(b) correspond to the five points and the regression line [eq(9.23)] presented in Fig 9.17(a); these have been mapped

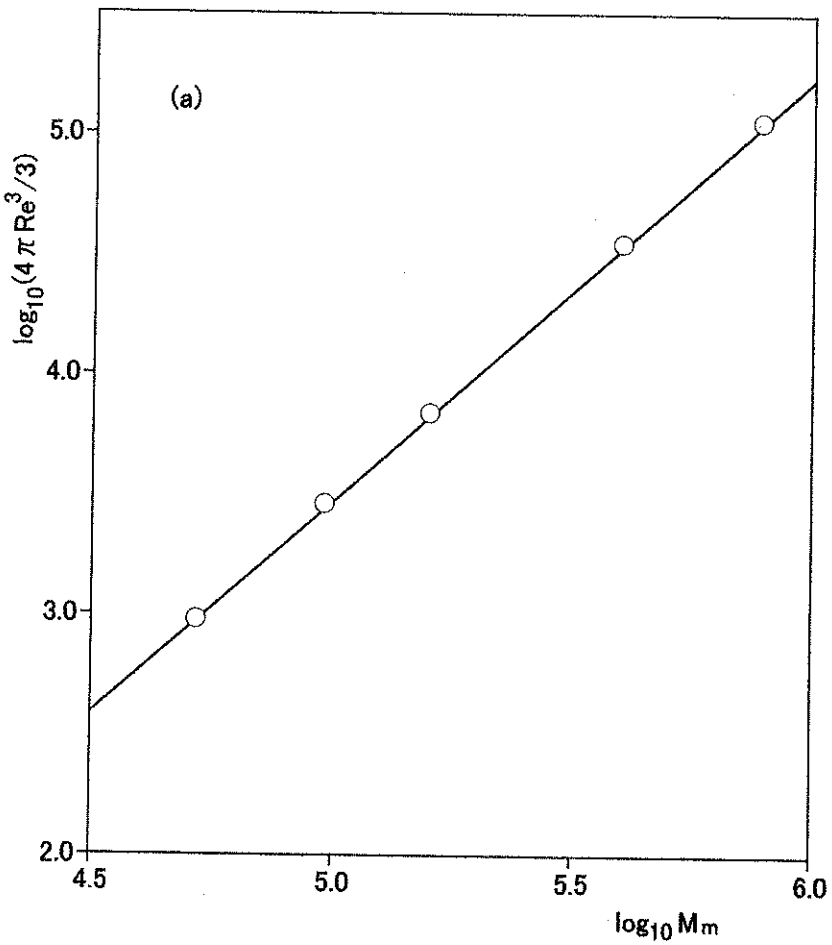


Fig 9.17. (a) Points: experimental plots of $\log_{10}(4\pi R_e^3/3)$ versus $\log_{10} M_m$ for polystyrene dissolved in THF at 23℃. Straight line: regression line of $\log_{10} M_m$ on $\log_{10}(4\pi R_e^3/3)$ for the five experimental points. (b) As (a) mapped to the $(M_m, 4\pi R_e^3/3)$ plane. (c) As (a) mapped to the $(M_m^{2/3}, \pi R_e^2/M_m^{2/3})$ plane.

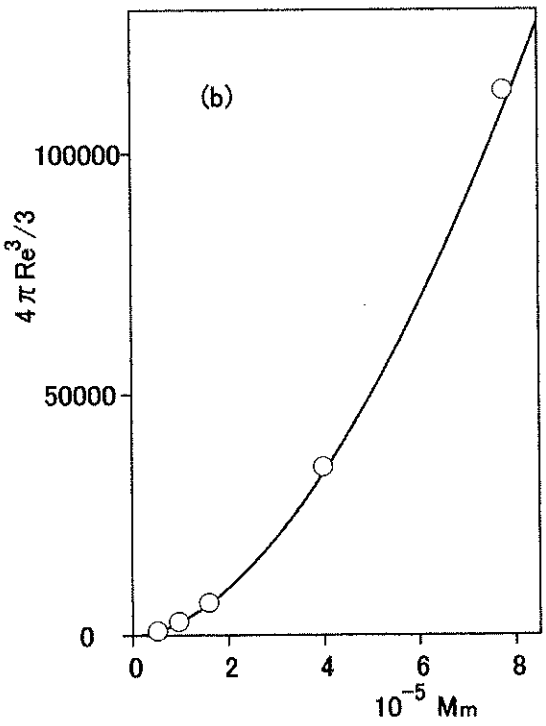


Fig 9.17. (b)

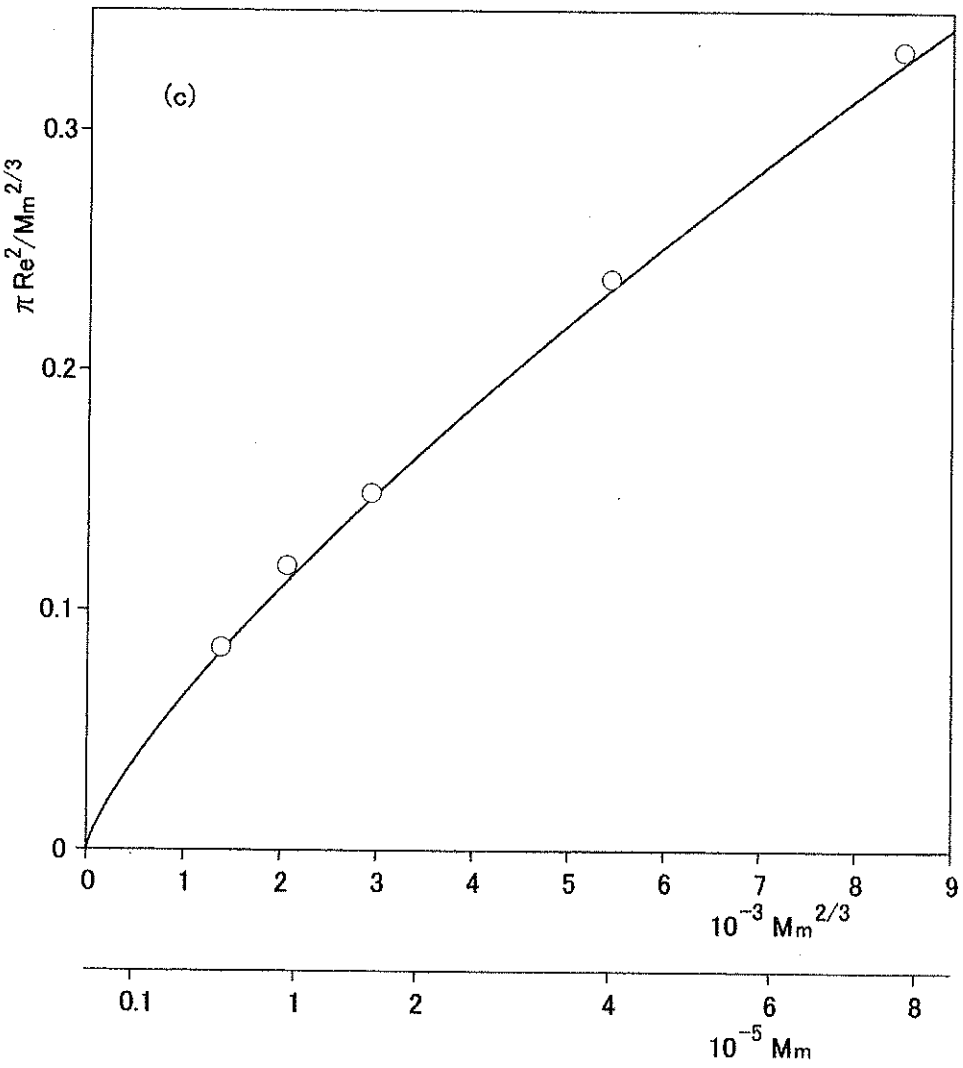


Fig 9.17. (c)

to the (M_m, $4\pi R_e^3/3$) plane. The fact that the effective volume of polystyrene in solution is proportional to the 1.76 power of M_m [eq(9.23'); Fig 9.17(b)] is parallel to the behaviors of a number of polymer-solvent systems manifestung that R_e^3, in general, is proportional to the approximately 1.7 power of M_m [cf. ref(9.15)]. This can be compared with the case of polystyrene adsorbed on the C_8 or C_{18} surface when it can be assumed that $4\pi(R_e)_{ad}^3/3$ is proportional to M_m [see Section(B)].

Eq(9.23') leads to

$$\pi R_e^2/M_m^{2/3} = 3.39\times10^{-4}(M_m^{2/3})^{0.76} \qquad (9.23'')$$

The five points and the curve [eq(9.23")] presented in Fig 9.17(c) correspond to those presented in either Fig 9.17(a) or (b); these have been mapped to the ($M_m^{2/3}$, $\pi R_e^2/M_m^{2/3}$) plane. Eq(9.23") can be compared with both eqs(9.22) and (9.22'). The M_m of polystyrene samples used for the analyses of the THF/H_2O chromatographic systems (Fig 9.1 top and Fig 9.2 top) ranges between 6×10^2 and 3.5×10^4 Da. Assuming that the conformation of polystyrene dissolved in THF is the same as that taking place in solution in the THF/H_2O mobile phase system, and by comparing either eq(9.22) or (9.22') with eq(9.23") or the curve drawn in Fig 9.17(c), it can be concluded that the polystyrene molecules (with M_m between 6×10^2 and 3.5×10^4 Da) that are adsorbed on the C_8 or C_{18} surface are much more swollen than those in solution or in the mobile phase.

With respect to reversed-phase chromatography of 1.75×10^4 Da polystyrene carried out on a C_{18} column by using the THF/H_2O mobile phase system, Stadalius et al. [ref (9.3) Appendices I and II] mentions that, *under adsorptive conditions*, the experimental data are compatible with the assumption that there is no exclusion effect of the molecules from pores as small as 6 nm in diameter, whereas the exclusion may take place *under non-adsorptive conditions*. By using eq(9.23') or Fig 9.17, it can be estimated that the diameter, $2R_e$, of the equivalent hydrodynamic sphere of the 1.75×10^4 Da polystyrene molecule dissolved in THF is 6.1 nm; this is almost equal to the lower limit, 6 nm, of the pore diameter on the C_{18} surface at which the molecular exclusion does not occur any more. In order for a molecule to penetrate freely without an exclusion effect, it would be necessary that its effective diameter be much smaller than 6 nm, and, for this to occur, it would be indispensable that the molecular conformation be hydrodynamically very flexible especially when the molecule stays on the C_{18} surface. It can be considered that this deduction is compatible with the conclusion obtained above that the polystyrene molecule in the adsorbed state is much more swollen than that in solution because the molecule should be hydrodynamically more flexible when it is swollen than when it is in the compact state. It should ne noted that the concept of the effectively small *diameter* of the molecule acquired when the molecular conformation is hydrodynamically flexible is qualitatively different from the concept of the *diameter* of the molecule in the swollen state taking place on the adsorbent surface. This latter is a concept with respect to the equilibrium state generating a high x' value. Cf. ref(9.3) Appendices I and II, and also cf. both

refs(9.16) and (9.17) for related problems.

(D) Analysis of the Experiment of Terabe et al.

Below is performed the analysis of Fig 9.6 for isocratic chromatographies of benzene and four peptides (or proteins) carried out on a C_{18} column in the presence of the ACN/ 0.005 M phosphate buffer (pH 3.0) mobile phase system (containing 0.1 M sodium sulphate). The regression line for the arrangement of the experimentl points for any molecule can be represented by eq(9.11) or (9.11'). The M_m, S, W, $\hat{S}$ and $\hat{W}$ values for the respective regression lines (estimated from the direct surveying of the diagram) are presented in the legend for Fig 9.6.

The points(△ and ○) in Fig 9.18(a) represent the plots of $\hat{S}$ (estimated from Fig 9.6) versus M_m for benzene and for four peptides (or proteins), respectively. As Terabe et al.(9.6) pointed out, it can be seen in Fig 9.18(a) that the points(○) for the four peptides or proteins give an almost linear arrangement. It appears, however, that the extrapolation of the linear arrangement intersects the $\hat{S}$ axis at a positive finite value rather than at the origin [see Fig 9.18(a)]. If it a priori is demanded that the extrapolation of the arrangement of the four points under consideration should pass through the origin, it would be reasonable to assume that the arrangement is concave in the total shape.

The points(△ and ○) in Fig 9.18(b) correspond to those plotted in Fig 9.18(a); these are mapped to the $(M_m^{2/3}, \hat{S})$ plane. It now appears that the points(○) for the four peptides or proteins give an almost linear arrangement the extrapolation of which passses through the origin. The straight line drawn in Fig 9.18(b) is the regression line (passing through the origin) of $M_m^{2/3}$ on $\hat{S}$ [eq(9.12)] for the arrangement of the four experimental points(○); the slope, ω_{Mm}, of the regression line can be evaluated to be 0.250. [The regression line for the arrangement of the five experimental points obtained with addition of the point(△) is almost identical with that obtained only for the four points(○), giving rise to the same value of ω_{Mm} (composed of three significant figures of the decimal fraction).] The curve (with a convex shape) drawn in Fig 9.18(a) corresponds to the regression line drawn in Fig 9.18(b).

In Fig 9.19, the points(△ and ○) represent the plots of $\hat{W}$ (estimated from Fig 9.6) versus $M_m^{2/3}$ for benzene and for four peptides (or proteins), respectively, and the straight line represents the regression line of $M_m^{2/3}$ on $\hat{W}$ [eq(9.15)] with respect to the four points(○). As the slope of the regression line, the "average" of $\gamma\,\omega_{Mm}$ can be evaluated to be 0.0944, or the "average" value of the parameters γ for the four peptides (or proteins) can be estimated to be $0.0944/\omega_{Mm}=0.0944/0.250=0.378$ [cf. both eq(9.15) and (9.17)]. On the other hand, as the intersection of the regression line with the $\hat{W}$ axis, the approximate value, -7.36, of $\ln\beta$ can be obtained [cf. both eq(9.15) and (9.18)]. Supprisingly, this value is included in the range between -9.09 and -7.34 of the $\ln\beta$ values estimated for another C_{18} column by using "homologous" polystyrene molecules (see

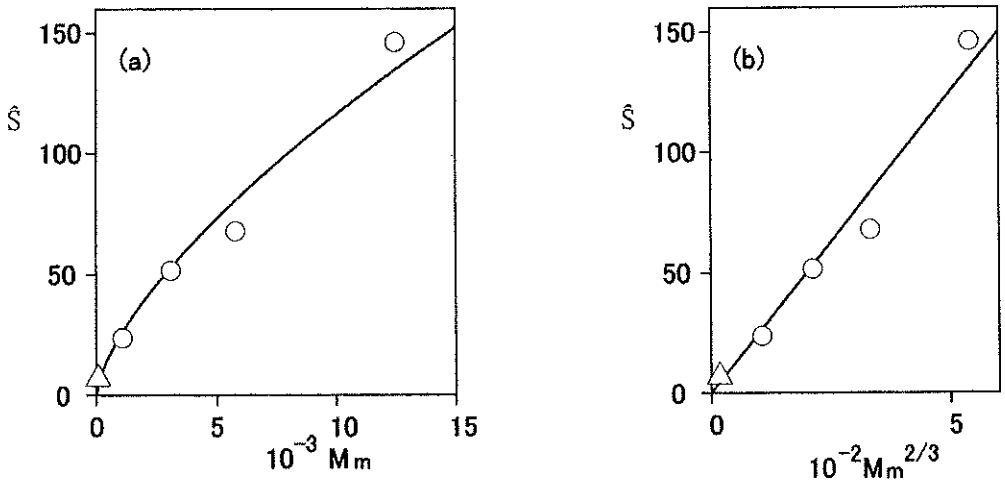


Fig 9.18. (a) Points(△ and ○): experimental plots of $\hat{S}$ (estimated from Fig 9.6) versus M_m for benzene(△) and four peptides or proteins(○) for a C_{18} column in the presence of the ACN/0.005 M phosphate buffer (pH 3.0) mobile phase system (containing 0.1 M sodium sulphate). Curve: regression curve corresponding to the regression line drawn in (b). (b) Points(△ and ○): experimental plots of $\hat{S}$ versus $M_m^{2/3}$ for the corresponding points in (a). Straight line: regression line (passing through the origin) of $M_m^{2/3}$ on $\hat{S}$ only for the four points(○). If the point(△) is added, virtually the same regression line can be calculated.

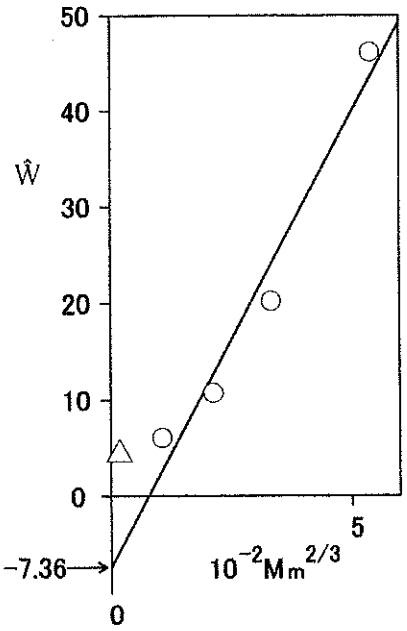


Fig 9.19. Points(△ and ○): experimental plots of $\hat{W}$ (estimated from Fig 9.6) versus $M_m^{2/3}$ for benzene(△) and four peptides or proteins(○) for a C_{18} column in the presence of the ACN/0.005 M phosphate buffer (pH 3.0) mobile phase system (containing 0.1 M sodium sulphate). Straight line: regression line of $M_m^{2/3}$ on $\hat{W}$ only for the four points (○).

Fig 9.14). It perhaps is rather fortuitous that such a reasonable $\ln\beta$ value was obtained by using non-homologous peptides or proteins. It perhaps happened that the γ values for the peptides or proteins under investigation do not fluctuate so much, and/or that the fluctiation occurs symmetrically around the average.

(E) Analysis of the Experiment of Larmann et al.

Experiment. Larmann et al.(9.4) carried out isocratic chromatographies of relatively low M_m polystyrenes (with P ranging between 2 and 12, or M_m between 208 and 1050 Da) on three types of C_{18} column (with 6, 15 and 30 nm pores, respectively) in the presence of the THF/H_2O mobile phase system while changing volume fraction, m, of THF at 23℃. [In ref(9.4), the experiment was also done on the C_{18} column with 100 nm pore. We do not here analyse this experiment since it was done only for a single m value.] The $\log_{10}$ k values obtained for a number of combinations of both m and P values for the three types of C_{18} column are summarized in ref(9.4) Table Ⅲ. These are reproduced in Tables 9.2(a)-(c) with conversion of $\log_{10}$ k to ln k.

The points in Figs 9.20(a), 9.21(a) and 9.22(a) represent the plots of ln k (Table 9.2) versus m for polystyrenes with eleven different degrees of polymerization, P, for 6, 15 and 30 nm pore columns, respectively, where it can be seen that the arangement of the exerimental points (for the molecule with any P value) is quite linear with a negative slope. The points in Figs 9.20(b), 9.21(b) and 9.22(b) represent the plots of ln k (Table 9.2) versus P for different m values for 6, 15 and 30 nm pore columns, respectively, where it can be seen that the arangement of the exerimental points for a constant m value, in general, is slightly convex in shape with positive tangential slopes.

The regression line of m on ln k for the arrangement of the experimental points for the molecule with any P value [Figs 9.20(a), 9.21(a) and 9.22(a)] can be represented by eq(9.11'), and the $\hat{S}$ and $\hat{W}$ values for all the regression lines are presented in the last two columns in Tables 9.2(a)-(c). The straight lines drawn in Figs 9.20(a), 9.21(a) and 9.22(a) represent these regression lines.

The points (○, □ and △) in Fig 9.23(a) represent the plots of $\hat{S}$ (Table 9.2) versus P for 6, 15 and 30 nm pore columns, respectively. Fig 9.23(b) corresponds to Fig 9.23(a), where the plots of $\hat{S}$ are done versus $P^{2/3}$ instead of P. It can be seen in either Fig 9.23(a) or (b) that the arrangement of the experimental points is almost independent of the pore size of the adsorbent. In contrast to the case of high M_m polystyrenes [Figs 9.10(a), 9.10(b), 9.13(a) and 9.13(b)], however, it now is difficult to represent the arrangement of the experimental points on the $(P, \hat{S})$ plane [Fig 9.23(a)] by using eq(9.9) in which $x'\varphi = \hat{S}$ and where function $f_{Mm}(M_m)$ or $f_P(P)$ is represented by a single term proportional to any power of M_m or P [cf. both eqs(9.12) and (9.13)].

The points (○, □ and △) in Fig 9.24(a) represent the plots of $\hat{W}$ (Table 9.2) versus P for 6, 15 and 30 nm pore columns, respectively. Fig 9.24(b) corresponds to Fig

Table 9.2

Reproduction of the experimental data obtained by Larmann et al.[ref(9.4) Table Ⅲ], and both $\hat{S}$ and $\hat{W}$ values calculated from the data. The experimental data are here represented as ln k values obtained from a number of combinations of both m and P values. (a), (b) and (c) represent the data for C_{18} columns with 6, 15 and 30 nm pores, respectively.

(a) 6 nm pore column

P	$P^{2/3}$	$(P-2)^{2/3}$	ln k for m (vol/vol) =				$\hat{S}$	$\hat{W}$
			0.70	0.72	0.75	0.78		
2	1.59	0	0.62	0.41	0.09	−0.23	10.63	8.06
3	2.08	1	0.85	0.62	0.28	−0.07	11.48	8.89
4	2.52	1.59	1.08	0.83	0.44	0.07	12.67	9.95
5	2.92	2.08	1.29	1.01	0.60	0.21	13.50	10.74
6	3.30	2.52	1.47	1.20	0.74	0.32	14.50	11.62
7	3.66	2.92	1.68	1.36	0.90	0.44	15.47	12.50
8	4.00	3.30	1.84	1.52	1.01	0.55	16.22	13.19
9	4.33	3.66		1.68	1.15	0.64	17.33	14.16
10	4.64	4.00		1.82	1.27	0.76	17.67	14.53
11	4.95	4.33			1.38	0.83	18.33	15.13
12	5.24	4.64			1.50	0.94	18.67	15.50

(b) 15 nm pore column

P	$P^{2/3}$	$(P-2)^{2/3}$	ln k for m (vol/vol) =					$\hat{S}$	$\hat{W}$
			0.65	0.68	0.70	0.72	0.75		
2	1.59	0	0.69	0.39	0.18	−0.05	−0.37	10.66	7.63
3	2.08	1	0.94	0.62	0.39	0.16	−0.21	11.50	8.43
4	2.52	1.59	1.22	0.83	0.60	0.35	−0.05	12.60	9.41
5	2.92	2.08	1.45	1.06	0.81	0.53	0.12	13.29	10.10
6	3.30	2.52	1.68	1.22	0.94	0.64	0.21	14.67	11.21
7	3.66	2.92	1.89	1.40	1.11	0.78	0.32	15.67	12.07
8	4.00	3.30	2.10	1.57	1.24	0.92	0.44	16.55	12.84
9	4.33	3.66		1.75	1.40	1.06	0.55	17.12	13.39
10	4.64	4.00		1.91	1.54	1.20	0.67	17.65	13.90
11	4.95	4.33		2.07	1.70	1.31	0.71	19.47	15.32
12	5.24	4.64				1.45	0.87	19.33	15.37

(cont.) **Table 9.2**

(c) 30 nm pore column

P	$P^{2/3}$	$(P-2)^{2/3}$	ln k for m (vol/vol) =				$\hat{S}$	$\hat{W}$
			0.63	0.65	0.68	0.70		
2	1.59	0	−0.09	−0.30	−0.62	−0.78	9.98	6.19
3	2.08	1	0.21	−0.05	−0.37	−0.58	11.19	7.24
4	2.52	1.59	0.46	0.21	−0.21	−0.39	12.43	8.28
5	2.92	2.08	0.71	0.41	0.02	−0.23	13.36	9.11
6	3.30	2.52	0.92	0.62	0.18	−0.07	14.22	9.87
7	3.66	2.92	1.13	0.81	0.35	0.07	15.17	10.68
8	4.00	3.30	1.31	0.99	0.48	0.21	15.91	11.33
9	4.33	3.66	1.50	1.15	0.64	0.35	16.57	11.89
10	4.64	4.00	1.68	1.31	0.78	0.46	17.47	12.67
11	4.95	4.33	1.84	1.45	0.92	0.58	17.95	13.13
12	5.24	4.64	2.03	1.63	1.04	0.69	19.22	14.13

(cont.) **Table 9.2**

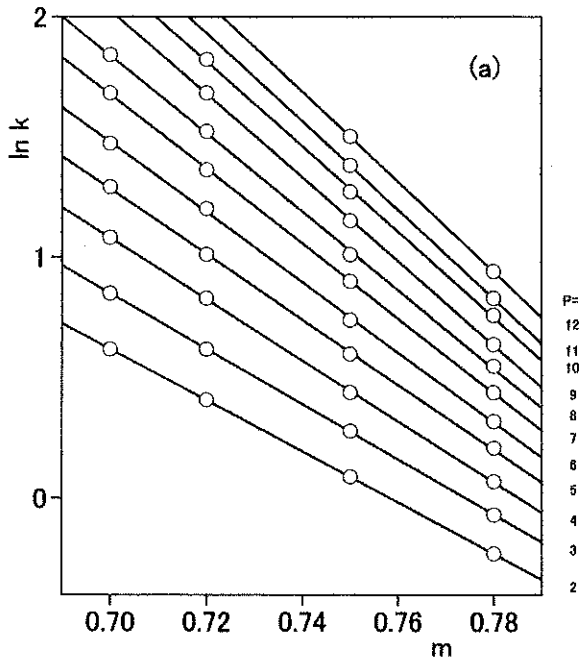


Fig 9.20. ln k [Table 9.2(a)] as a function of both volume fraction, m, of THF and degree of polymerization, P, of polystyrene, obtained for isocratic chromatography carried out on a C_{18} (6 nm pore) column in the presence of THF/H_2O mobile phase systems with different m values. (a) Points: plots of ln k versus m for different P values. Straight lines: regression lines [eq(9.11')] of m on ln k for the arrangements of the experimental points for respective P values; the $\hat{S}$ and $\hat{W}$ values for all the regression lines are presented in Table 9.2(a). (b) Points: plots of ln k versus P for different m values. Curves: regression curves corresponding to the regression lines drawn in (c); the regression is done with respect to the points on the right-hand side of the dotted vertical line. (c) Points: plots of ln k versus $(P-2)^{2/3}$ for different m values. Straight lines: regression lines [eq(9.46)] of $(P-2)^{2/3}$ on ln k for the arrangements of the experimental points with $P \geqq 4$ (i.e., the points on the right-hand side of the dotted vertical line) for respective m values, where $(\Psi_P, \Psi') = (1.89, 6.92)$ for m=0; (1.27, 4.11) for m=0.30; (0.447, 0.362) for m=0.70; (0.414, 0.158) for m=0.72; (0.348, −0.123) for m=0.75; and (0.283, −0.384) for m=0.78.

Fig 9.20. (b)

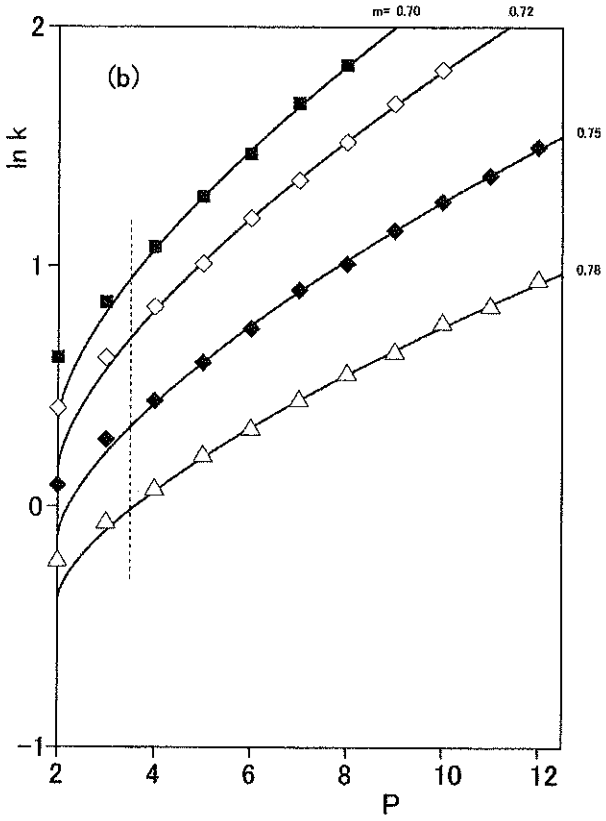
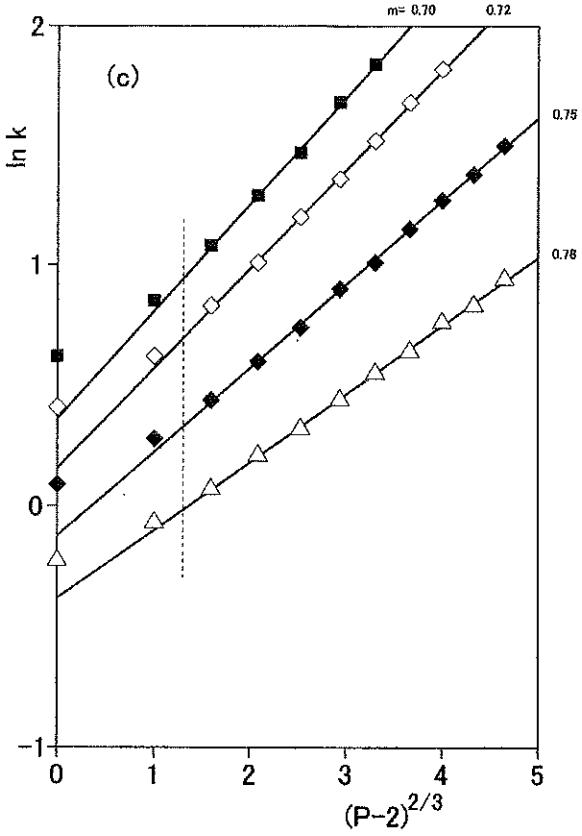


Fig 9.20. (c)



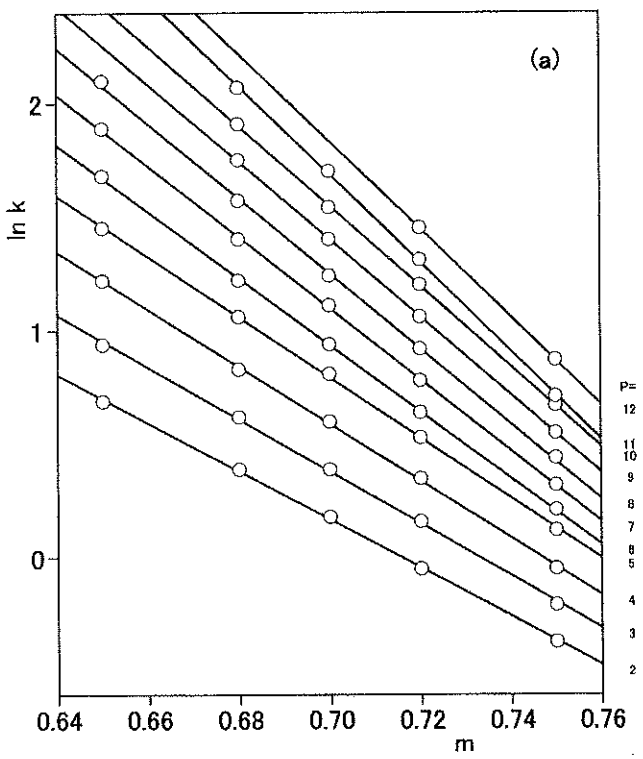


Fig 9.21. As Fig 9.20 for the experimental data presented in Table 9.2(b) for a C_{18} (15 nm pore) column. (a) Points: plots of ln k versus m for different P values. Straight lines: regression lines [eq(9.11')] of m on ln k for the arrangements of the experimental points for respective P values; the $\hat{S}$ and $\hat{W}$ values for all the regression lines are presented in Table 9.2(b). (b) Points: plots of ln k versus P for different m values. Curves: regression curves corresponding to the regression lines drawn in (c); the regression is done with respect to the points on the right-hand side of the dotted vertical line. (c) Points: plots of ln k versus $(P-2)^{2/3}$ for different m values. Straight lines: regression lines [eq(9.46)] of $(P-2)^{2/3}$ on ln k for the arrangements of the experimental points with $P \geqq 4$ (i.e., the points on the right-hand side of the dotted vertical line) for respective m values, where (Ψ_P, Ψ') = (2.04, 6.05) for m=0; (1.34, 3.43) for m=0.30; (0.514, 0.390) for m=0.65; (0.450, 0.103) for m=0.68; (0.394, −0.034) for m=0.70; (0.358, −0.239) for m=0.72; and (0.291, −0.511) for m=0.75.

Fig 9.21. (b)

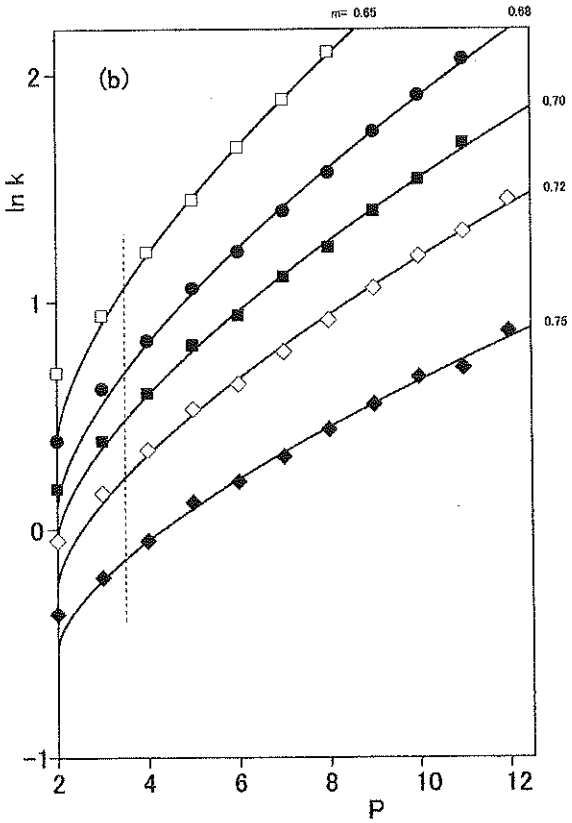
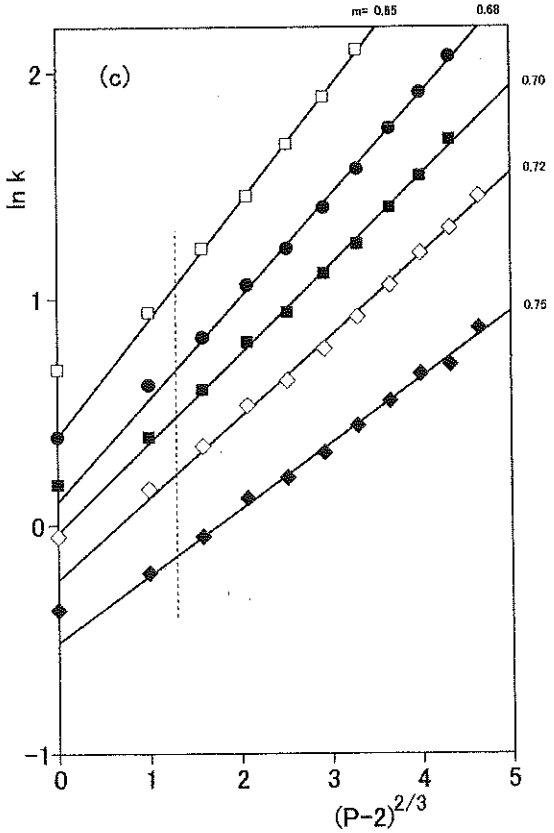


Fig 9.21. (c)



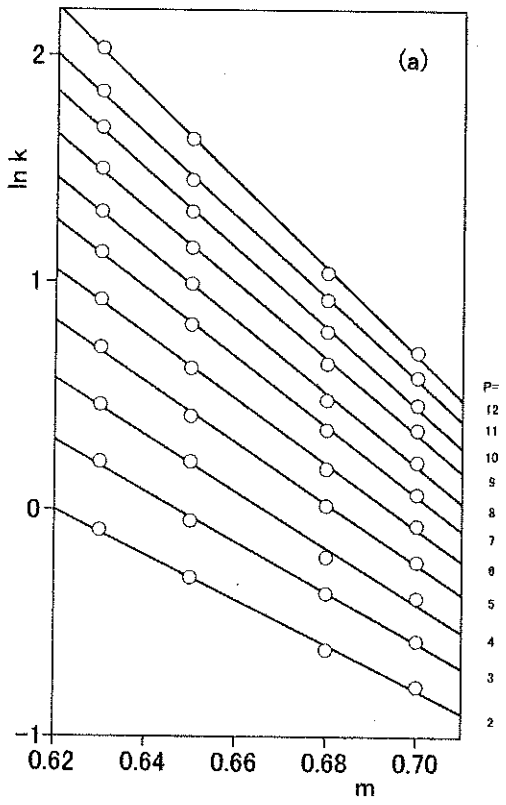


Fig 9.22. As Fig 9.20 for the experimental data presented in Table 9.2(c) for a C_{18} (30 nm pore) column. (a) Points: plots of ln k versus m for different P values. Straight lines: regression lines [eq(9.11')] of m on ln k for the arrangements of the experimental points for respective P values; the $\hat{S}$ and $\hat{W}$ values for all the regression lines are presented in Table 9.2(c). (b) Points: plots of ln k versus P for different m values. Curves: regression curves corresponding to the regression lines drawn in (c); the regression is done with respect to the points on the right-hand side of the dotted vertical line. (c) Points: plots of ln k versus $(P-2)^{2/3}$ for different m values. Straight lines: regression lines [eq(9.46)] of $(P-2)^{2/3}$ on ln k for the arrangements of the experimental points with $P \geqq 4$ (i.e., the points on the right-hand side of the dotted vertical line) for respective m values, where $(\Psi_F, \Psi') = (1.86, 5.23)$ for $m=0$; (1.22, 2.56) for $m=0.30$; (0.509, -0.357) for $m=0.63$; (0.463, -0.543) for $m=0.65$; (0.405, -0.842) for $m=0.68$; and (0.357, -0.966) for $m=0.70$.

Fig 9.22. (b)

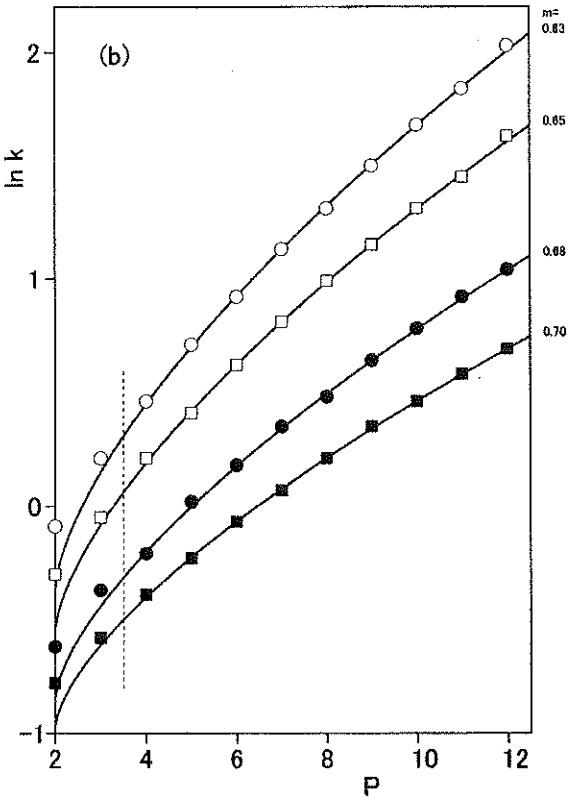
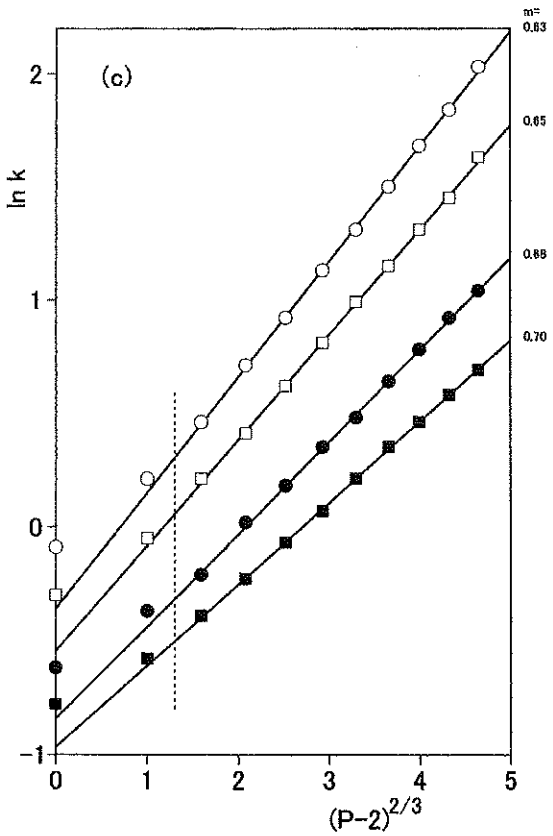


Fig 9.22. (c)



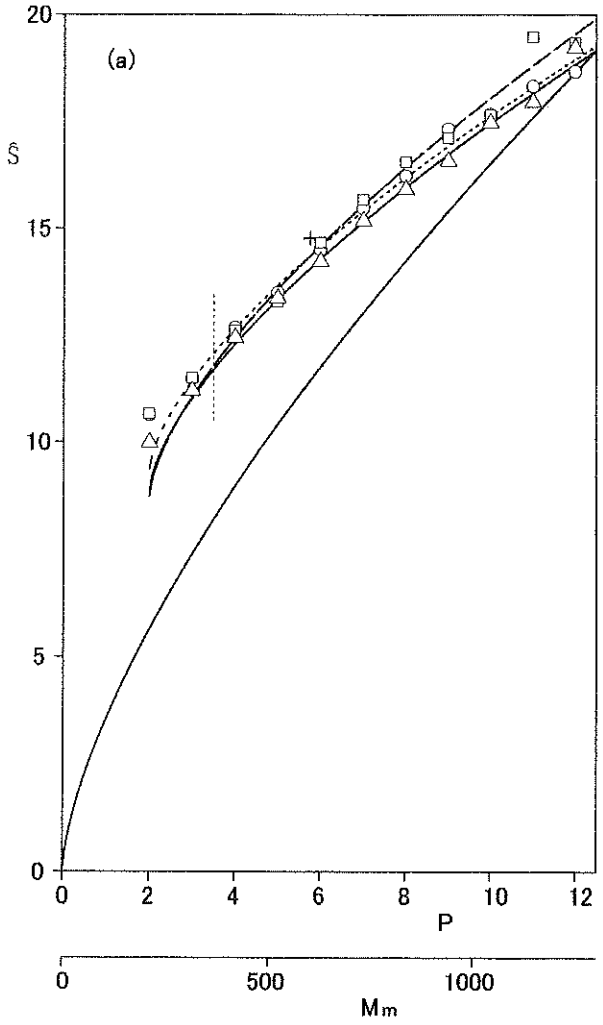


Fig 9.23. Analyses of the variations of $\hat{S}$ as functions of P [Tables 9.2(a)-(c)] for C_{18} columns with 6, 15 and 30 nm pores, respectively. (a) Points(○, □ and △): plots of $\hat{S}$ versus P for 6, 15 and 30 nm pore columns, respectively. Point(+): re-plot of the point(○) in Fig 9.13(a) for polystyrene with $M_n = 6 \times 10^2$ Da in the THF/H_2O system. Three curves drawn almost superposed on the experimental points: regression curves corresponding to the three regression lines drawn in (c); the regression is done with respect to the points on the right-hand side of the dotted vertical line. Curve passing through the origin: re-drawing of the regression curve drawn in Fig 9.13(a) for the THF/H_2O system. (b) Points(○, □ and △): plots of $\hat{S}$ versus $P^{2/3}$ for 6, 15 and 30 nm pore columns, respectively. Point(+): re-plot of the point(○) in Fig 9.13(b) for polystyrene with $M_n = 6 \times 10^2$ Da in the THF/H_2O system. Three curves drawn almost superposed on the experimental points: regression curves corresponding to the three regression lines drawn in (c); the regression is done with respect to the points on the right-hand side of the dotted vertical line. Straight line passing through the origin: re-drawing of the regression line drawn in Fig 9.13(b) for the THF/H_2O system. (c) Points(○, □ and △): plots of $\hat{S}$ versus $(P-2)^{2/3}$ for 6, 15 and 30 nm pore columns, respectively. Three straight lines: regression lines of $(P-2)^{2/3}$ on $\hat{S}$ for the three arrangements of the experimental points(○, □ and △) with $P \geqq 4$ (i.e., the points on the right-hand side of the dotted vertical line), respectively.

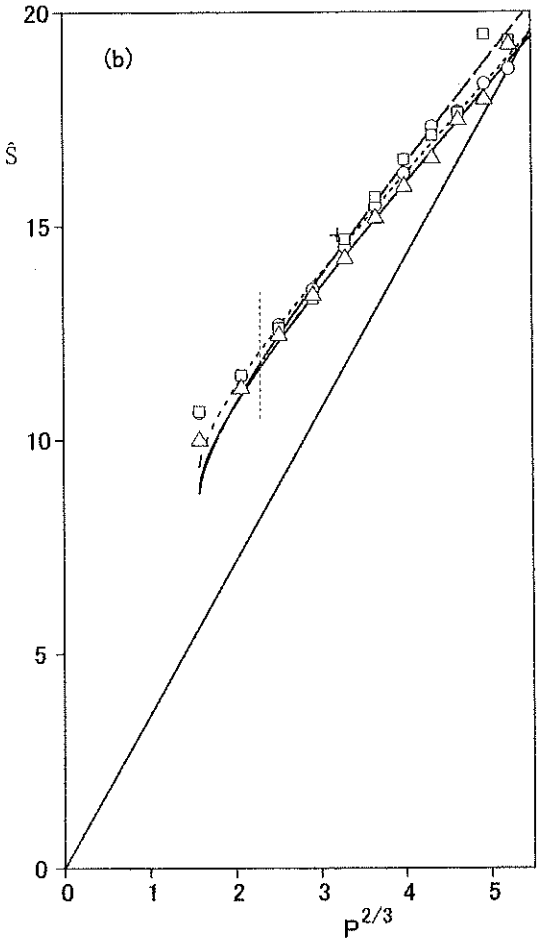


Fig 9.23. (b)

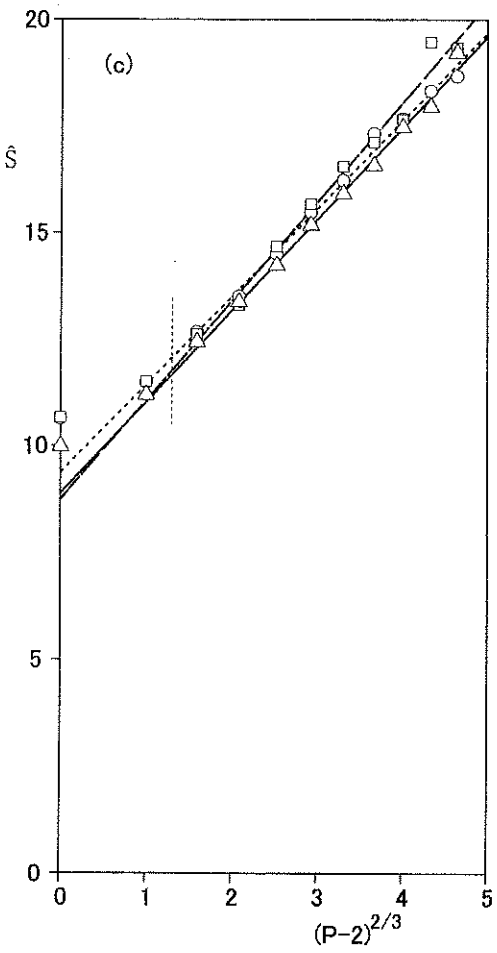


Fig 9.23. (c)

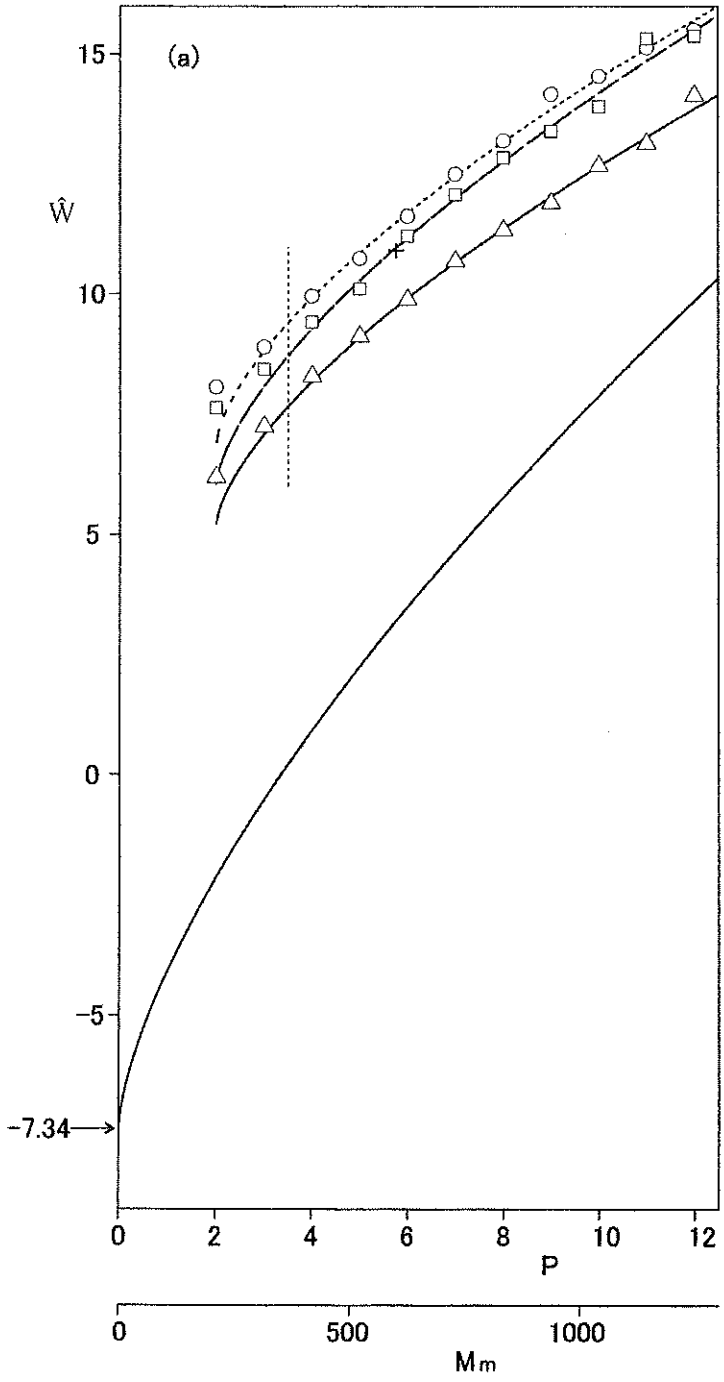


Fig 9.24. (a)

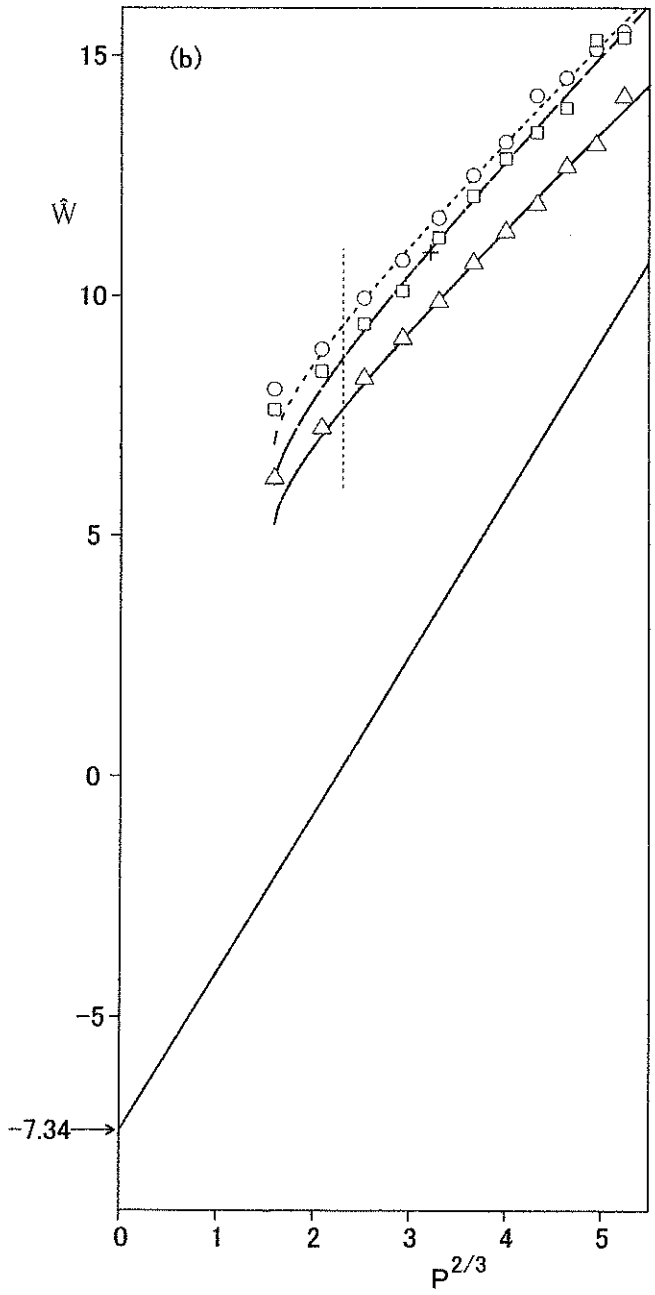


Fig 9.24. (b)

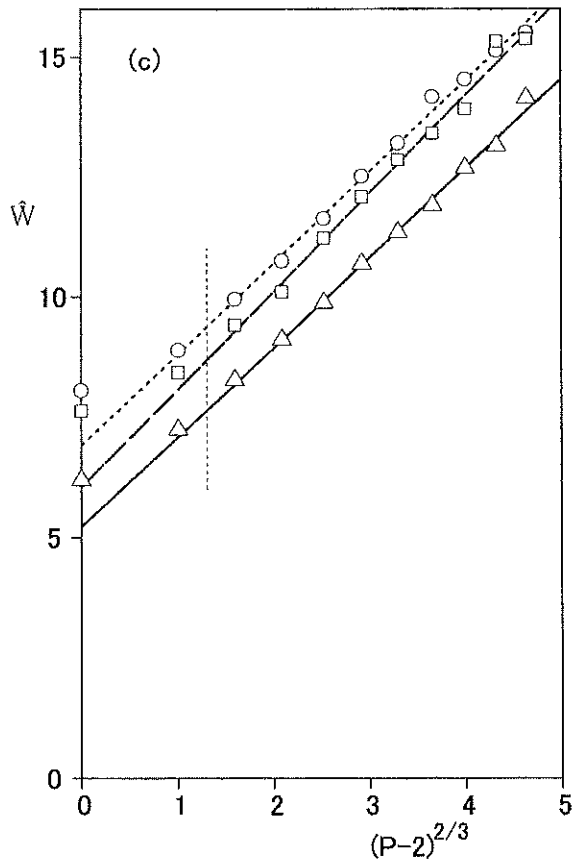


Fig 9.24. Analyses of the variations of $\hat{W}$ as functions of P [Tables 9.2(a)-(c)] for C_{18} columns with 6, 15 and 30 nm pores, respectively. (a) Points(○, □ and △): plots of $\hat{W}$ versus P for 6, 15 and 30 nm pore columns, respectively. Point(+): re-plot of the point(○) in Fig 9.14(a) for polystyrene with $M_n = 6 \times 10^2$ Da in the THF/H_2O system. Three curves drawn almost superposed on the experimental points: regression curves corresponding to the three regression lines drawn in (c); the regression is done with respect to the points on the right-hand side of the dotted vertical line. Curve drawn apart from the experimental points: re-drawing of the regression curve drawn in Fig 9.14(a) for the THF/H_2O system. (b) Points(○, □ and △): plots of $\hat{W}$ versus $P^{2/3}$ for 6, 15 and 30 nm pore columns, respectively. Point(+): re-plot of the point(○) in Fig 9.14(b) for polystyrene with $M_n = 6 \times 10^2$ Da in the THF/H_2O system. Three curves drawn almost superposed on the experimental points: regression curves corresponding to the three regression lines drawn in (c); the regression is done with respect to the points on the right-hand side of the dotted vertical line. Straight line drawn apart from the experimental points: redrawing of the regression line drawn in Fig 9.14(b) for the THF/H_2O system. (c) Points (○, □ and △): plots of $\hat{W}$ versus $(P-2)^{2/3}$ for 6, 15 and 30 nm pore columns, respectively. Three straight lines: regression lines of $(P-2)^{2/3}$ on $\hat{W}$ for the three arrangements of the experimental points(○, □ and △) with $P \geqq 4$ (i.e., the points on the right-hand side of the dotted vertical line), respectively.

9.24(a), where the plots of $\hat{W}$ are done versus $P^{2/3}$ instead of P. In contrast to the $\hat{S}$ versus P or $P^{2/3}$ plots [Fig 9.23(a) or (b)], the arrangement of the experimental points on the $(P,\hat{W})$ or $(P^{2/3},\hat{W})$ plane depends to some extent on the pore size of the adsorbent [see Fig 9.24(a) or (b)]. In contrast to the case of high M_m polystyrenes on the C_{18} column [Figs 9.14(a) and (b)], it now is difficult to consider that the extrapolation of the arrangement of the experimental points (for any pore size C_{18} column) intersects the $\hat{W}$ axis at the coordinate value of the order of magnitude of -9.08 to -7.34 [see Figs 9.24(a) and (b)].

Preliminary Consideration. It would be reasonable to consider that the proportionality between $\hat{S}$ and $M_m^{2/3}$ (or $P^{2/3}$) [eq(9.12)] holds asymptotically when $M_m \gtrsim 10^3$ Da or when $P \gtrsim 10$. Only asymptotically the conformation of polystyrene is three-dimensional in such a way that the effective volume occupied by the conformation is proportional to M_m and that the area of the adsorbent surface occupied by the molecule is proportional to the projection of the three-dimensional conformation. The experimental analyses performed in Section (C) [and also in Section(D)] are asymptotic analyses. With molecules with $M_m \lesssim 10^3$ Da or $P \lesssim 10$, it would be reasonable to asume that, when a minimal number (e.g., two) of monomer units are fixed on the adsorbent surface, then the other part of the molecular structure takes a three-dimensional conformation in such a way that the effective volume occupied by the conformation is proportional to the M_m of this part; the presence of the minimal number of monomer units under consideration is negligible when $M_m \gtrsim 10^3$ Da or when $P \gtrsim 10$.

Theoretical Preparation. Eqs(9.1)-(9.3) still hold, in which, with reference to the preliminary consideration done in the preceding subsection, it now would be possible to write

$$x' = x'^{*} + x'^{\circ} \tag{9.24}$$

$$E = E^{*} + E^{\circ} \tag{9.25}$$

$$\ln \tau = \ln \tau^{*} + \ln \tau^{\circ} \tag{9.26}$$

$$J^{*} = E^{*} + kT\ln \tau^{*} \tag{9.27}$$

$$J^{\circ} = E^{\circ} + kT\ln \tau^{\circ} \tag{9.28}$$

$$J = E + kT\ln \tau = J^{*} + J^{\circ} \tag{9.29}$$

and

$$\ln q = J^{*}/kT + \ln (\beta e^{J^{\circ}/kT}) \tag{9.30}$$

where x'°, E°, τ° and J° are constants with respect to the part of the molecular structure in which the minimal number of monomer units (considered in the preceding subsection) are involved. x'^{*}, E^{*}, τ^{*} and J^{*} are concerned with the other part of the structure taking a three-dimensional conformation on the adsorbent surface; these are direct functions of $P - P^{\circ}$ where P° stands for the minimal number of monomer units under consideration. Let

us consider an assembly of "homologous" molecules characterized as J^*/x''^*=constant, or as

$$J^*/(x''^*\varphi\, kT) = \gamma^* \tag{9.31}$$

in which γ^* represents a positive constant. Eq(9.30) can now be rewritten as

$$\ln q = \gamma^* x''^*\varphi + \ln (\beta e^{J^\circ/kT}) \tag{9.32}$$

where it can be considered that ln q is a function of $x''^*\varphi$ representing the "relative size" of the three-dimensional part of a member of "homologous" molecules. Eq(9.32) fulfills

$$\lim_{x''^*\varphi \to 0} \ln q = \ln (\beta e^{J^\circ/kT}) \tag{9.33}$$

Eq(9.1) can be rewritten as

$$\ln k = -(x''^*+x'^\circ)\varphi\, m + \gamma^* x''^*\varphi + \ln (\beta e^{J^\circ/kT}) \tag{9.34}$$

where it can be considered that ln k is a function of m, and that $x''^*\varphi$ is a parameter. When considering ln k to be a function of $x''^*\varphi$ and m to be a parameter, it is convenient to rewrite eq(9.34) as

$$\ln k = (\gamma^*-m)x''^*\varphi + \ln (\beta e^{J^\circ/kT}) - x'^\circ\varphi\, m \tag{9.34'}$$

Eq(9.34') fulfills

$$\lim_{x''^*\varphi \to 0} \ln k + x'^\circ\varphi\, m = \ln (\beta e^{J^\circ/kT}) \tag{9.35}$$

When $x''^*\varphi$ can be represented as a function of M_m or P as

$$x''^*\varphi\ [= f_{M_m}^*(M_m)] = f_P^*(P) \tag{9.36}$$

fulfilling

$$[\lim_{M_m \to M_m^\circ} f_{M_m}^*(M_m) =]\ \lim_{P \to P^\circ} f_P^*(P) = 0 \tag{9.37}$$

in which M_m° stands for M_m corresponding to P°, then eqs(9.32)-(9.34), (9.34') and (9.35) can be rewritten as

$$\ln q = \gamma^* f_P^*(P) + \ln (\beta e^{J^\circ/kT}) \tag{9.32a}$$

$$\lim_{P \to P^\circ} \ln q = \ln (\beta e^{J^\circ/kT}) \tag{9.33a}$$

$$\ln k = -[f_P^*(P)+x'^\circ\varphi]m + \gamma^* f_P^*(P) + \ln (\beta e^{J^\circ/kT}) \tag{9.34a}$$

$$\ln k = (\gamma^{*}-m)f_P^{*}(P) + \ln(\beta e^{J^{\circ}/kT}) - x'^{\circ}\varphi\, m \tag{9.34'a}$$

and

$$\lim_{P\to P^{\circ}} \ln k + x'^{\circ}\varphi\, m = \ln(\beta e^{J^{\circ}/kT}) \tag{9.35a}$$

respectively; P, P° and $f_P^{*}(P)$ can be replaced by M_m, M_m° and $f_{Mm}^{*}(M_m)$, respectively. Eq (9.37) gives a necessary condition for eq(9.31) to be justified. [f_{Mm}^{*} and f_P^{*} are symbols. In eq(9.37), do not misunderstand as if the subscripts M_m and P as parts of the symbols tend to M_m° and P° when M_m and P as variables tend to M_m° and P°, respectively.]

Experimental Analysis. The points(○, □ and △) in Fig 9.23(c) correspond to those plotted in either Fig 9.23(a) or (b); these are mapped to the $[(P-2)^{2/3}, \hat{S}]$ plane. It can be seen in Fig 9.23(c) that the arrangement of the experimental points for any pore column is almost linear at least when $P \geqq 4$ or when $(P-2)^{2/3} \geqq 1.59$ [i.e., on the right-hand side of the dotted vertical line]. The points(○, □ and △) in Fig 9.24(c) correspond to those plotted in either Fig 9.24(a) or (b); these are mapped to the $[(P-2)^{2/3}, \hat{W}]$ plane. It can also be seen in Fig 9.24(c) that the arrangement of the experimental points for any pore column is almost linear at least when $P \geqq 4$ or when $(P-2)^{2/3} \geqq 1.59$ [i.e., on the right-hand side of the dotted vertical line].

Both Figs 9.23(c) and 9.24(c) justify the consideration done in the subsection entitled "Theoretical Preparation". Thus, Fig 9.23(c) manifests that, at least when $P \geqq 4$, $\hat{S}$ can be represented as

$$\hat{S} = \omega_P^{*}(P-2)^{2/3} + \omega^{\circ} \tag{9.38}$$

[cf. eq(9.12)] in which

$$\omega^{\circ} = x'^{\circ}\varphi \tag{9.39}$$

and that function $f_P^{*}(P)$ can be represented as

$$f_P^{*}(P) = \omega_P^{*}(P-2)^{2/3} \tag{9.40}$$

with

$$P^{\circ} = 2 \tag{9.41}$$

In eq(9.40), ω_P^{*} is a positive constant expressed by using eq(9.36) as

$$\omega_P^{*} = x'^{*}\varphi/(P-2)^{2/3} \tag{9.42}$$

representing the "relative size" of the three-dimensional conformation part per monomer unit. When $P \leqq 3$ (especially when $P=2$), eq(9.38) or (9.40) does not hold exactly; the concept of the presence of the three-dimensional conformation part is ambiguous when $P \leqq 3$.

Eqs(9.32a), (9.34a) and (9.34'a) can be represented as

$$\ln q = \gamma^* \omega_P^* (P-2)^{2/3} + \ln (\beta c^{J^\circ/kT}) \tag{9.32b}$$

$$\ln k = \ln (\beta e^{J^\circ/kT}) - \omega^\circ m + \gamma^* \omega_P^* (P-2)^{2/3} - \omega_P^* m (P-2)^{2/3} \tag{9.34b}$$

and

$$\ln k = (\gamma^* - m) \omega_P^* (P-2)^{2/3} + \ln (\beta e^{J^\circ/kT}) - \omega^\circ m \tag{9.34'b}$$

respectively. Fig 9.24(c) shows that, at least when $P \geqq 4$, $\hat{W}$ can be represented as

$$\hat{W} = \Phi_P (P-2)^{2/3} + \Phi' \tag{9.43}$$

[cf. eq(9.15)]. With reference to eq(9.32b), it can be interpreted that $\hat{W}$ is represented by eq(9.16); both relationships:

$$\Phi_P = \gamma^* \omega_P^* \tag{9.44}$$

[cf. eq(9.17)] and

$$\Phi' = \ln (\beta e^{J^\circ/kT}) \tag{9.45}$$

[cf. eq(9.18)] hold.

The three straight lines drawn in Fig 9.23(c) are the regression lines of $(P-2)^{2/3}$ on $\hat{S}$ [eq(9.38)] for the three arrangements of the experimental points(○, □ and △) with $P \geqq 4$ or with $(P-2)^{2/3} \geqq 1.59$ for 6, 15 and 30 nm pore columns, respectively. It can be seen in Fig 9.23(c) that the experimental points with P=2 deviate from the regression lines. For 6, 15 and 30 nm pore columns, the parameter ω_P^* can be evaluated to be 2.07, 2.33 and 2.15 (as the slopes of the regression lines), and the parameter ω° can be evaluated to be 9.37, 8.71 and 8.88 (as the intersections with the $\hat{S}$ axis of the regression lines), respectively [see both Figs 9.23(c) and eq(9.38)]. These ω° values are slightly smaller than the ordinates $\hat{S}$ or the $x'\varphi$ values for the molecule with P=2 [written as $\hat{S}_{P=2}$ or $(x'\varphi)_{P=2}$]: 10.63, 10.66 and 9.98 for 6, 15 and 30 nm pore columns, respectively [see Fig 9.23(a), (b) or (c)]; this arises from the fact that eq(9.31) cannot be extended to P=2. The three curves almost superposed on the experimental points in Fig 9.23(a) and the three curves almost superposed on the experimental points in Fig 9.23(b) correspond to the three regression lines drawn in Figs 9.23(c); the two formers are mapped to $(P, \hat{S})$ and $(P^{2/3}, \hat{S})$ planes, respectively.

The straight line passing through the origin drawn in Fig 9.23(b) and the curve passing through the origin drawn in Fig 9.23(a) are identical with the regression line drawn in Fig 9.13(b) and the corresponding curve drawn in Fig 9.13(a) for high M_n polystyrenes in the THF/H_2O system on the 10 nm pore C_{18} column, respectively. In Figs 9.23(b) and (a), it would be possible to interpret that, with increase in P, the arrangements of the

experimental points approach asymptotically the regression line and the corresponding curve for high M_w polystyrenes, respectively.

The point(○) for plystyrene with $M_w = 6 \times 10^2$ Da in the THF/H_2O system on the 10 nm pore C_{18} column plotted in Fig 9.13(a) and the corresponding point(○) plotted in Fig 9.13(b) can be re-plotted as point(+) in Figs 9.23(a) and (b), respectively. The fact that the point(+) is present just in the vicinity of the arrangements of the points(○, □ and △) would justify to relate the argument performed in this Section to that for the THF/H_2O system with the 10 nm pore C_{18} column performed in Section(C). In Figs 9.23(b) and (a), the point(+) deviates considerably from the regression line and the corresponding curve (passing through the origin), respectively. In Figs 9.13(b) and (a), however, the experimental analysis is performed in larger scales with respect to M_w or P, where it is apparent that the deviation of the experimental point for 6×10^2 Da polystyrene deviates only slightly from the regression line and the corresponding curve, respectively.

It should be underlined that the regression lines or the corresponding curves drawn in Fig 9.23(a), (b) or (c) for polystyrenes with P ranging between 4 and 12 are valid only in the vicinity of these P values. These do not coincide with those for high M_w polystyrenes asymptotically when P approaces infinity; they only suggest that, with increase in P, the arrangement of the experimental points on the $(P, \hat{S})$, $(P^{2/3}, \hat{S})$ or $[(P-2)^{2/3}, \hat{S}]$ plane will approach asymptotically the ideal arrangement the extrapolation of which appears to pass through the origin.

The three straight lines drawn in Fig 9.24(c) are the regression lines of $(P-2)^{2/3}$ on $\hat{W}$ [eq(9.43)] for the three arrangements of the experimental points(○, □ and △) with $P \geqq 4$ or with $(P-2)^{2/3} \geqq 1.59$ for 6, 15 and 30 nm pore columns, respectively. As on the $[(P-2)^{2/3}, \hat{S}]$ plane [Fig 9.23(c)], the experimental points with P=2 are deviating from the regression lines [see Fig 9.24(c)]. For 6, 15 and 30 nm pore columns, $\gamma^* \omega_P^*$ can be evaluated to be 1.89, 2.04 and 1.86 (as the slopes of the regression lines) [see both Fig 9.24(c) and eq(9.44)], and the parameter γ^* $(= \gamma^* \omega_P^* / \omega_P^*)$ can be evaluated to be 1.89/2.07=0.913, 2.04/2.33=0.876 and 1.86/2.15=0.865, respectively. On the other hand, $\ln (\beta e^{J^*/kT})$ can be evaluated to be 6.92, 6.05 and 5.23 (as the intersections with the $\hat{W}$ axis of the regression lines), respectively. [see both Fig 9.24(c) and eq(9.45)]. These values are slightly smaller than the ordinates $\hat{W}$ or the ln q values for the molecule with P=2 [written as $\hat{W}_{P=2}$ or $(\ln q)_{P=2}$]: 8.06, 7.63 and 6.19 for 6, 15 and 30 nm pore columns, respectively [see Fig 9.24(a), (b) or (c)]; this arises from the fact that eq(9.31) cannot be extended to P=2. The three curves almost superposed on the experimental points in Fig 9.24(a) and the three curves almost superposed on the experimental points in Fig 9.24(b) correspond to the three regression lines drawn in Figs 9.24(c); the two formers are mapped to $(P, \hat{W})$ and $(P^{2/3}, \hat{W})$ planes, respectively.

The straight line drawn in Fig 9.24(b) and the curve drawn apart from the experimental points in Fig 9.24(a) are identical with the regression line drawn in Fig 9.14(b) and

the corresponding curve drawn in Fig 9.14(a) for high M_n polystyrenes in the THF/H_2O system on the 10 nm pore C_{18} column, respectively. As in Figs 9.23(b) and (a), in Fig 9.24(b) and (a) also, it would be possible to interpret that, with increase in P, the arrangements of the experimental points approach asymptotically the regression line and the corresponding curve for high M_n polystyrenes, respectively. The points(+) plotted just in the vicinities of the arrangements of the experimental points(○, □ and △) in Figs 9.24 (a) and (b), respectively, correspond to the points(○) in Figs 9.14(a) and (b) for polystyrene with $M_n = 6 \times 10^2$ Da in the THF/H_2O system on the 10 nm pore C_{18} column, justifying again to relate the the argument performed in this Section to that for the THF/H_2O system on the 10 nm pore C_{18} column performed in Section(C).

Let us pay attention to eq(9.34'b) from which it can be anticipated that, when m is constant and when $P \geqq 4$, the experimental plots of ln k versus $(P-2)^{2/3}$ will give a linear arrangement represented as

$$\ln k = \Psi_P (P-2)^{2/3} + \Psi' \tag{9.46}$$

in which

$$\Psi_P = (\gamma^* - m)\omega_P^* \tag{9.47}$$

and

$$\Psi' = \ln (\beta e^{J^\circ/kT}) - \omega^\circ m \tag{9.48}$$

[cf. eqs(9.19)-(9.21)]. Further, $\Psi_P/\omega_P^* + m$ will give a constant value independent of m, representing γ^*:

$$\gamma^* = \Psi_P/\omega_P^* + m \tag{9.47'}$$

[cf. eq(9.20')]. Therefore, when m tends to infinitesimal, then Ψ_P will coincide with $\gamma^*\omega_P^*$ i.e., the slope of the linear arrangement of the experimental points taking place on the $[(P-2)^{2/3}, \hat{W}]$ plane when $P \geqq 4$ [Fig 9.24(c)]. It can also be anticipated that $\Psi' + \omega^\circ m$ will give a constant value independent of m, representing $\ln (\beta e^{J^\circ/kT})$:

$$\ln (\beta e^{J^\circ/kT}) = \Psi' + \omega^\circ m \tag{9.48'}$$

When m tends to infinitesimal, then Ψ' will coincide with $\ln (\beta e^{J^\circ/kT})$ i.e., the intersection with the $\hat{W}$ axis of the extrapolation of the arrangement of the experimentl points taking place on the $[(P-2)^{2/3}, \hat{W}]$ plane when $P \geqq 4$ [Fig 9.24(c)].

The points in Figs 9.20(c), 9.21(c) and 9.22(c) correspond to those in Figs 9.20(b), 9.21(b) and 9.22(b), mapped to the $[(P-2)^{2/3}$, ln k] plane, respectively. As anticipated, it can be seen in Figs 9.20(c), 9.21(c) and 9.22(c) that the arrangement of the experimental points is almost linear for any m value for any pore column when $P \geqq 4$ or when $(P-2)^{2/3}$

$\geqq 1.59$.

The straight lines drawn in Figs 9.20(c), 9.21(c) and 9.22(c) are the regression lines of $(P-2)^{2/3}$ on ln k for the arrangements of the experimental points with $P \geqq 4$ for constant m values, respectively; the experimental points with $P=2$ are deviating from the regression lines. Both Ψ_P and Ψ' values for each regression line [eq(9.46)] are presented in the legends for Figs 9.20(c), 9.21(c) and 9.22(c); the regression lines for $m=0$ are identical with those taking place on the $[(P-2)^{2/3}, \hat{W}]$ plane [Fig 9.24(c)]. The curves drawn in Figs 9.20(b), 9.21(b) and 9.22(b) correspond to the regression lines drawn in Figs 9.20(c), 9.21(c) and 9.22(c), respectively.

In Tables 9.3(a)-(c) are summarized both γ^* and ln ($\beta e^{J^\circ/kT}$) values for all the m values estimated by using both eqs(9.47') and (9.48') for the regression lines drawn in Figs 9.20(c), 9.21(c) and 9.22(c), respectively; both parameters ω_P^* and ω° involved in the equations have been evaluated already (see above). In Table 9.3, however, the γ^* and ln ($\beta e^{J^\circ/kT}$) values for $m=0$ represent those obtained from Fig 9.24(c), and the values for $m=0.30$ were estimated on the basis of the regression lines drawn in Figs 9.20(a), 9.21(a) and 9.22(a) by extrapolating them to $m=0.30$. As anticipated, it can be seen in Table 9.3 that both γ^* and ln ($\beta e^{J^\circ/kT}$) values are almost constant, independent of m for any pore column. This again supports the competition model with reversed-phase chromatography.

Important Results Obtained from the Alalysis. The results of the experimental analyses are sumarized in Table 9.4; these can be compared with the results obtained for high M_m polystyrenes on the 10 nm pore C_{18} column in the presence of the THF/H_2O mobile phase system (summarized in the second line from the last in Table 9.1). Thus, it can be seen that the "relative size" of the three dimensional conformation part per monomer unit, $x''^*\varphi/(P-2)^{2/3}$, of low M_m polystyrens (Table 9.4 column<1>) is about 0.6 times as large as the "relative molecular size" per monomer unit, $x'\varphi/P^{2/3}$, of high M_m polystyrenes (column <1> in the second line from the last in Table 9.1). With respect to low M_m polystyrens, the "relative size" of the remainder of the molecular structure, $x''^\circ\varphi$, is about 4 times as large as $x''^*\varphi/(P-2)^{2/3}$ (Table 9.4 column<3b>).

The AVFA for the three dimensional conformation part per monomer unit, $J^*/(P-2)^{2/3}$, of low M_m polystyrens [ranging between 4.65 and 5.02 kJ/mol; Table 9.4 column<5>] are smaller by 3.11 to 3.48 kJ/mol than the AVFA per monomer unit, $J/P^{2/3}$, for high M_m polystyrens [8.13 kJ/mol; column<5> in the second line from the last in Table 9.1]. J or J^* (approximately equal to E or E^*) originally is defined as the absolute value of the difference in the free energy (or energy) of the total thermodynamic system between the two states when a sample molecule stays on the adsorbent surface and when it is in solution. It can be suggested that, on the C_{18} surface, the conformation of the three-dimensional conformation part of low M_m polystyrens is slightly different from the total molecular con-

Table 9.3

Summary of both γ^* and $\ln(\beta e^{J^\circ/kT})$ values obtaied for different m values. When $m \neq 0$, these were estimated by using eqs(9.47') and (9.48'), respectively. (a), (b) and (c) are for 6, 15 and 30 nm pore columns, and the experimental data used for the estimations are shown in Figs 9.20(c), 9.21(c) and 9.22(c), respectively. γ^* and $\ln(\beta e^{J^\circ/kT})$ values for $m=0$ represent those obtained from Fig 9.24(c). For detail, see text.

(a) 6 nm pore column

m (vol/vol)	0	0.30	0.70	0.72	0.75	0.78
γ^*	0.913	0.914	0.916	0.920	0.918	0.917
$\ln(\beta e^{J^\circ/kT})$	6.92	6.92	6.92	6.90	6.90	6.92

(b) 15 nm pore column

m (vol/vol)	0	0.30	0.65	0.68	0.70	0.72	0.75
γ^*	0.876	0.875	0.871	0.873	0.869	0.874	0.875
$\ln(\beta e^{J^\circ/kT})$	6.05	6.05	6.07	6.04	6.08	6.05	6.04

(c) 30 nm pore column

m (vol/vol)	0	0.30	0.63	0.65	0.68	0.70
γ^*	0.865	0.867	0.867	0.865	0.868	0.866
$\ln(\beta e^{J^\circ/kT})$	5.23	5.22	5.24	5.23	5.20	5.25

Table 9.4

Summary of the analysis of the experiments of low M_m polystyrenes performed in the THF/H_2O mobile phase system on C_{18} columns by Larmann et al. (Figs 9.20-9.22). The value of kT at 23℃ (2.46 kJ/mol) is used for the analysis.

	⟨1⟩	⟨1a⟩	⟨2⟩	⟨3b⟩	⟨4⟩	
Pore size (nm)	$\omega_P^* = x''^*\varphi/(P-2)^{2/3}$	$\omega_P^* = \omega_P^*/22.13$	$\omega^\circ = x'^\circ\varphi$	$x'^\circ\varphi/[x''^*\varphi/(P-2)^{2/3}]$	$\Phi_P = \gamma^*\omega_P^* = J^*/[(P-2)^{2/3}kT]$	
6	2.07	0.0935	9.37	4.53	1.89	⇒
15	2.33	0.105	8.74	3.75	2.04	⇒
30	2.15	0.0972	8.88	4.13	1.86	⇒

	⟨5⟩	⟨6⟩	⟨7⟩	⟨2'⟩	⟨8⟩	⟨8'⟩	
	$\gamma^*\omega_P^*kT = J^*/(P-2)^{2/3}$ (kJ/mol)	$\gamma^* = \gamma^*\omega_P^*/\omega_P^*$	$\gamma^*kT = J^*/(x''^*\varphi)$ (kJ/mol)	$\hat{S}_{P=2} = (x''^*\varphi)_{P=2}$	$\Phi' = \ln(\beta e^{J^\circ/kT})$	$\hat{W}_{P=2} = (\ln q)_{P=2}$	
⇒	4.65	0.913	2.25	10.63	6.92	8.06	⇒
⇒	5.02	0.876	2.15	10.66	6.05	7.63	⇒
⇒	4.58	0.865	2.13	9.98	5.23	6.19	⇒

	⟨9⟩	⟨9'⟩	⟨10⟩	⟨10'⟩	
	$J^\circ/kT=$ $\Phi'-\ln\ \beta=$ $\Phi'+7.34$	$J_{P=2}/kT=$ $\hat{W}_{P=2}-\ln\ \beta=$ $\hat{W}_{P=2}+7.34$	J° (kJ/mol)	$J_{P=2}$ (kJ/mol)	
⇒	14.26	15.40	35.1	37.9	⇒
⇒	13.39	14.97	32.9	36.8	⇒
⇒	12.57	13.53	30.9	33.3	⇒

	⟨11b⟩	⟨11'b⟩	⟨12⟩	⟨13⟩	⟨14⟩
	$J^\circ/[J^*(P-2)^{2/3}]$	$J_{P=2}/[J^*(P-2)^{2/3}]$	φ	$x''^*/(P-2)^{2/3}$	x'°
⇒	7.55	8.15	$\lesssim 0.63$	$\gtrsim 3.29$	$\gtrsim 14.9$
⇒	6.55	7.33	$\lesssim 0.63$	$\gtrsim 3.70$	$\gtrsim 13.9$
⇒	6.75	7.27	$\lesssim 0.63$	$\gtrsim 3.41$	$\gtrsim 14.1$

(cont.) **Table 9.4**

formation of high M_n polystyrens. As a result, it would be apparent that the (free) energy of adsorption of 3.11 to 3.48 kJ/mol per monomer unit is lost in the three-dimensional conformation part of low M_n polystyrens compared with the case of high M_n polystyrens perhaps due to the presence of the intra-molecular repulsive interactions specific to the former conformation.

By combininng the ln ($\beta e^{J^\circ/kT}$) values (Table 9.4 column<8>) with the ln β value of -7.34 estimated for the 10 nm pore C_{18} column in the presence of the THF/H_2O mobile phase system (column<8> in the second line from the last in Table 9.1), it can be estimated that the AVFA for the remainder of the molecular structure (other than the three-dimensional conformation part), J°, of low M_n polystyrens are between 30.9 and 35.1 kJ/mol (Table 9.4 column<10>); J° is 6.55 to 7.55 times as large as $J^*/(P-2)^{2/3}$ (Table 9.4 column<11b>). From a large difference between J° and $J^*/(P-2)^{2/3}$ values, it can be suggested that there, in general, may exist a considerably large intra-molecular repulsive interactions in the three-dimensional conformatin part of low M_n polystyrens taking place on the C_{18} surface. [For reference, the J value for the molecule with P=2 (written as $J_{P=2}$) and the ratio between $J_{P=2}$ and $J^*/(P-2)^{2/3}$ values are shown in Table 9.4 column <10'> and (11'b>, respectively. Cf. Note in the subsection entitled "Summary of the Important Results Obtained from the Analyses of Both Figs 9.1 and 9.2" in Section(C).]

Let us assume that the upper limit, $(\varphi\ m)_{u.l.}$, of the φ m value that brings about practically linear arrangements of the ln k versus m plots is 0.5. It can be seen in Figs 9.20(a), 9.21(a) and 9.22(a) that the maximum m value used for the experiment is lower than 0.8. The upper limits of the possible φ values can be estimated to be 0.5/0.8=0.63 (Table 9.4 column<12>). The lower limits of $x'^*/(P-2)^{2/3}$ and x'° can be evaluated, respectively; these are presented in Table 9.4 column<13> and <14> (cf. Table 9.4 col-umn<1> and <2>).

(F) Analysis of the Experiment of Jandera

Experiment(1). In ref(9.13), isocratic chromatographies of six n-alkanes (with number of carbon atoms, P, in the alkyl chain ranging between 5 and 10): n-pentane, n-hexane, n-heptane, n-octane, n-nonane and n-decane, and six n-alkylbenzenes (with P between 1 and 6) were carried out on a C_8 column in the presences of both MtOH/H_2O and ACN/H_2O mobile phase systems, respectively; the volume fractions, m, of both MtOH and ACN were changed between 0.5 and 0.9. With the MtOH/H_2O system, $\log_{10}$ k always decreased linearly with increase in m (see Fig 9.25 for the n-alkane series). With the ACN/H_2O system, however, the $\log_{10}$ k versus m plots, in general, tended to deviate slightly from the straight lines. [In ref(9.13), how the deviation occured is not mentioned. The data presentrd in Table 9.5(b) show, however, that the deviation occured in such a way that a concave arrangement of the experimental points is obtained, similarly to the arrangement presented in Fig 8.3(d).] With regard to the $\log_{10}$ k versus P plots, good linear arrange-

Table 9.5

Reproduction of the regression analysis performed by Jandera[ref(9.13) Table III] for both n-alkane and n-alkylbenzene series for (a) MtOH/H_2O and (b) ACN/H_2O mobile phase systems on a C_8 column.

(a) MtOH/H_2O system

Sample	α_{J0}	β_{J0}	α_{J1}	β_{J1}	$\hat{\alpha}_{J0}$	$\hat{\beta}_{J0}$	$\hat{\alpha}_{J1}$	$\hat{\beta}_{J1}$
n-alkanes	0.49	0.62	0.44	1.75	1.13	1.43	1.01	4.03
n-alkylbenzenes	0.50 | 0.52	1.44 | 1.53	0.46 | 0.49	2.52 | 2.62	1.15 | 1.20	3.32 | 3.52	1.06 | 1.13	5.80 | 6.03

(b) ACN/H_2O system

Sample	α_{J0}	β_{J0}	α_{J1}	β_{J1}	α_{J2}	β_{J2}	
n-alkanes	0.49	0.62	0.79	2.18	0.40	0.70	⇒
n-alkylbenzenes	0.50	1.53	0.90	3.39	0.49	0.99	⇒

	$\hat{\alpha}_{J0}$	$\hat{\beta}_{J0}$	$\hat{\alpha}_{J1}$	$\hat{\beta}_{J1}$	$\hat{\alpha}_{J2}$	$\hat{\beta}_{J2}$
⇒	1.13	1.43	1.82	5.02	0.92	1.61
⇒	1.15	3.52	2.07	7.81	1.13	2.28

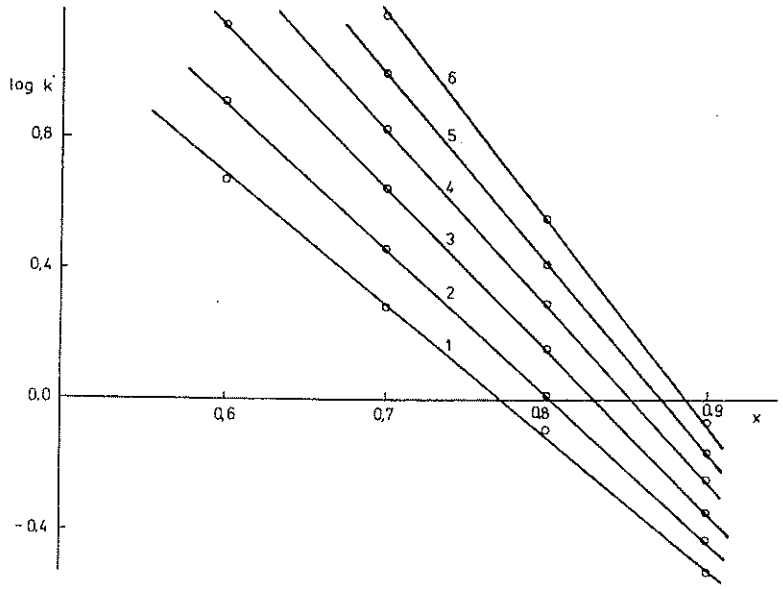


Fig 9.25. Plots of log k' i.e., $\log_{10}$ k versus volume fraction x i.e., m of MtOH for n-pentane (P=5; 1), n-hexane (P=6; 2), n-heptane (P=7; 3), n-octane (P=8; 4), n-nonane (P=9; 5), and n-decane (P=10; 6), obtained for isocratic chromatography carried out on a C_8 column in the presences of MtOH/H_2O mobile phase systems with different m values. The regression line for the molecule with any P value can be represented by eq(9.49) with the values of the parameters given in Table 9.5(a). [Reproduced from ref (9.13) Fig 1.]

ments of the experimental points with positive slopes always were obtained with both MtOH/H_2O and ACN/H_2O systems (see Fig 8.26 for the n-alkylbenzene series with the ACN/H_2O system).

On the basis of these data, Jandera(9.13) concluded that, for both n-alkane and n-alkylbenzene series with the MtOH/H_2O system, $\log_{10}$ k can be described as a function of both m and P by a simple equation. By converting $\log_{10}$ k to ln k and using our notations, this equation can be rewritten after rearrangement as

$$\begin{aligned} \ln k &= \hat{\beta}_{J0} + \hat{\alpha}_{J0}P - (\hat{\beta}_{J1} + \hat{\alpha}_{J1}P)m \\ &= \hat{\beta}_{J0} - \hat{\beta}_{J1}m + (\hat{\alpha}_{J0} - \hat{\alpha}_{J1}m)P \\ &= \hat{\beta}_{J0} - \hat{\beta}_{J1}m + \hat{\alpha}_{J0}P - \hat{\alpha}_{J1}mP \end{aligned} \tag{9.49}$$

With the ACN/H_2O system when the $\log_{10}$ k versus m plots tend to deviate slightly from the straight lines, $\log_{10}$ k can be described by adding a quadratic term with respect to m (9.13); the modified equation can be rewritten as

$$\begin{aligned} \ln k &= \hat{\beta}_{J0} + \hat{\alpha}_{J0}P - (\hat{\beta}_{J1} + \hat{\alpha}_{J1}P)m + (\hat{\beta}_{J2} + \hat{\alpha}_{J2}P)m^2 \\ &= \hat{\beta}_{J0} - \hat{\beta}_{J1}m + \hat{\beta}_{J2}m^2 + (\hat{\alpha}_{J0} - \hat{\alpha}_{J1}m + \hat{\alpha}_{J2}m^2)P \\ &= \hat{\beta}_{J0} - \hat{\beta}_{J1}m + \hat{\alpha}_{J0}P - \hat{\alpha}_{J1}mP + \hat{\beta}_{J2}m^2 + \hat{\alpha}_{J2}m^2P \end{aligned} \tag{9.50}$$

[Eq(9.49) can be derived from eqs(2), (7) and (8) in ref(9.13) in which $a_0 = \beta_0$, $a_1 = \alpha_0$, $m_0 = \beta_1$ and $m_1 = \alpha_1$. We here denote k', x, n_c, α_0, β_0, α_1 and β_1 in ref(9.13) by k, m, P, α_{J0}, β_{J0}, α_{J1} and β_{J1}, respectively. We also write $\hat{\alpha}_{J0}$, $\hat{\beta}_{J0}$, $\hat{\alpha}_{J1}$ and $\hat{\beta}_{J1}$ for (ln 10)α_{J0}, (ln 10)β_{J0}, (ln 10)α_{J1} and (ln 10)β_{J1}, respectively. Eq(9.50) can be derived from eqs(1), (7)-(9) in ref(9.13) in which $d_0 = \beta_2$ and $d_1 = \alpha_2$. We denote α_2 and β_2 by α_{J2} and β_{J2}, respectively, and write $\hat{\alpha}_{J2}$ and $\hat{\beta}_{J2}$ for (ln 10)α_{J2} and (ln 10)β_{J2}, respectively. The derivations of ref(9.13) eqs(1), (2), (7)-(9) performed by Jandera in both ref(9.13, 9.14) are presented in the subsection entitled "Interaction Indices Model" in Appendix XI (D).] The α_{J0}, β_{J0}, α_{J1} and β_{J1} values for the two homologous series in the MtOH/H_2O system and the α_{J0}, β_{J0}, α_{J1}, β_{J1}, α_{J2} and β_{J2} values for these series in the ACN/H_2O system both estimated from the regression analysis [summarized in ref(9.13) Table III] are reproduced in Table 9.5 with addition of the $\hat{\alpha}_{J0}$, $\hat{\beta}_{J0}$, $\hat{\alpha}_{J1}$, $\hat{\beta}_{J1}$, $\hat{\alpha}_{J2}$ and $\hat{\beta}_{J2}$ values.

Experiment(2). In ref(9.14), isocratic chromatographies of 1,2-naphthoylenebenzimidazole-6-sulphonamides of aliphatic n-amines (with P ranging between 1 and 10 at the maximum; called homologous series A) and 3,5-dinitrobenzoates of aliphatic n-alcohols (with P ranging between 1 and 6 at the maiximum; called homologous series B) were carried out on a C_{18} column. For series A, three types of mobile phase system were used: the MtOH/H_2O system with volume fraction, m, of MtOH changed between 0.7 and 0.9 at the maximum, the 1,4-deoxiane(DXN)/H_2O system with m of DXN changed between 0.5 and 0.75, and the ACN/H_2O system with m of ACN changed between 0.6 and 0.8 at the

maximum. For series B, four types of mobile phase system were used with addition of the THF/H_2O system with m of THF changed between 0.45 and 0.65. The experimental $\log_{10}$ k versus m plots were approximately linear with the MtOH/H_2O system (with negative slopes), slightly deviating from linearity with both DXN/H_2O and ACN/H_2O systems, and distinctly curved with the THF/H_2O system(9.14). With regard to the $\log_{10}$ k versus P plots, however, fairly linear positive correlations were found always(9.14).

Jandera(9.14) concluded that $\log_{10}$ k always can be represented by eq(9.49) approximately. With the THF/H_2O system, an attempt to improve the agreement with the $\log_{10}$ k versus m plots by using nonlinear quadratic regression analysis [eq(9.50)] was unsuccessful beacue of the large error in determination of constants from only five experimental points for each plots(9.14). The α_{J0}, β_{J0}, α_{J1} and β_{J1} values obtained from the linear regression analysis [summarized in ref(9.14) Tables II and III] are reproduced in Table 9.6 with addition of the $\hat{\alpha}_{J0}$, $\hat{\beta}_{J0}$, $\hat{\alpha}_{J1}$ and $\hat{\beta}_{J1}$ values.

Theoretical Preparation. The alalyses of the data for both n-alkane and n-alkylbenzene series obtained on the C_8 column with the MtOH/H_2O system in Experiment(1) and the analysys of the data for both homologous series A and B obtained on the C_{18} column with any mobile phase system in Experiment(2) are performed by using eq(9.1) combined with both eqs(9.2) and (9.3). We also use eqs(9.24)-(9.32), (9.32a), (9.33), (9.33a), (9.34), (9.34a), (9.34'), (9.34'a), (9.35), (9.35a), (9.36) and (9.37) with the following interpretations. Thus, when $P \geqq 2$, let us hypothesize to divide each of the two terminal monomer units of the aliphatic chain into two parts (called first and second parts); the terminal monomer units are both methyl groups in the case of n-alkanes, and benzyl and methyl groups in the case of n-alkylbenzenes for instances. Let us also hypothesize that the first part of a terminal monomer unit is equivalent with the inner monomer unit (methylene group) of the aliphatic chain not only in size but also in ability of being adsorbed on the adsorbent surface. [In general, the first part equivalent with the methylene group in size is not identical with that equivalent with the metylene group in ability of being adsorbed. It is only for simplicity that we assume them to be identical. If this is not the situation, all the arguments below will hold by modifying the interpretation slightly.] The second part of the terminal monomer unit is defined as the remainder of the structure of the unit. It is assumed that the terminal monomer unit is larger than the methylene group in size, which is a reasonable assumption. Especially when $P=1$, we consider to divide the total structure of the monomer molecule into two parts with one of them (first part) being equivalent with the methylene group. Here also, it is assumed that the monomer molecule is larger than the methylene group in size.

We interprete that, when $P \geqq 2$, then x'°, E°, τ° and J° represent constants with respect to the sum of the second parts of the two terminal monomer units. We also interpret that x'^{*}, E^{*}, τ^{*} and J^{*} correspond to the remainder of the total molecular structure from which the sum of the second parts of the two terminal monomer units are subtracted; x'^{*}, E^{*}, τ^{*} and J^{*} are functions of P. Especially when $P=1$, then x'^{*}, E^{*}, τ^{*} and J^{*}

Table 9.6

Reproduction of the regression analysis performed by Jandera[ref(9.14) Tables II and III] on a C_{18} column for (a) 1,2-naphthoylenebenzimidazole-6-sulphonamides of aliphatic n-amines (homologous series A) for MtOH/H_2O, DXN/H_2O and ACN/H_2O mobile phase systems, and (b) 3,5-dinitrobenzoates of aliphatic n-alcohols (homologous series B) for MtOH/H_2O, DXN/H_2O, ACN/H_2O and THF/H_2O mobile phase systems.

(a) Homologous series A

Mobile phase system	α_{J0}	β_{J0}	α_{J1}	β_{J1}	$\hat{\alpha}_{J0}$	$\hat{\beta}_{J0}$	$\hat{\alpha}_{J1}$	$\hat{\beta}_{J1}$
MtOH/H_2O	0.467	2.170	0.420	2.918	1.075	4.997	0.967	6.719
DXN/H_2O	0.463	1.420 | 1.426	0.481 | 0.482	3.185 | 3.213	1.066	3.270 | 3.283	1.108 | 1.110	7.334 | 7.398
ACN/H_2O	0.247	0.974	0.159	1.770	0.569	2.243	0.366	4.076

(b) Homologous series B

Mobile phase system	α_{J0}	β_{J0}	α_{J1}	β_{J1}	$\hat{\alpha}_{J0}$	$\hat{\beta}_{J0}$	$\hat{\alpha}_{J1}$	$\hat{\beta}_{J1}$
MtOH/H_2O	0.517	1.713	0.446	2.773	1.190	3.944	1.027	6.385
DXN/H_2O	0.551	1.700 | 1.701	0.580	2.980	1.269	3.914 | 3.917	1.335	6.862
ACN/H_2O	0.251 | 0.253	1.537 | 1.544	0.137	2.882 | 2.901	0.580 | 0.583	3.539 | 3.555	0.315	6.636 | 6.680
THF/H_2O	0.338 | 0.364	1.845 | 1.876	0.372 | 0.424	3.357 | 3.388	0.778 | 0.838	4.248 | 4.320	0.857 | 0.976	7.730 | 7.801

correspond to the first part of the total molecular structure, and x'°, E°, τ° and J° to the remainder of the molecular structure.

It should be noted that the assignment of the parameters x'°, E°, τ° and J° to the two terminal parts of the aliphatic chain is possible only when these keep in contact with the adsorbent surface in the adsorbed state of the molecule. Such a situation would be realizable when the conformation of the aliphatic chain on the adsorbent surface is either stretched or planar as deduced from the experimental analysis which will be performed in the subsequent subsection; the consideration in this subsection is self-consistent with the analysis which will be performed in the subsequent subsection.

For the alalyses of the data for both n-alkane and n-alkylbenzene series obtained on the C_8 column with the ACN/H_2O system in Experiment(1), let us begin with the original form, eq(8.52), of eq(9.1) or (8.65). Eq(8.52) can be rewritten approximately as

$$\begin{aligned} k &= q(\varphi m+1)^{-x'} \\ &= qe^{-x'\ln(\varphi m+1)} \\ &\approx qe^{-x'\varphi m+(x'\varphi^2/2)m^2} \end{aligned} \tag{9.51}$$

or

$$\ln k = -x'\varphi m + \tfrac{1}{2}x'\varphi^2m^2 + \ln q \tag{9.51'}$$

where it should be noted that the parameter φ is appearing in the form other than the form of $x'\varphi$ in the quadratic term with respect to m. Eq(9.51') can be obtained by adding the quadratic term, $\frac{1}{2}x'\varphi^2m^2$, to eq(9.1), and all the arguments can be performed on the basis of eq(9.51') instead of eq(9.1).

Experimental Analysis. With regard to the data for both n-alkane and n-alkylbenzene series obtained on the C_8 column with the MtOH/H_2O system in Experiment(1) and the data for both homologous series A and B obtained on the C_{18} column with any mobile phase system in Experiment(2), eq(9.49) is fulfilled at least approximately, and eq(9.11') holds when eq(9.38) is replaced by

$$\hat{S} = \omega_P^*P + \omega^{\circ} \tag{9.52}$$

with

$$\omega_P^* = \hat{\alpha}_{JI} \tag{9.53}$$

and

$$\omega^{\circ} = \hat{\beta}_{JI} \tag{9.54}$$

On the other hand, ω° can be represented by eq(9.39), and function $f_P^*(P)$ can be represented, instead of eq(9.40), by

$$f_P^*(P) = \omega_P^* P \tag{9.55}$$

This means that

$$P^\circ = 0 \tag{9.56}$$

[cf. eq(9.41)]. ω_P^* can be expressed, instead of eq(9.42), by

$$\omega_P^* = x''\varphi/P \tag{9.57}$$

[cf. eq(9.36)] representing the "relative size" per monomer unit (methylene group) of the aliphatic chain. Eq(9.32b) and eq(9.34b) or (9.34'b) can be replaced by

$$\ln q = \gamma^* \omega_P^* P + \ln (\beta c^{J^\circ/kT}) \tag{9.58}$$

and

$$\ln k = \ln (\beta e^{J^\circ/kT}) - \omega^\circ m + \gamma^* \omega_P^* P - \omega_P^* m P \tag{9.59}$$

respectively.

Eq(9.43) can be replaced by

$$\hat{W} = \Phi_P P + \Phi' \tag{9.60}$$

with

$$\Phi_P = \hat{\alpha}_{J0} \tag{9.61}$$

and

$$\Phi' = \hat{\beta}_{J0} \tag{9.62}$$

On the other hand, Φ_P and Φ' can be represented by eqs(9.44) and (9.45), respectively. Eq(9.53), eq(9.54), eq(9.61) [combined with eq(9.44)] and eq(9.62) [combined with eq(9.45)] can also be derived by comparing eq(9.59) with eq(9.49).

With regard to the data for both n-alkane and n-alkylbenzene series obtained on the C_8 column with the ACN/H_2O system in Experiment(1), eq(9.50) is fulfilled instead of eq (9.49), and eq(9.11') is replaced by

$$\ln k = -\hat{S} m + \hat{T} m^2 + \hat{W} \tag{9.63}$$

All eqs(9.52)-(9.62) still hold, and $\hat{T}$ [in eq(9.63)] can be represented as

$$\hat{T} = \hat{\alpha}_{J2} P + \hat{\beta}_{J2} \tag{9.64}$$

[cf. eq(9.63) with eq(9.50)]. On the other hand, by comparing eq(9.63) with eq(9.51') and using eqs(9.24), (9.39) and (9.57), $\hat{T}$ can also be written as

$$\hat{T} = \tfrac{1}{2} x' \varphi^2 = \tfrac{1}{2} \omega_P^* \varphi P + \tfrac{1}{2} \omega^\circ \varphi \tag{9.65}$$

from which it follows:

$$\tfrac{1}{2}\,\omega_P^{*}\varphi = \alpha_{J2} \tag{9.66}$$

and

$$\tfrac{1}{2}\,\omega^{\circ}\varphi = \beta_{J2} \tag{9.67}$$

[cf. eq(9.65) with eq(9.64)]. Eq(9.51') can be rewritten as

$$\ln k = \ln\left(\beta\, e^{J^{\circ}/kT}\right) - \omega^{\circ} m + \gamma^{*}\omega_P^{*} P - \omega_P^{*} mP + \tfrac{1}{2}\omega^{\circ}\varphi\, m^2 + \tfrac{1}{2}\omega_P^{*}\varphi\, m^2 P \tag{9.68}$$

which can be compared with eq(9.59).

In contrast to the case of low M_n polystyrenes when ln k is a direct function of $(P-2)^{2/3}$ [eq(9.34b) or (9.34'b)], ln k now is a direct function of P [eq(9.59) or (9.68)]. This implies that the area of the C_8 or C_{18} surface occupied by the adsorbed molecule [proportional to x' $(=x''^{*}+x'^{\circ})$] now is a linear function of P. For this to be realized actually, it would be necessary that the conformation of the molecule taking place on the C_8 or C_{18} surface be either stretched or planar (rather than three-dimensional).

The size and the ability of being adsorbed on the adsorbent surface assigned to the second part of the structure of the monomer molecule (with P=1), in general, are different from those assigned to the sum of the second parts of the two terminal residues of the polymer chain (with $P \geqq 2$), respectively. In the linear ln k versus P plots obtained for a constant m value, such differences may bring about a deviation of the experimental point for the monomer molecule. It can be seen in Fig 9.26 that some experimental points (corresponding to some m values) for the monomer molecule of the n-alkylbenzene series deviate slightly from linearity on the (P, $\log_{10}$ k) plane. The same phenomena can also be found in the $\log_{10}$ k versus P plots for a series of p-bromophenacyl esters of lower aliphatic carboxylic acids illustrated in ref(9.14) Fig 1. It might be possible that the phenomena under consideration take place caused by such a mechanism.

The fact that the ln k versus P plots always manifest a good linear arrangement (except for the experimental point for the monomer molecule) corresponds to the fact that ln k is a linear function of P in both eqs(9.59) and (9.68), reinforcing again the proof for the competition model with reversed-phase chromatogrphy.

Important Results Obtained from the Alalyses for the n-Alkane and n-Alkylbenzene Series on the C_8 Column with the MtOH/H_2O System [part of Experiment(1)]. These are summarized in Tables 9.7 and 9.8, respectively, where, as anticipated, it can be confirmed that the "relative size" per inner monomer unit (methylene group), $x''^{*}\varphi/P$, for n-alkanes is almost equal to that for n-alkylbenzenes (cf. Table 9.7 column<1> with Table 9.8 column<1>). These are about half the "relative size" per inner monomer unit, $x''^{*}\varphi/(P-2)^{2/3}$, for the three-dimensional conformation part of low M_n polystyrenes in the THF/H_2O sys-

Table 9.7

Summary of the analysis of the experiments of n-alkanes performed in the MtOH/H_2O mobile phase sysyem on the C_8 column by Jandera(9.13). The value of kT at 25℃ (2.48 kJ/mol) is used for the analysis.

⟨1⟩	⟨2⟩	⟨3⟩	⟨3a⟩	⟨3b⟩	
$\omega_P^* = x'^*\varphi/P = \hat{\alpha}_{J1}$	$\omega^\circ = x'^\circ\varphi = \hat{\beta}_{J1}$	$2x'^*\varphi/P + x'^\circ\varphi$	$(2x'^*\varphi/P + x'^\circ\varphi)/2$	$[(2x'^*\varphi/P + x'^\circ\varphi)/2]/(x'^*\varphi/P)$	
1.01	4.03	6.05	3.03	3.00	⇒

⟨4⟩	⟨5⟩	⟨6⟩	⟨7⟩	⟨8⟩	⟨9⟩	
$\gamma^*\omega_P^* = J^*/(PkT) = \hat{\alpha}_{J0}$	$\gamma^*\omega_P^*kT = J^*/P$ (kJ/mol)	$\gamma^* = \hat{\alpha}_{J0}/\hat{\alpha}_{J1}$	$\gamma^*kT = J^*/(x'^*\varphi)$ (kJ/mol)	$\ln(\beta e^{J^\circ/kT}) = \hat{\beta}_{J0}$	$J^\circ/kT = \hat{\beta}_{J0} - \ln\beta = \hat{\beta}_{J0} + 3.84$	
1.13	2.80	1.12	2.78	1.43	5.27	⇒

⇒

⟨10⟩	⟨11⟩	⟨11a⟩	⟨11b⟩	⟨12⟩	⟨13⟩	⟨14⟩
J° (kJ/mol)	$2J^*/P + J^\circ$ (kJ/mol)	$(2J^*/P + J^\circ)/2$ (kJ/mol)	$[(2J^*/P + J^\circ)/2]/(J^*/P)$	φ	x'^*/P	$(2x'^*/P + x'^\circ)/2$
13.07	18.67	9.34	3.34	$\lesssim 0.56$	$\gtrsim 1.80$	$\gtrsim 5.41$

⇒

Table 9.8

Summary of the analysis of the experiments of n-alkylbenzenes performed in the MtOH/H_2O mobile phase system on the C_8 column by Jandera(9.13). The value of kT at 25℃ (2.48 kJ/mol) is used for the analysis.

⟨1⟩	⟨2⟩	⟨3⟩	⟨3a⟩	⟨3a'⟩	⟨3b'⟩
$\omega_P^*=$ $x''\varphi/P=$ $\hat{\alpha}_{J1}$	$\omega^\circ=$ $x'^\circ\varphi=$ $\hat{\beta}_{J1}$	$2x''\varphi/P$ $+x'^\circ\varphi$	$3.00x''\varphi$ $/P$	$(2x''\varphi/P+x'^\circ\varphi)$ $-3.00x''\varphi/P=$ $x'^\circ\varphi-x''\varphi/P$	$(x'^\circ\varphi-x''\varphi/P)$ $/(x''\varphi/P)$
1.06 ∣ 1.13	5.80 ∣ 6.03	7.92 ∣ 8.29	3.18 ∣ 3.39	4.67 ∣ 4.97	4.13 ∣ 4.69

⇒

⟨4⟩	⟨5⟩	⟨6⟩	⟨7⟩	⟨8⟩	⟨9⟩
$\gamma^*\omega_P^*=$ $J^*/(PkT)=$ $\hat{\alpha}_{J0}$	$\gamma^*\omega_P^*kT=$ J^*/P (kJ/mol)	$\gamma^*=$ $\hat{\alpha}_{J0}/\hat{\alpha}_{J1}$	$\gamma'kT=$ $J^*/(x''\varphi)$ (kJ/mol)	$\ln(\beta e^{J^\circ/kT})=$ $\hat{\beta}_{J0}$	$J^\circ/kT=$ $\hat{\beta}_{J0}-\ln\beta=$ $\hat{\beta}_{J0}+3.84$
1.15 ∣ 1.20	2.85 ∣ 2.98	1.02 ∣ 1.13	2.53 ∣ 2.80	3.32 ∣ 3.52	7.16 ∣ 7.36

⇒ ⇒

⟨10⟩	⟨11⟩	⟨11a⟩	⟨11a'⟩	⟨11b'⟩
J° (kJ/mol)	$2J^*/P$ $+J^\circ$ (kJ/mol)	$3.34\ J^*/P$ (kJ/mol)	$(2J^*/P+J^\circ)-3.34J^*/P=$ $J^\circ-1.34J^*/P$ (kJ/mol)	$(J^\circ-1.34J^*/P)$ $/(J^*/P)$
17.76 ∣ 18.25	23.46 ∣ 24.21	9.52 ∣ 9.95	13.77 ∣ 14.43	4.62 ∣ 5.06

⇒ ⇒

⟨12⟩	⟨13⟩	⟨14⟩	⟨15⟩
φ	x''/P	$3.00x''/P$	$x'^\circ-x''/P$
$\lesssim 0.56$	$\gtrsim 1.89$ ∣ 2.02	$\gtrsim 5.68$ ∣ 6.05	$\gtrsim 8.34$ ∣ 8.88

⇒

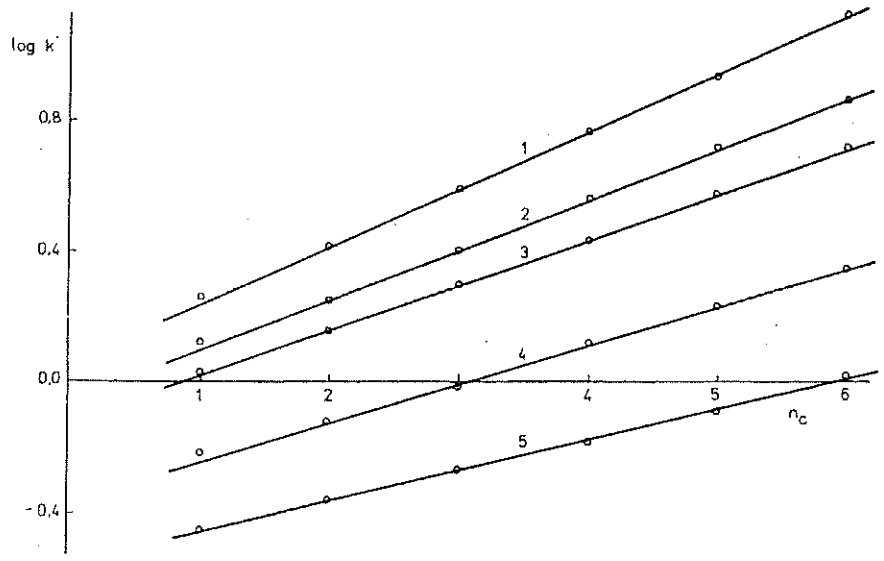


Fig 9.26. Plots of log k' i.e., $\log_{10}$ k versus number, n_c i.e., P, of carbon atoms in the alkyl chains for n-alkylbenzenes, obtained for isocratic chromatography carried out on a C_8 column in the presences of ACN/H_2O mobile phase systems with volume fraction, m, of ACN equal to 0.50 (1), 0.55 (2), 0.60 (3), 0.70 (4) and 0.80 (5). The regression line for any m value can be represented by eq(9.50) with the values of the parameters given in Table 9.5(b). [Reproduced from ref(9.13) Fig 3.]

tem (Table 9.4 column<1>), about equal to or smaller than half that per inner monomer unit, $x'\varphi/P^{2/3}$, for high M_m polystyrenes in the THF/H_2O system, and about equal to $x'\varphi/P^{2/3}$ for high M_m polystyrenes in the $MeCl_2$/ACN system (Table 9.1 column <1>).

The "relative size" of each of the two terminal methyl groups of n-alkanes [which can be represented as $(2x''\varphi/P+x'^{\circ}\varphi)/2$; Table 9.7 column <3a>] is three times as largre as that of the inner methylene group ($x''\varphi/P$; see Table 9.7 column <3b>); this is a reasonable conclusion. Assuming that the "relative size" of the methyl group at one of the two terminals of n-alkylbenzenes is also three times as large as that of the inner methylene group, the "relative size" of the benzyl group at the other terminal can be represented as $2x''\varphi/P+x'^{\circ}\varphi-3.00x''\varphi/P=x'^{\circ}\varphi-x''\varphi/P$; this (Table 9.8 column<3a'>) is 4.1 to 4.7 times as large as that for the inner methylene group ($x''\varphi/P$; see Table 9.8 column <3b'>). This implies that the "relative size" of the benzyl group is larger than that of the methyl group, which is a reasonable conclusion again.

As anticipated, the AVFA per inner methylene group, J^*/P, for n-alkanes is almost equal to that for n-alkylbenzenes (cf. Table 9.7 column<5> with Table 9.8 column<5>). These are about 0.6 times as large as the AVFA per inner monomer unit, $J^*/(P-2)^{2/3}$, for the three-dimensional conformation part of low M_m polystyrenes in the THF/H_2O system (Table 9.4 column<5>), 0.3 to 0.6 times as large as that per inner monomer unit, $J/P^{2/3}$, for high M_m polystyrenes in the THF/H_2O system, and 1.2 to 2 times as large as $J/P^{2/3}$ for high M_m polystyrenes in the $MeCl_2$/ACN system (Table 9.1 column<5>).

By using the $\ln\beta$ value of -3.84 estimated for the C_8 column (Table 9.1 column <8>), J° for n-alkkanes can be evaluated (Table 9.7 column<10>). By using this J° value along with the J^*/P value (Table 9.7 column<5>), the AVFA for each of the two terminal methyl groups of n-alkanes [which can be represented as $(2J^*/P+J^\circ)/2$] can be estimated (Table 9.7 column<11a>); this is 3.34 times as large as that for the inner methylene group (J^*/P; see Table 9.7 column<11b>). Assuming that the AVFA for the methyl group at one of the two terminals of n-alkylbenzenes is also 3.34 times as large as that for the inner methylene group, the AVFA for the benzyl group at the other terminal can be represented as $2J^*/P+J^\circ-3.34J^*/P=J^\circ-1.34J^*/P$; this (Table 9.8 column<11a'>) is 4.6 to 5.1 times as large as that for the inner methylene group (J^*/P; see Table 9.8 column <11b'>)

Let us assume that the upper limit, $(\varphi\ m)_{u.l.}$, of the φ m value that brings about practically linear arrangements of the ln k versus m plots is 0.5. As the maximum m value used for the experiment is 0.9 [see the subsection entitled "Experiment(1)"], the upper limit of the possible φ values can be estimated to be $0.5/0.9=0.56$ (see both Table 9.7 column<12> and Table 9.8 column<12>). The lower limits of the "sizes" can now be evaluated for the inner methylene group of n-alkanes (Table 9.7 column<13>), each of the two terminal methyl groups of n-alkanes (Table 9.7 column<14>), the inner methylene group of n-alkylbenzenes (Table 9.8 column<13>), the terminal methyl group of n-alkylbenzenes (Table 9.8 column<14>), and the terminal benzyl group of n-alkylbenzenes (Table 9.8 column<15>).

Important Results Obtained from the Alalyses for the n-Alkane and n-Alkylbenzene Series on the C_8 Column with the ACN/H_2O System [the other part of Experiment(1)]. These are summarized in Tables 9.9 and 9.10, respectively, where, as anticipated, it can be confirmed again that the "relative size" per inner monomer unit (methylene group), $x''\varphi/P$, for n-alkanes is about equal to that for n-alkylbenzenes (cf. Table 9.9 column <1> with Table 9.10 column<1>). These are larger than those for the MtOH/H_2O system (see both Table 9.7 column<1> and Table 9.8 column<1>), and close to the "relative size" per inner monomer unit, $x''\varphi/(P-2)^{2/3}$, for the three-dimensional conformation part of low M_n polystyrenes in the THF/H_2O system (Table 9.4 column<1>).

The "relative size" of each of the two terminal methyl groups of n-alkanes [$(2x''\varphi/P + x'^{\circ}\varphi)/2$; Table 9.9 column <3a>] now is 2.38 times as largre as that of the inner methylene group ($x''\varphi/P$; see Table 9.9 column <3b>). Assuming that the "relative size" of the methyl group at one of the two terminals of n-alkylbenzenes is also 2.38 times as large as that of the inner methylene group, the "relative size" of the benzyl group at the other terminal can be represented as $2x''\varphi/P + x'^{\circ}\varphi - 2.38x''\varphi/P = x'^{\circ}\varphi - 0.38x''\varphi/P$; this (Table 9.10 column<3a'>) is 3.4 times as large as that for the inner methylene group($x''\varphi/P$; see Table 9.10 column <3b'>).

As anticipated, the AVFA per inner methylene group, J^*/P, for n-alkanes is almost equal to that for n-alkylbenzenes (cf. Table 9.9 column<5> with Table 9.10 column<5>). These are also almost equal to those for the MtOH/H_2O system (see both Table 9.7 column<5> and Table 9.8 column<5>).

The J° value for n-alkanes estimated by using the $\ln\beta$ value of -3.84 (see above) is presented in Table 9.9 column<10>; this is equal to the corresponding value with the MtOH/H_2O system (Table 9.7 column<10>). The AVFA for each of the two terminal methyl group of n-alkanes [$(2x''\varphi/P + x'^{\circ}\varphi)/2$] can now be estimated (Table 9.9 column <11a>); this is equal to the corresponding value with the MtOH/H_2O system (Table 9.7 column<11a>) and 3.34 times as large as that for the inner methylene group (J^*/P; see Table 9.9 column<11b>). Assuming that the AVFA for the methyl group at one of the two terminals of n-alkylbenzenes is also 3.34 times as large as that for the inner methylene group, the AVFA for the benzyl group at the other terminal can be estimated (Table 9.10 column<11a'>); this is almost equal to the corresponding value with the MtOH/H_2O system (Table 9.8 column<11a'>) and 5.1 times as large as that for the inner methylene group (J^*/P; see Table 9.10 column<11b'>).

From the two quadratic terms (with respect to m) in eq(9.68), the parameter φ can be evaluated independently [cf. both eqs(9.66) and (9.67)]; these two φ values should be identical. Of course, φ should also be independent of the type of sample molecule applied to the experiment. It can be seen in Table 9.9 column<12a> and <12b>, and Table 9.10 column<12a> and <12b>, however, that the two φ values [arising from eqs(9.66) and (9.67), respectively] are different to some extent both when n-alkanes are applied and when n-alkylbenzenes are applied; the range of the variations of the φ values are almost the same

Table 9.9

Summary of the analysis of the experiments of n-alkanes performed in the ACN/H_2O mobile phase system on the C_8 column by Jandera(9.13). The value of kT at 25℃ (2.48 kJ/mol) is used for the analysis.

⟨1⟩	⟨2⟩	⟨3⟩	⟨3a⟩	⟨3b⟩
$\omega_P^* = x'^*\varphi/P = \hat{\alpha}_{J1}$	$\omega^\circ = x'^\circ\varphi = \hat{\beta}_{J1}$	$2x'^*\varphi/P + x'^\circ\varphi$	$(2x'^*\varphi/P + x'^\circ\varphi)/2$	$[(2x'^*\varphi/P + x'^\circ\varphi)/2]/(x'^*\varphi/P)$
1.82	5.02	8.66	4.33	2.38

⇒

⟨4⟩	⟨5⟩	⟨6⟩	⟨7⟩	⟨8⟩	⟨9⟩
$\gamma^* \omega_P^* = J^*/(PkT) = \hat{\alpha}_{J0}$	$\gamma^* \omega_P^* kT = J^*/P$ (kJ/mol)	$\gamma^* = \hat{\alpha}_{J0}/\hat{\alpha}_{J1}$	$\gamma^* kT = J^*/(x'^*\varphi)$ (kJ/mol)	$\ln(\beta e^{J^\circ/kT}) = \hat{\beta}_{J0}$	$J^\circ/kT = \hat{\beta}_{J0} - \ln\beta = \hat{\beta}_{J0} + 3.84$
1.13	2.80	0.621	1.54	1.43	5.27

⇒ ⇒

⟨10⟩	⟨11⟩	⟨11a⟩	⟨11b⟩	⟨12a⟩	⟨12b⟩	⟨13⟩	⟨14⟩
J° (kJ/mol)	$2J^*/P + J^\circ$ (kJ/mol)	$(2J^*/P + J^\circ)/2$ (kJ/mol)	$[(2J^*/P + J^\circ)/2]/(J^*/P)$	$\varphi = 2\hat{\beta}_{J2}/\omega^\circ$	$\varphi = 2\hat{\alpha}_{J2}/\omega_P^*$	x'^*/P	$(2x'^*/P + x'^\circ)/2$
13.07	18.67	9.34	3.34	0.64	1.01	1.80 | 2.84	4.29 | 6.77

⇒

Table 9.10

Summary of the analysis of the experiments of n-alkylbenzenes performed in the ACN/H_2O mobile phase system on the C_8 column by Jandera(9.13). The value of kT at 25℃ (2.48 kJ/mol) is used for the analysis.

⟨1⟩	⟨2⟩	⟨3⟩	⟨3a⟩	⟨3a'⟩	⟨3b'⟩
$\omega_P' = x''\varphi/P = \hat{\alpha}_{J1}$	$\omega^\circ = x'^\circ\varphi = \hat{\beta}_{J1}$	$2x''\varphi/P + x'^\circ\varphi$	$2.38x''\varphi/P$	$(2x''\varphi/P + x'^\circ\varphi) - 2.38x''\varphi/P = x'^\circ\varphi - 0.38x''\varphi/P$	$(x'^\circ\varphi - 0.38x''\varphi/P)/(x''\varphi/P)$
2.07	7.81	11.95	4.93	7.02	3.39

⇒

⟨4⟩	⟨5⟩	⟨6⟩	⟨7⟩	⟨8⟩	⟨9⟩
$\gamma' \omega_P' = J'/(PkT) = \hat{\alpha}_{J0}$	$\gamma' \omega_P' kT = J'/P$ (kJ/mol)	$\gamma' = \hat{\alpha}_{J0}/\hat{\alpha}_{J1}$	$\gamma' kT = J'/(x''\varphi)$ (kJ/mol)	$\ln(\beta e^{J^\circ/kT}) = \hat{\beta}_{J0}$	$J^\circ/kT = \hat{\beta}_{J0} - \ln\beta = \hat{\beta}_{J0} + 3.84$
1.15	2.85	0.556	1.38	3.52	7.36

⇒ ⇒

⟨10⟩	⟨11⟩	⟨11a⟩	⟨11a'⟩	⟨11b'⟩
J° (kJ/mol)	$2J'/P + J^\circ$ (kJ/mol)	$3.34\ J'/P$ (kJ/mol)	$(2J'/P + J^\circ) - 3.34J'/P = J^\circ - 1.34J'/P$ (kJ/mol)	$(J^\circ - 1.34J'/P)/(J'/P)$
18.25	23.95	9.52	14.43	5.06

⇒ ⇒

⟨12a⟩	⟨12b⟩	⟨13⟩	⟨14⟩	⟨15⟩
$\varphi = 2\hat{\beta}_{J2}/\omega^\circ$	$\varphi = 2\hat{\alpha}_{J2}/\omega_P'$	x''/P	$2.38x''/P$	$x'^\circ - 0.38x''/P$
0.58	1.09	1.90 | 3.57	4.52 | 8.50	6.44 | 12.1

⇒

between the experiments of the two types of polymer molecule. Taking into account the technical difficulty of measuring the exact values of both parameters $\hat{\alpha}_{12}$ and $\hat{\beta}_{12}$ [as mentioned in both refs(9.13, 9.14)], it would be reasonable to consider that the difference of the φ values estimated from the two quadratic terms reside within the range of the experimental error. When the parameter φ is evaluated, the "sizes" can be evaluated for the inner methylene group of n-alkanes (Table 9.9 column<13>), each of the two terminal methyl groups of n-alkanes (Table 9.9 column<14>), the inner methylene group of n-alkylbenzenes (Table 9.10 column<13>), the terminal methyl group of n-alkylbenzenes (Table 9.10 column<14>), and the terminal benzyl group of n-alkylbenzenes (Table 9.10 column <15>).

Important Results Obtained from the Alalyses for the Homologous Series A and B on the C_{18} Column with MtOH/H_2O, DXO/H_2O, ACN/H_2O and THF/H_2O Systems [Experiment(2)]. The results for homologous series A and B are summarized in Tables 9.11 and 9.12, respectively, where, with respect to MtOH/H_2O, DXO/H_2O and ACN/H_2O systems, it can be confirmed that the "relative size" per inner monomer unit (methylene group), $x''\varphi/P$, for homologous series A is approximately equal to that for homologous series B (cf. Table 9.11 column<1> with Table 9.12 column<1>). The $x''\varphi/P$ values for both series A and B in the MtOH/H_2O system are almost equal to that for either n-alkane or n-alkylbenzene series in the MtOH/H_2O system on the C_8 column (see both Table 9.7 column<1> and Table 9.8 column<1>). On the other hand, the $x''\varphi/P$ values for both series A and B in the ACN/H_2O system are about one third the corresponding values in the MtOH/H_2O system (see both Table 9.11 column<1> and Table 9.12 column<1>). This is in contrast to the fact that, with both n-alkane and n-alkylbenzene series on the C_8 column, the $x''\varphi/P$ values in the ACN/H_2O system are roughly twice the corresponding values in the MtOH/H_2O system (cf. Table 9.7 column<1> with Table 9.9 column<1>, and cf. Table 9.8 column<1> with Table 9.10 column<1>). For both series A and B in any mobile phase system, the "relative size" of the sum of the two terminal monomer units ($2x''\varphi/P+x'^{\circ}\varphi$) is ten to twenty times as large as that of the methylene group ($x''\varphi/P$) (see Table 9.11 column<1> and <3>, and Table 9.12 column<1> and <3>).

The AVFA per inner methylene group, J^*/P, for series A are approximately equal to those for series B in MtOH/H_2O, DXO/H_2O and ACN/H_2O systems, respectively (see both Table 9.11 column<5> and Table 9.12 column<5>); these are fluctuating around the corresponding values for both n-alkane and n-alkylbenzene series in MtOH/H_2O and ACN /H_2O systems (see Tables 9.7-9.10 column<5>, respectively).

By using the $\ln\beta$ value of -9.08 to -7.34 estimated for the C_{18} column (Table 9.1 column <8>), J° for both series A and B can be evaluated (see both Table 9.11 column<10> and Table 9.12 column<10>). By using these J° values along with the J^*/P values (Table 9.11 column<5> and Table 9.12 column<5>), the AVFA for the sum of the two terminal monomer units ($2J^*/P+J^{\circ}$) can be estimated (Table 9.11 column<11> and Table 9.12 column<11>); these are more than ten times as large as those for the inner methyl-

Table 9.11

Summary of the analysis of the experiments of 1,2-naphthoylenebenzimidazole-6-sulphonamides of aliphatic n-amines (homologous series A) performed in MtOH/H_2O, DXN/H_2O and ACN/H_2O mobile phase systems on the C_{18} column by Jandera(9.14). The value of kT at 25℃ (2.48 kJ/mol) is used for the analysis.

	⟨1⟩	⟨2⟩	⟨3⟩	⟨4⟩	⟨5⟩
Mobile phase system	$\omega_P^* = x''^*\varphi/P = \hat{\alpha}_{J1}$	$\omega^\circ = x''^\circ\varphi = \hat{\beta}_{J1}$	$2x''^*\varphi/P + x''^\circ\varphi$	$\gamma^*\omega_P^* = J'/(PkT) = \hat{\alpha}_{J0}$	$\gamma^*\omega_P^*kT = J^*/P$ (kJ/mol)
MtOH/H_2O	0.967	6.719	8.653	1.075	2.67
DXN/H_2O	1.108 | 1.110	7.334 | 7.398	9.550 | 9.618	1.066	2.64
ACN/H_2O	0.366	4.076	4.808	0.569	1.41

	⟨6⟩	⟨7⟩	⟨8⟩	⟨9⟩	⟨10⟩	⟨11⟩
	$\gamma^* = \hat{\alpha}_{J0}/\hat{\alpha}_{J1}$	$\gamma^*kT = J'/(x''^*\varphi)$ (kJ/mol)	$\ln(\beta e^{J^\circ/kT}) = \hat{\beta}_{J0}$	$J^\circ/kT = \hat{\beta}_{J0} - \ln\beta = \hat{\beta}_{J0} + (7.34 \text{ to } 9.08)$	J° (kJ/mol)	$2J^*/P + J^\circ$ (kJ/mol)
⇒	1.112	2.76	4.997	12.34 | 14.08	30.60 | 34.92	35.94 | 40.26
⇒	0.960 | 0.962	2.38 | 2.39	3.270 | 3.283	10.61 | 12.36	26.31 | 30.65	31.59 | 35.93
⇒	1.555	3.86	2.243	9.58 | 11.32	23.76 | 28.07	26.58 | 30.89

Table 9.12

Summary of the analysis of the experiments of 3,5-dinitrobenzoates of aliphatic n-alcohols (homologous series B) performed in MtOH/H_2O, DXN/H_2O, ACN/H_2O and THF/H_2O mobile phase systems on the C_{18} column by Jandera(9.14). The value of kT at 25℃ (2.48 kJ/mol) is used for the analysis.

	⟨1⟩	⟨2⟩	⟨3⟩	⟨4⟩	⟨5⟩		⟨6⟩	⟨7⟩	⟨8⟩	⟨9⟩	⟨10⟩	⟨11⟩
Mobile phase system	$\omega_P^* = x'^*\varphi/P = \hat{\alpha}_{J1}$	$\omega^\circ = x'^\circ\varphi = \hat{\beta}_{J1}$	$2x'^*\varphi/P + x'^\circ\varphi$	$\gamma^*\omega_P^* = J^*/(PkT) = \hat{\alpha}_{J0}$	$\gamma^*\omega_P^* kT = J^*/P$ (kJ/mol)		$\gamma^* = \hat{\alpha}_{J0}/\hat{\alpha}_{J1}$	$\gamma^* kT = J^*/(x'^*\varphi)$ (kJ/mol)	$\ln(\beta e^{J^\circ/kT}) = \hat{\beta}_{J0}$	$J^\circ/kT = \hat{\beta}_{J0} - \ln\beta = \hat{\beta}_{J0} + (7.34 \text{ to } 9.08)$	J° (kJ/mol)	$2J^*/P + J^\circ$ (kJ/mol)
MtOH/H_2O	1.027	6.385	8.439	1.190	2.95	⇒	1.159	2.87	3.944	11.28 | 13.02	27.97 | 32.29	33.87 | 38.19
DXN/H_2O	1.335	6.862	9.532	1.269	3.15	⇒	0.951	2.36	3.914 | 3.917	11.25 | 13.00	27.90 | 32.24	34.20 | 38.54
ACN/H_2O	0.315	6.636 | 6.680	7.266 | 7.310	0.580 | 0.583	1.44 | 1.45	⇒	1.841 | 1.851	4.57 | 4.59	3.539 | 3.555	10.88 | 12.64	26.98 | 31.35	29.86 | 34.25
THF/H_2O	0.857 | 0.976	7.730 | 7.801	9.444 | 9.753	0.778 | 0.838	1.93 | 2.08	⇒	0.797 | 0.978	1.98 | 2.43	4.248 | 4.320	11.59 | 13.40	28.74 | 33.23	32.60 | 37.39

ene group (J^*/P; Table 9.11 column<5> and Table 9.12 column<5>).

With regard to the THF/H_2O system, the $x'^*\varphi/P$ and J^*/P values for homologous series B (last lines in Table 9.12 column<1> and <5>) are slightly smaller than halves the $x'^*\varphi/(P-2)^{2/3}$ and $J^*/(P-2)^{2/3}$ values for the three-dimensional conformation part of low M_n polystyrenes (in the THF/H_2O system on the C_{18} column; Table 9.4 column<1> and <5>), respectively.

For all the arguments in this Section, recall Note in the subsection entitled "Summary of the Important Results Obtained from the Analyses of Both Figs 9.1 and 9.2" in Section(C)

Chapter X. Ion-Exchange Chromatography versus Competition Model

(A) General Aspect of Ion-Exchange Chromatography

Different from reversed-phase chromatography [Chapter IX], with ion-exchange chromatography, it is the plots of log k versus log m (rather than the plots of log k versus m) that often give a linear arrangement of the experimental points with a negative slope; m now represents the concentration or molarity of the active gradient substance i.e., the cation or the anion from the buffer with cation- and anion-exchange chromatographies, respectively. Let us begin with taking brief looks at several typical examples of ion-exchange chromatographies of proteins and peptides.

Fig 10.1 [reproduced from ref(10.1)] illustrates the plots of $\log_{10}$ k (written as Log k') versus $\log_{10}$ (1/[NaCl]) (written as Log 1/[NaCl]; [ ] represents molarity) for β-lactoglobulin A [$M_m = 3.5 \times 10^4$ Da when it is in the dimer state, and $M_m = 1.75 \times 10^4$ Da when it is in the monomer state], obtained for isocratic chromatography carried out on an anion-exchange column while changing [NaCl] at four different pH: 5, 6, 7 and 8, respectively. It can be assumed that the chloride ion will play a role of the active gradient substance if the gradient elution mode is applied; $\log_{10}$ (1/[NaCl]) can be rewritten as $-\log_{10}$ [Cl^-] or $-\log_{10}$ m. It can be seen in Fig 10.1 that the plots at any pH give an almost linear arrangement with a positive slope; this means that the arrangement of the experimental points give a negative slope if it is mapped to the ($\log_{10}$ m, $\log_{10}$ k) plane. Let us denote by $\bar{x}'$ the absolute value ($= -d\log_{10} k/d\log_{10} m$) of the negative slope of the arrangement on the ($\log_{10}$ m, $\log_{10}$ k) plane. $\bar{x}'$ also represents the absolute value ($= -d\ln k/d\ln m$) of the negative slope of the arrangement mapped again to the (ln m, ln k) plane. It can also be seen in Fig 10.1 that all the arrangements of the experimental points taking place when pH$\geqq$6 are quasi-identical with one another with $\bar{x}' = 8.2$ to 8.3, whereas the arrangement taking place when pH=5 gives $\bar{x}'$ a value of 3.6 (see the legend for Fig 10.1). It would be reasonable to assume that, when pH$\geqq$6, β-lactoglobulin A is in the dimer state, whereas it is in the monomer state when pH=5 [see the subsection entitled "Interpretation on Fig 10.1" in the subsequent Section(B)].

Fig 10.2 [reproduced from ref(10.2)] illustrates the plots of k (written as k') versus [Ca^{2+}] (written as [Ca^{+2}]) (part A) and the plots of $\log_{10}$ k (written as Log k') versus $\log_{10}$ (1/[Ca^{2+}]) [written as Log (1/[Ca^{+2}])] (part B) for α-chymotrypsinogen A (○; $M_m = 2.5 \times 10^4$ Da), pancreatic trypsin inhibitor (■; $M_m = 6.3 \times 10^3$ Da), cytochrome c (▲; $M_m = 1.25 \times 10^4$ Da) and lysozyme (●; $M_m = 1.43 \times 10^4$ Da), obtained for isocratic chromatography carried out on a cation-exchange column while changing [Ca^{2+}] or the molarity of the calcium acetate buffer at pH 4.90, respectively; $\log_{10}$ (1/[Ca^{2+}]) can be rewritten as $-\log_{10}$ m. It can be seen in Fig 10.2(B) that the plots for any protein give an almost linear arrangement with $\bar{x}' = 3.27$ for α-chymotrypsinogen A, $\bar{x}' = 2.69$ for pancreatic trypsin inhibitor, $\bar{x}' = 3.24$ for cytochrome c and $\bar{x}' = 3.39$ for lysozyme [see ref(10.2) Table I].

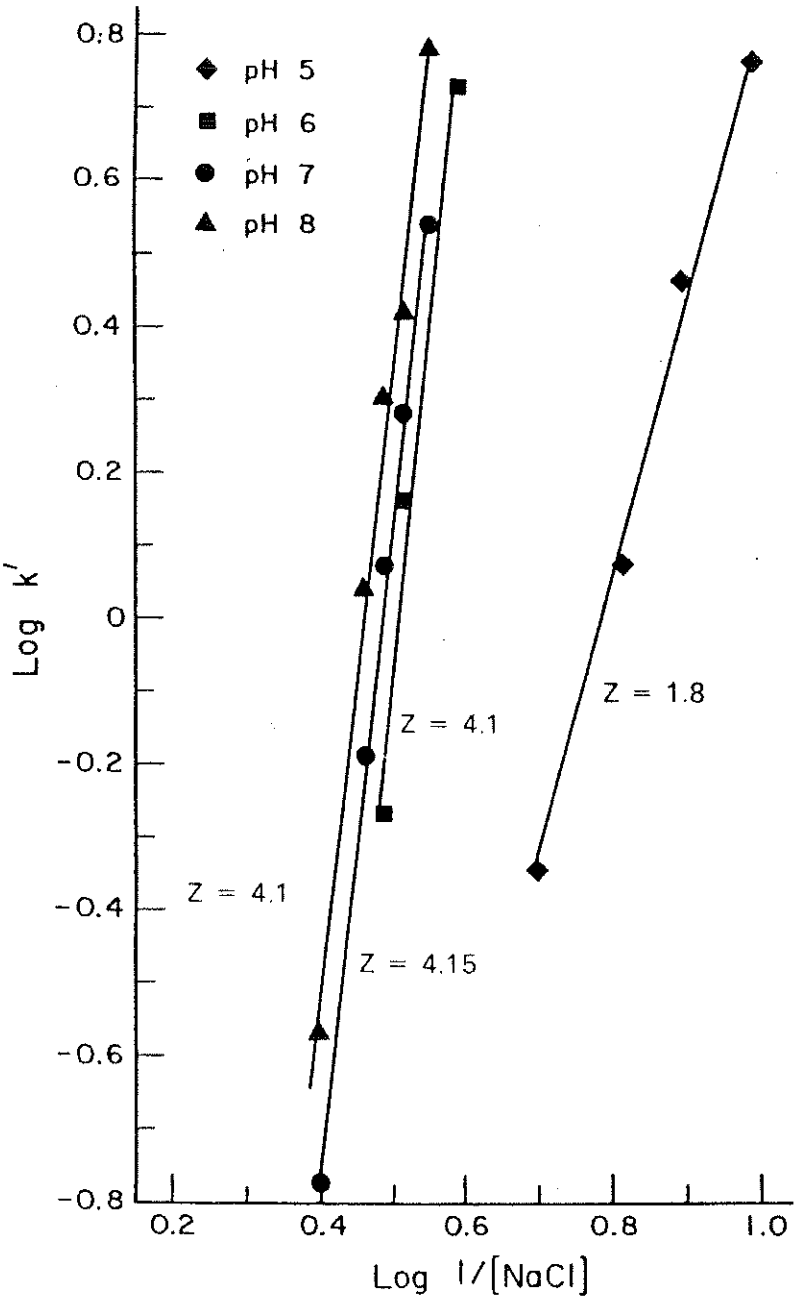


Fig 10.1. Plots of Log k' i.e., $\log_{10}$ k versus Log 1/[NaCl] i.e., $\log_{10}$ (1/[NaCl]) for β-lactoglobulin A, obtained for isocratic chromatography carried out on an anion-exchange column while changing the [NaCl] value at four different pH: 5, 6, 7 and 8, respectively. It can be assumed that the chloride ion will play a role of the active gradient substance if the gradient elution mode is applied; $\log_{10}$ (1/[NaCl]) can be rewritten as $-\log_{10}$ $[Cl^-]$ or $-\log_{10}$ m. The regression lines for the experimental plots re-drawn on the (ln m, ln k) plane can be represented by eq(10.6) in which $\bar{x}$ corresponds to 2Z; Z is indicated in the diagram. [Reproduced from ref(10.1) Fig 11.]

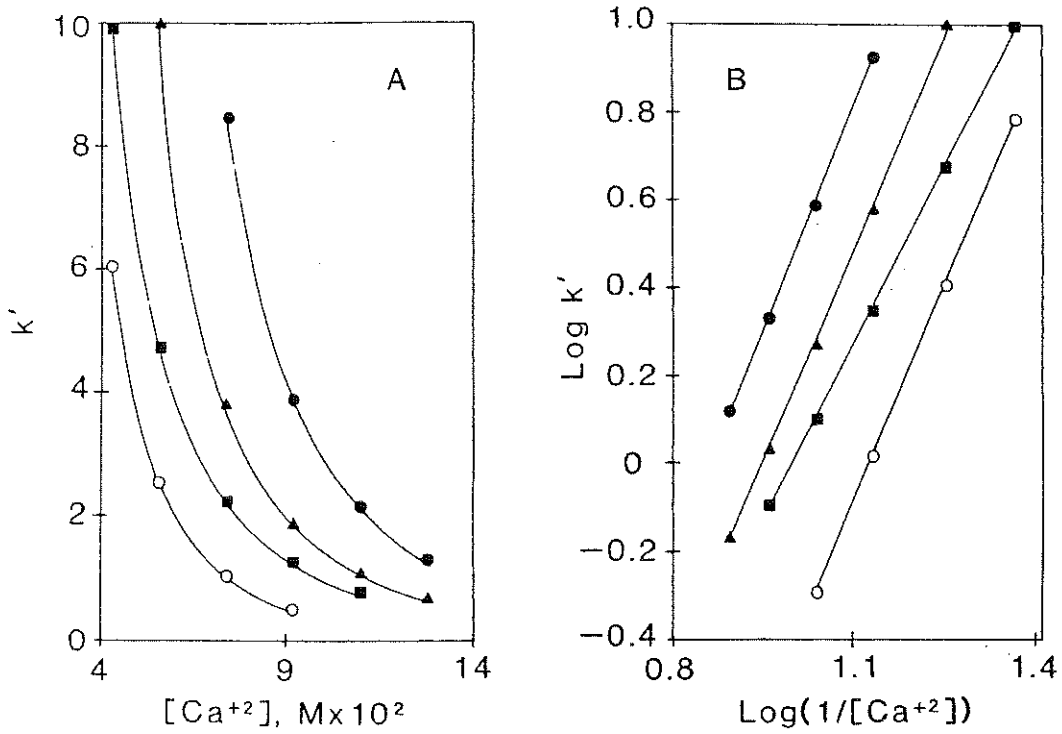


Fig 10.2. Plots of k' i.e., k versus $[Ca^{+2}]$ i.e, $[Ca^{2+}]$ (part A) and plots of Log k' i.e., $\log_{10}$ k versus Log $(1/[Ca^{+2}])$ i.e., $\log_{10}$ $(1/[Ca^{2+}])$ (part B) for α-chymotrypsinogen A (○), pancreatic trypsin inhibitor(■), cytochrome c(▲) and lysozyme(●), obtained for isocratic chromatography carried out on a cation-exchange column while changing the $[Ca^{2+}]$ value or the molarity of the calcium acetate buffer at pH 4.90, respectively. It can be assumed that the calcium ion will play a role of the active gradient substance if the gradient elution mode is applied; $\log_{10}$ $(1/[Ca^{2+}])$ can be rewritten as $-\log_{10}$ m. The regression lines for the experimental plots re-drawn on the (ln m, ln k) plane can be represented by eq(10.6). [Reproduced from ref(10.2) Fig 2.]

Fig 10.3 [reproduced from ref(10.3)] illustrates the plots(□) of k (written as k') in logarhithmic scale versus molarity c in logatithmic scale of sodium acetate buffer at pH 6.4 for ribonuclease A ($M_m=1.35\times10^4$ Da) and lysozyme ($M_m=1.43\times10^4$ Da), obtained for isocratic chromatography carried out on a cation-exchange column while changing c, respectively; c also represents the active sodium molarity or m. It can be seen in Fig 10.3 that the plots for either ribonuclease A or lysozyme give an almost linear arrangement. [In Fig 10.3 are also shown the plots(●) of apparent k (written as $\bar{k}$) versus apparent c (written as $\bar{c}$) obtained by using the "gradient measurement method based on the LSS gradient hypothesis" [see Note 1 in Chapter IX(B)]. The $\bar{k}$ versus $\bar{c}$ plots now are superposed well on the k versus c plots. For detail, see ref(10.3).] From the direct surveying of the regression lines drawn in Fig 10.3, it can be estimated that $\bar{x}'=3.75$ for ribonuclease A and that $\bar{x}'=4.12$ for lysozyme.

Fig 10.4 [reproduced from ref(10.4)] illustrates the plots of $\log_{10}$ k (written as Log k) versus $\log_{10}$ (1/c) (written as Log 1/c) with c representing the molarity of sodium bromide for ovalbumin (●; $M_m=4.35\times10^4$ Da) and carbonic anhydrase (○; $M_m=3.0\times10^4$ Da), obtained for isocratic chromatography carried out on an anion-exchange column while changing c at pH 9.60, respectively; c also represents the active bromide molarity or m. It can be seen in Fig 10.4 that the plots for either ovalbumin or carbonic anhydrase give an almost linear arrangement. [In Fig 10.4 are also shown the plots of apparent $\log_{10}$ k versus apparent $\log_{10}$ (1/c) for both ovalbumin(▲, ■) and carbonic anhydrase(△, □) obtained by using the "gradient measurement method based on the LSS gradient hypothesis". For detail, see ref(10.4).] From the direct surveying of the regression lines drawn in Fig 10.4, it can be estimated that $\bar{x}'=5.73$ for ovalbumin and that $\bar{x}'=2.78$ for carbonic anhydrase.

Fig 10.5 [reproduced from ref(10.5)] illustrates the plots of k (written as k') in logarithmic scale versus [NaCl] [written as Concentration (M)] in logarithmic scale for ACTH (▲; $M_m=4.5\times10^3$ Da), angiotensin Ⅲ (■; $M_m=9\times10^2$ Da) and neurotensin (●; $M_m=1.7\times10^3$ Da), obtained for isocratic chromatography carried out on a cation-exchange column while changing [NaCl] at pH 6.0, respectively; [NaCl] also represents the active sodium molarity or m. It can be seen in Fig 10.5 that the plots for any peptide give an almost linear arrangement. The $\bar{x}'$ values estimated from the regression lines for the arrangements of the experimental points (Fig 10.5) are presented in ref(10.5) Table Ⅰ, where it can be seen: $\bar{x}'=2.69$ for ACTH, $\bar{x}'=1.01$ for angiotensin Ⅲ and $\bar{x}'=0.54$ for neurotensin. [$\bar{x}'$ is written as Z in ref(10.5) Table Ⅰ, and the regression lines are not drawn in Fig 10.5.]

Fig 10.6 summarizes all the experiments above, illustrating the $\bar{x}'$ versus M_m plots for both cation- and anion-exchange chromatographies at the same time. Fig 10.6 shows that $\bar{x}'$, in general, tends to increase with increase in M_m.

The fact that $\log_{10}$ k (or ln k) decreases linearly with increase in $\log_{10}$ m (or ln m; Figs 10.1-10.5) and that $\bar{x}'$ ($=-d\log_{10} k/d\log_{10} m=-d\ln k/d\ln m$), in general, tends to

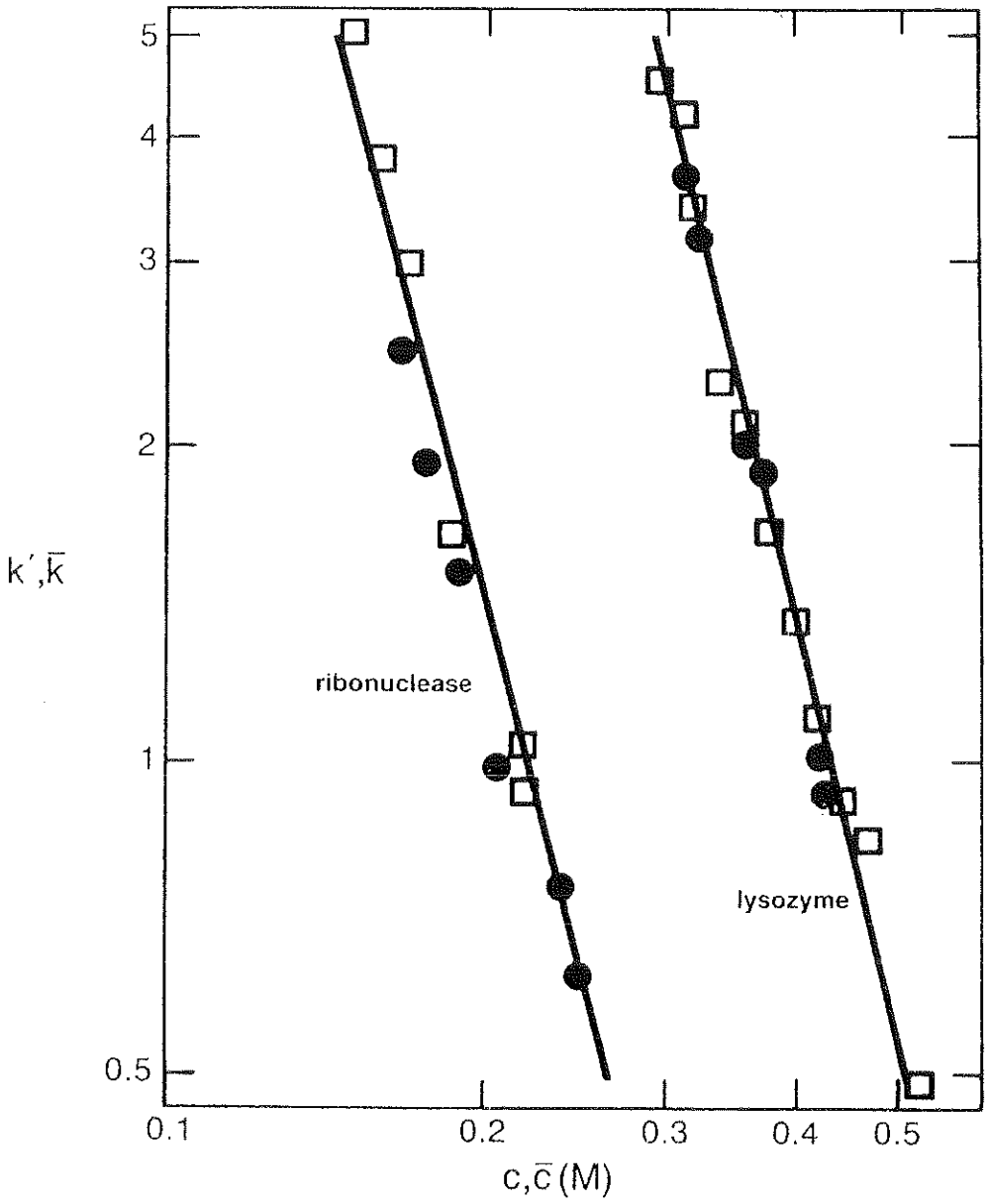


Fig 10.3. Points(□): plots of k' i.e., k in logarithmic scale versus molarity c in logarithmic scale of sodium acetate buffer at pH 6.4 for ribonuclease A and lysozyme, obtained for isocratic chromatography carried out on a cation-exchange column while changing c, respectively. It can be assumed that the sodium ion will play a role of the active gradient substance if the gradient elution mode is applied; c can be rewritten as m. Points (●): plots of apparent k (written as $\bar{k}$) versus apparent c (written as $\bar{c}$), obtained by using the "gradient elution measurement method based on the LSS gradient hypothesis". The $\bar{k}$ versus $\bar{c}$ plots now are superposed well on the k versus c plots. The regression lines for the experimental plots re-drawn on the (ln m, ln k) plane can be represented by eq(10.6). [Reproduced from ref(10.3) Fig 1.]

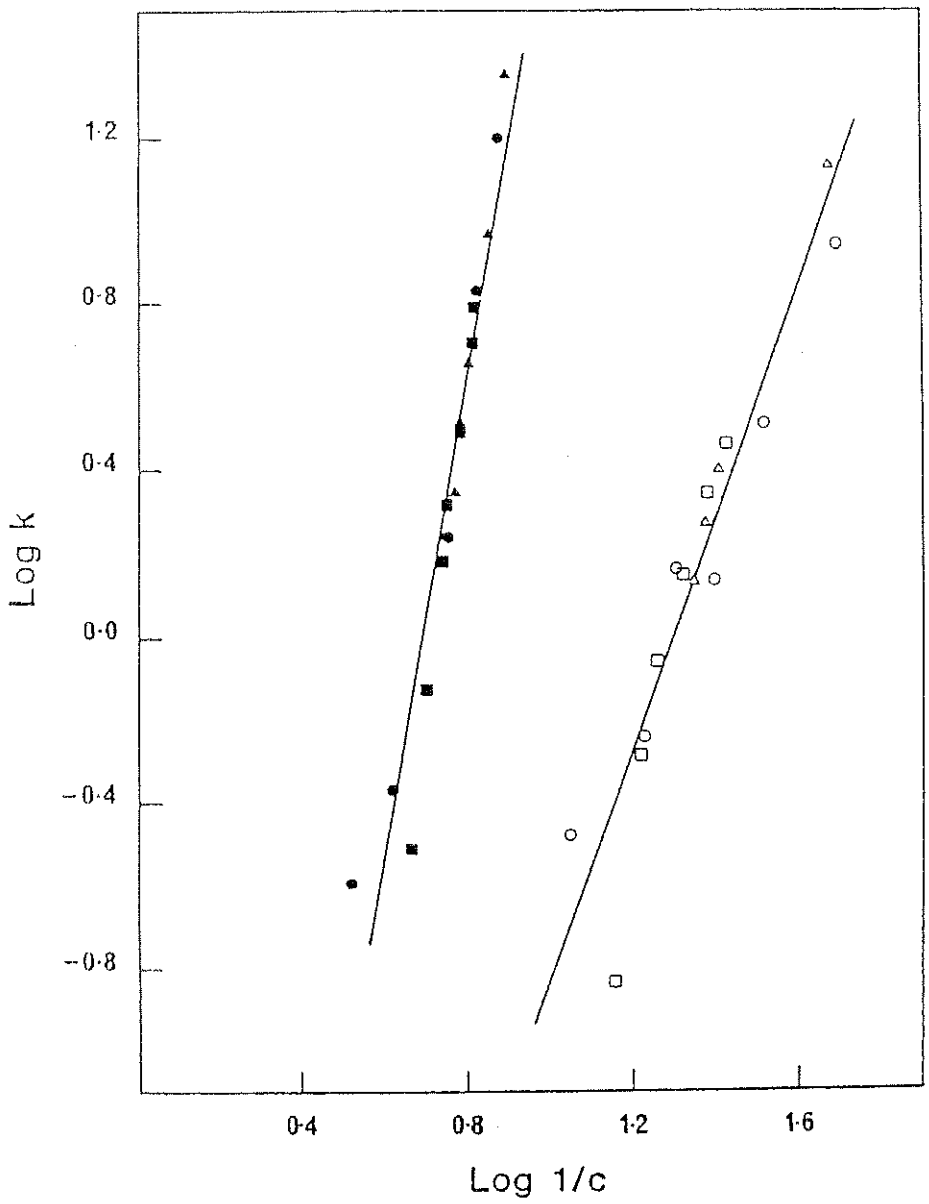


Fig 10.4. Points(● and ○): plots of Log k i.e., $\log_{10}$ k versus Log 1/c i.e., $\log_{10}$ (1/c) with c reprersenting the molarity of sodium bromide for ovalbumin and carbonic anhydrase, obtained for isocratic chromatography carried out on an anion-exchange column while changing c at pH 9.60, respectively. It can be assumed that the bromide ion will play a role of the active gradient substance if the gradient elution mode is applied; c can be rewritten as m. The other points: plots of apparent $\log_{10}$ k versus apparent $\log_{10}$ (1/c) for ovalbumin(▲, ■) and carbonic anhydrase(△, □), obtained by using the "gradient elution measurement method based on the LSS gradient hypothesis". The regression lines for the experimental plots re-drawn on the (ln m, ln k) plane can be represented by eq (10.6). [Reproduced from ref(10.4) Fig 2.]

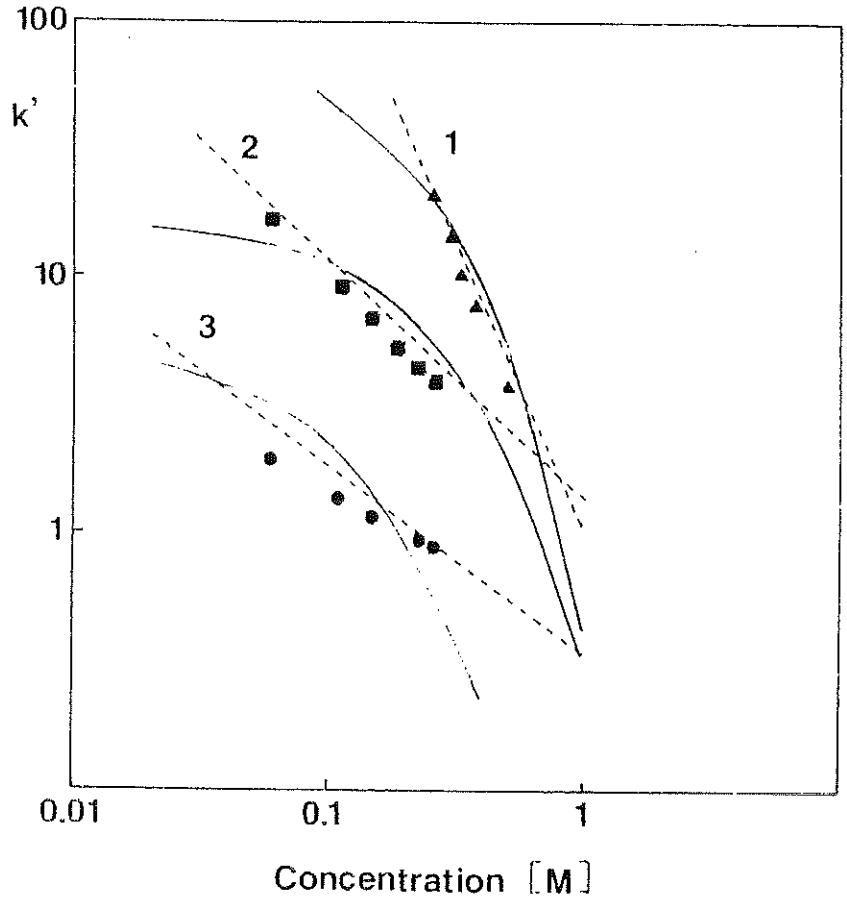


Fig 10.5. Plots of k' i.e., k in logarithmic scale versus NaCl molarity in logarithmic scale for ACTH(▲), angiotensin Ⅲ(■) and neurotensin(●), obtained for isocratic chromatography carried out on a cation-exchange column while changing the NaCl molarity at pH 6.0, respectively. It can be assumed that the sodium ion will play a role of the active gradient substance if the gradient elution mode is applied; the abscissa can be rewritten as m in logarithmic scale. The solid curves are theoretical, calculated by using the "gradient elution measurement method based on the LSS gradient hypothesis" which is established on the basis of the equation equivalent to eq(8.65) or (9.1). The dashed lines are also theoretical, calculated by using another method similar to that used for the calculation of the solid curves. In this method, however, the LSS gradient model is replaced by the model established on the basis of the equation equivalent to eq(8.67) or (10.1) [instead of eq(8.65) or (9.1)]. The regression lines for the experimental plots (not shown in the diagram) can be represented by eq(10.6) if it is drawn on the (ln m, ln k) plane. [Reproduced from ref(10.5) Fig 1.]

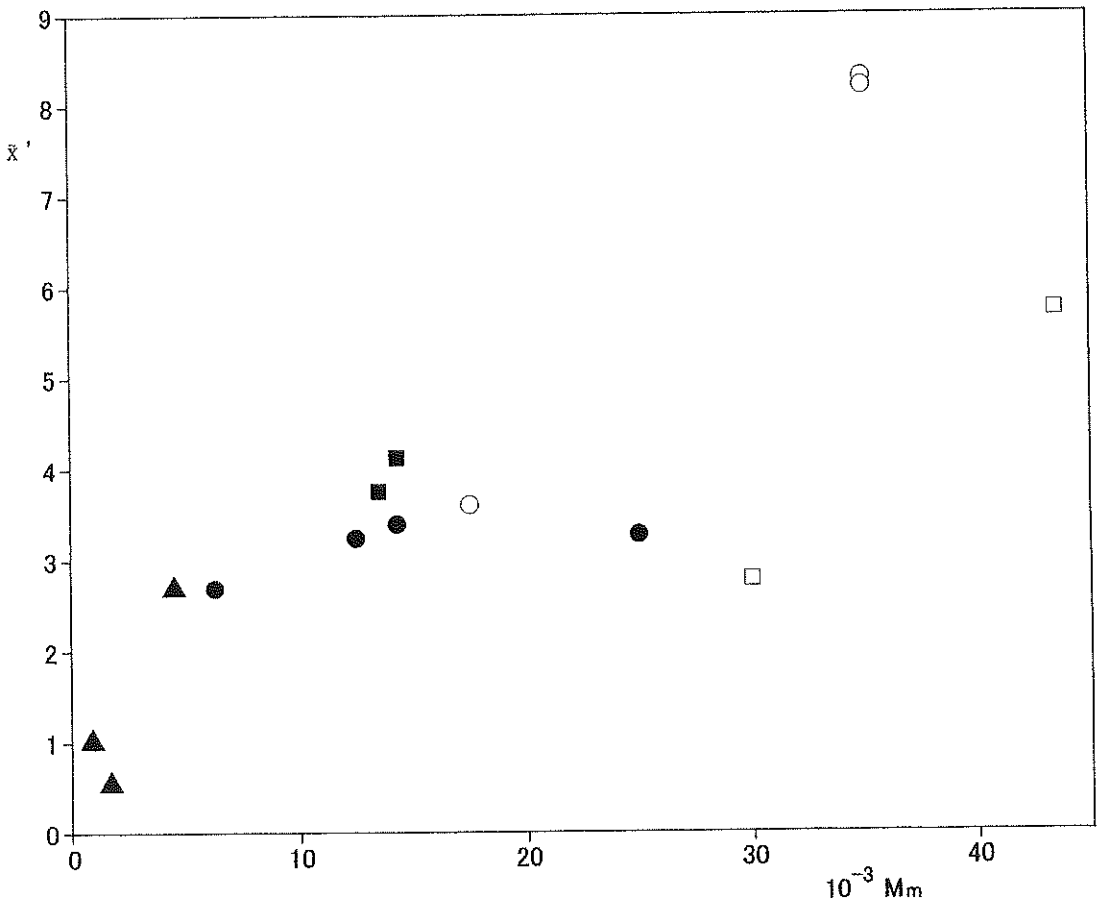


Fig 10.6. $\bar{x}$ versus M_m plots for the experimens of Kopaciewicz et al. (Fig10.1; anion-exchanger; ○), Parente et al. (Fig 10.2; cation-exchanger; ●), Stout et al. (Fig 10.3; cation-exchanger; ■); Hodder et al. (Fig 10.4; anion-exchanger; □), Sasagawa et al. (Fig 10.5; cation-exchanger; ▲) for proteins and peptides.

increase with increase in M_m (Fig 10.6) can be explained by eq(8.67) or (10.1) if $\bar{x}'$ is identified with x'; this is because, due to its physical meaning, x', in general, should tend to increase with increase in M_m. (With regard to homologous series of molecules, x' always should increase with increase in M_m or P; cf. below.) Figs 10.1–10.6 imply that protein (or peptide) molecules and active ions (cations or anions) from the buffer are both adsorbed "strongly" on the cation- or anion-exchanger surface while performing the competition [see Chapter Ⅷ(H)]. [*Note.* In ref(10.4), it was shown that, with anion-exchange chromatography, $\bar{x}'$ for protein molecules depends (to some extent) on the type of not only anion but also cation present in the mobile phase system and that the abnormal $\bar{x}'$ value is obtained in some instances [$\bar{x}'$ corresponds to the parameter Zc in ref(10.4)]. In ref(10.6) also, similar results were obtained in connection with the investigation performed in ref(10.1). The dependence on the type of anion might be explained by the competition mechanism at least partially because x', in general, should depend on the size of the competing substance [cf. Fig 8.2]. The dependences on the type of cation might arise, however, from the secondary effect of the interaction between sample molecule and the solvent [cf. Chapter Ⅷ(B)].]

Let us take looks at chromatographies of substances other than protein or peptide. Fig 10.7 [reproduced from ref(10.7)] illustrates the polts of $\log_{10}$ k (written as log k') versus $\log_{10}$ C (written as log C) with C representing the molarity of the phosphate buffer at pH 6.8 for polyadenylates with degrees of polymerization, P, between 1 and 7, obtained for isocratic chromatography carried out on an anion-exchange column while changing C in the presence of 20% ACN, respectively; C also represents molarity, m, of active phosphate ion. Fig 10.8 [reproduced from ref(10.7)] illustrates the plots of $\log_{10}$ k (written as log k') versus P (written as n) for various C or m values for polyadenylates obtained from the same or similar experiments as those generating Fig 10.7. Fig 10.9(b) [reproduced from ref(10.7)] shows an example of the mutual separation of a mixture of polyadenylates with P ranging between 1 and 35 on the same anion-exchange column as that used in both Figs 10.7 and 10.8, obtained by applying a convex concentration gradient from 0.01 to 0.3 M of the phosphate buffer at pH 6.8 containing 20% ACN. [For Fig10.9(a), see the legend for the figure.] All the experiments in Figs 10.7–10.9 were carried out at 40℃.

It can be seen in Fig 10.7 that, for polyadenylate with any P value, $\log_{10}$ k decreases linearly with increase in $\log_{10}$ C or $\log_{10}$ m, and that $\bar{x}'$ ($=-d\log_{10} k/d\log_{10} m$) increases with increase in P; this implies that both polyadenylate and phosphate ion from the buffer are adsorbed "strongly" on the anion-exchanger surface while performing the competition (see above). It can be seen in Fig 10.8 that, for any m value, $\log_{10}$ k increases linearly with increase in P, and that the slope of the linear arrangement of the experimental points (for a given m) decreases with increase in m. It should be noted that the aspect of the mutual separation of the mixture of polyadenylates with different P values obtained in Fig 10.9(b) is quite parallel to those obtained on HA columns for poly-L-

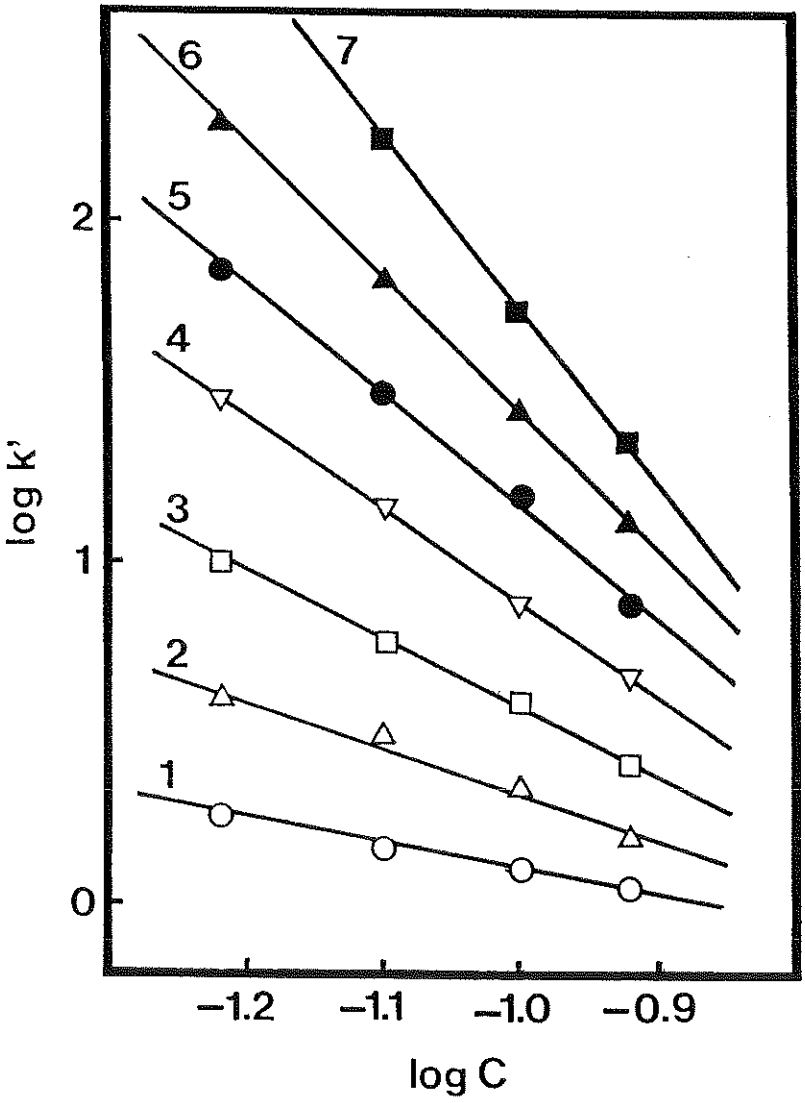


Fig 10.7. Plots of log k' i.e., $\log_{10}$ k versus log C i.e., $\log_{10}$ C with C representing the molarity of phosphate buffer at pH 6.8 for polyadenylates with degrees of polymerization, P, between 1 and 7, obtained for isocratic chromatography carried out at 40℃ on an anion-exchange column while changing C in the presence of 20% ACN, respectively. It can be assumed that the phosphate ion will play a role of the active gradient substance if the gradient elution mode is applied; C can be rewritten as m. The regression lines for the experimental plots re-drawn on the (ln m, ln k) plane can be represented by eq (10.6). [Reproduced from ref(10.7) Fig 3.]

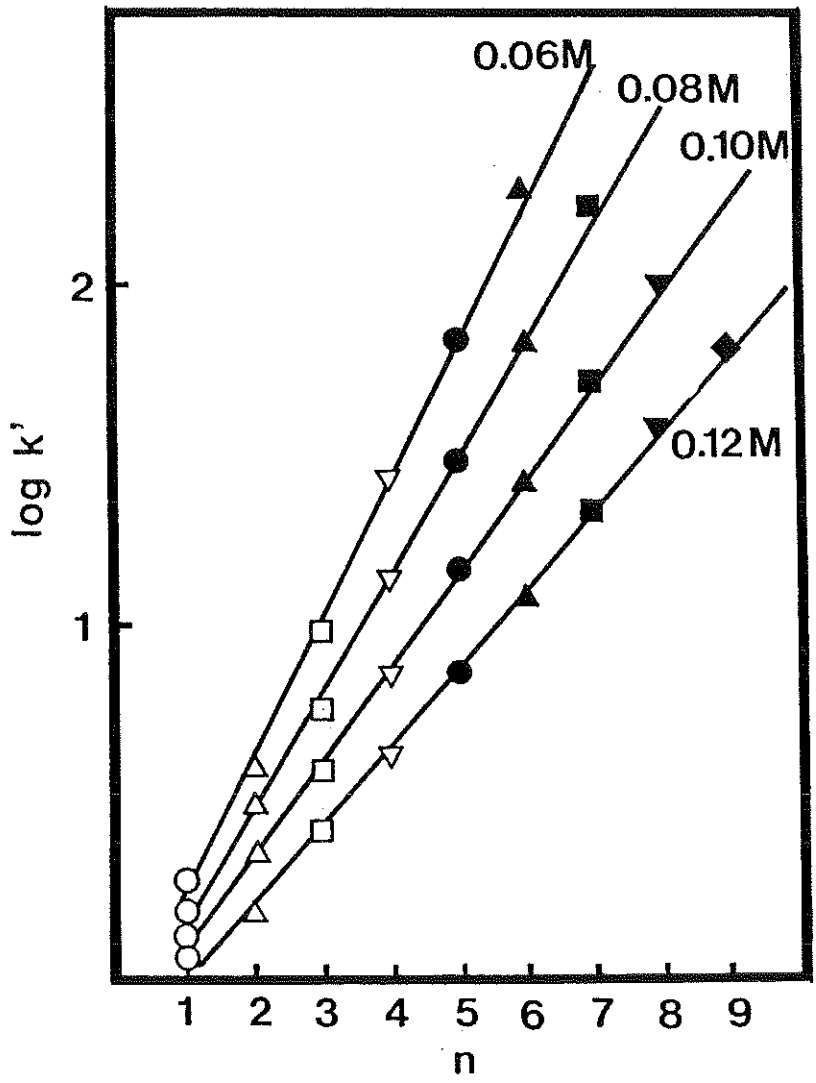


Fig 10.8. Plots of log k' i.e., $\log_{10}$ k versus degree of polymerization n i.e., P for various C or m values for polyadenylates, obtained at 40℃ from the same or similar experiments as those generating Fig 10.7. The regression lines for the plots re-drawn on the (P, ln k) plane can be represented by eq(10.31). [Reproduced from ref(10.7) Fig 4.]

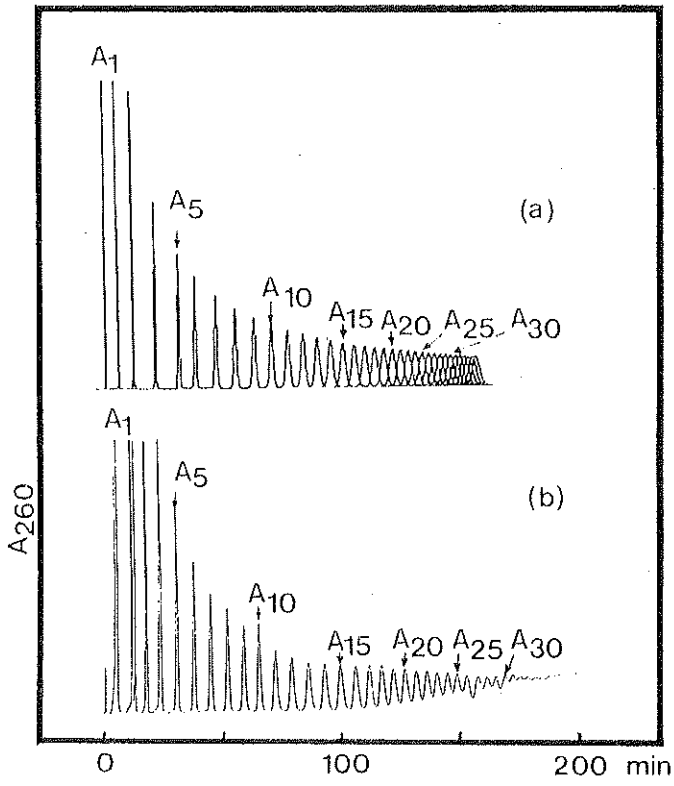


Fig 10.9. (a) Theoretical chromatogram corresponding to (b) in which the width of each chromatogrphic peak has been calculated by using the equation equivlent to Appendix XI(B) eq(A11.33); for detail, see ref(10.7). (b) An example of the mutual separation of a mixture of polyadenylates with P varying between 1 and 35 on the same anion-exchange column as that used in both Figs 10.7 and 10.8, carried out at 40℃ by applying a convex concentration gradient (from 0.01 to 0.3 M) of the phosphate buffer at pH 6.8 containing 20% ACN. In the diagram, the value of the parameter P is represented as suffix of the parameter A.

lysine (Fig 8.9), poly-L-glutamate (Fig 9.4) and poly-L-arginine (Fig 9.5), and that obtained on a reversed-phase column for polystyrene (Fig 9.3). This strongly suggests that the fundamental separation mechanisms of ion-exchange, HA and reversed-phase chromatographies are similar to one another.

Fig 10.10 [reproduced from ref(10.8)] illustrates the plots of $\log_{10}$ k (written as log k') versus $\log_{10}$ C (written as log C) with C representing the molarity of KCl for polyphosphates with degrees of polymerization, P, between 1 and 9, obtained at 25℃ for isocratic chromatography carried out on an anion-exchange column while changing C in the presence of 0.1% (weight/volume) sodium ethylenediaminetetraacetate (Na_4EDTA) at pH 10, respectively; C also represents molarity, m, of active chloride ion. Fig 10.11 [reproduced from ref(10.9)] illustrares the plots of k (written as k') in ligarithmic scale versus P−2 (written as n−2) representing the number of inner phosphorous atoms for various C or m values for polyphosphates, obtained from the same or similar experiments as those generating Fig 10.10; the column temperature is 25℃. Fig 10.12 [reproduced from ref(10.9)] illustrates the plots corresponding to those shown in Fig 10.11, obtained at several temperatures when C or m=0.30 M (in the presence of 0.1% Na_4EDTA). In Fig 10.13 [reproduced from ref(10.8)] is depicted the dependence of ln k (written as ln k') on the reciprocal of the absolute temperature, T, of the column, obtained when C or m=0.30 M (in the presence of 0.1% Na_4EDTA).

Fig 10.10 is parallel to Fig 10.7 manifesting that $\log_{10}$ k of polyphosphate with any P value decreases linearly with increase in $\log_{10}$ C or $\log_{10}$ m, and that $\bar{x}'$ (=$-d\log_{10} k/d\log_{10} m$), in general, increases with increase in P; the slight decrease of $\bar{x}'$ taking place when P=9 can be assumed to arise from the experimental error. This implies that both polyphosphate and chloride ion are adsorbed "strongly" on the anion-exchanger surface while performing the competition. Fig 10.11 is also parallel to Fig 10.8, showing that, for any m value, $\log_{10}$ k increases linearly with increase in P−2 or P, and that the slope of the linear arrangement of the experimental points (for a given m) decreases with increase in m. Fig 10.12 shows that the linear increase of $\log_{10}$ k with increase in P−2 or P takes place at any temperature, and Fig 10.13 (along with Fig 10.12) manifests that ln k (for any P) decreases linearly with increase in 1/T.

In ref(10.5), by using an indirect method, it is shown that the $\bar{x}'$ value of polyadenylates (with P ranging between 17 and 100) increases with increase in P on an anion-exchange column at pH 9.0. In ref(10.5), it also is mentioned that the $\bar{x}'$ value of α (1→6)-linked homologous α-D-gluco-polysaccharides (with number of structural unit, P, ranging between 10 and 43) incrreases with increase in P on an anion-exchange column at an alkaline pH. [$\bar{x}'$ corresponds to the parameter Z in ref(10.5).]

The experiment of Kopaciewicz et al. (Fig 10.1) will be analyzed in the subsequent Section(B), and the experiments of Baba et al. (Figs 10.7-10.13) will be analyzed in the susequent Section(C) on the basis of competition model, respectively.

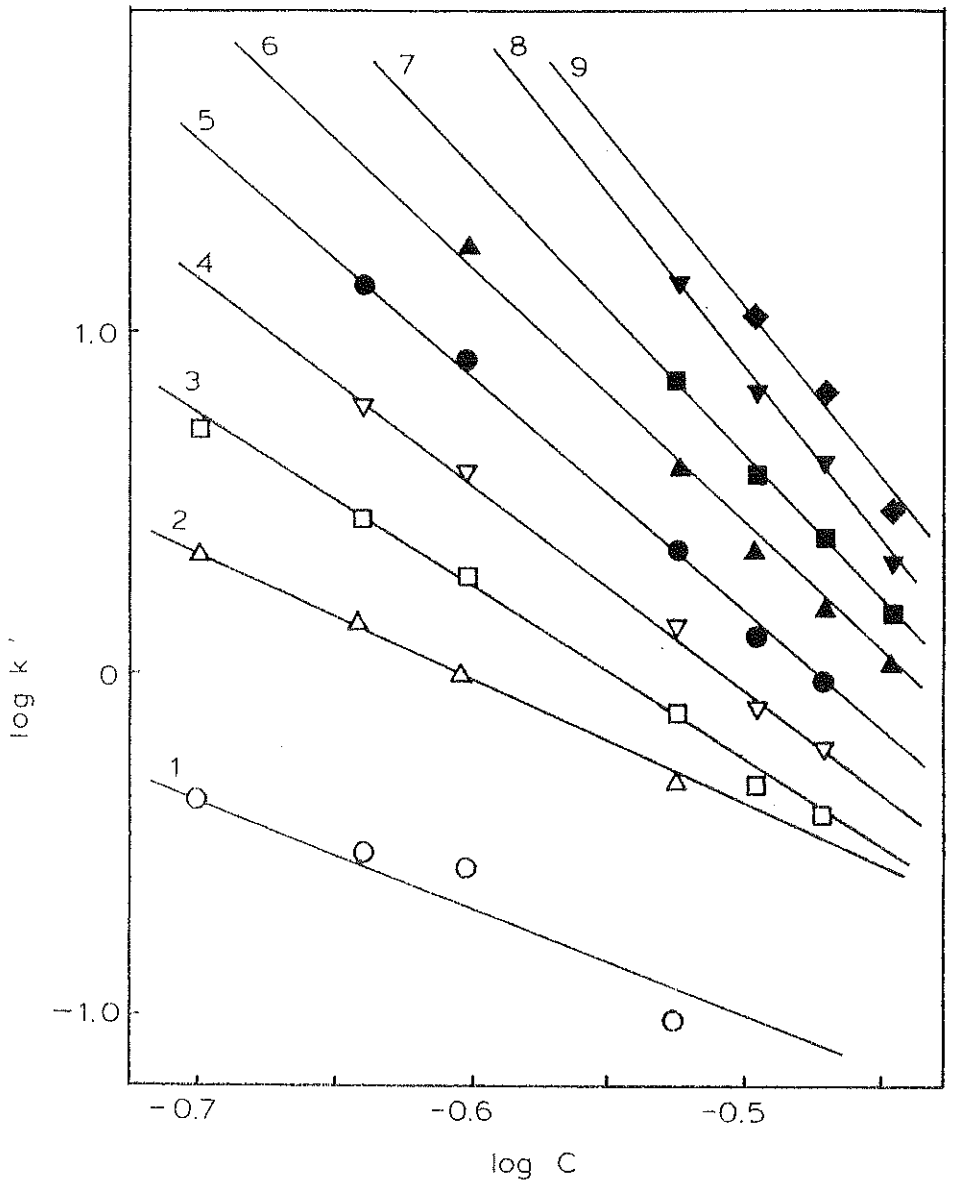


Fig 10.10. Plots of log k' i.e., $\log_{10}$ k versus log C i.e., $\log_{10}$ C with C representing the molarity of KCl for polyphosphates with degrees of polymerization, P, between 1 and 9, obtained for isocratic chromatography carried out at 25℃ on an anion-exchange column while changing C in the presence of 0.1% (weight/volume) Na_4EDTA at pH 10, respectively. It can be assumed that the chloride ion will play a role of the active gradient substance if the gradient elution mode is applied; C can be rewritten as m. The regression lines for the experimental plots re-drawn on the (ln m, ln k) plane can be represented by eq(10.6). [Reproduced from ref(10.8) Fig 3.]

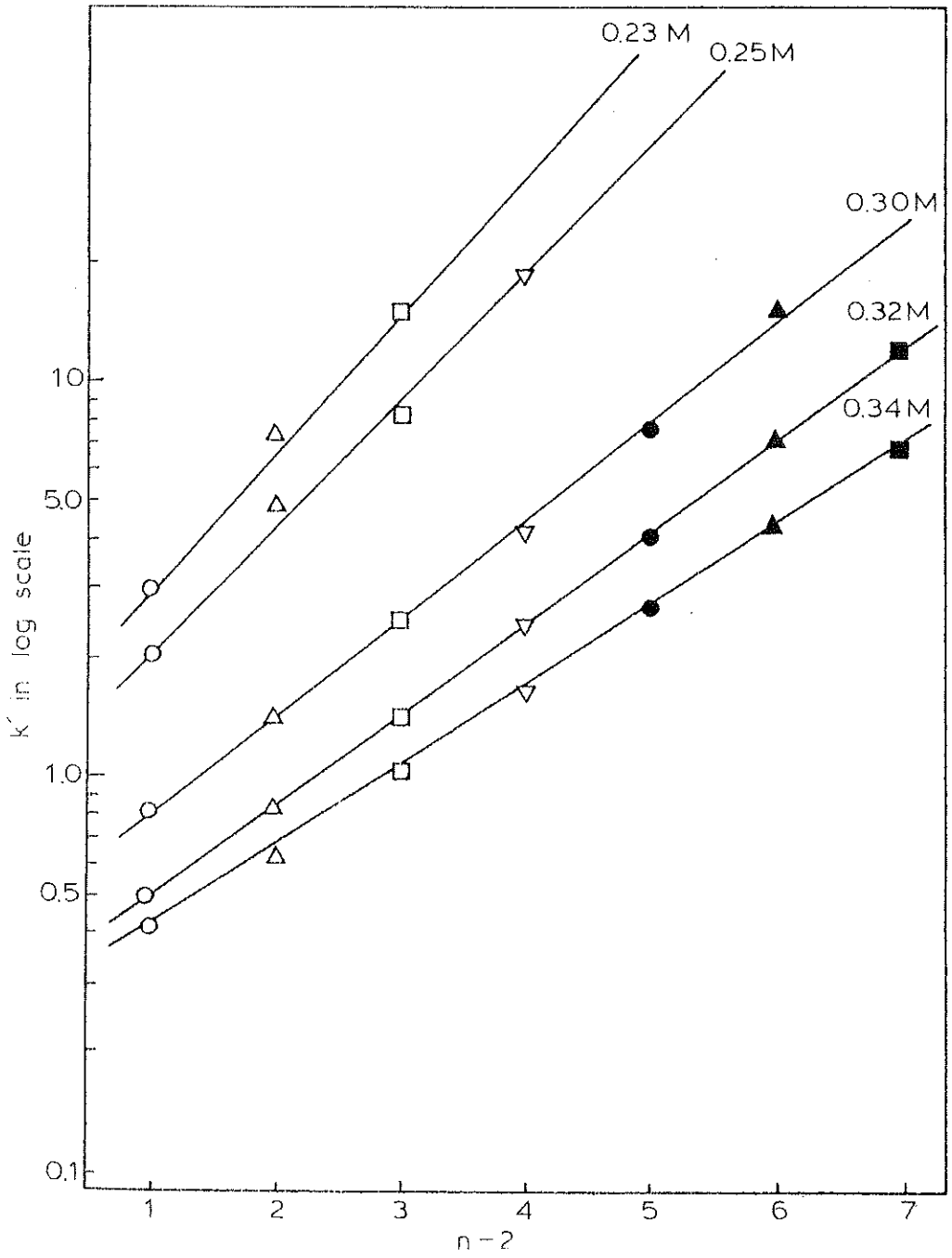


Fig 10.11. Plots of k' i.e., k in logarithmic scale versus number, n−2 i.e., P−2, of inner phosphate atoms for various C or m values for polyphosphates, obtained at 25℃ from the same or similar experiments as those generating Fig 10.10. The regression lines for the experimental plots re-drawn on the (P, ln k) plane can be represented by eq (10.31). [Reproduced from ref(10.9) Fig 1.]

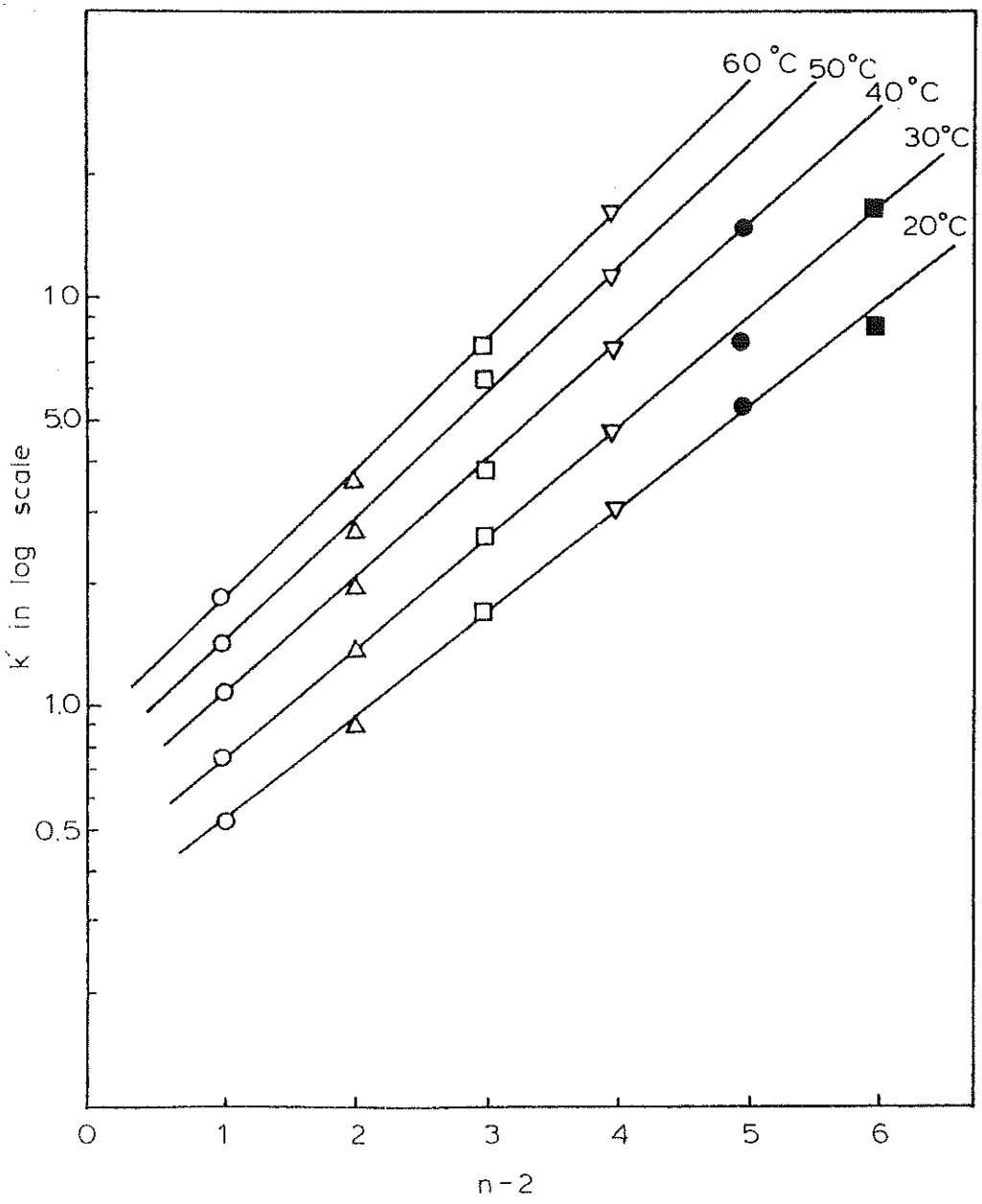


Fig 10.12. Plots corresponding to those shown in Fig 10.11 obtained at various temperatures when C or m=0.30 M (in the presence of 0.1% Na_4EDTA). The regression lines for the experimental plots re-drawn on the (P, ln k) plane can be represented by eq (10.31). [Reproduced from ref(10.9) Fig 2.]

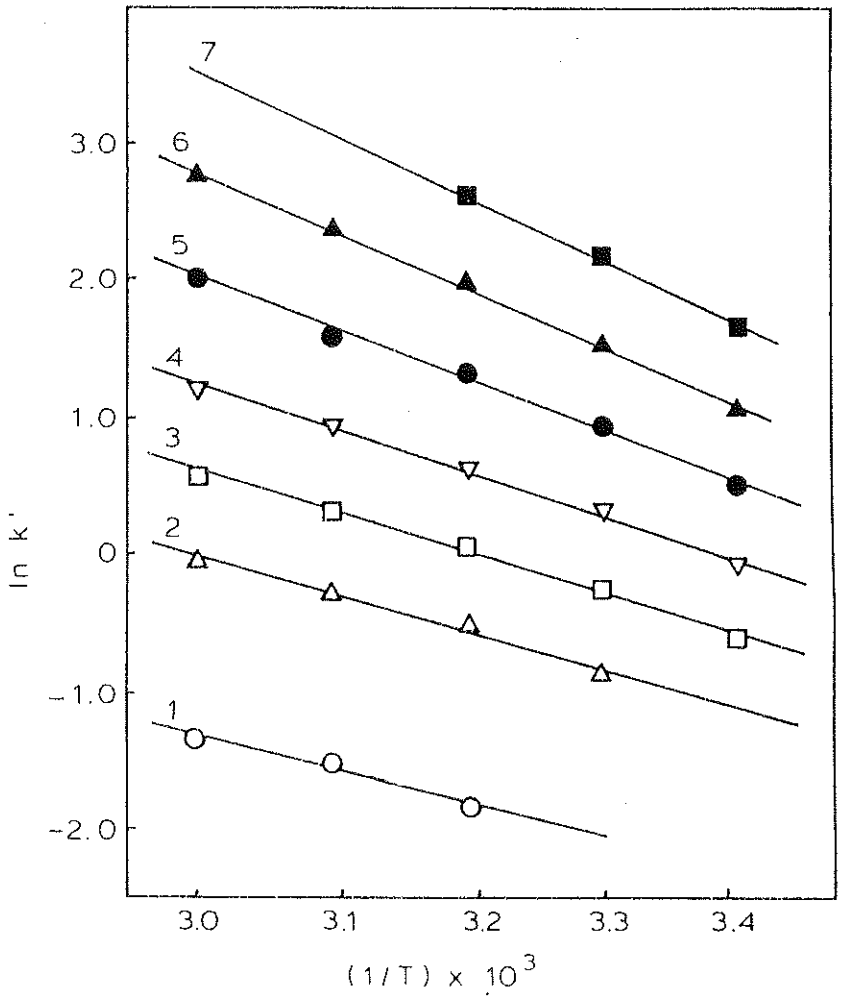


Fig 10.13. Plots of ln k' i.e., ln k versus reciprocal of the absolute temperature T for polyphosphates with various degrees of polymerization P taking place when C or m = 0.30 M (in the presence of 0.1% Na_4EDTA), obtained for isocratic chromatography carried out on the same anion-exchange column as that used in Figs 10.10-10.12. The regression lines for the experimental plots can be represented by eq(10.22). [Reproduced from ref (10.8) Fig 5.]

(B) Analysis of the Experiment of Kopaciewicz et al.

Interpretation on Fig 10.1. Summarizing the study of Green and Aschaffenburg(10.10) and the study of Townend and Timasheff(10.11), it can be assumed that β-lactoglobulin A usually is in the dimer state (with $M_m = 3.5 \times 10^4$ Da) when it is dissolved at pH between 3.5 and 7.5, and that the molecule is in the monomer state (with $M_m = 1.75 \times 10^4$ Da) when the pH is below 3.5. On the other hand, McKenzie and Sawyer(10.12) mention that all variants of β-lactoglobulin (involving variant A, B and C) tend to dissociate to the monomer below pH 3.5 *at moderately low concentration*, and that, with increasing pH, the dimer becomes the predominant form *except at very low concentration*. By using the ultracentrifugation method, Zimmerman et al.(10.13) shows that, at either pH 6.9 or 8.2, both sedimentation constant and weight average M_m of β-lactoglobulin A decrease with decrease in molecular concentration in solution; the extrapolations of these values to infinitesimal concentration imply the presence of a considerable amount of monomer molecules beside dimer molecules in the very diluted state. Mills and Creamer(10.14) mention that approximately 90% of β-lactoglobulin A molecules are in the monomer state at pH 2.0 while 50% are in the monomer state at pH 6.5. It can be deduced from the experiment of Bull(10.15) that β-lactoglobulin is in the monomer state when it is not in solution or when the molecules are in surface films spread out on ammonium sulphate solutions.

It can be seen in Fig 10.1 that all the arrangements of the experimental points taking place when pH=6 to 8 are qusi-identical with one another with $\bar{x}' = 8.2$ to 8.3, whereas that taking place at pH=5 gives a roughly half $\bar{x}'$ value of 3.6. According to competition model, $\bar{x}'$ or x' should measure the molecular size [Section (A)], and, referring to all the informations obtained from the preceding paragraph, it would be reasonable to assume that, *in the chromatographic system,* β-lactoglobulin A virtually is in the dimer state when pH=6 to 8 and that it is in the monomer state when pH=5. From the analogy to the deduction that β-lactoglobulin molecules are in the monomer state when they are in surface films (see above), the fact that the molecules are partially in the adsorbed state (and not in solution) in the chromatographic system might promote the monomer state at acidic enough pH of 5. [In refs(10.1, 10.6), however, another interpretation is given to the different chromatographic behavior of β-lactoglobulin A at pH 5.]

Theoretical Preparation. In eq(8.67) i.e.,

$$\ln k = -x' \ln m + \ln q - x' \ln \varphi \qquad (10.1)$$

the term ln q can be represented by eq(9.2) in which the AVFA is defined by eq(9.3). Let us consider an assembly of "homologous" molecules characterized by eq(8.53) as $J/x' = \text{constant}$, or as

$$J/(x'kT) - \ln \varphi = \rho \qquad (10.2)$$

in which ρ represents a constant [cf. eq(9.4)]. The term $\ln q - x'\ln \varphi$ in eq(10.1) can now be rewritten as

$$\ln q - x'\ln \varphi = \rho x' + \ln \beta \tag{10.3}$$

[cf. eq(9.5)], and it can be considered that $\ln q - x'\ln \varphi$ is a function of x'. Eq(10.3) fulfills

$$\lim_{x' \to 0} (\ln q - x'\ln \varphi) = \ln \beta \tag{10.4}$$

[cf. eq(9.6)], and eq(10.1) can be rewritten as

$$\ln k = -x'\ln m + \rho x' + \ln \beta \tag{10.5}$$

[cf. eq(9.7)].

Analysis of Fig 10.1. Let us assume that β-lactoglobulin A is in dimer and monomer states when pH=6-8 and when pH=5, respectively, that the slight dependence on pH of the $\log_{10} k$ versus $\log_{10} (1/[NaCl])$ plots taking place when pH is between 6 and 8 (Fig 10.1) arises either from a minor secondary effect added to the competition mechanism or from the experimental error, and that the dimer and monomer states of β-lactoglobulin A can be regarded as two "homologous" molecules fulfilling eq(10.2). The regression lines for the experimental plots taking place at any pH (Fig 10.1) can be re-expressed on the (ln m, ln k) plane as

$$\ln k = -\bar{x}'\ln m + \hat{U} \tag{10.6}$$

in which

$$\bar{x}' = x' \tag{10.7}$$

and

$$\hat{U} = \rho \bar{x}' + \ln \beta = \rho x' + \ln \beta \tag{10.8}$$

respectively [see eq(10.5)]. Given two $\bar{x}'$ values ($\bar{x}'_1$ and $\bar{x}'_2$) and two $\hat{U}$ values ($\hat{U}_1$ and $\hat{U}_2$) for a pair of molecules (1 and 2), eq(10.8) leads to simultaneous equations with respect to two unknowns ρ and $\ln \beta$:

$$\left.\begin{aligned} \hat{U}_1 &= \rho \bar{x}'_1 + \ln \beta \\ \hat{U}_2 &= \rho \bar{x}'_2 + \ln \beta \end{aligned}\right\} \tag{10.9}$$

By solving eq(10.9),

$$\rho = \frac{\hat{U}_1 - \hat{U}_2}{\bar{x}'_1 - \bar{x}'_2} \tag{10.10}$$

and

$$\ln\beta = \frac{\bar{x}'_1\hat{U}_2 - \bar{x}'_2\hat{U}_1}{\bar{x}'_1 - \bar{x}'_2} \qquad (10.11)$$

are obtained.

Table 10.1 summarizes the $\bar{x}'$ values for the regression lines in Fig 10.1 re-drawn on the (ln m, ln k) plane and the corresponding $\hat{U}$ values (the intersections with the ln k axis taking place when ln m=0); these latters have been estimated from the direct surveying of the diagram. By using the data for the pair at pH 5 and pH 6, those for the pair at pH 5 and pH 7, and those for the pair at pH 5 and pH 8 presented in Table 10.1, both ρ and $\ln\beta$ can be evaluated from both eqs(10.10) and (10.11), respectively; the results are summarized in Table 10.2 with addition of the β values. These β values (much smaller than unity, and ranging between 8.74×10^{-3} and 1.85×10^{-2}) are reasonable ones; these can be compared with the corresponding values (1.14×10^{-4} to 2.15×10^{-2}) obtained for reversed-phase columns (see Table 9.1) and the value of the order of magnitude of 10^{-2} deduced for the HA column [see Chapter Ⅷ(E)].

In order for eq(10.1) to hold precisely or for a precisely linear arrangement of the experimental log k versus log m plots to be obtained, it is necessary that the term φ m be much larger than unity [see Chapter Ⅷ(H)]. Let us assume that the lower limit, $(\varphi\ m)_{lL}$, of the φ m value that brings about *practically* linear arrangements of the experimental points is 2. It can be seen in Fig 10.1 that the maximum $\log_{10}$ (1/[NaCl]) value used for the experiment is lower than unity. This means that the minimum $\log_{10}$ m value is higher than -1, or that the minimum m value is higher than 0.1 M. The lower limit of the possible φ value can be estimated to be $2/0.1=20$ (M^{-1}), or the lower limit of ln φ can be evaluated to be about 3. As $\rho=-0.689$ to -0.480 (Table 10.2), by using eq (10.2), the lower limit of $J/(x'kT)$ can be evaluated to be 2.3 to 2.5, and, by using the kT value of 2.48 kJ/mol at 25℃, the lower limit of J/x' can be evaluated to be 5.7 to 6.2 kJ/mol (see Table 10.3). These values can be compared with the corresponding values of 2.47 and 6.13 kJ/mol estimated for lysozyme on the HA column [see Chapter Ⅷ(D)].

(C) Analysis of the Experiment of Baba et al.

Theoreical Preparation. In the presence of eq(10.1), let us consider the case when eqs(9.24)-(9.30) hold with the interpretation similar to that used for the analysis of the experiment of Jandera [Chapter Ⅸ(F)]. Thus, when $P\geqq2$, let us hypothesize to divide each of the two terminal monomer units of either polyadenylate or polyphosphate chain into two parts (denoted by first and second parts). The first part is equivalent with the inner monomer unit of the polymer chain not only in size but also in ability of being adsorbed on the adsorbent surface. For simplicity, we assume that the first part equivalent with the inner monomer unit in size is identical with the first part equivqlent with the inner monomer unit in ability of being adsorbed. The second part is defined as the remainder of the terminal monomer unit; it is assumed that the terminal monomer unit is larger

Table 10.1

$\hat{x}'$ values for the regression lines in Fig 10.1 re-drawn on the (ln m, ln k) plane[eq(10.6)] obtained for anion-exchange chromatography of β-lactoglobulin A, and the corresponding $\hat{U}$ values (the intersections with the ln k axis taking place when ln m=0) estimaterd from the direct surveying of the diagram.

pH	$\hat{x}'$	$\hat{U}$	Index	Molecular state
5	3.6	−6.47	1	monomer
6	8.2	−9.64	2	dimer
7	8.3	−9.25	2	
8	8.2	−8.68	2	

Table 10.2

ρ values for β-lactoglobulin A on an anion-exchange column estimated from the three pairs of data presented in Table 10.1. The simultaneously estimated ln β and β values for the column are also shown.

Pair of molecules	ρ	ln β	β
monomer at pH 5 dimer at pH 6	−0.689	−3.99	1.85×10^{-2}
monomer at pH 5 dimer at pH 7	−0.591	−4.34	1.30×10^{-2}
monomer at pH 5 dimer at pH 8	−0.480	−4.74	8.74×10^{-3}

Table 10.3

Evaluations of the lower limits of J/(x'kT) and J/x' for β-lactoglobulin A on an anion-exchange column. The value of kT at 25℃ (2.48 kJ/mol) is used for the calculation of the last column.

ρ	φ (M^{-1})	ln φ	J/(x'kT)= ρ + ln φ	J/x' (kJ/mol)
−0.689 ∣ −0.480	≳20	≳3	≳2.3 ∣ 2.5	≳5.7 ∣ 6.2

than the inner monomer unit in size. When $P=1$, we consider to divide the total molecular structure into two parts with one of them (first part) being equivalent with the inner monomer unit taking place provided that $P \geqq 2$; it is assumed that the monomer molecule is larger than the inner monomer unit in size.

In eqs(9.24)-(9.30), x'°, E°, τ° and J° represent constants with respect to the sum of the second parts of the two terminal monomer units (when $P \geqq 2$) and the second part of the total molecular structure (when $P=1$). x'^{*}, E^{*}, τ^{*} and J^{*} correspond to the remainder of the total molecular structure both when $P \geqq 2$ and when $P=1$; these are functions of P. The assignment of the parameters x'°, E°, τ° and J° to the two terminal parts of the polymer chain is compatible with the situation where the conformation of the polymer chain on the anion-exchanger surface is either stretched or planar (rather than three-dimensional).

Let us consider an assembly of "homologous" molecules characterized as $J^{*}/x'^{*}=$constant, or as

$$J^{*}/(x'^{*}kT) - \ln \varphi = \rho^{*} \tag{10.12}$$

in which ρ^{*} represents a constant [cf. eq(9.31)]. The term $\ln q - x'\ln \varphi$ in eq(10.1) can be rewritten as

$$\ln q - x'\ln \varphi = \rho^{*}x'^{*} + \ln (\beta c_{\varphi}^{J^{\circ}/kT - x'^{\circ}}) \tag{10.13}$$

[cf. eq(9.32)], and it can be considered that $\ln q - x'\ln \varphi$ is a function of x'^{*}. Eq(10.13) fulfills

$$\lim_{x'^{*}\to 0} (\ln q - x'\ln \varphi) = \ln (\beta e_{\varphi}^{J^{\circ}/kT - x'^{\circ}}) \tag{10.14}$$

[cf. eq(9.33)]. Eq(10.1) can be rewritten as

$$\ln k = -(x'^{*}+x'^{\circ})\ln m + \rho^{*}x'^{*} + \ln (\beta e_{\varphi}^{J^{\circ}/kT - x'^{\circ}}) \tag{10.15}$$

[cf. eq(9.34)] where it can be considered that $\ln k$ is a function of m, and that x'^{*} is a parameter. When considering $\ln k$ to be a function of x'^{*} and m to be a parameter, it is convenient to rewrite eq(10.15) as

$$\ln k = (\rho^{*} - \ln m)x'^{*} + \ln (\beta e_{\varphi}^{J^{\circ}/kT - x'^{\circ}}) - x'^{\circ}\ln m \tag{10.15'}$$

[cf. eq(9.34')]. Eq(10.15') fulfills

$$\lim_{x'^{*}\to 0} \ln k + x'^{\circ}\ln m = \ln (\beta e_{\varphi}^{J^{\circ}/kT - x'^{\circ}}) \tag{10.16}$$

[cf. eq(9.35)].

When x'^{*} can be represented as a function of P as

$$x'' = h_P^*(P) \tag{10.17}$$

[cf. eq(9.36)] fulfilling

$$\lim_{P\to 0} h_P^*(P) = 0 \tag{10.18}$$

[cf. eq(9.37)], then eqs(10.13)-(10.15), (10.15') and (10.16) can be rewritten as

$$\ln q - x'\ln \varphi = \rho^* h_P^*(P) + \ln (\beta e^{J^\circ/kT}_{\varphi^{-x'^\circ}}) \tag{10.13a}$$

$$\lim_{P\to 0}(\ln q - x'\ln \varphi) = \ln (\beta e^{J^\circ/kT}_{\varphi^{-x'^\circ}}) \tag{10.14a}$$

$$\ln k = -[h_P^*(P)+x'^\circ]\ln m + \rho^* h_P^*(P) + \ln (\beta e^{J^\circ/kT}_{\varphi^{-x'^\circ}}) \tag{10.15a}$$

$$\ln k = (\rho^* - \ln m)h_P^*(P) + \ln (\beta e^{J^\circ/kT}_{\varphi^{-x'^\circ}}) - x'^\circ \ln m \tag{10.15'a}$$

and

$$\lim_{P\to 0} \ln k + x'^\circ \ln m = \ln (\beta e^{J^\circ/kT}_{\varphi^{-x'^\circ}}) \tag{10.16a}$$

[cf. eqs(9.32a)-(9.34a), (9.34'a) and (9.35a)], respectively. Eq(10.18) gives a necessary condition for eq(10.12) to be justified. [h_P^* is a symbol. In eq(10.18), do not misunderstand as if the subscript P as part of the symbol tends to zero when P as variable tends to zero.]

The absolute activity, $\lambda_{(0)}$, for the competing substance is related to the corresponding chemical potential, $\mu_{(0)}$, by eq(8.23) as

$$\lambda_{(0)} = e^{\mu_{(0)}/kT} \tag{10.19}$$

and the assumption of the constant value of the parameter φ [see Chapter Ⅷ(B)] corresponds to the approximate expression of the chemical potential $\mu_{(0)}$ in the form of

$$\mu_{(0)} \approx \mu_{(0)}^\circ + kT\ln m \tag{10.20}$$

in which $\mu_{(0)}^\circ$ represents a constant. By using both eqs(10.19) and (10.20), φ [eq(8.45)] can be rewritten as

$$\varphi \approx ze^{(\mu_{(0)}^\circ + \varepsilon)/kT} \tag{10.21}$$

or $\mu_{(0)}^\circ + \varepsilon$ can be represented as

$$\mu_{(0)}^\circ + \varepsilon \approx kT\ln(\varphi/z) \tag{10.21'}$$

With reference to eq(10.12), eq(10.15) or (10.15') can be rewritten as

$$\ln k = \Pi/kT + \Sigma \tag{10.22}$$

in which

$$\Pi = [J^*/x'^* - (\mu_{(0)}^\circ + \xi)]x'^* + J^\circ - (\mu_{(0)}^\circ + \xi)x'^\circ \tag{10.23}$$

and

$$\Sigma = -[\ln (zm)]x'^* + \ln\beta - x'^\circ \ln (zm) \tag{10.24}$$

The term J^*/x'^* in eq(10.23) is virtualy constant, independent of x'^*; this is because J, J° or J^* can be identified with E, E° or E^* virtually.

Analysis of Figs 10.7 and 10.8 for Polyadenylates. The regression line for any P value in Fig 10.7 re-drawn on the (ln m, ln k) plane can be expressed by eq(10.6) in which $\hat{x}'$ and $\hat{U}$ can be interpreted to represent

$$\hat{x}' = h_P^*(P) + x'^\circ \tag{10.25}$$

and

$$\hat{U} = \rho^* h_P^*(P) + \ln (\beta e^{J^\circ/kT} \varphi^{-x'^\circ}) \tag{10.26}$$

respectively [see eq(10.15a)]. Both $\hat{x}'$ and exp $\hat{U}$ values for the regression line for any P value drawn in Fig 10.7 [estimated in ref(10.7) Table I where $\hat{x}'$ and exp $\hat{U}$ are written as b and a, respectively] are reproduced in Table 10.4 with addition of the $\hat{U}$ value.

The points in Fig 10.14 represent the $\hat{x}'$ versus P plots for the values presented in Table 10.4. It can be seen in Fig 10.14 that all the experimental points are arranged almost linearly, and that the extrapolation of the linear arrangement passes through the origin virtually; this means that

$$x'^\circ = 0 \tag{10.27}$$

virtually, and that function $h_P^*(P)$ can be represented as

$$h_P^*(P) = \upsilon_P^* P \tag{10.28}$$

in which υ_P^* stands for a positive constant [see eq(10.25)]. Eq(10.28) implies that the area of the anion-exchanger surface occupied by the adsorbed molecule [proportional to x' (=x'*)] is proportional to P, and that the conformations of polyadenylates taking place on the anion-exchanger surface are either stretched or planar (rather than three-dimensional). This is consistent with the consideration done in the subsection entitled "Theoretical Preparation". Writing υ_P for υ_P^* when eq(10.27) holds, eqs(10.25) and (10.26) can be re-expressed as

Table 10.4

$\bar{x}'$, $\exp\hat{U}$ and $\hat{U}$ values for the regression lines in Fig 10.7 re-drawn on the (ln m, ln k) plane[eq(10.6)], obtained for anion-exchange chromatography of polyadenylates with different P values at 40℃. The molecule with P=1 represents monoadenylate. Both $\bar{x}'$ and $\exp\hat{U}$ values were reproduced from ref (10.7) Table I where $\bar{x}'$ and $\exp\hat{U}$ are written as b and a, respectively.

P	$\bar{x}'$	$\exp\hat{U}$	$\hat{U}$
1	0.737	2.32×10^{-1}	−1.461
2	1.37	8.95×10^{-2}	−2.414
3	1.92	4.50×10^{-2}	−3.101
4	2.71	1.44×10^{-2}	−4.241
5	3.25	8.09×10^{-3}	−4.817
6	3.90	3.41×10^{-3}	−5.681
7	5.01	5.38×10^{-4}	−7.528

$$\hat{x}' = \upsilon_P P \tag{10.29}$$

and

$$\hat{U} = \rho^* \upsilon_P P + \ln (\beta e^{J^\circ/kT}) \tag{10.30}$$

respectively. The straight line drawn in Fig 10.14 is the regression line (passing through the origin) of P on $\hat{x}'$ for the experimental points. As the slope of the regression line, the parameter υ_P can be evaluated to be 0.677 [see eq(10.29)].

The points in Fig 10.15 represent the plots of $\hat{U}$ versus P for the values presented in Table 10.4. It can be seen in Fig 10.15 that all the experimental points are arranged almost linearly. This is consistent with competition model because the model predicts that $\hat{U}$ should be a linear function of P if $\hat{x}'$ is a linear function of P and vice versa [see both eqs(10.29) and (10.30).] The straight line drawn in Fig 10.15 is the regression line of P on $\hat{U}$ for the experimental points. As the slope of the regression line, $\rho^* \upsilon_P$ can be evaluated to be -0.945 [see eq(10.30)], and, by using υ_P ($=0.677$), the parameter ρ^* can be evaluated to be -1.40. On the other hand, as the intersection of the regression line with the $\hat{U}$ axis, $\ln (\beta e^{J^\circ/kT})$ can be evaluated to be -0.399 [eq(10.30); see Table 10.5].

In Fig 10.8, the experimental points for any m value are arranged almost linearly on the (P, $\log_{10}$ k) plane, and the linear arrangement should take place on the (P, ln k) plane also. This is consistent with competition model again because the model predicts that ln k should be a linear function of P if $h_P'(P)$ (i.e., $\hat{x}'$) is a linear function of P and vice versa [see eqs(10.15a), (10.25) and (10.28)]. The regression line for the experimental points for any m value in Fig 10.8 re-drawn on the (P,ln k) plane can be expressed as

$$\ln k = \hat{c} P + \hat{d} \tag{10.31}$$

in which $\hat{c}$ and $\hat{d}$ can be interpreted to represent

$$\hat{c} = (\rho^* - \ln m) \upsilon_P \tag{10.32}$$

and

$$\hat{d} = \ln (\beta e^{J^\circ/kT}) \tag{10.33}$$

respectively [see eqs(10.15'a), (10.27) and (10.28); in eq(10.28) υ_P^* is replaced by υ_P]. In ref(10.7) Table II are estimated both slope (denoted by c) and intersection with the $\log_{10}$ k axis at P=0 (denoted by d) for the regression line for any m value drawn in Fig 10.8; c and d are related to $\hat{c}$ and $\hat{d}$ as $\hat{c} = (\ln 10)c$ and $\hat{d} = (\ln 10)d$, respectively. In Table 10.6, the c and d values [ref(10.7) Table II] are reproduced with addition of

Table 10.5

Evaluations of υ_P, $\rho^*\upsilon_P$, ρ^* and $\ln(\beta e^{J^\circ/kT})$ for polyadenylates on an anion-exchange column at 40℃. υ_P can be evaluated from Fig 10.14, and both $\rho^*\upsilon_P$ and $\ln(\beta e^{J^\circ/kT})$ can be evaluated from Fig 10.15. ρ^* can be evaluated by using both υ_P and $\rho^*\upsilon_P$ values.

$\upsilon_P = x'/P$	$\rho^*\upsilon_P$	$\rho^* = J^*/(x'kT) - \ln\varphi$	$\ln(\beta e^{J^\circ/kT})$
0.677	−0.945	−1.40	−0.399

Table 10.6

Analysis of the regression lines drawn in Fig 10.8 for anion-exchange chromatography of polyadenylates at 40℃. c and d represent slope and intersection with the $\log_{10}$ k axis at P=0 for the regression lines for constant m values, reproduced from ref(10.7) Table II, respectively. $\hat{c}$ [=(ln 10)c] and $\hat{d}$ [=(ln 10)d] represent slope and intersection with the ln k axis for the regression lines re-drawn on the (P, ln k) plane [expressed by eq(10.31)]. ρ^* can be represented as $\ln m + \hat{c}/\upsilon_P$ (fifth column) with $\upsilon_P = 0.677$ (see Table 10.5), and $\ln(\beta e^{J^\circ/kT})$ can be represented by $\hat{d}$ (last column).

m (M)	c	d	$\hat{c}$	$\ln m + \hat{c}/\upsilon_P = \rho^*$	$\hat{d} = \ln(\beta e^{J^\circ/kT})$
0.06	0.409	−0.189	0.942	−1.42	−0.435
0.08	0.343	−0.209	0.790	−1.36	−0.481
0.10	0.278	−0.212	0.640	−1.36	−0.488
0.12	0.229	−0.252	0.527	−1.34	−0.580

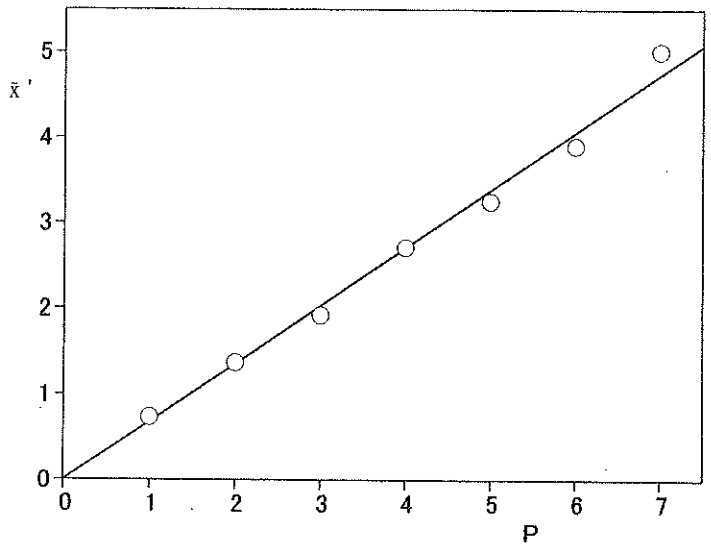


Fig 10.14. Points: plots of $\bar{x}$ versus P for the values presented in Table 10.4 for anion-exchange chromatography of polyadenylates (involving monoadenylate). Straight line: regression line (passing through the origin) of P on $\bar{x}$ for the experimental points.

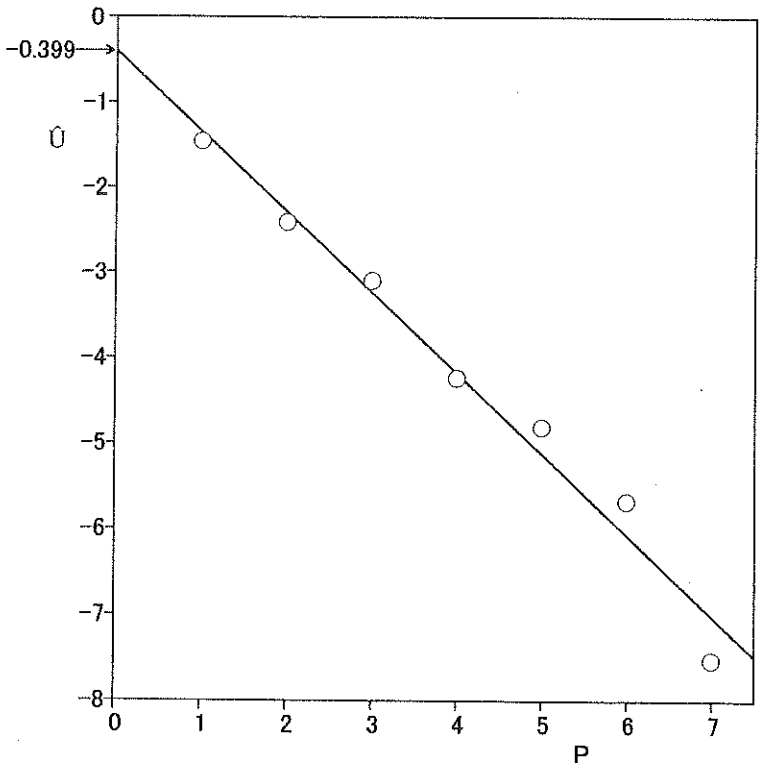


Fig 10.15. Points: plots of Û versus P for the values presented in Table 10.4 for anion-exchange chromatography of polyadenylates (involving monoadenylate). Straight line: regression line of P on Û for the experimental points.

$\hat{c}$, $\ln m + \hat{c}/\upsilon_P$ [$= \rho^*$; see eq(10.32)] and $\hat{d}$ [$= \ln(\beta e^{J^\circ/kT})$; see eq(10.33)] values; $\upsilon_P = 0.677$. Theoretically, both ρ^* and $\ln(\beta c^{J^\circ/kT})$ should be constant, independent of m. It can be seen in both Tables 10.5 and 10.6 that, when m varies between 0.06 and 1 M, then ρ^* and $\ln(\beta e^{J^\circ/kT})$ fluctuate between -1.42 and -1.34, and between -0.580 and -0.399, respectively; Table 10.5 represents the case when $\ln m = 0$ or m = 1 M. The fluctuation might arise from minor secondary mechanisms other than those assumed in competition model (Chapter Ⅷ) and/or from the experimental error.

By using the value, -4.74 to -3.99, of $\ln\beta$ obtained from the experiment of Kopaciewicz (see Table 10.2), it can be estimated that $J^\circ/kT = \ln(\beta e^{J^\circ/kT}) - \ln\beta = (-0.580$ to $-0.399) - (-4.74$ to $-3.99) = 3.41$ to 4.34. As $kT = 2.60$ kJ/mol at 40℃, it follows that $J^\circ = 8.87$ to 11.28 kJ/mol (see Table 10.7 column<1>-<4>).

It can be seen in Fig 10.7 that the minimum $\log_{10}$ C or $\log_{10}$ m value used for the experiment is higher than -1.3, or that the minimum m value is higher than 0.05 M. Under assumption of $(\varphi m)_{lL} = 2$, the lower limit of the possible φ value can be estimated to be $2/0.05 = 40$ (M^{-1}), or the lower limit of $\ln\varphi$ can be evaluated to be about 3.7. As $\rho^* = -1.42$ to -1.34 (see above), by using eq(10.12), the lower limit of $J^*/(x'kT)$ can be evaluated to be 2.3 to 2.4, and, by using the kT value of 2.60 kJ/mol at 40℃, the lower limit of J^*/x' can be evaluated to be 6.0 to 6.2 kJ/mol. By using eq(10.29) into which x'' or x' is substituted for $\hat{x}'$ [cf. eq(10.27)] and where $\upsilon_P = 0.677$, the lower limit of the AVFA per univalent phosphate group of polyadenylate, J^*/P, can be estimated to be 4.0 to 4.2 kJ/mol. The lower limit of the AVFA per terminal divalent phosphate group (which can be represented as $J^*/x' + J^\circ$) can be estimated to be 12.9 to 15.5 kJ/mol (see Table 10.7 column<5>-<10>). The lower limits of J^*/P and $J^*/x' + J^\circ$ (Table 10.7 column<9> and <10>) can be compared with the absolute values of energy of adsorption of uni- and divalent phosphate groups on a C site of HA, 3.8-4.2 kJ/mol and 13.5-14.9 kJ/mol, respectively [see Chapter Ⅷ(E)]. [*Note.* As reversed-phase chromatography, with ion-exchange chromatography also, we have no knowledge about how many functional groups that are present on the local molecular surface facing the adsorbent surface are superposable well on adsorbing sites (i.e., ion-exchangers); $J/P^{2/3}$ only represents the average of the AVFA assigned to a monomer unit that is present on the molecular surface facing the adsorbent surface. It, however, is reasonable to consider that, on the adsorbent surface, the geometrical arrangement of the ion-exchangers can fluctuate to a considerable extent around the mean arrangement in order for a large number of functional groups that are present on the molecular surface facing the adsorbent surface to be superposed well on the ion-excangers since an ion-exchanger is part of an organic substrate with a more or less flexible stereochemical structure [cf. the subsection entitled "Ion-Exchange and Reversed-Phase Chromatographies in Contrast to HA Chromatography" in Chapter Ⅷ(E)]. This suggests that a large proportion of functional groups that are present on the molecu-

Table 10.7

Summary of the analysis of anion-exchange chromatography of polyadenylates at 40℃ where kT=2.60 kJ/mol.

⟨1⟩	⟨2⟩	⟨3⟩	⟨4⟩	⟨5⟩
$\ln(\beta e^{J^\circ/kT})$	$\ln \beta$	J°/kT	J° (kJ/mol)	ρ^*
−0.580 | −0.399	−4.71 | −3.99	3.41 | 4.34	8.87 | 11.28	−1.42 | −1.34

⇒

⟨6⟩	⟨7⟩	⟨8⟩	⟨9⟩	⟨10⟩
φ (M^{-1})	$J^*/(x'kT)=\rho^*+\ln\varphi$	J^*/x' (kJ/mol)	J^*/P (kJ/mol)	$J^*/P+J^\circ$ (kJ/mol)
⇒ ≳40	≳2.3 | 2.4	≳6.0 | 6.2	≳4.0 | 4.2	≳12.9 | 15.5

lar surface facing the adsorbent surface are participating in the reaction with ion-exchangers actually. Cf. Note in the subsection entitled "Summary of the Important Results Obtained from the Analyses of Both Figs 9.1 and 9.2" in Chapter IX(C).]

Analysis of Figs 10.10, 10.11 and 10.13 for Polyphosphates. The regression line for any P value in Fig 10.10 re-drawn on the (ln m, ln k) plane can be expressed by eq (10.6) in which $\bar{x}'$ and $\hat{U}$ can be represented by eqs(10.25) and (10.26), respectively. Both $\bar{x}'$ and exp $\hat{U}$ values at 25℃ for the regression line for any P value drawn in Fig 10.10 [estimated in ref(10.8) Table I where $\bar{x}'$ and exp $\hat{U}$ are written as b and a, respectively] are reproduced in Table 10.8(a) with addition of the $\hat{U}$ value. In ref(10.8) Table I are also listed the $\bar{x}'$ and exp $\hat{U}$ values obtained at 60 and 70℃. These are reproduced in Tables 10.8(b) and (c) with addition of the corresponding $\hat{U}$ values, respectively.

Fig 10.16(a) represent the plots of $\bar{x}'$ versus P at 25, 60 and 70℃ for the values presented in Tables 10.8(a), (b) and (c), respectively. It can be seen in Fig 10.16(a) that the experimental points are arranged almost linearly at any temperature with the arrangements at 60 and 70℃ being almost superposed on one another and with the arrangement at 25℃ slightly different from the others; the extrapolation of the linear arrangement at any temperature intersects the $\bar{x}'$ axis at a popsitive value. This means that eq(10.28) holds but that $x'^{\circ}>0$ in eq(10.25) at any temperature with polyphosphates. Eq(10.28) implies that the area of the anion-exchanger surface occupied by the adsorbed molecule [proportional to x' $(=x'^{*}+x'^{\circ})$] is a linear function of P, and that the the conformations of polyphosphates taking place on the anion-exchanger surface are either stretched or planar similarly to the case of polyadenylates. Eqs(10.25) and (10.26) can be re-expressed as

$$\bar{x}' = \upsilon_P^{*}P + x'^{\circ} \tag{10.34}$$

and

$$\hat{U} = \rho^{*}\upsilon_P^{*}P + \ln\left(\beta e^{J^{\circ}/kT}_{\varphi} - x'^{\circ}\right) \tag{10.35}$$

[cf. eqs(10.29) and (10.30)], respectively. The solid, dashed and dotted straight lines drawn in Fig 10.16(a) are the regression lines of P on $\bar{x}'$ for the experimental points at 25, 60 and 70℃, respectively. As the slope and the intersection with the $\bar{x}'$ axis of the regression line, the parameter υ_P^{*} and x'° can be evaluated, respectively [see eq(10.34)]. Both υ_P^{*} and x'° values at 25, 60 and 70℃ obtained from Fig 10.16(a) are presented in Table 10.9 column<2> and <3>.

$\upsilon_P^{*}=x''/P$ [see both eqs(10.17) and (10.28)] represents the "size" of the inner univalent phosphate in the polyphosphate chain. The "size" of the divalent phospate at each of the two terminals of the polyphosphate chain can be represented as $x''/P+x'^{\circ}/2$, and the "size" of the orthophosphate molecule can be represented approximately as $x''/P+x'^{\circ}$.

Table 10.8

(a) $\bar{x}'$, $\exp\hat{U}$ and $\hat{U}$ values for the regression lines in Fig 10.10 re-drawn on the (ln m, ln k) plane[eq(10.6)], obtained for anion-exchange chromatography of polyphosphates with different P values at 25℃. The molecule with P=1 represents orthophosphate. (b) and (c) $\bar{x}'$, $\exp\hat{U}$ and $\hat{U}$ values for the similar experiments carried out at 60℃ and 70℃, respectively. All the $\bar{x}'$ and $\exp\hat{U}$ values were reproduced from ref(10.8) Table I where $\bar{x}'$ and $\exp\hat{U}$ are written as b and a, respectively.

(a) 25℃

P	$\bar{x}'$	$\exp\hat{U}$	$\hat{U}$
1	2.10	1.47×10^{-2}	−4.220
2	3.83	5.11×10^{-3}	−5.277
3	5.01	1.80×10^{-3}	−6.320
4	6.01	9.40×10^{-4}	−6.970
5	6.97	5.30×10^{-4}	−7.543
6	7.77	3.72×10^{-4}	−7.897
7	8.54	2.52×10^{-4}	−8.286
8	10.2	6.62×10^{-5}	−9.623
9	11.3	3.16×10^{-5}	−10.362

(b) 60℃

P	$\bar{x}'$	$\exp\hat{U}$	$\hat{U}$
1	3.68	2.96×10^{-3}	−5.823
2	4.71	3.18×10^{-3}	−5.751
3	5.38	2.64×10^{-3}	−5.937
4	6.18	1.99×10^{-3}	−6.220
5	7.17	1.27×10^{-3}	−6.669
6	8.32	7.01×10^{-4}	−7.263

(c) 70℃

P	$\bar{x}'$	$\exp\hat{U}$	$\hat{U}$
1	3.70	3.75×10^{-3}	−5.586
2	4.62	4.34×10^{-3}	−5.440
3	5.38	3.41×10^{-3}	−5.681
4	6.15	2.71×10^{-3}	−5.911
5	7.18	1.73×10^{-3}	−6.360
6	8.41	8.93×10^{-4}	−7.021

Table 10.9

Summary of the analysis of anion-exchange chromatography of polyphosphates on the basis of both Figs 10.16 and 10.17.

⟨1⟩	⟨2⟩	⟨3⟩	⟨4⟩	⟨5⟩	
℃	$\upsilon_P^* = x''^*/P$	x'^0	$x''^*/P + x'^0/2$	$x''^*/P + x'^0$	
25	1.079	1.465	1.812	2.544	⇒
60	0.897	2.769	2.282	3.666	⇒
70	0.914	2.707	2.268	3.621	⇒
25 to 70	0.974	2.281	2.115	3.255	

	⟨6⟩	⟨7⟩	⟨8⟩
	$\rho^* \upsilon_P^*$	$\rho^* = J^*/(x''^* kT) - \ln \varphi$	$\ln (\beta e^{J^0/kT} \varphi^{-x'^0})$
⇒	−0.708	−0.656	−3.850
⇒	−0.292	−0.326	−5.253
⇒	−0.290	−0.317	−4.983

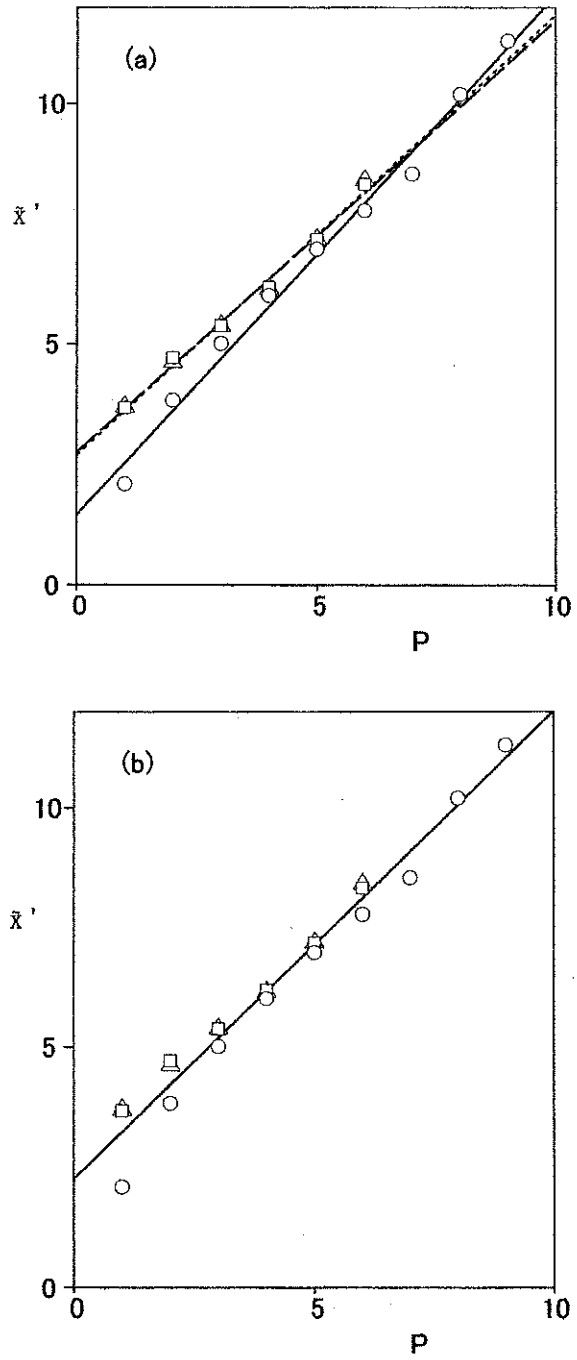


Fig 10.16. (a) Points(○, □ and △): plots of $\bar{x}$ versus P at 25, 60 and 70℃ for the values presented in Tables 10.8(a), (b) and (c) for anion-exchange chromatography of polyphosphates (involving orthophosphate), respectively. Solid, dashed and dotted straight lines: regression lines of P on $\bar{x}$ for the experimental points at 25, 60 and 70℃, respectively. (b) Points(○, □ and △): as (a). Straight line: regression line of P on $\bar{x}$ for all the experimental points taking place between 25 and 70℃.

Both $x''^{*}/P+x'^{\circ}/2$ and $x''^{*}/P+x'^{\circ}$ values at 25, 60 and 70℃ obtained from Fig 10.16(a) are presented in Table 10.9 column<4> and <5>. When considering their physical meanings, the ratios among the x''^{*}/P, $x''^{*}/P+x'^{\circ}/2$ and $x''^{*}/P+x'^{\circ}$ values (Table 10.9) are reasonable ones.

The points(○, □ and △) plotted in Fig 10.16(b) are identical with those plotted in Fig 10.16(a). The straight line drawn in Fig 10.16(b) is the regression line of P on $\hat{x}'$ for all the experimental points taking place between 25 and 70℃. As the slope and the intersection with the $\hat{x}'$ axis of the regression line, the average values of the parameter v_P^{*} $(=x''^{*}/P)$ and x'° taking place between 25 and 70℃ can be estimated, respectively, and, by using these values, the average values of $x''^{*}/P+x'^{\circ}/2$ and $x''^{*}/P+x'^{\circ}$ can be estimated (see the last line in Table 10.9). [*Note.* From their physical meanings, it would be reasonable to assume that both v_P^{*} $(=x''^{*}/P)$ and x'° are almost independent of the temperature. Slight dependences might arise, however, from the slight dependence of the molecular conformation on the temperature.]

The points(○, □ and △) in Fig 10.17 represent the plots of $\hat{U}$ versus P at 25, 60 and 70℃ for the values presented in Table 10.8(a), (b) and (c), respectively. It can be seen in Fig 10.17 that the experimental points are arranged quasi-linearly at any temperature, consistent with competition model virtually. The solid, dashed and dotted straight lines drawn in Fig 10.17 are the regression lines of P on $\hat{U}$ for the experimental plots at 25, 60 and 70℃, respectively. As the slope of the regression line, $\rho^{*}v_P^{*}$ can be evaluated [see eq(10.35)], and, by using the v_P^{*} value (see above), the parameter ρ^{*} can be evaluated. On the other hand, as the intersection of the regresion line with the $\hat{U}$ axis, $\ln\left(\beta e^{J^{\circ}/kT}_{\varphi}{}^{-x'^{\circ}}\right)$ can be evaluated [see eq(10.35)]. The $\rho^{*}v_P^{*}$, ρ^{*} and $\ln\left(\beta e^{J^{\circ}/kT}_{\varphi}{}^{-x'^{\circ}}\right)$ values at 25, 60 and 70℃ obtained from Fig 10.17 are presented in Table 10.9 column<6>-<8>.

In Fig 10.11, the experimental points for any m value at 25℃ are arranged almost linearly on the (P−2, k in logarithmic scale) plane. The linear arrangement should also be obtained on the (P, ln k) plane, consistent with competition model. The regression line for the experimental points for any m value (Fig 10.11) re-drawn on the (P, ln k) plane can be expressed by eq(10.31) where it can be interpreted that $\hat{c}$ and $\hat{d}$ represent

$$\hat{c} = (\rho^{*}-\ln m)\,v_P^{*} \tag{10.36}$$

and

$$\hat{d} = \ln\left(\beta e^{J^{\circ}/kT}_{\varphi}{}^{-x'^{\circ}}\right) - x'^{\circ}\ln m \tag{10.37}$$

respectively [see eqs(10.15'a) and (10.28); cf. eqs(10.32) and (10.33)]. In Fig 10.11, it is possible to shift the abscissa by 2 to obtain the new abscissa representing P, and the ordinate can simply be replaced by that representing $\log_{10}$ k. By the direct surveying of Fig

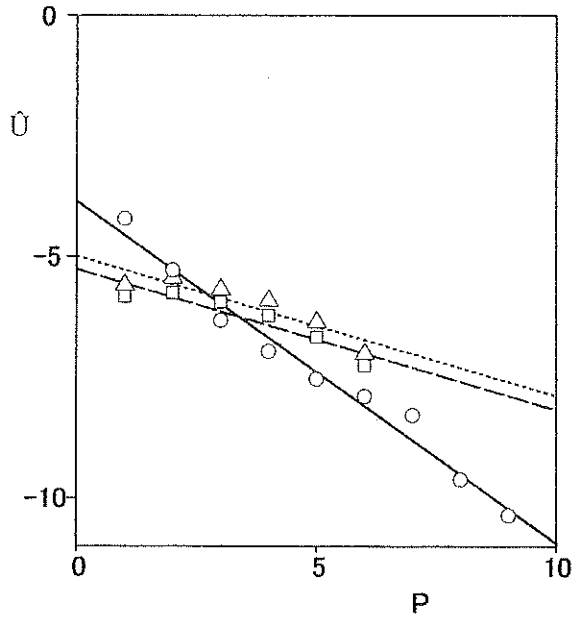


Fig 10.17. Points(○, □ and △): plots of Û versus P at 25, 60 and 70℃ for the values presented in Tables 10.8(a), (b) and (c) for anion-exchange chromatography of polyphosphates (involving orthophosphate), respectively. Solid, dashed and dotted straight lines: regression lines of P on Û for the experimental points at 25, 60 and 70℃, respectively.

10.11 with the new coordinate system, both slope (denoted by c) and intersection with the $\log_{10}$ k axis at P=0 (denoted by d) for the regression line for any m value can be obtained; c and d are related to $\hat{c}$ and $\hat{d}$ as $\hat{c}=(\ln 10)c$ and $\hat{d}=(\ln 10)d$, respectively. These c, d, $\hat{c}$ and $\hat{d}$ values associated to any m value obtained from Fig 10.11 are presented in Table 10.10 with addition of the $\ln m+\hat{c}/\upsilon_P^*$ [$=\rho^*$; see eq(10.36)] and $x'^{\circ}\ln m+\hat{d}$ [$=\ln(\beta e^{J^{\circ}/kT}_{\varphi}{}^{-x'^{\circ}})$; see eq(10.37)] values; see Table 10.9 for the υ_P^* and x'° values at 25℃. Theoretically, both ρ^* and $\ln(\beta e^{J^{\circ}/kT}_{\varphi}{}^{-x'^{\circ}})$ should be constant, independent of m. It can be seen in both Tables 10.9 and 10.10 that, when m varies between 0.23 and 1 M at 25℃, then ρ^* and $\ln(\beta e^{J^{\circ}/kT}_{\varphi}{}^{-x'^{\circ}})$ fluctuate between -0.723 and -0.648, and between -3.946 and -3.498, respectively (Table 10.11); Table 10.9 represents the case when ln m=0 or m=1 M. The The fluctuation might arise from minor secondary mechanisms other than those assumed in competition model (Chapter Ⅷ) and/or from the experimental error.

By using both eqs(10.17) and (10.28), eqs(10.23) and (10.24) can be re-expressed as

$$\Pi = [J^*/P-(\mu_{(w)}^{\circ}+\xi)\upsilon_P^*]P + J^{\circ} - (\mu_{(w)}^{\circ}+\xi)x'^{\circ} \qquad (10.38)$$

and

$$\Sigma = -[\ln(zm)]\upsilon_P^*P + \ln\beta - x'^{\circ}\ln(zm) \qquad (10.39)$$

respectively; the term J^*/P in eq(10.38) is virtually constant, independent of P (since $J^*\approx E^*$). The regression line for any P value drawn in Fig 10.13 [obtained for m=0.3 M] can be expressed by eq(10.22) in which it can be interpreted that Π and Σ are represented by eqs(10.38) and (10.39), respectively. By the direct surveying of Fig 10.13, both slope Π/k [where k [$=8.314\times10^{-3}$ kJ/(deg·mol)] represents the Boltzmann constant] and intersection Σ with the ln k axis at 1/T=0 (where k represents the capacity ratio) can be obtained; these are presented in Table 10.12 with addition of the Π values.

The points in Fig 10.18 represent the plots of Σ versus P for the values presented in Table 10.12. It can be seen in Fig 10.18 that all the experimental points are arranged almost linearly, consistent with competition model. The straight line drawn in Fig 10.18 is the regression line of P on Σ for the experimental points. From its slope and intersection witht the Σ axis at P=0, it can be estimated that $-[\ln(zm)]\upsilon_P^*=1.857$ and that $\ln\beta-x'^{\circ}\ln(zm)=3.932$ [see eq(10.39)]. By using the first relationship and the average, 0.974, of the υ_P^* values taking place between 25 and 70℃ (Table 10.9), it can be estimated that $\ln(zm)=-1.857/\upsilon_P^*=-1.857/0.974=-1.907$. As m=0.3 M, z can be evaluated to be 0.495. On the other hand, by using the second relationship, the average, 2.281, of the x'° values taking place between 25 and 70℃ (Table 10.9) and the ln (zm) value of -1.907, it can be estimated that $\ln\beta=x'^{\circ}\ln(zm)+3.932=-2.281\times1.907+3.932=-0.418$, or that $\beta=0.658$ (see Table 10.13). Due to its physical meaning (coor-

Table 10.10

Analysis of the regression lines drawn in Fig 10.11 for anion-exchange chromatography of polyphosphates at 25℃. c and d represent slope and intersection with the $\log_{10}$ k axis (which is expressed as the k axis in logarithmic scale) at P=0 for the regression lines for constant m values, estimated by the direct surveying of the diagram, respectively. $\hat{c}$ [=(ln 10)c] and $\hat{d}$ [=(ln 10)d] represent slope and intersection with the ln k axis for the regression lines redrawn on the (P, ln k) plane [expressed by eq(10.31)]. ρ^* and $\ln(\beta e^{J^\circ/kT}\varphi^{-x'^\circ})$ can be represented as $\ln m + \hat{c}/\upsilon_P^*$ and $x'^\circ \ln m + \hat{d}$ (the two last columns) with υ_P^* and x'° values estimated in Table 10.9 column <2> and <3>, respectively. The symbol c and d correspond to the symbol c and d−2c in ref(10.9), respectively.

m (M)	c	d	$\hat{c}$	$\hat{d}$	$\ln m + \hat{c}/\upsilon_P^* = \rho^*$	$x'^\circ \ln m + \hat{d} = \ln(\beta e^{J^\circ/kT}\varphi^{-x'^\circ})$
0.23	0.350	−0.584	0.806	−1.345	−0.723	−3.498
0.25	0.321	−0.651	0.739	−1.499	−0.701	−3.530
0.30	0.247	−0.826	0.569	−1.902	−0.677	−3.666
0.32	0.229	−0.989	0.527	−2.277	−0.651	−3.946
0.34	0.202	−0.976	0.465	−2.247	−0.648	−3.827

Table 10.11

ρ^* and $\ln(\beta e^{J^\circ/kT}\varphi^{-x'^\circ})$ values for polyphosphates on an anion-echange column at 25℃.

ρ^*	$\ln(\beta e^{J^\circ/kT}\varphi^{-x'^\circ})$
−0.723	−3.946
|	|
−0.648	−3.498

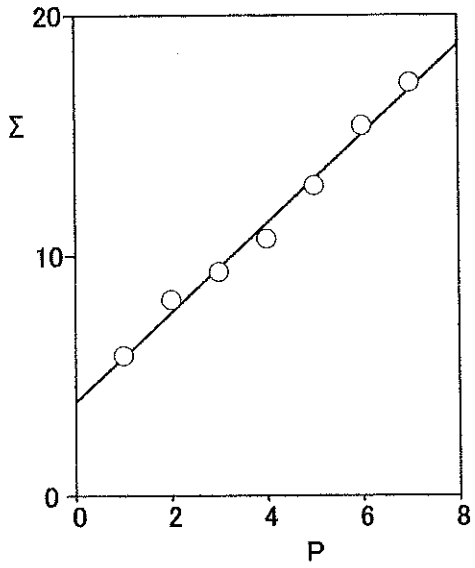


Fig 10.18. Points: plots of Σ versus P for the values pesented in Table 10.12 for anion-exchange chromatography of polyphosphates (involving orthophosphate). Straight line: regression line of P on Σ for the experimental points.

dinate number of the adsorbing sites), it would be reasonable to interpret that the value, 0.495, of z estimated above represents the value of unity approximately; the error might arise at least partially from the rough approximation of the use of the averages of both υ_P^* and x'^0 values.

The value, 0.658, of the parameter β is not much smaller than unity. Let us consider eq(8.51) in which $q=\beta$ [i.e., $J(\equiv E+kT\ln\tau)=0$; see eq(8.49)] and $m=0$. By substituting $\beta=0.658$ into this equation, $\dot{B}$ or $B=1/(1+0.658)=0.603$ is obtained. This means that, even provided that all the phosphate groups on the polyphosphate chain are deprived of the function of adsorption (of the type which can be prevented by the presence of chloride ions through the competition mechanism), partition, B, of polyphosptate molecules in the mobile phase taking place in the absence of competing chloride ions is not close to unity, about 40% of the molecules being adsorbed on the anion-exchanger surface. This implies that the polyphosphate chain is adsorbed on the anion-exchanger surface partially through another mechanism where the adsorption is not prevented by the presence of chloride ions. It can be assumed that this mechanism is independent of the total length of the polyphosphate chain because the dependence of the chromatographic behavior of polyphosphate on degree of polymerization P (Fig 10.11) can be explained satisfactorily in terms of the competition mechanism only (see above). This strongly suggests that the second adsorption mechanism takes place at both terminals of the polyphosphate chain where divalent phosphate groups are present, respectively. (This consideration may be consistent with the result of the analysis of Fig 10.19 which will be performed below.) The second mechanism of adsorption might be induced (perhaps indirectly) by the presence of the strongly chelating agent, Na_4EDTA, in the chromatographic system.

The points in Fig 10.19 represent the plots of Π versus P for the values presented in Table 10.12. It can be seen in Fig 10.19 that all the experimental points are arranged quasi-linearly, consistent with competition model virtually. The straight line drawn in Fig 10.19 is the regression line of P on Π for the experimental points. From its slope and intersection with the Π axis at $P=0$, it can be estimated that $J^*/P-(\mu_{(0)}^\circ+\xi)\upsilon_P^*=-3.021$ and that $J^\circ-(\mu_{(0)}^\circ+\xi)x'^0=-15.887$ [see eq(10.38)].

It can be seen in Fig 10.10 that the minimum $\log_{10}$ C or $\log_{10}$ m value used for the experiment is almost equal to -0.7, or that the minimum m value is almost equal to 0.2 M. Under assumption of $(\varphi\ m)_{LL}=2$, the lower limit of the possible φ value can be estimated to be $2/0.2=10$ (M^{-1}). $\mu_{(0)}^\circ+\xi$ is almost equal to $kT\ln(\varphi/z)$ [eq(10.21')] and $z=0.495$ (Table 10.13). On the other hand, the lower limit of the temperature applied in Fig 10.13 is 20℃, so that the lower limit of the KT value is 2.44 kJ/mol. This means that the lower limit of the $\mu_{(0)}^\circ+\xi$ value is $2.44\times\ln(10/0.495)=7.33$ kJ/mol. By using the first relationship obtained from the analysis of the regression line drawn in Fig 10.19 (see the last of the preceding paragraph) and the average, 0.974, of the υ_P^* values taking place between 25 and 70℃ (Table 10.9), it can be estimated that $J^*/P=(\mu_{(0)}^\circ+\xi)\upsilon_P^*-3.021\gtrsim 7.33\times 0.974-3.021=4.12$ kJ/mol. On the other hand, by using the second rela-

Table 10.12

Π/k [where $k=8.314\times10^{-3}$ kJ/(deg·mol) represents the Boltzmann constant], Π and Σ values for the regression lines[eq(10.22)] drawn in Fig 10.13, obtained for anion-exchange chromatography of polyphosphates with different P values. The molecule with P=1 represents orthophosphate. Π/k and Σ were evaluated by the direct surveying of Fig 10.13.

P	Π/k	Π (kJ/mol)	Σ
1	−2388	−19.85	5.859
2	−2725	−22.66	8.165
3	−2900	−24.11	9.310
4	−3150	−26.19	10.700
5	−3638	−30.25	12.924
6	−4200	−34.92	15.390
7	−4550	−37.83	17.170

Table 10.13

Summary of the analysis of anion-exchange chromatography of polyphosphates on the basis of Fig 10.18.

ln (zm)	z	ln β	β
−1.907	0.495	−0.418	0.658

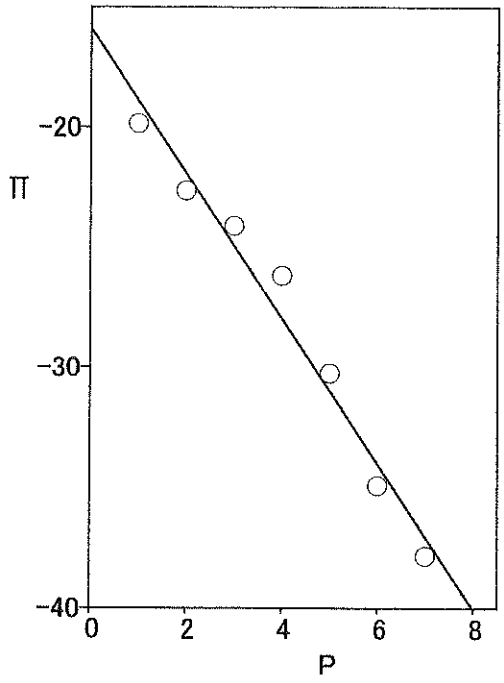


Fig 10.19. Points: plots of Π versus P for the values presented in Table 10.12 for anion-exchange chromatography of polyphosphates (involving orthophosphate). Straight line: regression line of P on Π for the experimental points.

tionship (the last of the preceding paragraph) and the average, 2.281, of the x'° values taking place between 25 and 70℃ (Table 10.9), it can be estimated that $J^{\circ}=(\mu\omega^{\circ}+\xi)x'^{\circ}-15.887\gtrsim 7.33\times 2.281-15.887=0.83$ kJ/mol. J^{*}/P represents the AVFA per inner univalent phosphate in the polyphosphate chain. The AVFA per divalent phosphate taking place at each of the two terminals of the chain can be represented as $J^{*}/P+J^{\circ}/2$, and the AVFA for the orthophosphate molecule can be represented approximately as $J^{*}/P+J^{\circ}$. It can be estimated that $J^{*}/P+J^{\circ}/2\gtrsim 4.54$ kJ/mol and that $J^{*}/P+J^{\circ}\gtrsim 4.95$ kJ/mol. All the results obtained in this paragraph are summarized in Table 10.14. [Cf. Note at the end of the preceding subsection entitled "Analysis of Figs 10.7 and 10.8 for Polyadenylates".]

The lower limit, 4.12 kJ/mol, of the AVFA estimated for the univalent phospahe on the polyphosphate chain (Table 10.14 column<4>) is almost equal to the lower limit, 4.0 to 4.2 kJ/mol, estimated for the univalent phosphate on the polyadenylate chain (Table 10.7 column<9>). In contrast, the lower limit, 4.54 kJ/mol, of the AVFA estimated for the divalent phosphate at each of the two terminals of the polyphosphate chain (Table 10.14 column<6>) is only slightly larger than that for the univalent phosphate on the same polyphosphate chain (4.12 kJ/mol; Table 10.14 column<4>). The former is fairly smaller than the lower limit, 12.9 to 15.5 kJ/mol, of the AVFA for the divalent phosphate at one of the two terminals of the polyadenylate chain (Table 10.7 column<10>). It is presumable that the apparently abnormally small lower limit of the AVFA for the terminal divalent phosphates of the polyphosphate chain arises in connection with the presence of the second adsorption mechanism (see above).

For other studies of the temperature effect on both ion-exchange and reversed-phase chromatographies, see refs(10.16-10.19).

Table 10.14

Summary of the analysis of anion-exchange chromatography of polyphosphates on the basis of Fig 10.19.

⟨1⟩	⟨2⟩	⟨3⟩	⟨4⟩	⟨5⟩	⟨6⟩	⟨7⟩
φ (M^{-1})	T (K°)	$\mu_{(0)}^{\circ} + \varepsilon$ (kJ/mol)	J^{*}/P (kJ/mol)	J° (kJ/mol)	$J^{*}/P + J^{\circ}/2$ (kJ/mol)	$J^{*}/P + J^{\circ}$ (kJ/mol)
≳10	≳293	≳7.33	≳4.12	≳0.83	≳4.54	≳4.95

APPENDIX

Appendix I. Partial Differentiation of Compound Function

When function $z(x,y)$ is totally differentiable and when both x and y are partially differentiable functions of u and v [$x=x(u,v)$ and $y=y(u,v)$], then a set of relationships:

$$\left.\begin{aligned}(\partial z/\partial u)_v &= (\partial z/\partial x)_y(\partial x/\partial u)_v + (\partial z/\partial y)_x(\partial y/\partial u)_v \\ (\partial z/\partial v)_u &= (\partial z/\partial x)_y(\partial x/\partial v)_u + (\partial z/\partial y)_x(\partial y/\partial v)_u\end{aligned}\right\} \quad \text{(A1.1)}$$

hold.

Appendix II. Solutions of Differential Equations

(A) General Solution of Eq(3.31) When B Is Represented by Eq(3.32), and Other Similar Cases

Eq(3.31) can be rewritten by using eq(3.32) as

$$k'(\hat{m})\partial C/\partial \hat{m} + \partial C/\partial s = -(dk'/d\hat{m})C \tag{A2.1}$$

which is called a linear partial differential equation of the first order. The corresponding auxiliary equation can be represented as

$$\frac{d\hat{m}}{k'(\hat{m})} = ds = -\frac{dC}{(dk'/d\hat{m})C} \tag{A2.2}$$

The integrations of the equality between left-hand side and middle, and of the equality between left- and right-hand sides of eq(A2.2) lead to

$$s - \int_0^{\hat{m}} d\hat{m}/k'(\hat{m}) = K_1 \tag{A2.3}$$

and

$$Ck'(\hat{m}) = K_2 \tag{A2.4}$$

in which K_1 and K_2 represent integral constants, respectively. Both eqs(A2.3) and (A2.4) lead to

$$K_2 = U(K_1) \tag{A2.5}$$

or eq(3.33).

The solution, eq(3.37), of eq(3.31) when B is represented by eq(3.36), the solution, eq(3.41), of eq(3.31) when B is represented by eq(3.40), the solution, eq(3.54), of eq (3.52), the solution, eq(3.55), of eq(3.51), the solution, eq(3.82), of eq(3.80), and the solution, eq(3.83), of eq(3.81) can be obtained by using similar methods, respectively.

(B) General Solution of Eq(3.77)

Eq(3.77) can be rewritten by using both eqs(3.17) and (3.21) as

$$\frac{1-B''(\bar{s})}{B''(\bar{s})}\cdot\frac{\partial C}{\partial \hat{m}} + \frac{\partial C}{\partial s} = \frac{1}{B''(\bar{s})}\cdot\frac{dB''(\bar{s})}{d\bar{s}}C \tag{A2.6}$$

which is a linear partial differential equation of the first order. The corresponding auxiliary equation can be represented as

$$\frac{d\bar{m}}{\frac{1-B''(\bar{s})}{B''(\bar{s})}} = ds = \frac{dC}{\frac{1}{B''(\bar{s})} \cdot \frac{dB''(\bar{s})}{d\bar{s}} C} \tag{A2.7}$$

The equality between left-hand side and middle of eq(A2.7) can be rewritten by using eq (3.19) as

$$ds = d\bar{s} \tag{A2.8}$$

which, with integration, leads to

$$s - \bar{s} = K''_1 \tag{A2.9}$$

where K''_1 represents the integral constant. On the other hand, the equality between middle and rigth-hand side of eq(A2.7) can be rewritten by using eq(A2.8) as

$$d\ln C = d\ln B''(\bar{s}) \tag{A2.10}$$

which, with integration, leads to

$$C/B''(\bar{s}) = K''_2 \tag{A2.11}$$

where K''_2 represents the integral constant. Both eqs(A2.9) and (A2.11) lead to

$$K''_2 = F(K''_1) \tag{A2.12}$$

or eq(3.78').

Eq(3.77) can also be rewritten by using both eqs(3.17) and (3.20) as

$$\frac{1-B'(\bar{m})}{B'(\bar{m})} \cdot \frac{\partial C}{\partial \hat{m}} + \frac{\partial C}{\partial s} = \frac{1-B'(\bar{m})}{[B'(\bar{m})]^2} \cdot \frac{dB'(\bar{m})}{d\bar{m}} C \tag{A2.13}$$

Corresponding to eqs(A2.9) and (A2.11),

$$\hat{m} - \bar{m} = K'_1 \tag{A2.14}$$

and

$$C/B'(\bar{m}) = K'_2 \tag{A2.15}$$

can be derived, where K'_1 and K'_2 represent the integral constants, and, for the derivation of both eqs(A2.14) and (A2.15), eq(3.18) has been used instead of eq(3.19). Both eqs (A2.14) and (A2.15) lead to

$$K'_2 = F(-K'_1) \tag{A2.16}$$

or eq(3.78).

(C) Solution of Homogeneous Linear Partial Differential Equation of the Second Order with A Parabolic Form

The homogeneous linear partial differential equation of the second order with a parabolic form:

$$\mathrm{div}_r\,[\,\phi(t)Y-\phi(t)\mathrm{grad}_r\,Y]\;+\;\partial Y/\partial t\;=\;0 \tag{A2.17}$$

or

$$\phi(t)\,\partial Y/\partial r\;+\;\partial Y/\partial t\;=\;\phi(t)\,\partial^2 Y/\partial r^2 \tag{A2.17'}$$

can be solved under initial condition:

$$\lim_{t\to 0} Y(t,r)\;=\;Y_0(r) \tag{A2.18}$$

to give a solution:

$$Y\;=\int_{-\infty}^{\infty} Y_0(r')G\left(\,r;\int_0^t \phi(t)dt\;+\;r',\;\sqrt{2\int_0^t \phi(t)dt}\,\right)dr' \tag{A2.19}$$

in which

$$G(x;\;\mu,\;\sigma)\;\equiv\;\frac{1}{\sqrt{2\pi}\,\sigma}\exp[-\frac{(x-\mu)^2}{2\sigma^2}] \tag{A2.20}$$

represents the normalized Gauss function with mean value μ and standard deviation σ. When

$$Y_0(r)\;=\;\delta(r) \tag{A2.21}$$

then eq(A2.19) reduces to

$$Y\;=\;G\left(\,r;\int_0^t \phi(t)dt,\;\sqrt{2\int_0^t \phi(t)dt}\,\right) \tag{A2.22}$$

The solution, eq(A2.19), can be obtained by using the Fourier transformation method. Thus, introducing Fourier transformations:

$$\mathcal{F}(Y)\;=\;U(t,u)\;\equiv\;\frac{1}{\sqrt{2\pi}}\int_{-\infty}^{\infty}\exp(-iur)Y(t,r)dr \tag{A2.23}$$

$$\mathcal{F}(\partial Y/\partial r)\;=\;iuU(t,u) \tag{A2.24}$$

and

$$\mathcal{F}(\partial^2 Y/\partial r^2) = -u^2 U(t,u) \tag{A2.25}$$

eq(A2.17') becomes

$$iu\phi(t)U + \partial U/\partial t = -u^2\phi(t)U \tag{A2.26}$$

from which

$$U(t,u) = h(u)\exp\left(-\int_0^t [u^2\phi(t)+iu\phi(t)]dt\right) \tag{A2.27}$$

is obtained where h is any function. On the other hand, as it can be considered that

$$\begin{aligned} Y_0(r) &= \frac{1}{\sqrt{2\pi}}\int_{-\infty}^{\infty}\exp(iur)U(0,u)du \\ &= \frac{1}{\sqrt{2\pi}}\int_{-\infty}^{\infty}\exp(iur)h(u)du \end{aligned} \tag{A2.28}$$

then we have

$$h(u) = \frac{1}{\sqrt{2\pi}}\int_{-\infty}^{\infty}\exp(-iur')Y_0(r')dr' \tag{A2.29}$$

which, with eq(A2.27), leads to

$$\begin{aligned} Y(t,r) &= \frac{1}{\sqrt{2\pi}}\int_{-\infty}^{\infty}\exp(iur)U(t,u)du \\ &= \frac{1}{\sqrt{2\pi}}\int_{-\infty}^{\infty}Y_0(r')\left\{\frac{1}{\sqrt{2\pi}}\int_{-\infty}^{\infty}\exp\left(-u^2\int_0^t\phi(t)dt\right)\right. \\ &\qquad \left.\cdot\exp\left(iu[r-\int_0^t\phi(t)dt - r']\right)du\right\}dr' \end{aligned} \tag{A2.30}$$

We show below that the right-hand side of eq(A2.30) is identical with the right-hand

side of eq(A2.19). Thus, the integral, $\oint \exp(-z^2/2)dz$ (where $z=x+iy$), along the four sides of a rectangle on the complex xy-plane is zero (Cauchy theorem). Therefore, if the rectangle is symmetric around the y axis while superposing one of the sides on the x axis and setting the oposite side (parallel to the x axis) on the negative y domain, and if the lengths of the two sides under consideration tend to infinity, then the relationship:

$$\frac{1}{\sqrt{2\pi}} \int_{-\infty}^{\infty} \exp(-x^2/2)\exp(ixy)dx = \exp(-y^2/2) \qquad \text{(A2.31)}$$

is fulfilled. Therefore, defining x and y as

$$x \equiv \sqrt{2\int_0^t \phi(t)dt} \qquad \text{(A2.32)}$$

and

$$y \equiv \left(r - \int_0^t \phi(t)dt - r' \right) \Big/ \sqrt{2\int_0^t \phi(t)dt} \qquad \text{(A2.33)}$$

respectively, then the term { } in eq(A2.30) can be calculated as

$$\{\ \} = \frac{1}{\sqrt{2\pi}} \int_{-\infty}^{\infty} \exp(-x^2/2)\exp(ixy)dx \Big/ \sqrt{2\int_0^t \phi(t)dt}$$

$$= \exp(-y^2/2) \Big/ \sqrt{2\int_0^t \phi(t)dt}$$

$$= \sqrt{2\pi}\ G\left(r; \int_0^t \phi(t)dt + r', \sqrt{2\int_0^t \phi(t)dt} \right) \qquad \text{(A2.34)}$$

This means that the right-hand side of eq(A2.30) is identical with the right-hand side of eq(A2.19).

It is easy to confirm that eq(A2.22) is a solution to eq(A2.17') by substituting eq (A2.22) into eq(A2.17') directly. Eq(A2.19), being a convolution of eq(A2.22), is also a solution to eq(A2.17') since this latter has a homogeneous linear form.

(D) Solution of Eq(5.26) Combined with Eq(5.20)

Linear differential equation of the first order:

$$dy/dx + P(x)y = Q(x) \tag{A2.35}$$

has a general solution:

$$y = e^{-\int P(x)dx} \left(\int e^{\int P(x)dx} Q(x)dx + K \right) \tag{A2.36}$$

in which K represents the integral constant. Considering s, $\Delta(s; g')$, $[dB'(\mu)/d\mu]/B'[\mu(s)]$ and $\sqrt{g'\Theta^\circ}/2\cdot(1/\sqrt{s})$ for x, y, P(x) and Q(x), respectively, the general solution of eq(5.26) can be obtained, where the term corresponding to $\int P(x)dx$ can be calculated by using eq(5.20) as $\int [dB'(\mu)/d\mu]ds/B'[\mu(s)] = \int dB'/(1-B') = -\ln(1-B') + K'$; K' represents another integral constant. Under initial condition given by eq(5.18), the solution, eq(5.27), is obtained.

Appendix Ⅲ. Complementary Arguments on Gradient Chromatography

(A) Complementary Chromatogram as First Concept versus Complementary Abstract Flux

It would be possible to extend eq(2.25) to

$$\mathrm{div}_{\hat{m}}\left(\frac{B}{1-B}\chi\right)+\frac{\partial\chi}{\partial\hat{m}}=0 \tag{A3.1}$$

representing the complementary abstract flux with gradient chromatography in OPV(CPV). As

$$\Omega = C/B = \chi/(1-B) \tag{A3.2}$$

[cf. both eqs(2.2) and (2.4)], eq(A3.1) is identical with eq(3.31).

The Case When Only the Gradient in the Liquid Phase Is Applied. Eq(3.32) holds, and eq(A3.1) has a general solution:

$$\chi = U\left(s-\int_0^{\hat{m}}\frac{d\hat{m}}{k'(\hat{m})}\right) = U\left(s-\int_0^{\hat{m}}\frac{B'(\hat{m})}{1-B'(\hat{m})}d\hat{m}\right) \tag{A3.3}$$

which is identical with eq(3.33) [cf. eq(A3.2)]. Corresponding to eq(3.34), we have

$$\lim_{\hat{m}\to 0}\chi = U(s) = (1-B_0)F[(1-B_0)s] = \left(\frac{k_0}{1+k_0}F\left(-\frac{k_0}{1+k_0}s\right)\right) \tag{A3.4}$$

which implicitly states that $\lim_{\hat{m}\to 0}\chi = 0$ when $s<0$. Under initial condition given by eq (A3.4), eq(A3.3) can be rewritten as

$$\chi = (1-B_0)F\left((1-B_0)\left[s-\int_0^{\hat{m}}\frac{B'(\hat{m})}{1-B'(\hat{m})}d\hat{m}\right]\right)$$

$$\left(=\frac{k_0}{1+k_0}F\left(\frac{k_0}{1+k_0}\left[s-\int_0^{\hat{m}}\frac{d\hat{m}}{k'(\hat{m})}\right]\right)\right) \tag{A3.5}$$

which is identical with eq(3.35) [cf. eq(A3.2)]. Eq(A3.5) represents χGM1st both width, Δ_x, and shape of which are constant, independent of $\hat{m}$; these can be measured and determined by reciprocal of $1-B_o$ in function F, respectively. With the isocratic case when $B'(\hat{m})=B_o=B^\circ$ and $k'(\hat{m})=k_o=k^\circ$, eq(A3.4) coincides with eq(2.26), and eq(A3.5) reduces to eq(2.22).

The Case When Only the Gradient in the Solid Phase Is Applied. Eq(3.36) holds, and eq(A3.1) has a general solution:

$$\chi = \kappa''(s)\, U\left(\int_0^s k''(s)ds - \hat{m} \right)$$

$$= \frac{1-B''(s)}{B''(s)} U\left(\int_0^s \frac{1-B''(s)}{B''(s)} ds - \hat{m} \right) \qquad \text{(A3.6)}$$

which is identical with eq(3.37) [cf. eq(A3.2)]. Corresponding to eq(3.38), we have

$$\lim_{\hat{m}\to 0} \chi = \frac{1-B''(s)}{B''(s)} U\left(\int_0^s \frac{1-B''(s)}{B''(s)} ds \right)$$

$$= (1-B_o)F[(1-B_o)s] = \left(\frac{k_o}{1+k_o} F\left(\frac{k_o}{1+k_o} s \right) \right) \qquad \text{(A3.7)}$$

where $B''(s)$ appearing explicitly in eq(A3.7) represents B_o. Under eq(A3.7), eq(A3.6) can be rewritten as

$$\chi = \frac{B_o[1-B''(s)]}{B''(s)} F\left(B_o[\int_0^s \frac{1-B''(s)}{B''(s)} ds - \hat{m}] \right)$$

$$\left(= \frac{k''(s)}{1+k_o} F\left(\frac{1}{1+k_o} [\int_0^s k''(s)ds - \hat{m}] \right) \right) \qquad \text{(A3.8)}$$

which is identical with eq(3.39) [cf. eq(A3.2)]. Eq(A3.8) represents χGM1st the width, Δ_x, of which increases monotonically to approach infinity with increase in $\hat{m}$; this can be measured by reciprocal of the product by B_o of integrand $[1-B''(s)]/B''(s)$ in function F. [It should be noted that $B''(s)/[1-B''(s)]$ increases monotonically to approach infinity with increase in s and that the s coordinates over which χGM1st appears, in general, increase with increase in $\hat{m}$.] With the isocratic case when $B''(s)=B_o=B^\circ$ and $k''(s)=k_o=k^\circ$, eq(A3.7) coincides with eq(2.26), and eq(A3.8) reduces to eq(2.22).

The Case When Both the Gradient in the Liquid Phase and the Gradient in the Solid

Phase Are Applied at the Same Time. Eq(3.40) holds, and eq(A3.1) has a general solution:

$$\chi = \kappa''(s)\ U\left(\int_0^s \kappa''(s)ds - \int_0^{\hat{m}} \frac{d\hat{m}}{\kappa'(\hat{m})} \right) \tag{A3.9}$$

which is identical with eq(3.41) because the relationship:

$$\kappa'(\hat{m})C = \chi / \kappa''(s) \tag{A3.10}$$

can be derived from both eqs(3.25) and (A3.2). Corresponding to eq(3.43), we have

$$\lim_{\hat{m}\to 0} \chi = \kappa''(s)\ U\left(\int_0^s \kappa''(s)ds \right)$$

$$= (1-B_o)F[(1-B_o)s] = \left(\frac{k_o}{1+k_o} F\left(\frac{k_o}{1+k_o} s \right) \right) \tag{A3.11}$$

where $\kappa''(s)$ appearing explicitly in eq(A3.11) represents κ_o''. Under eq(A3.11), eq(A3.9) can be rewritten as

$$\chi = \frac{\kappa''(s)}{1/\kappa_o' + \kappa_o''} F\left(\frac{1}{1/\kappa_o' + \kappa_o''} \left[\int_0^s \kappa''(s)ds - \int_0^{\hat{m}} \frac{d\hat{m}}{\kappa'(\hat{m})} \right] \right) \tag{A3.12}$$

which is identical with eq(3.44) due to both eqs(3.42) and (A3.10). Eq(A3.12) represents χGM1st the width, Δ_x, of which can be measured by reciprocal of the product by $1/(1/\kappa_o' + \kappa_o'')$ of integrand $\kappa''(s)$ in the first integral in function F i.e., by the product by $1/\kappa_o' + \kappa_o''$ of $1/\kappa''(s)$. The s coordinates over which χGM1st appears, in general, increase with increase in the $\hat{m}$ coordinates over which χGM1st appears. Δ_x, therefore, increases monotonically with increase in the $\hat{m}$ coordinates; this means that Δ_x increases monotonically with increase in coordinate $\hat{m}$ (on the carrier liquid) at which the monitoring is performed.

There are two cases. *First case*: The functions $\kappa'(\hat{m})$ corresponding to the $\hat{m}$ coordinates over which χGM1st appears decrease more rapidly than the functions $\kappa''(s)$ corresponding to the s coordinates over which χGM1st appears with increases in both $\hat{m}$ and s coordinates in such a way that the $\kappa''(s)$ values are still finite when the $\kappa'(\hat{m})$ values tend to infinitesimal (corresponding to the second case with CGM1st). These coordinates over which χGM1st appears and the corresponding functions $\kappa''(s)$ with finite values tend to be constant. χGM1st with both constant finite width Δ_x and constant shape stays over these constant s coordinates. *Second case*: The functions $\kappa'(\hat{m})$ decrease less rapidly than the functions $\kappa''(s)$ with increases in both $\hat{m}$ and s in such a

way that the $\kappa'(\hat{m})$ values are still finite when the $\kappa''(s)$ values tend to infinitesimal (corresponding to the first case with CGM1st). The case when both $\kappa'(\hat{m})$ and $\kappa''(s)$ tend to infinitesimal at comparable rates is here regarded as an extreme of the second case. χGM1st with infinite Δ_x takes place.

When $\kappa''(s)=\kappa^{\circ\prime\prime}=\kappa_\circ''$ and eq(3.28) into which $\kappa_\circ''$ is substituted for $\kappa^{\circ\prime\prime}$ holds, then, due to eq(3.42), eq(A3.12) reduces to eq(A3.5). On the other hand, when $\kappa'(\hat{m})=\kappa^{\circ\prime}=\kappa_\circ'$ and eq(3.29) into which $\kappa_\circ'$ is substituted for $\kappa^{\circ\prime}$ holds, then eq(A3.12) reduces to eq(A3.8). With the isocratic case when $\kappa'(\hat{m})=\kappa_\circ'=\kappa^{\circ\prime}$, $\kappa''(s)=\kappa_\circ''=\kappa^{\circ\prime\prime}$, $B_\circ=B^\circ$ and $k_\circ=k^\circ$, eq(A3.11) coincides with eq(2.26), and eq(A3.12) reduces to eq(2.22).

(B) Complementary Chromatogram as Second Concept versus Molecular Band as Flux

The Case When Only the Gradient in the Liquid Phase Is Applied. χGM2nd (as a function of ξ for a given position $\hat{m}$; CPV) can be obtained by combining eq(3.54) with the relationship: $\chi=[1-B'(\hat{m})]\Omega$ as

$$\chi = (1-B_\circ)F\left((1-B_\circ)[\xi - \int_0^{\hat{m}} \frac{d\hat{m}}{1-B'(\hat{m})}] \right)$$

$$\left(= (1-B_\circ)F\left((1-B_\circ)[\xi - \hat{m} - \int_0^{\hat{m}} \frac{B'(\hat{m})}{1-B'(\hat{m})} d\hat{m}] \right) \right) \qquad \text{(A3.13)}$$

Eq(A3.13) can also be derived by substituting $\xi-\hat{m}$ for s into eq(A3.5), or, to the contrary, eq(A3.5) can be derived by substituting $\hat{m}+s$ for ξ into eq(A3.13) [see the right-hand side in parentheses in eq(A3.13)]. With the isocratic case when $B'(\hat{m})=B_\circ=B^\circ$ and $k'(\hat{m})=k_\circ=k^\circ$, eq(A3.13) reduces to eq(2.38).

The Case When Only the Gradient in the Solid Phase Is Applied. χGM2nd can be obtaied by combining eq(3.56) with the relationship: $\chi=[1-B''(\xi-\hat{m})]\Omega$ as

$$\chi = \frac{B_\circ[1-B''(\xi-\hat{m})]}{B''(\xi-\hat{m})} F\left(B_\circ[\int_0^{\xi-\hat{m}} \frac{ds}{B''(s)} - \xi] \right)$$

$$\left(= \frac{B_\circ[1-B''(\xi-\hat{m})]}{B''(\xi-\hat{m})} F\left(B_\circ[\int_0^{\xi-\hat{m}} \frac{1-B''(s)}{B''(s)} ds - \hat{m}] \right) \right) \qquad \text{(A3.14)}$$

Eq(A3.14) can also be derived by substituting $\xi-\hat{m}$ for s into eq(A3.8), or to the contrary, eq(A3.8) can be derived by substituting $\hat{m}+s$ for ξ into eq(A3.14) [see the right-hand side in parentheses in eq(A3.14)]. With the isocratic case when $B''(s)=B''(\xi-\hat{m})=$

$B_o = B^\circ$ and $k''(s) = k''(\xi - \hat{m}) = k_o = k^\circ$, eq(A3.14) reduces to eq(2.38).

The Case When Both the Gradient in the Liquid Phase and the Gradient in the Solid Phase Are Applied at the Same Time. χGM2nd can be obtaied by combining eq(3.58) with the relationship: $\chi = (1-B)\Omega = \kappa'(\hat{m})\kappa''(\xi - \hat{m})\Omega/[1+\kappa'(\hat{m})\kappa''(\xi - \hat{m})]$ as

$$\chi = \frac{\kappa''(\xi - \hat{m})}{1/\kappa_o' + \kappa_o''} F\left(\frac{1}{1/\kappa_o' + \kappa_o''} \left[\int_0^{\xi - \hat{m}} \kappa''(s)ds - \int_0^{\hat{m}} \frac{d\hat{m}}{\kappa'(\hat{m})} \right] \right) \qquad (A3.15)$$

Eq(A3.15) can also be derived by substituting $\xi - \hat{m}$ for s into eq(A3.12), or, to the contrary, eq(A3.12) can be derived by substituting $\hat{m} + s$ for ξ into eq(A3.15). With the isocratic case when $\kappa'(\hat{m}) = \kappa_o = \kappa^\circ$ and $\kappa''(s) = \kappa''(\xi - \hat{m}) = \kappa_o = \kappa^\circ$, eq(A3.15) reduces to eq(2.38) [cf. eq(3.30)].

From the mutual derivations between eqs(A3.5) and (A3.13), those between eqs(A3.8) and (A3.14), and those between eq(A3.12) and (A3.15), it can be understood that the shape of distribution in χ as a function of ξ (χGM2nd) is identical with the shape of distribution in χ as a function of s (χGM1st); the ξ values over which χGM2nd [eq (A3.13), (A3.14) or (A3.15)] appears are larger by a constant value of $\hat{m}$ (representing the dead volume of the column) than the s values over which χGM1st [eq(A3.5), (A3.8) or (A3.12)] appears.

(C) The Case of Molecular Band with A Small Width

Complementary Chromatogram as First Concept. When the width of MB(o) or MB(c) is small, eq(A3.1) can be rewritten as

$$\mathrm{div}_s \left(\frac{\hat{B}(\hat{m}+s)}{1-\hat{B}(\hat{m}+s)} \chi \right) + \frac{\partial \chi}{\partial \hat{m}} = 0 \qquad (A3.16)$$

in which function $\hat{B}(\hat{m}+s)$ fulfills eq(3.17) combined with eq(3.16). Due to eq(A3.2) into which $\hat{B}(\hat{m}+s)$ is substituted for B, eq(A3.16) is identical with eq(3.77). The solution:

$$\chi = [1-B'(\bar{\hat{m}})]F[-(\hat{m} - \bar{\hat{m}})] \qquad (A3.17)$$

or

$$\chi = [1-B''(\bar{s})]F(s - \bar{s}) \qquad (A3.17')$$

of eq(A3.16) is identical with eq(3.78) or (3.78') due to both eq(A3.2) into which $\hat{B}(\hat{m}+s)$ is substituted for B and eq(3.17). Either eq(A3.17) [combined with the equality between first and third terms in eq(3.16) where $\hat{m}_o = 0$] or eq(A3.17') [combined with the equality between first and last terms in eq(3.16) where $s_o = 0$] represents χGM1st obtained when the initial MB(o) and MB(c) are represented by eqs(2.15) and (2.17), respectively;

χGM1st is expressed as a function of s for a given value of $\hat{m}$. With the isocratic case when $B'(\bar{m})=B''(\bar{s})=B^{\circ}$, both eqs(A3.17) and (A3.17') [combined with eq(3.16) in which $\hat{m}_{\circ}=s_{\circ}=0$] reduce to eq(2.22).

Complementary Chromatogram as Second Concept. By combining eq(3.83) or eq(3.82) into which $\xi-\hat{m}$ is substituted for s with $\chi=[1-\hat{B}(\xi)]\Omega$, χGM2nd (as a function of ξ for a given value of $\hat{m}$):

$$\chi = [1-\hat{B}(\xi)]F\left(-[\hat{m}-\int_0^{\xi}(1-\hat{B}(\xi))d\xi]\right) \qquad (A3.18)$$

can be obtained. The equation derived by substituting $\hat{m}+s$ for ξ into eq(A3.18):

$$\chi = [1-\hat{B}(\hat{m}+s)]F\left(-[\hat{m}-\int_0^{\hat{m}+s}(1-\hat{B}(\xi))d\xi]\right)$$

$$= [1-\hat{B}(\hat{m}+s)]F\left(s-\int_0^{\hat{m}+s}\hat{B}(\xi)d\xi\right) \qquad (A3.19)$$

is identical with either eq(A3.17) [combined with the equality between first and third terms in eq(3.16) where $\hat{m}_{\circ}=0$] or eq(A3.17') [combined with the equality between first and last terms in eq(3.16) where $s_{\circ}=0$], representing χGM1st. To the contrary, by substituting $\xi-\hat{m}$ for s into eq(A3.19), eq(A3.18) can be derived. Eq(A3.18) can also be represented as eq(A3.17) combined with the equality between the first term (rewritten as ξ instead of $\hat{m}+s$) and the third term in eq(3.16) (where $\hat{m}_{\circ}=0$). With the isocratic case when $\hat{B}(\xi)=B^{\circ}$, eq(A3.18) reduces to eq(2.38). The shape of distribution in χ as a function of ξ [χGM2nd; eq(A3.18)] is identical with the shape as a function of s [χGM1st; eq(A3.19) i.e., either eq(A3.17) or (A3.17') combined with eq(3.16) in which $\hat{m}_{\circ}=s_{\circ}=0$]. The ξ values over which χGM2nd apears are larger by a constant value of $\hat{m}$ (representing the dead volume of the column) than the s values over which χGM1st appears.

Appendix IV. Visual Understanding of the Relationship between Molecular Band and Chromatogram as First Concept versus Role of the Gradient

(A) General Case

The purpose of this Appendix is to attain a deeper understanding of the role of the gradient for the three cases (a) when only the gradient in the liquid phase is applied, (b) when only the gradient in the solid phase is applied, and (c) when both the gradient in the liquid phase and the gradient in the solid phase are applied at the same time. Some examples are shown of the calculations of CGM1st [eqs(3.35), (3.39) and (3.44)] and the corresponding MB(o) and MB(c) [eqs(3.53)-(3.58)] for step gradients which can be considered to represent simplified models of continuous gradients. Any discontinuous step-function appearing in the process of the calculation is regarded as a limit of a series of hypothetical continuous functions. The calculations lead to a visual understanding of the relationships among MB(o), MB(c) and CGM1st taking place through the intervention of the gradient.

Figs A4.1(a)-(c) schematically illustrate examples of the three characteristic surfaces [eqs(3.12), (3.13) and (3.3)] present in the ($\hat{m}$,s,B) space, overlooked along the B axis for the three cases (a)-(c), respectively; all the surfcaces consist of flat sub-surfaces. In Fig A4.1, the dashed lines represent steps between different sub-surfaces; the numerical figure outside the paraentheses, and the first and second numerical figures inside the parentheses printed on each sub-surface represent B, $\tilde{B}'$ and $\tilde{B}''$ values for the sub-surface, respectively. The numerical figure outside the brackets, and the first and second numerical values inside the brackets represent the corresponding k, κ' and κ'' values, respectively [see eqs(3.22'), (3.26) and (3.27)]. In the lower margin of each part of Fig A4.1, the numerical figures outside and inside the parentheses represent B (i.e., B_o) and $\tilde{B}'$ values taking place potentially in the sample solution to be injected into the column, respectively; the numerical figures outside and inside the brackets represent the corresponding k (i.e., k_o) and κ' (i.e., κ_o') values, respectively. Here, the potential values of B etc. imply the values which would take place immediately after the inflow of the sample solution into the column.

The Case(a) When Only the Gradient in the Liquid Phase Is Applied. This is summarized in Fig A4.2 where it is possible to apply to the gradient the concept similar to that of FCB migrating along gradient G. Thus, let us consider that the gradient under consideration is originating from a curve (called *gradient curve*) present in the ($\hat{m}$,s,B) space, constrained on the plane parallel to the B axis the intersection of which with the ($\hat{m}$,s) plane coincides with gradient G. Let us also consider that gradient curve moves in the s direction in the ($\hat{m}$,s,B) space at a rate equal to g' times the flow-rate. If it is considered that gradient G migrates in the s direction on the ($\hat{m}$,s) plane at a rate equal to g' times the flow-rate, then the projection on the ($\hat{m}$,s) plane of gradient curve always stays

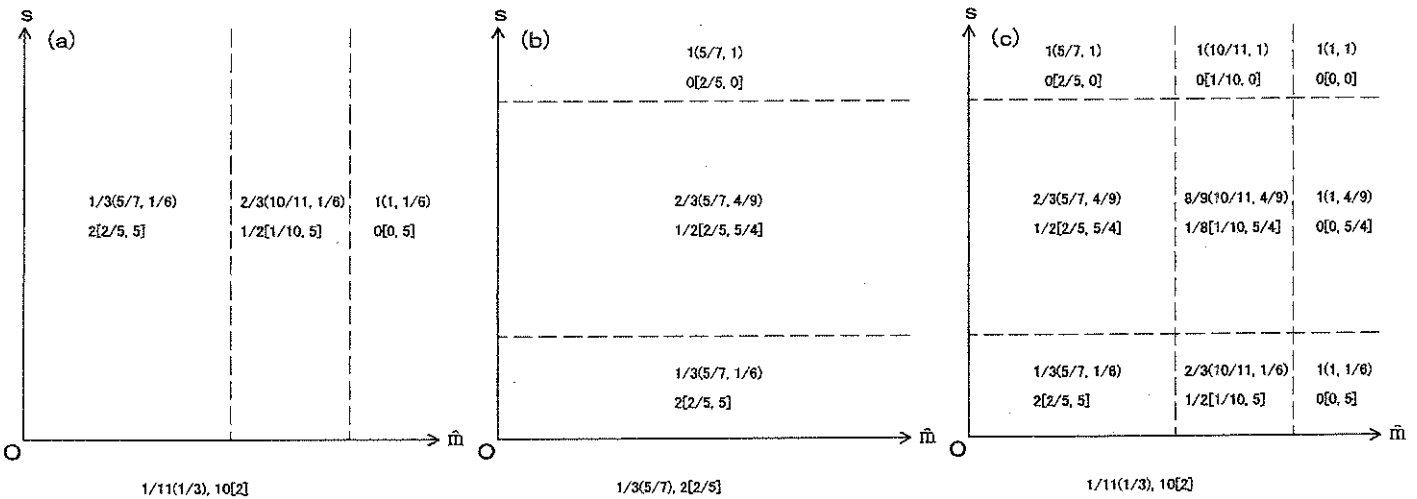


Fig A4.1. Three characteristic surfaces overlooked along the B axis for the three cases (a) when only the gradient in the liquid phase is applied, (b) when only the gradient in the solid phase is applied, and (c) when both the gradient in the liquid phase and the gradient in the solid phase are applied at the same time.

over the same positions on gradient G, whereas, if it is considered that gradient G migrates in the $\hat{m}$ direction on the ($\hat{m}$,s) plane, then the projection of gradient curve migrates along gradient G. In Fig A4.2(a), point $\bar{P}'$ (defined as projection of the slice of gradient curve which stayed on the B axis initially or at proper time $\xi = 0$) draws a trajectory (called *trajectory* T_0') coinciding with the s axis on the ($\hat{m}$,s) plane; the demixing effect[Chapter III(A)] is neglected for simplicity. The projections of gradient curve on ($\hat{m}$, B) and (s,B) planes are drawn in extreme-lower and extreme-left parts of Fig A4.2(a), respectively. The projection of gradient curve on the ($\hat{m}$,B) plane always stays at the same position, whereas the projection on the (s,B) plane migrates along s at a rate equal to g' times the flow-rate [see Fig A4.2(a)]. Gradient curve scans the ($\hat{m}$,s,B) space while moving in the s direction, generating the characteristic surface[eq(3.12)] illustrated in Fig A4.1(a).

Let us consider the ($\hat{m}$,s,W) space where W represents B, $\bar{B}'$ and $\tilde{B}'$ commonly. In this space, the characteristic surface[eq(3.12)] can be represented as W=B, and it is possible to consider that the surface W=B is synthesized from the two surfaces W=$\bar{B}'$ and W=$\tilde{B}'$ by using eqs(3.22'), (3.25)-(3.27) where $\kappa''(s) = \kappa^{o''}$ [see eq(3.28)]. Surface W=$\bar{B}'$ is flat, parallel to the ($\hat{m}$,s) plane. The projection of the surface W=$\tilde{B}'$ on the (s,W) plane is represented by the dotted straight line drawn in the middle-left part of Fig A4.2(a); this also represents the projection of the gradient curve with respect to surface W=$\tilde{B}'$. The projections on ($\hat{m}$,W) and (s,W) planes of the gradient curve with respect to surface W=$\bar{B}'$ are drawn in middle-lower and middle-left parts of Fig A4.2(a), respectively. The former always stays at the same position, whereas the latter migrates along s at a rate equal to g' times the flow-rate [see Fig A4.2(a)]. It can be considered that point $\bar{P}'$ is also concerned with the gradient curve with respect to surface W=$\bar{B}'$, drawing trajectory T_0' [see Fig 4.2(a)].

It is possible to map FCB taking place in the ($\hat{m}$,s,Ω) space to the ($\hat{m}$,s,B) space. The map is constrained on the plane parallel to the B axis the intersection of which with the ($\hat{m}$,s) plane defines gradient G, and the projection of the map on the ($\hat{m}$,s) plane migrates along gradient G while gradient G migrates in either $\hat{m}$ or s direction on the ($\hat{m}$,s) plane. The map of FCB scans the ($\hat{m}$,s,B) space, generating a sub-surface involved in the characteristic surface obtained by the scan of the gradient curve. The sub-surface is an assembly of characteristic curves each of which projects itself on the ($\hat{m}$,s) plane to draw trajectory T_0 or T. The projections on the ($\hat{m}$,s) plane of the characteristic curves corresponding to rear and front borders of MB(o) [cf. Fig A4.2(c)] are drawn in Fig A4.2 (b), representing trajectory T_0 and T, respectively. The projections on the (s,B) plane of the corresponding characteristic curves are drawn in the left part of Fig A4.2(b). The projection on the ($\hat{m}$,B) plane of any characteristic curve is the same [lower part of Fig A4.2(b)], and it is identical with the projection of gradient curve [extreme-lower part of Fig A4.2(a)]; this arises from the fact that the characteristic surface[eq(3.12); Fig A4.1(a)] is parallel to the s axis. Fig A4.2(b) partially corresponds to Fig 3.2.

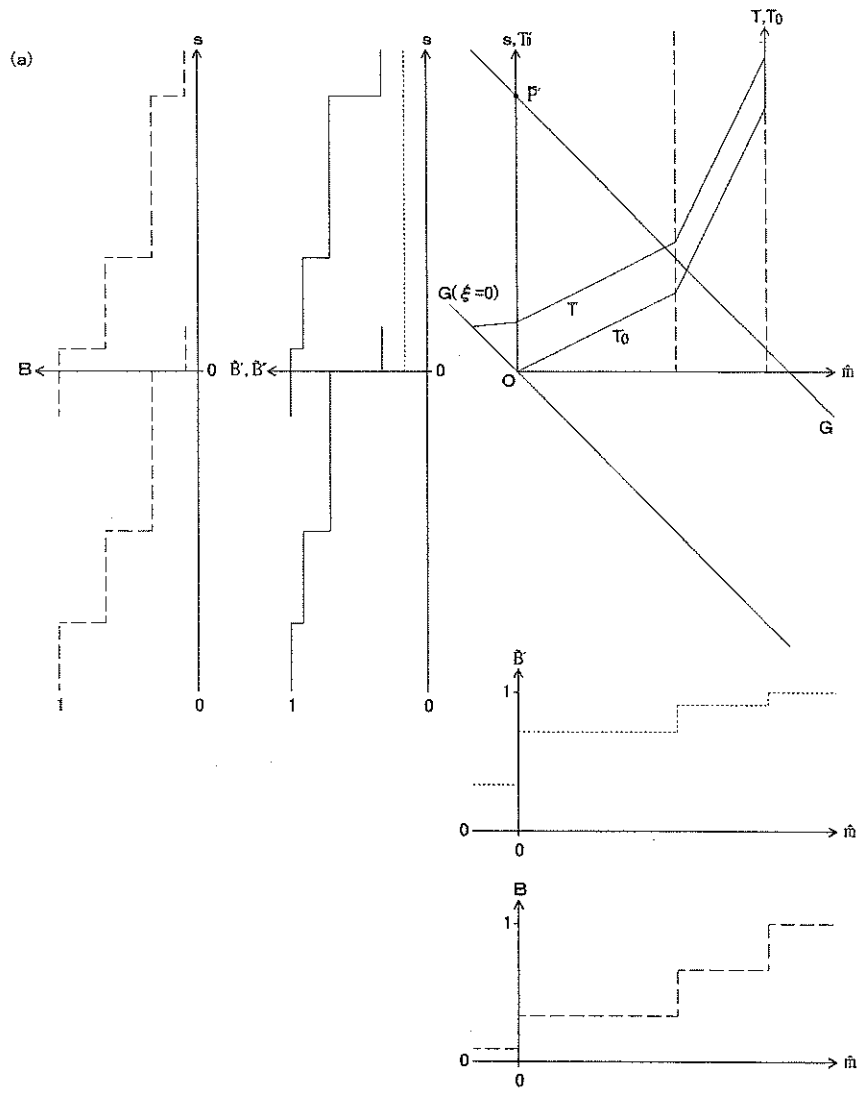


Fig A4.2. Relationships among MB(o), MB(c) and CGM1st versus role of the gradient for the case when only the gradient in the liquid phase is applied. (a) Gradient curves projected on ($\hat{m}$,s), ($\hat{m}$,W) and (s,W) planes, where W=B, $\tilde{B}'$ or $\tilde{B}''$. The projection of the gradient curve on the ($\hat{m}$,s) plane is superposed on gradient G. The projection on the ($\hat{m}$,s) plane of a slice of the gradient curve (with respect to surface W=B or W=$\tilde{B}'$) gives trajectory T_0' (superposed on the s axis). For reference, both trajectories T_0 and T are drawn at the same time. (b) Two characteristic curves (corresponding to the two borders of FCB) projected on ($\hat{m}$,s), ($\hat{m}$,B) and (s,B) planes, giving trajectories T_0 and T on the ($\hat{m}$,s) plane, respectively; cf. Fig 3.2. (c) CGM1st versus FCB projected on ($\hat{m}$,s), ($\hat{m}$,Ω) and (s,Ω) planes. The projections of FCB on ($\hat{m}$,Ω) and (s,Ω) planes give MB(c) and MB(o), respectively, and the projections of the two borders of FCB on the ($\hat{m}$,s) plane give trajectories T_0 and T, respectively. For reference, the projections of the gradient curve on ($\hat{m}$,B) and (s,B) planes are shown at the same time.

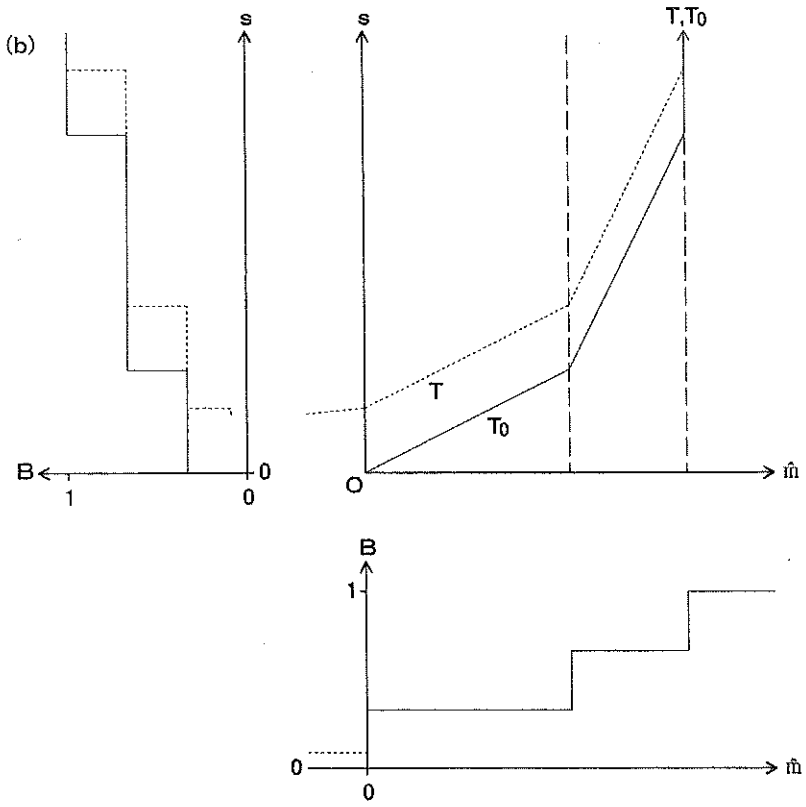


Fig A4.2. (b)

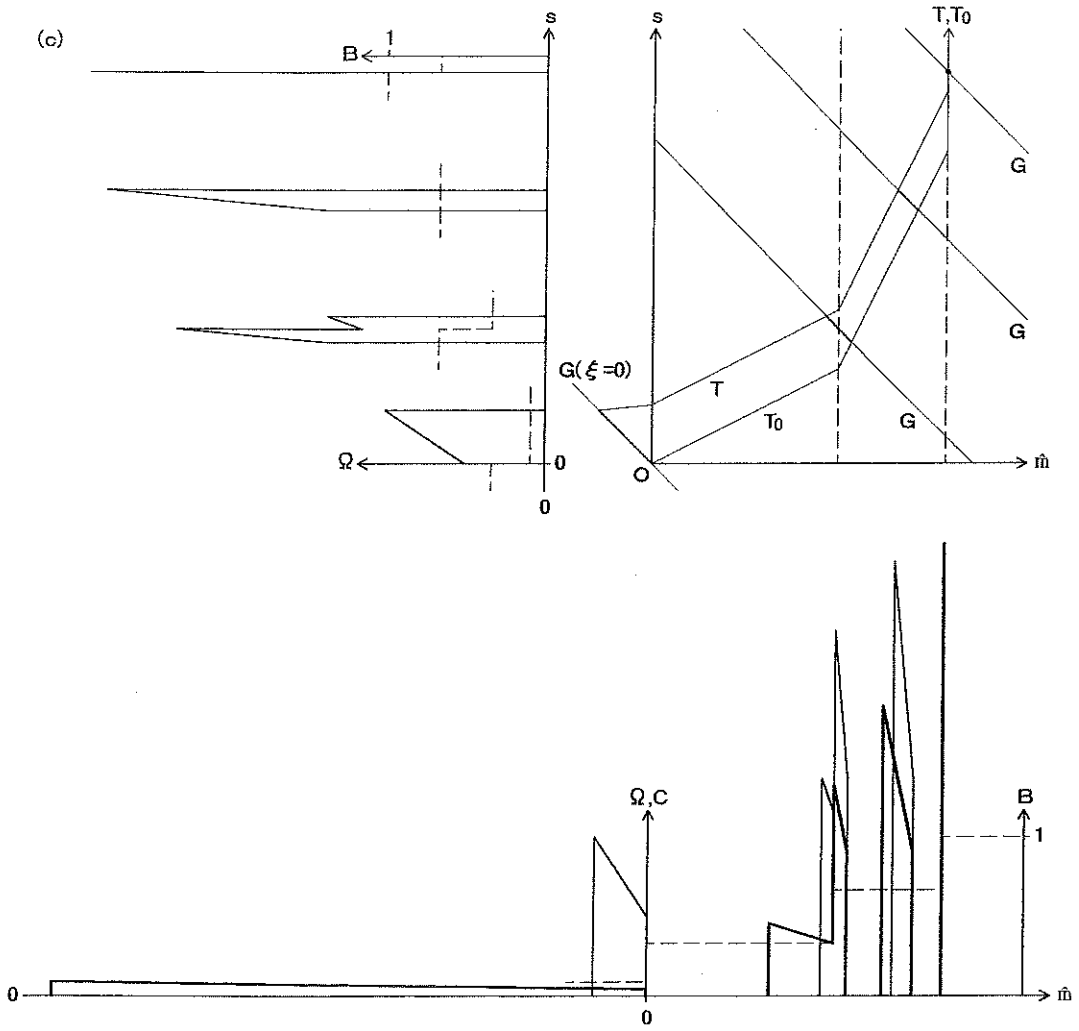


Fig A4.2. (c)

Two assemblies of trapezoids drawn lightly in left and lower parts of Fig A4.2(c), being mirror images of one another, represent the migration of MB(o) on the column(OPV) and the migration of MB(c) on the carrier liquid(CPV), calculated by using eqs(3.53) and (3.54), respectively; both the compound of two trapezoids and the straight half-line (as extreme shape of the trapezoid obtained when width and height of it tend to infinitesimal and infinity, respectively) are here called as trapezoids. It can be seen in Fig A4.2(c) that MB(o) and MB(c) are projections on (s,Ω) and $(\hat{m},\Omega)$ planes of FCB taking place in the $(\hat{m},s,\Omega)$ space, conjugate to gradient G. The initial MB(o) and MB(c) which keep in contact with the Ω axis are identical with those drawn by dotted lies in Fig 2.4, respectively. In Fig A4.2(c), MB(o) and MB(c) migrate on the column and the carrier liquid while changing their shapes, respectively, and their widths decrease monotonically to tend to infinitesimal with migration or with a lapse of proper time ξ (compression of band; cf. Table 3.1).

The trapezoids drawn with thick lines in the lower part of Fig A4.2(c) represent CGM1st each conjugate to each MB(c), calculated by using eq(3.35); the initial CGM1st (keeping in contact with the C axis) can be interpreted to be obtained by using a column with infinitesimal length(EPV). The width of CGM1st, in general, is larger than the width of conjugate MB(c) (chromatographic dilatation), and the width of CGM1st decreases more rapidly than the width of conjugate MB(c) when migrating on the carrier liquid as a result of the enhancement of the two effects of compression of band and decrease of chromatographic dilatation. CGM1st and conjugate MB(c) coincide with one another finaly when the widths of both of them tend to infinitesimal [see lower part of Fig A4.2(c); cf. Table 3.1].

The Case(b) When Only the Gradient in the Solid Phase Is Applied. This is summarized in Fig A4.3. Thus, gradient curve now moves in the $\hat{m}$ direction in the $(\hat{m},s,B)$ space at a rate equal to g' times the flow-rate. If it is considered that gradient G migrates in the $\hat{m}$ direction on the $(\hat{m},s)$ plane at a rate equal to g' times the flow-rate, then the projection on the $(\hat{m},s)$ plane of gradient curve always stays over the same positions on gradient G, whereas, if it is considered that gradient G migrates in the s direction on the $(\hat{m},s)$ plane, then the projection of gradient curve migrates along gradient G. In Fig A4.3(a), point $\bar{P}'$ (defined as projection of the slice of gradient curve which stayed on the B axis initially or at proper time $\xi=0$) draws a trajectory (called *trajectory* T_0'') coinciding with the $\hat{m}$ axis on the $(\hat{m},s)$ plane. The projections of gradient curve on $(\hat{m},B)$ and (s,B) planes are drawn in extreme-lower and extreme-left parts of Fig A4.3 (a), respectively. The projection of gradient curve on the $(\hat{m},B)$ plane migrates along $\hat{m}$ at a rate equal to g' times the flow-rate, whereas the projection on the (s,B) plane always stays at the same position [see Fig A4.3(a)]. Gradient curve scans the $(\hat{m},s,B)$ space while moving in the $\hat{m}$ direction, generating the characteristic surface[eq(3.13)] illustrated in Fig A4.1(b).

In the $(\hat{m},s,W)$ space, the characteristic surface, $W=B$ [eq(3.13)], is synthesized

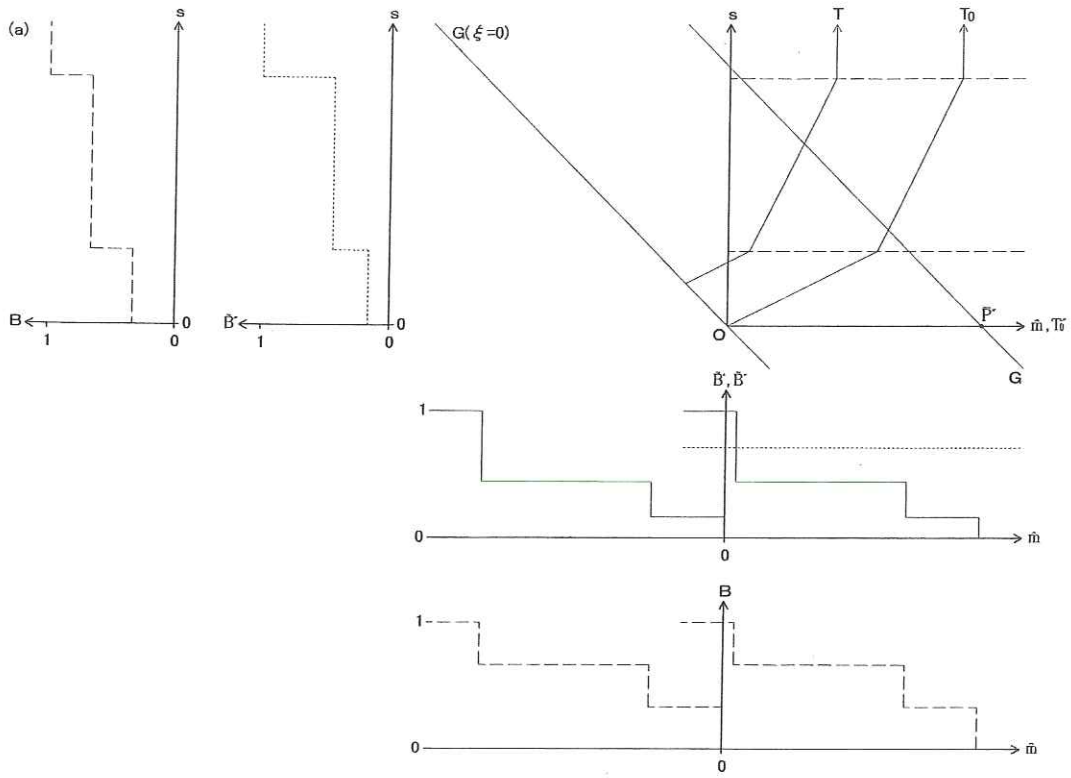


Fig A4.3. (a)

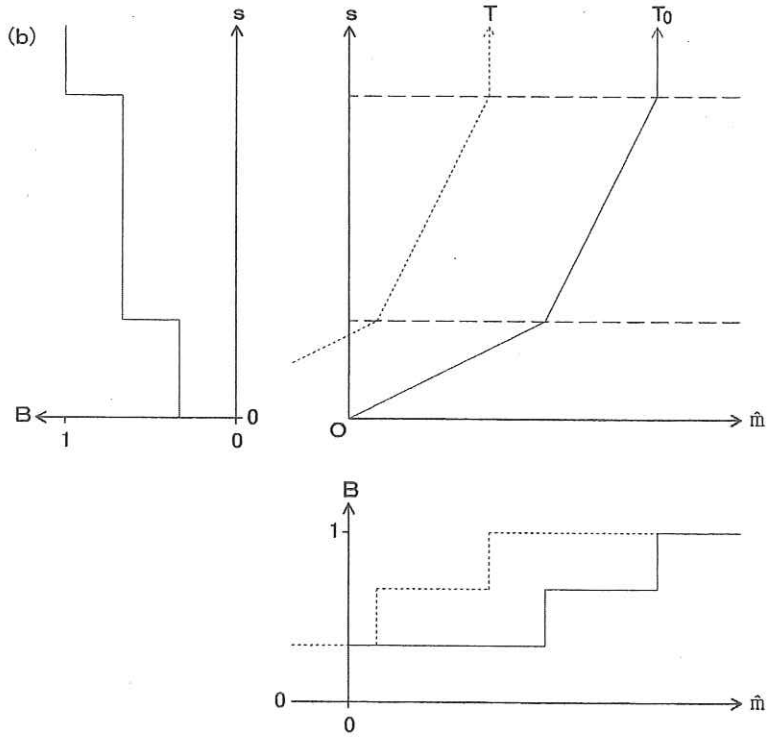


Fig A4.3. (b)

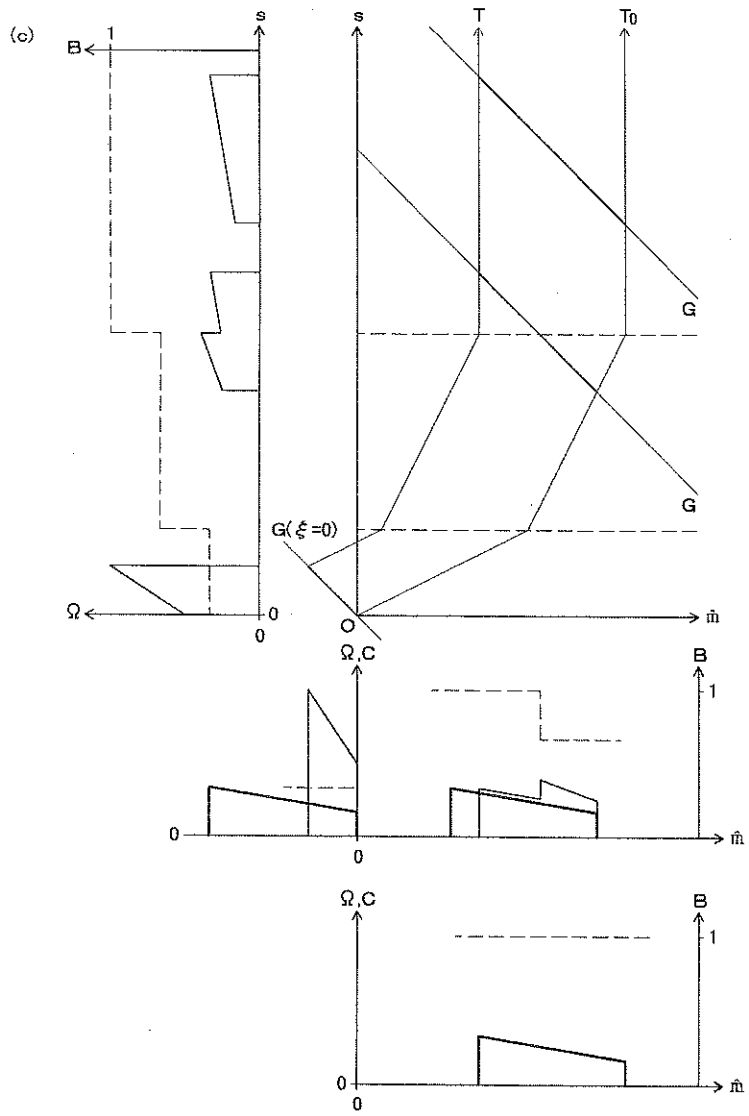


Fig A4.3. Relationships among MB(o), MB(c) and CGM1st versus role of the gradient for the case when only the gradient in the solid phase is applied. (a) Gradient curves projected on ($\hat{m}$,s), ($\hat{m}$,W) and (s,W) planes, where W=B, $\hat{B}'$ or $\hat{B}''$. The projection of the gradient curve on the ($\hat{m}$,s) plane is superposed on gradient G. The projection on the ($\hat{m}$,s) plane of a slice of the gradient curve (with respect to surface W=B or W=$\hat{B}''$) gives trajectory T_0'' (superposed on the $\hat{m}$ axis). For reference, both trajectories T_0 and T are drawn at the same time. (b) Two characteristic curves (corresponding to the two borders of FCB) projected on ($\hat{m}$,s), ($\hat{m}$,B) and (s,B) planes, giving trajectories T_0 and T on the ($\hat{m}$,s) plane, respectively; cf. Fig 3.2. (c) CGM1st versus FCB projected on ($\hat{m}$,s), ($\hat{m}$,Ω) and (s,Ω) planes. The projections of FCB on ($\hat{m}$,Ω) and (s,Ω) planes give MB(c) and MB(o), respectively, and the projections of the two borders of FCB on the ($\hat{m}$,s) plane give trajectories T_0 and T, respectively. For reference, the projections of the gradient curve on ($\hat{m}$,B) and (s,B) planes are shown at the same time.

from the two surfaces $W=\check{B}'$ and $W=\check{B}''$ by using eqs(3.22'), (3.25)-(3.27) where $\kappa'(\hat{m})=\kappa^{0'}$ [see eq(3.29)]. Surface $W=\check{B}'$ is flat, parallel to the $(\hat{m},s)$ plane. The projection of surface $W=\check{B}'$ on the $(\hat{m},W)$ plane is represented by the dotted straight lines drawn in the middle-lower part of Fig A4.3(a); this also represents the projection of the gradient curve with respect to surface $W=\check{B}'$. The projections on $(\hat{m},W)$ and (s,W) planes of the gradient curve with respect to surface $W=\check{B}''$ are drawn in middle-lower and middle-left parts of Fig A4.3(a), respectively. The former migrates along $\hat{m}$ at a rate equal to g' times the flow-rate, whereas the latter always stays at the same position [see Fig A4.3 (a)]. It can be considered that point $\check{P}''$ is also concerned with the gradient curve with respect to surface $W=\check{B}''$, drawing trajectory T_0'' [see Fig A4.3(a)].

The projections on the $(\hat{m},s)$ plane of the characteristic curves corresponding to rear and front borders of MB(o) [cf. Fig A4.3(c)] are drawn in Fig A4.3(b), representing trajectory T_0 or T, respectively. The projections on the $(\hat{m},B)$ plane of the corresponding characteristic curves are drawn in the lower part of Fig A4.3(b). The projection on the (s, B) plane of any characteristic curve is the same [left part of Fig A4.3(b)], and it is identical with the projection of gradient curve [extreme-left part of Fig A4.3(a)]; this arises from the fact that the characteristic surface[eq(3.13); Fig A4.1(b)] is parallel to the $\hat{m}$ axis. Fig A4.3(b) partially corresponds to Fig 3.2.

Fig A4.3(c) corresponds to Fig A4.2(c), where MB(o), MB(c) and CGM1st were calculated by using eqs(3.55), (3.56) and (3.39), respectively, and where the initial MB(o) and MB(c) are identical with those assumed in Fig A4.2(c). In Fig A4.3(c), MB(o) and MB(c) migrate on the column and the carrier liquid while changing their shapes, respectively, and their widths increase monotonically to tend to be finitely constant with migration or with a lapse of proper time ξ (expansion of band; cf. Table 3.1). On the other hand, both shape and width of CGM1st are constant when it migrates on the carrier liquid, and the constant width of CGM1st, in general, is larger than the width of conjugate MB(c) [chromatographic dilatation; see the lower part of Fig A4.3(c)]. The constancy of the width of CGM1st arises as a result of the cancellation of the two effects of expansion of band and decrease of chromatographic dilatation. CGM1st and conjugate MB(c) coincide with one another finaly when both shape and width of MB(c) tend to be constant [see lower part of Fig A4.3(c); cf. Table 3.1].

The Case(c) When Both the Gradient in the Liquid Phase and the Gradient in the Solid Phase Are Applied at the Same Time. This is summarized in Fig A4.4. Thus, the pair of Figs A4.4(a) and (a') correspond to both Figs A4.2(a) and A4.3(a), where the characteristic surface, $W=B$ [eq(3.3)], is synthesized from the two surfaces $W=\check{B}'$ and $W=\check{B}''$ by using eqs(3.22'), (3.25)-(3.27). The projection on the $(\hat{m},W)$ plane of the gradient curve with respect to surface $W=\check{B}'$ always stays at the same position [lower part of Fig A4.4(a)], whereas the projection on the (s,W) plane of the same gradient curve migrates along s at a rate equal to g' times the flow-rate [solid curves in the middle-left part of Fig A4.4(a)]. Point $\check{P}'$ with respect to surface $W=\check{B}'$ draws trajectory T_0' coin-

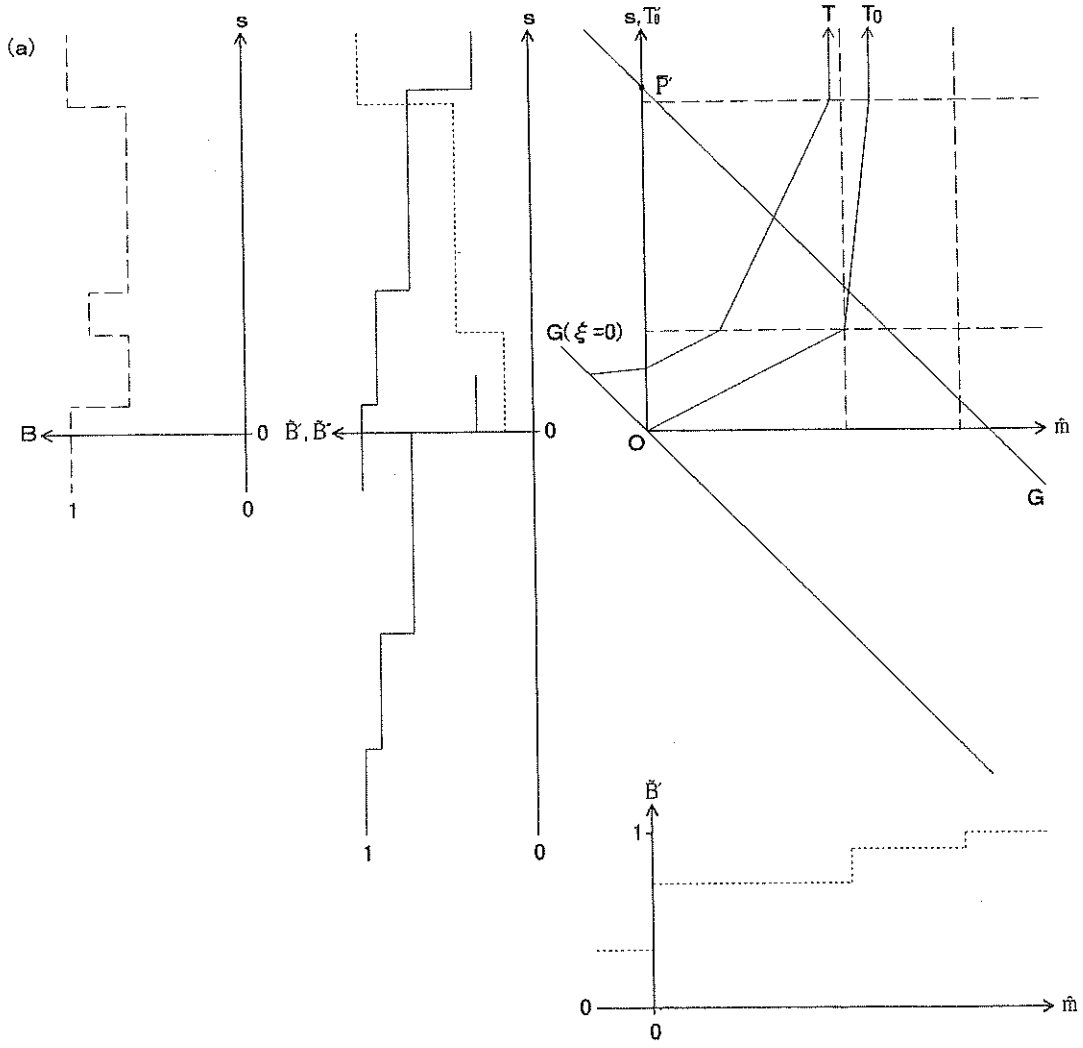


Fig A4.4. Relationships among MB(o), MB(c) and CGM1st versus role of the gradient for the case when both the gradient in the liquid phase and the gradient in the solid phase are applied at the same time. (a) and (a') Gradient curves projected on ($\hat{m}$,s), ($\hat{m}$, W) and (s,W) planes, where W=B, $\tilde{B}'$ or $\tilde{B}''$. The projection of the gradient curve on the ($\hat{m}$,s) plane is superposed on gradient G. The projection on the ($\hat{m}$,s) plane of a slice of the gradient curve (with respect to surface W=$\tilde{B}'$) gives trajectory T_0' [superposed on the s axis; see (a)], whereas the projection on the ($\hat{m}$,s) plane of a slice of the gradient curve (with respect to surface W=$\tilde{B}''$) gives trajectory T_0'' [superposed on the $\hat{m}$ axis; see (a')]. For reference, both trajectories T_0 and T are drawn at the same time. (b) Two characteristic curves (corresponding to the two borders of FCB) projected on ($\hat{m}$, s), ($\hat{m}$,B) and (s,B) planes, giving trajectories T_0 and T on the ($\hat{m}$,s) plane, respectively; cf. Fig 3.2. (c) CGM1st versus FCB projected on ($\hat{m}$,s), ($\hat{m}$,Ω) and (s,Ω) planes. The projections of FCB on ($\hat{m}$,Ω) and (s,Ω) planes give MB(c) and MB(o), respectively, and the projections of the two borders of FCB on the ($\hat{m}$,s) plane give trajectories T_0 and T, respectively. For reference, the projections of the gradient curve on ($\hat{m}$,B) and (s,B) planes are shown at the same time.

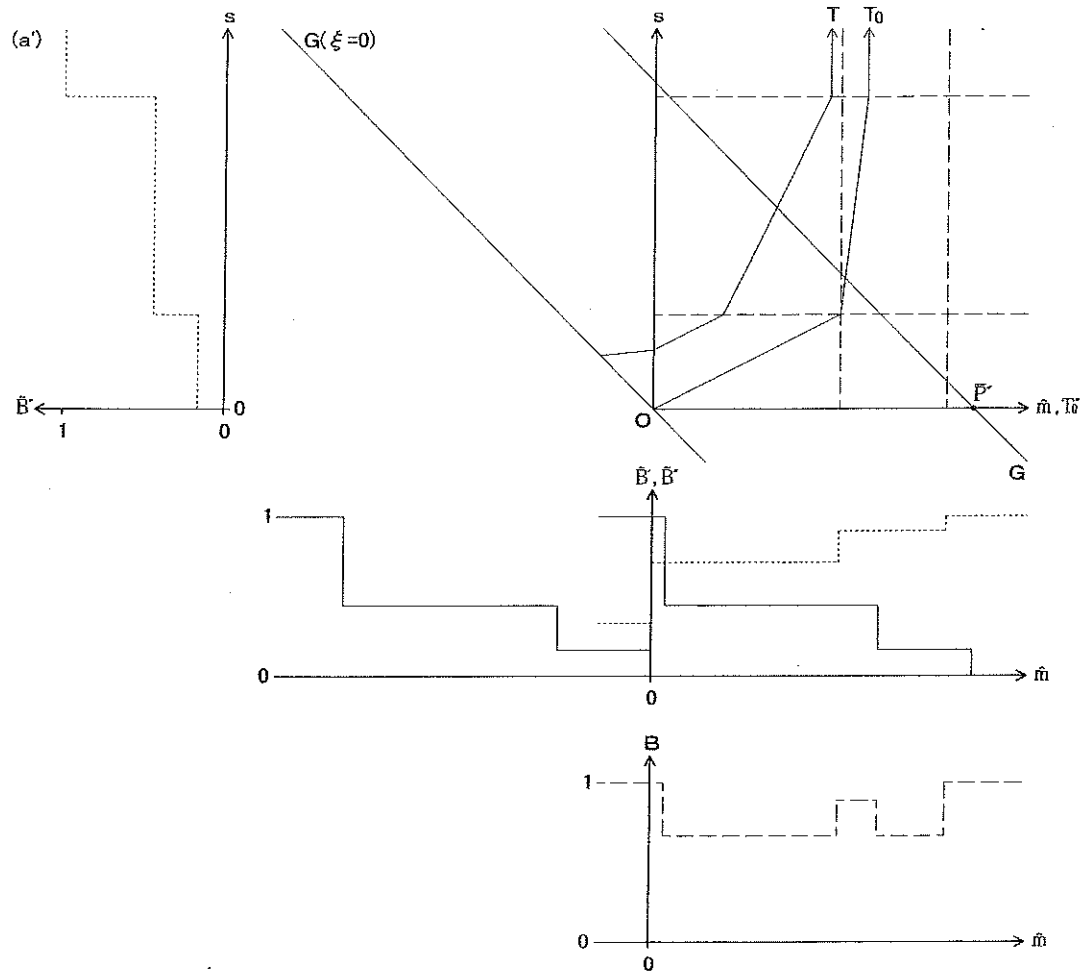


Fig A4.4. (a')

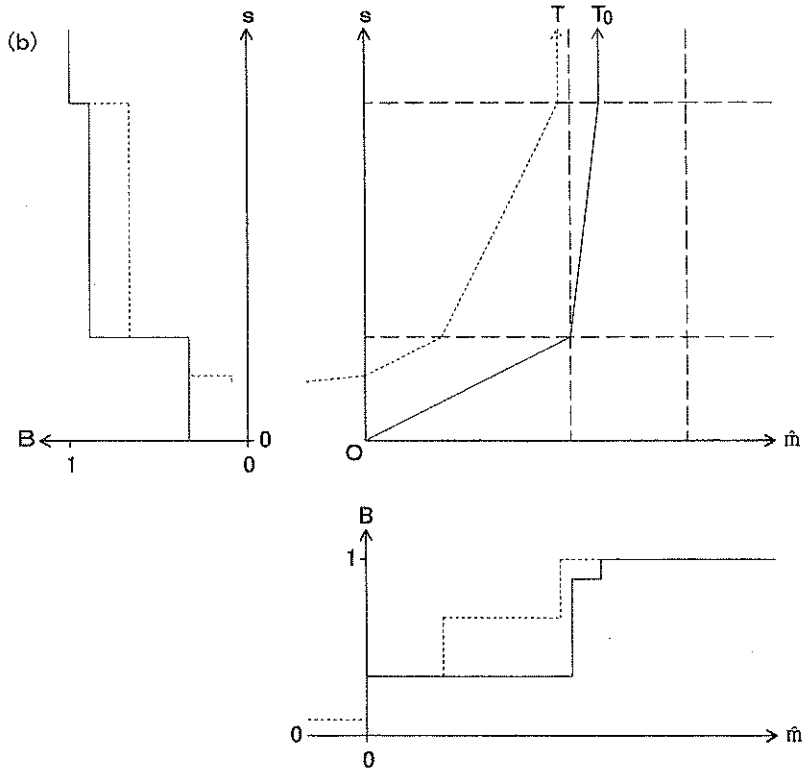


Fig A4.4. (b)

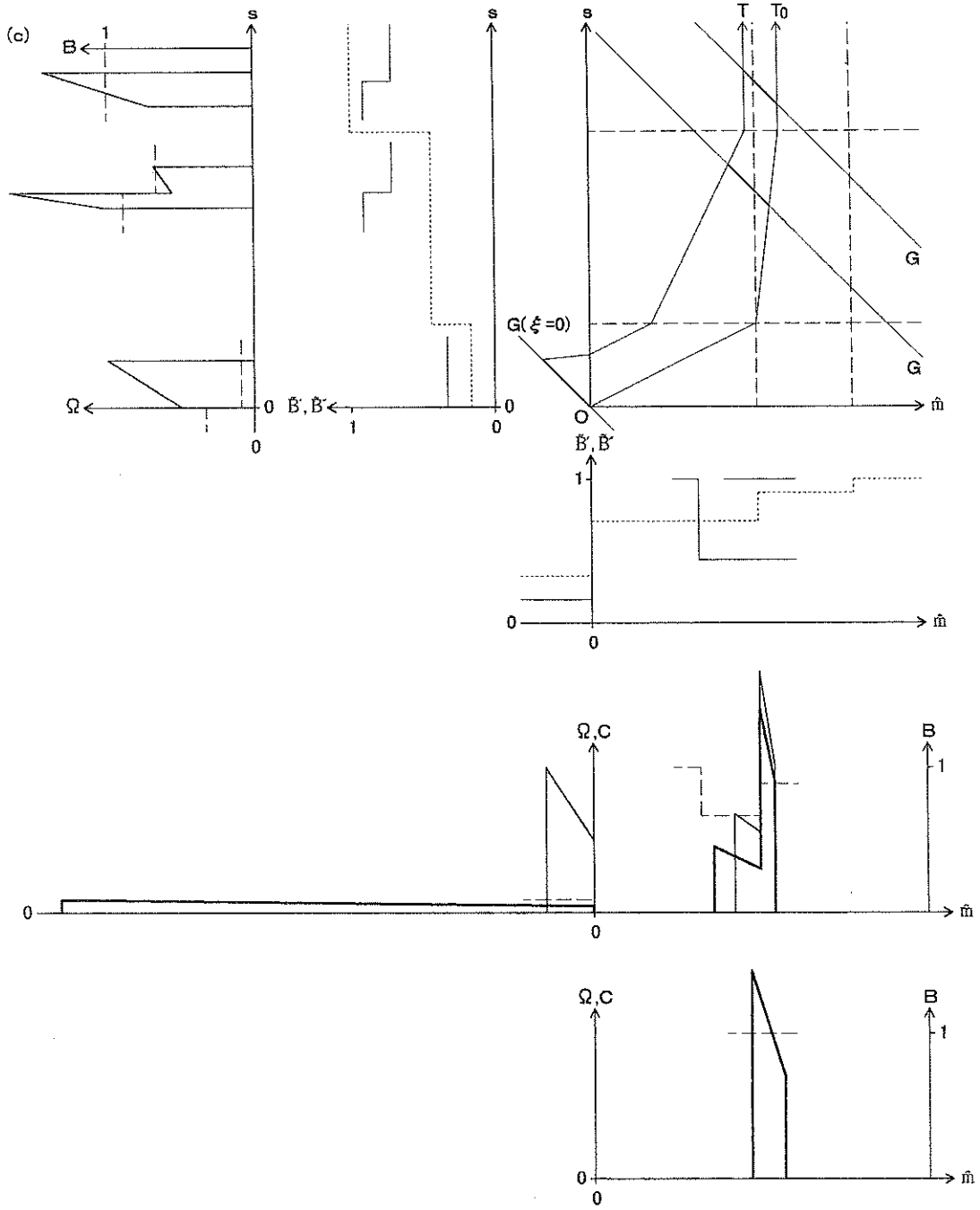


Fig A4.4. (c)

ciding with the s axis on the ($\hat{m}$,s) plane [see Fig A4.4(a)]. On the other hand, the projection on the ($\hat{m}$,W) plane of the gradient curve with respect to surface $W=\check{B}'$ migrates along $\hat{m}$ at a rate equal to g' times the flow-rate [solid curve in the middle-lower part of Fig A4.4(a')], whereas the projection on the (s,W) plane of the same gradient curve always stays at the same position [left part of Fig A4.4(a')]. Point $\check{P}'$ with respect to surface $W=\check{B}'$ draws trajectory T_0'' coinciding with the $\hat{m}$ axis on the ($\hat{m}$,s) plane [see Fig A4.4(a')]. The projection on the (s,W) plane of the gradient curve with respect to surface $W=\check{B}'$ is also drawn in the midle-left part of Fig A4.4(a) (dotted curve), and the projection on the (s,W) plane of the total gradient curve with respect to surface $W=B$ is drawn in the extreme-left part of Fig A4.4(a). On the other hand, the projection on the ($\hat{m}$,W) plane of the gradient curve with respect to surface $W=\check{B}'$ is also drawn in the middle-lower part of Fig A4.4(a') (dotted curve), and the projection on the ($\hat{m}$,W) plane of the total gradient curve with respect to surface $W=B$ is drawn in the extreme-lower part of Fig A4.4(a').

Fig A4.4(b) corresponds to both Figs A4.2(b) and A4.3(b), drawing the projections of the two characteristic curves on ($\hat{m}$,s), ($\hat{m}$,B) and (s,B) planes; the projections on the ($\hat{m}$,s) plane give trajectories T_0 and T. Fig A4.4(b) partially corresponds to Fig 3.2.

Fig A4.4(c) corresponds to both Figs A4.2(c) and A4.3(c) where MB(o), MB(c) and CGM1st were calculated by using eqs(3.57), (3.58) and (3.44), respectively, and where the initial MB(o) and MB(c) are identical with those assumed in both Figs A4.2(c) and A4.3(c). In Fig A4.4(c), MB(o) and MB(c) migrate on the column and the carrier liquid while changing their shapes, respectively; their widths change non-monotonically to tend to be finitely constant with migration or with a lapse of proper time ξ. This is because both compression and expansion of band take place alternately in the process of migration (cf. Table 3.1). The width of CGM1st, in general, is larger than the width of conjugate MB(c) [chromatographic dilatation; see lower part of Fig A4.4(c)]. Different from MB(o) or MB(c), the width of CGM1st decreases monotonically, and both shape and width of CGM1st tend to be constant with its migration. This, in general, arises through an alternation of the two processes: the enhancement of the two effects of compression of band and decrease in chromatographic dilatation, and the cancellation of the two effects of expansion of band and decrease in chromatographic dilatation. CGM1st and conjugate MB(c) coincide with one another finally when both shape and width of both of them tend to be constant [see lower part of Fig A4.4(c); cf. Table 3.1].

(B) The Case of Molecular Band with A Small Width

Some examples of the calculation of CGM1st [eq(3.78) or (3.78') combined with eq (3.16) in which $\hat{m}_0=s_0=0$, or eq(3.85)] and the corresponding MB(c) [eq(3.83)] are shown below. Thus, Figs A4.5(a)-(c) correspond to the lower parts of Figs A4.2(c), A4.3(c) and A4.4(c), representing both CGM1st (thick-drawn trapezoids) and conjugate MB(c) (lightly-

drawn trapezoids) for the three cases (a) when only the gradient in the liquid phase is applied, (b) when only the gradient in the solid phase is applied, and (c) when both the gradient in the liquid phase and the gradient in the solid phase are applied at the same time, respectively. The initial CGM1st and the initial MB(c) drawn in Figs A4.5(a)-(c) are identical with those drawn in Figs A4.2(c), A4.3(c) and A4.4(c), respectively; this means that the width of MB(c) is exagerated in the diagrams in contrast to the assumption that it is very small. It can be seen in Fig A4.5 that both shape and width of MB(c) are kept constant when it migrates on the carrier liquid, independent of the type of gradient applied; this arises from the fact that both compression and expansion of band are negligible with MB with a small width. The width of CGM1st, in general, is larger than the width of conjugate MB(c) (chromatographic dilatation), and the width of CGM1st decreases monotonically with its migration on the carrier liquid only due to decrease in chromatographic dilatation; both shape and width of CGM1st coincide with those of MB(c) finally, independent of the type of gradient applied (see Fig A4.5).

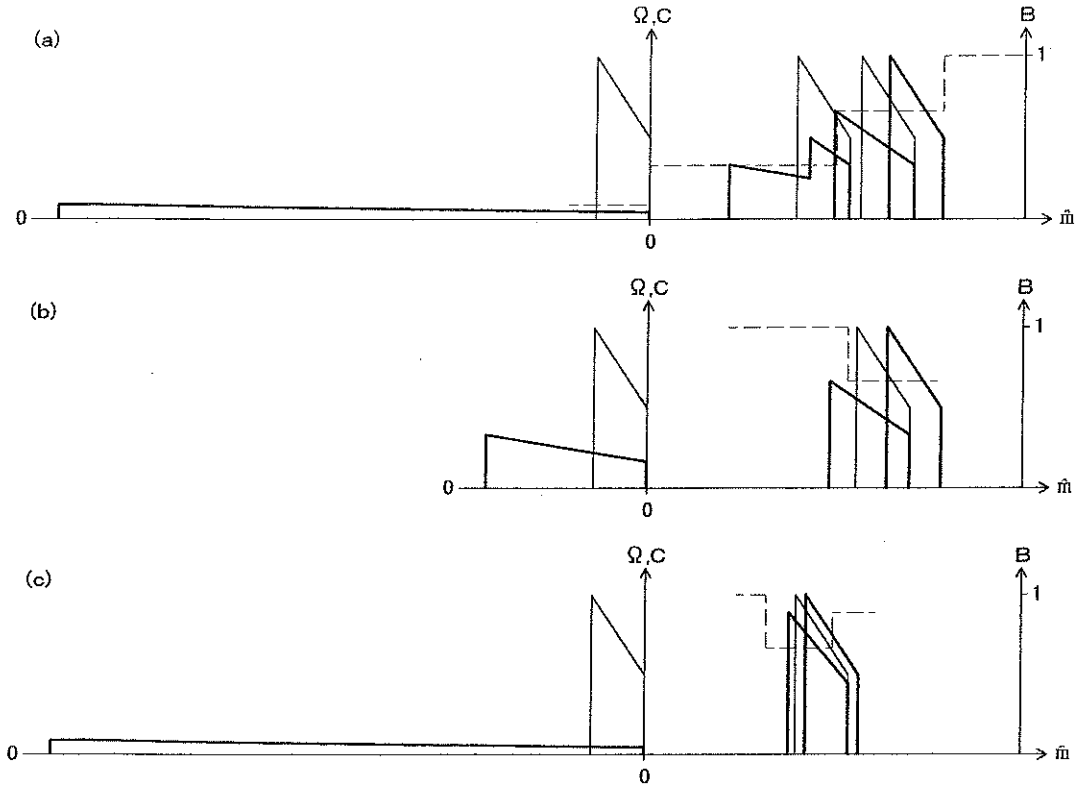


Fig A4.5. Relationship between MB(c) with a small width and the corresponding CGM1st for the three cases (a) when only the gradient in the liquid phase is applied, (b) when only the gradient in the solid phase is applied, and (c) when both the gradient in the liquid phase and the gradient in the solid phase are applied at the same time. Three stages (initial, middle and final stages) of development of chromatography are shown, where the widths of both MB(c) and CGM1st are exagerated while keeping correctly the ratio of the widths between MB(c) and CGM1st. For reference, the projection of the gradient curve on the ($\hat{m}$,B) plane is shown for the middle stage of development. The projection stays at the same position at any stage of development in (a), however.

Appendix V. Some Arguments on Eq(5.14) or (5.14') in Connection with Eq(4.16)

Eq(5.14) or (5.14') [representing CGM1st of gradient chromatography obtained when a MB(o) with a small width is formed initially at the inlet of the column] is a solution of the continuity equation, eq(5.17), of abstract flux, obtained under initial condition given by eq(4.16). Let us consider the case when concentration gradient chromatography is carried out on a column with a very small length, s, under usual experimental condition where molecular partition, B, in the mobile phase taking place in the initial MB(o) is close to zero. With the column with a very small length s, molecular partition $B''(s)$ or $B'[\mu(s)]$ in the mobile phase taking place at the outlet, s, of the column is also close to zero during most of the chromatographic process. As a result, CGM1st with a very large width $\Delta(s;g')/B''(s)$ [eq(5.14)] or $\Delta(s;g')/B'[\mu(s)]$ [eq(5.14')] takes place. As position μ (>0) at the center of CGM1st [see eq(5.14')] is present in the vicinity of origin, $\hat{m}=0$, of coordinate $\hat{m}$, however, a considerable portion of theoretical CGM1st leaks out to negative values of coordinate $\hat{m}$. In other words, the left portion of CGM1st is present over a wide range of negative values of coordinate $\hat{m}$ even before the application of the concentration gradient. Such a situation is unrealizable actually, and the initial condition, eq (4.16), is not valid as far as the very short column is concerned. With increase in length, s, of the column used, however, width, $\Delta(s;g')/B''(s)$ or $\Delta(s;g')/B'[\mu(s)]$, of the resultant CGM1st decreases rapidly. At the same time, the position, $\hat{m}=\mu$, at the center of CGM1st migrates to large $\hat{m}$ values, and the portion of CGM1st leaking out to negative $\hat{m}$ values becomes negligibly small. It is usual practice that chromatography is carried out by using a column with a large enough length s; eq(5.14) or (5.14') obtained under initial condition given by eq(4.16) can represent the actual CGM1st. The similar argument holds with respect to eq(5.11) also. (Cf. both Figs 7.6 and 7.11 in Chapter Ⅶ, and both Figs A6.2 and A6.5 in Appendix Ⅵ.)

Below is shown that eq(5.14) or (5.14') is even valid for a short column if an interpretation is introduced that the portion of the theoretical CGM1st appearing over positive $\hat{m}$ values represents the corresponding portion of the actual CGM1st, but that the other portion leaking out to negative $\hat{m}$ values can be replaced by a sharp peak with an infinitesimal width taking place at the beginning, $\hat{m}=0$, of the concentration gradient. The total CGM1st therefore is a sum of the part (taking place over positive $\hat{m}$ values) of Gaussian distribution and the sharp peak (taking place at $\hat{m}=0$ or the cut end of Gaussian distribution). The sharp peak reduces gradually to vanish with increase in s. [The prototype of the argument below can be found in refs(6.10, 8.47, A5.1, A5.2).]

Thus, let us denote by δs the length or the total interstitial volumes of a very short column through which the carrier liquid with a volume much larger than δs passes during the chromatographic process where almost all the sample molecules loaded on the column are eluted out of δs; molecular partition B in the mobile phase taking place in

the column is close to zero during this process. In eq(5.17) [in CPV(OPV)], the diffusion term (the second term in brackets on which $\mathrm{div}_{\hat{m}}$ operates) now is negligible. Instead of the replacement of B by either B″(s) or B'[Ω(s)], the replacement of B by B'($\hat{m}$) can be done because B hardly depends on the axial position on the short column, whereas $\hat{m}$ corresponds to m in a one-to-one manner through eq(3.1). Eq(5.17) can be rewritten as

$$\frac{\partial}{\partial \hat{m}}\left(\frac{1-B'(\hat{m})}{B'(\hat{m})}C\right)+\frac{\partial C}{\partial s}=0 \tag{A5.1}$$

In OPV[CPV(OPV)], the variable $\hat{m}$ and s in eq(A5.1) have meanings of time and axial position on the column, respectively, and it is possible to consider that C=0 at the inlet, s=0, of the column when once the sample injection is completed, thus leading to

$$C(\hat{m},\ s=0)=0 \tag{A5.2}$$

By using eq(A5.2), the term, $\partial C/\partial s$, in eq(A5.1) can be replaced by

$$\begin{aligned}\partial C/\partial s &= [C(\hat{m},\ s=\delta s)-C(\hat{m},\ s=0)]/\delta s\\ &= C(\hat{m},\ s=\delta s)/\delta s\end{aligned} \tag{A5.3}$$

and eq(A5.1) reduces to

$$-\frac{d}{d\hat{m}}\left(\frac{1-B'(\hat{m})}{B'(\hat{m})}C\right)_{s=\delta s}=C(\hat{m},\ s=\delta s)/\delta s \tag{A5.4}$$

Let us calculate the solution of eq(A5.4) fulfilling

$$\int_0^\infty C(\hat{m},\ s=\delta s)d\hat{m}=1 \tag{A5.5}$$

For this purpose, introducing molecular density in the solid phase:

$$\chi=\frac{1-B'(\hat{m})}{B'(\hat{m})}C \tag{A5.6}$$

eq(A5.4) can be rewritten as

$$-\left(\frac{d\chi}{d\hat{m}}\right)_{s=\delta s}=\frac{1}{\delta s}\cdot\frac{B'(\hat{m})}{1-B'(\hat{m})}\chi(\hat{m},\ s=\delta s) \tag{A5.4'}$$

which can easily be integrated to give

$$\chi(\hat{m},\ s=\delta s)=\chi_{in}\exp\left(-\frac{1}{\delta s}\int_0^{\hat{m}}\frac{B'(\hat{m})}{1-B'(\hat{m})}d\hat{m}\right) \tag{A5.7}$$

where χ_{in} represents the integral constant. By using eq(A5.6), eq(A5.7) can be transformed to the general solution of eq(A5.4). By substituting this solution into eq(A5.5) and executing the integration, the integral constant χ_{in} can be determined to be equal to $1/\delta s$, and the solution of eq(A5.4) which we desired:

$$C(\hat{m},\ s=\delta s) = \frac{1}{\delta s}\cdot\frac{B'(\hat{m})}{1-B'(\hat{m})}\exp\left(-\frac{1}{\delta s}\int_0^{\hat{m}}\frac{B'(\hat{m})}{1-B'(\hat{m})}d\hat{m}\right) \qquad (A5.8)$$

is obtained finally.

Eq(5.4) or (5.4') can be re-expressed as

$$-\left(\frac{d\chi}{d(\hat{m}/\delta s)}\right)_{s=\delta s} = C(\hat{m},\ s=\delta s) \qquad (A5.4'')$$

which manifests that the amount of molecules that are eluted out of the interstice (with volume δs) of the column during a chromatographic process where a volume δs of the carrier liquid passes [left-hand side of eq(A5.4'')] is virtually equal to the amount of molecules staying in the mobile phase in the interstice of the column during this process [right-hand side of eq(A5.4'')]. The reason why, in the left-hand side of eq(A5.4''), the amount, χ, of molecules in the solid phase is considered instead of the total amount, Ω, in both mobile and stationary phases is that the molecular flux under consideration is the abstract flux (with density C) and not the real flux (with density Ω). By using eq(A5.8) in part, let us define molecular density C as a function of $\hat{m}$ as

$$\left.\begin{aligned} C &= \frac{1}{\delta s}\cdot\frac{B'(\hat{m})}{1-B'(\hat{m})}\exp\left(-\frac{1}{\delta s}\int_0^{\hat{m}}\frac{B'(\hat{m})}{1-B'(\hat{m})}d\hat{m}\right) \quad (\text{when } \hat{m}\geqq 0)\\ C &= 0 \qquad\qquad\qquad\qquad\qquad\qquad\qquad\qquad\qquad\qquad (\text{when } \hat{m}<0)\end{aligned}\right\} \qquad (A5.9)$$

In OPV[CPV(OPV)], it can be interpreted that eq(A5.9) represents CGM1st obtained by using a column with length δs. At the limit of $\delta s\to 0$, eq(A5.9) becomes

$$\lim_{\delta s\to 0} C = \delta(\hat{m}) \qquad (A5.10)$$

which coincides with eq(4.16).

Let us consider to join the column with an infinitesimal length $\delta s\to 0$ (into which the injection of sample molecules has been completed) to the inlet of the column with a finite small length s. By reconsidering that the total column system represents the actual column, it can be understood that the CGM1st obtained by using this column is a sum of the part (taking place over positive $\hat{m}$ values) of Gaussian distribution represented by eq (5.14) or (5.14') and the sharp peak with an infinitesimal width (taking place at $\hat{m}=0$ or at the cut end of the Gaussian distribution). The sharp peak reduces gradually to vanish

with increase in length s of the column used.

Appendix VI. Analysis of the Earlier Experiment

It would be worthwhile here to supply the experimental analysis of a series of linear concentration gradient chromatographies of lysozyme carried out by using the column packed with HA crystals with a plate-like shape [published in ref(6.8)]. This is because, in ref(6.8), much wider ranges of both overall length, L, of the column (0.5-216 cm) and slope, g, of the potassium gradient of KP buffer [0.0387-3.866 mM/cm; this range corresponds to 0.0375-3.75 mM/ml for the parameter $g'_{(P)}$($\varnothing$=1 cm) (see the legend for Table 7.1)] are applied; these can be compared with the ranges applied in Chapter VII: L=0.5-33 cm and g=0.196-1.185 mM/cm.

The experimental analysis is carried out by using eqs(6.2), (6.7'), (6.8'), (6.9'), (6.11), (6.18) and (6.23) with m_{in}=0.0015 M; eqs(6.7'), (6.18) and (6.23) lead to eq(6.24) or (6.24'). The value, 0.2474 cm^2, of the parameter γ estimated from the sucrose experiment is used; this value is different from that estimated in Chapter VII(D) since the type of HA is different. [By using the value of γ, the ratio of the void volume to the total packed volume of the plate-like HA crystals in the column can be estimated to be 0.875. This value is smaller than the value, 0.925, derived in ref(6.8) from the measurement of the dry weight of the packed crystals in the column, and is larger than the value, 0.838, obtained for the spherical HA; see Chapter VII(D).] For the parameters x', ln q, φ, $\theta°$ and $\Theta°$, optimum values 4.8, 7.68, 25 M^{-1}, 0.12 cm and 0.0297 cm^3 are used. [These can be compared with the corresponding values 6.4, 9.82, 25 M^{-1}, 0.015 cm and 0.00356 cm^3 used for the analysis of the spherical HA packed column [see Chapter VII(E)]. It can be assumed that the difference between the two values of x' (4.8 for plate-like HA and 6.4 for spherical HA) is not significant because the possible lower and upper limiting values of x' can be estimated to be 4 and 8, respectively [see Chapter VII(D)]. The difference between the two values of ln q might be significant, however. The value, 0.12 cm (or 0.0297 cm^3), of the parameter $\theta°$ (or $\Theta°$) for the plate-like HA packed column which is larger than the corresponding value, 0.015 cm (or 0.00356 cm^3), for the spherical HA packed column can be assumed to arise from the fact that the channels of the flow among the packed crystals in the column are distributed less uniformly with the former column.]

Fig A6.1 corresponds to Fig 7.3(a) or Fig 7.4 (the middle diagrams). In Fig A6.1, the abscissa represents virtually both μ and $\hat{\mu}$ since the value, 0.0015 M, of m_{in} is close to zero from the practical viewpoint.

Fig A6.2 corresponds to Fig 7.5(a) or Fig 7.6 (the middle diagram). In Fig A6.2, the abscissa represents virtually both μ and $\hat{\mu}$. If the $\hat{m}$ axis is considered instead of the $\hat{\mu}$ axis, Fig A6.2 represents trajectory T_0.

Fig A6.3 corresponds to Fig 7.8 or Fig 7.9 (the middle diagram). In Fig A6.3, the abscissa represents virtually both m and $\hat{m}$.

Fig A6.4 corresponds to Fig 7.10(a).

Figs A6.5 and A6.6 correspond to Figs 7.11(a) and 7.12(a), respectively. [*Note.* For

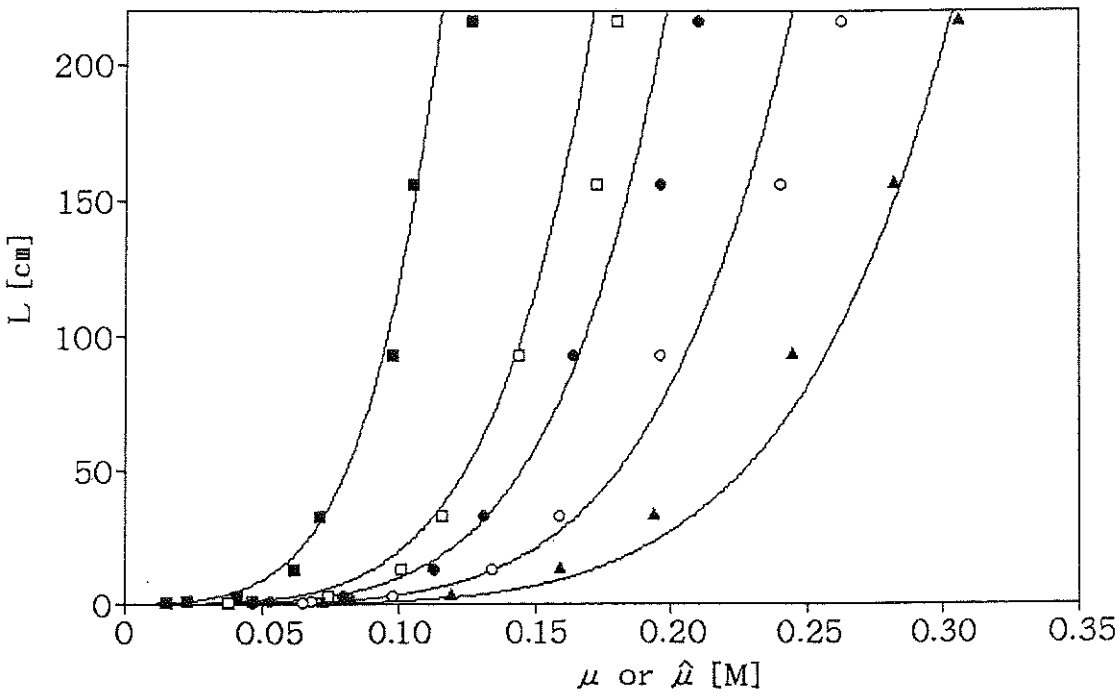


Fig A6.1. Points: experimental plots of L versus μ or $\hat{\mu}$ for lysozyme obtained when the slope, g, of the linear potassium gradient is 0.0387 mM/cm(■), 0.232 mM/cm(□), 0.464 mM/cm(●), 1.289 mM/cm(○) and 3.866 mM/cm(▲). The corresponding $g'_{(P)}(\sigma=1\ \text{cm})$ values (cf. the legend for Table 7.1) are 0.0375, 0.225, 0.45, 1.25 and 3.75 mM/ml, respectively. [Reproduced from ref(6.8) Fig 3(a) with modifications.] Curves: theoretical curves calculated by using eq(6.7') combined with eq(6.2); functions ϕ and $\hat{B}$ are defined by eqs(6.18) and (6.23), respectively.

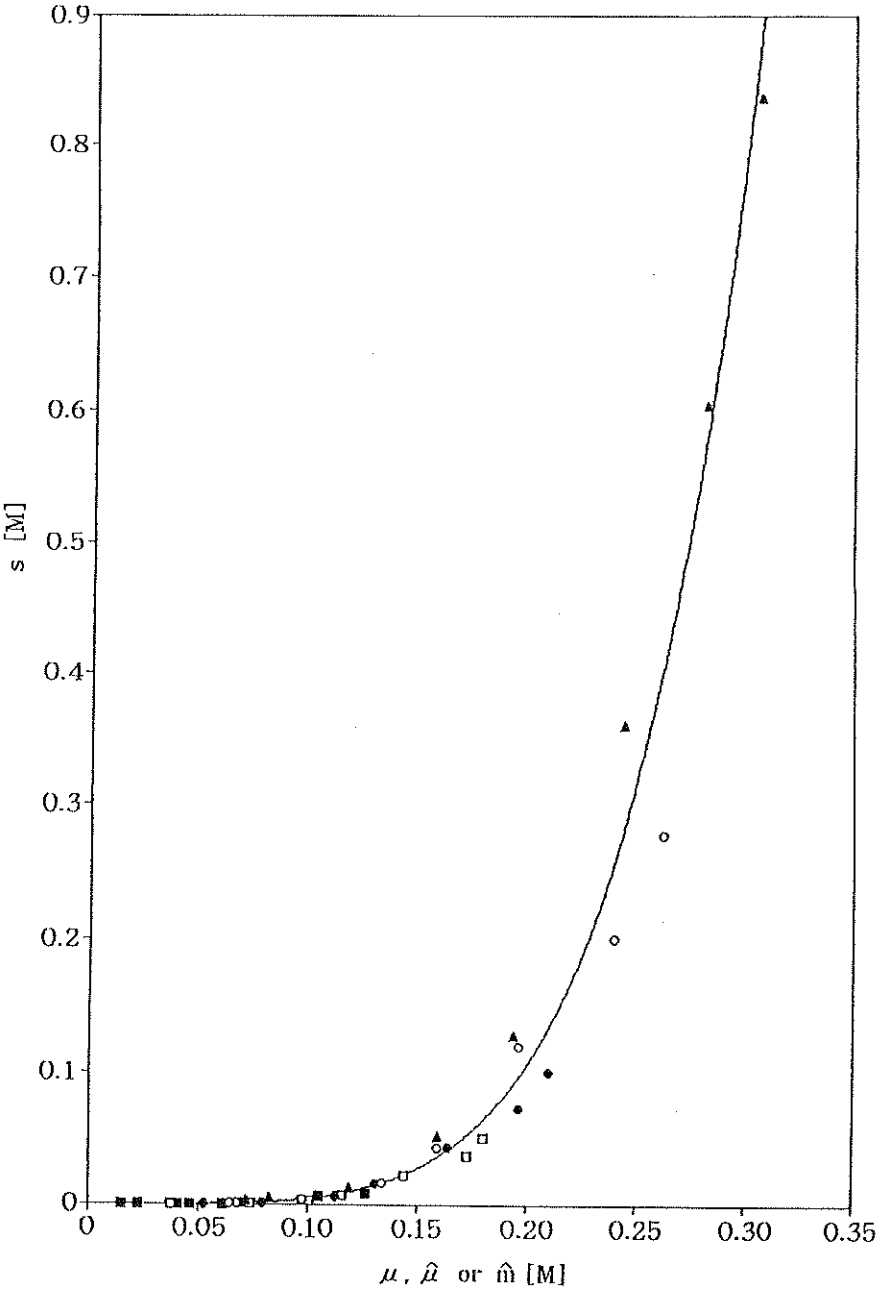


Fig A6.2. Points: experimental plots of s versus μ or $\hat{\mu}$ for lysozyme obtained when the slope, g, of the linear potassium gradient is 0.0387 mM/cm(■), 0.232 mM/cm(□), 0.464 mM/cm(●), 1.289 mM/cm(○) and 3.866 mM/cm(▲). If the $\hat{m}$ axis is considered instead of the $\hat{\mu}$ axis, these represent trajectory T_0. [Reproduced from ref(6.8) Fig 4(b) with modifications.] Curve: theoretical curve calculated by using the equality between extreme left- and extreme right-hand sides, or the equality between extreme left-hand side and middle in eq(6.7'); functions ϕ and $\hat{B}$ are defined by eqs(6.18) and (6.23), respectively.

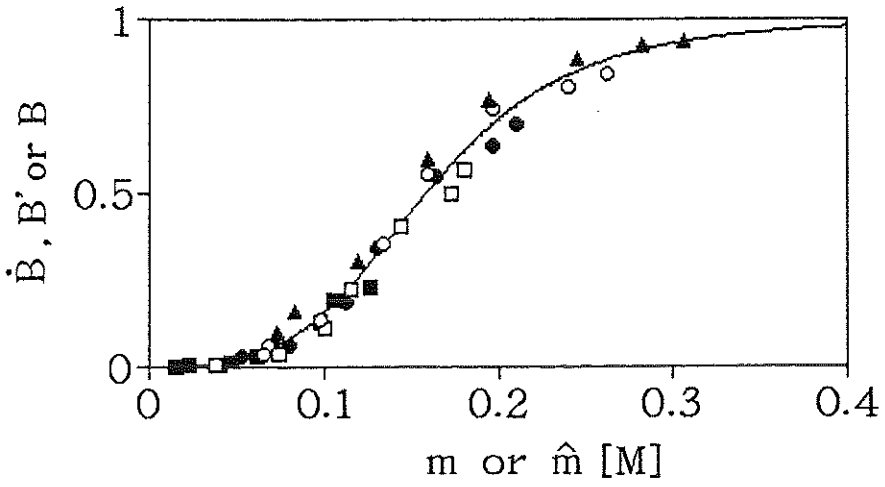


Fig A6.3. Curve: theoretical curve calculated by using eq(6.23), or eq(6.23) into which $B'(\hat{m})$ is substituted for $\dot{B}(m)$; function ϕ is defined by eq(6.18). Points: experimental plots obtained by mapping the points plotted in Fig A6.2. The symbols are common to those used in Fig A6.2.

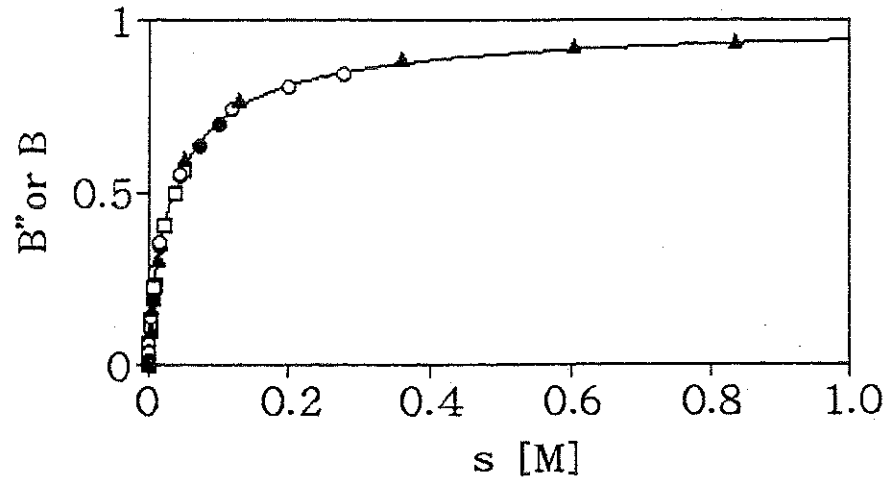


Fig A6.4. Curve: theoretical curve calculated by using the fact that $B''(s)$ can be represented as $B'[T_0^{-1}(s)]$. Points: experimental plots obtained by mapping the points plotted in Fig A6.3. The symbols are common to those used in both Figs A6.2 and A6.3.

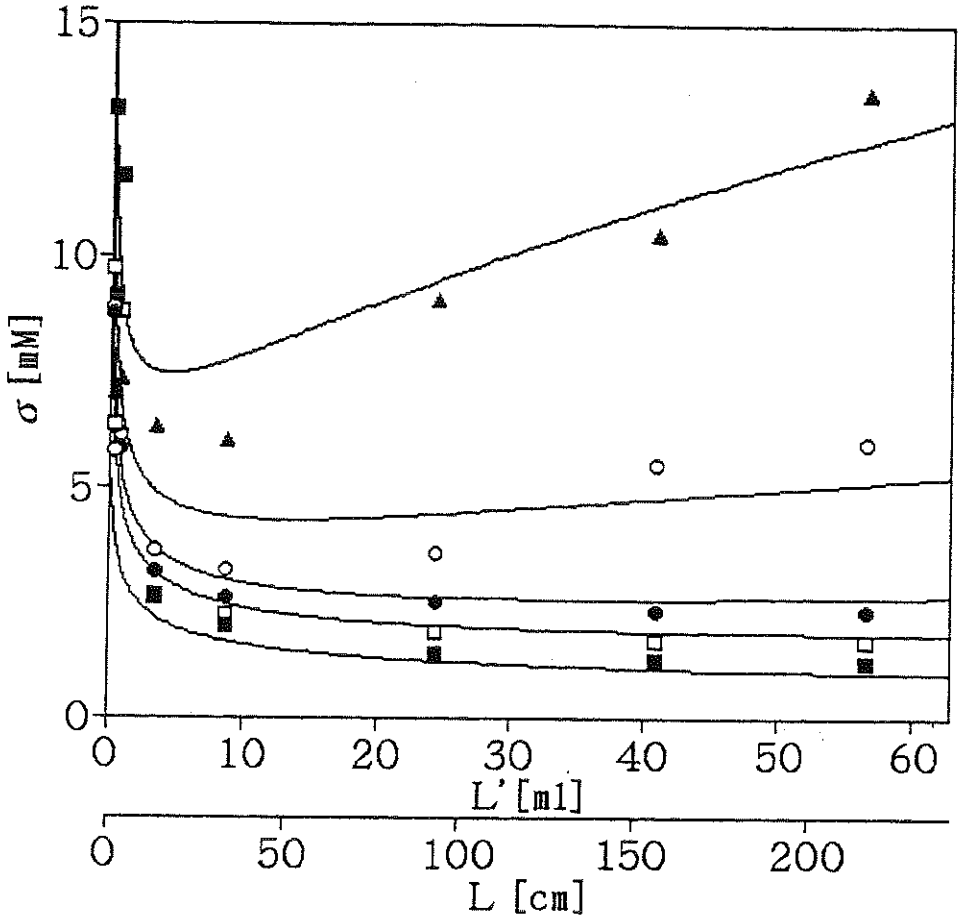


Fig A6.5. Points: experimental plots of σ versus L' or L for lysozyme obtained when the slope, g, of the linear potassium gradient is 0.0387 mM/cm(■), 0.232 mM/cm (□), 0.464 mM/cm(●), 1.289 mM/cm(○) and 3.866 mM/cm(▲). [Reproduced from ref (6.8) Fig 3(b) with modifications.] Curves: theoretical curves calculated by using eq(6.8'); functions ϕ and $\dot{B}$ are defined by eqs(6.18) and (6.23), respectively.

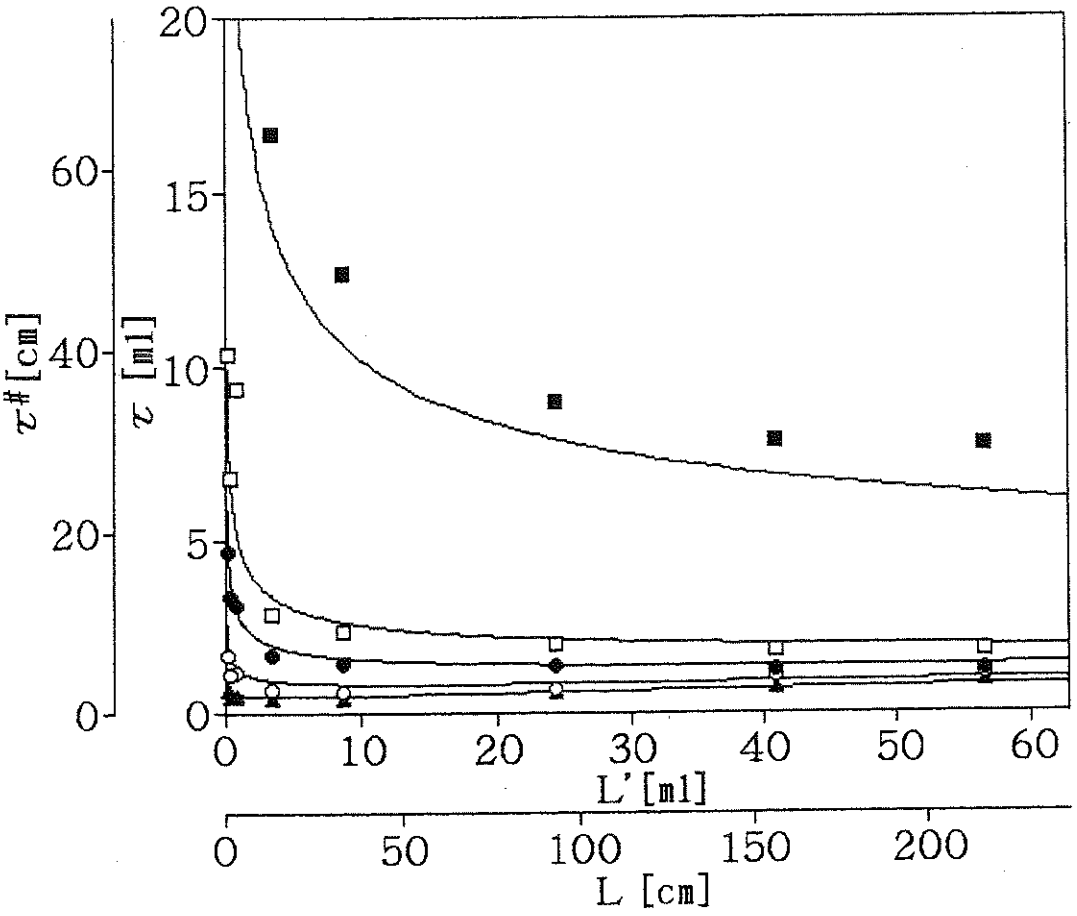


Fig A6.6. Points: experimental plots of τ or $\tau^{\#}$ versus L' or L for lysozyme obtained when the slope, g, of the linear potassium gradient is 0.0387 mM/cm(■), 0.232 mM/cm(□), 0.464 mM/cm(●), 1.289 mM/cm(○) and 3.866 mM/cm(▲). [Reproduced from ref(6.8) Fig 3(b) with modifications.] Curves: theoretical curves calculated by using eq(6.8') combined with eq(6.11); functions ϕ and $\dot{B}$ are defined by eqs(6.18) and (6.23), respectively.

the calculation of the curves in both Figs A6.5 and A6.6, account is not taken of the leaking-out effect of the theoretical chromatogram to negative $\hat{m}$ values taking place when s is extremely small (see Appendix V). As with both Figs 7.11 and 7.12, the leaking-out effect is negligible in practice as far as the curves drawn in the diagrams are concerned.]

It can be seen in Figs A6.1-A6.6 that the coincidence between theory and experiment is satisfactory even in considerably wide ranges of both L and g. As far as standard deviation, σ or τ, is concerned, however, the experimental value tends to be slightly larger than the theoretical prediction when the smallest g, 0.0387 mM/cm, is applied(Figs A6.5 and A6.6). The tendency is parallel to that for the spherical HA packed column [see both Chapter Ⅶ(E) and (F)].

In ref(6.8), the theoretical curves corresponding to those drawn in Figs A6.1-A6.3 and A6.5 were calculated by using the earlier theory [see Chapter Ⅵ(D)]. The theoretical curves in Figs A6.1-A6.3 are almost identical with those drawn in ref(6.8) Figs 3(a), 4(b) and 4(g), respectively; the negligible difference arises from the fact that the values of the experimental parameters used in ref(6.8) are slightly different from those used in this Appendix. The theoretical curves drawn in Fig A6.5 are considerably different from those drawn in ref(6.8) Fig 3(b), however.

Ref(6.8) Figs 1(a) and (b) manifest that μ decreases slightly and that σ increases considerably with increase in sample load of lysozyme; both μ and σ tends to a finite value when sample load tends to infinitesimal. From these data, it can be confirmed that all the experiments in Figs A6.1-A6.6 are carried out under conditions of small enough sample load where both μ and σ are virtualy independent of sample load. Ref(6.8) Fig 2 (a) manifests that μ for the lysozyme chromatogram (obtained under condition of small enough sample load) is virtually independent of flow-rate; this is consistent with the fundamental consideration that a thermodynamic equilibrium is attained apparently at the center of MB(o) with a Gaussian shape [see Chapter Ⅰ(A)]. Ref(6.8) Fig 2(b) shows, however, that σ for the lysozyme chromatogram (obtained under condition of small enough sample load) increases with increase in flow-rate. This implies that the flow heterogeneity [which contributes to bringing about axial molecular diffusion in the column; see Chapter Ⅰ(A)] increases with increase in flow-rate. Provided that the resistance to mass transfer between mobile and stationary phases takes place, its contribution to axial molecular diffusion in the column would also increase with increase in flow-rate. With HPLC, however, it can be assumed that the contribution of the resistance to mass transfer effect is small [see Chapter Ⅰ(A)].

Appendix Ⅶ. Justification of Eq(8.17)

Let us introduce the functions:

$$\ln X_{(\omega)}[\mathbf{n}''] = \ln (n_0 z/M) + \mu_{(\omega)}/kT + \varepsilon/kT + \ln y_{(\omega)}[\mathbf{n}''] \tag{A7.1}$$

and

$$\ln X_{(\omega)}[\mathbf{n}''] = \ln (n_0 z/M) + \mu_{(\omega)}/kT + (E + kT\ln\tau)/kT + \ln y_{(\omega)}[\mathbf{n}''] \tag{A7.2}$$

Eq(8.2) into which eqs(8.3'), (8.15) and (8.16) are substituted can now be rewritten as

$$\Xi = \sum_{n'_{(\omega)}+n'_{(\omega)} \leqq M} \Psi_1(n'_{(\omega)}, n'_{(\omega)}) \tag{A7.3}$$

in which

$$\Psi_1(n'_{(\omega)}, n'_{(\omega)}) = \frac{M!}{n'_{(\omega)}! n'_{(\omega)}! (M - n'_{(\omega)} - n'_{(\omega)})!} \prod_{\rho=0}^{1} \prod_{n''_{(\rho)}=1}^{n'_{(\rho)}} X_{(\rho)}[\mathbf{n}''] \tag{A7.4}$$

Statistical mechanics, in general, concludes that, when $M \gg 1$, $\Psi_1(n'_{(\omega)}, n'_{(\omega)})$ manifests a sharp distribution around a set $(n_{(\omega)}, n_{(\omega)})$, the elements of which represent the expectation values of $n'_{(\omega)}$ and $n'_{(\omega)}$, respectively; the set $(n_{(\omega)}, n_{(\omega)})$ gives Ψ_1 a maximum value. $n_{(\omega)}$ and $n_{(\omega)}$ can be represented as solutions of the simultaneous equations:

$$\partial \ln \Psi_1 / \partial n'_{(\rho)} = 0 \tag{A7.5}$$

($\rho = 0, 1$). As $\sum_{\rho'=0}^{1} \sum_{n''(\rho')=1}^{n'(\rho')} \ln X_{(\rho')}[\mathbf{n}'']$ is a state quantity, then corresponding to eqs(8.31) and (8.33), the relationmships:

$$\sum_{\rho'=0}^{1} \sum_{n''_{(\rho')}=1}^{n'_{(\rho')}} \ln X_{(\rho')}[\mathbf{n}''] = \sum_{I=1}^{n'_{(\omega)}+n'_{(\omega)}} \{\ln X_{(\rho')}[\mathbf{n}'']\}_I \tag{A7.6}$$

and

$$\frac{\partial \sum_{I=1}^{n'_{(\omega)}+n'_{(\omega)}} \{\ln X_{(\rho')}[\mathbf{n}'']\}_I}{\partial n'_{(\rho)}} = \ln p_{(\rho)}[\mathbf{n}'] \tag{A7.7}$$

(ρ =0, 1) are fulfilled, respectively. By using both eqs(A7.6) and (A7.7) along with Stirling's approximation, and writing $n_{(0)}$ and $n_{(1)}$ for $n'_{(0)}$ and $n'_{(1)}$, respectively, eq(A7.5) can be re-expressed as

$$-\ln n_{(\rho)}+\ln (M-n_{(0)}-n_{(1)})+\ln X_{(\rho)}[\mathbf{n}] = 0 \qquad \text{(A7.8)}$$

(ρ =0, 1).

On the other hand, eq(8.2) into which eq(8.3'), (8.15') and (8.16') are substituted [i.e., eq(8.2')] can be rewritten as

$$\Xi = \sum_{n'_{(0)}+n'_{(1)} \leqq M} \Psi_2(n'_{(0)},n'_{(1)}) \qquad \text{(A7.9)}$$

in which

$$\Psi_2(n'_{(0)},n'_{(1)}) = \frac{M!}{n'_{(0)}!n'_{(1)}!(M-n'_{(0)}-n'_{(1)})!} \prod_{\rho=0}^{1} (X_{(\rho)}[\mathbf{n}])^{n'_{(\rho)}} \qquad \text{(A7.10)}$$

When $M \gg 1$, $\Psi_2(n'_{(0)},n'_{(1)})$ manifests a sharp distribution around a set $(n^*_{(0)},n^*_{(1)})$, the elements of which represent the expectation values of $n'_{(0)}$ and $n'_{(1)}$, respectively; the set $(n^*_{(0)},n^*_{(1)})$ gives Ψ_2 a maximum value. $n^*_{(0)}$ and $n^*_{(1)}$ can be represented as solutions of the simultaneous equations:

$$\partial \ln \Psi_2 / \partial n'_{(\rho)} = 0 \qquad \text{(A7.11)}$$

(ρ =0, 1). By using Stirling's approximation and writing $n^*_{(0)}$ and $n^*_{(1)}$ for $n'_{(0)}$ and $n'_{(1)}$, respectively, eq(A7.11) can be re-expressed as

$$-\ln n^*_{(\rho)}+\ln (M-n^*_{(0)}-n^*_{(1)})+\ln X_{(\rho)}[\mathbf{n}] = 0 \qquad \text{(A7.12)}$$

(ρ =0, 1).

It is evident that the solutions, $n_{(0)}$ and $n_{(1)}$, of eq(A7.8) are identical with the solutions, $n^*_{(0)}$ and $n^*_{(1)}$, of eq(A7.12), thus justifying eq(8.17).

Appendix Ⅷ. Reconsideration on the Methodology for the "Determination" of the Collagen Primary Structure versus Collagen Biosynthesis

(A) "Determination" of the Primary Structure

The microheterogeneous collagen model with the π value of 0.8 can be considered to be compatible with the fact that the primary structure of the α chains can be "determined" by the organochemical method. The process of this "determination" is reviewed in detail by Fietzek and Kühn(8.35, 8.38). Thus, the determination of the amino acid sequence is carried out for relatively small peptide fragments of the α chains, mainly with the aid of the Beckman Sequenator (Sequencer), by repeating successively the Edman-type degradation cycles. In a cycle, N terminal residue of the peptide fragment is released and converted finally to a phenylthiohydratoinine(PTH) derivative, which is extracted and identified. The residual peptide which is now one amino acid shorter is subjected to the next degradation cycle. For the identification of the PTH-amino acid, thin layer or gas-liquid chromatography is used. It is reported(8.38), however, that, as the peptide degradation proceeds, the detection of the liberated amino acid residue becomes more and more hampered by overlaps and a general rise of background. This is a reason why the amino acid sequence determination can be performed only for small peptide fragments (see above). Yield relative to the first step of the degradation declines to 50% after only 20 degradation steps, and to 5% at the 45 th step. The decrease of the yield may be accounted for by the cumulative effect of only a slight blocking of the reaction at each step. A concomitant increase of the background would be due (at least partially) to unspecific cleavage of the peptide chain(8.38).

According to microheterogeneous collagen model, the recovery of the chromatographic spot or the peak for a "correct" amino acid appearing in thin layer or gas-liquid chromatography (see above) should be equal to π or 80% with aspartic or glutamic acid, provided that the experiment is ideal and that there is no unspecific cleavage of the peptide chain or slight blocking of the degradation reaction (see above). The spots or the peaks for "incorrect" amino acids would be distributed around the main one (for the "correct" amino acid) in diluted states. It practically would be difficult to observe "incorrect" spots or peaks, and/or to distinguish them from the artificial backgrounds. In conclusion, it would be the most-frequently-occurring primary structure that is picked up or "determined". It would be rare but the possibility does exist (cf. Appendix Ⅸ) that the "incorrect" amino acid sequence can be found out by using the organochemical method.

(B) Biosynthesis

The collagen biosynthesis can be characterized by at least two prominent features: (i) The protein is first synthesized as a precursor form, procollagen; this is made up of two pro-α_1 and one pro α_2 peptide chains being longer at the N and C terminals by

several hundred amio acids (about 40% larger in size than the α cahins), and (ii) the biosynthesis involves several unusual posttranslational modifications which occur after assembly of amio acids into the three polypeptide chains of the molecule(8.32, A8.1, A8.2). These modifications involve (a) conversion of proline to hydroxyproline, (b) conversion of lysine to hydroxylysine, (c) glycosylation of hydroxylysine to yield both galactosylhydroxylysine and glucosylgalactosylhydroxylysine, and (d) oxidative deamination of lysine and hydroxylysine to yield the cross-link-precursor aldehydes, allysine and hydroxyallysine(8.32; cf. Appendix IX). Pro-α_1 and pro-α_2 chains are synthesized separately as single chains by sequential amino acid additions from the amino terminal ends (like syntheses of polypeptides of other proteins) (A8.1, A8.3, A8.4). The estimation that polysomes participating in collagen synthesis are larger than a 23-ribosomal aggregate but smaller than a 50-60-ribosomal aggregate is consistent with a monocistronic message coding for a pro-α chain (A8.1, A8.2, A8.5). For cDNA for collagen, cf. Appendix IX.

The heterogeneous collagen chromatograms(Figs 8.14 and 8.15) cannot satisfactorily be explained in terms of posttranslational modifications nor of deaminations of asparginyl and/or glutaminyl residues if they take place spontaneously. This is because the maximum possible degree of molecular heterogeneity that can arise from these mechanisms is much too small to explain the experimental chromatograms [see the subsequent Section(C)]. It can be suggested[ref(8.25) Appendix III] that the equivocal primary structures of the α chains may arise at a translational level of biosynthesis. For this to occur, two possibilities exist: (a) binding between "incorrect" amino acid and tRNA, and (b) binding between "incorrect" codon and anticodon. In order for (a) to occur, the activation energies for bindings of "correct" pairs of molecules provided by aminoacyl-tRNA synthetases(A8.6) would not be so different from the activation energies for "incorrect" pairs, and/or the binding energies for "correct" pairs would not be so different from the binding energies for "incorrect" pairs. In order for (b) to occur, the binding energies for "correct" pairs of codon and anticodon would not perhaps be so different from those for "incorrect" pairs.

For globular proteins (ovalbumin and hemoglobin), Loftfield(A8.7, A8.8) estimates that the frequency of replacement of a "correct" amino acid with a sterically similar "incorrect" amino acid on a polypeptide chain should be at most of the order of 3×10^{-4} (the case of substitution of valine for isoleucine). On the other hand, Pauling(A8.9) estimates, on a physicochemical basis, that the probability of occurrence of the Michaelis-Menten complex of "incorrect" amino acid and aminoacyl-tRNA synthetase should be at least 5% in some instances. In this estimation, an effort is made to decrease as much as possible the possibility of the entrance of the "incorrect" amino acid into the template of the enzyme. Numerous "incorrect" aminoacylations occurring due to misrecognition of the "correct" tRNA by the valyl-tRNA synthetase are reported in heterologous system(A8.10). For instance, by using valyl-tRNA synthetase from *Bacillus stearothermophilus*, $tRNA^{Ile}$ and $tRNA_f^{Met}$ from *Escherichia coli* are acylated to the extents of 78 and 20%, respectively(A8.10). In both bacterial and mammalian cells, extreme starvation for certain amino acids results in trans-

lational errors that can be easily detected by two-dimensional polyacrylamide gel electrophoresis(A8.11). These errors can be predicted from misreading of pyrimidines for purines at the third position of the codon(A8.11). In order to explain high precisions for occurrences of "correct" amino acid residues on a polypeptide chain that can be seen at least with globular proteins (see above), some proofreading mechanisms are proposed (A8.12-A8.16).

A highly unequivocal primary structure would teleologically be necessary with a number of globular proteins in order to acquire a highly unique stereochemical structure. The situation is different with collagen, however. Thus, the greater part of both α_1 and α_2 collagen peptides consist of the triplet structures of Gly-X-Y where X and Y can be any residue [see Chapter Ⅷ(F)]. Nevertheless, the tertiary triple-helical structure[Chapter Ⅷ(F)] is shown(8.30, A8.17) to be identical with the conformation that $(Gly\text{-}Pro\text{-}Pro)_n$ takes. Further, it is demonstrated experimentally(A8.18) that the triple-helical collagen structure [naturally consisting of two α_1 and one α_2 chains; see Chapter Ⅷ(F)] can be formed from both three α_1 and three α_2 chains. This again manifests that precise amino acid sequences in the α chains are not reqired for the formation of the collagen streochemical structure, since the amino acid compositions and the sequences are different between α_1 and α_2 chains. However, the existence of glycyl residues in glycyl positions in the $(Gly\text{-}X\text{-}Y)_n$ structure is necessary for the formation of the collagen stereochemical structure (8.30, A8.17). This suggests that the π value with respect to glycine is close to unity. A high π value for imino acid residues can also be suggested because the stability of the collagen structure is sensitive to the imino acid content(A8.19). With regard to amino acids other than glycine and imino acids, we find no reasons why they should exist at "correct" peptide positions in high probabilities.

(C) Possibility of Explaining the Heterogeneous Collagen Chromatograms(Figs 8.14 and 8.15) on the Basis of Other Models Than Microheterogeneous Model

Deaminations. With a number of synthetic peptides, spontaneous deaminations of asparginyl and glutaminyl residues do occur under physiological solvent conditions(A8.20). The deamination half-times vary between 6 days to 9 years depending markedly on the sequence in amino acid residues in peptides. The in vivo behaviors of cytochrome c, aldolase and lysozyme are consistent with the deamination half-times of model peptides with the same amide sequences as these peptides(A8.20).

It can be deduced, however, that deaminations do not occur or that they occur only very slightly with collagen. Thus, in Table A8.1 are shown amide contents (obtained by amino acid analysis) of collagen from different sources and their subunit components, expressed as numbers per 1000 amino acid residues (for detail, see the legend for Table A8.1). It can be seen in Table A8.1 that the amide contents are almost constant among

Table A8.1

Amide Contents (obtained by amino acid analysis) of collagens from several different sources and their subunit components, expressed as numbers per 1000 amino acid residues. [Reproduced from ref(8.33).]

Source of collagen	Total	α_1	β_{11}	β_{12}	α_2
calf-skin	44.2		α =42.9,	β =42.2	
rat-skin	41	42	41	42	43
rat-tail tendon	40	39	40	41	41
carp swim bladder	40	37	39	43	46
cod skin	46	α_1=43,	α_2=46,	α_3=54	
dog fish shark skin	38	39	39	36	
human skin	36.9	37.9	37.2	44	45
		β_{22}=45			

Note. Cod-skin collagen is composed of α_1, α_2 and α_3 components in contrast with other collagens composed of two α_1 and one α_2. β_{11}, β_{12} and β_{22} represent dimers: α_1-α_1, α_1-α_2 and α_2-α_2, respectively. α and β (for calf-skin collagen) show mixtures before fractionations of α_1 and α_2, and β_{11} and β_{12}, respectively.

collagen peptides originating from different sources. Theoretically, the amide contents of β_{11} (dimer of α_1) and β_{22} (dimer of α_2) should be equal to those of α_1 and α_2, respectively. The amide content of β_{12} (dimer of α_1 and α_2) should be intermediate of those of α_1 and α_2. These points, in fact, are well reflected in amino acid analysis(Table A8.1). This would mean that the precision in the experimental data in Table A8.1 is high. If spontaneous deamination occurred, almost constant amide contents among different collagens seen in Table A8.1 should be highly fortuitous. It seems unlikely that such a high fortuity actually occurs. In conclusion, it is difficult to explain the heterogeneous collagen chromatograms(Figs 8.14 and 8.15) in terms of the deamination mechanism.

Posttranslational Modifications. It is difficult to attribute the collagen heterogeneity (Figs 8.14 and 8.15) to posttranslational modifications [modifications(a)-(d) in Section(B)]. Thus, when the terminal parts of the collagen rod where the cross-links are formed are eliminated by pepsin treatment, essentially the same chromatogram as that occurring before treatment is obtained [see ref(8.26); cf. Fig 8.15(a) with Fig 8.15(b)]. This excludes the possibility that collagen heterogeneity(Figs 8.14 and 8.15) arises from modification(d). It can be assumed that modification(c) scarcely changes the elution phosphate molarity ($m_{elu(P)}$ or μ) from HA column because the carbohydrate content of a collagen molecule is exremely small. Only some hydroxylysyl residues (out of about 3000 amino and imino acid residues) are attached to carbohydrates in the form of galactosylhydroxylysine and glucosylgalactosylhydroxylysine [see Chapter Ⅷ(F)]. It is reported(A8.21) that a slight heterogeneity in an α chain can be detected on a DEAE-cellulose column, which is mainly concerned with the variation in hydroxylations of lysyl residues. Even assuming that hydroxylations of both prolyl and lysyl residues [modifications(a) and (b)] occur heterogeneously among different molecules, it is difficult to explain the heterogeneous HA chromatograms(Figs 8.14 and 8.15) in terms of this heterogeneity. First, if the heterogeneous hydroxylations do occur, this should not influence the distribution of functional carboxyl groups on the collagen surface. From a titration experiment, it can be assumed that all carboxyl groups are exposed on the molecular surface [see Chapter Ⅷ(F)]. Second, no synthetic polypeptides without electric charge are retained on the HA column(7.1). This would mean that the hydroxyl group without charge does not virtually react with the HA surface. If it reacts, the absolute value of reaction energy should be much smaller than that of adsorption energy, 2.9 kJ/mol, for a carboxyl group [see Chapter Ⅷ(F)]. It is difficult to assume that, due to the heterogeneity in hydroxylations, the heterogeneous chromatograms(Figs 8.14 and 8.15) are obtained.

(D) Comment on Some Experimental Data Giving An Apparent Impression of High Homogeneities of Both α_1 and α_2 Peptides

Sharp peaks or bands of both α_1 and α_2 peptides with random coil conformations can be obtained both chromatographically [on a CM-cellulose cation-exchange column

(8.31, 8.34)] and electrophoretically. The electrophoreses are carried out on polyacrylamide gels in both the absence(8.31, A8.18, A8.22, A8.23) and the presence(A8.24) of sodium dodecylsulfate(SDS), and on starch gels in the absence of SDS(8.31, A8.25, A8.26). With polyacrylamide gels in the presence of SDS, it can be suggested(A8.24) that the separation of the α_1 and α_2 peptides (with essentially the same M_m) arises from the difference in rigidities in molecular structures depending on the imino acid content, and not from the difference in electric charges. It can be suggested that, with starch gel electrophoresis in the absence of SDS also, the separation of the two peptides is not due to the charge difference. Thus, a good resolution can be achieved only in a small range of pH (pH=4-5) (A8.26). In this range, the α_2 peptide [with the higher content of basic amino acid residues and the lower content of acidic amino acid residues(8.33)] migtares more rapidly than the α_1 peptide. When pH is more acid (pH=3.58), however, it is not the basic α_2 but rather the acidic α_1 peptide that migrates most rapidly(A8.26). This datum suggests that the molecular conformations and the change in conformations taking place with change in pH are both fundamentally different between α_1 and α_2 peptides. On the other hand, the pH value of 4.8 [see ref(8.34)] that is appllied to CM-cellulose chromatography for the separation of α_1 and α_2 peptides is just within the small pH range between 4 and 5 only where a good electrophoretic separation can be achieved on starch gels. It is probable that the chromatographic separation is also attributed finally to the difference in molecular conformations because the effective number (or density) of positively charged groups that are present on the "surface" of a molecule with a "random coil" conformation would depend markedly on the type of "random coil" conformation. [Here, it should be recalled that, with ion-exchange chromatography, the charges on the total molecular surface can be considered to be used fairly uniformly for bonding with ion-exchangers throughout a development on the column. See the subsection entitled "Ion-Exchange and Reversed-Phase Chromatograohies in Contrast to HA Chromatography" in Chapter Ⅷ (E).]

In conclusion, it is probable that both chromatography (on a CM-cellulose column) and electophoresis data giving an apparent impression of high homogeneities of both α_1 and α_2 peptides arise from the difference in molecular conformations between the peptides. It can be suggested that the difference in molecular conformations is mainly due to the difference in the imino acid content. These data are not incompatible with microheterogeneous collagen model.

Appendix IX. Experiment of Yamauchi et al. Manifesting A Heterogeneity of the Collagen Primary Structure

In bovine skin collagen fibers, type I collagen molecules are mostly cross-linked to one another while forming "polymers". These are insoluble in the aqueous solvent, and are called "insoluble" collagen [cf. Chapter Ⅷ(F)]. By using a tryptic digest method, Yamauchi et al.(A9.1) isolated a mixture of polypeptides containing a three-chained polypeptide chain [cross-linked by hydroxylaldolhistidine(OHAlHis)] from bovine skin collagen fibers. Thus, in a step of the purification of the peptide as object, DEAE-cellulose anion-exchange column chromatography was performed, generating a chromatogram consisting of at least seven definite peaks in three of which OHAlHis was contained; it was confirmed that the amino acid compositions of the three peaks were extremely similar to one another. The three-chained cross-link peptide contained in one of the three peaks (called peak Ⅵ) was completely derivatized by using di-tert-butylcarbonate. This was submitted to a series of chemical reactions with cleavage into a two-chained cross-link peptide and a single peptide. By using a Sephadex G-50 gel-filtration column, the two-chained cross-link peptide was separated as a chromatographic peak (called peak Ⅲ). The authors emphasize(A9.1) that sequence analyses and amino acid composition of peak Ⅲ unequivocally demonstrated that it was a two-chained cross-link peptide.

By the simultaneous sequent analyses of the two peptide chains cross-linked to one another (carried out by using a Beckman 890C sequencer), it was found out that the cross-link consists of an aldehyde derived from hydroxylysine No.87 in a fragment of an α_1 peptide chain (called cyanogen bromide fragment α_1CB5) and an aldehyde derived from lysine No.18[c] in the C terminal nonhelical region of a fragment of another α_1 peptide chain (called α_1CB6) (see Fig A9.1). Thus, starting with amino acid residue No.15[c] and ending at residue No.19[c] in α_1CB6, the sequence was found to be Glu-Glu-Ala-Lys(ald)-His where "ald" indicates the aldehyde form (see Fig A9.1). On the other hand, the published sequence is Glx-Glx-Lys(ald)-Ala-His where Glx signifies either Glu or Gln (undeterminable at this stage of development of the sequence analysis). This is consistent with the sequence of the bases in a portion of cDNA that codes for the α_1 chain in chicken type I collagen i.e., the peptide sequence represented by the base triplets for the corresponding residues is Glu-Glu-Lys-Ala-His [see ref(A9.2)].

Yamauchi et al.(A9.1) suggest that there may exist small amounts of another structural gene that codes for an α_1 type I peptide whose expression is the altered sequence of ...Ala-Lys... instead of ...Lys-Ala...; this is based on the hypothesis that the amino acid sequence of a collagen α peptide should reflect the base triplet arrangement on the corresponding cDNA highly unequivocally. This hypothesis is in contrast to microheterogeneous model according to which the amino acid sequence of the α peptide does not reflect the base triplet arrangement unequivocally.

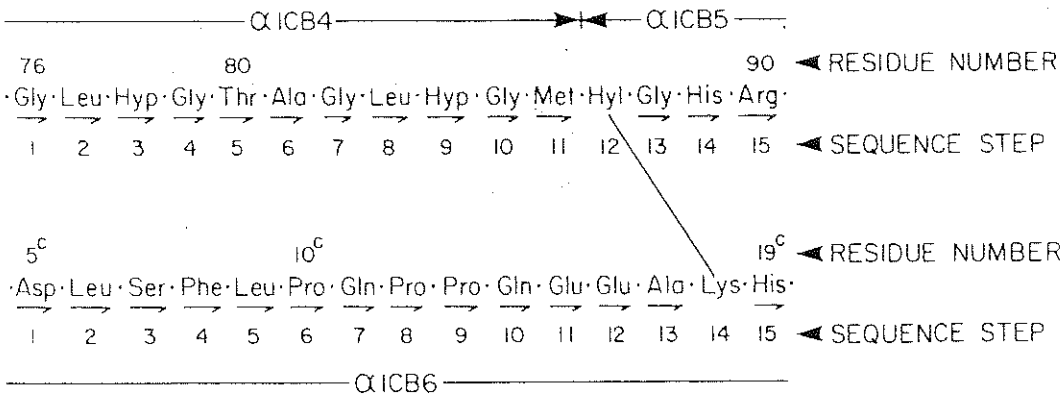


Fig A9.1. Sequence of two-chained crosslinked peptide obtained by specific cleavage of three-chained OHAlHis crosslink peptide. The residue numbers in the collagen sequence are above the amino acid residues. The half-headed arrows with the numbers of the sequence step below are results obtained from the sequenator. The arrows denote that the residue was identified in the sequence step assigned. [Reproduced from ref (A10.1) Fig 5.]

Appendix X. Detail on the Calculation of Fig 8.19

(A) Calculation

Let us introduce an integer ν that has the closest value to $1/\phi$ [see eq(8.63)]:

$$\nu \approx 1/\phi \tag{A10.1}$$

Replacing $1/\phi$ by an integer ν means replacing the lateral collagen surface by an abstract surface consisting of ν elementary domains; each elementary domain consists of a number of elementary surfaces with an area of h^2 $(=h_1h_2)$ nm^2, respectively. ϕ now represents the probability that, in a given molecular configuration on the HA surface, a given carboxyl group belongs in a particular one of the ν elementary domains. It is only in that elementary domain that the bonding of carboxyl group with a C site is possible. Denoting by X the total number of carboxyl groups per molecule, it is possible to define the probability that X carboxyl groups are partitioned among the ν elementary domains with ratios of $x_1 : x_2 : \ldots : x_\nu$ fulfilling

$$\sum_{j=1}^{\nu} x_j = X \tag{A10.2}$$

where each x_j can be virtually

$$x_j = 0, 1, 2, \ldots, X \tag{A10.3}$$

This is because the total number of elementary surfaces on the lateral surface of the collagen rod [about $300\times4.71/h^2\approx300\times4.71/(0.26\times0.344)\approx1.58\times10^4$] is much (i.e., about 69 times) as large as the number, X(=230), of elementary surfaces among which the carboxyl groups are partitioned.

In eq(A10.2), j and ν have meanings of the j th geometrical configuration of the molecule on the HA surface and the total number of possible configurations, respectively. x_j represents the number of carboxyl groups per molecule bonding with C sites provided that the j th configuration is being realized. x_1, $x_2,\ldots,$ x_ν are related to x and $\ln\tau$ through eqs(8.59) and (8.7), respectively; γ_j in eq(8.7) is defined by eq(8.8) in which $E_j=x_j\varepsilon$.

It is necessary to know the distribution law of the X "correct" elementary surfaces on the abstract molecular surface or the partition law of these surfaces among the ν elementary domains. For this purpose, let us rearrange the j value, which indicates the ν respective elementary domains, in decreasing order following the magnitude of the number of partitioned "correct" elementary surfaces. Writing ζ_1, $\zeta_2,\ldots,$ ζ_ν for these numbers, we therefore have

$$\zeta_1 \geqq \ldots \geqq \zeta_j \geqq \zeta_{j+1} \geqq \ldots \geqq \zeta_\nu \tag{A10.4}$$

where

$$\sum_{j=1}^{\nu} \zeta_j = X \tag{A10.5}$$

and each ζ_j can be virtually

$$\zeta_j = 0,\ 1,\ 2,\ \ldots\ ,\ X \tag{A10.6}$$

We now make N ($N \gg 1$) attempts to partition at random the X "correct" elementary surfaces among the ν elementary domains, and we define the mean value, $\bar{\zeta}_j$, of "correct" elementary surfaces partitioned to the j th elementary domain as

$$\bar{\zeta}_j = \lim_{N\to\infty} \sum_{m=1}^{N} (\zeta_j)_m/N \tag{A10.7}$$

where $j=1,\ 2,\ldots,\ \nu$, and m indicates the m th trial. We finally assume that the number, ζ_j, of "correct" elementary surfaces partitioned to the j th elementary domain is

$$\zeta_j = [\bar{\zeta}_j + 0.5] \tag{A10.8}$$

where $j=1,\ 2,\ldots,\ \nu$, and the square brackets indicate that the decimal values are discounted in order for ζ_j to be an integer. According to eq(A10.8), the sum of ζ_j for j may, in general, be slightly different from X. Fortunately, however, the sum in our calculation(Fig A10.1) is exactly equal to X.

If $\pi = 1$, then $x_j = \zeta_j$ for any value of j and for any molecular species. If $\pi < 1$, the values of x_j for different species are distributed statistically around the mean value ζ_j. It should be emphasized that what is important for our purpose is the distribution of the x_j values around ζ_j for each j, and not the exact value of ζ_j.

Fig A10.1 [reproduced from ref(8.25)] illustrates a type of calculation of ζ_j as a function of j when $X=230$ and $\nu = 18$. Thus, the plane consisting of a number of squares represents the total abstract collagen surface. The squares represent the elementary surfaces [with an area of h^2 ($=h_1h_2$) nm^2, respectively]. A verical column of squares piled up above a particular value of j on the abscissa represents the j th elementary domain. The ordinate value of the thick folded line gives the value of ζ_j for each j. The total domain under the thick folded line is composed of X ($=230$) "correct" elementary surfaces in each of which each of X carboxyl groups shuold be present provided that $\pi = 1$.

If a set $(x_1,\ldots,x_j,\ldots,x_\nu)$ is assigned to each model molecule in the mixture, the ϕ value for each molecule can be calculated by using eq(8.58) combined with eqs(8.7), (8.8) and (8.59); $E_j = x_j\varepsilon$. If the data for a large number of molecules with a constant π value

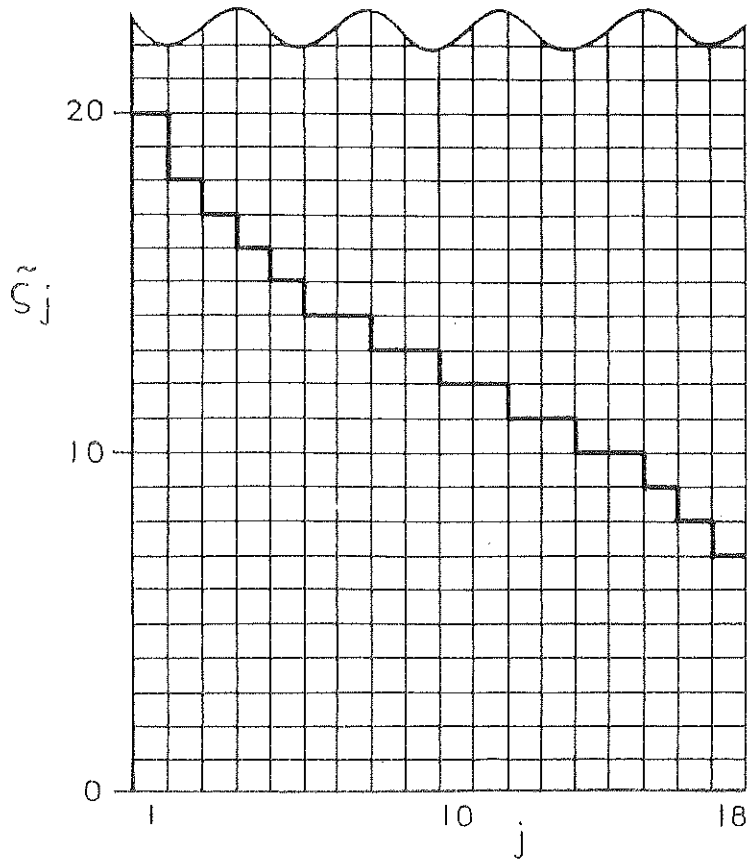


Fig A10.1. Abstract surface of collagen. For detail, see text. [Reproduced from ref (8.25) Fig 2.]

are accumulated, the distribution function $D(\phi)$ for that π value can be obtained. It should be noted that the above consideration is valid only when π has large enough values, and setting π to zero leads to the preliminary random model. This is because the total area of the domain where "corerect" elementary surfaces are present (the domain under the thick folded line in Fig A10.1) is much smaller than that of the other domain (the domain above the thick folded line in Fig A10.1). Each part of Fig 8.19 was calculated by accumulating 5000 model molecules [with $\nu=18$ and $\varepsilon=2.9$ kJ/mol ($e^{\varepsilon/kT}=3.6$)]; these were produced by the computer by using the Monte Carlo method.

(B) Some Comment

The consideration in Section(A) is done with reference to the experimantal data showing that the amino acid compositions of the α chains estimated from the amino acid analysis are similar to those deduced from the primary structures that have been "determined" by using the organochemical method(8.32, 8.35, 8.38-8.40). Unless a certain new mechanism of biosynthesis is hypothesized, however, it would be difficult to consider that the total number, X, of acidic amino residues (i.e., both glutamic and aspartic acid residues) on any molecular species of collagen is exactly constant (equal to 230) while giving rise to equivocal primary structures. Provided that the equivocal primary structures of the α peptides arise at a translational level of biosynthesis, the standard deviation for the fluctuation of the X values around the mean value of 230 can roughly be estimated. Preliminarily, let us examine the hypothetical case when the amino acids are chosen completely at random from the amino acid pool [presumably with a composition similar to that of the collagen molecule, not being so different from the amino acid composition of procollagen(A8.1)]. In this instance, the probability that X acidic amino acids are incorpolated into a collagen molecule (consisting of 3000 amino acid residues) should be $\binom{3000}{X}P^X(1-P)^{3000-X}$ forming a binomial distribution with respect to X where $P=230/3000=0.0767$. This can be replaced approximately by a Gaussian distribution with a standard deviataion equal to $[3000P(1-P)]^{1/2}\approx 14.6$, which is much smaller than the mean value, 230, of X. When acidic amino acids are incorporated into the "correct" positions on the α chains in probability $\pi=0.8$, it would be possible to consider in a rough manner that, beside the "corerect" incorpolation, the acidic amino acids are incorpolated into "incorrect" positions on the α chains in probability of $(1-\pi)P=0.2P=0.0153$ (instead of $P=0.0767$). This leads to a still smaller value of standard deviatioin for the fluctuation of X: $[3000(1-\pi)P\{1-(1-\pi)P\}]^{1/2}\approx 6.7$. [With respect to an individual α peptide, standard deviation for the fluctuation of the total number of acidic amino residues that are contained in it can be estimated approximately as $[1000(1-\pi)P\{1-(1-\pi)P\}]^{1/2}\approx 3.9$; this is because the difference in contents of the acidic amino residues between $\alpha 1$ and $\alpha 2$ chains is not so large(8.32, 8.34, 8.35, 8.38-8.40).]

The consideration performed in the preceding paragraph justifies the approximation us-

ed in Section(A) where the effect of the fluctuation of the X values is neglected. As suggested in ref(8.25), the fluctuation of the X values may be detectable by isoelectric focusing electrophoresis. A possibility exists, however, that the detection is disturbed by strong enough attractive interactions taking place between a sample macromolecule and ions from the buffer in such a way that the macromolecule behaves in association with a number of ions [cf. Chapter Ⅷ(F)].

Appendix XI. Theoretical Studies of Other Authors: Relationship with the Present Theory

(A) Isocratic Chromatography

The origin of chromatography goes back to the work of Tswett, the Russian investigator, of which the comprehensive review can be found in ref(A11.1). The theoretical investigation began with two different types of approach, the one originated by Wicke (A11.2), Wilson(A11.3), Weiss(A11.4) and DeVault(A11.5) [carried out on the basis of the concept of continuity of flow] and the other by Martin and Synge(A11.6) [carried out on the basis of a hypothesis that a chromatographic column is constructed from a series of theoretical plates, and that axial diffusion in the column is attributed to the height or thickness of each plate]. The first type prepares a basis of the present theory developed in this monograph. It will be understood below, however, that there is a fundamental difference in concept between classical and present theories. Thus, in the classical theory, although the concept of continuity of flow is used, what is emphasized is is the mass balance of molecules taking place among the sub-processes organizing the total process of chromatography. In contrast, in the present theory, the occurrences of several types of total molecular flow are emphasized, and attempt is made to find a first principle of chromatography in the presences themselves of plural types of total flow.

Investigations of Wilson and of Weiss. Wilson proposed a continuity equation of chromatogrphy (called as a mass balance equation by a number of authors) on the basis of the assumption that pointwise equilibrium between mobile and stationary phases are attained at any instant in the column, and that axial diffusion is absent in the column[ref(A11.3) eq(3)]. Wilson's equation virtually plays a role of the starting point of a series(A11.3-A11.5, A11.7, A11.8) of classical theories of isocratic chromatography developed nearly sixty five to fifty years ago by using continuity equations of flow (or mass balance equations). Wilson's equation succeeded by Weiss[ref(A11.4) eq(1)] can be reproduced with slight modofications as

$$\partial q/\partial v + \partial c/\partial x = 0 \qquad \text{(A11.1)}$$

in which c represents the concentration of sample molecules in the liquid phase (corresponding to C of our notation); q represents the amount of molecules adsorbed per unit length of the column (corresponding to $\gamma\chi$); and x represents the distance from the inlet of any position on the column (corresponding to L or L'/γ). What is questionable, however, is the quantity v representing the volume of the carrier liquid in some manner. Thus, eq(A11.1) can be rewritten by using our notations as

$$\partial\chi/\partial v + \partial C/\partial L' = 0 \qquad \text{(A11.1')}$$

Both eqs(2.2) and (2.4) show that $\chi=[(1-B^o)/B^o]C$ or that $C=[B^o/(1-B^o)]\chi$. Therefore, if v corresponds to V of our notation, then eq(A11.1') or (A11.1) is identical with

either eq(2.23) or (2.25) into which V and L' are substituted for $\hat{m}$ and s, respectively; only the case with linear adsorption isotherm is treated in this monograph. In both refs (A11.3, A11.4), it is the concept of Z rather than V that is assigned to v; the classical interpretation on eq(A11.1) should be modified.

In both refs(A11.3, A11.4), the case when the molecular solution injected into the column is developed isocratically by using another solvent is treated; this can be compared to the argument performed in Appendix IV.

Investigation of DeVault. DeVault's equation[ref(A11.5) eq(1)] is also based on the assumption of pointwise equilibria and no axial diffusion in the column; this can be reproduced as

$$\partial c/\partial x + \alpha\, \partial c/\partial V + \partial Q/\partial V = 0 \qquad \text{(A11.2)}$$

in which c, Q and x correspond to c, q and x in eq(A11.1), or C, $\gamma\chi$ and L'/γ of our notations, respectively; V and α correspond to Z and γ of our notations, respectively. Eq(A11.2) can be rewritten by using our notations as

$$\partial C/\partial L' + \partial C/\partial Z + \partial \chi/\partial Z = 0 \qquad \text{(A11.2')}$$

Due to both eqs(2.1) and (2.2), eq(A11.2') or (A11.2) is identical with eq(2.33) into which Z and L' are substituted for ξ and s, respectively; only the case with linear adsorption isotherm is treated in this monograph.

Investigation of Lapidus and Amundson. After several previous works had been done by other authors [for instances, see refs(A11.9, A11.10)], Lapidus and Amundson(A11.7) extended DeVault's equation[eq(A11.2)] to the equation dealing with the actual case when axial diffusion takes place in the column. The extended equations[ref(A11.7) eqs(1), (2) and (2')] can be reproduced as

$$D\partial^2 c/\partial z^2 = V\partial c/\partial z + \partial c/\partial t + (\partial n/\partial t)/\alpha \qquad \text{(A11.3)}$$

$$n = k_1 c + k_2 \qquad \text{(A11.4)}$$

and

$$\partial n/\partial t = k_1 c - k_2 n \qquad \text{(A11.5)}$$

respectively. The pair of eqs(A11.3) and (A11.4) treat the equilibrium case when poinwise equilibria are attained at any instant while giving rise to linear adsorption isotherm represented by eq(A11.4). The pair of eqs(A11.3) and (A11.5) treat the nonequilibrium case when the rate of mass transfer between liquid and solid phases is finite, following the first order kinetics represented by eq(A11.5).

In eq(A11.3), c (concentration of adsorbate in the fluid stream, moles per unit volume of solution) corresponds to C, and z (distance variable along the bed) corresponds to L or L'/γ of our notations. n represents the amount of adsorbate on the adsorbent (moles

per unit volume of bed as packed), and α represents the fractional void volume in the bed. Therefore, n/α corresponds to χ of our notation. Let us rewrite V (flow-rate) as u. t (time) should be called as proper time in our nomenclature, and t can be rewritten as $Z/(\gamma u)$ in our notations. Let us rewrite D (diffusion constant in the liquid phase expressed in units of length^2/time) as $u\bar{\theta}^\circ$ or $u\bar{\Theta}^\circ/\gamma$, where $\bar{\theta}^\circ$ (with dimension of length) or $\bar{\Theta}^\circ$ (with dimensions of volume) represent the diffusion constant of ordinary diffusion (induced by a combination of thermal Brownian motion of molecules and random motion of molecules brought about by flow heterogeneity). [See Chapter I (A), and cf. eq(A11.19) or (A11.19')]. Eq(A11.3) can be rewritten by using our notations as

$$\bar{\Theta}^\circ \partial^2 C/\partial L'^2 = \partial C/\partial L' + \partial C/\partial Z + \partial \chi/\partial Z \qquad \text{(A11.3')}$$

In the absence of diffusion when D or $\bar{\Theta}^\circ$ tends to zero, eq(A11.3') reduces to DeVault's equation, eq(A11.2').

In eq(A11.4), k_1 is a positive constant representing the slope of the adsorption isotherm, and it can be rewritten by using our notations as $\alpha(1-B^\circ)/B^\circ$, whereas the other constant k_2 can be considered to be equal to zero. Eq(A11.4) can be rewritten as

$$\chi = \frac{1-B^\circ}{B^\circ} C \qquad \text{(A11.4')}$$

Eq(A11.4') can also be derived from both eqs(2.2) and (2.4). With reference to eq(2.2), substitution of eq(A11.4') into eq(A11.3') leads to

$$\frac{\partial}{\partial L'}\left(B^\circ \Omega - \bar{\Theta}^\circ B^\circ \frac{\partial \Omega}{\partial L'} \right) + \frac{\partial \Omega}{\partial Z} = 0 \qquad \text{(A11.6)}$$

which is identical with eq(4.1') into which $\bar{\Theta}^\circ$ is substituted for Θ°. Eq(4.5) into which $\bar{\Theta}^\circ$, Z and L' are substituted for $g'\Theta^\circ$, ξ and s, respectively:

$$\Omega = G(L'; B^\circ Z, \sqrt{2\bar{\Theta}^\circ B^\circ Z}) \qquad \text{(A11.7)}$$

is a solution to eq(A11.6); this represents MB(o) taking place when its initial width is small. Corresponding to eq(4.8) combined with eq(4.10), CGM2nd can be derived from eq(A11.7); this can be written as

$$\begin{aligned} C &= G(Z; L'/B^\circ, \sqrt{2\bar{\Theta}^\circ L'}/B^\circ) \\ &= G(Z; \gamma L/B^\circ, \gamma\sqrt{2\bar{\theta}^\circ L}/B^\circ) \end{aligned} \qquad \text{(A11.8)}$$

In eq(A11.5), k_1 and k_2 represent rate constants of adsorption and desorption which we rewrite here as $\in \phi_{\mathrm{I}}$ and ϕ_{II}, respectively. ϕ_{I} and ϕ_{II} are related to mean time (to be precise, mean proper time) z_{I} and z_{II} necessary for the molecule to move from

mobile to stationary phase and from stationary to mobile phase [see Chapter I (A)] by

$$\phi_{I}/(\gamma u) = 1/z_{I} \tag{A11.9}$$

and

$$\phi_{II}/(\gamma u) = 1/z_{II} \tag{A11.10}$$

respectively. [*Note.* Eq(A11.9) is parallel to the second equation from the last in eq(1.58) into which $\epsilon/[(1-\epsilon)z_{PI}]$ is substituted for λ_{I} [see eq(1.43)], and eq(A11.10) is parallel to the last equation in eq(1.58) into which $\epsilon/[(1-\epsilon)z_{PII}]$ is substituted for λ_{II} [see eq (1.44)].] Eq(A11.5) can be rewritten as

$$\partial\chi/\partial Z = (\phi_{I}C-\phi_{II}\chi)/(\gamma u) = C/z_{I} - \chi/z_{II} \tag{A11.5'}$$

in which ϕ_{I} and ϕ_{II} are related to capacity ratio, k°, or molecular partition, B°, in the mobile phase (taking place provided that the equilibrium is attained) through

$$k^{\circ} = (1-B^{\circ})/B^{\circ} = \phi_{I}/\phi_{II} = z_{II}/z_{I} \tag{A11.11}$$

which is identical with eq(1.24). It should be noted that the meaning of relative rate, R_{F}, of migration is not assigned to B° now.

Investigation of van Deemter et al.. In the concept of partition chromatography [see Chapter I (A)], van Deemter et al. rewrote the nonequilibrium pair of Lapidus and Amundson's equations[eqs(A11.3) and (A11.5)] as a pair of eqs(29) and (30) in ref(A11.8); these can be reproduced as

$$F_{I}\partial c_{I}/\partial t = F_{I}D\partial^{2}c_{I}/\partial z^{2}-F_{I}u\partial c_{I}/\partial z+\alpha(Kc_{II}-c_{I}) \tag{A11.12}$$

and

$$F_{II}\partial c_{II}/\partial t = \alpha(c_{I}-Kc_{II}) \tag{A11.13}$$

In both eqs(A11.12) and (A11.13), z, t and D are identical with those appearing in both eqs(A11.3) and (A11.5), corresponding to L'/γ, $Z/(\gamma u)$ and $u\bar{\Theta}^{\circ}/\gamma$ of our notations, respectively. u [written as V in eq(A11.3)] corresponds to u of our notation. The subscript I and II stand for mobile and stationary phases, respectively. c_{I} and c_{II} represent molecular concentrations, and F_{I} and F_{II} represent volume fractions of the corresponding phases. $F_{I}c_{I}$ and $F_{II}c_{II}$ correspond to C and χ of our notations, respectively; this is because, in the concept of partition chromatography, C and χ stand for numbers of molecules in mobile and stationary phases per unit total volume (as a sum of volumes of both mobile and stationary phases), respectively. α (mass transfer coefficient per unit volume of packing) is related to ϕ_{I} of our notation through the correspondence of α/F_{I} to ϕ_{I}. K (distribution factor) represents the ratio, c_{I}/c_{II}, taking place, provided that the equilibrium is attained. Therefore, $\alpha K/F_{II}$ corresponds to ϕ_{II} of our notation, or K corresponds to $\phi_{II}F_{II}/(\phi_{I}F_{I})$ or $[B^{\circ}/(1-B^{\circ})]F_{II}/F_{I}$ [see eq(A11.11]. $\alpha(c_{I}-Kc_{II})$ corre-

sponds to $\phi_I C - \phi_{II} \chi$. It follows that the pair of eqs(A11.12) and (A11.13) are identical with the pair of eqs(A11.3') and (A11.5').

van Deemter et al.(A11.8) showed that the general solution [obtained originally by Lapidus and Amundson(A11.7)] of the pair of eqs(A11.12) and (A11.13) [i.e., the pair of eqs(A11.3') and (A11.5')] can be expressed approximately by using a Gauss function when a concentration pulse $c_0 t_0$ (where c_0=concentration in feed and t_0=sufficiently short duration of time i.e., proper time in our notation; $t_0 \to 0$) is injected into the column, provided that $z \gg 2D/u$ (i.e., $L \gg 2\bar{\theta}^\circ$ or $L' \gg 2\bar{\Theta}^\circ$) and that $z \gg F_I u/\alpha$ [i.e., $L \gg u/\phi_I = z_I/\gamma$ or $L' \gg \gamma u/\phi_I = z_I$; see ref(A11.8) Appendix]. The first condition indicates that the effect of the ordinary axial diffusion [induced by a combination of thermal Brownian motion of molecules and random motion of molecules brought about by flow heterogeneity; see Chapter I (A)] is small, provided that the column with large enough length is used (usual practice). The second indicates that the rate of mass transfer between mobile and stationary phases is high in comparison with the flow-rate [since when ϕ_I is large, then ϕ_{II} is large and vice versa for k° to be kept constant; see eq(A11.11)], or that the effect of the deviation from pointwise equilibrium is small, provided again that the column with large enough length is used. Later, an argument related to the above was done by Houghton (A11.11).

The Gauss function obtained in the preceding paragraph[eq(33) combined with three equations, eq(34), in ref(A11.8); representing CGM2nd] can be reproduced as

$$c_I/c_0 = \frac{\beta t_0}{\sqrt{2\pi(\sigma_1^2+\sigma_2^2)}} \exp\left(-\frac{(z/u-\beta t)^2}{2(\sigma_1^2+\sigma_2^2)}\right) \tag{A11.14}$$

with

$$1/\beta = 1 + F_{II}/(F_I K) \tag{A11.15}$$

$$\sigma_1^2 = 2Dz/u^3 \tag{A11.16}$$

and

$$\sigma_2^2 = 2\beta^2 F_{II}^2 z/(\alpha F_I K^2 u) \tag{A11.17}$$

As C of our notation is normalized with respect to Z ($=\gamma ut$), $c_I/(c_0 t_0 \gamma u)$ now corresponds to C [see eq(A11.14)]. As K corresponds to $[B^\circ/(1-B^\circ)]F_{II}/F_I$ (see above), eq (A11.15) can be rewritten as $\beta = B^\circ$. After some calculations, it can be shown that $\sigma_1^2 + \sigma_2^2 = 2L'[\bar{\Theta}^\circ + (1-B^\circ)^2 \gamma u/\phi_I]/(\gamma u)^2 = 2L'[\bar{\Theta}^\circ + (1-B^\circ)^2 z_I]/(\gamma u)^2$. Eq(A11.14) can be rewritten as

$$\begin{aligned} C &= G(Z;\ L'/B^\circ,\ \sqrt{2\Theta^\circ L'}/B^\circ) \\ &= G(Z;\ \gamma L/B^\circ,\ \gamma\sqrt{2\theta^\circ L}/B^\circ) \end{aligned} \tag{A11.18}$$

in which Θ° and θ° are defined as

$$\Theta^\circ = \bar{\Theta}^\circ + (1-B^\circ)^2\gamma u/\phi_I = \bar{\Theta}^\circ + B^\circ(1-B^\circ)\gamma u/\phi_{II}$$
$$= \bar{\Theta}^\circ + (1-B^\circ)^2 z_I = \bar{\Theta}^\circ + B^\circ(1-B^\circ)z_{II} \qquad \text{(A11.19)}$$

and

$$\theta^\circ = \bar{\theta}^\circ + (1-B^\circ)^2 u/\phi_I = \bar{\theta}^\circ + B^\circ(1-B^\circ)u/\phi_{II}$$
$$= \bar{\theta}^\circ + (1-B^\circ)^2 z_I/\gamma = \bar{\theta}^\circ + B^\circ(1-B^\circ)z_{II}/\gamma \qquad \text{(A11.19')}$$

respectively [cf. both eqs(4.8) and (4.10)]. Eq(A11.19) is identical with eq(1.33), and eq (A11.19) or (A11.19') show that diffusion coefficient, Θ° or θ°, for total diffusion can be represented as a sum of diffusion constant, $\bar{\Theta}^\circ$ or $\bar{\theta}^\circ$, for ordinary diffusion and diffusion coefficient, $(1-B^\circ)^2\gamma u/\phi_I = (1-B^\circ)^2 z_I$ [$=\bar{\bar{\Theta}}^\circ$; see eq(1.31)] or $(1-B^\circ)^2 u/\phi_I = (1-B^\circ)^2 z_I/\gamma$, for apparent diffusion; these can be re-expressed as $B^\circ(1-B^\circ)\gamma u/\phi_{II} = B^\circ(1-B^\circ)z_{II}$ [$=\bar{\bar{\Theta}}^\circ$; see eq(1.31)] and $B^\circ(1-B^\circ)u/\phi_{II} = B^\circ(1-B^\circ)z_{II}/\gamma$, respectively. It therefore is apparent that equilibrium is attained instantaneously at any slice of MB(o) migrating on the column despite the presence of RMT, and that molecular partition in the mobile phase takes place equally among all the slices of MB(o). When the rate of mass transfer between the two phases is extremely high in comparison with the flow-rate (i.e., when $\phi_I, \phi_{II} \gg u$), the diffusion coefficient for apparent diffusion vanishes, and Θ° or θ° coincides with $\bar{\Theta}^\circ$ or $\bar{\theta}^\circ$. It follows that eq(A11.18) coincides with eq(A11.8).

Due to eq(6.16), eq(A11.19) or (A11.19') is identical with ref(A11.8) eq(38); this can be reproduced as

$$H = 2D/u + \frac{2uF_I/\alpha}{(1+KF_{II}/F_I)^2} \qquad \text{(A11.20)}$$

in which $\hat{H}$ [height equivalent to a theoretical plate; for detail, see ref(A11.6)] is written as H; 2D/u (equal to $2\bar{\theta}^\circ$) is called as height of a mixing stage, and uF_I/α (equal to $u/\phi_I = z_I/\gamma$) as height of a mass transfer unit. Arguing in the other direction, the relationship between diffusion constant, θ°, and height equivalent to a theoretical plate, $\hat{H}$[eq (6.16)], can be obtained by comparing eq(A11.19') with eq(A11.20).

Theoretical plate number, N, can be represented in our notations as

$$N = L/\hat{H} = L/(2\theta^\circ) = L'/(2\Theta^\circ) \qquad \text{(A11.21)}$$

[for detail on theoretical plate number, see ref(A11.6)].

By substituting V+L' for Z into eq(A11.18) (representing CGM2nd), CGM1st:

$$C = G\left(V;\ \frac{1-B^\circ}{B^\circ}L',\ \sqrt{2\Theta^\circ L'}/B^\circ\right) \qquad \text{(A11.22)}$$

can be obtained. Eq(A11.22) can also be derived by substituting Θ°, V and L' for $g'\Theta^\circ$,

$\hat{m}$ and s into eq(4.15) combined with eq(4.10), respectively. Eq(A11.22) is a solution to

$$\frac{\partial}{\partial V}\left(\frac{1-B^{\circ}}{B^{\circ}}C-\frac{\Theta^{\circ}}{B^{\circ 2}}\cdot\frac{\partial C}{\partial V}\right)+\frac{\partial C}{\partial L'}=0 \qquad \text{(A11.23)}$$

Eq(A11.23) can be derived by substituting Θ°, V and L' for $g'\Theta^{\circ}$, $\hat{m}$ and s into eq(4.19), respectively.

In the arguments above (and in the argument below also), it is assumed that the molecular distribution C as a functionof Z or V obtained at a given position L' on the hypothetical column with infinite length(TPV) is identical with that obtained by using a column with length L'(EPV) [cf. ChapterIV(A)].

Several Versions. Sørensen derived the equation equivalent to eq(A11.20) by using another method[ref(A11.12) eq(32)]. A treatment intimately connected to those of Lapidus and Amundson(A11.7) and of van Deemter et al.(A11.8) was performed by Aris(A11.13) from a different viewpoint. The study on the broadening of MB(o) taking place, induced by RMT was also performed by Giddings and Eyring(A11.14) and by Giddings(A11.15,A11.16) on the basis of a stochastic consideration.

Investigations of Ku č era and of Kub í n. Below are presented the studies for the case when the packed particles in the column are porous, performed almost at the same time by Ku č era(A11.17) and by Kub í n(A11.18) independently by modifying a series of studies of Lapidus and Amundson(A11.7), and van Deemter et al.(A11.8). For convenience' sake, we first present the studies(A11.17,A11.18) while giving some modifications and using both system of units and notations applied in this monograph. A direct consideration on the original papers(A11.17,A11.18) will be done later. Thus, the fundamental simultaneous differential equations in a series of studies(A11.7,A11.8) can be rewritten as a pair of eqs (A11.3') and (A11.5') by using our system of units and notations. In refs(A11.17,A11.18), eq(A11.5') of the pair was replaced by a set of equations:

$$\frac{\partial \chi}{\partial Z}=\frac{3}{R}\cdot\frac{\bar{\Theta}^{\circ}_{P}}{\epsilon_{P}}\cdot\frac{\partial \chi_{P}}{\partial r}\Big|_{r=R} \qquad \text{(A11.24)}$$

$$\bar{\Theta}^{\circ}_{P}\frac{\partial \chi_{P}}{\partial r}\Big|_{r=R}=\omega\left(\frac{B^{\circ}_{P}(1-B^{\circ})}{B^{\circ}}C-\chi_{P}|_{r=R}\right) \qquad \text{(A11.25)}$$

$$\frac{\bar{\Theta}^{\circ}_{P}}{\epsilon_{P}}\left(\frac{\partial^{2}\chi_{P}}{\partial r^{2}}+\frac{2}{r}\cdot\frac{\partial \chi_{P}}{\partial r}\right)=\frac{\partial \chi_{P}}{\partial Z}+\frac{\partial \chi_{s}}{\partial Z} \qquad \text{(A11.26)}$$

and

$$\frac{\partial \chi_{s}}{\partial Z}=\lambda_{I}\chi_{P}-\lambda_{E}\chi_{s}$$

$$= \lambda_I \left(\chi_P - \frac{B^\circ_P}{1-B^\circ_P} \chi_s \right) = \lambda_{II} \left(\frac{1-B^\circ_P}{B^\circ_P} \chi_P - \chi_s \right) \qquad \text{(A11.27)}$$

where

$$\chi = \chi_P + \chi_s \qquad \text{(A11.28)}$$

and

$$\frac{\partial \chi_P}{\partial r}\Big|_{r=0} = 0 \qquad \text{(A11.29)}$$

In eqs(A11.24)-(A11.29), the case when the packed particles in the column are spherical in shape is treated, and the symbols used are common to those used in Chapter I (A) except for r, χ_P and χ_s. Thus, r represents the current radial coordinate being set in the packed particle in the column; r=0 and r=R at the center and the surface of the particle, respectively. χ_P and χ_s stand for the number of sample molecules that are present in solution inside the pores of the particles and the number of molecules that are adsorbed on the solid surfaces inside the pores per unit volume of column packing, respectively; eq(A11.28) holds.

In eq(A11.24), the term 3/R represents the surface to volume ratio of the sphere, and eq(A11.24) expresses the balance of the time change, $\partial \chi / \partial Z$, of total molecular density in the stationary phase with flux, $\bar{\Theta}^\circ_P \partial \chi_P / \partial r$, of molecules in solution inside the pore taking place at the border, r=R, to the outside. The reason why diffusion constant $\bar{\Theta}^\circ_P$ for diffusion taking place inside the pore is contained in the flux expression is that the flux under consideration occurs, induced by diffusion inside the pore. $\bar{\Theta}^\circ_P/\epsilon_P$ represents apparent diffusion constant occurring, provided that the inside of the packed particle has a uniform structure with absorbing property (in the absence of the concept of the pores). Eq(A11.25) expresses the balance between flux $\bar{\Theta}^\circ_P \partial \chi_P / \partial r$ and RMT type a taking place at border r=R, where it is important to point out that diffuson constant $\bar{\Theta}^\circ_P$ and rate constant ω are forming a quotient $\bar{\Theta}^\circ_P/\omega$ (or $\omega/\bar{\Theta}^\circ_P$) substantially (for this problem, see below). It should be recalled[Chapter I (A)] that rate constant ω represents the number of molecules passing in either direction over the wrapping film of RMT type a per unit time (to be precise, per unit proper time) per unit area of the sphere surface per unit mean molecular density inside the sphere. Eq(A11.26) expresses a type of Fick's second law for diffusion taking place inside the pore and playing a role of RMT type c. In the Laplacian, $\partial^2 \chi_P / \partial r^2 + (2/r) \partial \chi_P / \partial r$, appearing in eq(A11.26), the terms for diffusions in both azimuthal and zenithal directions are lacking because these effects should be canceled out due to symmetry of the sphere. Eq(A11.27) expresses the balance with RMT type b of the time change, $\partial \chi_s / \partial Z$, of molecular density on the solid surface inside the pore. Finally, eq(A11.29) arises from the consideration that flux, $\bar{\Theta}^\circ_P \partial \chi_P / \partial r$, of molecules in solution inside the pore should vanish at the center of pore due to symmetry of the sphere.

When a concentration pulse C_0Z_0 (where C_0=concentration in feed and Z_0=duration of proper time) is injected into the column, the initial and boundary conditions for a set of eqs(A11.3'), (A11.24)-(A11.29) can be written as

$$\left.\begin{array}{ll} C = 0 & (\text{for } Z \leqq 0) \\ \chi_P = 0 & (\text{for } Z \leqq 0) \\ C = C_0 & (\text{for } 0 < Z \leqq Z_0 \text{ and } L' = 0) \\ C = 0 & (\text{for } Z > Z_0 \text{ and } L' = 0) \end{array}\right\} \quad \text{and} \qquad \text{(A11.30)}$$

Although it is difficult to obtain an analytical solution for the system of eqs(A11.3'), (A11.24)-(A11.30), it is possible [cf. ref(A11.19)] to find an expansion of the solution as a function of Z for a fixed value of L', which we write C(Z). Thus, C(Z) can be expressed as

$$C(Z) = \exp\left(-\frac{(Z-\mu'_1)^2}{2\mu_2}\right) \sum_{n=0}^{\infty} a_n H_n\left(\frac{Z-\mu'_1}{\sqrt{2\mu_2}}\right) \qquad \text{(A11.31)}$$

in which $H_n(x)$ represents the Hermite polynomials defined as

$$H_n(x) \equiv (-1)^n \exp(x^2) d^n \exp(-x^2)/dx^n \qquad \text{(A11.32)}$$

or as

$$\left.\begin{array}{l} H_0(x) = 1 \\ H_1(x) = 2x \\ H_2(x) = 4x^2 - 2 \\ H_3(x) = 8x^3 - 12x \\ H_4(x) = 16x^4 - 48x^2 + 12 \\ \quad \cdots \end{array}\right\} \qquad \text{(A11.32')}$$

μ'_1 and μ_2 represent the first moment (i.e., the center of gravity) and the second moment around the first moment (i.e., the second central moment or variance) of function C(Z), respectively. As function C(Z) now is normalized, the k th moment, μ'_k (k=0,1,2, ...) can, in general, be defined as

$$\mu'_k = \int_{-\infty \text{ (or } 0)}^{\infty} Z^k C(Z) dZ \qquad \text{(A11.33)}$$

with

$$\mu'_0 = 1 \qquad \text{(A11.34)}$$

and the k th central moment, μ_k (k=0,1,2,...) can be defined as

$$\mu_k = \int_{-\infty\ (\text{or } 0)}^{\infty} (Z-\mu'_1)^k C(Z)dZ = \sum_{i=0}^{k} \binom{k}{i} (-\mu'_1)^i \mu'_{k-i} \qquad \text{(A11.35)}$$

In the above, the lower limit of integral, $-\infty$, can be replaced by 0 since, when $Z<0$, then $C(Z)=0$ in general [cf. the first equality in eq(A11.30)].

Due to the orthogonality of Hermite polynomials:

$$\int_{-\infty}^{\infty} H_n(x)H_m(x)\exp(-x^2)dx = \begin{cases} 0 & (\text{for } m\neq n) \\ 2^n n!\sqrt{\pi} & (\text{for } m=n) \end{cases} \qquad \text{(A11.36)}$$

the coefficient a_n in eq(A11.31) can be calculated as

$$a_n = \frac{1}{2^n n!\sqrt{2\pi\mu_2}} \int_{-\infty\ (\text{or } 0)}^{\infty} C(Z)H_n\left(\frac{Z-\mu'_1}{\sqrt{2\mu_2}}\right)dZ \qquad \text{(A11.37)}$$

This means that a_n can be expressed in terms of μ_2 and of other central moments μ_k with $k\leqq n$ [see eq(A11.32')] or moments μ'_k with $k\leqq n$ [see eq(A11.35)]. [For instances, $a_0=1/\sqrt{2\pi\mu_2}$, $a_1=a_2=0$, $a_3=[1/(2^2\cdot 3!\sqrt{\pi})]\cdot\mu_3/\mu_2^2$, $a_4=[1/(2^{5/2}\cdot 4!\sqrt{\pi\mu_2})]\cdot(\mu_4/\mu_2^2-3)$ etc. are obtained.]

On the other hand, by executing the Laplace transformation with respect to Z, the expression in the Laplace domain for the system of eqs(A11.3'), (A11.24)-(A11.30) can be obtained; these are soluble analytically with respect to the Laplace transformation of C(Z):

$$\check{C}(Y) = \int_0^{\infty} C(Z)e^{-YZ}dZ \qquad \text{(A11.38)}$$

[We do not here present the concrete expression for the analytical solution $\check{C}(Y)$ since it is much complicated. See ref(A11.17) eq(2) or (2a) accompanied with several equations.] Unfortunately, it still is difficult to carry out the inverse transformation of $\check{C}(Y)$ to find the analytical expression of C(Z). It, however, is possible to calculate moments μ'_k (k=0, 1,2,...) from $\check{C}(Y)$ by using the property of the Laplace transformation:

$$\mu'_k \equiv \int_0^\infty Z^k C(Z)dZ = (-1)^k \lim_{Y\to 0} d^k \tilde{C}(Y)/dY^k \qquad \text{(A11.39)}$$

It follows that μ_k (k=0,1,2...) can be calculated by using eq(A11.35).

The results of the calculations of μ'_1 (center of gravity) and μ_2 (variance) obtained when width, Z_0, of the initial concentration pulse is infinitesimal ($Z_0 \to 0$) are:

$$\mu'_1 = (L'+2\bar{\Theta}^\circ)/B^\circ \approx L'/B^\circ \qquad \text{(A11.40)}$$

($L' \gg 2\bar{\Theta}^\circ$) and

$$\begin{aligned}\mu_2 &= (2\bar{\Theta}^\circ L'+8\bar{\Theta}^{\circ 2})/B^{\circ 2} \\ &+ (2L'+4\bar{\Theta}^\circ)\frac{(1-B^\circ)\epsilon_P}{B^\circ_P B^\circ}\left(\frac{R}{3\omega}+\frac{R^2}{15\bar{\Theta}^\circ_P}+\frac{B^\circ_P(1-B^\circ_P)}{\lambda_{II}}\right) \\ &\approx 2\bar{\Theta}^\circ L'/B^{\circ 2} + 2L'\frac{(1-B^\circ)\epsilon_P}{B^\circ_P B^\circ}\left(\frac{R}{3\omega}+\frac{R^2}{15\bar{\Theta}^\circ_P}+\frac{B^\circ_P(1-B^\circ_P)}{\lambda_{II}}\right) \\ &= 2\bar{\Theta}^\circ L'/B^{\circ 2} + 2L'\left(\frac{1-B^\circ}{B^\circ}\right)^2\frac{\epsilon}{1-\epsilon}\left(\frac{R}{3\omega}+\frac{R^2}{15\bar{\Theta}^\circ_P}+\frac{B^\circ_P(1-B^\circ_P)}{\lambda_{II}}\right)\end{aligned} \qquad \text{(A11.41)}$$

($L' \gg 4\bar{\Theta}^\circ$). Eq(1.55) has been utilized for the derivation of the last term in eq(A11.41).

If it is admitted that function C(Z) (representing CGM2nd) is Gausian in shape virtually, C(Z) should coincide with C represented by eq(A11.18). This means that $(\sqrt{2\Theta^\circ L'}/B^\circ)^2 = \mu_2$ or that difusion coefficient Θ° can be represented as

$$\begin{aligned}\Theta^\circ &= \frac{B^{\circ 2}}{2L'}\mu_2 \left(= \frac{\mu_2}{2\mu'^2_1}L'\right) \\ &= \bar{\Theta}^\circ + (1-B^\circ)^2\frac{\epsilon}{1-\epsilon}\left(\frac{R}{3\omega}+\frac{R^2}{15\bar{\Theta}^\circ_P}+\frac{B^\circ_P(1-B^\circ_P)}{\lambda_{II}}\right)\end{aligned} \qquad \text{(A11.42)}$$

Eq(A11.42) is identical with eq(1.33) (the equality between first and fourth terms) combined with eqs(1.38'), (1.41), (1.42) and (1.45), and with eq(1.50) (the equality between first and fourth terms). [Actually, by comparing eq(A11.42) with eq(1.33) combined with eqs (1.38'), (1.41), (1.45) and (1.50), eq(1.42) has been obtained i.e., the parameter η has been evaluated.]

By using eq(1.8) into which I and x are substituted for R and $\hat{R}$, respectively, and also using eqs(1.58) and (1.63), eq(A11.42) can be rewritten as

$$\theta^\circ = \bar{\theta}^\circ + (1-B^\circ)^2 \frac{1}{\gamma} \cdot \frac{\epsilon}{1-\epsilon}\left(\frac{R}{3\omega} + \frac{R^2}{15\bar{\Theta}^\circ_P} + \frac{B^\circ_P(1-B^\circ_P)}{\lambda_{II}} \right)$$

$$= \bar{D}^\circ/u + (1-B^\circ)^2 u \frac{\epsilon}{1-\epsilon}\left(\frac{\hat{R}}{3k_f} + \frac{\hat{R}^2}{15\bar{D}^\circ_P} + \frac{B^\circ_P(1-B^\circ_P)}{v_{II}} \right) \qquad \text{(A11.42')}$$

Eq(A11.42') is identical with eq(1.33″) (the equality between left-hand side and middle terms) combined with eq(1.61) (the equality between left-hand side and middle terms).

In eq(A11.25), diffusion constant $\bar{\Theta}^\circ_P$ and rate constant ω are forming a quotient $\bar{\Theta}^\circ_P/\omega$ (or $\omega/\bar{\Theta}^\circ_P$) substantially. As long as the value of $\bar{\Theta}^\circ_P/\omega$ is kept constant, eq (A11.25) therefore corresponds to the phenomena taking place when $\bar{\Theta}^\circ_P$ is small in the same fashion as the correspondence to the phenomena taking place when $\bar{\Theta}^\circ_P$ is large. On the other hand, diffusion constant $\bar{\Theta}^\circ_P$ with a large enough value should induce a thermodynamic equilibrium inside the pore of the packed particle in the column. This means that a tacit assumption of thermodynamic equilibrium inside the pore resides behind eq(A11.25) even when $\bar{\Theta}^\circ_P$ is small, or that Approximation(a) or (b) used in the subsection entitled "Times z_I and z_{II} as Sums of Times of Stay at Different Resistances to Mass Transfer That Are Joined in Series" in Chapter I (A) is also used in eq(A11.25) tacitly. As a result, eq(A11.42) coincides with eq(1.33), or eq(A11.42') coincides with eq(1.33″); both eqs (1.33) and (1.33″) are accompanied with several equations (see above).

Consideration on the original papers of Kučera and of Kubín: Although almost the same investigations are done in both refs(A11.17) and (A11.18), the latter study is considerably simplified in comparison with the former. We here mainly refer to Kučera's paper(A11.17). Thus, in ref(A11.17), the set corresponding to the set of eqs(A11.3'), (A11.24)-(A11.27) are expressed in such a way that

$$\frac{\partial C'}{\partial t} + u\frac{\partial C'}{\partial L} - \bar{D}^\circ \frac{\partial^2 C'}{\partial L^2} = Q_c \qquad \text{(A11.43)}$$

$$Q_c = -\epsilon_P \frac{1-\epsilon}{\epsilon} \cdot \frac{3}{\hat{R}} D_r \frac{\partial c}{\partial f}\Big|_{f=R}$$

$$= -\frac{1-\epsilon}{\epsilon} \cdot \frac{3}{\hat{R}} D_r \frac{\partial(\epsilon_P c)}{\partial f}\Big|_{f=R} \qquad \text{(A11.44)}$$

$$Q_c = -H_c(C'-c|_{f=R}) \qquad \text{(A11.45)}$$

$$\frac{\partial c}{\partial t} - D_r\left(\frac{\partial^2 c}{\partial f^2} + \frac{2}{f} \cdot \frac{\partial c}{\partial f} \right) = Q_n = -\frac{\partial n}{\partial t} \qquad \text{(A11.46)}$$

and

$$Q_n = -H_n(K_n c - n) \qquad \text{(A11.47)}$$

Eq(A11.43) corresponds to the equation on page 237, and eqs(A11.44)-(A11.47) corre-

spond to the third, fifth, first and sixth equations on page 238 in ref(A11.17), respectively; the right-hand side of the third equation on page 238 in ref(A11.17) should be supplied with a minus sign. In eqs(A11.43)-(A11.47), the original symbols z, D_p, r, R, α and β are replaced by the symbols used in this monograph: L, $\bar{D}^\circ$, f, $\hat{R}$, ϵ and ϵ_p, respectively; the original symbol u is common to ours; symbol C is replaced by C' in order to distinguished it from symbol C used in this monograph; and symbols ν and K_c are replaced by 3 and 1, respectively (see below).

In eqs(A11.43)-(A11.47), t represents time (to be precise, proper time); C' represents the concentration of compound (sample molecule) in the free volume (mobile phase) given per unit free volume; c is the molecular concentration in the pores and n is the concentration of the sorbed molecules on the internal suerface of the pores, and both concentrations are given per unit volume of the pores; D_r is the apparent difusion constant for the flow of the compound inside the pores taking place in the direction normal to the external surface of the pores, expressed as if the inside of the packed particle had a uniform structure with absorbing property (in the absence of the concept of the pores; see below); K_n is an equilibrium constant; and H_c and H_n are mass transfer coefficients. In the original paper(A11.17), the term $3/\hat{R}$ [eq(A11.44)] and $2/f$ [eq(A11.46)] are written as $\nu/\hat{R}$ and $(\nu-1)/f$, respectively, and, when $\nu=1$, 2 and 3, then the packed particle in the column is interpreted to represent an infinite plate ($2\hat{R}$ showing the thickness of the plate), an infinite cylinder ($\hat{R}$ showing the radius of the cylinder) and a sphere, respectively. Also the term C' in eq(A11.45) is replaced by K_cC' in which K_c stands for another equilibrium constant. It can be considered, however, that $K_c=1$ when RMT type a taking place in the two opposite directions of the molecular flow are equal. It should be noted that, in eq(A11.44), the middle term can be rewritten as the right-hand side in which $\epsilon_p c$ represents the molecular concentration in the pores given *per unit volume of packed particle*, or the apparent molecular concentration inside the particle, expressed as if the inside of the particle had a uniform structure with absorbing property (see above). Thus, the right-hand side of eq(A11.44) is an expression in the absence of the concept of the pores.

In eq(A11.43), C' corresponds to C/ϵ of our notation, and Q_c has a meaning of $-[(1-\epsilon)/\epsilon]\partial\chi'/\partial t$ where χ' represents the molecular density in the stationary phase given per unit volume of stationary phase or packed particles in the vertical slice of the column. χ' is related to χ by $\chi'=\chi/(1-\epsilon)$; this means that Q_c corresponds to $-(\partial\chi/\partial t)/\epsilon$ of our notation. As $L=L'/\gamma$, $t=Z/(\gamma u)$ and $\bar{D}^\circ=u\bar{\Theta}^\circ/\gamma$ [see eqs (1.8), (1.9) and (1.58)], eq(A11.43) can be rewritten as eq(A11.3'). In both eqs(A11.44) and (A11.45), c corresponds to $\chi_p/[\epsilon_p(1-\epsilon)]$ and D_r corresponds to $\bar{D}^\circ_p/\epsilon_p = u\bar{\Theta}^\circ_p/(\gamma\epsilon_p)$ [see eq(1.58)] of our notations, respectively. As it can be considered that $H_c=[(1-\epsilon)/\epsilon]\cdot(3/\hat{R})k_f=\gamma u[(1-\epsilon)/\epsilon]\cdot(3/R)\omega$ [see eqs(1.8) and (1.58)], the pair of eqs (A11.44) and (A11.45) can be rewritten as eq(A11.25). In eq(A11.46), n corresponds to $\chi_s/[\epsilon_p(1-\epsilon)]$ of our notation. This means that eq(A11.46) can be rewritten as eq

(A11.26). Finally, in eq(A11.47), it can be considered that $K_n=(1-B^{\circ}_P)/B^{\circ}_P$ and that $H_n = v_{II}/\epsilon_P$. As $v_{II}=\gamma u \lambda_{II}$ [see eq(1.58)], by substituting $-\partial n/\partial t$ for Q_n [see eq (A11.46)], eq(A11.47) can be rewritten as eq(A11.27).

On the basis of eqs(A11.43)-(A11.47), corresponding to eqs(A11.40) and (A11.41), ref (A11.17) eqs(3b) and (3c) can be derived, respectively. These can be reproduced by using our notations as

$$\mu'_{K1} = \left(\frac{L}{u}+\frac{2\bar{D}^{\circ}}{u^2}\right)\cdot\left(1+\frac{B^{\circ}_P(1-B^{\circ})}{B^{\circ}}\left\{1+\frac{1-B^{\circ}_P}{B^{\circ}_P}\right\}\right)$$

$$= \left(\frac{L}{u}+\frac{2\bar{D}^{\circ}}{u^2}\right)\frac{1}{B^{\circ}} \approx \frac{L}{uB^{\circ}} \qquad \text{(A11.48)}$$

$(L \gg 2\bar{D}^{\circ}/u)$ and

$$\mu_{K2} = \left(\frac{2\bar{D}^{\circ}L}{u^3}+\frac{8\bar{D}^{\circ 2}}{u^4}\right)\cdot\left(1+\frac{B^{\circ}_P(1-B^{\circ})}{B^{\circ}}\left\{1+\frac{1-B^{\circ}_P}{B^{\circ}_P}\right\}\right)^2$$

$$+\left(\frac{2L}{u}+\frac{4\bar{D}^{\circ}}{u^2}\right)\frac{B^{\circ}_P(1-B^{\circ})}{B^{\circ}}\left(\frac{\hat{R}^2}{\bar{D}^{\circ}_P/\epsilon_P}\cdot\frac{1}{15}\left\{1+\frac{1-B^{\circ}_P}{B^{\circ}_P}\right\}^2\right.$$

$$+\frac{B^{\circ}_P(1-B^{\circ})}{B^{\circ}}\cdot\frac{B^{\circ}}{B^{\circ}_P(1-B^{\circ})}\cdot\frac{\hat{R}}{3}\cdot\frac{\epsilon_P}{k_f}\left\{1+\frac{1-B^{\circ}_P}{B^{\circ}_P}\right\}^2$$

$$\left.+\frac{1-B^{\circ}_P}{B^{\circ}_P}\cdot\frac{\epsilon_P}{v_{II}}\right)$$

$$= \left(\frac{2\bar{D}^{\circ}L}{u^3}+\frac{8\bar{D}^{\circ 2}}{u^4}\right)\frac{1}{B^{\circ 2}}$$

$$+\left(\frac{2L}{u}+\frac{4\bar{D}^{\circ}}{u^2}\right)\frac{(1-B^{\circ})\epsilon_P}{B^{\circ}_P B^{\circ}}\left(\frac{\hat{R}}{3k_f}+\frac{\hat{R}^2}{15\bar{D}^{\circ}_P}+\frac{B^{\circ}_P(1-B^{\circ}_P)}{v_{II}}\right)$$

$$\approx \frac{2\bar{D}^{\circ}L}{u^3B^{\circ 2}}+\frac{2L}{u}\left(\frac{1-B^{\circ}}{B^{\circ}}\right)^2\frac{\epsilon}{1-\epsilon}\left(\frac{\hat{R}}{3k_f}+\frac{\hat{R}^2}{15\bar{D}^{\circ}_P}+\frac{B^{\circ}_P(1-B^{\circ}_P)}{v_{II}}\right) \qquad \text{(A11.49)}$$

$(L \gg 4\bar{D}^{\circ}/u)$. In the original paper(A11.17), μ'_{K1} and μ_{K2} are written as μ'_1 and μ_2, respectively, and $\epsilon_P(1-\epsilon)/\epsilon$ is written as ε. As $\epsilon_P(1-\epsilon)/\epsilon = B^{\circ}_P(1-B^{\circ})/B^{\circ}$ [eq(1.55)], ε in ref(A11.17) is rewritten as $B^{\circ}_P(1-B^{\circ})/B^{\circ}$ in both eqs(A11.48) and (A11.49). For the derivation of the last term in eq(A11.49) also, eq(1.55) has been utilized [cf. eq(A11.41)]. As $\mu'_{K1}=\mu'_1/(\gamma u)$ and $\mu_{K2}=\mu_2/(\gamma u)^2$, eqs(A11.48) and (A11.49) are identical with eqs (A11.40) and (A11.41), respectively [cf. eqs(1.8), (1.9) and (1.58)].

In Kubín's paper(A11.18), the case when all RMT type a, b and c vanish is examined. In this instance, it is possible to carry out the inverse transformation of $\check{C}(Y)$ [eq (A11.38)] to obtain the analytical expression of C(Z) [ref(A11.18) eq(18a)]; this is identical

with eq(4.6) into which L', Z and Θ° are substituted for s, ξ and $g'\Theta^\circ$, respectively, and $\bar{\Theta}^\circ$ is substituted for Θ° again.

Versions and Relevant Studies. A number of versions of refs(A11.17, A11.18) are published[e.g., refs(A11.20)-(A11.23)], and relevant semi-empirical studies are done by a number of authors[e.g., refs(10.19, A11.24, A11.25)].

Supplement. In ref(A11.26), the theoretical studies of isocratic chromatographies developed by a number of authors are reviewed from another viewpoint with references to a number of original papers that are not cited above. Studies on overload chromatography in which account is taken of mutual interactions among sample molecules [cf. Chapter Ⅷ(F)] originate in the classical papers(A11.3-A11.5). Typical studies treating this problem can be found in refs(A11.26-A11.29).

(B) Gradient Chromatography

Concentration gradient chromatography was originally introduced by the Tiselius' group(A11.30, A11.31), Donaldson et al.(A11.32), and Busch et al.(A11.33). A report on the chromatography carried out by using a gradient in the solid phase can be found in the paper of Stahl(A11.34). It is rare, however, that the gradient in the solid phase is used in practice. [In connection, it should be noted that a column packed with particles the surface of which was modified by a polymer with a temperature dependent conformation was developed recently; the affinity of hydrophobic molecules for the polymer increased with an increasing temperature due to a change in the polymer conformation(A11.35). It was reported(A11.36, A11.37) that good chromatographic separations of steroids etc. were achieved by decreasing gradually the temperature of the oven in which the column was set i.e., by applying the second type of gradient [see Chapter I (A)]. If a duration of time is needed for the oven temperature to be transmitted to the interior of the column, however, a gradient in the solid phase can be anticipated to be made at the same time. Especially if the oven temperature is kept constant, only the gradient in the solid phase would be realized.

Investigations of Drake and of Freiling. The first theoretical investigations on concentration gradient chromatography can be found in the paper of Drake(A11.38) and the papers of Freiling(A11.39, A11.40). In ref(A11.38), chromatographies carried out by using concentration gradients of substances with linear and nonlinear adsorption isotherms were investigated theoretically for model sample molecules with linear and nonlinear adsorption isotherms. The concept, w, of "corrected volume" introduced in ref(A11.38) corresponds to our concept, V, of "time" or "elution volume" as far as the concentration gradient with a linear adsorption isotherm is concerned involving the case when the adsorption of the gradient substance on the adsorbent surface does not take place at all. Ref(A11.38) eq(5):

$$v = w + \frac{v_{0,s}h}{h_0}(1+Q\alpha_s) \qquad \text{(A11.50)}$$

(in which v, w and $v_{0,s}h/h_0$ correspond to Z, V and L' of our notations, respectively, and where $Q\alpha_g$ represents the capacity ratio with respect to the gradient substance) coincides with eq(2.3) when $Q\alpha_g$ tends to zero i.e., when the adsorption of the gradient substance on the adsorbent surface does not take place at all. It should be noted, however, that the concentration gradient of the substance which is unadsorbable on the adsorbent surface usually is not used in practice (at least when the competition mechanism takes place; cf. Chapter Ⅷ-X). It can usually be assumed that the adsorption of the gradient substance does occur but that there is an upper limit of the amount of the substance that can be asorbed per unit area of the adsorbent surface; concentration, m, in solution of the gradient substance is high enough for the majority of the substances to be in solution or the liquid phase except just at the beginning of the concentration gradient [see Chapter Ⅲ(A)]. In this instance, it is apparent that the gradient substance is not adsorbed at all except at the beginning of the concentration gradient, thus giving rise to the coincidence of eq(A11.50) (in which $Q\alpha_g=0$) with eq(2.3).

Ref(A11.38) eq(18) taking place when the adsorption isotherm of the sample molecule is linear and when the gradient substance is (apparently; see above) unadsorbable on the adsorbent surface ($Q\alpha_g=0$) can be reproduced when $w_1=0$ as

$$\Delta h_1 = \frac{h_0}{v_{0,s}Q}\int_0^{w_2}\frac{dw}{\alpha_1[c_g(w)]} \qquad (A11.51)$$

in which $v_{0,s}\Delta h_1/h_0$, w, w_2 and and $Q\alpha_1[c_g(w)]$ correspond to L', V, $\dot{V}$ and $k'(g'V)\equiv[1-B'(g'V)]/B'(g'V)$ of our notations; $g'V=\hat{m}$ [eq(2.6) or (6.3)] and $g'\dot{V}=\hat{\mu}$ [eq(6.10)]. Let us rewrite k'(g'V) and B'(g'V) *symbolically* as k'(V) and B'(V), respectively. Eq (A11.51) can now be re-expressed as

$$L' = \int_0^{\dot{V}} dV/k'(V) \equiv \int_0^{\dot{V}} \frac{B'(V)}{1-B'(V)}dV \qquad (A11.51')$$

which is identical with eq(6.7) into which V, $\dot{V}$ and B'(V) are substituted for $\hat{m}$, $\hat{\mu}$ and $B'(\hat{m})$, respectively.

A qualitative study of the width of MB(o) migrating on the column was done in ref (A11.38) by using the "working-isotherm" concept. Further, the demixing of the gradient substance taking place at the beginning of the concentration gradient [cf. Chapter Ⅲ(A)] was argued briefly in ref(A11.38) Fig 2 for the case when the adsorption isotherm of the gradient substance is of the Langmuir type. Recently, the demixing problem was treated in detail by Velayudhan and Ladisch(A11.41).

In refs(A11.39, A11.40) also, the concept corresponding to our concept of V was attained, and the equation equivalent to eq(A11.51') was derived for the case when the ad-

sorption isotherm of the sample molecule is linear[ref(A11.39) eq(4) and ref(A11.40) eq(1)]; for the derivation of the equation, it was considered that a continuous concentration gradient represents a limit of an infinite number of infinitesimal steps, and account was not taken of the adsorption of the gradient substance on the adsorbent surface. In refs (A11.39, A11.40), some arguments with respect to the width of MB(o) are involved. In contrast to the treatment in ref(A11.38), the arguments in refs(A11.39, A11.40) are partially based on the theoretical plate concept [cf. Section(A)].

Eq(A11.51') (derived nearly fifty years ago by the two authors) can be compared with the prototype, eq(6.36), of eq(6.7) [derived about thirty years ago by Kawasaki; see Chapter VI(D)]. Thus, whereas eq(A11.51') represents *only one relationship* between $\dot{V}$ and L' taking place when both shape ϕ [cf. eqs(6.18)-(6.20)] and steepness g' of the concentration gradient are given arbitrarily, eq(6.36) [combined with eq(6.2), eq(3.1) into which μ, β and $\dot{V}$ are substituted for m, $\hat{m}$ and V, respectively, and eq(6.18) into which β is substituted for $\hat{m}$] represents *an assembly of relationships* between $\dot{V}$ and L' obtained for an assembly of g' values but only for linear concentration gradients. Eq(6.7) [combined with both eqs(6.2) and (3.1) into which μ, β and $\dot{V}$ are substituted for m, $\hat{m}$ and V, respectively] is a unified expression involving both eqs(A11.51') and (6.36). Moreover, eq(6.7) represents a special case of eq(3.6') or (3.6) [into which β and $\hat{s}$ are substituted for $\hat{m}$ and s, respectively; for $\hat{s}$, see Chapter IV(B) and V(A)]; eq(3.6') or (3.6) is valid for the general case when both the gradient in the liquid phase (i.e., the concentration gradient) and the gradient in the solid phase are applied at the same time.

The fundamental theories(A11.38-A11.40) were succeeded by several authors involving Said(A11.42), Schwab et al.(A11.43), the Snyder's group(A11.44)-(A11.48), Jandera and Churá č ek(A11.49), Jandera et al.(A11.50), Pitt(A11.51), and Poppe et al.(A11.52). Eq (A11.51') is appearing in most of these papers while changing its expression slightly, and it plays a central role of the theories [see the equation just below eq(10) in ref(A11.42), ref(A11.43) eq(9), ref(A11.44) eq(8), ref(A11.45) eq(3), ref(A11.46) eq(9), ref(A11.47) Appendix I eq(i-1), ref(A11.48) eqs(9) and (9a), ref(A11.49) eq(8), and ref(A11.52) eq(14)]. The investigations performed by Pitt(A11.51), the Snyder's group(A11.44-A11.48), Poppe et al.(A11.52), and Jandera et al.(A11.49, A11.50) are reconsidered below in our own viewpoint, respectively.

Investigation of Pitt. Attempt(A11.51) was made to extend the treatment of van Deemter et al.[ref(A11.8); cf. eqs(A11.12)-(A11.20)] to the case of concentration gradient chromatography, and to calculate the chromatogram taking place in the presence of the concentration gradient [which corresponds to the chromatogram represented by eq(A11.14) or (A11.18) with the isocratic case] by using the computer.

The starting partial differential equation, ref(A11.51) eq(8), can be reproduced as

$$\frac{\partial(\alpha c)}{\partial t} + u_0 \frac{\partial c}{\partial z} = \left(D_m \varepsilon + \frac{u_0^2}{\alpha^2} \cdot \frac{k_A}{k_D^2} \right) \frac{\partial^2 c}{\partial z^2} \qquad \text{(A11.52)}$$

in which

$$\alpha = k_A/k_D + \varepsilon \tag{A11.53}$$

and

$$u_0 = \varepsilon u \tag{A11.54}$$

In eqs(A11.52)-(A11.54), c (bulk concentration of sample molecules in the fluid phase) correspond to C, t (time i.e., proper time in our nomenclature) to $Z/(\gamma u)$, z (distance from the inlet of the column) to L or L'/γ, u (average interstitial fluid velocity) to u, D_z (axial diffusivity) to $u\bar{\Theta}^\circ/\gamma$, and ε (externl void fraction of the bed) to ϵ of our notations, respectively. As in both eqs(A11.5') and (A11.11), let us rewrite k_A (rate coefficient for adsorption) and k_D (rate coefficient for desorption) as $\epsilon\,\phi_I$ and ϕ_{II}, respectively; ϕ_I and ϕ_{II} are related to k and B as

$$k = (1-B)/B = \phi_I/\phi_{II} \tag{A11.55}$$

[cf. eq(A11.11)]. It follows that $k_A/(\varepsilon k_D)$ corresponds to k or $(1-B)/B$ and that α/ε corresponds to $1/B$ of our notations, respectively. Eq(A11.52) can be rewritten by using our notations as

$$\frac{\partial (C/B)}{\partial Z} + \frac{\partial C}{\partial L'} = \left(\bar{\Theta}^\circ + \frac{B(1-B)\gamma u}{\phi_{II}} \right) \frac{\partial^2 C}{\partial L'^2} \tag{A11.52'}$$

where it should be noted that B is a function of both Z and L'. It should also be noted that B represents partition of molecules in the mobile phase taking place, provided that the equilibrium is attained; the meaning of relative rate, R_F, of migration is not assigned to B.

Let us first examine the isocratic case as a special case. In eq(A11.52'), the function B can be replaced by a constant B°. The terms in large parentheses in the right-hand side of eq(A11.52') can be rewritten simply as Θ° since they now coincide with the third term in eq(A11.19). Further, C can be rewritten as $B^\circ\Omega$, and eq(11.52') coincides with eq(4.1'). It should be recalled that eq(4.1) leads to eq(4.8) representing CGM2nd. In the same manner, eq(4.1') or eq(A11.52') into which B° is substituted for B leads to eq (A11.18) or (A11.14) representing the theoretical chromatogram derived originally by van Deemter et al.(A11.8).

Let us return to concentration gradient chromatography. When ϕ_{II}/u approaches infinity (while keeping B constant) i.e., when RMT vanishes, then the second term in large parentheses in the right-hand side of eq(A11.52') vanishes. Further C can be rewritten as $B\Omega$, and eq(A11.52') becomes

$$\partial\Omega/\partial Z + \partial(B\Omega)/\partial L' = \bar{\Theta}^\circ \partial^2(B\Omega)/\partial L'^2 \tag{A11.56}$$

The argument below is done for the purpose of comparing eq(A11.56) with eq(5.1). For

this purpose, we define the mean position of MB(o) migrating on the column as position superposed on the position of the ideal MB(o) with an infinitesimal width which would take place provided that there is no axial diffusion in the column. It is possible to consider that molecular partition, B, taking place at the mean position of the actual MB(o) is a function of Z (=V+L') because molecular partition B taking place in the ideal MB(o) with infinitesimal width is a function of ξ (=$\hat{m}$+s) [if the column is equipped with coordinate s; cf. both eqs(3.7) and (3.6')]. Let us denote B as a function of Z by $\hat{B}(Z)$ *symbolically* [cf. the symbol B'(V) in eq(A11.51')]. Actually when MB(o) with a very small width is formed initially at the inlet of the column and when the width of MB(o) migrating on the column is also small enough because of the small $\bar{\Theta}^\circ$ value, then it would be possible to consider that molecular partition B taking place at any position within MB(o) is virtualy equal to molecular partition $\hat{B}(Z)$ taking place at the mean position of MB(o). In the usual experimental condition as such, it appears to be possible to replace B by $\hat{B}(Z)$ in eq(A11.56) thus leading to

$$\frac{\partial}{\partial L'}\left(\hat{B}(Z)\Omega - \bar{\Theta}^\circ \hat{B}(Z) \frac{\partial \Omega}{\partial L'} \right) + \frac{\partial \Omega}{\partial Z} = 0 \qquad \text{(A11.57)}$$

It should be noted, however, that the description of the "compression of band" effect is deprived of eq(A11.57), caused by the replacement of B by $\hat{B}(Z)$. Substituting s, ξ and $g'\bar{\Theta}^\circ$ for L', Z and $\bar{\Theta}^\circ$ into eq(A11.57), respectively, and writing $\hat{B}(\xi)$ for $\hat{B}(Z)$

$$\text{div.}\,[\hat{B}(\xi)\Omega - g'\bar{\Theta}^\circ \hat{B}(\xi)\,\text{grad.}\,\Omega] + \partial\Omega/\partial\xi = 0 \qquad \text{(A11.58)}$$

is obtained. Eq(A11.58) is identical with eq(5.1) except for the fact that $\hat{\Theta}(\xi)$ is replaced by $\bar{\Theta}^\circ$. Function $\hat{\Theta}(\xi)$ is approximately identical with function $\Theta(s)$[eq(5.9)], and function $\Theta(s)$ now arises from the balance between axial diffusion and compression of band taking place in the column [see Chapter V(C)]. Thus, in eq(5.1), the deprived description of the "compression of band" effect is compensated by the replacement of $\bar{\Theta}^\circ$ by $\hat{\Theta}(\xi)$. [*Note.* On calculating $\Theta(s)$, the approximation of the displacement of Θ° [eq(1.33)] by a mean value of Θ° taking place in the whole process of chromatography is used; see the subsection entitled "Quasi-Static Chromatography versus Nonequilibrium Thermodynamics" in Chapter I (A). It is the concept of the mean value of Θ° rather than the value obtained when RMT vanishes that now corresponds to the concept of $\bar{\Theta}^\circ$.]

The standard deviation, $\sqrt{2\Theta^\circ L'}/B^\circ$, of the isocratic chromatogram represented by eq(A11.18) is proportional to the square-root of the total length, L', of the column used. In ref(A11.51) eq(18) or (19), the same situation is translated in such a way that the variance (denoted by σ^2) of the chromatogram as a function of dimensionless effluent column volume (denoted by τ) is inversely proportional to the total length (denoted by Z) of the column used. The numerical calculation in ref(A11.51) shows that the inverse relationship between σ^2 and Z holds even in the presence of the concentration gradient [see ref

(A11.51) Fig 5]. With reference to Appendix VI Fig A6.5 or A6.6, it is probable that the calculation in ref(A11.51) was performed in experimental conditions where total column length L' (in our notation) is large enough for a given value of g'. In these conditions, the standard deviation σ or τ (in our notations) increases with increase in L' at a rate of the order of the square-root of L' (see Appendix VI Fig A6.5 or A6.6 where it should be noted that the increase of σ or τ with increase in L' takes place outside the figure frame when g' is small). This means that, in notations in ref(A11.51), σ^2 decreases with increase in Z, or that the inverse relationship between σ^2 and Z takes place.

Investigation of the Snyder's Group. In his early study, Snyder(A11.45) attempted to estimate four times the standard deviation (in units of volume; denoted by w_i) of the Gaussian chromatogram with concentration gradient chromatography [taking place when MB(o) with a small width is formed initially at the inlet of the column] by extending the expression obtained for the isocratic case; the expression for the isocratic case, ref (A11.45) eq(2), can be reproduced as

$$w_i = 4R_i/\sqrt{p} \qquad \text{(A11.59)}$$

in which retention volume R_i is defined by ref(A11.45) eq(1) as

$$R_i = K_iW + V^\circ \qquad \text{(A11.60)}$$

In eqs(A11.59) and (A11.60), V° (total quantity of moving phase contained within the column, in units of volume) corresponds to L'; K_i (distribution coefficient for equilibrium partitioning between stationary and mobile phases) corresponds to $k^\circ L'/W$ with W representing the total quantity of stationary phase contained within the column, in unit of mass; and p (theoretical plate number) corresponds to $N=L'/(2\Theta^\circ)$ [see eq(A11.21)] of our notations, respectively. Writing τ for $w_i/4$, eq(A11.59) can be re-expressed as $\tau = \sqrt{2\Theta^\circ L'/B^\circ}$ which coincides with the expression of the standard deviation in eq(A11.18) or (A11.22); eq(A11.22) can be derived by substituting V, L' and Θ° for $\hat{m}$, s and $g'\Theta^\circ$ into eq(4.15) combined with eq(4.10), respectively.

Snyder(A11.45) considered that, with concentration gradient chromatography, R_i can be replaced by the effective or instntaneous value, R_t, of R_i taking place when molecules leave the column at the outlet, and that K_i can be replaced by the value taking place when $R_i=R_t$. He also assumed(A11.45) that R_i and K_i are approximately constant during the time when the elution of MB(o) from the column is being performed. Thus, eq(A11.59) can be modified to ref(A11.45) eq(11):

$$w_i = 4R_t/\sqrt{p} \qquad \text{(A11.61)}$$

which can be rewritten by using our notations as

$$\tau = \sqrt{2\Theta^{\circ}L'}\ /B'[\dot{V}(L')] \qquad \text{(A11.61')}$$

In eq(A11.61'), $\dot{V}$ represents the elution volume taking place at the center of MB(o) as a function of total length, L', of the column used, which can be defined implicitly by eq (A11.51'). Due to the assumption, molecular partition, $B'[\dot{V}(L')]$, in the mobile phase taking place at the center of MB(o) just prior to elution is virtually equal to that taking place at any part of MB(o) just prior to elution. With reference to ref(A11.45) eq(3) which is identical with eq(A11.61'), the theoretical chromatogram obtained in ref(A11.45) can be represented by using our notations as

$$C = G(V;\ \dot{V},\ \tau) \qquad \text{(A11.62)}$$

in which $\dot{V}$ and τ are defined as functions of L' by eqs(A11.51') and (A11.61'), respectively; eq(A11.62) can be compared with eq(A11.22). It should be noted that eq(A11.61') is equivalent with eq(6.39) when concentration gradint applied is linear. When $\Theta^{\circ}=\bar{\Theta}^{\circ}$ [cf. eq(A11.19)], eq(A11.62) is a solution to eq(6.41) into which V, L', Θ $(=\bar{\Theta}^{\circ})$ and $B'[\dot{V}(L')]$ are substituted for m, s, $g'\Theta^{*}$ and $B''(s)$, respectively; $B''(s)=B'[\mu(s)]=B'[\phi^{-1}\{\mu(s)\}]$ [cf. eqs(3.1), (5.14) and (5.14')].

In eq(A11.61) or (A11.61'), account is not taken of the "compression of band" effect. Snyder et al.(A11.47) modified eq(A11.61) by multiplying it by a band compression factor, G, leading to ref(A11.47) eq(5):

$$\sigma_t = (1+k_f)\,\sigma_x G t_0/L \qquad \text{(A11.63)}$$

The physical meanings of the symbols in eq(A11.63) are: σ_t=standard deviation of the chromatogram (in unit of time); σ_x=standard deviation of MB(o) taking place just prior to elution (in unit of length); k_f=value of capacity ratio for MB(o) at the moment when it leaves the column [which is assumed to be the same for any part of MB(o)]; t_0=column dead time (in unit of time); and L=column length (in unit of length). It is evident that eq(A11.63) can be translated to eq(A11.61) the right-hand side of which is multiplied by G, or, by using our notations, to

$$\tau = \sqrt{2\Theta^{\circ}L'}\ \Gamma/B'[\dot{V}(L')] \qquad \text{(A11.64)}$$

in which G is rewritten as Γ [cf. eq(A11.61')]. A method for the numericl calculation of G i.e., Γ was developed in ref(A11.46) by considering that a continuous concentration gradient represents a limit of an infinite number of infinitesimal steps.

Snyder et al.(A11.44-A11.48) called as linear solvent strength(LSS) gradient the concentration gradient formed in such a way that the logarithm of *potential* capacity ratio, k_i, at the inlet of the column (which would be realized, provided that sample molecules are

present at the column inlet always) decreases linearly with increase in volume (denoted by V) of mobile phase eluted from the column after sample injection or the simultaneous start of concentration gradient. When the total volume of mobile phase contained within the column is V_m, LSS gradient can be represented by ref(A11.47) Appendix I eq(i-3) as

$$\log_{10} k_i = \log_{10} k_0 - bV/V_m \qquad (A11.65)$$

in which k_0 and b are positive constants, and V, V_m and k_0 correspond to Z, L' and k_o of our notations, respectively. Eq(A11.65) can be rewritten as

$$\log_{10} k_i = \log_{10} k_o - bZ/L' \qquad (A11.65')$$

It should be noted that b measures the steepness of the concentration gradient used for the column with length L'. [b is proportional to s i.e., the product by g' of L'; see eqs (A11.71) and (A11.71') below.]

With LSS gradient chromatogrphy, capacity ratio k'(V) [$\equiv$(1−B'(V))/B'(V)] taking place at the center of MB(o) migrating on the column [provided that the initial width of MB(o) is very small] fulfills eq(A11.65') into which V and k'(V) are substituted for Z and k_i, respectively:

$$\log_{10} k'(V) = \log_{10} k_o - bV/L' \qquad (A11.66)$$

in which V represents the volume of the carrier liquid that has passed the center of MB(o) since the beginning of the migration on the column, and L' now has a physical meaning of the sum of interstitial volumes inserted between the position at the center of MB(o) and the column inlet.

Proof of eq(A11.66). Fig A11.1 illustrates schematically the migration of LSS gradient through a column with length L', where the symbol L' is used to represent not only the length of the actual column but also the current coordinate on the hypothetical column with infinite length; the actual column is part [0, L'] of the hypothetical column. In Fig A11.1, three oblique straight lines on the (L', $\log_{10}$ k) plane represent LSS gradients taking place at proper time or proper elution volume Z=0 (left straight line), Z=L' (middle straight line) and Z>L' (right straight line); k, k_i, k'(V) and k_o stand for potential capacity ratios which would take place provided that sample molecules are present. Z is related to time or elution volume V by eq(2.3) as Z=V+L'. The right oblique straight line drawn in Fig A11.1 shows that, when $\log_{10} k_o - \log_{10} k_i$ (Z>L')=bZ/L' [eq(A11.65')], then $\log_{10} k_o - \log_{10} k'(V>0)$=bV/L' [eq(A11.66)] and vice versa. This general statement is true involving the special case when the center of MB(o) is present just at the outlet of the column with length L' (EPV) or when the center of MB(o) is present at position L' on the hypothetical column with infinite length (TPV). In TPV, V represents the volume of the carrier liquid that has passed the center of MB(o) since the beginning of the migration on the column. It should be noted, however, that this special case is not illustrated in Fig A11.1 quantitatively. Thus, the proportion between the magnitudes of V and

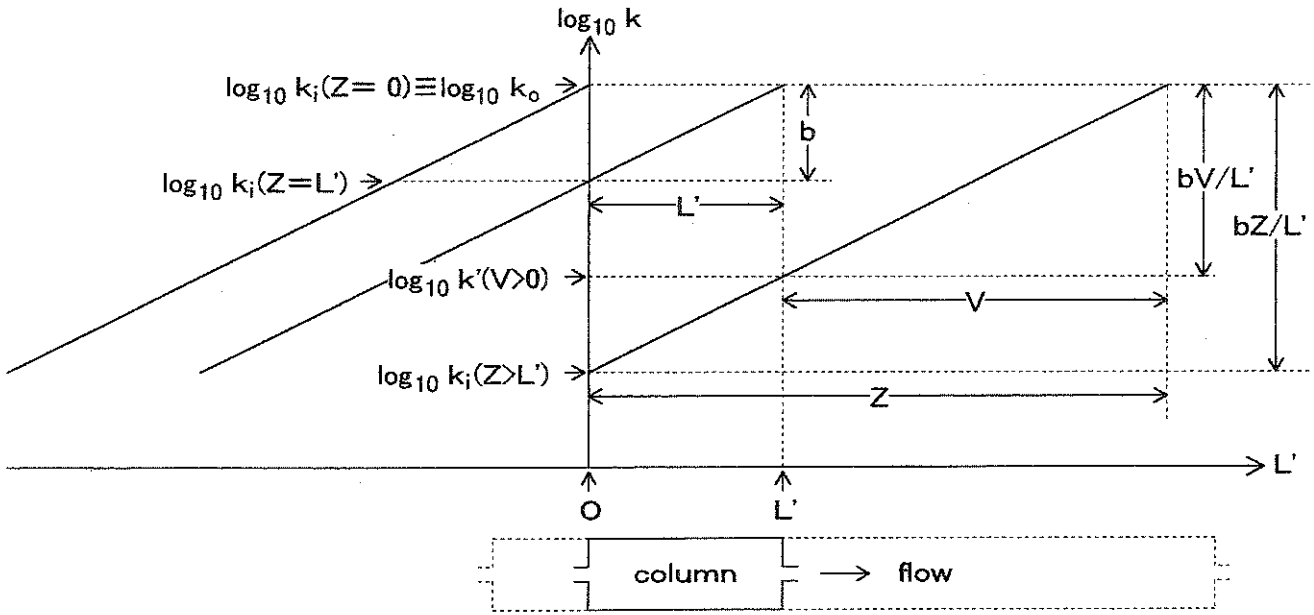


Fig A11.1. Migration of LSS gradient through a column with length L'. For detail, see text.

Z such as associated to the right oblique straight line does not take place in this special case. *Q.E.D.*

It was shown(A11.47, A11.48) that, with LSS gradient chromatography, the instantaneous value (denoted by k_f) of the capacity ratio for the band maximum [center of MB(o)] at the moment when it leaves the column can be represented by ref(A11.47) eq(6) as

$$k_f = 1/[(\ln 10)b + 1/k_0] \tag{A11.67}$$

As k_f and k_0 correspond $k'(\dot{V})$ [cf. eq(A11.51')] and k_o of our notations, eq(A11.67) can be rewritten as

$$k'(\dot{V}) = 1/[(\ln 10)b + 1/k_o] \tag{A11.67'}$$

which can be derived by substituting eq(A11.66) into eq(A11.51') and by executing the integration.

Snyder et al.(A11.47, A11.48) payed attention to the fact (see Chapter IX) that, with many reversed-phase chromatographies, the logarithm of potential (see above) capacity ratio decreases linearly with increase in volume fraction, Φ_b, of the organic component in the binary solvent involving water as the other component, following ref(A11.47) eq(12):

$$\log_{10} k = \log_{10} k_w - S\Phi_b \tag{A11.68}$$

in which k_w represents capacity ratio which would take place in pure water (usually an extrapolated value), and S is a positive constant [cf. eq(9.11)]. They(A11.47, A11.48) emphasized that, when eq(A11.68) holds, then LSS gradient corresponds to linear solvent composition gradient where volume fraction, Φ_b, of the organic component increases linearly with a lapse of proper time at the inlet of the column (to be precise, proper time for a hypothetical molecule fixed at the inlet of the column) or with a lapse of time at the center of MB(o) migrating on the column. Let us translate the above argument by using our notations. Thus, it, in general, is reasonable to assume that Φ_b is almost proportional to concentration, m, of gradient substance expressed anyhow; Φ_b can be rewritten as αm where α represents a positive constant. [In Chapter IX, Φ_b is written as m by setting α to unity.] When a linear solvent composition gradient or a linear gradient of concentration m is applied and when potential capacity ratio k[eq(A11.68)] represents capacity ratio k'(V) taking place at the center of MB(o), then Φ_b in eq(A11.68) can be re-expressed as

$$\Phi_b = \alpha m = \alpha(\hat{m} + m_{in}) = \alpha(g'V + m_{in}) \tag{A11.69}$$

[cf. both eqs(3.1) and (6.18)]. In this instance, eq(A11.68) coincides with eq(A11.66) if

$$k_o = k_w e^{-(\ln 10)S\alpha m_{in}} \tag{A11.70}$$

and

$$b = S\alpha g'L' = S\alpha s \qquad \text{(A11.71)}$$

By replacing k and Φ_b by $\dot{k}(m)$ and αm, respectively, eq(A11.68) can be rewritten as

$$\log_{10} \dot{k}(m) = \log_{10} k_w - S\alpha m \qquad \text{(A11.68')}$$

Reversed-phase chromatography can be explained by competition model for the special case when both sample molecule and gradient substance are adsorbed "weakly" on the adsorbent surface while performing the competition, leading to eq(8.65):

$$\ln \dot{k}(m) \approx -x'\varphi m + \ln q \qquad \text{(A11.72)}$$

[see both Chapter Ⅷ(H) and Ⅸ]. By comparing eq(A11.72) with eq(A11.68'), it can be concluded that the parameters k_w and S can be expressed in terms of competition model as

$$k_w = q \qquad \text{(A11.73)}$$

and

$$S = x'\varphi/[(\ln 10)\alpha] \qquad \text{(A11.74)}$$

respectively. By substituting both eqs(A11.73) and (A11.74) into eqs(A11.70) and (A11.71)

$$k_o = qe^{-x'\varphi m_{in}} \qquad \text{(A11.70')}$$

and

$$b = x'\varphi s/(\ln 10) \qquad \text{(A11.71')}$$

are obtained, respectively. Eq(A11.67) or (A11.67') can be rewritten as

$$k'[\mu(s)]\left(= \frac{1-B'[\mu(s)]}{B'[\mu(s)]}\right) = 1/(x'\varphi s + e^{x'\varphi m_{in}}/q) \qquad \text{(A11.67'')}$$

where it can be considered that $k'(\dot{V})$ [eq(A11.67')] is a symbolical expression of $k'[\mu(s)]$ [$=k'\{g'\dot{V}\}$] [cf. the symbol $k'(V)$ in eq(A11.51')]. Eq(A11.67'') can be derived directly from eqs(6.25), (6.25') and (6.31).

Investigation of Poppe et al. Attempt(A11.52) was made to calculate analytically the band compression factor Γ[eq(A11.64)] for the case of LSS gradient, in which two key points are involved. The first key point consists in the introduction of the approximation given by ref(A11.52) eq(18):

$$\kappa(x) = \kappa(1+ax) \qquad \text{(A11.75)}$$

or, to be precise, by

$$\kappa(x,\mu_1) = \kappa(\mu_1)(1+ax) \qquad \text{(A11.75')}$$

in which κ and $\bar{\kappa}$ represent capacity ratios for molecules at any position and at the center of gravity of MB(o) migrating on the column, respectively; μ_1 is the distance (in unit of length) of the center of gravity of MB(o) from the column inlet; x is the axial coordinate (in unit of length) relative to the center of gravity of MB(o) on the column; and a is a positive constant. Although it is mentioned in ref(A11.52) that "the results are applicable to all cases where the retention can be calculated in advance", eq(A11.75) or (A11.75') anticipates tacitly the case of LSS gradient. In fact, the relationship:

$$(\partial \kappa / \partial x)_{\mu_1} = a \bar{\kappa}(\mu_1) \tag{A11.76}$$

derived from eq(A11.75') shows that the partial derivative of κ is proportional to $\bar{\kappa}$ occurring at the center of gravity of MB(o); such a situation takes place when

$$(\partial \kappa / \partial x)_{\mu_1} = a \kappa(x, \mu_1) \tag{A11.77}$$

or when

$$\kappa(x, \mu_1) = \bar{\kappa}(\mu_1) e^{ax} \tag{A11.78}$$

It can therefore be considered that eq(A11.75') or (A11.75) is an approximate expression of eq(A11.78). It is with LSS gradient that eq(A11.78) holds. In fact, with LSS gradient, capacity ratio, k_i, at the inlet of the column [taking place provided that MB(o) is extending over an infinite range around the center of gravity even though its density Ω decreases to infinitesimal when going to both borders] can be represented as

$$k_i(\mu_1) = \bar{\kappa}(\mu_1) e^{-a\mu_1} \tag{A11.79}$$

By using eq(A11.79), eq(A11.78) can be rewritten as

$$\kappa(x, \mu_1) = k_i(\mu_1) e^{a(\mu_1 + x)} \tag{A11.78'}$$

Writing L'/γ and $k''(L')$ for $\mu_1 + x$ and κ, respectively, eq(A11.78') can be re-expressed as

$$k''(L') = k_i e^{aL'/\gamma} \tag{A11.78''}$$

and, when eq(A11.78'') holds, then

$$k'(V) = k_e e^{-aV/\gamma} \tag{A11.80}$$

holds and vice versa. If

$$a = (\ln 10) b \gamma / L'_T \tag{A11.81}$$

in which L'_T represents the total length (in units of volume) of the column used, then eq (A11.80) is identical with eq(A11.66) in which L' is rewritten as L'_T [i.e., with eq (A11.66') below]; eq(A11.66) leads to eq(A11.65') representing LSS gradient.

Proof of the equivalence between eqs(A11.78″) and (A11.80). Let us consider $B'(\hat{m})$ $[=1/\{1+k'(\hat{m})\}]$ and $B''(s)$ $[=1/\{1+k''(s)\}]$ instead of k'(V) and k″(L'), respectively, where k'(V) and k″(L') are symbolical expressions of $k'(\hat{m})$ $[=k'(g'V)]$ and k″(s) $[=k''(g'L')]$, respectively. It is possible to consider that the curves $B=B'(\hat{m})$ and $B=B''(s)$ represent projections on $(\hat{m},B)$ and (s,B) planes of the gradient curve taking place in the $(\hat{m},s,B)$ space; the curves $B=B'(\hat{m})$ and $B=B''(s)$ are the mirror images of one another because the projection of the gradient curve on the $(\hat{m},s)$ plane coincides with gradient G i.e., a straight line with a slope of $-45°$ drawn on the $(\hat{m},s)$ plane [see Appendix IV(A)]. With concentration gradient chromatography, the gradient curves moves in the s direction in the $(\hat{m},s,B)$ space at a rate equal to g' times the flow-rate. As a result, the curve $B=B''(s)$ moves in the s direction on the (s,B) plane at a rate equal to g' times the flow-rate, while the curve $B=B'(\hat{m})$ always stays at the same position on the $(\hat{m},s)$ plane [see Appendix IV(A) Fig A4.2(a)]. The argument similar to the above holds if the $(\hat{m},s,B)$ space, the curves $B=B'(\hat{m})$ and $B=B''(s)$, and g' times the flow-rate are replaced by the (V, L', $\log_{10}$ k) space, the curves $\log_{10} k=\log_{10} k'(V)$ and $\log_{10} k=\log_{10} k''(L')$, and the flow-rate, respectively. Thus, it can be considered that LSS gradient taking place at any proper time Z (any oblique straight line drawn in Fig A11.1) is the projection, $\log_{10} k=\log_{10} k''(L')$, of the gradient curve on the (L', $\log_{10}$ k) plane with k″(L') represented by eq(A11.78″) combined with eq(A11.81):

$$\log_{10} k''(L') = \log_{10} k_1 + bL'/L'_T \qquad (A11.78''')$$

in which

$$\log_{10} k_1 = \log_{10} k_0 - bZ/L'_T \qquad (A11.82)$$

Here, it should be noted that flow-rate u or γu can be represented as $\gamma u=Z/t$; t represents time in the usual sense (see Fig A11.1). It now is evident that the projection, $\log_{10} k=\log_{10} k'(V)$, of the gradient curve on the (V, $\log_{10}$ k) plane, being the mirror image of the projection on the (L', $\log_{10}$ k) plane, can be represented by using k'(V) defined as

$$\log_{10} k'(V) = \log_{10} k_0 - bV/L'_T \qquad (A11.66')$$

which is identical with eq(A11.80) combined with eq(A11.81). *Q.E.D.*

The second key point in the calculation of Γ consists in the form of ref(A11.52) eq (22):

$$\frac{d\mu_2}{d\mu_1} = H - 2\frac{\kappa}{1+\kappa}a\mu_2 \qquad (A11.83)$$

in which μ_2 represents the variance (in units of length^2) of MB(o), and H represents height equivalent to a theoretical plate, corresponding to $\hat{H}$ or $2\Theta^\circ/\gamma$ of our notation [see both eqs(6.15) and (6.16)]; both μ_2 and κ are functions of μ_1. Eq(A11.83) can be re-expressed as

$$\mu_2(\mu_1) + \frac{1+\kappa(\mu_1)}{2a\kappa(\mu_1)} \cdot \frac{d\mu_2}{d\mu_1} = \frac{1+\kappa(\mu_1)}{\gamma a \kappa(\mu_1)} \Theta^\circ \qquad \text{(A11.83')}$$

Eq(A11.83) or (A11.83') arises from the approximate expression of the term B [$\equiv 1/(1+\kappa)$] which relates C and Ω as $C = B\Omega$; the approximation leads to

$$\begin{aligned} \frac{1}{1+\kappa} &\approx \frac{1}{1+\kappa(1+ax)} \\ &= \frac{1}{(1+\kappa)\left(1+\dfrac{\kappa}{1+\kappa}ax\right)} \\ &\approx \frac{1}{1+\kappa}\left(1-\frac{\kappa}{1+\kappa}ax\right) \end{aligned} \qquad \text{(A11.84)}$$

[see ref(A11.52) eqs(19) and (29), where C and Ω are written as $c_m(x)$ and $c_i(x)$, respectively]. It can usually be assumed that, when MB(o) with a small width is formed initially at the inlet of the column, then it spreads into a Gaussian shape with migration on the column. On the other hand, the convolution of two Gaussian distributions brings about a Gaussian distribution with variance equal to the sum of the variances of the distributions taking place before convolution [cf. Chapter I (A)]. Eq(A11.83') appears to imply a possibility that a Gaussian MB(o) with variance μ_2 and a certain Gaussian distribution with variance $[(1+\kappa)/(2a\kappa)]\cdot d\mu_2/d\mu_1$ are convoluted with one another to generate a Gaussian distribution with variance $[(1+\kappa)/(\gamma a\kappa)]\Theta^\circ$. In conclusion, however, it is difficult to find out a physical mechanism that corresponds to the mathematical structure of eq (A11.83') or (A11.83) even if it is valid only simply as an approximation and if Poppe et al.(A11.52) mention that eq(A11.83) "gives very good insight, as it gives the increase of the second moment with the migrated distance as a sum of the normal dispersion effect (H term) and the band compression effect (−last term), proportional to μ_2 and a".

On the basis of eq(A11.83), Poppe et al.(A11.52) derived a conclusion that, when LSS gradient is applied or when eq(A11.80) combined with eq(A11.81) [which corresponds to ref(A11.52) eq(26)] holds, then variance, μ_2, of MB(o) taking place at the moment when the elution of its center of gravity is being done at the outlet of the column with length L can be represented by ref(A11.52) eq(30). Here, the precise meaning of variance μ_2 under consideration is that taking place at the moment when the center of gravity of MB(o) passes position L on the hypothetical column with infinite length, and it is assumed that MB(o) with an infinitesimal width is formed initially at the inlet of the actual column.

Ref(A11.52) eq(30) can be reproduced as

$$\mu_2 = HL \frac{1+p+p^2/3}{(1+p)^2} \qquad \text{(A11.85)}$$

in which

$$p = \frac{\kappa_0}{1+\kappa_0} bt_0 \qquad \text{(A11.86)}$$

In eq(A11.85), L and H correspond to L'/γ and $2\Theta^\circ/\gamma$ of our notations, respectively, and, in eq(A11.86), κ_0 and bt_0 correspond to k_0 and $(\ln 10)b$ of our notations, respectively. Writing $\Delta_{L'}^2/\gamma^2$ for μ_2, eq(A11.85) can be re-expressed as

$$\Delta_{L'} = \sqrt{2\Theta^\circ L'}\ \Gamma \qquad \text{(A11.85')}$$

with

$$\Gamma = \frac{(1+p+p^2/3)^{1/2}}{1+p} \qquad \text{(A11.87)}$$

and

$$p = (\ln 10)bk_0/(1+k_0) \qquad \text{(A11.86')}$$

When molecular partition, $B'[\dot{V}(L')]$, in the mobile phase taking place at the center of gravity of MB(o) just prior to elution from the column with length L' is virtually equal to that taking place at any part of MB(o) just prior to elution, then the relationship:

$$\tau = \Delta_{L'}/B'[\dot{V}(L')] \qquad \text{(A11.88)}$$

is fulfilled. By substituting eq(A11.85') into eq(A11.88), eq(A11.64) can be derived. This means that Γ defined by eq(A11.87) represents the band compression factor.

As $s=g'L'$, $\Delta(s;g')=g'\Delta_{L'}$ [cf. eq(6.9)] and $\sigma(s;g')=g'\tau$ [cf. both eqs(6.8) and (6.11)], and as $B'[\dot{V}(L')]$ is a symbolical expression of $B'[\mu(s)]$ [cf. eq(6.8)], then eqs (A11.85') and (A11.88) can be rewritten as eqs(6.27') and (6.28') with Γ defined by eq (A11.87), respectively. On the other hand, Γ appearing precedently in both eqs(6.27') and (6.28') is defined by eq(6.34), and the parameter p appearing in eq(6.34) [defined by eq(6.32)] is identical with that appearing in eq(A11.87) [defined by eq(A11.86')]. In fact, eq(A11.86') is identical with eq(6.32) because k_0 is identical with $k'(0)$, and, due to eq (A11.71'), $(\ln 10)b$ is equal to $x'\varphi s$.

The discrepancy between the two Γ defined by eqs(A11.87) and (6.34), respectively, arises from the difference in the method of estimation of the band compression effect, the one based on eq(A11.83) or (A11.83') and the other based on eq(5.26). It should be emphasized that, in contrast to eq(A11.83) or (A11.83'), eq(5.26) represents a well-defined

physical mechanism of the balance between axial diffusion and compression of band taking place on the column with concentration gradient chromatography. Moreover, eq(5.26) is quite general. Thus, when limiting ourselves to concentration gradient chromatography, eq (5.26) is valid for any shape of concentration gradient which is not necessrily an LSS gradient. Further, eq(5.26) is even valid for the case of the gradient in the solid phase when expansion of band takes place instead of compression, and for the case when both gradient in the liquid phase (i.e., concentration gradient) and gradient in the solid phase are applied at the same time.

Investigation of Jandera et al. According to chemical equilibrium equation model[Section (C)], capacity ratio k can be represenred as a functrion of $X\langle 0,m_b\rangle$ or m by eq (A11.104) as

$$k = \alpha' m^{-\breve{x}'} \tag{A11.89}$$

in which α' and $\breve{x}'$ are positive constants. Jandera and Churá č ek(A11.49) considered that eq(A11.89) [i.e., ref(A11.49) eq(1)] applies to both ion-exchange and so-called adsorption chromatoraphies. They(A11.49) attempted to calculate both elution volume, $\dot{V}$, at the center of MB(o) [represented by eq(A11.51')] and standard deviation, τ, of the chromatogram or chromatographic peak [assumed to be represented by eq(A11.61')] for the case when eq(A11.89) holds and when concentration gradient delivered from the device is represented by ref(A11.49) eq(4) as

$$m = (\breve{g}'Z + m_{in}^{1/\iota})^{\iota} \tag{A11.90}$$

in which

$$\breve{g}' = (m_f^{1/\iota} - m_{in}^{1/\iota})/V_T \tag{A11.91}$$

[ref(A11.49) eq(5)]. ι is a positive constant, and when $\iota > 1$, $\iota = 1$ and $\iota < 1$, eq (A11.90) combined with eq(A11.91) represents concave, linear and convex gradients, respectively; $\breve{g}'$ (with a positive value) measures the mean slope of gradient. $\breve{g}'$, in general, is different from g' [defined by eq(6.22)], however, and only in the case of the linear gradient when $\iota = 1$, $\breve{g}'$ coincides with g'. In this instance, eq(A11.91) coincides with eq (6.22) combined with eq(6.21).

Corresponding to eq(A11.65'), potential capacity ratio, k_i, at the inlet of the column can be calculated by substituting eq(A11.90) into eq(A11.89) and writing k_i for k as

$$k_i = \alpha'(\breve{g}'Z + m_{in}^{1/\iota})^{-\iota\,\breve{x}'} \tag{A11.92}$$

[ref(A11.49) eq(6)], and, corresponding to eq(A11.66), k'(V) can be represented as

$$k'(V) = \alpha'(\breve{g}'V + m_{in}^{1/\iota})^{-\iota\,\breve{x}'} \tag{A11.93}$$

Substituting eq(A11.93) into eq(A11.51') [which corresponds to ref(A11.49) eq(8)], and executing the integration, the explicit expression of $\dot{V}$:

$$\dot{V} = [(\iota\,\breve{x}'+1)\alpha'\breve{g}'L'+m_{in}^{(\iota\,\breve{x}'+1)/\iota}]^{1/(\iota\,\breve{x}'+1)}/\breve{g}' - m_{in}^{1/\iota}/\breve{g}' \quad (A11.94)$$

[ref(11.49) eq(10)] can be obtained finally. When $\iota=1$ and $\breve{g}'=g'$, eq(A11.94) reduces to

$$\dot{V} = [(\breve{x}'+1)\alpha'g'L'+m_{in}^{\breve{x}'+1}]^{1/(\breve{x}'+1)}/g' - m_{in}/g' \quad (A11.95)$$

When volume, V_z, of connecting tubing between the outlet of the gradient-generating device and the inlet of the column is negligible, τ [eq(A11.61')] can be represented by ref (A11.49) eq(17) as

$$\tau = (L'/\sqrt{N})\cdot[1+\alpha'(\breve{g}'\dot{V}+m_{in}^{1/\iota})^{-\iota\,\breve{x}'}]$$

$$= \sqrt{2\Theta^{\circ}L'}\,[1+\alpha'(\breve{g}'\dot{V}+m_{in}^{1/\iota})^{-\iota\,\breve{x}'}] \quad (A11.96)$$

[In fact, eq(A11.96) can be obtained by substituting $1/[1+k'(\dot{V})]$ [where $k'(\dot{V})$ is defined by eq(A11.93)] for $B'[\dot{V}(L')]$ into eq(A11.61').] When $\iota=1$ and $\breve{g}'=g'$, eq(A11.96) reduces to

$$\tau = \sqrt{2\Theta^{\circ}L'}\,[1+\alpha'(g'\dot{V}+m_{in})^{-\breve{x}'}] \quad (A11.97)$$

On the other hand, by replacing the terms $\varphi(\mu+m_{in})+1$ and $\varphi\,m_{in}+1$ in eq(6.24) by $\varphi(\mu+m_{in})$ and $\varphi\,m_{in}$, respectively

$$s = \frac{\varphi^{x'}}{(x'+1)q}[(\mu+m_{in})^{x'+1} - m_{in}^{x'+1}] \quad (A11.98)$$

or

$$\mu(s) = [(x'+1)q\,\varphi^{-x'}\,s + m_{in}^{x'+1}]^{1/(x'+1)} - m_{in} \quad (A11.98')$$

can be derived. Eq(A11.98') coincides with eq(A11.95) if $g'L'$, $g'\dot{V}$, $\breve{x}'$ and α' are substituted for s, $\mu(s)$, x' and $q\,\varphi^{-x'}$, respectively [cf. both eqs(6.2) and (6.10)]. This is intimately related to the fact that chemical equilibrium equation model coincides with competition model in the special case when both sample molecule and competing substance are adsorbed "strongly" on the adsorbent surface [see Section(C)]. In this instance, except when m is close to zero, the relationship $\varphi\,m \gg 1$ holds, and eq(8.52) tends to eq(8.67) or eq(A11.108) in Section(C). This latter coincides with eq(A11.89) if $\breve{x}'$ and α' are substituted for x' and $q\,\varphi^{-x'}$, respectively [cf. Section(C) eqs(A11.106) and (A11.107)]. Eq

(A11.98) or (A11.98') can also be derived in the following way. Thus, eq(6.18) holds with linear concentration gradient chromatography; this means that $\dot{k}(m)=\dot{k}(\hat{m}+m_{in})=k'(\hat{m})$ and that $dm=d\hat{m}$. In this instance, if eq(A11.108) [in which k stands for $\dot{k}(m)$] is substituted into eq(6.7) [in which $B'(\hat{m})/[1-B'(\hat{m})]$ stands for $1/k'(\hat{m})$], then, after executing the integration, eq(A11.98) or (A11.98') can be obtained.

With regard to the first method for the derivation of eq(A11.98) or (A11.98'), the replacement of $\varphi(\beta+\dot{m}_{in})+1$ by $\varphi(\beta+m_{in})$ is consistent with the consideration that both sample molecule and competing substance are adsorbed "strongly" on the adsorbent surface, giving rise to the relationship $\varphi\, m\gg 1$ when m is not close to zero. In contrast, the replacement of $\varphi\, m_{in}+1$ by $\varphi\, m_{in}$ corresponds to the assumption specific to the treatment of Jandera and Churá č ek(A11.49). Thus, in ref(A11.49), it simply is assumed that eq (A11.89) [corresponding to eq(8.67) or (A11.108)] holds always, involving the case when $m=m_{in}$ and when m_{in} is close to zero. According to competition model, eq(8.67) or (A11.108) does not hold when $m=m_{in}$ and when m_{in} is close to zero (even if both sample molecule and competing substance are adsorbed "strongly" on the adsorbent surface). In this instance, the relationship $\varphi\, m\gg 1$ does not hold. With regard to the second method for the derivation of eq(A11.98) or (A11.98'), the reciprocal of k [defined by eq(8.67) or (A11.108)] was used despite the fact that the domain of integration involves $\hat{m}=0$ (corresponding to $m=m_{in}$); this corresponds to the assumption specific to ref(A11.49).

It is easy to show that, when $\varphi\,\beta(s)\gg 1$, then eq(6.40) (in which σ^* and Θ^* are rewritten as σ and Θ°, respectively) coincides with eq(A11.97) since σ is related to τ through eq(6.11).

For so-called partition chromatography (liquid-liquid, salting-out and solubilization chromatography on ion-exchange resins in mixed aqueous-organic media), Jandera and Churá č ek(A11.49) proposed a semi-empirical expression of capacity ratio:

$$k = \gamma' \cdot 10^{-\upsilon m} \qquad \text{(A11.99)}$$

[ref(A11.49) eq(2)] in which γ' anf υ are positive constants. Eq(A11.99) has the same mathematical form as eq(A11.68'); this means that, when eq(A11.99) holds, the linear concentration gradient represents a LSS gradient. In ref(A11.49), the argument similar to that performed above on the basis of eq(A11.89) was repeated on the basis of eq(A11.99). Further, Jandera et al.(A11.50) developed the argument by applying eq(A11.99) to reversed-phase chromatography.

Supplement. Yamamoto et al.(A11.53) published another type of theory treating both linear and step concentration gradient chromatographies. Although experimental verifications thereof are also published(A11.54), the theory itself(A11.53) contains a number of basic assumptions and/or approximations in the abstract. The general purpose of this monograph is to understand the fundamental principle of chromatography, and, even though the theory (A11.53) may be valid from a practical viewpoint [as is emphasized by the authors(A11.53,

A11.54)], it is difficult to decipher the signification of each assumption, not to speak of that of the assembly of assumptions.

(C) Adsorption and Desorption Mechanism: Chemical Equilibrium Equation Model

Probably, it is Boardman and Partridge(A11.55) who first introduced in an explicit manner the concept (which is also used in competition model; Chapter Ⅷ) that sample molecule and a component from the carrier liquid (here called active component molecule from the carrier liquid, abbreviated as ACMCL) compete for adsorption on the adsorbent packed in the column, and who attempted to represent this concept by using a chemical equilibrium equation. [Only for convenience' sake, we here use the terminology "competition model" to represent only the model developed in Chapter Ⅷ.] Thus, in ref(A11.55), a competition mechanism of cytochrome c and sodium ion from the carrier liquid for adsorption on cation-exchange resin packed in the column was proposed by using a chemical equilibrium equation [the first equation without numbering in the Discussion Section in ref (A11.55)]. Snyder also considered chemical equilibrium equations of the similar type for so-called adsorption chromatography although somewhat different meanings are implied in the equations [ref(A11.56) eq(2) and ref(A11.57) eq(4)].

The chemical equilibrium equations proposed above [especially that proposed in ref(A11.55)] can be written by changing the notations as

$$X\langle 1,m_b\rangle + \chi' X\langle 0,s_t\rangle \rightleftarrows X\langle 1,s_t\rangle + \chi' X\langle 0,m_b\rangle \qquad \text{(A11.100)}$$

in which the suffixes 0 and 1 refer to ACMCL and sample molecule, respectively. $X\langle \rho, m_b\rangle$ and $X\langle \rho, s_t\rangle$ represent molecule ρ in mobile and stationary phases, respectively; $\rho = 0$ or 1. In Snyder's image(A11.56, A11.57), χ' represents the ratio of the volume, $\Phi\langle 1\rangle$, occupied by an adsorbed sample molecule to the volume, $\Phi\langle 0\rangle$, occupied by an ACMCL taking place within the monomolecular layer formed on the adsorbent surface, where it is assumed that both sample molecules and ACMCL are forming a monomolecular layer (with a constant thickness) on the adsorbent surface while saturating the surface always. It therefore is possible to re-interpret that $\Phi\langle 1\rangle$ and $\Phi\langle 0\rangle$ represent the areas on the adsorbent surface occupied by a sample molecule and an ACMCL, respectively. Introducing integers $\nu\langle 0\rangle$ and $\nu\langle 1\rangle$, χ' can be expressed as an irreducible fraction as

$$\chi' \equiv \Phi\langle 1\rangle/\Phi\langle 0\rangle = \nu\langle 1\rangle/\nu\langle 0\rangle \qquad \text{(A11.101)}$$

and eq(A11.100) can be rewritten as

$$\nu\langle 0\rangle X\langle 1,m_b\rangle + \nu\langle 1\rangle X\langle 0,s_t\rangle \rightleftarrows \nu\langle 0\rangle X\langle 1,s_t\rangle + \nu\langle 1\rangle X\langle 0,m_b\rangle \qquad \text{(A11.100')}$$

On the other hand, assigning to $\nu\langle 0\rangle$ and $\nu\langle 1\rangle$ the meanings of electric charges per ACMCL and per sample molecule, respectively, Jandera and Churáček proposed eq (A11.100') as equation specific to ion-exchange chromatography[ref(A11.58) eq(18) or ref

(A11.59) eq(21)] [where, $\nu\langle 0\rangle$ and $\nu\langle 1\rangle$ [eq(A11.100')] are defined as positive, representing the absolute values of positive and negative charges with cation- and anion-exchange chromatographies, respectively.] By using eq(A11.100') and limiting themselves to the case when only a trace amount of sample molecules are present, Jandera and Churá ć ek(A11.58, A11.59) calculated capacity ratio k of sample molecule as a function of concentration, $[X\langle 0,m_b\rangle]$, of ACMCL in the mobile phase. Thus, in eq(A11.100'), the equilibrium constant K (called selectivity constant) can be expressed by ref(A11.58) eq(19) or ref(A11.59) eq(22) as

$$K = \frac{[X\langle 0,m_b\rangle]^{\nu\langle 1\rangle}\,[X\langle 1,s_t\rangle]^{\nu\langle 0\rangle}}{[X\langle 0,s_t\rangle]^{\nu\langle 1\rangle}\,[X\langle 1,m_b\rangle]^{\nu\langle 0\rangle}} \qquad \text{(A11.102)}$$

in which the brackets represent concentration or density. By using eq(A11.102), capacity ratio k can be represented by ref(A11.58) eq(20) or ref(A11.59) eq(23) as

$$\begin{aligned} k \equiv \chi/C &= \alpha[X\langle 1,s_t\rangle]/[X\langle 1,m_b\rangle] \\ &= \alpha K^{1/\nu\langle 0\rangle}[X\langle 0,s_t\rangle]^{\nu\langle 1\rangle/\nu\langle 0\rangle}[X\langle 0,m_b\rangle]^{-\nu\langle 1\rangle/\nu\langle 0\rangle} \end{aligned} \qquad \text{(A11.103)}$$

in which α represents a positive constant. In the presence of a trace amount of sample molecules, it can be assumed(A11.58, A11.59) that the term $[X\langle 0,s_t\rangle]$ in eq(A11.103) can be replaced by the total exchange capacity, Q (with a constant value), of the ion-exchanger for ACMCL. In this instance, the term $\alpha K^{1/\nu\langle 0\rangle}[X\langle 0,s_t\rangle]^{\nu\langle 1\rangle/\nu\langle 0\rangle}$ in the extreme right-hand side of eq(A11.103) can be replaced by a new positive constant α', and eq(A11.103) becomes

$$k = \alpha'[X\langle 0,m_b\rangle]^{-\bar{x}'} \qquad \text{(A11.104)}$$

[see ref(A11.58) eqs(7) and (21), or ref(A11.59) eq(23); cf. eq(A11.101)]. [*Note.* In order for the replacement of $[X\langle 0,s_t\rangle]$ by Q to be feasible, it would be necessary that concentration, $[X\langle 0,m_b\rangle]$, of ACMCL in the mobile phase be high enough for almost all the adsorbent surface (with a finite capacity Q) to be occupied by ACMCL. The high enough concentration of $[X\langle 0,m_b\rangle]$ is consistent with the fact that, with concentration gradient chromatography, concentration $[X\langle 0,m_b\rangle]$ is high enough for it to be virtually independent of the adsorption and desorption of sample molecules except at the beginning of concentration gradient. Cf. Chapter Ⅲ(A).]

Eq(A11.104) can be rewrittren as

$$\ln k = -\bar{x}'\ln[X\langle 0,m_b\rangle] + \ln\alpha' \qquad \text{(A11.104')}$$

manifesting that ln k decreases linearly with increase in $\ln[X\langle 0,m_b\rangle]$. Eq(A11.104') is consistent with the linear $\log_{10} k$ versus $\log_{10}[X\langle 0,m_b\rangle]$ plots obtained for a number of

ion-exchange chromatographies [see Chapter X where [X<0,m_b>] is written as m].

The argument similar to that performed until now was also done by Boardman and Partridge(A11.55) for cation-exchange chromatography and by Soczewiński(A11.60) for so-called adsorption chromatography, both leading to eq(A11.104) or (A11.104') [see the last two equations without numbering in the Discussion Section in ref(A11.55), and also see both eq(5) and the last equation without numbering in ref(A11.60)]; Snyder's image for the parameter $\bar{x}'$ (see above) is used in ref(A11.60). Versions of eq(A11.100) or (A11.100') were proposed by the Regnier's group for both ion-exchange chromatography[ref(10.1) eq (7)] and reversed-phase chromatography[ref(9.8) eqs(A)-(E)], leading to eq(A11.104) or (A11.104') again [see ref(10.1) eq(17) or (18), and ref(9.8) eq(14) or (15)]. With reversed-phase chromatography, however, eq(A11.104) or (A11.104'), in general, is not consistent with experimental data obtained by a number of authors; this is consistent only with the exceptional data obtained in ref(9.8) [see Chapter IX(A)].

Regnier(A11.61) pays attention to the fact that eq(A11.104) [i.e., ref(A11.61) eq(4)] shows an exponentional relation between chromatographic retention (k) and the number ($\bar{x}'$) of molecules of displacing agent in solution for desorption of a sample molecule. He mentions(A11.61) that eq(A11.104) explains the fact that desorption curves for macromolecules become increasingly concave with increasing M_m and are different from those for small molecules ["on-off" mechanism versus "partition" mechanism; see Chapter IX(A)]. He suggests that eq(A11.104) is applicable to not only ion-exchange chromatography but also reversed-phase chromatography [see ref(A11.61)].

Chemical Equilibrium Equation Model versus Competition Model. Eq(A11.100) or (A11.100') representing a *chemical equation* implies tacitly a chemical equilibrium among the four *independent* "molecules" each of which is constructed from an "atom" or "atoms"; the total number of any "atom" participating in the chemical reaction is conserved. In order to emphasize this concept, let us rewrite eq(A11.100) or (A11.100') as

$$\nu\langle 0\rangle X\langle 1\rangle + X\langle 0\rangle_{\nu\langle 1\rangle} A \rightleftarrows X\langle 1\rangle_{\nu\langle 0\rangle} A + \nu\langle 1\rangle X\langle 0\rangle \qquad \text{(A11.100a)}$$

in which A represents the adsorbent; this is expressed as an abstract concept of "atom" particle. X<0> and X<1> represent free ACMCL and free sample molecule behaving as "molecules" in the mobile phase, respectively. $X\langle 0\rangle_{\nu\langle 1\rangle} A$ represents a compound "molecule" formed by association between $\nu\langle 1\rangle$ ACMCL as "atoms" and an adsorbent "atom" particle, whereas $X\langle 1\rangle_{\nu\langle 0\rangle} A$ represents another compound "molecule" formed by association between $\nu\langle 0\rangle$ sample molecules as "atoms" and an adsorbent "atom" particle. Eqs(A11.102)-(A11.104) can now be rewritten as

$$K = \frac{[X\langle 0\rangle]^{\nu\langle 1\rangle}[X\langle 1\rangle_{\nu\langle 0\rangle} A]}{[X\langle 0\rangle_{\nu\langle 1\rangle} A][X\langle 1\rangle]^{\nu\langle 0\rangle}} \qquad \text{(A11.102a)}$$

$$k \equiv \chi/C = \alpha[X\langle 1\rangle_{\nu\langle 0\rangle} A]^{1/\nu\langle 0\rangle}/[X\langle 1\rangle]$$

$$= \alpha K^{1/\nu\langle 0\rangle}[X\langle 0\rangle_{\nu\langle 1\rangle} A]^{1/\nu\langle 0\rangle}[X\langle 0\rangle]^{-\nu\langle 1\rangle/\nu\langle 0\rangle} \quad \text{(A11.103a)}$$

and

$$k = \alpha'[X\langle 0\rangle]^{-\bar{x}'} \quad \text{(A11.104a)}$$

respectively; $\bar{x}'$ is defined by eq(A11.101).

It should be pointed out that, if

$$[X\langle 0, m_k\rangle] = [X\langle 0\rangle] = m \quad \text{(A11.105)}$$

$$\bar{x}' = x' \quad \text{(A11.106)}$$

and

$$\alpha' = q\varphi^{-x'} \quad \text{(A11.107)}$$

then eq(A11.104) or (A11.104a) becomes

$$k = q\varphi^{-x'} m^{-x'} \quad \text{(A11.108)}$$

which is identical with eq(8.67).

Fig A11.2(a) illustrates schematically the concept correspondong to eq(A11.100a) for so-called adsorption chromatography in Snyder's image assuming: $\nu\langle 0\rangle = 2$ and $\nu\langle 1\rangle = 3$. Thus, in Fig A11.2(a), largest, middle and smallest rectangles represent adsorbent, sample molecule and ACMCL, respectively; left and right parts of the diagram correspond to left- and right-hand sides of eq(A11.100a), respectively. Figs A11.2(b) and (b') illustrate the same concept for ion-exchange chromatography in Jandera and Churá č ek's image assuming: $\nu\langle 0\rangle = 1$ and $\nu\langle 1\rangle = 2$, and assuming: $\nu\langle 0\rangle = 2$ and $\nu\langle 1\rangle = 3$, respectively. Thus, in both Figs A11.2(b) and (b'), the rectangle with triangular protuberances represents adsorbent (triangular protuberances expressing adsorbing sites or ion-exchangers), whereas the rectangle with round protuberances represents sample molecule (round protuberances expressing electric charges or charged adsorption groups). ACMCL is represented by a small circle[Fig A11.2(b)] or a semi-circle with two round proturberances (expressing electric charges or charged adsorption groups as parts of divalent ACMCL) [Fig A11.2(b')]. In Figs A11.2(b) and (b'), an electric charge or a charged adsorption group of the sample molececule bonds with a single ion-exchanger when the molecule is adsorbed, and the molecule as a whole does not cover other vacant ion-exchangers. The situation is the same with ACMCL: the univalent[Fig A11.2(b)] and divalent[Fig A11.2(b')] ACMCL bond with one and two ion-exchangers without covering other vacant ion-exchangers, respectively.

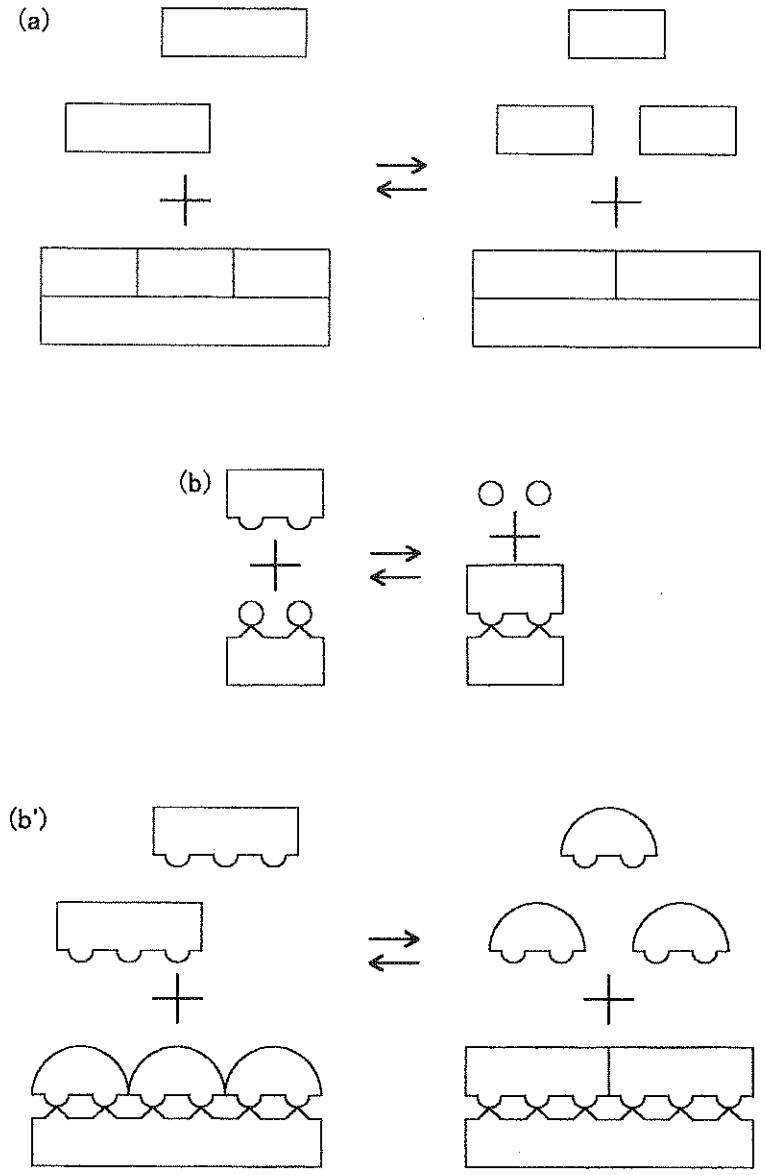


Fig A11.2. The relationship between chemical equilibrium equation model and competition model. For detail, see text.

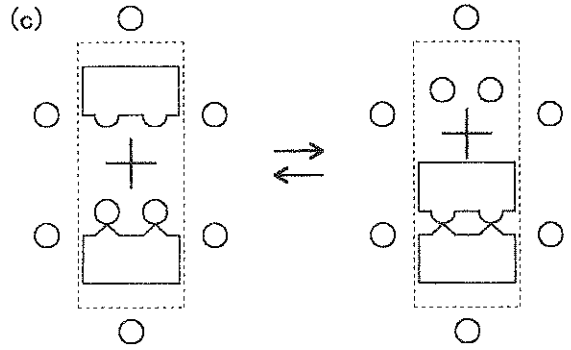


Fig A11.2. (c)

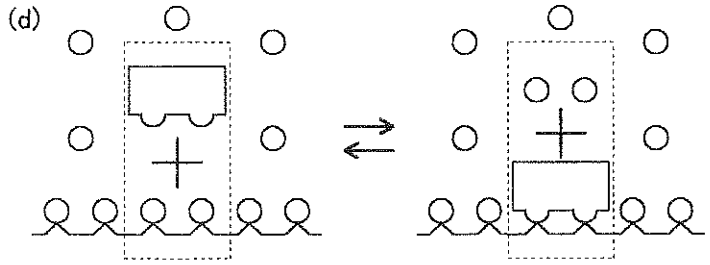


Fig A11.2. (d)

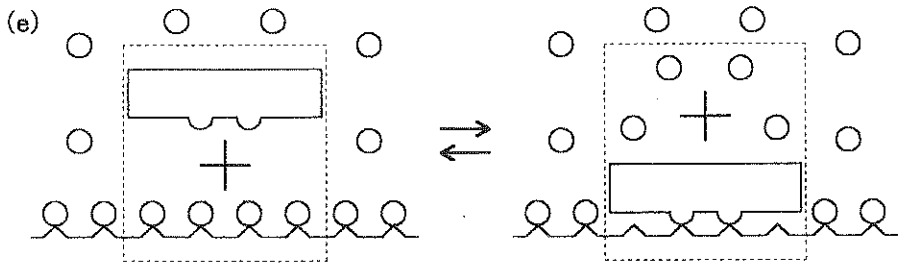


Fig A11.2. (e)

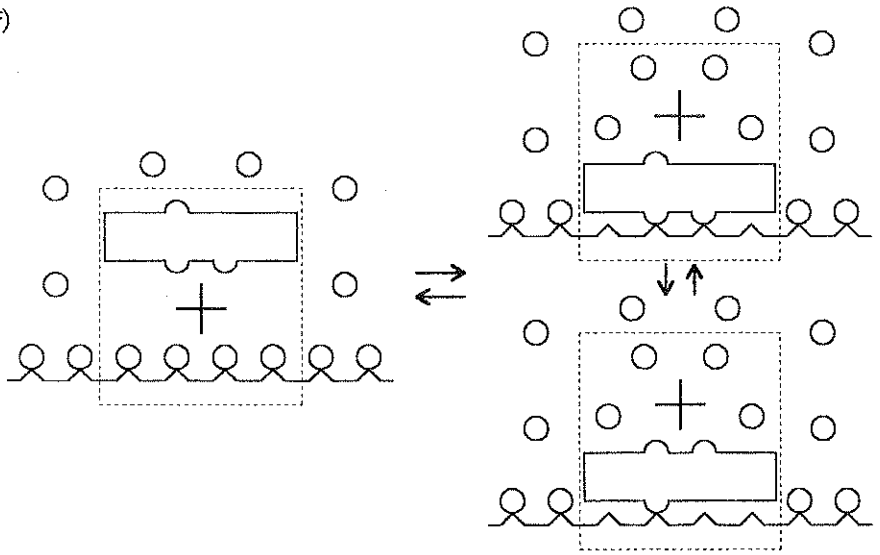


Fig A11.2. (f)

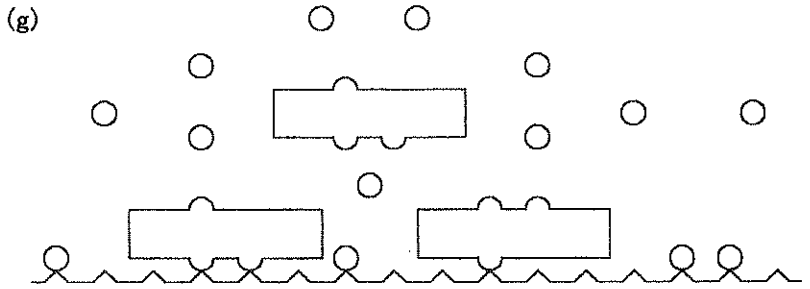


Fig A11.2. (g)

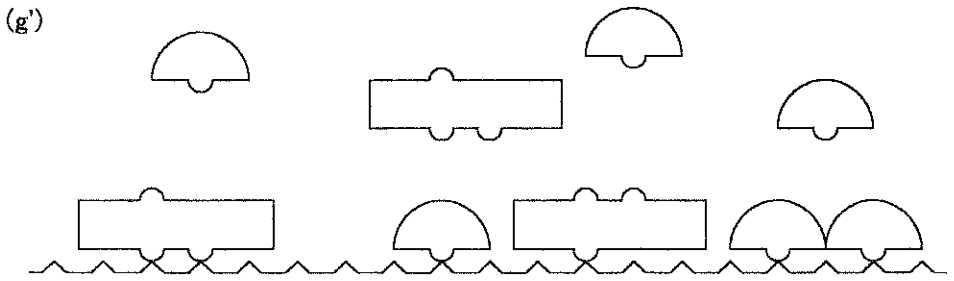


Fig A11.2. (g')

As mentioned in Note just below eq(A11.104), chemical equilibrium equation model is valid only when concentration of ACMCL in the mobile phase is high. Therefore, let us consider that the chemical reaction (in equilibrium) takes place while surrounded by an environment where concentration or density of ACMCL is high enough for it to be virtually constant, independent of the chemical reaction. Fig A11.2(b) can now be re-drawn as Fig A11.2(c) where the environment is expressed as the domain outside the dotted rectangle. Further, Fig A11.2(c) can be re-drawn as Fig A11.2(d) where the abstract concept of the adsorbent "atom" particle[Fig A11.2(c)] is replaced by the real concept of the adsorbent with an infinite surface area. In Fig A11.2(d), the adsorbent surface around the adsorbed sample molecule is saturated with adsorbed ACMCL in such a way that $[X\langle 0,s_b\rangle] \equiv [X\langle 0\rangle_{\nu\langle 1\rangle} A]^{1/\nu\langle 1\rangle} \approx Q$ [cf. Note just below eq(A11.104)]. This means that both mobile and stationary phases as environment surrounding the sample molecule are constant, independent of adsorptions and desorptions of both sample molecule and ACMCL, thus justifying the replacement between Figs A11.2(b) and (d).

When considering competition model, it is possible to interpret that Fig A11.2(d) represents the special case taking place when $\varphi\ m \gg 1$. In fact, the situation where $\varphi\ m \gg 1$ takes place either when competing substance (synonym of ACMCL) is adsorbed strongly on the adsorbent surface bringing about a large φ value [see eq(8.45)] [provided that concentration, m, of competing substance in the mobile phase (synonym of $[X\langle 0,m_b\rangle]$ or $[X\langle 0\rangle]$) is not close zero] or when m is very high. In this instance, the adsorbent surface would be almost saturated with competing substances. Thus, Fig A11.2(d) represents the point of contact between chemical equilibrium equation model and competition model; this can be rationalized by eqs(A11.105)-(A11.108).

Even limiting ourselves to the case when $\varphi\ m \gg 1$, competition model implies a wider concept than that illustrated in Fig A11.2(d), dealing with the case when the sample molecule adsorbed on the adsorbent surface covers not only the sites bonding with the functional groups of the molecule but also vacant adsorbing sites. Such a situation is illustrated in both Figs A11.2(e) and (f); Fig A11.2(f) is more general than Fig A11.2(e). Thus, whereas Fig A11.2(e) represents the case when the sample molecule can take only one adsorption configuration, Fig A11.2(f) represents the case when it can take plural configurations; a Boltzmann distribution occurs among the configurations [see eq(8.8)]. [In competition model, the number, x', of competing substances the adsorption of which is impossible owing to the presence of an adsorbed sample molecule is important. For the sake of simplicity, however, the average of the x' values is considered when x' depends on the configuration. See Chapter Ⅷ(B).] Competition model is even valid when the molecular conformation is flexible and when the conformation on the adsorbent surface is different from that taking place in the mobile phase [cf. Chapter Ⅸ(B)]. It should be noted, however, that all these concepts may be latent in both parameters α' and $\bar{x}'$ appearing in chemical equilibrium equation model [see eq(A11.104), (A11.104') or (A11.104a); cf. eqs

(A11.105)-(A11.108)].

Fig A11.2(g) corresponds to Fig A11.2(f), representing a most general case when the relationship $\varphi\ m \gg 1$ does not necessarily hold. Thus, in Fig 11.2(g), the adsorbent surface around the adsorbed sample molecule is not saturated with ACMCL (or competing substances), and the stability of the adsorbed state of the sample molecule depends on the density of ACMCL coexisting on the adsorbent surface *for entropical reason.* In this instance, it is impossible to apply chemical equilibrium equation model. [*Note.* With concentration gradient chromatography, the mobile phase of ACMCL as environment surrounding a sample molecule can be regarded as constant, independent of adsorptions and desorptions of both sample molecule and ACMCL even though the relationship $\varphi\ m \gg 1$ does not hold. In fact, it is common practice that, even when the adsorbent surface is not saturated with both sample molecules and ACMCL, concentration, m, of ACMCL in the mobile phase is high enough for it to be virtually independent of adsorptions and desorptions of both sample molecule and ACMCL [except at the beginning of the concentration gradient; see Chapter Ⅲ(A)].]

Finally, Fig A11.2(g') corresponds to Fig A11.2(g), representing the case when an ACMCL covers more than one site when it is adsorbed on the adsorbent surface (cf. Fig 8.2). Similarly to the relationship between Figs A11.2(b) and (g), it is possible to argue the relationship between Figs A11.2(b') and (g'); it is only for convenience' sake that ACMCL is represented differently between Figs A11.2(b') and (g').

Supplement. More recently, Kasai and Oda(A11.62) developed another type of chemical equilibrium equation model for affinity chromatography to investigate and characterize specific interaction between biomolecules. Thus, in ref(A11.62), four types of interacting substance were considered in the chromatographic system: A, a ligand that interacts with an affinity adsorbent packed in the column: B, an immobilized ligand on the affinity adsorbent; I, a counter-ligand that compete with A and inhibits the binding of A to B (i.e., a competitive inhibitor of enzymes); and E, an effector that affects the binding of A to B, with three dissociation constants: that between A and B, that between A and I, and that between A and E. Attempt was made to relate these dissociation constants to frontal-analytical chromatographic data. The analytical method is analogous to that used in enzyme kinetics performed on the basis of Lineweaver-Burk or Michaelis-Menten equation. Equilibrium constants obtained from chromatographic analysis are consistent with those obtained from enzyme kinetics and from equilibrium dialysis. [For detail, see ref(A11.62).]

(D) Models Insisting on the Predominant Role of the Mobile Phase for the Adsorption of Sample Molecule on the Adsorbent

General. With both HA and ion-exchange chromatographies, it a priori would be reasonable to assume that the adsorption of sample molecule on the adsorbent surface is brought about mainly by the *active* attractive energetical interaction. As Horváth et al.

(A11.63) pointed out, it may be possible to assume that, with reversed-phase chromatography, it is the solvent in the mobile phase that forces sample molecule to associate with the adsorbent; the adsorption of sample molecule on the adsorbent surfcae is brought about in a *passive* manner. Thus, in the typical case of the binary solvent system of organic molecule (good solvent) and water (poor solvent) (cf. Chapter IX), it can be assumed that the free energy level of the total chromatographic system (taking place in a slice of the column) is raised when the contact with water molecules of both the nonpolar part of sample molecule and the nonpolar surface of the adsorbent occurs. The driving force of the adsorption of sample molecule on the adsorbent surface is generated by the mechanism of minimizing the total area of the two kinds of contact with water molecules in order for the free energy of the total chromatographic system to be at a minimum. This type of adsorption is said to be done by a hydrophobic interaction. Of course, water can be replaced by another poor solvent, and the terminology "hydrophobic" may be replaced by "solvophobic". With respect to the role of good solvent in the binary solvent sysyem, there are two ways of consideration in connection with the consideration on the dependence of capacity ratio k (or molecular partition B in the liquid phase) on concentration or volume fraction, m, of good solvent, which will be argued in the following paragraph. [In connection, it should be pointed out that the meaning of "solvophobicity" mentioned above is different from that used in the treatment of Horváth et al.(A11.63-A11.65) performed in great reference to the study of Siano & Iu(A11.66); see the subsequent subsection entitled "Solvophobic Model".]

Assuming that the adsorption of sample molecule on the adsorbent surface is brought about by the passive mechanism, there may be two ways of consideration on the mechanism of the dependence of k (or B) on m. In the first way, both sample molecule and good solvent molecule are treated equally, and we assume explicitly that good solvent molecule is also adsorbed on the adsorbent surface in order to reduce the total area of the contact with water molecules of both the nonpolar part of good solvent molecule and the nonpolar surface of the adsorbent. This implies that competition does take place between sample molecule and good solvent molecule for adsorption on the adsorbent surface (provided that both sample molecule and good solvent molecule are dissolved in water in the liquid phase, and that the aggregation does not take place among them even on the adsorbent surface). As a result, k would decrease (or B would increase) with increase in m. A possibility cannot be excluded that, besides the passive adsorption mechanism, the active mechanism interferes at the same time where van der Waals and other types of energetical interaction are used. In the second way of consideration, the mixture of good and poor solvents is treated as a medium; this is distinguished from solute (i.e., sample molecule) conceptually. All models presented below (focused on reversed-phase chromatography) are based on the second way of consideration. [It should be pointed out that the second way of consideration is less natural than the first since we a priori have no reason why the mixture of good and poor solvents (being an assembly of molecules) should con-

ceptually be different from solute (also being an assembly of molecules). Let us begin, however, with simply accepting the second way of consideration.]

Solvophobic Model. According to the solvophobic theory of Siano ğlu(A11.66) which is reviewed in ref(A11.63), the stability of the dissolved state of a solute molecule in the solvent depends importantly on the surface tension, γ, of the cavity formed in the bulk solvent surrounding the solute molecule. The energetical interaction taking place between solute molecule and the surrounding solvent also contribute to the stability, and it involves both van der Waals and electrostatic interactions(A11.63, A11.66). With reference to this theory, Horváth et al.(A11.63, A11.65) hypothesized as follows. With reversed-phase chromatography (especially with that performed on the column packed with C_{18} particles), the association between sample molecule and the packed particle in the column should occur on the hydrocarboneous ligand protruded on the particle. (For simplicity, it can be assumed that the one-to-one association takes place between sample molecule and the ligand). The total surfaces of both sample molecule and ligand that are exposed to the solvent in the association state is smaller by the contact area between them (denoted by ΔA) than those taking place before association. This means that the surface of the cavity of the solvent surrounding the complex of sample molecule and ligand (except the part joined to the support particle) should also be smaller by ΔA than the total surfaces of the cavities for both sample molecule and ligand before association.

When the solvent is poor, the decrease, ΔG_c^{assoc}, of the free energy of the total system contributed from the decrease in the total tension energies of the cavities (due to the decrease in the total surface area of the cavities, which is brought about by the association between sample molecule and ligand) can be represented by ref(A11.65) eq(4) as

$$\Delta G_c^{assoc} = -\gamma \Delta A - \gamma A_s(\kappa^e - 1) \qquad \text{(A11.109)}$$

in which A_s is the surface area per solvent molecule and κ^e is the factor which adjusts the macroscopic surface tension to the dimensions of the solvent molecule. The contribution, ΔG_{vdw}^{assoc}, from the van der Waals interaction can be represented by ref(A11.65) eq (7) as

$$\Delta G_{vdw}^{assoc} = -W - a\Delta A \qquad \text{(A11.110)}$$

in which W and a are solvent dependent parameters. The contribution, ΔG_{es}^{assoc}, from the electrostatic interaction can be represented by ref(A11.65) eq(9) as

$$\Delta G_{es}^{assoc} = \Delta Z/\varepsilon \qquad \text{(A11.111)}$$

in which ε is the dielectric constant of the medium, and ΔZ stands for the change of the total effective electric charges and/or dipoles on both sample molecule and ligand brought about by the association between them.

On the other hand, the change, ΔG, of the free energy of the total system taking place in the chromatographic binding process is related to capacity ratio, k, as

$$\ln k = \ln \phi - \Delta G/kT \qquad \text{(A11.112)}$$

in which ϕ represents the phase ratio [see Chapter I (A), and ref(A11.65) eqs(1) and (2)], and it can be hypothesized(A11.63, A11.65) that the sum of ΔG_{e}^{assoc}, ΔG_{vdw}^{assoc} and ΔG_{es}^{assoc} should offer the major contribution to ΔG. Substituting the sum of eqs(A11.109)-(A11.111) for ΔG into eq(A11.112), and adding the term $\ln[kT/(P_0V)]$ [which arises from Siano & lu's theory(A11.66) and which offers a minor contribution to ΔG; P_0=atmospheric pressure, V=volume per solvent molecule], ln k can finally be represented by ref(A11.65) eq(11) as

$$\ln k = \ln \phi + [(\gamma + a)\Delta A + A_s(\kappa' - 1)\gamma + W - \Delta Z/\varepsilon]/kT + \ln[kT/(P_0V)] \qquad \text{(A11.113)}$$

In the practical viewpoint, however, the greatest effect on capacity factor k can be considered(A11.63, A11.65) to arise from the changes in the surface tension energy $\gamma \Delta A$ and the conjugate function $A_s(\kappa' - 1)\gamma$, and eq(A11.113) can be rewritten practically as

$$\ln k = \text{constant} + [A_s(\kappa' - 1)\gamma + a\Delta A + \gamma \Delta A]/kT \qquad \text{(A11.113')}$$

In eq(A11.113) or (A11.113'), ΔA would increase with increase in size of sample molecule, to be precise, size of the hydrocarboneous part of sample molecule [provided that the size of the (hydrocarboneous part of) sample molecule is smaller than that of the ligand always]. Therefore, ln k would increase with increase in size of the (hydrocarboneous part of) sample molecule [see eq(A11.113')]. On the other hand, γ or $(\kappa' - 1)\gamma$ would depend on volume fraction, m, of good solvent in the binary solvent system (where it should be recalled that the argument is performed in the second way of consideration; see the prededing subsection entitled "General"). Thus, according to the calculation of Horváth et al. [see ref(A11.65) Figs 8 and 9; cf. ref(A11.63) Figs 15 and 16], with either MtOH/H_2O or ACN/H_2O system, γ or $\gamma \Delta A$ decreases monotonically with increase in m (for MtOH or ACN), whereas $A_s(\kappa' - 1)\gamma$ first increases and then decreases with increase in m. Despite the presence of a maximum in the change of $A_s(\kappa' - 1)\gamma$, however, the sum of $\gamma \Delta A$ and $A_s(\kappa' - 1)\gamma$ decreases quasi-linearly with increase in m [see ref (A11.65) Figs 8 and 9; cf. ref(A11.63) Figs 15 and 16]; this means that ln k decreases quasi-linearly with increase in m [see eq(A11.113')]. All the above conclusions appear to be compatible with experimental data at least qualitatively [see refs(10.19, A11.63, A11.64, A11.67-A11.69)]. With regard to reversed-phase chromatography data shown in Figs 9.1, 9.2, 9.20-9.22, 9.25 and 9.26, and in Tables 9.5 and 9.6], both the linear decrease of ln k as a function of m and the increase of ln k as a function of P (which would bring about an increase in ΔA) appear to be explained qualitatively by the solvophobic theory. (But see the subsequent subsection entitled "Interactioin Indices Model" for further criteria of the theory.)

It should be underlined again that, in the second way of consideration [used in refs (A11.63)-(A11.65)], the solvophobicity is concerned with the mean (or macroscopic) prop-

erty of the binary solvent system. In this instance, the passive adsorption mechaism of sample molecule on the adsorbent surface implies that the mobile phase plays a predominant role for the adsorption. In the first way of consideration, however, the solvophobicity is concerned with the poor solvent in the binary solvent system, and the terminology "solvophobic" can be replaced by that of "hydrophobic" in most cases of reversed-phase chromatography when the poor solvent represents water. In the first way of consideration, the passive adsorption mechanism, in general, does not mean that the mobile phase plays a predominant role for the adsorption of sample molecule on the adsorbent surface.

Karger et al.(A11.70) also assumed the hydrophobic interaction between sample molecule and adsorbent with reversed-phase chromatography, and introduced the topological index (called molecular connectivity) to represents the surface area of sample molecule (or its functional group); this would account for the hydrophobicity of each molecule and the chromatographic selectivity among different molecules. With regard to the binary solvent system, semi-empirical arguments were performed in the second way of consideration [see ref(A11.70)].

Interaction Indices Model. In the abstract, while stating that this model is not theoretical but rather empirical, Jandera et al.(A11.71) hypothesized that, with reversed-phase chromatography, either sample or solvent molecule (denoted by A) in the mobile phase should be characterized by a parameter I_A (called interaction index). The energy of interaction between molecule A_1 and A_2 taking place in the mobile phase should be represented as $C_{A1}I_{A1}\cdot C_{A2}I_{A2}$, where C_{A1} and C_{A2} are constants depending on the relative chemical functionalities of molecule A_1 and A_2 occurring when they meat each other(A11.71). The free energy of transfer from mobile to stationasry phase per sample molecule, ΔG, should be represented by ref(A11.71) eq(4) as

$$\Delta G = -(C_M^2 I_M^2 - C_M C_X I_M I_X) V_X \qquad \text{(A11.114)}$$

in which the subscript X stands for sample molecule and V_X represents its volume; the subscript M stands for solvent molecule. With the binary solvent system of organic substance (denoted by ORG) and water, I_M should be represented as arithmetic mean of I_{H_2O} and I_{ORG} as

$$I_M = (1-m)I_{H_2O} + mI_{ORG} \qquad \text{(A11.115)}$$

[ref(A11.71) eq(6)] where m stands for the volume fraction of organic substance or good solvent (second way of consideration; see the subsection entitled "General"). On the other hand, ln k can be represented by ref(A11.71) eq(5) or eq(A11.112); this can be rewritten by using both eqs(A11.114) and (A11.115) as

$$\ln k = \ln \phi + (V_X I_{H_2O} C_M / kT)(C_M I_{H_2O} - C_X I_X)$$

$$- (V_X C_M / kT)(2I_{H_2O} C_M - I_X C_X)(I_{H_2O} - I_{ORG})m$$

$$+(V_X C_M^2/kT)(I_{H_2O}-I_{ORG})^2 m^2 \qquad \text{(A11.116)}$$

[ref(A11.71) eq(8)].

Jandera(9.14) hypothesized that, with a homologous saturated aliphatic series with different degrees of polymerization P [such as considered in Chapter IX(F)], both V_X and I_X should increase linearly with increase in P following ref(9.14) eqs(3) and (4) as

$$V_X = V_{0X} + P\Delta V_X \qquad \text{(A11.117)}$$

and

$$I_X = I_{0X} + P\Delta I_X \qquad \text{(A11.118)}$$

respectively, where V_{0X}, ΔV_X, I_{0X} and ΔI_X represent constants. Substituting both eqs (A11.117) and (A11.118) into eq(A11.116), and neglecting the quadratic term with respect to P, eq(9.50) can be derived, and, if the quadratic term with respect to m is also neglected, eq(9.50) reduces to eq(9.49), where

$$\hat{\alpha}_{J0} = (C_M I_{H_2O}/kT)[(C_M I_{H_2O}-C_X I_{0X})\Delta V_X - C_X V_{0X}\Delta I_X] \quad [=J^s/(PkT)] \qquad \text{(A11.119)}$$

$$\hat{\beta}_{J0} = \ln\phi + (V_{0X}C_M I_{H_2O}/kT)(C_M I_{H_2O}-C_X I_{0X}) \quad [=\ln(\beta e^{J^s/kT})] \qquad \text{(A11.120)}$$

$$\hat{\alpha}_{J1} = [C_M(I_{H_2O}-I_{ORG})/kT][(2C_M I_{H_2O}-C_X I_{0X})\Delta V_X - C_X V_{0X}\Delta I_X] \quad [=x''^s\varphi/P] \qquad \text{(A11.121)}$$

$$\hat{\beta}_{J1} = (V_{0X}C_M/kT)(2C_M I_{H_2O}-C_X I_{0X})(I_{H_2O}-I_{ORG}) \quad [=x''^s\varphi] \qquad \text{(A11.122)}$$

$$\hat{\alpha}_{J2} = (C_M^2\Delta V_X/kT)(I_{H_2O}-I_{ORG})^2 \quad [=\tfrac{1}{2}x''^s\varphi^2/P] \qquad \text{(A11.123)}$$

and

$$\hat{\beta}_{J2} = (V_{0X}C_M^2/kT)(I_{H_2O}-I_{ORG})^2 \quad [=\tfrac{1}{2}x''^s\varphi^2] \qquad \text{(A11.124)}$$

[cf. ref(9.14) eqs(6a)-(6f)]. In the thick brackets in the exreme right-hand sides of eqs (A11.119)-(A11.124) are presented the interpretations obtained on the basis of competition model(Chapter VIII) [see eqs(9.53), (9.54), (9.61), (9.62), (9.66) and (9.67); cf. eqs(9.31), (9.39), (9.44), (9.45) and (9.57)].

As mentioned in Chapter IX(F), both eqs(9.49) and (9.50) manifest excellent fits with experiment. Is the physical mechanism hypothesized in interaction indices model realizable actually, however? In this model, the hypothesis that the energy of interaction between a pair of molecules A_1 and A_2 should be represented by a product of $C_{A1}I_{A1}$ and $C_{A2}I_{A2}$ (see above) appears to come from the analogy with the fact that the energy of interaction between a pair of particles with electric charges q_1 and q_2, respectively, is proportional to the product q_1q_2. On the other hand, eq(A11.114) states that the free energy, ΔG, of adsorption should be generated by the replacement of a pair of solvent molecule M and sample molecule X (where the absolute value of the interaction energy is small) by a pair of solvent molecule M and another solvent molecule M (where the absolute value of the

interaction energy is large). If this statement holds approximately when both sample and solvent molecules are comparable in size, it would be difficult to consider that the statement still holds when sample molecule is much larger than solvent molecule in size. In order to dodge this difficulty, it simply is assumed that interaction index I_x should increase linearly with increase in "size" P of sample molecule[eq(A11.118)], which evidently is questionable. The authors themselves mention(A11.71) that they "wish to point out that, although some of the assumptions made in the derivation of the basic equations may be questionable, the agreement between the calculated and experimental values of the capacity ratios is often surprisingly good". They also mention(A11.71) that "the assumption of the negligible contribution of the stationary phase to the retention process can be undoubtedly refused in some cases".

Eq(A11.113') resembles eq(9.49) if γ and ΔA are proportional to m and P, respectively and if both $A_s(\kappa^s-1)$ and a are constant. The contradiction arises between the two equations, however. Thus, in eq(11.113') with replacements, the sign of the coefficient of mP should be positive, whereas, in eq(9.49), the experimentally estimated value of the corresponding coefficient, $-\hat{a}_{j1}$, is negative always (see both Tables 9.5 and 9.6). More fundamentally, according to the calculation of Horváth et al. [see ref(A11.63) Figs 13 and 14], it is difficult to regard $A_s(\kappa^s-1)$ as constant. In deference to the precision experiments of homologous polymers performed by Jandera(9.13, 9.14) which are consistent with either eq(9.49) or (9.50) [see Chapter IX(F)] and not with eq(A11.113'), it now is difficult to accept the solvophobic model proposed by the Horváth's group (see the subsection entitled "Solvophobic Model"). On the other hand, interaction indices model is questionable with respect to the physical mechanism proposed by the model (see above). Taking into account all the arguments performed in Chapter IX, it is reasonable to accept competition model(Chapter Ⅷ) for reversed-phase chromatography, which is consistent with both eqs (9.49) and (9.50). Cf. the subsequent Section(F).

(E) Solubility Parameter Model

With reversed-phase chromatography, in an image of partition chromatography [see Chapter I (A)], Tijssen et al.(A11.72) and Schoenmakers et al.(A11.73) hypothesized that partition of sample molecules between mobile and stationary phases should be brought about by the balance of the values of the solubility parameters taking place in the respective phases. The solubility parameter is defined thermodynamically as square-root of internal potential energy compared with the ideal gas state (called cohesive energy density); the partial solubility parameters for dispersion, orientation, induction, and acid and base interactions together determine the total solubility parameter(A11.72, A11.73). Assuming that any partial solubility parameter for the binary mobile phase system (usually the organic solvent/water system) is an arithmetic mean of those for the respective components of the system (weighted with volume fractions), ln k can be represented as a quadratic

form of volume fraction, m, of the less polar solvent; partrial and total solubility parameters for both mobile and stationary phases are involved in the coefficients of the terms of the 0th, 1st and 2nd power of m [see eqs(19)-(26) and Table II in ref(A11.73), respectively]. It can be seen in ref(A11.73) Figs 2 and 3 that the dependence of ln k on m can be well represented by the quadratic equation for phenol in MtOH/H_2O, ethanol/H_2O and n-propanol/H_2O mobile phase systems, and for m-cresol, 2,4-dimethylphenol, alanine, diethylphthalate and dibutylphthalate in the MtOH/H_2O mobile phase system.

Schoenmakers et al.(A11.73) mention, however, that "chemically bonded (C_{18}) phases may not have the properties of bulk phases for which the solubility parameter theory has been derived" and that "it is more likely that they constitute an interfacial layer between the mobile phase and the silica support material". They hypothesized(A11.73) that the discrepancy to theory of the experimental data with respect to enthalpy and entropy contributions may arise from this problem, and that the problem should be reduced by assuming that the effective properties of the stationary phase change with the composition of the mobile phase. Assuming that the variation of the effective stationary phase properties with volume fraction m of organic solvent in the organic solvent/water mobile phase system occurs linearly[ref(A11.73) eq(20)], the direction of the change of the coefficients of the quadratic expression of ln k taking place in connection with enthalpy and entropy contributions can be corrected to the reasonable direction in fact(A11.73). Despite this correction, however, the change is generally too small to provide a reasonable description of the experimental data [for detail, see ref(A11.73)].

(F) Statistical Mechanical Model

Boehm and Martire Model. Making reference to the previous theory of DiMarzio (A11.74) on the lattice statistics for rigid rod-like polymer molecules and employing a cubic lattice model to enumerate the possible molecular arrangements in both mobile and stationary phases, Boehm and Martire(A11.75, A11.76) developed a statistical mechanical study on the adsorption and desorption of rigid molecules taking place in the chromatographic column. Thus, supposing that cubic unit lattices are piled up in x, y and z directions in the (x,y,z) space to complete a three-dimensional lattice space, it is possible to consider that the partial lattice space occurring when $z \geqq 0$ represents the interstice in the column; the (x,y) plane defined at $z=0$ represents the adsorbent surface. In this concept, it was hypothesized(A11.75, A11.76) as follows. In the column interstice, either good or poor solvent molecule (the case of the binary solvent system) occupies a unit lattice, whereas a sample molecule, in general, occupies plural lattices. For instance, a rigid rod-like molecule constructed of P contiguous monomers occupies P contiguous lattices arranged in x, y or z direction; only molecular orientations either parallel or normal to the adsorbent surface are considered. The column interstice is filled with solvent and sample molecules without any vacancy. When solvent molecule (with cubic shape) and sample mol-

ecule (with cubic, tetragonal or orthorhombic shape) keep in contact with the adsorbent surface through one of the six sub-surfaces, they can be regarded as being in the stationary phase, respectively. Otherwise, they are in the mobile phase. In res(A11.75, A11.76), the limiting case of infinite dilution of sample molecules is treated when the mutual contact between sample molecules is negligible in both mobile and staionary phases.

In refs(A11.75, A11.76), the nearset neighbor energetical interactions among solvent and sample molecules (through the six sub-surfaces of the respective substances) were studied along with the energetical interactions of the substances with the adsorbent surface, and the Bragg-Williams random mixing approximation was used to estimate the number of molecular pairings of each type. The competitive equilibrium among solvent and sample molecules distributed between mobile and stationary phases was examined. Thus, the canonical partition functions for both mobile and styationary phases were calculated, and, by using the equilibrium condition of equal chemical potentials for any component of the mixture between mobile and stationary phases, mole fraction distribution coefficient, K, for sample molecule was calculated. K is defined as $K \equiv x_{3s}/x_{3m}$ where x_{3s} and x_{3m} stand for mole fractions of sample molecules taking place in stationary and mobile phases, respectively; K is proportional to capacity ratio k.

Denoting by 1 and 2 the two components of the binary solvent system, mole fractions x_{is} and x_{im} for each component (where $i=1$ or 2) taking place in stationary and mobile phases are conceivable, respectively, and it is possible to regard K as a function of x_{im} (where $i=1$ or 2). As parameters, function $K(x_{im})$ involves nearest neighbor interaction energies, w_{ij}, between an i-j pair (where i, j=1, 2, 3; the suffix 3 is assigned to a monomer unit or a segment of sample molecule), and adhesion energies, $\dot{e}_i$, between solvent molecule and adsorbent surface (when $i=1$ or 2) and between a segment of sample molecule and adsorbent surface (when $i=3$); to be precise, $\dot{e}_i$ represents temperature dependent free energy rather than energy. The parameters w_{ij} and $\dot{e}_i$ appear in the forms:

$$w_{ij} - \tfrac{1}{2}(w_{ii}+w_{jj}) \equiv \Delta_{ij} \qquad \text{(A11.125)}$$

in which i, j=1, 2, 3 with $i \neq j$, and

$$\dot{e}_3 - \dot{e}_i + w_{ii} - w_{i3} \equiv -\Delta\,\dot{e}(i,3) \qquad \text{(A11.126)}$$

in which i=1, 2. Δ_{ij} represents the interchange energy required to generate an i-j nearest neighbor pair from i-i and j-j nearest neighbor pairs. $-\Delta\,\dot{e}(i,3)$ represents the net (free) energy change taking place when a segment of sample molecule is adsorbed accompanied with the concomitant desorption of type i solvent molecule at the common site on the adsorbent surface, provided that the other type j ($\neq$i) of solvent is absent. The process under consideration can be represented symbolically as $3(m)+i(s) \rightleftarrows 3(s)+i(m)$ where i=1 or 2, and m and s stand for mobile and stationary phases, respectively. When $\Delta\,\dot{e}(i,3)>0$ and $\Delta\,\dot{e}(i,3)<0$, the the adsorption of the segment of the sample molecule and the adsorption of the i type solvent molecule are energetically preferred, provided

that the other type j ($\neq$i) of solvent is absent, respectively.

The reciprocal of mole fraction distribution coefficient K was calculated as a function of mole or volume fraction x_{2m} while changing the combination of parameter values for both cases when sample molecule is a cubic monomer (constructed of only one segment) [ref(A11.76) Fig 1] and when sample molecule is rod-like in shape (constructed of some contiguous segments); this latter involves two sub-cases when segments are homogeneous and heterogeneous in property[ref(A11.76) Fig 4]. Several intricate curves can be found in both Figs1 and 4 in ref(A11.76). The case when sample molecule has other shapes and the case when the adsorbent surface is heterogeneous constituted of a random mixture of lattices with different properties were also examined in refs(A11.75, A11.76). Although suggestive, the results of the calculations are abstract; the comparison of theory and experiment is not done in a concrete manner (such as those performed in Chapter Ⅷ-X).

Boehm, Martire, Armstrong and Bui Model. While conserving the concept of cubic lattice space, Boehm and Martire in collaboration with Armstrong and Bui(A11.77-A11.79) reformed the theory for rigid molecules (the preceding sebsection) to the theory for flexible chain-like homopolymer molecules; a unit lattice of the space now is occupied by a segment of the flexible polymer chain. The new theory, in principle, is adequate to reversed-phase chromatography of polystyrene, and the authors' interest is partially focused on the mechanism of the abrupt change from $\approx\infty$ to ≈ 0 of capacity ratio k (or the abrupt change from ≈ 0 to ≈ 1 of molecular partition B in the mobile phase) taking place with increase in volume fraction m of good solvent in the binary solvent system especially when degree of polymerization P of homopolymer is very high ["on-off" mechanism; see Chapter Ⅸ(B) and (C)]. The interest is also focused on the mechanism of the increse (taking place with increase in P) of the m values over which is brought about the transition of k from $\approx\infty$ to ≈ 0 (or the transition of B from ≈ 0 to ≈ 1), and the mechanism of the asymptotic approach of these m values to a limiting finite value taking place when P approaches infinity [cf. Chapter Ⅸ(B) and (C)]. As will be mentioned below, the authors(A11.77-A11.79) consider that the increase of the m values of transition (or the m value at which $k=1$ or $B=1/2$) taking place with increase in P is mainly brought about by the flexibility of the polymer chain (at least when P is large enough), which enables the molecule to change its configurational geometry and size in response to the solvent and/or adsorbent surface environment.

As for the treatment of flexible polymers, both Flory-Huggins' lattice model(A11.80) and McMillan-Mayer's solution theory(A11.81) were applied to great extents. In ref (A11.77), the case of infinite dilution of sample molecules is treated, and, in ref(A11.78), the theory is extended to the case of semi-dilute polymer solutions when account is taken of inter-molecular interactions. In ref(A11.79), some improvements were added to the theories developed in both ref(A11.77, A11.78). We here consider only the case of infinite dilution of sample molecules.

Thus, the authors(A11.77-A11.79) hypothesized as follows. In either mobile or sta-

tionary phase, the polymer molecule entrains the binary solvent system containing both good and poor solvent molecules, where the ratio of volume fractions between the two types of solvent molecule is kept equal to that taking place in the exterior solvent environment. The complex of sample molecule and entrained solvent can be regarded as an independent thermodynamic or statistical mechanical system; the total canonical partition function can be regarded as a product of the canonical partition function for the complex by that for the exterior solvent environment. Both configurational geometry and size of the flexible polymer-entrained solvent system depends on not only the exterior solvent environment (i.e., the composition of the binary solvent) but also the type of phase in which the system belongs (i.e., mobile or stationary phase). These are determined by (a) the energetical interaction of each segment of polymer molecule with nearest neighbor solvent molecules (when polymer molecule is in the mobile phase) or that with both nearest neighbor solvent molecules and adsorbent surface (when polymer molecule is in the stationary phase), (b) the excluded volume effect taking place within the polymer molecule, and (c) the configurational entropy of the flexible polymer-entrained solvent system estimated by using the Bragg-Williams approximation. Especially, the size of the system depends on the number of entrained solvent molecules directly, and favorable and unfavorable solvent environments bring about expansion and contraction of the system, respectively. These cannot proceed indefinitely because they are opposed by the corresponding decrease in configurational entropy. The relative phase preference of the polymer molecule depends on all the above factors.

It can further be hypothesized(A11.77-A11.79) that, with reversed-phase chromatography, the less polar component (i.e., good solvent molecule) in the binary solvent system is predominantly adsorbed on the adsorbent surface while fulfilling both relationships:

$$\dot{e}_1 \ll \dot{e}_2 \quad \text{or} \quad \exp[-(\dot{e}_1 - \dot{e}_2)/kT] \gg 1 \tag{A11.127}$$

and

$$x_{2s} \ll x_{1s} \approx 1 \tag{A11.128}$$

where subscript 1 and 2 stand for the less polar component (good solvent molecule) and the more polar component (poor solvent molecule), respectively. It therefore is apparent that the adsorbent surface is mostly constructed of strongly adsorbed good solvent molecules which are replacable with segments of polymer molecule. Moreover, reversed-phase chromatography is usually carried out in favorable environments (in both mobile and stationary phases), and the flexible polymer-entrained solvent system behaves as a swollen spherical gel and a thin cylindrical gel in mobile and stationary phases, respectively (A11.77-A11.79). Under these assumptions, especially when degree of polymerization P is high enough, ln k divided by P can be represented approximately by ref(A11.79) eq(26) as

$$P^{-1}\ln k = \ln[u(1+u)^{-1}\exp\{-\Delta\dot{e}(1)/kT + (c_s c_m^{-1}(1+u)^{-1} - 1 + x_{1m})(\chi_{13}^{m} + \chi_{12}^{m} - \chi_{23}^{m})\}$$

$$+(1+u)^{-1}\exp[-\Delta\dot{e}(2)/kT+(c_s c_m^{-1}u(1+u)^{-1}-x_{1m})(\chi_{23}^{m}+\chi_{12}^{m}-\chi_{13}^{m})]]$$

$$-2g_s^{1/2}P^{-1/2}+(5/2)g_m^{2/5}P^{-4/5}+P^{-1}\ln(Jg_s^{1/2}g_m^{-3/5}P^{1/5}) \qquad \text{(A11.129)}$$

The physical meanings and the definitions of the symbols in eq(A11.129) are as follow. c_m and c_s stand for the lattice coordinate numbers in mobile and stationary phases, equal to 6 and 5 with cubic lattice model, respectively. x_{1m} corresponds to our usual notation m (representing mole or volume fraction of good solvent in the mobile phase). J is defined as

$$J \equiv \phi c_s(c_m-1)^2(2\pi/3)^{1/2}/[c_m(c_s-1)^2] \qquad \text{(A11.130)}$$

in which ϕ is a positive constant representing the phase ratio [cf. eq(A11.112)]. $\Delta\dot{e}(i)$ (i=1,2) is defined as

$$\Delta\dot{e}(i) \equiv \Delta\dot{e}(i,3)+kT\ln[(c_m-1)/(c_s-1)] \qquad \text{(A11.131)}$$

χ_{ij}^{a} (where i,j=1,2,3 with $i\neq j$, and a=m or s, m and s representing mobile and stationary phases, respectively) is defined as

$$\chi_{ij}^{a} = c_a\Delta_{ij}/kT \qquad \text{(A11.132)}$$

u is defined by using the relationship $c_m-c_s=1$ (see above) as

$$u \equiv x_{1m}(1-x_{1m})^{-1}\exp[(1-2x_{1m})\chi_{12}^{m}+\chi_{12}^{s}+(\dot{e}_{1s}-\dot{e}_{2s})/kT+\tfrac{1}{2}(w_{11}-w_{22})/kT] \qquad \text{(A11.133)}$$

It can be assumed(A11.79) that, in addition to both eqs(A11.127) and (A11.128), the approximations:

$$x_{1s} \approx u(1+u)^{-1} \qquad \text{(A11.134)}$$

and

$$x_{2s} \approx (1+u)^{-1} \qquad \text{(A11.135)}$$

hold with reversed-phase chromatography [which have been used for the derivation of eq (A11.129)]. Finally, g_a (a=m,s) is defined as

$$g_a = 1/2-x_{1a}\chi_{13}^{a}-x_{2a}\chi_{23}^{a}+x_{1a}x_{2a}\chi_{12}^{a} \qquad \text{(A11.136)}$$

characterizing the quality of the binary solvent system vis-à-vis to the polymer molecule. Thus, if $g_a>0$ and $g_a<0$, then the binary solvent system is favorable and unfavorable to the polymer molecule in either phase a, respectively. If $g_a=0$, the binary solvent system represents a theta solvent.

When degree of polymerization P is not high enough, the expression of ln k divided by P is much more complicated [see ref(A11.79) eq(27) accompanied with several equations].

For the hypothetical polymer molecule that is not swollen nor distorted while main-

taining the same average configuration in both mobile and stationary phases, ln k divided by P can be represented by ref(A11.79) eq(29) as

$$P^{-1}\ln k = \ln [u(1+u)^{-1}\exp\{-\Delta \dot{e}(1)/kT+(c_s c_m^{-1}(1+u)^{-1}-1+x_{1m})(\chi_{13}^{m}+\chi_{12}^{m}-\chi_{23}^{m})\}$$
$$+(1+u)^{-1}\exp\{-\Delta \dot{e}(2)/kT+(c_s c_m^{-1}u(1+u)^{-1}-x_{1m})(\chi_{23}^{m}+\chi_{12}^{m}-\chi_{13}^{m})\}]$$
$$+ (1-\delta_{1P})P^{-1}\ln [(2\pi/3)^{-1/2}J] + \delta_{1P}\ln\phi \qquad \text{(A11.137)}$$

where δ_{1P} denotes Kronecker's delta (with $\delta_{1P}=1$ when $P=1$ and $\delta_{1P}=0$ otherwise), and $\Delta \dot{e}(i)\equiv \Delta \dot{e}(i,3)$ when $P=1$. It can be interpreted [see ref(A11.79)] that the molecule with a rigid structure belongs in this type of molecule.

The three curves drawn in Fig A11.3 [reproduced from ref(A11.79)] represent the critical volume fractions (at which $k=1$ or $B=1/2$; denoted by x_c) of good solvent in the binary solvent system as functions of P (written as M) obtained by solving eq(A11.129) (curve 1), ref(A11.79) eq(27) [precision expression of eq(A11.129); curve 2] and eq (A11.137) (curve 3) into which $k=1$ is substituted, respectively. All the calculations were performed assuming: $\phi=0.5$, $x_{1s}\approx 0.97$, $\chi_{12}^{m}=0.5$, $\chi_{13}^{m}=0.0$, $\chi_{23}^{m}=1.0$, $\Delta \dot{e}(1,3)/kT=-0.1$ and $\Delta \dot{e}(2,3)/kT=-1.683$. These selections are consistent with solvents 1 and 2 being completely miscible, being respectively good and poor for the polymeric solutes, and respectively possessing comparable and considerably less affinity for the adsorbent surface than the solute on a per segment basis(A11.79). The mixed mobile phase also provides a favorable solvent environment when $g_m \geqq 0$ which is satisfied for $1 \geqq x_{1m} \geqq (3-\sqrt{5})/2 = 0.382$ for the χ_{ij}^{m} values selected above [see ref(A11.79)].

It can be seen in Fig A11.3 that, for the flexible solute homologues(curve 1 and 2), x_c passes through a minimum in the oligomer range and then increases monotonically to an asymptotic value $x_c^{\infty}=0.8504$ with increase in P. A simple monotonical increase of x_c with increase in P is obtained for the solute homologues with rigid structures where, however, x_c is almost independent of P when $P \gtrsim 10$(curve 3). The asymptotic parts of the three curves are almost identical. The authors(A11.79) mention that the x_c-P dependence of the flexible homopolymers is related to their ability to adjust their dimensions in response to their solvent and/or adsorbent surface environment. They(A11.79) also mention: "This feature distinguishes flexible polymers and oligomers from their structurally rigid counterparts and assists, in principle, in their fractionation for large P by gradient elution HPLC, and the chromatographic separation of the structurally rigid chain-like homopolymers is predicted to be considerably more difficult than for their flexible counterparts" (when P is large enough); similar limitations on the separability of rigid rod-like solutes as P increases have been predicted previously(A11.77). [Fig A11.3 can be compared with Fig 8.5 where it can be seen that the critical potassium molarity at which $B=1/2$ increases monotonically with increase in x' (or M_m) of the solute homologue and that the critical m tends to a finite value m' as x' (or M_m) approaches infinity. It should be noted, however,

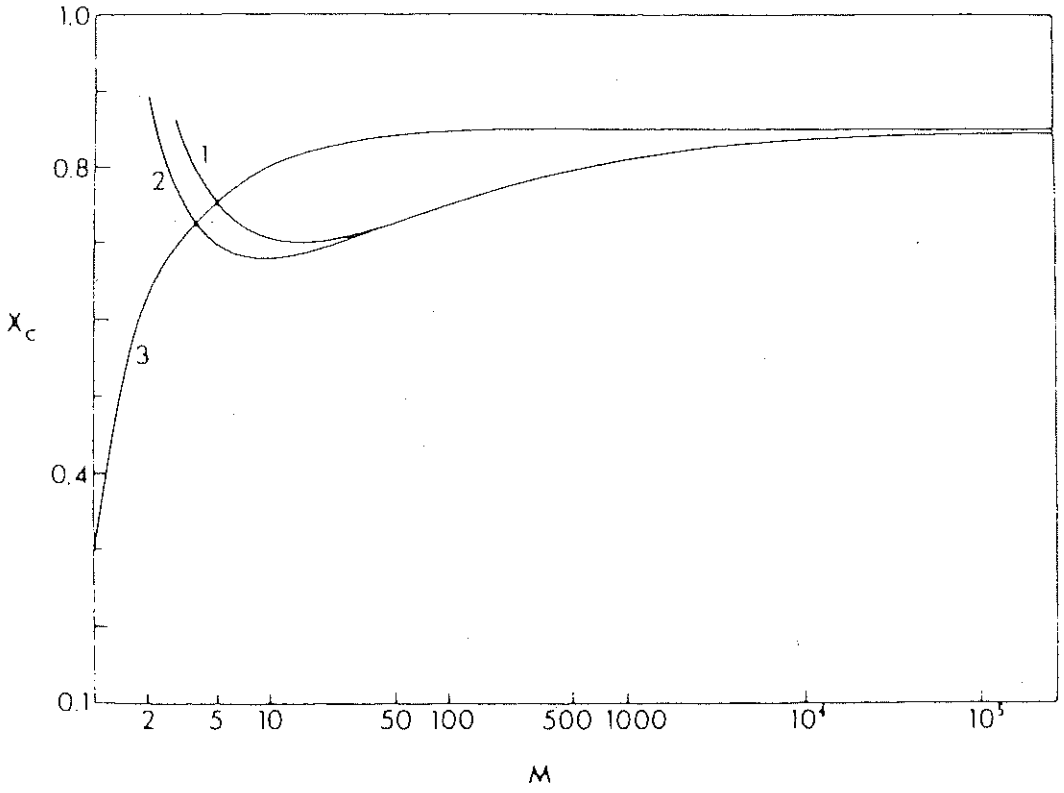


Fig A11.3. Critical volume fractions, x_c, of good solvent as a functions of degree of polymerization, P, of homologues; P is written as M. Curve 1, 2 and 3 were obtained by solving eq(A11.129), ref(A11.79) eq(27), and eq(A11.137) into which k=1 is substituted, respectively. For detail, see text. [Reproduced from ref(A11.79) Fig 1.]

that, in Chapter Ⅷ, the terminology "critical" is used to represent m* (corresponding to x_c^{∞}) rather than the m value at which B=1/2 or k=1.]

In the immediate vicinity of x_c, by using a Taylor expansion, ln k can be expressed as

$$\ln k = P \sum_{j=1}^{\infty} A_j (x_{1m} - x_c)^j \qquad \text{(A11.138)}$$

in which

$$A_j = (j!)^{-1} [\partial^j (P^{-1} \ln k) / \partial x_{1m}^j]_{x_{1m}=x_c} \qquad \text{(A11.139)}$$

In order to obtain simple expressions of both x_c and A_j for flexible polymer molecules, let us consider(A11.77, A11.79) the limiting case when x_{1s} tends to unity. In this instance, u approaches infinity [see eq(A11.134)], and eq(A11.129) reduces to ref(A11.79) eq(26*) or

$$P^{-1} \ln k = -\Delta \dot{e}(1)/kT - (1 - x_{1m})(\chi_{13}^m + \chi_{12}^m - \chi_{23}^m) - 2g_s^{1/2} P^{-1/2} + (5/2) g_m^{2/5} P^{-4/5} + P^{-1} \ln (J g_s^{1/2} g_m^{-3/5} P^{1/5}) \qquad \text{(A11.140)}$$

in which g_s can be represented by using eqs(A11.132), (A11.134)-(A11.136) as

$$g_s = 1/2 - (c_s/c_m)[u(1+u)^{-1} \chi_{13}^m + (1+u)^{-1} \chi_{23}^m - u(1+u)^{-2} \chi_{12}^m] \approx 1/2 - (c_s/c_m) \chi_{13}^m \qquad \text{(A11.141)}$$

A simple expression of x_c can now be obtained as x_{1m} fulfilling eq(A11.140) into which k=1 is substituted; this leads to ref(A11.79) eq(32) or

$$x_c = x_c^{\infty} + (\chi_{13}^m + \chi_{12}^m - \chi_{23}^m)^{-1} [2 g_s^{1/2} P^{-1/2} - (5/2) g_m^{2/5} P^{-4/5} - P^{-1} \ln (J g_s^{1/2} g_m^{-3/5} P^{1/5})] \qquad \text{(A11.142)}$$

in which

$$x_c^{\infty} = \lim_{P \to \infty} x_c = 1 + (\chi_{13}^m + \chi_{12}^m - \chi_{23}^m)^{-1} [\Delta \dot{e}(1,3) + kT \ln \{(c_m - 1)/(c_s - 1)\}]/kT \qquad \text{(A11.143)}$$

[see eq(A11.131)]. From its physical meaning x_c^{∞} should be comprised between 0 ana 1; this means that $-1 \leqq (\chi_{13}^m + \chi_{12}^m - \chi_{23}^m)^{-1} [\Delta \dot{e}(1,3) + kT \ln \{(c_m - 1)/(c_s - 1)\}]/kT \leqq 0$. On the other hand, by using both eqs(A11.140) and (A11.141), A_1 can be calculated as

$$A_1 = \chi_{13}^m + \chi_{12}^m - \chi_{23}^m + [g_m^{-3/5} P^{-4/5} - (3/5) g_m^{-1} P^{-1}] (\partial g_m / \partial x_{1m})_{x_{1m}=x_c} \qquad \text{(A11.144)}$$

[see ref(A11.79) eq(34)], and A_j ($j \geqq 2$) can be calculated as

$$A_1 = P^{-4/5}[\partial^{j-1}(g_m^{-3/5}\partial g_m/\partial x_{1m})/\partial x_{1m}^{j-1}]_{x_{1m}=x_c} - (3/5)P^{-1}(\partial^j \ln g_m/\partial x_{1m}^j)_{x_{1m}=x_c} \quad (A11.145)$$

[see ref(A11.79) eq(35)].

The authors(A11.77, A11.79) mention that, when P is large, then, in eq(A11.138), only the leading term of expansion contributes significantly, and that it still remains an excellent approximation to use

$$\ln k = PA_1(x_{1m} - x_c) \quad (A11.146)$$

in which x_c and A_1 are given by eqs(A11.142) and (A11.144), respectively. For reasonable selections of the binary solvent system, $\chi_{13}^m + \chi_{12}^m - \chi_{23}^m < 0$ (see above). In this instance, x_c is a monotonically increasing function of P, which asymptotically approaches x_c^∞ as P approaches infinity [see eq(A11.142)]. Under condition of $0 < x_c \leqq x_c^\infty \leqq 1$, an abrupt transition from very high to very low solute retention is predicted to occur across a narrow mobile phase composition interval centered about x_c [see eq(A11.146)]. As long as P is large, A_1 has a negative value, and $-PA_1$ increases monotonically with increase in P [see eq(A11.144)]. In this instance, eq(A11.146) [along with eqs(A11.142)-(A11.144)] appears to explain the following general trends of reversed-phase chromatography at least qualitatively. Thus, ln k decreases linearly with increase in volume fraction, x_{1m}, of good solvent; the absolute value $\hat{S} \equiv -d\ln k/dx_{1m}$ $(= -PA_1)$ of the negative slope of ln k as a function of x_{1m} increases monotonically with increase in M_m or P; and, with respect to a series of homopolymers like polystyrene, x_c shifts to high values while decreasing the rate of shift with increase in P (see Chapter IX; cf. Fig A11.3).

Alhedai et al.(9.2) attempted to make empirical fits of eq(A11.142) to the experimental x_c-P data obtained from reversed-phase chromatography of polystyrene homologues; this was carried out on C_{18} columns with 10 and 30 nm pores in the presence of the $MeCl_2$/MtOH mobile phase system in which $MeCl_2$ is the good solvent [for detail, see the legend for Fig A11.4; cf. Chapter IX(B)]. Thus, the authors rewrote eq(A11.142) as ref (9.2) eq(2) or

$$x_c = x_c^\infty + aP^{-1/2} + bP^{-4/5} + c_1P^{-1} + c_2P^{-1}\ln P \quad (A11.142')$$

in which

$$a = 2g_s^{1/2}/(\chi_{13}^m + \chi_{12}^m - \chi_{23}^m) \quad (A11.147)$$

$$b = -(5/2)g_m^{2/5}/(\chi_{13}^m + \chi_{12}^m - \chi_{23}^m) \quad (A11.148)$$

$$c_1 = -\ln(Jg_s^{1/2}g_m^{-3/5})/(\chi_{13}^m + \chi_{12}^m - \chi_{23}^m) \quad (A11.149)$$

and

$$c_2 = -1/(\chi_{13}^m + \chi_{12}^m - \chi_{23}^m) \quad (A11.150)$$

x_c^∞ [see eq(A11.143)] and c_2 are independent of the mobile phase composition or x_{1m}. The

authors(9.2) considered further that a, b and c_1 should depend only weakly on x_{1m} [cf. eq(A11.136)], and the empirical fit of eq(A11.142') was attempted. In ref(9.2), howener, it simply is mentioned that the results are not significantly better than those achieved by neglecting the last two terms, c_1P^{-1} and $c_2P^{-1}\ln P$, in eq(A11.142'). In Fig A11.4 [reproduced from ref(9.2)] are presented the results obtained by neglecting the last two terms in eq(A11.142') for both 10 and 30 nm pore columns, where ϕ_e and M stand for x_e and P of our notations, respectively.

In Fig A11.4, the points(● and ■) represent the experimental data for 10 and 30 nm columns, respectively. Curve 1 represents the best fit to the data for the 10 nm column over the range of M_m between 2×10^3 and 3.9×10^5 Da ($20\lesssim P\lesssim3.8\times10^3$) and was calculated assuming: $x_e^\infty=0.671$, $a=-0.895$ and $b=1.33$. Curve 2 represents the best fit to the data for the 30 nm column over the same M_m (or P) range and was calculated assuming: $x_e^\infty=0.701$, $a=-1.78$ and $b=2.33$. It can be seen in Fig A11.4 that the theoretical curve 1 has a minimum. When regarding only the experiment, however, the x_e (or ϕ_e) values of the arrangements of both points(● and ■) appear to increase monotonically with increase in ln P (or ln M) without passing through minima, respectively (see Fig A11.4). Below will be critisized the Boehm, Martire, Armstrong and Bui model(A11.77-A11.79) while comparing it with other experimental data.

Criticism(1). It should be recalled that eq(9.7b) or (9.7'b) has been verified by precision experiments for polystyrene homologues with high M_m ranging between 6×10^2 and 3×10^5 Da (or with degrees of polymerization P ranging between about 6 and 2.9×10^3) in the presences of both THF/H_2O and $MeCl_2$/ACN mobile phase systems (see Figs 9.1, 9.2, 9.10-9.16). It therefore is possible to endow eq(9.7b) or (9.7'b) with the qualification as an empirical formula with a high precision. Substituting $\ln k=0$ into eq(A9.7b) or (9.7'b), writing x_e for m, and replacing $\omega_M M^{2/3}$ by $\omega_P P^{2/3}$ [see both eqs(9.14) and (9.14')] lead to

$$x_e = \gamma + [(\ln\beta)/\omega_P]P^{-2/3} \qquad \text{(A11.151)}$$

in which γ (>0), $\ln\beta$ (<0) and ω_P (>0) are constants. Eq(A11.151) which corresponds to eq(A11.142) or (A11.142') can also be regarded as an empirical formula. Eq(A11.151) [in which $(\ln\beta)/\omega_P<0$] manifests that x_e decreases linearly with increase in $P^{-2/3}$, and its form is very different from that of eq(A11.142) or (A11.142').

Eq(9.7b) or (9.7'b) (empirical formula) can be rewritten as

$$\ln k = -\omega_P P^{2/3}(x_{1m}-x_e) \qquad \text{(A11.152)}$$

Eq(A11.152) corresponds to eq(A11.146) in which A_1 is represented by eq(A11.144). Again the form of eq(A11.152) is different from that of eq(A11.146) combined with eq(A11.144). Especially when P is large, eq(A11.146) combined with eq(A11.144) predicts that the absolute value of the negative slope of ln k as a function of x_{1m} increases linearly with increase in P, whereas eq(A11.152) manifests that the absolute value of the negative slope under consideration increases linearly with increase in $P^{2/3}$ always.

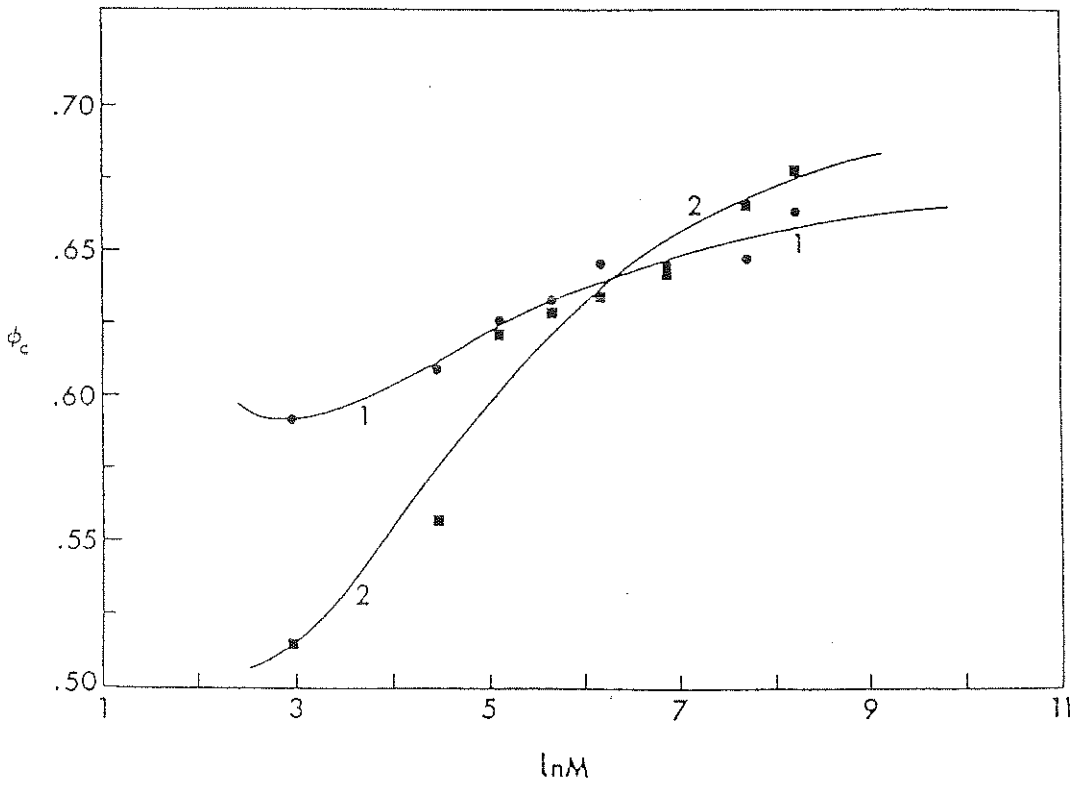


Fig A11.4. Points(● and ■): experimental plots of critical volume fractions, x_c (written as ϕ_c), of good solvent($MeCl_2$) as functions of the logarithm of degree of polymerization, P (written as M), of polystyrene homologues. These were obtained on C_{18} columns with 10 and 30 nm pores in the presence of the $MeCl_2$/MtOH mobile phase system, respectively. The plots over the range of M_n between 2×10^3 and 10^5 Da ($20\lesssim P\lesssim10^3$) were obtaied from isocratic chromatography data whereas the plots for M_n higher than 10^5 Da ($P\gtrsim10^3$) were obtained by using the "gradient elution measurement method based on the LSS gradient hypothesis" [see Chapter IX(B) Note 1]. It can be assumed(9.2) that the error arising in the latter method is small when P is large. Curve 1: the best fit to the experimental data for the 10 nm column over the range of M_n between 2×10^3 and 3.9×10^5 Da ($20\lesssim P\lesssim3.8\times10^3$) calculated assuming: $x_c=0.671-0.895P^{-1/2}+1.33P^{-4/5}$. Curve 2: the best fit to the experimental data for the 30 nm column over the same M_n (or P) range calculated assuming: $x_c=0.701-1.78P^{-1/2}+2.33P^{-4/5}$. [Reproduced from ref(9.2) Fig 5].

Finally, both curves 1 and 2 drawn in Fig A11.3 (along with curve 1 drawn in Fig A11.4) (giving x_c as a function of P for flexible homologous molecules) show minima, respectively. Curves 1 and 2 in Fig A11.3 have been calculated by using eq(A11.129) and ref(A11.79) eq(27), respectively, so that they should be more precise than that which would have been calculated by using eq(A11.142) or (A11.142'). Experimentally, however, x_c (i.e., the m value at which k=1) increases monotonically with increase in M_m or P, and the minimum does not take place at all [as judged from Figs 9.1, 9.2, 9.20(a), 9.21 (a), 9.22(a) and 9.25; also see both Tables 9.5 and 9.6]. On the other hand, curve 3 drawn in Fig A11.3 calculated for rigid molecules by using eq(A11.137) increases monotonically with increase in M_m or P. When $P \gtrsim 10$, however, x_c is almost constant, independent of P; this is not consistent with the experiment either [as underlined in refs(A11.77, A11.79)].

Criticism(2). Boehm, Martire, Armstrong and Bui model emphasizes the importance of nearest neighbor energetical interactions Δ_{ij} [eq(A11.125)] or χ_{ij}^m [eq(A11.132)] taking place in the mobile phase other than the energetical interaction $\Delta \dot{e}(i,3)$ with the adsorbent surface [eq(A11.126)]. In fact, as pointed out by the authors(A11.77), if $\chi_{13}^m + \chi_{12}^m - \chi_{23}^m = 0$ or $\chi_{12}^m = \chi_{13}^m = \chi_{23}^m = 0$, which represents an ideal ternary mixture, then the Taylor expansion of $P^{-1}\ln k$ [eqs(A11.138) and (A11.139)] does not exist, and eq(A11.146) does not apply. On the other hand, it can be considered that the solubility parameter [defined in Section(E)] intimately is related to the energetical interaction χ_{ij}^m. Schoenmakers et al.(A11.73) mention that, in the binary solvent system, water behaves so uniquely that it is difficult to describe in terms of solubility parameters; nonetheless, other authors have successfully applied the solubility parameter theory to aqueous systems. It can be seen in both Figs 9.1 and 9.2, however, that the chromatographic behavior of polystyrenes in the THF/H_2O system is quite parallel to the behavior in the nonaqueous $MeCl_2$/ACN system. This implies that, the energetical interaction, χ_{ij}^m, taking place in the mobile phase, if it contributes, does not contribute directly to the adsorption and desorption of sample molecules in the manner such as described by Boehm, Martire, Armstrong and Bui model.

Comparison with Competition Model. Both Boehm and Martire model (for rigid molecules) and Boehm, Martire, Armstrong and Bui model (for both flexible and rigid molecules) resemble competition model(Chapter Ⅷ) in that the competitive equilibrium among sample and solvent molecules distributed between mobile and stationary phases is examined on the basis of statistical mechanical considerations. [Only for convenience' sake, however, we here use the terminology "competition model" to represent only the model developed in Chapter Ⅷ. Cf. Section(C)]. Competition model is different from the former models in the following respects. Thus, competition model *formally* is established by neglecting the presence of the components other than gradient substance or ACMCL (corresponding to good solvent) in the solvent system which contains plural components in general; the energetical interaction between sample molecule and gradient substance is also neglected;

and the energetical interaction taking place on the adsorbent surfcace and both energetical and geometrical interaction taking place in the liquid phase, respectively, among gradient substances are incorpolated in parameter φ [see eq(8.45)]. In competition model, the geometrical interaction between sample molecule and gradient substance taking place on the adsorbent surface is emphasized in particular (in which the terminology "competition model" has its rise), and the geometrical interactions among gradient substances taking place on the adsorbent surface also plays an important role in the adsorption and desorption of sample molecules [cf. the subsection entitled "Chemical Equilibrium Equatioin Model versus Competition Model" in Section(C)]. This can be compared with Boehm, Martire, Armstrong and Bui model in which the nearest neighbor energetical interaction χ_{ij}^{m} taking place in the liquid phase is emphasized [see the subsection entitled "Criticism (2)"].

It should be underlined that, in competition model, account is taken implicitly of the presence of the compoments other than gradient substance in the solvent system (although it is neglected formally). In fact, in competition model, $J \equiv E + kT\ln\tau$ and ℓ represent the absolute values of the *differences* of the free energies of the total thermodynamic system between the two states when sample molecule and gradient substance are on the adsorbent surface and when they are in solution, respectively; the difference of the free energy is called as free energy of adsorption. The components other than gradient substance interfere in determining the free energy of adsorption. The effect from the components other than gradient substance is also incorpolated in parameter φ [eq(8.45)]. It can be considered that both the interaction between sample molecule and the components other than gradient substance in the solvent system and the interaction among these components contribute to the effect. In some instance, account is also taken of the energetical interaction between sample molecule and gradient substance (i.e., the adsorption of gradient substances on the surface of sample molecule) taking place in both mobile and stationary phases [see ChapterⅧ(B) and (F)]. What is arbitrary in competition model would be that the assumption of a constant value of φ (to be precise, the assumption of a slowly enough change of the φ value in the range of m applied) is used.

It, in general, would be reasonable to consider that φ is a function of m ($\equiv x_{1m}$), and that $\dot{B}$ or $\dot{k}$ can be represented as

$$\dot{B}(m) = \frac{1}{1+q[\varphi(m)\cdot m+1]^{-x'}} \qquad \text{(A11.153)}$$

or

$$\dot{k}(m) = q[\varphi(m)\cdot m+1]^{-x'} \qquad \text{(A11.153')}$$

[To be precise, Γ [eq(8.43)] should also be considered to be a function of m; this means that both β and q are functions of m [see eqs(8.49) and (8.50)]. It can be assumed, however, that Γ is almost constant since the case of the dilute solution of sample

molecules is treared [see eq(8.43)].] The judgement about whether the approximation of constant φ (and constant Γ) is justifiable or not should be entrusted to the experiment finally. For both HA and ion-exchange chromatographies, it was verified that all the experiments (carried out in certain ranges of m values) can be explained satisfactorily by using competition model with a constant φ value (see Chapter Ⅷ and X). For reversed-phase chromatography also, the experiments can be explained satisfactorily by using competition model with a constant φ value (Chapter Ⅸ) except for some cases when it can be suggested that φ depends on m slightly (provided that there is no systematic experimental error; cf. Figs 9.12, 9.15 and 9.16).

It can be considered that the conclusion in favor of the virtually constant φ value is intimately connected to the unimportance [in the sense argued in the subsection entitled "Criticism (2)"] of the energetical interaction χ_{ij}^{m} taking place in the mobile phase as judged with reversed-phase chromatography from the similar chromatographic behaviors of polystyrene between aqueous THF/H_2O and nonaqueous $MeCl_2$/ACN systems. With HA chromatography, the unimportance of the energetical interaction χ_{ij}^{m} is implied in the fact that the chromatopgrphic behaviors of DNA and other acidic substances are almost independent of the presence of KCl in the carrier liquid [see Chapter Ⅷ(A); also see ref (7.1)]. The fact that essentially the same chromatogram of collagen can be obtained in both presence and absence of 1 M urea in the carrier liquid (see the legend for Fig 8.14) also supports the unimportance of χ_{ij}^{m} with HA chromatography. In fact, it is very reasonable to assume that both KCl and urea change the solubility or the χ_{ij}^{m} value for sample molecules considerably. It would be possible to say that competition model with a virtually constant φ value is applicable to a wide range of chromatographies whether the adsorption of sample molecule on the adsorbent surfcae is brought about by an "active" or a "passive" mechanism [cf. the subsection entitled "General" in Section(D)].

References

Chapter I

1.1 A.Katchalsky and P.F.Curran, Nonequilibrium Thermodynamics in Biophysics, Harvard University Press, Cambridge, Massachusetts and London, 1981, p.74

Chapter VI

6.1. T.Kawasaki and G.Bernardi, Biopolymers **9**, 257 (1970)
6.2. T.Kawasaki, Biopolymers **9**, 277 (1970)
6.3. T.Kawasaki, Biopolymers **9**, 291 (1970)
6.4. T.Kawasaki, J.Chromatogr., **93**, 313 (1974)
6.5. T.Kawasaki, J.Chromatogr., **93**, 337 (1974)
6.6. T.Kawasaki, Sep.Sci.Technol., **16**, 817 (1981)
6.7. T.Kawasaki, Sep.Sci.Technol., **22**, 121 (1987)
6.8. T.Kawasaki and S.Takahashi, Sep.Sci.Technol., **23**, 193 (1988)
6.9. T.Kawasaki, M.Niikura and Y.Kobayashi, J.Chromatogr., **515**, 91 (1990)
6.10. T.Kawasaki, Sep.Sci.Technol., **17**, 337 (1982)

Chapter VII

7.1. T.Kawasaki, J.Chromatogr., **544**, 147 (1991)
7.2. T.Kawasaki, Sep.Sci.Technol., **16**, 439 (1981)

Chapter VIII

8.1. M.I.Kay, R.A.Young and A.S.Posner, Nature (London), **204**, 1050 (1964)
8.2. K.Sudarsanan and R.A.Young, Acta Crystallogr., **B25**, 1534 (1969)
8.3. A.Tiselius, S.Hjertén and Ö.Levin, Arch.Biochem.Biophys., **65**, 132 (1956)
8.4. G.Bernardi, Methods Enzymol., **21**, 95 (1971)
8.5. G.Bernardi, Methods Enzymol., **22**, 325 (1971)
8.6. G.Bernardi, Methods Enzymol., **27**, 471 (1973)
8.7. G.Bernardi, Nature (London), **206**, 779 (1965)
8.8. D.A.Wilson and C.A.Thomas,Jr, Biochim.Biophys.Acta, **331**, 333 (1973)
8.9. G.Bernardi, M.G.Giro and C.Gaillard, Biochim.Biophys.Acta, **278**, 409 (1972)
8.10. R.K.Main and L.J.Cole, Arch.Biochem.Biophys., **68**, 186 (1957)
8.11. G.Bernardi, Biochim.Biophys.Acta, **91**, 686 (1964)
8.12. M.Niikura and T.Kawasaki, Chromatography (Japanese edition in Japanese), **11**, 64 (1990) (Orally presented in Nihon-Toshi Center, Tokyo)
8.13. T.Kawasaki, J.Chromatogr., **82**, 167 (1973)
8.14. T.Kawasaki, J.Chromatogr., **82**, 191 (1973)
8.15. T.Kawasaki, Sep.Sci.Technol., **23**, 601 (1988)
8.16. T.Kawasaki, Sep.Sci.Technol., **23**, 617 (1988)

8.17. T.Kawasaki, Sep.Sci.Technol., **23**, 1105 (1988)
8.18. T.Kawasaki, J.Chromatogr., **157**, 7 (1978)
8.19. T.Imoto, L.N.Johnson, A.C.T.North, D.C.Phillips and J.A.Pulpley, in P.D.Boyer, H.Lardy and K.Myrbäck (Editors), The Enzymess, Vol. 7, Academic Press, New York, 1972, p.692
8.20. T.Kawasaki, J.Chromatogr., **151**, 95 (1978)
8.21. S.M.Krane and M.J.Glimcher, J.Biol.Chem., **237**, 2991 (1962)
8.22. D.R.Taves and R.C.Reedy, Calcif.Tissue Res., **3**, 284 (1969)
8.23. T.Kawaski, Sep.Sci.Technol., **17**, 785 (1982)
8.24. E.Daniel and Z.Alexandrowicz, Biopolymers **1**, 473 (1963)
8.25. T.Kawasaki, Sep.Sci.Technol., **17**, 407 (1982)
8.26. T.Kawasaki and G.Bernardi, Biopolymers, **9**, 269 (1970)
8.27. G.Bernardi and T.Kawasaki, Biochim.Biophys.Acta, **160**, 301 (1968)
8.28. T.Kadoya, Y.Amano, T.Isobe, Y.Kato, K.Nakamura, and T.Okuyama, Bunseki Kagaku (Japanese edition in English), **33**, E287 (1984)
8.29. T.Sasagawa, T.Okuyama, and D.C.Teller, J.Chromatogr., **240**, 329 (1982)
8.30. W.Traub and K.A.Piez, Adv.Protein Chem., **25**, 243 (1971)
8.31. K.A.Piez, in G.N.Ramachandran (Editor), Treatise on Collagen Vol. 1, Academic Press, New York, 1967, p.267
8.32. K.A.Piez, in G.N.Ramachandran and A.H.Raddi (Editors), Biochemistry of Collagen, Plenum Press, New York, 1976, p.1
8.33. J.E.Eastoe, in G.N.Ramachandran (Editor), Treatise on Collagen Vol. 1, Academic Press, New York, 1967, p.1
8.34. K.A.Piez, E.Eigner, and M.S.Lewis, Biochemistry **2**, 58 (1963)
8.35. P.P.Fietzek and K.Kühn, Int.Rev.Connect.Tissue Res., **7**, 1 (1976)
8.36. A.L.Rubin, M.P.Drake, P.F.Davidson, D.Pfahl, P.T.Speakman, and F.O.Schmitt, Biochemistry **4**, 181 (1965)
8.37. M.P.Drake, P.F.Davidson, and F.O.Schmitt, Biochemistry **5**, 301 (1966)
8.38. P.P.Fietzek and K.Kühn, Top.Curr.Chem., **29**, 1 (1972)
8.39. K.A.Piez and B.L.Trus, J.Mol.Biol., **122**, 419 (1978)
8.40. H.Hofman, P.P.Fietzek, and K.Kühn, J.Mol.Biol., **125**, 137 (1978)
8.41. A.Veis, in G.N.Ramachandran (Editor), Treatise on Collagen Vol. 1, Academic Press, New York, 1967, p.367
8.42. T.Kawasaki, S.Takahashi and K.Ikeda, Eur.J.Biochem **152**, 361 (1985)
8.43. T.Kawasaki, J.Chromatogr., **82**, 219 (1973)
8.44. T.Kawasaki, J.Chromatogr., **82**, 237 (1973)
8.45. T.Kawasaki, J.Chromatogr., **93**, 257 (1974)
8.46. T.Kawasaki, J.Chromatogr., **93**, 275 (1974)
8.47. T.Kawasaki, Sep.Sci.Technol., **17**, 575 (1982)
8.48. T.Kawasaki, Sep.Sci.Technol., **17**, 1397 (1982)

8.49. T.Kawasaki, Sep.Sci.Technol., **23**, 2365 (1988)
8.50. T.Kawasaki, Sep.Sci.Technol., **24**, 1109 (1989)
8.51. T.Kawasaki and M.Niikura, Sep.Sci.Technol., **25**, 397 (1990)
8.52. W.S.Hancock, C.A.Bishop, R.L.Prestidge, D.R.K.Harding and M.T.W.Hearn, J.Chromatogr., **153**, 391 (1978)
8.53. A.Oyane, K.Onuma, T.Kokubo, and A.Ito, J.Phys.Chem.B, **103**, 8230 (1999)
8.54. K.Onuma, A.Oyane, K.Tsutsui, K.Tanaka, G.Treboux, N.Kanzaki, and A.Ito, J.Phys.Chem.B, **104**, 10563 (2000)
8.55. K.Ohta, H.Monma, S.Takahashi, H.Kobayashi, Y.Ohkatsu, and T.Kawasaki, Transactions of the 14 th Symposium on Apatite, 1998, p.15 (in Japanese) (Orally presented in Hokkaido University, Sapporo)
8.56. K.Ohta, H.Monma and S.Takahashi, J.Biomed.Mater.Res., **55**, 409 (2001)

Chapter IX

9.1. C.H.Lochmüller and M.B.McGranaghan, Anal.Chem., **61**, 2449 (1989)
9.2. A.Alhedai, R.E.Boehm, and D.E.Martire, Chromatographia **29**, 313 (1990)
9.3. M.A.Stadalius, M.A.Quarry, T.H.Mourey, and L.R.Snyder, J.Chromatogr., **358**, 17 (1986)
9.4. J.P.Larmann, J.J.DeStefano, A.P.Goldberg, R.W.Stout, L.R.Snyder, and M.A.Stadalius, J.Chromatogr., **255**, 163 (1983)
9.5. M.A.Quarry, R.L.Grob, and L.R.Snyder, Anal.Chem., **58**, 907 (1986)
9.6. S.Terabe, H.Nishi, and T.Ando, J.Chromatogr., **212**, 295 (1981)
9.7. J.Koyama, J.Nomura, Y.Shiojima, Y.Ohtsu, and I.Horii, J.Chromatogr., **625**, 217 (1992)
9.8. X.Geng and F.E.Regnier, J.Chromatogr., **296**, 15 (1984)
9.9. H.Colin and G.Guiochon, J.Chromatogr.Sci., **18**, 54 (1980)
9.10 A.Tchapla, H.Colin, and G.Guiochon, Anal.Chem., **56**, 621 (1984)
9.11 P.Dufek and E.Smolková, J.Chromatogr., **257**, 247 (1983)
9.12. P.Dufek, J.Chromatogr., **281**, 49 (1983)
9.13. P.Jandera, Chromatographia **19**, 101 (1984)
9.14. P.Jandera, J.Chromatogr., **314**, 13 (1984)
9.15. K.A.Boni, F.A.Sliemers, and P.B.Stickney, J.Polym.Sci. (part A-2), **6**, 1579 (1968)
9.16. D.S.Cannell and F.Rondelez, Macromolecules **13**, 1599 (1980)
9.17. T.D.Long and J.L.Anderson, J.Polym.Sci. (Polym.Phys.Ed.), **22**, 1261 (1984)

Chapter X

10.1. W.Kopaciewicz, M.A.Rounds, J.Fausnaugh, and F.E.Regnier, J.Chromatogr., **266**, 3 (1983)
10.2. E.S.Parente and D.B.Wetlaufer, J.Chromatogr., **355**, 29 (1986)
10.3. R.W.Stout, S.I.Sivakoff, R.D.Ricker, and L.R.Snyder, J.Chromatogr., **353**, 439 (1986)

10.4. A.N.Hodder, M.I.Aguilar, and M.T.W.Hearn, J.Chromatogr., **476**, 391 (1989)
10.5. T.Sasagawa, Y.Sakamoto, T.Hirose, T.Yoshida, Y.Kobayashi, Y.Sato, and K.Koizumi, J.Chromatogr., **485**, 533 (1989)
10.6. M.A.Rounds and F.E.Regnier, J.Chromatogr., **283**, 37 (1984)
10.7. Y.Baba, M.Fukuda, and N.Yoza, J.Chromatogr., **458**, 385 (1988)
10.8. Y.Baba, N.Yoza, and S.Ohashi, J.Chromatogr., **348**, 27 (1985)
10.9. Y.Baba, N.Yoza, and S.Ohashi, J.Chromatogr., **350**, 461 (1985)
10.10. D.W.Green and R.Aschaffenburg, J.Mol.Biol., **1**, 54 (1959)
10.11. R.Townend and S.N.Timasheff, J.Am.Chem.Soc., **79**, 3613 (1957)
10.12. H.A.McKenzie and W.H.Sawyer, Nature (London), **214**, 1101 (1967)
10.13. J.K.Zimmerman, G.H.Barlow, and I.M.Klotz, Arch.Biochem.Biophys., **138**, 101 (1970)
10.14. O.E.Mills and L.K.Creamer, Biochim.Biophys.Acta, **379**, 618 (1975)
10.15. H.B.Bull, J.Am.Chem.Soc., **68**, 745 (1946)
10.16. C.G.Horvath, B.A.Preiss and S.R.Lipsky, Anal.Chem., **39**, 1422 (1967)
10.17. R.Dybczy ń ski, J.Chromatogr., **31**, 155 (1967)
10.18. D.E.Henderson and D.J.O'Connor, Adv.Chromatogr., **23**, 65 (1984)
10.19. K.Miyabe and G.Guiochon, Adv.Chromatogr., **40**, 1 (2000)

Appendix V

A5.1 T.Kawasaki, Sep.Sci.Technol., **17**, 319 (1982)
A5.2 T.Kawasaki, Sep.Sci.Technol., **17**, 695 (1982)

Appendix Ⅷ

A8.1. D.J.Prockop, R.A.Berg, K.I.Kivirikko, and J.Uitto, in G.N.Ramachandran and A.H.Raddi (Editors), Biochemistry of Collagen, Plenum Press, New York, 1976, p.163
A8.2. P.Bornstein, Annu.Rev.Biochem., **43**, 567 (1974)
A8.3. J.Vuust and K.A.Piez, J.Biol.Chem., **245**, 6201 (1970)
A8.4. J.Vuust and K.A.Piez, J.Biol.Chem., **247**, 856 (1972)
A8.5. E.Lazarides and L.N.Lukens, Nature (New Biol.), **232**, 37 (1971)
A8.6. L.L.Kisselev and O.O.Favorova, Adv.Enzymol., **40**, 141 (1974)
A8.7. R.B.Loftfield, Biochem.J., **89**, 82 (1963)
A8.8. R.B.Loftfield, Biochem.J., **128**, 1353 (1972)
A8.9. L.Pauling, Festschrift Arthur Stoll, Birkhauser Press, Basel, 1957, p.597
A8.10. R.Gierge, D.Kern, J.P.Ebel, H.Grosjean, S.DeHenau, and H.Chantrenne, Eur.J.Biochem., **45**, 351 (1974)
A8.11. J.Parker, J.W.Pollard, J.D.Friesen, and C.P.Stanners, Proc.Natl.Acad.Sci.U.S.A., **75**, 1091 (1978)
A8.12. J.J.Hopfield, Proc.Natl.Acad.Sci.U.S.A., **71**, 4135 (1974)
A8.13. J.Ninio, Biochimie, **57**, 587 (1975)

A8.14. A.R.Fersht and M.M.Kaethner, Biochemistry, **15**, 3342 (1976)
A8.15. F.von der Haar and F.Cramer, Biochemistry, **15**, 4131 (1976)
A8.16. T.Yamane and J.J.Hopfield, Proc.Natl.Acad.Sci.U.S.A., **74**, 2246 (1977)
A8.17. G.N.Ramachandran and C.Ramakrishnan, in G.N.Ramachandran and A.H.Raddi (Editors), Biochemistry of Collagen, Plenum Press, New York, 1976, p.45
A8.18. C.Trocz and K.Kühn, Eur.J.Biochem., **7**, 454 (1969)
A8.19. P.H.von Hippel, in G.N.Ramachandran (Editor), Treatise on Collagen Vol. 1, Academic Press, New York, 1967, p.253
A8.20. A.B.Robinson, Proc.Natl.Acad.Sci.USA, **71**, 885 (1974)
A8.21. R.A.Trelstad, A.H.Kang, B.P.Toole, and J.Gross, J.Biol.Chem., **247**, 6469 (1972)
A8.22. M.L.Tanzer, D.Monroe, and J.Gross, Biochemistry **5**, 1919 (1966)
A8.23. M.Stark and K.Kühn, Eur.J.Biochem., **6**, 534 (1968)
A8.24. H.Furthmayer and R.Timpl, Anal.Biochem., **41**, 510 (1971)
A8.25. V.Näntö, J.Maatela, and E.Kulonen, Acta.Chem.Scand., **17**, 1604 (1963)
A8.26. V.Näntö, J.Pikkarainen, and E.Kulonen, J.Am.Leather Chem.Assoc., **60**, 63 (1965)

Appendix IX

A9.1. M.Yamauchi, C.Noyes, Y.Kuboki, and G.L.Mechanic, Proc.Natl.Acad.Sci.USA, **79**, 7684 (1982)
A9.2. F.Fuller and H.Boedtker, Biochemistry, **20**, 996 (1981)

Appendix XI

A11.1. K.Sakodynskii, J.Chromatogr., **73**, 303 (1972)
A11.2. von E.Wicke, Kolloid Z., **86**, 295 (1939)
A11.3. J.N.Wilson, J.Am.Chem.Soc., **62**, 1583 (1940)
A11.4. J.Weiss, J.Chem.Soc. (London), p.297 (1943)
A11.5. D.DeVault, J.Am.Chem.Soc., **65**, 532 (1943)
A11.6. A.J.P.Martin and R.L.M.Synge, Biochem.J., **35**, 1358 (1941)
A11.7. L.Lapidus and N.R.Amundson, J.Phys.Chem., **56**, 984 (1952)
A11.8. J.J.van Deemter, F.J.Zuiderweg, and A.Klinkenberg, Chem.Eng.Sci., **5**, 271 (1956)
A11.9. H.C.Thomas, Ann.N.Y.Acad.Sci., **49**, 161 (1948)
A11.10. E.Glueckauf, K.H.Barker, and G.P.Kitt, Disc.Faraday Soc., **7**, 199 (1949)
A11.11. G.Houghton, J.Chromatogr., **15**, 5 (1964)
A11.12. T.S.Sørensen, J.Chromatogr., **88**, 197 (1974)
A11.13. R.Aris, Proc.R.Soc. (London), **A252**, 538 (1959)
A11.14. J.C.Giddings and H.Eyring, J.Phys.Chem., **59**, 416 (1955)
A11.15. J.C.Giddings, J.Chem.Phys., **26**, 169 and 1755 (1957)
A11.16. J.C.Giddings, Dynamics of Chromatography: Part I , Principles and Theory, Marcel Dekker Press, New York, 1965
A11.17. E.Kućera, J.Chromatogr., **19**, 237 (1965)

A11.18. M.Kubín, Collect.Czech.Chem.Commun., **30**, 1104 (1965)
A11.19. G.Szegö, Orthogonal Polynomials, Colloquium Publications Vol.XXIII, American Mathematical Society Press, New York, 1939, p.101
A11.20. O.Grubner, Adv.Chromatogr., **6**, 173 (1968)
A11.21. E.Grushka, J.Phys.Chem., **76**, 2586 (1972)
A11.22. E.Grushka, L.R.Snyder and J.H.Knox, J.Chromatogr.Sci., **13**, 25 (1975)
A11.23. H.Vink, J.Chromatogr., **135**, 1 (1977)
A11.24. J.H.Knox, J.Chromatogr.Sci., **15**, 352 (1977)
A11.25. C.Horváth and H.J.Lin, J.Chromatogr., **149**, 43 (1978)
A11.26. G.Guiochon, S.Golshan-Shirazi, and A.M.Katti, Fundamentals of Preparative and Nonlinear Chromatography, Academic Press, New York, 1994
A11.27. P.C.Haarhoff and H.J.van der Linde, Anal.Chem., **38**, 573 (1966)
A11.28. J.L.Wade, A.F.Bergold, and P.W.Carr, Anal.Chem., **59**, 1286 (1987)
A11.29. S.Golshan-Shirazi and G.Guiochon, Anal.Chem., **61**, 1276 and 1368 (1989)
A11.30. R.S.Alm, R.J.P.Williams, and A.Tiselius, Acta Chem.Scand., **6**, 826 (1952)
A11.31. L.Hagdahl, R.J.P.Williams, and A.Tiselius, Ark.Kemi, **4**, 193 (1952)
A11.32. K.O.Donaldson, V.J.Tulane, and L.M.Marshall, Anal.Chem., **24**, 185 (1952)
A11.33. H.Busch, R.B.Hurlbert, and van R.Potter, J.Biol.Chem., **196**, 717 (1952)
A11.34. E.Stahl, Angew.Chem. (International Ed.), **3**, 784 (1964)
A11.35. H.Kanazawa, T.Sunamoto, and Y.Matsushima, Anal.Chem., **72**, 5961 (2000)
A11.36. H.Kanazawa, Chromatography (Japanese edition in Japanese), **23**, 13 (2002) (Orally presented in Tokyo Metropolitan University, Hachioji)
A11.37. Y.Okada, C.Sakamoto, H.Kanazawa, A.Kikuchi, T.Okano, E.Ayano, T.Nishimura, and M.Ando, Chromatography (Japanese edition in Japanese), **23**, 69 (2002) (Orally presented in Tokyo Metropolitan University, Hachioji)
A11.38. B.Drake, Ark.Kemi, **8**, 1 (1955)
A11.39. E.C.Freiling, J.Am.Chem.Soc., **77**, 2067 (1955)
A11.40. E.C.Freiling, J.Phys.Chem., **61**, 543 (1957)
A11.41. A.Velayudhan and M.R.Ladisch, Anal.Chem., **63**, 2028 (1991)
A11.42. A.S.Said, A.I.Ch.E.J., **2**, 477 (1956)
A11.43. H.Schwab, W.Rieman III, and P.A.Vaughan, Anal.Chem., **29**, 1357 (1957)
A11.44. L.R.Snyder, J.Chromatogr., **13**, 415 (1964)
A11.45. L.R.Snyder, Chromatogr.Rev., **7**, 1 (1965)
A11.46. L.R.Snyder and D.L.Saunders, J.Chromatogr.Sci., **7**, 195 (1969)
A11.47. L.R.Snyder, J.W.Dolan, and J.R.Gant, J.Chromatogr., **165**, 3 (1979)
A11.48. L.R.Snyder and J.W.Dolan, Adv.Chromatogr., **38**, 115 (1998)
A11.49. P.Jandera and J.Churáček, J.Chromatogr., **91**, 223 (1974)
A11.50. P.Jandera, J.Churáček, and L.Svoboda, J.Chromatogr., **174**, 35 (1979)
A11.51. W.W.Pitt,Jr, J.Chromatogr.Sci., **14**, 396 (1976)
A11.52. H.Poppe, J.Paanakker, and M.Bronckhorst, J.Chromatogr., **204**, 77 (1981)

A11.53. S.Yamamoto, K.Nakanishi, R.Matsuno, and T.Kamikubo, Biotechnol.Bioeng., **25**, 1465 (1983)
A11.54. S.Yamamoto, K.Nakanishi, R.Matsuno, and T.Kamikubo, Biotechnol.Bioeng., **25**, 1373 (1983)
A11.55. N.K.Boardman and S.M.Partridge, Biochem.J., **59**, 543 (1955)
A11.56. L.R.Snyder, J.Chromatogr., **6**, 22 (1961)
A11.57. L.R.Snyder, J.Chromatogr., **8**, 178 (1962)
A11.58. P.Jandera and J.Churá č ek, J.Chromatogr., **91**, 207 (1974)
A11.59. P.Jandera and J.Churá č ek, Adv.Chromatogr., **19**, 125 (1980)
A11.60. E.Soczewi ń ski, Anal.Chem., **41**, 179 (1969)
A11.61. F.E.Regnier, Science **222**, 245 (1983)
A11.62. K.Kasai and Y.Oda, J.Chromatogr. (Biomed.Appl.), **376**, 33 (1986)
A11.63. C.Horváth, W.Melander, and I.Molnár, J.Chromatogr., **125**, 129 (1976)
A11.64. C.Horváth, W.Melander, and I.Molnár, Anal.Chem., **94**, 142 (1977)
A11.65. C.Horváth and W.Melander, J.Chromatogr.Sci., **15**, 393 (1977)
A11.66. O.Siano ğ lu, in B.Pullman (Editor), Molecular Association in Biology, Academic Press, New York, 1968, p.427
A11.67. S.V.Galushko, J.Chromatogr., **552**, 91 (1991)
A11.68. S.V.Galushko, Chromatographia, **36**, 39 (1993)
A11.69. S.V.Galushko, A.A.Kamenchuk, and G.L.Pit, J.Chromatogr. A, **660**, 47 (1994)
A11.70. B.L.Karger, J.R.Gant, A.Hartkopf, and P.H.Weiner, J.Chromatogr., **128**, 65 (1976)
A11.71. P.Jandera, H.Colin, and G.Guiochon, Anal.Chem., **54**, 435 (1982)
A11.72. R.Tijssen, H.A.H.Billiet, and P.J.Schoenmakers, J.Chromatogr., **122**, 185 (1976)
A11.73. P.J.Schoenmakers, H.A.H.Billiet, R.Tijssen, and L.De Galan, J.Chromatogr., **149**, 519 (1978)
A11.74. E.A.DiMarzio, J.Chem.Phys., **35**, 658 (1961)
A11.75. D.E.Martire and R.E.Boehm, J.Liq.Chromatogr., **3**, 753 (1980)
A11.76. R.E.Boehm and D.E.Martire, J.Phys.Chem., **84**, 3620 (1980)
A11.77. R.E.Boehm, D.E.Martire, D.W.Armstrong, and K.H.Bui, Macromolecules, **16**, 466 (1983)
A11.78. R.E.Boehm, D.E.Martire, D.W.Armstrong, and K.H.Bui, Macromolecules, **17**, 400 (1984)
A11.79. R.E.Boehm and D.E.Martire, Anal.Chem., **61**, 471 (1989)
A11.80. P.J.Flory, Principles of Polymer Chemistry, Cornell University Press, New York, 1971
A11.81. T.L.Hill, An Introduction to Statistical Thermodynamics, Addison-Wesley Press, Massachusetts, 1960, Chapter 14, 19 and 21